Εθνικό Μετσόβιο Πολυτεχνείο
Σχολή Πολιτικών Μηχανικών

National Technical University of Athens
School of Civil Engineering

Διπλωματική Εργασία

ΑΝΤΩΝΙΟΥ ΜΑΡΙΑ – ΠΛΟΥΜΑΚΗ ΜΑΡΙΑ

Επιβλέποντες :

Καθηγητής Γ. Γκαζέτας

Δρ. Φ. Καρυδάκης

Επ. Καθ. Ι. Αναστασόπουλος

ΑΡΙΘΜΗΤΙΚΗ ΚΑΙ ΠΕΙΡΑΜΑΤΙΚΗ ΔΙΕΡΕΥΝΗΣΗ ΚΑΙΝΟΤΟΜΟΥ ΣΥΣΤΗΜΑΤΟΣ ΔΥΣΚΑΜΨΙΑΣ ΚΑΙ ΑΠΟΣΒΕΣΗΣ INSTED – FUSEIS ΜΕ ΘΕΩΡΗΣΗ ΑΛΛΗΛΕΠΙΔΡΑΣΗΣ ΕΔΑΦΟΥΣ-ΚΑΤΑΣΚΕΥΗΣ

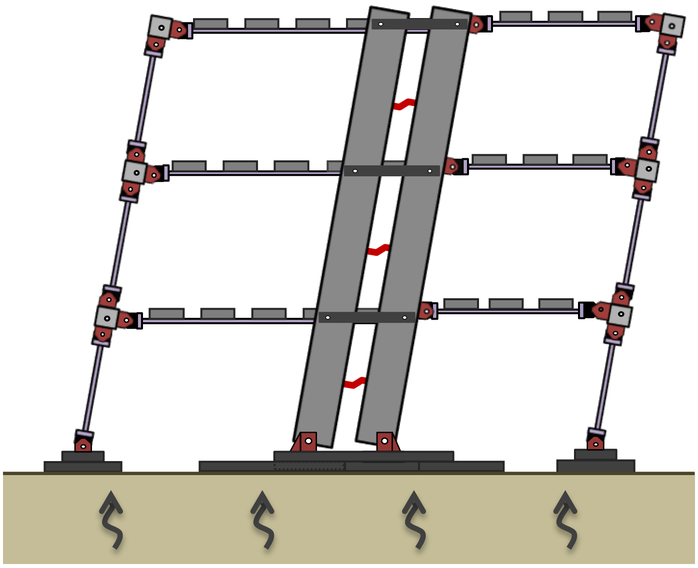

NUMERICAL AND EXPERIMENTAL ANALYSIS OF AN INNOVATIVE STIFFNESS AND ENERGY DISSIPATION SYSTEM INSTED – FUSEIS CONSIDERING SOIL-STRUCTURE INTERACTION

Diploma Thesis

ANTONIOU MARIA – PLOUMAKI MARIA

Supervised by :

Professor G.Gazetas

Dr. Ph. Karydakis

Ass. Prof. I. Anastasopoulos

ΑΘΗΝΑ ΜΑΡΤΙΟΣ 2013

ATHENS MARCH 2013

Ευχαριστίες

Ολοκληρώνοντας τη διπλωματική μας εργασία, νιώθουμε βαθιά την ανάγκη να ευχαριστήσουμε τους ανθρώπους που συνέβαλαν στη επίτευξη του στόχου αυτού.

Αρχικά, θα θέλαμε να ευχαριστήσουμε θερμά τον καθηγητή Γ. Γκαζέτα και τον Δρ. Φ. Καρυδάκη,για την ευκαιρία που μας έδωσαν να συνεργαστούμε μαζί τους. Ήταν τιμή μας που τους συναναστραφήκαμε κατά τα χρόνια των σπουδών μας. Επιπλέον, εκτιμούμε ιδιαίτερα το γεγονός ότι στήριξαν από την αρχή την ιδέα αυτής της διπλωματικής και συνέβαλαν καθοριστικά στην επιτυχή συνεργασία των δύο τομέων, Γεωτεχνικού και Δομοστατικού.

Ιδιαίτερες ευχαριστίες οφείλουμε στον επίκουρο καθηγητή Ι. Αναστασόπουλο, για την εξαιρετική συνεργασία που αναπτύξαμε μαζί του τους τελευταίους μήνες. Η πολύτιμη καθοδήγηση, οι υποδείξεις και η αμέριστη συμπαράστασή του ήταν καθοριστικές για την επιτυχή ολοκλήρωση αυτής της εργασίας.

Φυσικά, δε θα μπορούσαμε να μην ευχαριστήσουμε θερμά τον Δρ. Βασίλη Δρόσο για την πολύτιμη συμβολή του στη διεξαγωγή των πειραμάτων αλλά και για τις συμβουλές που μας παρείχε. Βεβαίως, ευχαριστούμε πολύ και όλα τα υπόλοιπα μέλη του Εργαστηρίου Εδαφομηχανικής που μας στήριξαν ενεργά κατά τη διάρκεια της εργασίας αυτής. Σημαντικό ρόλο για την εκπόνηση των πειραμάτων διαδραμάτισε σαφέστατα και το εργαστήριο Μεταλλικών Κατασκευών και τα μέλη του. Συγκεκριμένα, οφείλουμε ένα μεγάλο ευχαριστώ στον κ. Στέλιο Κατσατσίδη για τη σημαντική βοήθεια που μας παρείχε.

Επίσης, θα θέλαμε να ευχαριστήσουμε όλους τους φίλους μας για την ανεκτίμητη συμπαράσταση τους όλο αυτό το διάστημα.

Ολοκληρώνοντας, νιώθουμε την ανάγκη να ευχαριστήσουμε περισσότερο απ΄ όλους τις οικογένειές μας για την διαρκή στήριξη που μας παρέχουν.

ΑΝΑΛΥΤΙΚΗ & ΠΕΙΡΑΜΑΤΙΚΗ ΔΙΕΡΕΥΝΗΣΗ ΚΑΙΝΟΤΟΜΟΥ ΣΥΣΤΗΜΑΤΟΣ ΔΥΣΚΑΜΨΙΑΣ ΚΑΙ ΑΠΟΣΒΕΣΗΣ
INSTED – FUSEIS
ΜΕ ΘΕΩΡΗΣΗ ΑΛΛΗΛΕΠΙΔΡΑΣΗΣ ΕΔΑΦΟΥΣ–ΚΑΤΑΣΚΕΥΗΣ

ΠΕΡΙΛΗΨΗ

Βασική ιδέα:

Το αντικείμενο της παρούσας διπλωματικής εργασίας είναι η διερεύνηση της σεισμικής συμπεριφοράς ενός καινοτόμου συστήματος δυσκαμψίας και απορρόφησης ενέργειας σε πολυώροφα κτίρια, μια ιδέα του Καθηγητή κ. Ιωάννη Βάγια, που μελετήθηκε αρχικά από τον κ. Φαίδωνα Καρυδάκη.

Αρχική προσέγγιση:

Μέχρι τώρα, η συνηθισμένη πρακτική για την επίτευξη της απαιτούμενης αντοχής και δυσκαμψίας έναντι οριζόντιων φορτίων στις μεταλλικές και τις κατασκευές από σκυρόδεμα είναι είτε πλαίσια ικανά να παραλάβουν ροπή στους κόμβους τους (πλαίσια ροπής), είτε τοιχώματα δυσκαμψίας, είτε συστήματα διαγωνίων ράβδων (χιαστί σύνδεσμοι δυσκαμψίας), με ή χωρίς εκκεντρότητα. Λαμβάνοντας υπ’ όψη τα πλεονεκτήματα και τα μειονεκτήματα κάθε τέτοιου συστήματος, εξετάζεται ένα νέο, που αποτελείται από δύο ισχυρούς κατακόρυφους στύλους συνδεόμενους καθ’ ύψος με οριζόντιες δοκούς (πλάστιμα στοιχεία) - στην ουσία μία κατακόρυφη δοκός Vierendeel.

Το συγκεκριμένο είναι ένα καινοτόμο σύστημα δυσκαμψίας και απορρόφησης ενέργειας, συνοπτικά καλούμενο στη συνέχεια **INSTED** (**IN**novative **ST**iffness and **E**nergy **D**issipation system). Διαθέτει τα χαρακτηριστικά ενός τοιχώματος δυσκαμψίας αλλά με πρόσθετα πλεονεκτήματα. Αφ’ ενός, έχει την ικανότητα απορρόφησης μεγάλης ποσότητας ενέργειας μέσω των πλαστικών παραμορφώσεων των πλάστιμων μελών (οριζόντιων δοκών) και αφ’ ετέρου, εφ’ όσον απαιτηθεί μετά από μία μεγάλη σεισμική καταπόνηση, την ευκολία επισκευής ή και πλήρους αντικατάστασης των μελών αυτών. Το σύστημα αυτό έχει μελετηθεί για μεταλλικές κατασκευές αλλά η εφαρμογή του βρίσκεται ακόμα σε πρώιμο στάδιο.

Η πειραματική του διερεύνηση ξεκίνησε στο Εργαστήριο Μεταλλικών Κατασκευών του ΕΜΠ, όπου εκπονήθηκαν στατικές μονοτονικές και ανακυκλικές φορτίσεις σε πραγματικής κλίμακας μοντέλα,

με βάση δύο διαφορετικά πρωτόκολλα φόρτισης. Αυτή συσχετίστηκε στη συνέχεια και με ανάλογες μη γραμμικές αναλύσεις.

Από τα πειράματα αυτά εξακριβώθηκε ότι η αντίσταση στα οριζόντια φορτία και οι πλαστικοποιήσεις κατά τη διάρκεια της φόρτισης συγκεντρώνονται σε συγκεκριμένα προεπιλεγμένα στοιχεία και θέσεις, δηλαδή στις οριζόντιες δοκούς, προστατεύοντας τα υπόλοιπα στοιχεία από διαρροή. Επιπλέον, το σύστημα απορρόφησης ενέργειας (οι οριζόντιες δοκοί) δεν συμμετέχει στην παραλαβή των κατακόρυφων φορτίων διαφοροποιώντας έτσι τα στοιχεία του φορέα με βάση την κύρια λειτουργία τους. Επομένως, το προτεινόμενο σύστημα παρουσιάζει σημαντικά πλεονεκτήματα, όπως είναι η ικανότητα απορρόφησης σημαντικής ποσότητας ενέργειας, παράλληλα με την ευχέρεια αντικατάστασης των πλαστικοποιηθέντων στοιχείων εφόσον αυτά δεν αποτελούν μέρος του φέροντος οργανισμού (όπως π.χ. τα υποστυλώματα).

<u>Σκοπός της διπλωματικής:</u>

Φυσικά, η διερεύνηση της συμπεριφοράς ενός τέτοιου συστήματος δεν θα μπορούσε να μην περιλαμβάνει δυναμικές αναλύσεις και περάματα, όπου θα φαινόταν ξεκάθαρα η πλάστιμη συμπεριφορά του και η προστασία της κατασκευής, στην οποία θα τοποθετούνταν σαν ενίσχυση. Αυτό ήταν και το κύριο έργο της διπλωματικής μας εργασίας. Προκειμένου, μάλιστα, τα αποτελέσματα να είναι όσο το δυνατόν πιο ρεαλιστικά, επιδιώξαμε να εντάξουμε το προτεινόμενο σύστημα, τόσο αναλυτικά όσο και πειραματικά, σε ένα υπάρχον μοντέλο τριώροφου κτιρίου (κλίμακας 1:10), που αντιστοιχεί σε πραγματική τριώροφη κατασκευή.

Η διάρθρωση της διπλωματικής εργασίας χωρίζεται σε δύο μέρη: Το μέρος Α' περιλαμβάνει τις αριθμητικές αναλύσεις, που έγιναν στον κώδικα *Abaqus*, ώστε να διερευνηθεί αρχικά αναλυτικά το προτεινόμενο σύστημα ενίσχυσης. Στη συνέχεια (μέρος Β') συγκεντρώνονται τα αποτελέσματα από τα στατικά και δυναμικά πειράματα που εκπονήθηκαν στο Εργαστήριο Εδαφομηχανικής του ΕΜΠ καθώς και κάποιες αντιπροσωπευτικές αναλύσεις των πειραμάτων αυτών.

Α' ΜΕΡΟΣ

Το αναλυτικό μέρος αυτής της εργασίας περιλαμβάνει τρισδιάστατες αριθμητικές αναλύσεις πεπερασμένων στοιχείων στο πρόγραμμα *Abaqus*, οι οποίες προσομοιώνουν τη συμπεριφορά:

- ✓ του συστήματος INSTED, σύμφωνα με την διάταξή του στα πειράματα πραγματικής κλίμακας, που είχαν διεξαχθεί στο Εργαστήριο Μεταλλικών Κατασκευών,
- ✓ του τριώροφου κτιρίου, σε κλίμακα μοντέλου (1:10)
- ✓ του ενισχυμένου κτιρίου μέσω του συστήματος INSTED και
- ✓ του ενισχυμένου κτιρίου μέσω ενός τοιχώματος δυσκαμψίας.

Σκοπός είναι, μέσω των αναλύσεων, να συγκριθεί η σεισμική απόκριση του ενισχυμένου κτιρίου με εκείνη του αρχικού (μη ενισχυμένου) και να εξεταστούν οι επιπλέον δυνατότητες του ενισχυμένου. Τόσο το πρωτότυπο όσο και το ενισχυμένο υποβάλλονται στην ίδια σειρά ελληνικών σεισμών μέτριας έντασης, η οποία είχε χρησιμοποιηθεί και κατά την πειραματική του διερεύνηση (Μοναστηράκι 1999, Αίγιο 1995, Καλαμάτα 1986, Λευκάδα 2003). Μάλιστα το ενισχυμένο υποβάλλεται και σε διεγέρσεις ισχυρότερης έντασης (Rinaldi, Jma, Takatori). Μέσω αυτών επιβεβαιώνεται η ικανότητα του συστήματος INSTED να απορροφά σημαντική ποσότητα ενέργειας κατά την ανακυκλική φόρτιση λόγω της μεγάλης πλαστιμότητας που διαθέτει. Αυτό έχει ως αποτέλεσμα, η ενισχυμένη κατασκευή να επιβιώνει μετά από ιδιαίτερα ισχυρές σεισμικές δονήσεις (με επιταχύνσεις πολύ μεγαλύτερες από τη επιτάχυνση σχεδιασμού του συστήματος ενίσχυσης) και μάλιστα αποκτώντας επιτρεπτές παραμορφώσεις. Αντιθέτως, το πρωτότυπο κτίριο αδυνατεί να ανταπεξέλθει ακόμη και στους μέτριας εντάσεως ελληνικούς σεισμούς και αστοχεί τελικά στο σεισμό της Λευκάδας με μηχανισμό “μαλακού ορόφου” (πλαστικοποίηση των υποστυλωμάτων του ισογείου).

Στη συνέχεια η σύγκριση του συστήματος INSTED με το τοίχωμα δυσκαμψίας αποδεικνύει την υπεροχή του πρώτου τύπου ενίσχυσης, τόσο σε επίπεδο παραμορφώσεων της κατασκευής όσο και σε επίπεδο επισκευής και επαναχρησιμοποίησης. Συγκεκριμένα, το τοίχωμα δυσκαμψίας παρουσιάζει αρκετά μικρότερη πλαστιμότητα και δυνατότητα επαναφοράς, με αποτέλεσμα να καταρρέει στο σεισμό του Takatori σε αντίθεση με το INSTED.

Β’ ΜΕΡΟΣ

Αφού έχουμε ολοκληρώσει τις αρχικές αριθμητικές αναλύσεις, προχωράμε στην πειραματική διερεύνηση, που αποτελείται τόσο από στατικά όσο και από δυναμικά πειράματα. Τα στατικά πειράματα περιλαμβάνουν μονοτονικές και ανακυκλικές φορτίσεις και πραγματοποιούνται με τη βοήθεια ενός εμβόλου που επιβάλλει μετακίνηση στο δεύτερο όροφο της πακτωμένης κατασκευής, προσομοιώνοντας τριγωνική κατανομή μετακίνησης. Όσο για τα δυναμικά πειράματα, το φυσικό μοντέλο της υπό κλίμακα κατασκευής τοποθετείται πάνω σε ένα στρώμα άμμου, που διαμορφώνεται χρησιμοποιώντας ένα κατάλληλο σύστημα διαβροχής της άμμου. Με αυτό τον τρόπο μελετάται η αλληλεπίδραση του συστήματος εδάφους-θεμελίωσης-ανωδομής. Μάλιστα το μοντέλο του ενισχυμένου κτιρίου δοκιμάζεται, μεταβάλλοντας την αντοχή του και τη δυσκαμψία του, έτσι ώστε να επιτύχουμε την επιθυμούμενη σχέση αντοχής και δυσκαμψίας κατασκευής-ενίσχυσης και να μελετήσουμε τα αποτελέσματα της αλληλεπίδρασης εδάφους-κατασκευής. Ως σεισμικές διεγέρσεις, χρησιμοποιούμε πραγματικά επιταχυνσιογραφήματα ποικίλης έντασης (ελληνικούς σεισμούς, του Northridge στις ΗΠΑ, και του Kobe στην Ιαπωνία).

Λαμβάνοντας υπόψη τα καινούρια δεδομένα του πειράματος, όσον αφορά το σύστημα INSTED, όπως τις ιδιότητες των υλικών κατασκευής, προχωράμε σε κάποιες αντιπροσωπευτικές αναλύσεις, που σκοπό κυρίως έχουν την προσομοίωση της πειραματικής διάταξης όσο το δυνατόν πιο ρεαλιστικά. Μέσω αυτών των αναλύσεων γίνεται πιο ξεκάθαρη η λειτουργία της κατασκευής σε αλληλεπίδραση με το έδαφος θεμελίωσης.

Σε τελικό στάδιο μελετάμε πειραματικά το σύστημα INSTED, αυτόνομο, χωρίς τη συμμετοχή της υπόλοιπης κατασκευής, αλλά με εφαρμογή της αντίστοιχης μάζας στην κορυφή του. Η διαμόρφωση αυτού του μονοβάθμιου συστήματος μας επιτρέπει να εξετάσουμε μεμονωμένα τη σεισμική του συμπεριφορά, ανεξάρτητα από τυχόν επιρροές της κατασκευής. Για τη επίτευξη αυτού του σκοπού επιβάλλουμε στο σύστημα τη ίδια χρονοΪστορία σεισμών, όπως και στα προηγούμενα δυναμικά πειράματα, καταλήγοντας σε πολύ χρήσιμα συμπεράσματα.

Table of contents

CHAPTER A.3

CHAPTER A.4

PART B'

CHAPTER B.1

CHAPTER B.2

CHAPTER B.3

Introduction

SCOPE OF THE THESIS

1. Earthquake Design of Structures

Due to the lack of knowledge and experience, but also due to the limited existing data of seismic records worldwide, earthquake hazard was greatly underestimated in the past. However, this perception altered after some great earthquakes (such as the Kobe earthquake in Japan, 1995), which resulted to the collapse of many buildings and severe damage of others. Existing buildings proved unable to withstand seismic excitations of such great amplitude and the need for careful seismic design of structures arose. Of course, the alternative of increasing a building' strength with regard to the amplitude of the seismic records is not always the case, since this leads to a huge increase of the acceleration and velocity that the structure develops, therefore, to greater displacements. Consequently, this design method does not always result in safer design. This realization led to the development of a new seismic design methodology, which mainly aims at controlling earthquake damage rather than avoiding it (ductility and capacity design). Ductility design ensures that critical structural members can sustain loads that exceed their capacity, without collapsing, and capacity design aims at guiding failures to less important structural members (beams instead of columns) and to non-brittle mechanisms (bending instead of shearing) [Park & Paulay, 1976].

However, most of the existing structures have been designed according to older seismic codes, thus do not comply with the aforementioned newer seismic design model. For example, in Greece, about 85% of the building stocks date before 1985 and therefore lack adequate ductility and capacity design. Such structures are vulnerable even to relatively small seismic motions and develop brittle failure mechanisms (Figure 1.1), a fact that was also clearly proved during the M_s 5.9 earthquake near Athens in 1999; the earthquake led to 145 fatalities due to collapse of 100 buildings and damage beyond repair to 13000 buildings [Papadopoulos et al., 2000]. Hence, the need for reinforcement in terms of strength, stiffness or ductility appears imperative for this kind of structures.

1.1 Typical resistance systems

The ductility and capacity design aims at increasing the stiffness and strength of a structure and is being implemented in various ways. As far as concrete structures are concerned, shear resistance walls (Figure 1.2a) are a usual type of seismic retrofit. In regard to steel structures, this design methodology is established through the introduction of some typical horizontal resistance systems, such as moment-resisting frames and anti-diagonal bracings, with or without eccentricity (Figure 1.2 b,c,d). Each one of these systems has its own advantages and disadvantages in regards to seismic response:

Moment resisting frames (Figure 1.2b) are the most flexible among the aforementioned systems and therefore perform in a ductile manner, dissipating energy through the creation of plastic hinges at the edges of their beams. It has been proved, though, that under strong seismic shaking, these systems do not always work as desired. The horizontal beams can demonstrate sufficient strength, thus rigid beam-column connections are inevitably charged with the whole amount of seismic energy and shear cracks are created. Since these connections are designed to undertake both horizontal and vertical loading it becomes quite difficult to repair any damage, without disturbing the normal operation of the building.

Frames using ***anti-diagonal bracings without eccentricity*** (Figure 1.2c) as a horizontal resistance system are much stronger and stiffer than moment-resisting frames, so less sensitive towards large displacements, but less ductile. For bracings of type (X), energy dissipation takes place through yielding of the tensile diagonal, which is designed to be weaker than the rest of the structural members, hence is the first to reach its yield stress during a seismic motion, while the rest of the structure remains elastic. The system is not designed to bear any vertical loading, therefore is easier to repair after a serious damage. For bracings of type (V) or (Λ), the compression diagonal needs to participate in the bearing of seismic loading and therefore becomes the critical member of the system, due to its brittle type of failure (buckling). Hence, these kinds of systems cannot be used for energy dissipation design (q=1.5). Of course, they still have the advantage of resisting only to horizontal seismic loads, offering ease of replacement after damage, without affecting the rest of the structure, which bears the vertical loads.

Finally, the ***anti-diagonal bracings with eccentricity*** (Figure 1.2d) dissipate seismic energy through plastification of the link beam, which is deliberately designed to be the weakest member of the system. This type of horizontal resistance systems combine some advantages of the previous ones, since they are stronger and stiffer than moment - resisting frames, but also more ductile than anti-diagonal bracings without eccentricity. Nevertheless, they are quite difficult to repair, as the link beam is not easily accessible and is also part of the vertical loading bearing mechanism.

2. Proposal of this thesis: INSTED-FUSEIS system

The aforementioned design methodology of retrofitting structures with stiffer systems surely establishes the concentration of seismic force on these systems. Our aim, though, is to move one step further into the earthquake design of structures, by investigating the seismic performance of considerably ductile structural systems. The proposal of this thesis is to examine a system that, apart from the necessary stiffness and strength, will mainly display great ductility. This means that this system will be, of course, stiffer and stronger than the existing structure, but at the same time, very ductile, establishing that the structure will be able to deform and dissipate large amounts of energy, without collapsing. Actually, this parameter appears to be equally significant with the previous ones.

The INnovative STiffness and Energy Dissipation (INSTED) system (Figure 1.2e) is a recent novelty that corresponds to the proposed, but a not yet established design methodology (since the existing laws do not allow behaviour factor values larger than q=4). The system consists of two strong columns, closely positioned, articulated at the base and joined together with horizontal beams in a relatively tight arrangement; it is practically a vertical vierendeel beam. Combining the advantages of the previously mentioned systems, in terms of stiffness and strength, it can be theoretically used both as a horizontal resistance system for newly built structures or as reinforcement for existing buildings. Indeed, it has already been studied for steel structures, though, not yet implemented in reality. The object of investigation, in this thesis, is the possibility of introducing the INSTED - FUSEIS system in a concrete structure, as a means of retrofit under seismic loading.

2.1 Main Structure of the Thesis

The INSTED system has already been tested under real scale pushover tests in the Steel Structures Laboratory of NTUA [Karydakis, 2011]. The scope of this thesis is to examine, both numerically and experimentally, the seismic performance of an existing building, retrofitted with the INSTED system, taking also account of the effects of soil structure interaction (SSI). For this purpose, a scaled-down model of an idealised 3-storey structure (Figure 1.3) is considered [Nonika Antonaki, 2012] for both the numerical and experimental program. The numerical analyses constitute *Part A* and the experimental program is compiled in *Part B*.

Part A: Before testing the physical model of the retrofitted structure in the shaking table of the Laboratory of Soil Mechanics of NTUA, a number of numerical dynamic analyses are conducted (*ABAQUS)*. Firstly, the real-scale experiments (conducted in the Steel Structures Laboratory) of the INSTED system alone are simulated in order to result to a correct numerical model of this retrofitting system. Afterwards, a numerical model of the original building is made (Figure 1.4), in which the INSTED system will be introduced on next step. Also, the proposed retrofit is compared to another one, that of an RC shear wall, in order to result to the most effective one.

More specifically, the ***numerical analyses*** include simulation - in model scale – of:

- ✓ the original building
- ✓ the retrofitted building, after the attachment of the INSTED system and
- ✓ the retrofitted building, after the attachment of an RC shear wall.

The numerical models of the original building and the retrofitted one, with the RC wall, are compared to the experimental results, derived from the already completed experiments in the shaking table of the Laboratory of Soil Mechanics [N.Antonaki, 2012]. At the same time, comparisons are made, in numerical terms, between the performance of the original and the retrofitted building (with the INSTED system), in order to ascertain the contribution of the INSTED system in the structure's seismic behaviour. Finally, the performance of the building with both kinds of retrofit (with the RC wall and the INSTED system) is compared.

***Part B**:* The final step is that of the ***experimental program*,** conducted in the Laboratory of Soil Mechanics of NTUA. This includes monotonic and cyclic pushover tests, as well as shaking table testing. Various model configurations are tested, varying the strength of the INSTED retrofit, in order to result to the optimum design of this system. The pushover tests are conducted with the pushover apparatus, utilizing a loading protocol, similar to the one utilized in the pushover tests of the INSTED system alone, in the Steel Structures Laboratory. As for the dynamic tests of the building, the entire soil-foundation-structure system is modeled, placing the physical model of the building on top of a sand stratum, prepared using a carefully-calibrated sand raining system. A variety of real records of varying intensity (from earthquakes in Greece, Northridge US, and Kobe) are used as seismic excitation.

Introduction

Figures

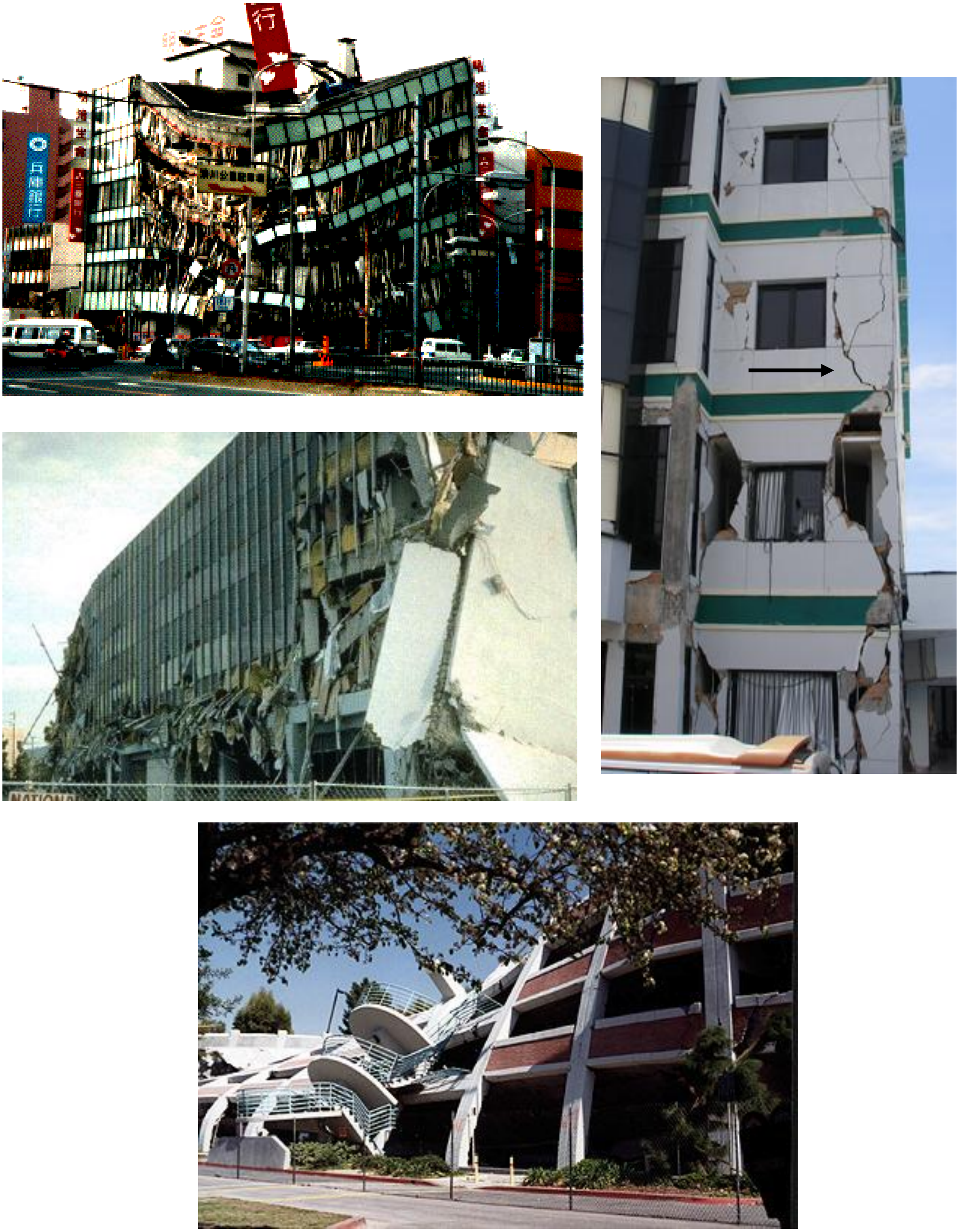

Figure 1.1 Brittle failures in structures as appears after earthquakes.

Need for Retrofit

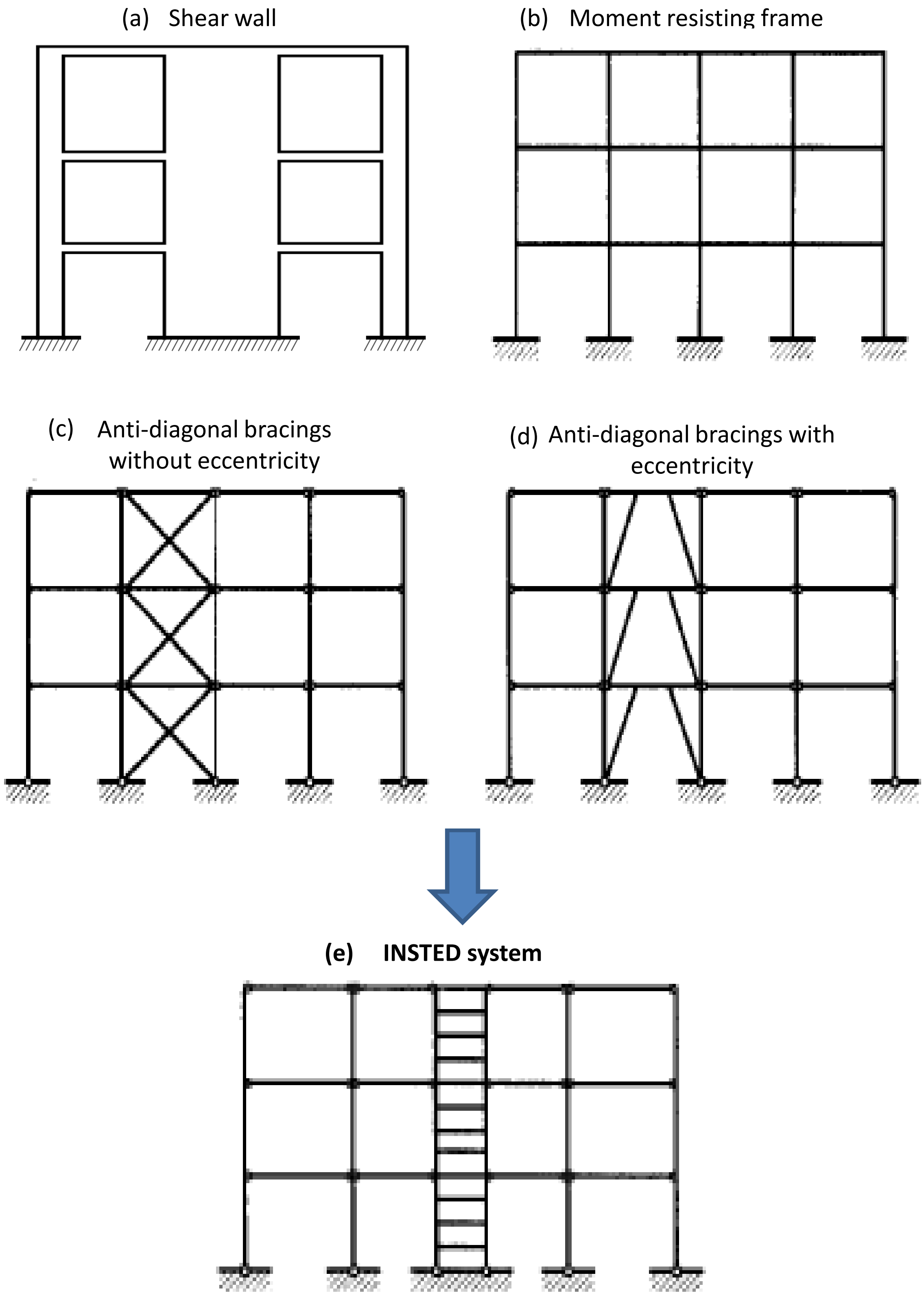

Figure 1.2 Usual types of horizontal resistance systems used for retrofit against horizontal loading and *the proposed retrofitting system.*.

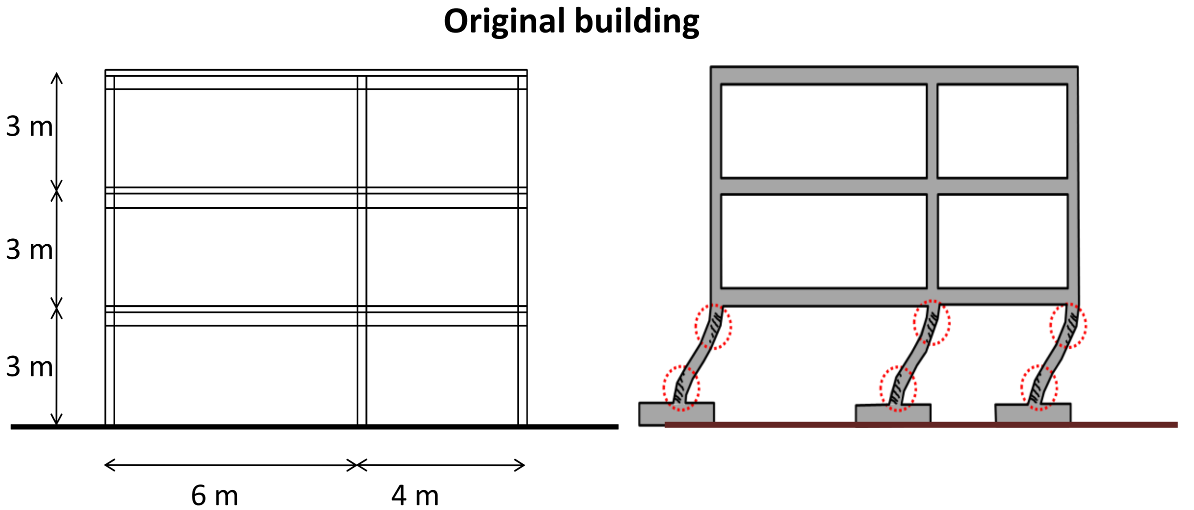

Figure 1.3 Schematic illustration of the under study building and its failure mechanism.

PROPOSAL

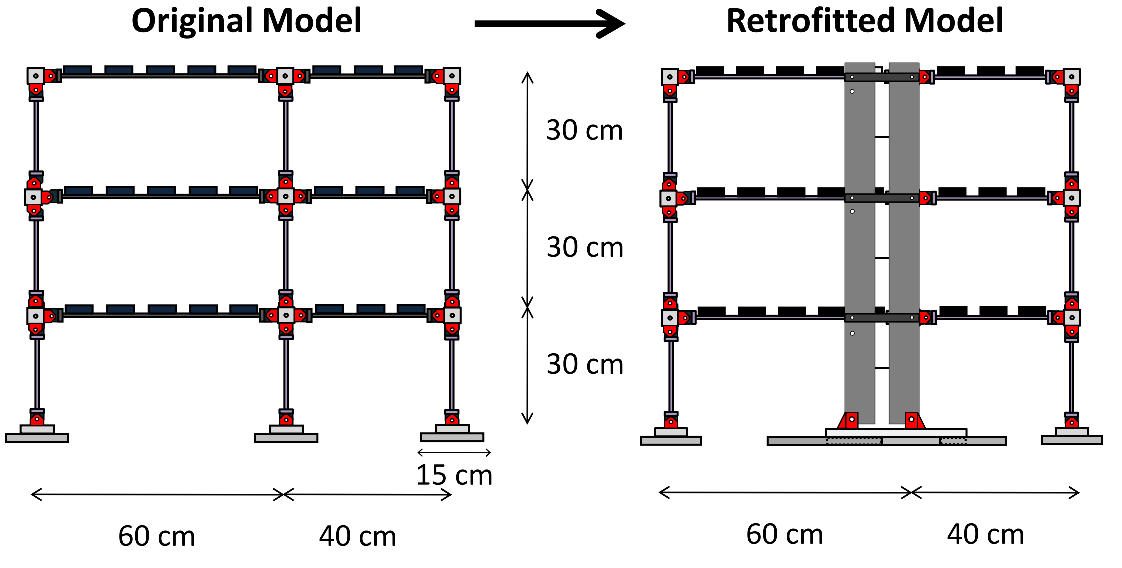

Figure 1.4 Schematic illustration of real scale frame and the proposed retroffited one. introduction of the “INSTED” system to the original building.

CHAPTER A.1

PERFORMANCE OF THE INSTED ON ANALYTICAL APPROACH – COMPARISON WITH THE EXPERIMENTS

1.1 The INSTED system

The Innovative Stiffness and Energy Dissipation (INSTED) system examined in our thesis is constituted of two strong columns, closely positioned, articulated at the base and joined together with horizontal beams in a relatively tight arrangement; it is practically a vertical vierendeel beam. The columns of the INSTED system are designed to remain elastic during seismic loading (rotate around the hinge) while *potential failure is guided to the horizontal beams*, where energy dissipation takes place through the plastic hinges that are formed.

When the acceleration amplitude of a seismic motion is lower than the design acceleration, the horizontal beams are designed to remain elastic and within limits of serviceability. But, when the seismic motions exceed this yield limit, these beams (fuse elements) dissipate energy by creating plastic hinges. Their strength is considerably smaller than the one of the columns, which means that the basic principle of capacity design is followed – failure is guided to less important structural members and non-brittle failure mechanisms are developed (bending instead of shearing). The length, number and type of section of these fuse elements (expendable beams) actually determine the strength and stiffness of the whole system. As long as the stiffness of the rest of the structure (in the case of moment resisting frames) is smaller than the one of the INSTED system, the damage is localized on the INSTED system and the rest of the structure remains elastic.

The horizontal elements can be beams of any section, like I-beams or hollow sections, or solid rods or bars (Figure 1.2). In order to avoid the creation of plastic hinges near the beam – column connection, these expandable beams were initially located at the middle of the span, with the use of receptacle beams welded to the columns, considerably stronger than the connecting elements (Figure 1.4). The receptacle beams also remain elastic, restraining the creation of plastic hinges in the expandable middle section. Therefore, it becomes clear that the more the expandable horizontal beams are moved away from the columns, by increasing the length of the receptacle beams that remain elastic, the bending moment developed is smaller and so is the cross-section needed (Figure 1.4). On the other hand, because of the larger relative vertical displacement, more plasticity is required from the fuse elements. Additionally, considerable axial force is developed, increasing the stiffness and strength of the INSTED system.

Due to the great ductility expected from the horizontal beams, the material that is preferred is steel, due to its hardening after yield. In fact, mild steel (S235) is preferred, since this ensures quicker yield of the retrofitting system, along with ductility and stiffness. This ductile behaviour of the system enables us to design with very a high behaviour factor (q), which means that we result to a smaller design acceleration, therefore, reduced moments and cross-sections (economic design). Of course, the fact that we do not expect large strength from our system could result in failure under static loading. However, this is not the case under dynamic motions. In fact, the cyclic behaviour of an earthquake is what guarantees its safety, since the ductility limits of the system are not easily overcome. Any static loading of similar acceleration amplitude would result to ultimate failure.

Besides the fact that this system is able to resist under strong seismic motions, it appears also that a structure that includes this system will be functional again after some intervention. Since the expendable connecting elements, to which the damage is localized, *do not participate in the dead load bearing mechanism*, it is quite easy and cheap to replace or repair them, after a strong earthquake. Therefore, this system may be an introduction to sustainable design. Taking all the above into consideration, we may conclude that this system resembles a shear resistance wall, but has the additional advantages of (a) being able to dissipate a larger amount of energy, through plastic deformation of the horizontal beams and (b) being easily repaired or replaced, if needed, after a strong earthquake.

1.1.1 Optimum design

After the series of real-scale experiments that took place in the Steel Structures Laboratory of NTUA, it became clear that *the optimum design of the INSTED system should include solid rods or bars as fuse elements* (Figure 1.5a), since these elements have the obvious advantage of length adjustment, which is crucial for parts of the system that are meant to be replaced or repaired. Between those two options, rods are easier to machine than rectangular bars, as are the supporting edges of the receptacle beams, rounded to prevent local damage from fatigue (Figure 1.6). In the case of rods, ring slots are easily constructed, leading to the formation of plastic hinges away from the supports and allowing for a long plastic zone with high plasticity and progressive section plastification. Therefore, the final design proposal (Figure 1.10) of the INSTED system [Karydakis et al, 2011] includes *a rod as the connecting element, between two strengthened vertical columns that remain elastic, length adjusting screws at both ends and weakened crossection away from the* *supports* [Figure 2]. This setup, conclusively, is the one that we will adopt for the analytical and experimental work made in our thesis.

1.2 Numerical Simulation of the real-scale experimental model setup

In order to have a right model of the structure as a whole, it is important that we result in a corresponding, to the experiments, analytical behaviour of the INSTED system itself. This is the reason why we simulated in *Abaqus* the experimental setup used for the pushover tests in the Steel Structure Laboratory (Figure 1.1). (The initial geometry was firstly created in *Ansys*.)

The structural members of the setup, i.e. the columns, receptacle beams and fuse elements of the INSTED system (Figure 1.7), as well as the steel frame, were simulated by 3-dimensional, 2-node linear beam elements (B31). The extensometer, used to measure the relative vertical displacements (Figure 1.8) of the receptacle beams, was simulated by a 3-dimensional stress/displacement truss element (T3D2) which had a negligible thickness, so as not to affect the measurements. The existence of an identical steel frame normal to the first one (Figure 1.3), guaranteeing the stability of the setup, was also taken into account by the constraint of the out-of-plane displacement of the nodes. Additionally, the diaphragmatic function of the storey plates was established with the kinematic conjunction of the nodes on top and base of the INSTED system.

Intending to describe the non-linear behaviour of the B31 members, we used the multi-yield elastic-plastic stress-strain curve that derived from the tensile strength test, conducted in the Steel Structure Laboratory of NTUA (Figure 1.11). As for the extensometer, an elastic constitutive model with the nominal steel Young's modulus was adopted (Figure 1.15).

1.3 Performance of the numerical model

1.3.1 Pushover testing

The push-over displacement was imposed at the base of the right column of the INSTED system. The loading protocol used consisted of a number of steps, in groups of three, each one imposing cyclic displacements on an increasing range (Figure 1.12). The final level of the loading implemented in each series of analyses differed, due to the fact that the setup could not reach the maximum displacement imposed (Figure 1.13). The factor that defined the loading magnitude was the relative vertical displacement (Δv), which needed to be the independent variable in the analysis, and was measured by the extensometers in each experiment (Figure 1.5b). Therefore the loading was calculated according to the one measured by the extensometers, and the maximum the setup would undertake if we imposed 150mm displacement (4% interstorey drift).

The image of the deformed INSTED system, with one or five fuse elements, after the end of the loading, is depicted in the following figures (Figure 1.14). The results of the analyses, in terms of system strength and vertical displacement (Δv) (Figure 1.15), as well as the experimental measurements, are also compiled in the set of figures at the end of chapter 2, for each type of the connecting elements of the INSTED system.

1.3.2 Comparison between the experiment and the numerical analyses

Having already obtained the results from the real-scale pushover experiments conducted in the Steel Structures Laboratory, we come to compare them with the numerical simulation ones. The graphs, exported from each case, much resemble the experimental ones at first sight, considering the uncertainties and flaws an experiment may include.

With a more detailed look, we can deduce that the analytical initial stiffness as well as the ultimate strength of the system is in good agreement with the measured data in most cases, especially in the first circles. Experimentally, the gradual strength degradation of the system is attributed to the non-linear steel behaviour, which cannot be realistically simulated in *Abaqus,* due to the way the program manages with it. This is the reason why the steel curve we imported in the analysis reached the ultimate stress yield, but did not include the descending branch after hardening.

As for the experiments that included rods as fuse elements [Figure 2], the initial stiffness and the form of the graph near the horizontal axis present slight differences compared to the analyses. It is a fact, indeed, that the experimental setup encases lots of imperfections due to the number of connections needed. These connections were not so rigid, as assumed in the analyses, resulting to a reduced real stiffness of the system. Additionally, the small gaps that inevitably existed around the rod enlarged as the rods deformed during the cyclic loading. When the rod detached the beam, it was subjected to no bending due to the gap, therefore, allowed deformation under no resisting force. The inability of the numerical analyses to simulate this factor justifies the deviations between the analyses and the experiments.

Chapter A.1

Figures

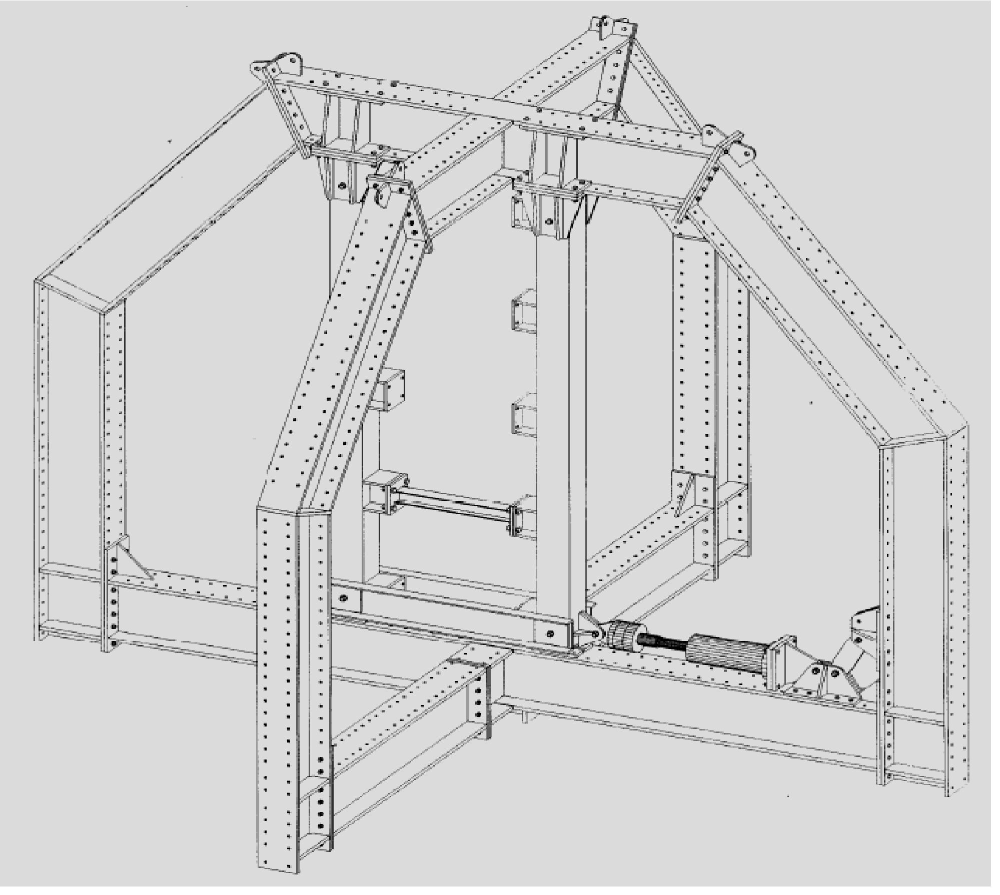

Figure 1.1 Axonometric design of the experimental setup.

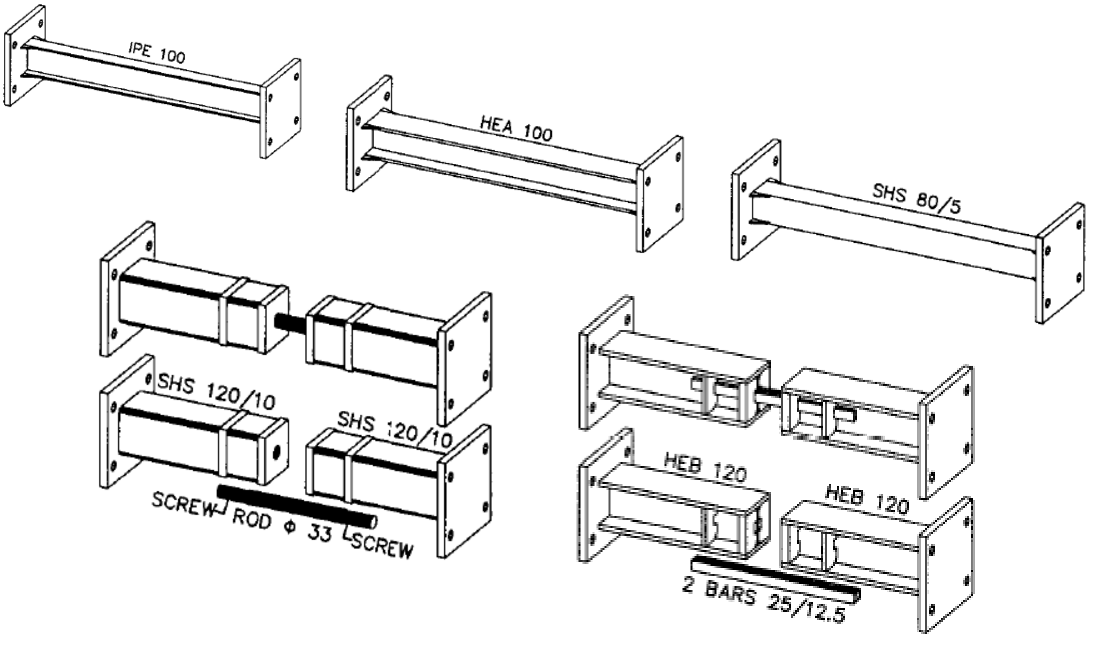

Figure 1.2 Typical cross sections of the fuse elements used in the real-scale experiments.

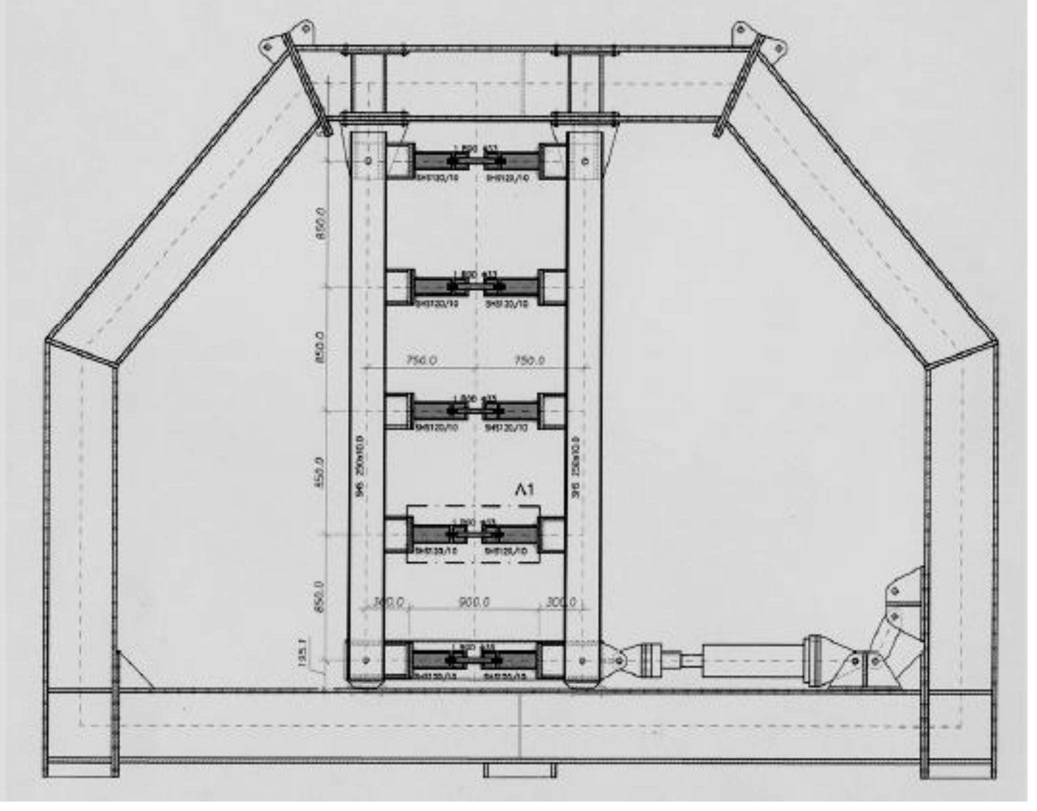

Figure 1.3 Schematic 2-D illustration of the experimental setup.

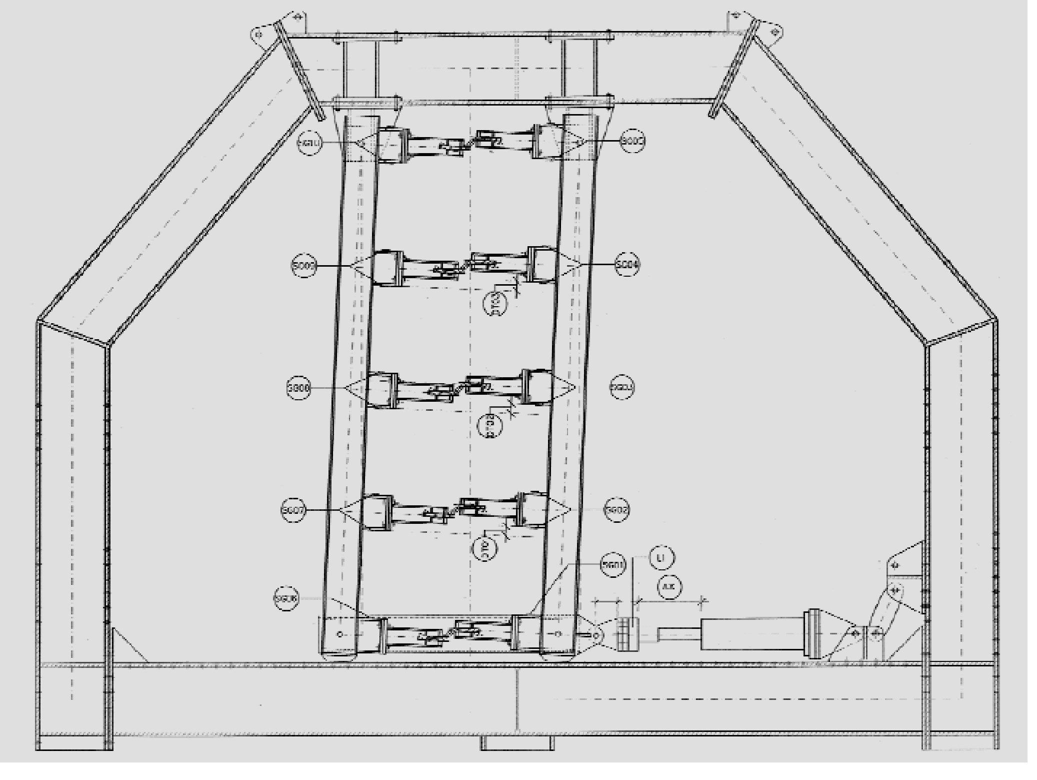

Figure 1.4 Deformed shape of the experimental setup during the pushover testing.

THE INSTED SYSTEM

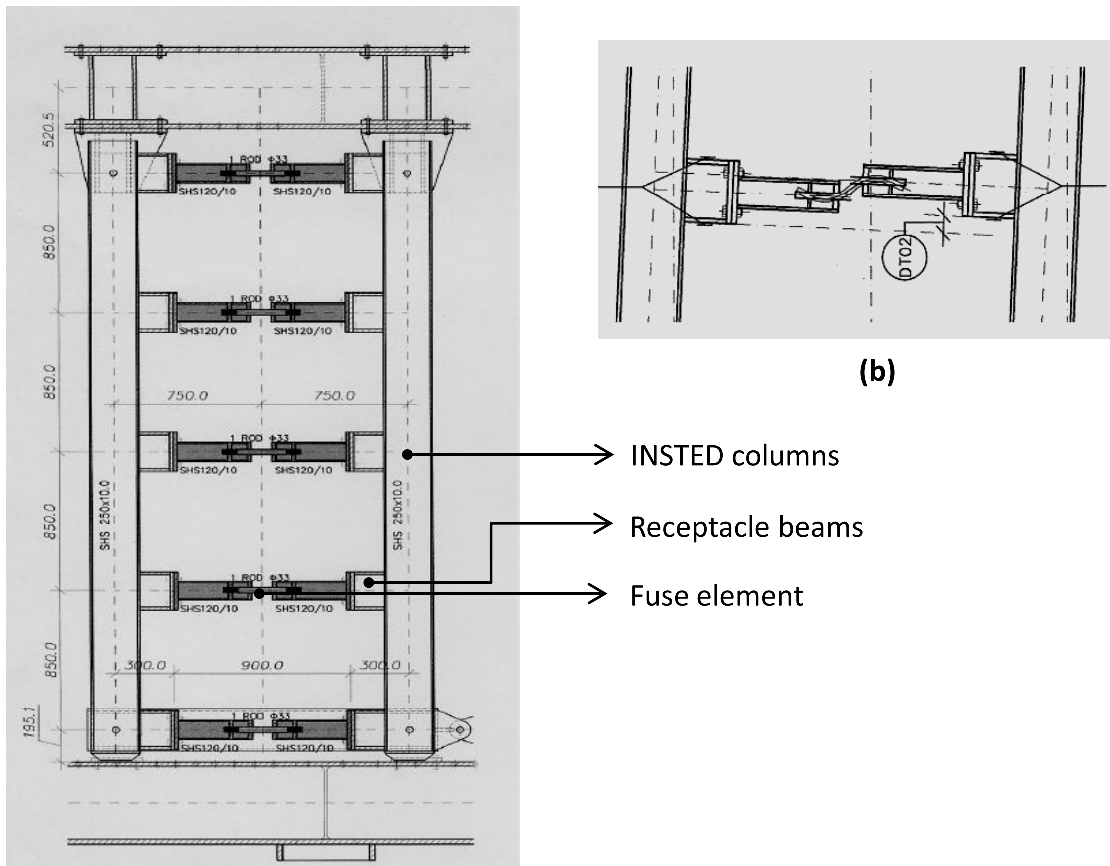

(a)

Figure 1.5 (a) The INSTED system with rods as fuse elements and **(b)** relative vertical displacement measured in the experiments (Δv).

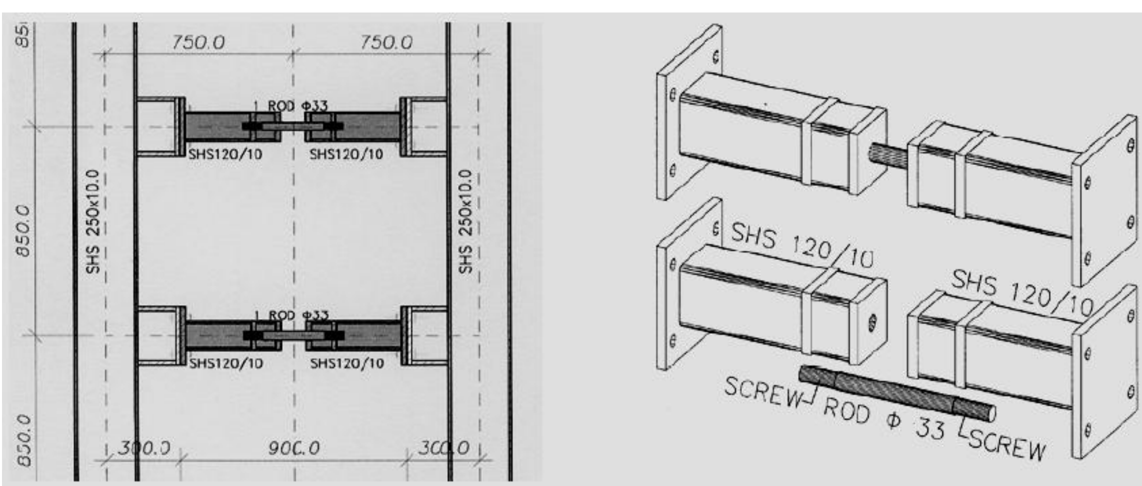

Figure 1.6 Detailed design of the most efficient type of fuse elements (INERD beams - RODS Φ33)

Figure 1.7 Experimental setup of the INSTED system (photograph from the Steel Structures Laboratory, NTUA).

Figure 1.8 Photograph of the device measuring relative vertical displacements (extensometer).

OPTIMUM DESIGN OF THE FUSE ELEMENTS

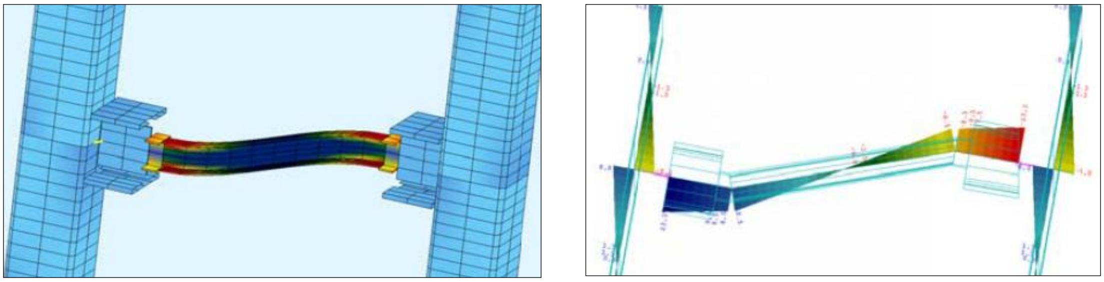

(a)

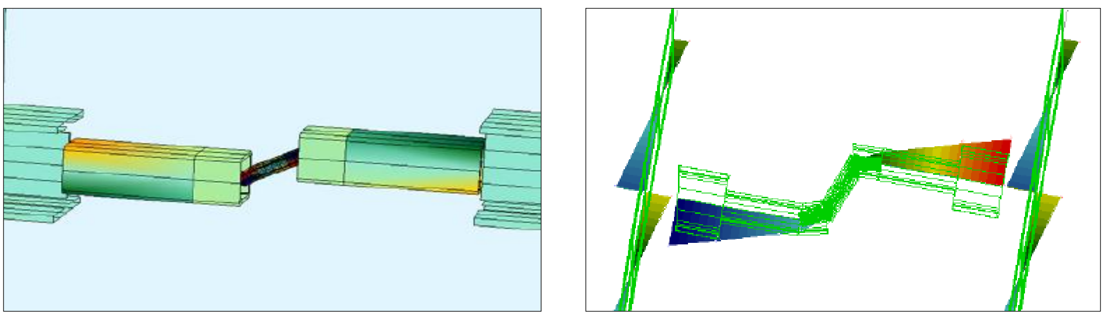

(b)

Figure 1.9 Design moment capacity values depending on the type of fuse element and thus the position where the plastic hinge is formed (analyses with *Sofistik software*). The superiority of setup (b) in terms of required moment capacity is obvious.

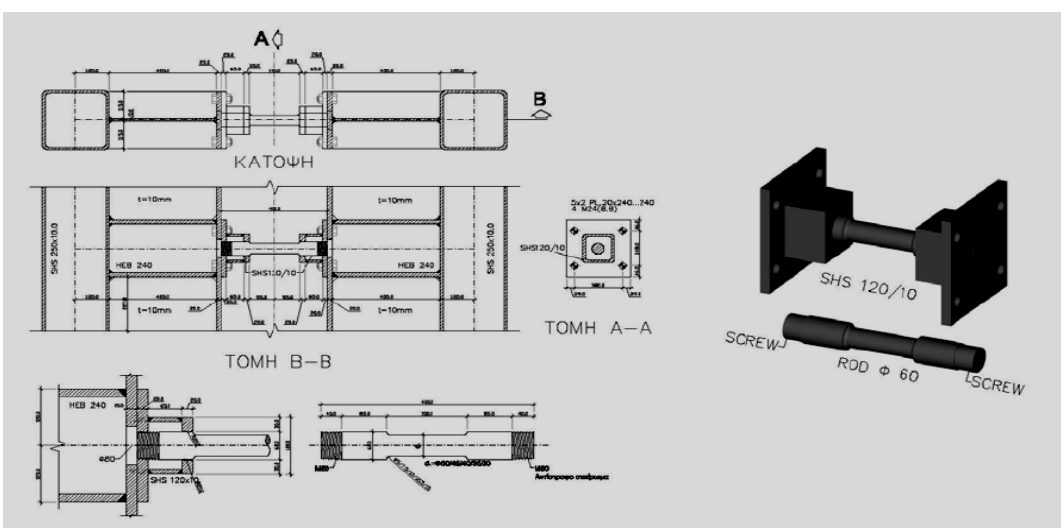

Figure 1.10 Final design proposal for the fuse elements of the INSTED system.

TENSILE STRENGTH TEST IN THE STEEL STRUCTURES LABORATORY

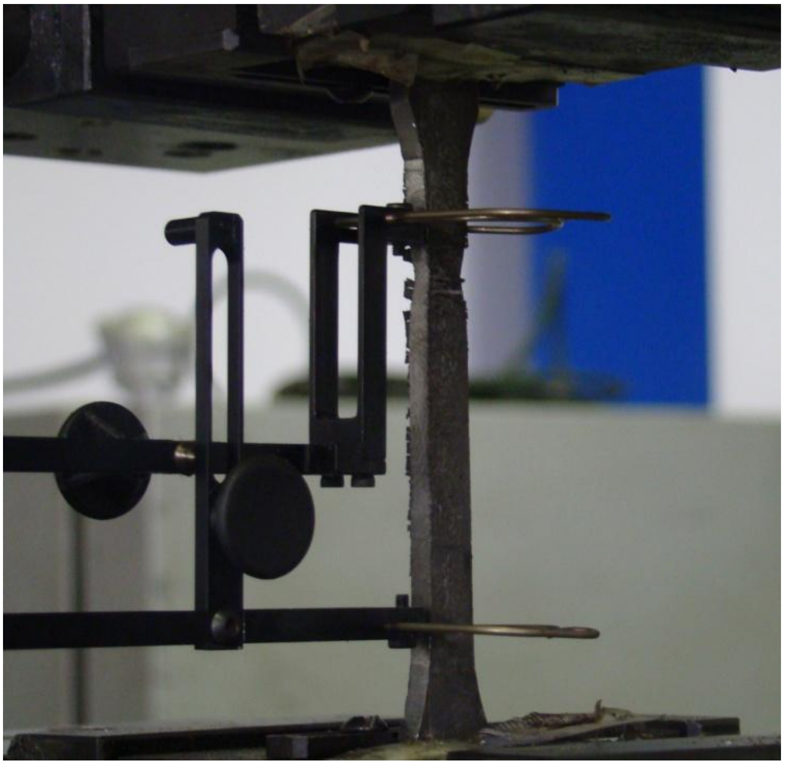

(a)

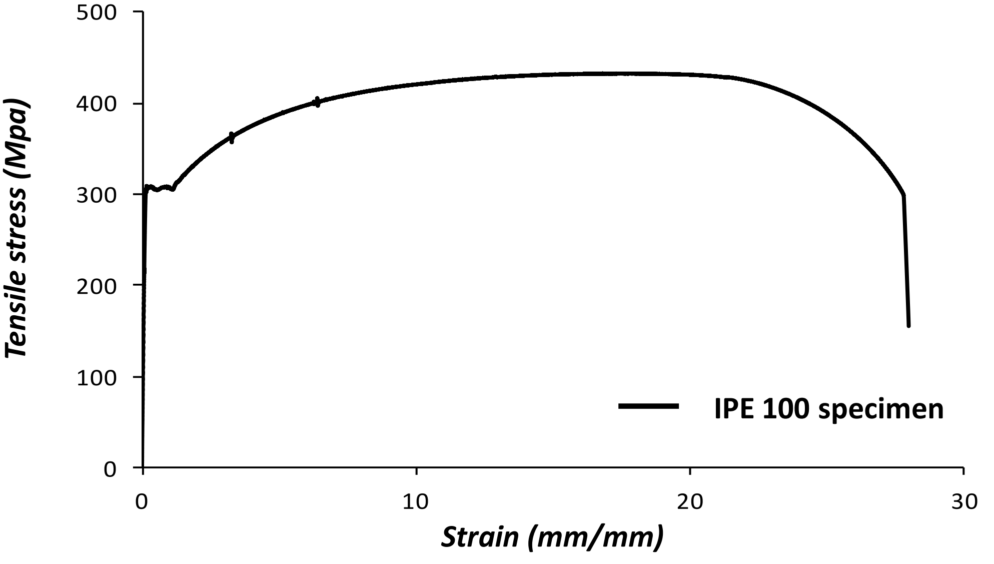

(b)

Figure 1.11 (a) Photograph of the IPE 100 specimen during the tensile strength test at the Steel Structures Laboratory of NTUA and **(b)** Tensile stress – strain curve derived from the respective test.

PUSHOVER TEST:
COMPARISON BETWEEN THE NUMERICAL ANALYSES AND THE EXPERIMENTS

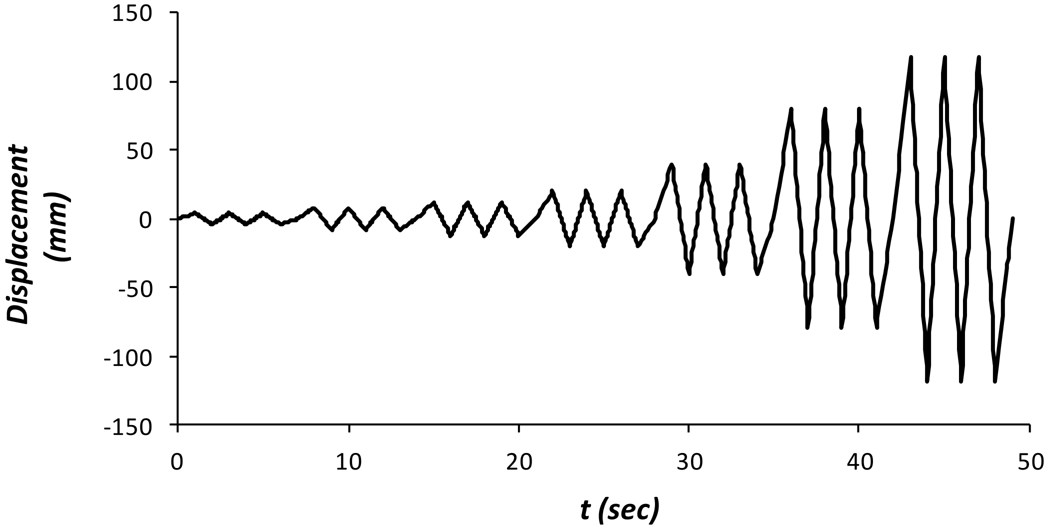

Figure 1.12 The time history displacement protocol used in the numerical analysis.

EXPERIMENT	DISPLACEMENT (mm)
1 IPE 100	78
5 IPE 100	92
5 SHS 80/5	118
1 ROD 33	99
5 ROD 33	95

Figure 1.13 Maximum displacement imposed on each test.

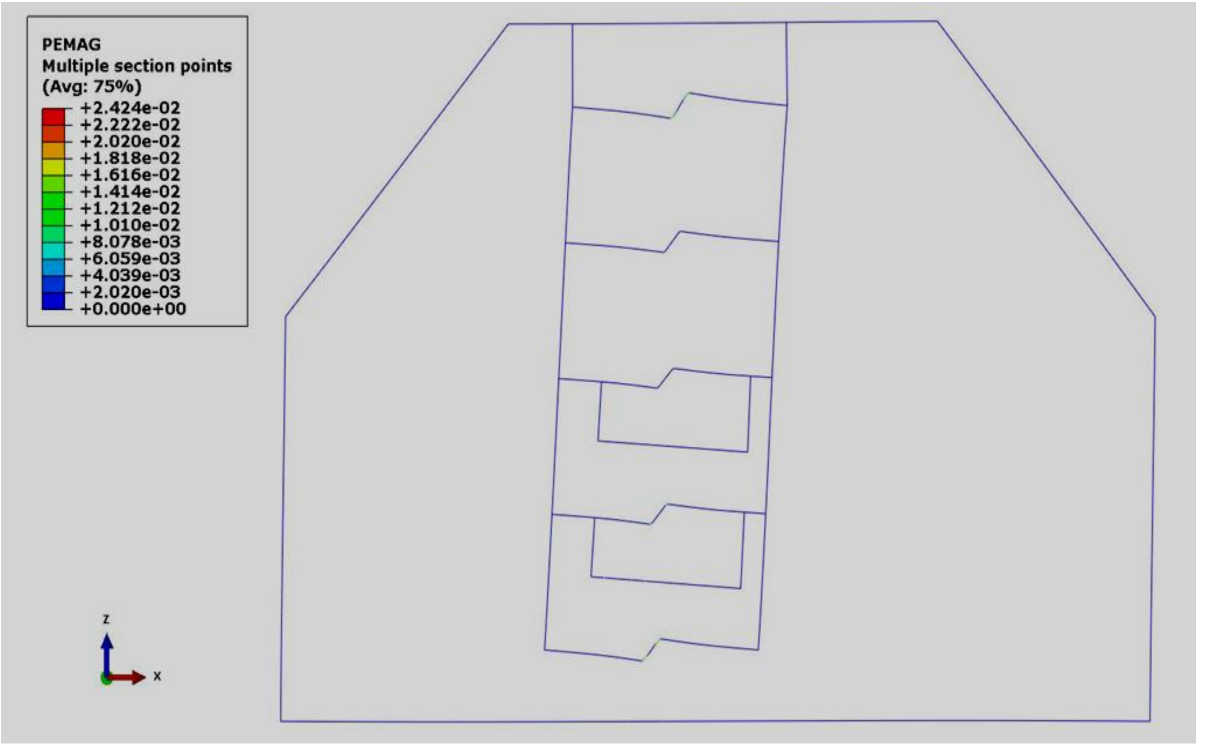

Figure 1.14 Deformed shape of the experimental setup in Abaqus (5 fuse elements).

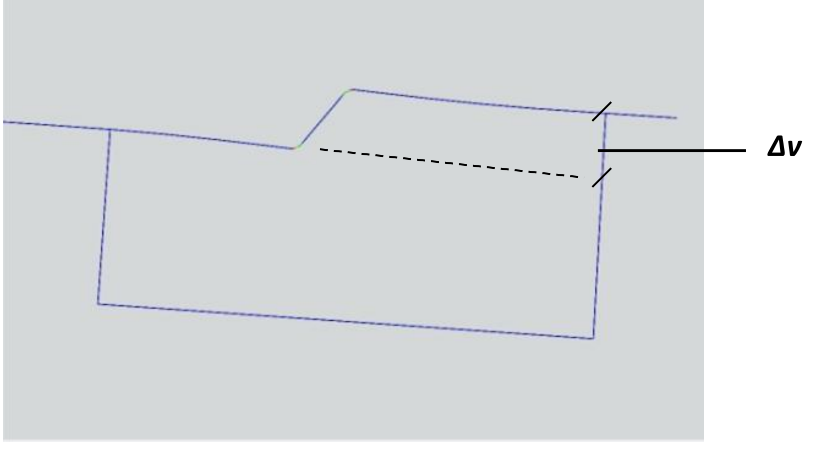

Figure 1.15 Measurement of the extensometer placed on the INSTED system.

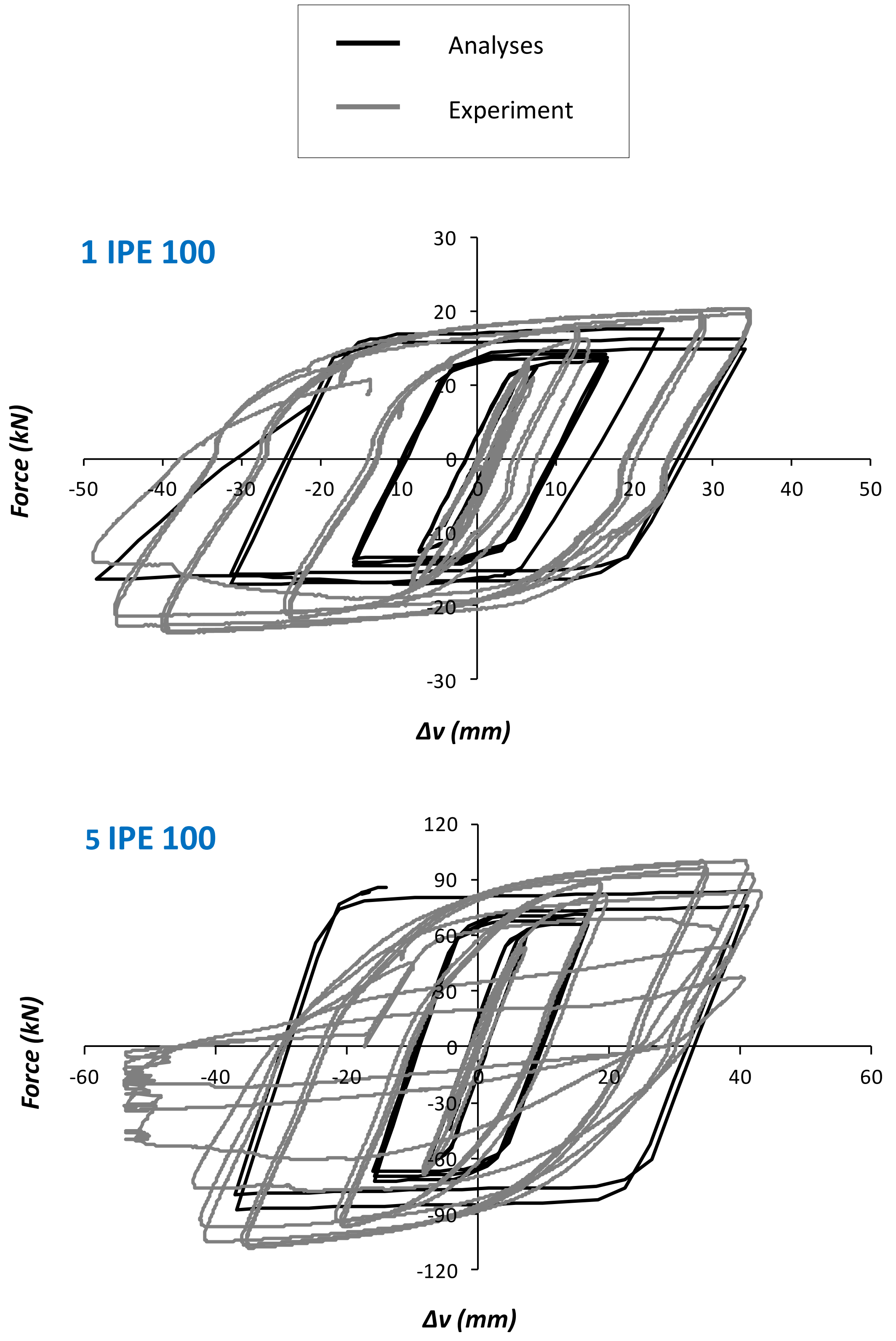

Figure 1.16 Resisting force of the INSTED system in accordance to the relative vertical displacement of the rod.

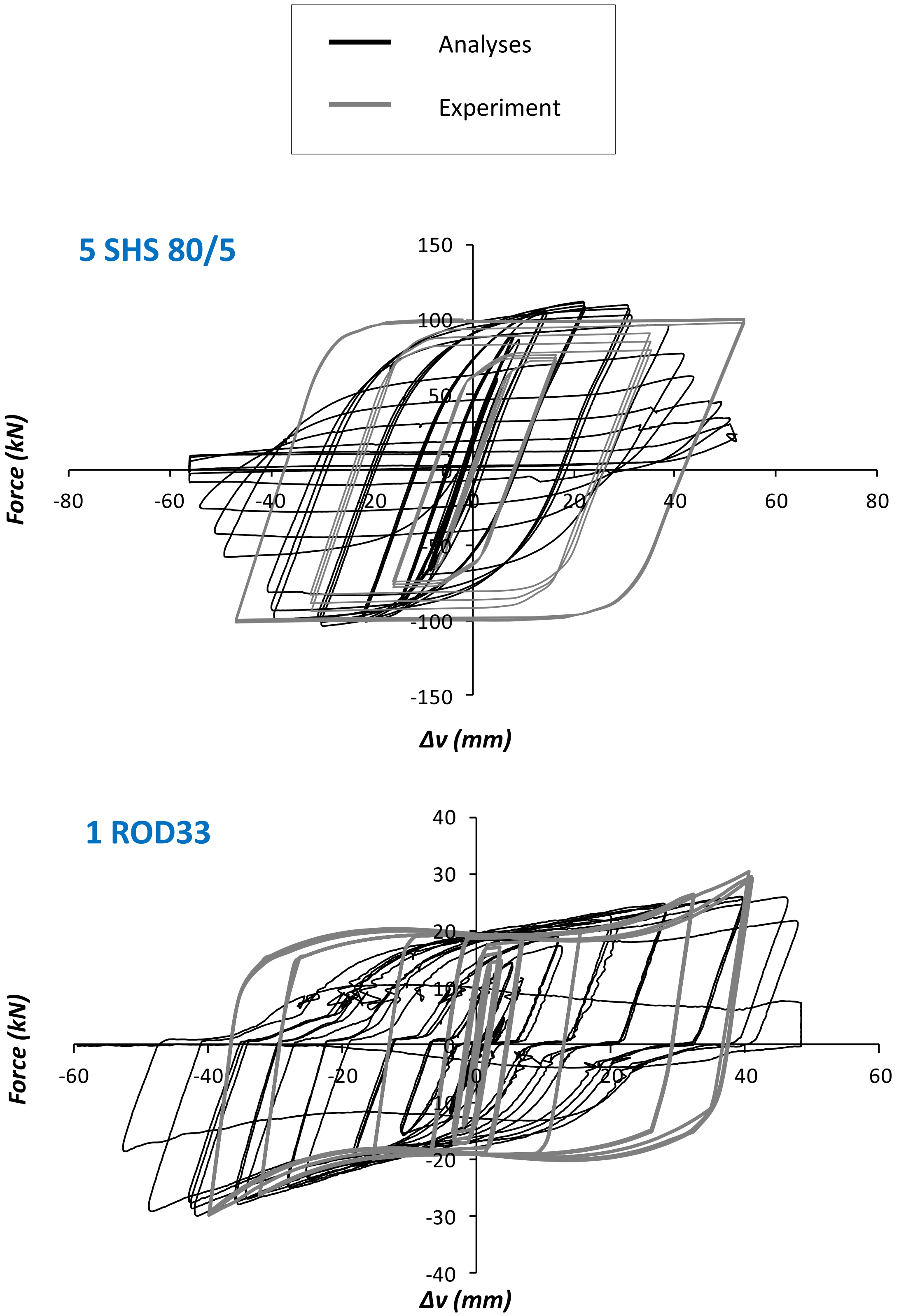

Figure 1.17 Resisting force of the INSTED system in accordance to the relative vertical displacement of the rod.

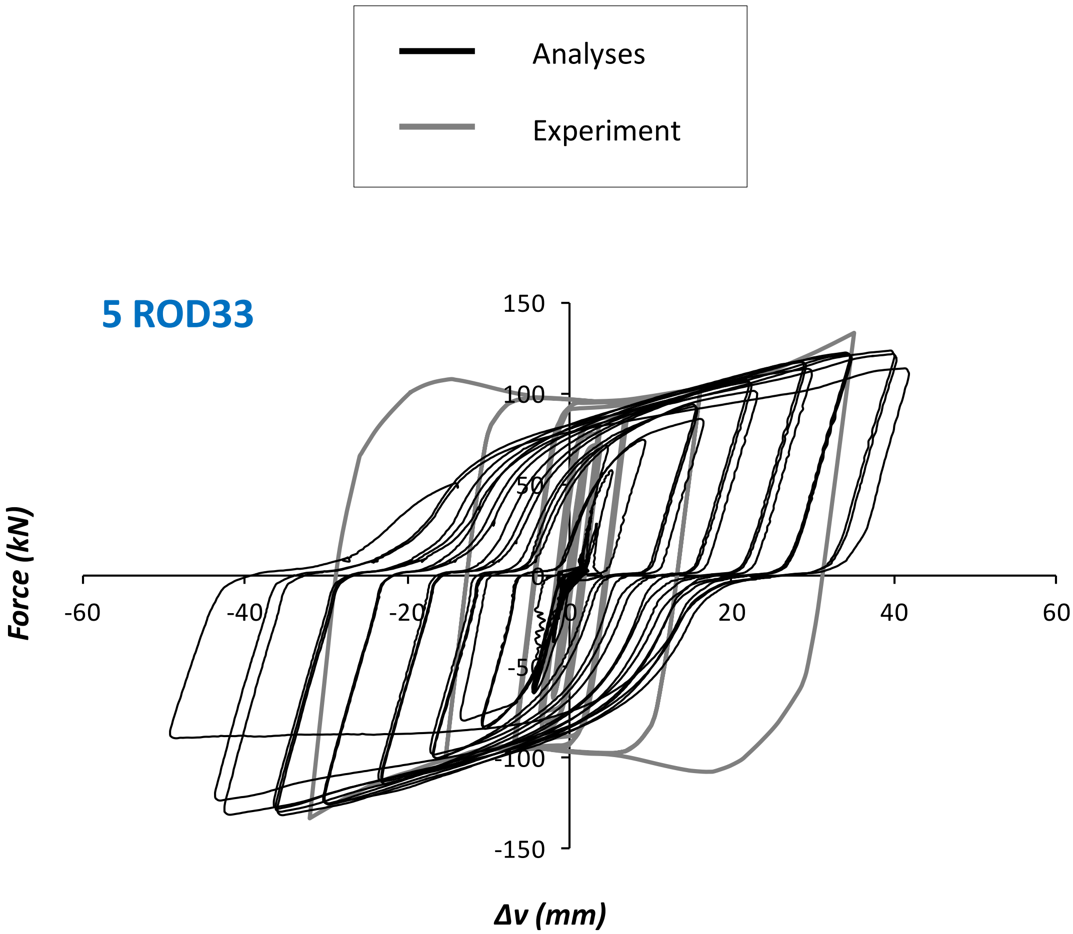

Figure 1.18 Resisting force of the INSTED system in accordance to the relative vertical displacement of the rod.

CHAPTER A.2

PERFORMANCE OF THE ORIGINAL BUILDING ON ANALYTICAL AND EXPERIMENTAL APPROACH – COMPARISON

2.1 The original building

The under study building is a a typical 3 – storey building of Southern Europe, designed and constructed during the 70's . The structure does not comply with capacity design principles and is prone to collapse with a mechanism resembling a "soft" storey. A representative "slice" of the building had been modelled [Ageliki Rodogianni, 2011], corresponding to the 1/3 of the whole structure. The square columns of the prototype are 25 cm in width, while the beams have a 25 cm x 50 cm (width x height) cross section. The construction materials of the building were reinforced concrete, with a nominal strength of 25 MPa, and smooth reinforced steel bars of nominal strength equal to 320 MPa. The foundation consists of square surface foundations of width B = 1.5 m, considered realistic for competent soil. The bending moment of the members of the building was calculated using these values and corresponding safety factors.

2.1.1 The experimental setup

The reduced-scale model has been designed with a scale factor N = 10 and tested in the shaking table of the Laboratory of Soil Mechanics of NTUA [Nonika Antonaki, 2012]. This physical model (Figure 2.1) consists of two identical 3-storey frames, connected together through evenly distributed steel plates. These plates are used to represent the mass of each storey, which is equal to 22tn, in real scale [Aggeliki Rodogianni, 2011]. Consequently, the total mass of each frame is equal to 66kg in model scale. The bearing elements (columns and beams) are made of compact aluminum plates that are connected together as in a moment-resisting frame.

The dimensions of the bearing elements were calculated so as to comply with the stiffness of the real structure [Gibson, 1997]. However, it is practically impossible to model stiffness correctly and achieve the desired (scaled-down) bending moment capacity of the structural members at the same time. This is the reason why each beam-column connection was modeled with custom-built artificial plastic hinges (Figure 2.1), whereas the rest of the structure was intended to behave elastic. The ultimate bending moment of each plastic hinge was calibrated through adjustment of the applied torque. The calibration of each assembly was performed through static and slow-cyclic pushover testing, utilizing a screw-jack pushover apparatus. As for the foundation, it consists of square surface footings of 0.15m width (in model scale), a much realistic value for competent soil and the corresponding safety factors.

After the structural members were put together, the building was placed onto the soil inside the sandbox, in order carry out the experiments. The soil-structure system was subjected to a sequence of moderate seismic motions [MNSA-Athens 1999, Aegion-1995, Kalamata-1986, Lefkada-2003] due to the fact that it was found incapable of surviving stronger ones. The motions were imposed at the base of the sandbox and a number of instruments were used to measure the accelerations and displacements on every storey.

The building finally collapsed after it was submitted to the record of Lefkada, having already accumulated deformations by the previously induced seismic records of Aegion and Kalamata. The failure mechanism was that of a soft storey formed in the base floor. After the abrupt increase in displacement of the first storey, the upper ones followed, resulting to total failure.

2.2 Numerical Simulation of the experimental setup

It cannot be doubted that the numerical model of the original building had to be tested alone, before the introduction of the INSTED system in this, in order to ensure that its behavior corresponds to the real one.

The geometry of the building was first modeled in *Ansys*. The cross-sections and properties of all elements were defined straight in Abaqus, along with the whole geometry. All elements were simulated by 3-dimensional, 2-node linear beam elements (B31The column – beam connections were modeled as intersections of rigid elements (their Young's modulus was 10 times the aluminum one, reassuring that they do not deform), connected at their ends to smaller ones that simulated the artificial plastic hinges. Both had the cross-section of the structural member that ended up to the connection.

As far as the constitutive models are concerned, a linear elastic one was applied in the structural (beams and columns) and rigid members, while a bilinear elastic-plastic law was utilized for the plastic elements. The yield stress derived from the calibration of the plastic hinges, so that the ultimate scaled bending moment of the real building is reached.

2.3 Performance of the numerical model

2.3.1 Pushover testing

Before subjecting the numerical model to dynamic loading, we had to validate its strength, according to the original [Aggeliki Rodogianni, 2011]. This had to be verified through a static pushover testing. In order to succeed a triangular displacement distribution by height, according to the first displacement eigenvalue, each storey was connected, on the left, to a horizontal spring. Thereafter the edges of these springs were rigidly connected to a node, on which the displacement was imposed. The above springs had all different stiffness coefficients (K_1=10kN/m, K_2=20kN/m, K_3=30kN/m), so that the above triangular eigenmode is established.

The data we needed in order to estimate the strength of the building were the resisting force of the whole structure and its horizontal displacement. The combination of those two values would determine the displacement were the plastic elements (rods) yield, as well as the maximum force that this building resists. After this point, the diagram acquires a much smaller gradient, equal to the one of the after-yield gradient of the rods in the stress-strain diagram. The yielding force of the original building turned out to be *0.08kN* (Figure 2.1), which resembles much to that of the real one [Aggeliki Rodogianni, 2011]. Also, the yield acceleration that this corresponds to is the ratio of the above resisting force to the total mass of the building. Therefore, the original building appears to yield in:

$$\boldsymbol{Ay = \frac{0.08}{0.66} = 0.12g}$$

2.3.2 Dynamic Testing of the building – Comparison to the experiments

In the first sequence of dynamic analyses, the soil was not taken into account. However, this case is not unrealistic, since the footings used in the experiment had a big safety factor (FS=14) and the sand was dense enough (Dr = 93%). Therefore, the base of the model could be considered as fixed. After defining the kinematic boundaries of our model, we proceeded to the seismic motions. Naturally, we used the same seismic record sequence as in the experiment, so that similarity in the loading conditions is established and the right comparisons are made. The excitation, which was imported to the numerical model, derived from the acceleration measured by the accelerometers that were placed in the middle of the sand stratum, so as to ensure that the soil nonlinearity and seismic amplification is taken into account.

The comparison between the computed and measured results has been initially conducted in terms of interstorey drifts. All acceleration and drift time-histories, for every record imposed, are compiled at the end of Chapter A.2. Taking a look at the first three records, where the interstorey drifts are generally negligible with a maximum value of *2.5mm* (Figures 2.5, 2.8 & 2.11), we can infer that the analysis simulates the experiment quite correctly. Also when the residual drifts on storey level come in comparison (Figure 2.17), we can indicate some deviations in the response between the analytical and experimental model, but these are generally insignificant, considering their amplitude.

The collapse of the building numerically comes, as expected, when it is being imposed to the record of Lefkada (2003). As for the model with the fixed base, the failure mechanism resembles the one observed in the experiment, since the first storey gains significant displacements, before the others start drifting away. This can be clearly seen from the response of the numerical model in terms of interstorey drifts, which has a great similitude with the one observed in the experiment. What the numerical model fails to capture is the drift amplitude of the experiment. Actually this unlikeness is fictitious since the physical model was not let to collapse, even though it was bound to, due to the aluminum bars that were placed vertically at both sides. A more realistic view is obtained when the residual drifts are compared, since they practically coincide (Figure 2.15).

The analysis where the base of the structure was simulated with springs gives the same results as the fixed one, as it can be inferred from the interstorey drifts' time histories, during the seismic record of Lefkada (2003). We simulated three springs for each base, one horizontal, one vertical and one rotational. The horizontal and vertical springs were considered linear and very stff. As for the rotational one, this was calibrated according to pushover tests of the footings used in the experiments; therefore, it had a non-linear behavior.

Conclusively, we may deduce that the above evidence consist a verification that the numerical model of the original building is correct, therefore, we may proceed to the next step, which is the introduction of the INSTED system to it.

Chapter A.2

Figures

ORIGINAL BUILDING

COMPARISON BETWEEN THE EXPERIMENT AND THE NUMERICAL ANALYSES

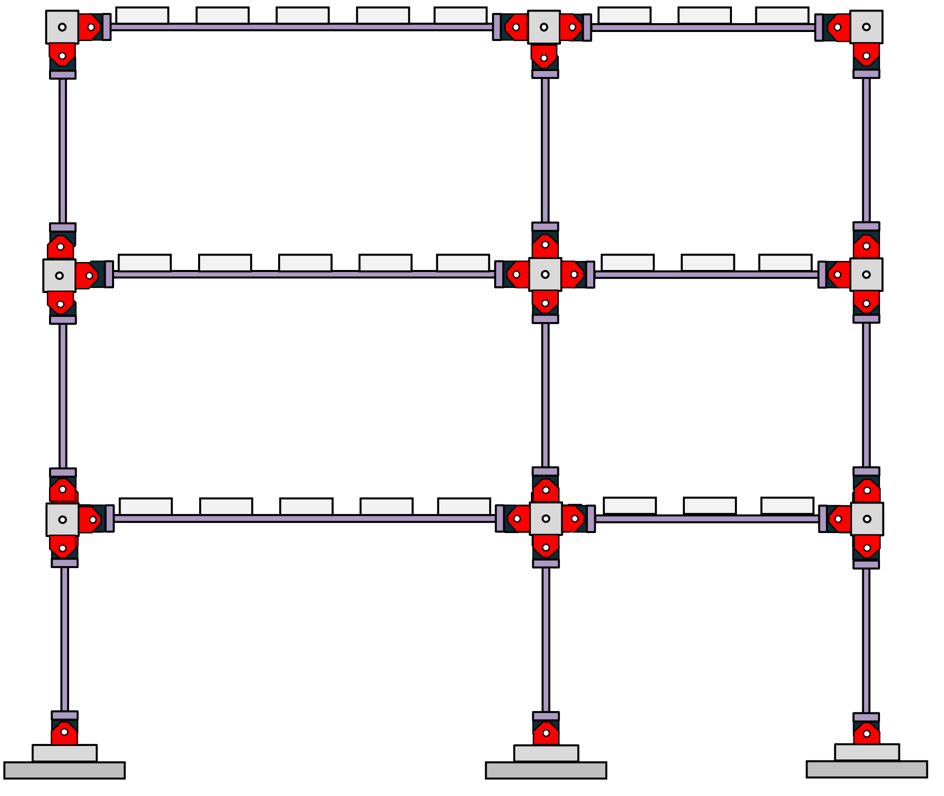

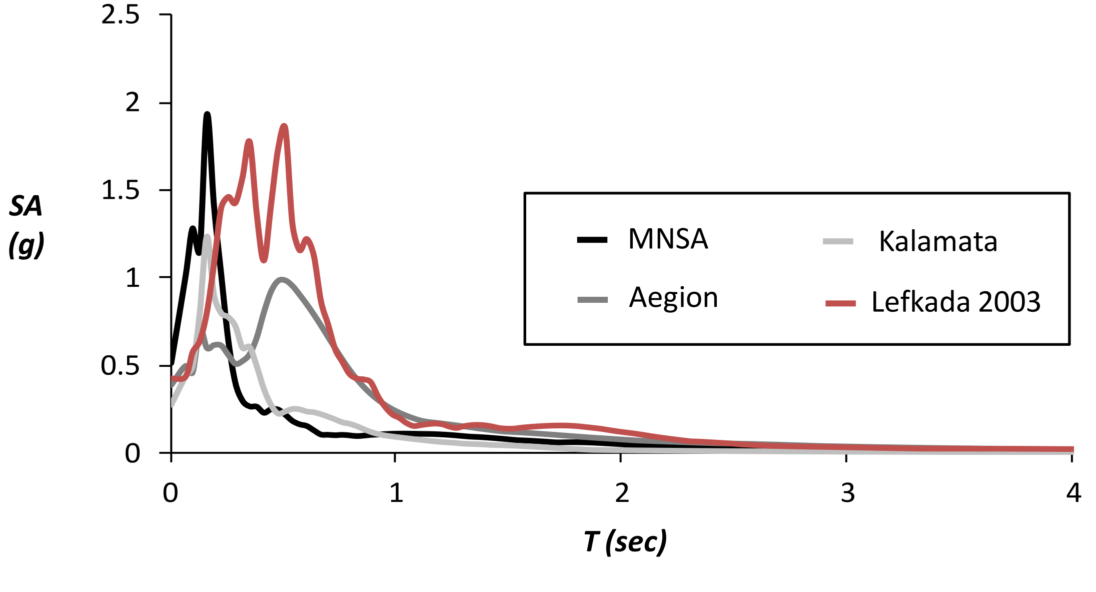

Figure 2.1 The original model building and the imposed seismic excitations.

PUSHOVER TEST (Abaqus)

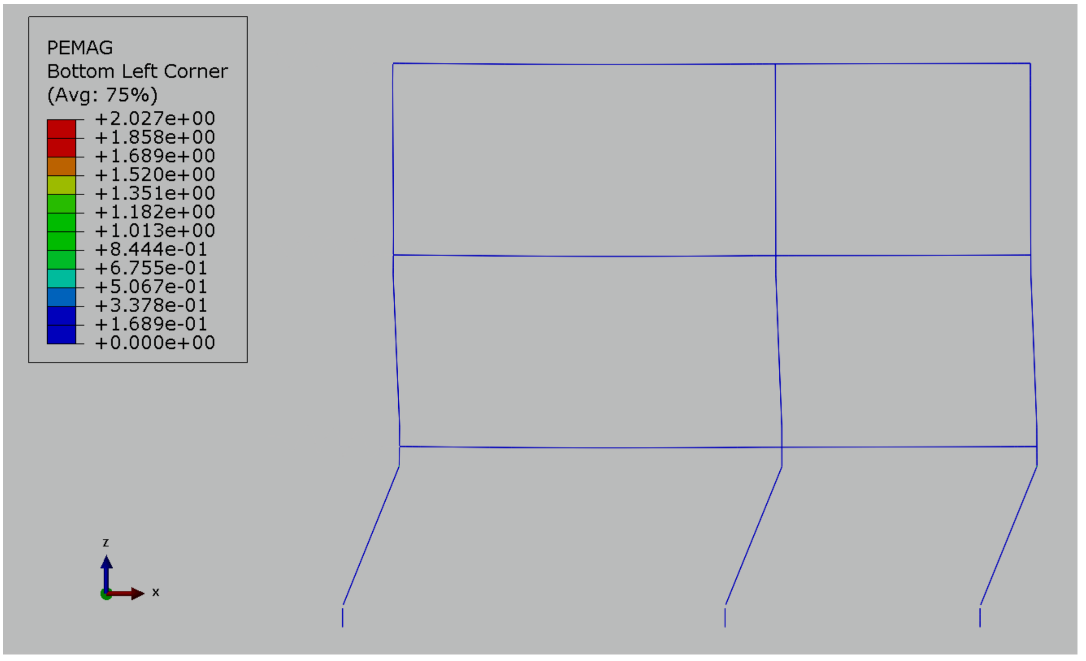

Figure 2.1. Deformed shape of the retrofitted structure after the **pushover testing**.

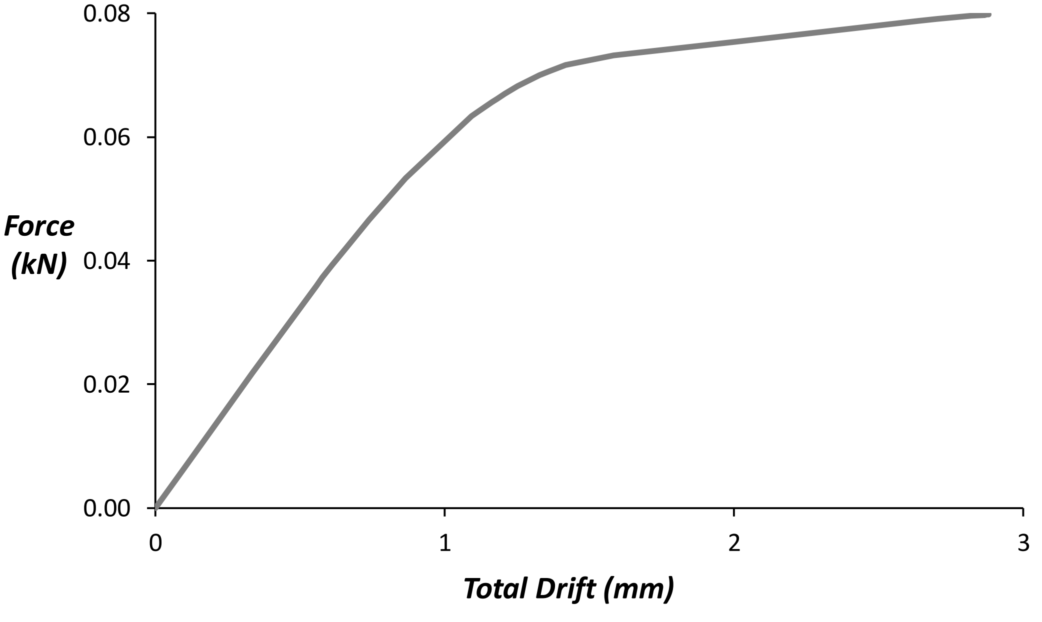

Figure 2.2. The force of the original model with regard to the displacement on top of the structure, as derived from the pushover test in Abaqus.

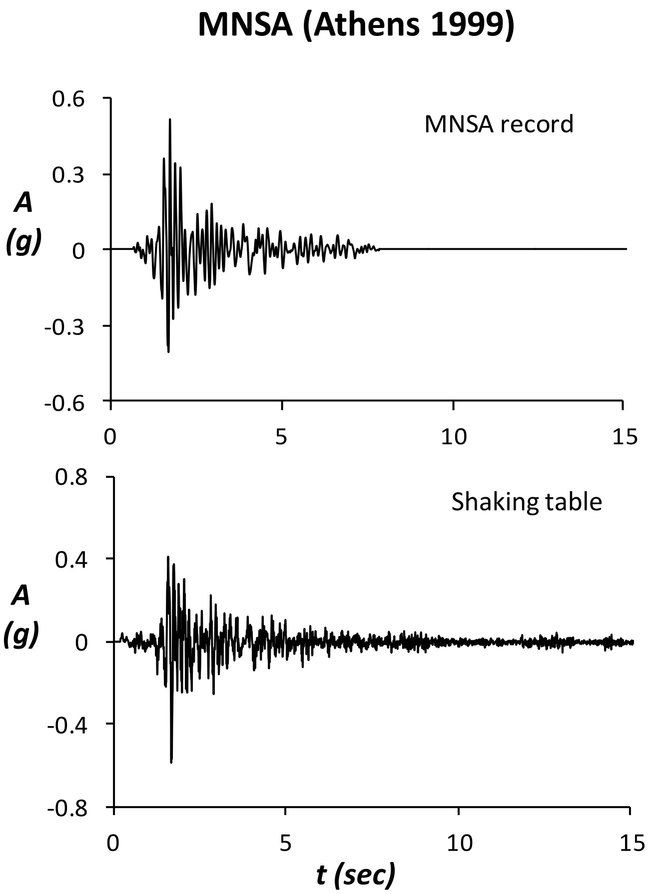

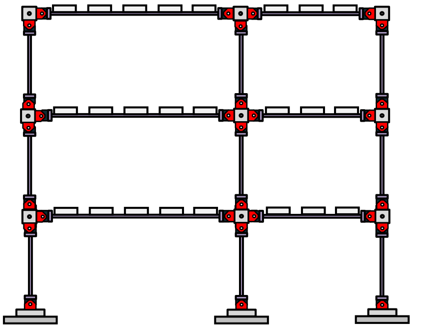

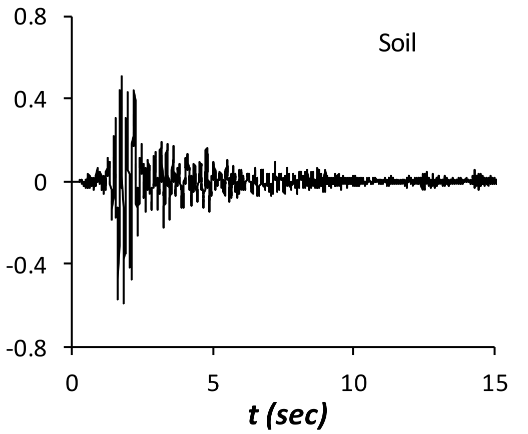

Fig.2.3 Acceleration time history imposed on the model of the original building during the experiment.

Fig.2.4 Acceleration time history imposed on the model of the original building in the Abaqus analysis.

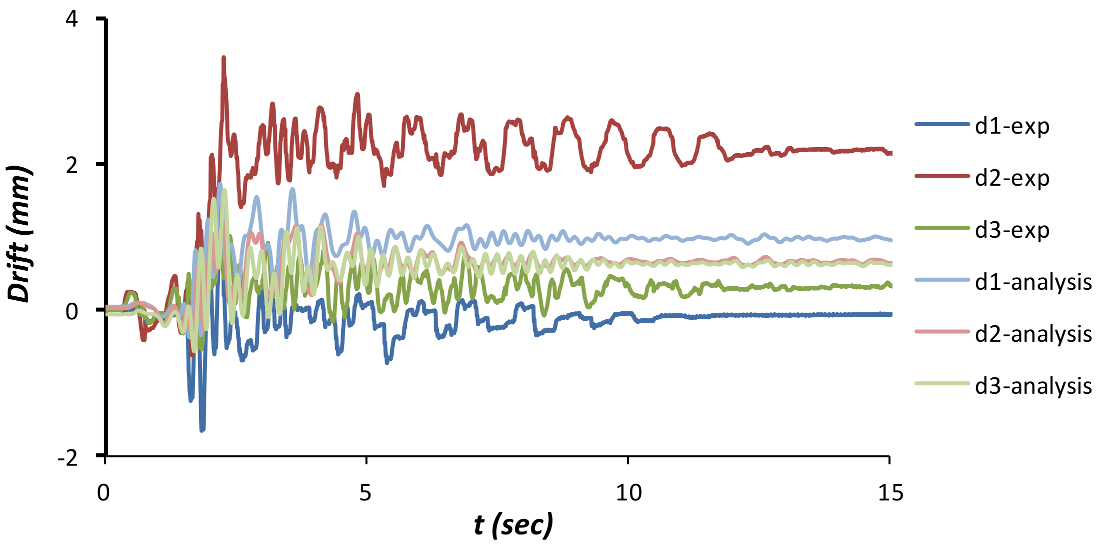

Fig.2.5 Comparison of interstorey drifts between the Abaqus analysis and the experiment results for the record of MNSA (Original building).

AEGION (1995)

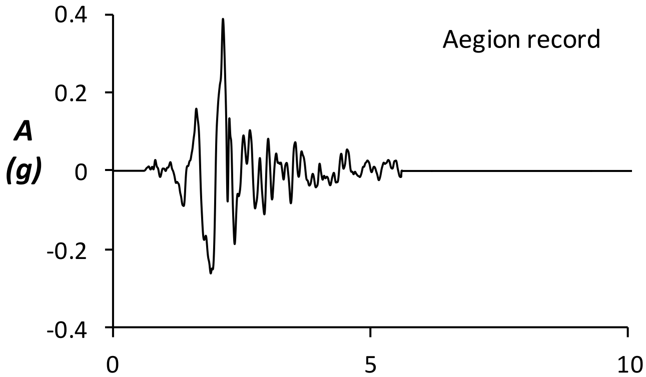

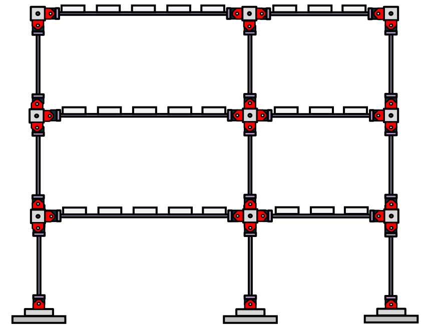

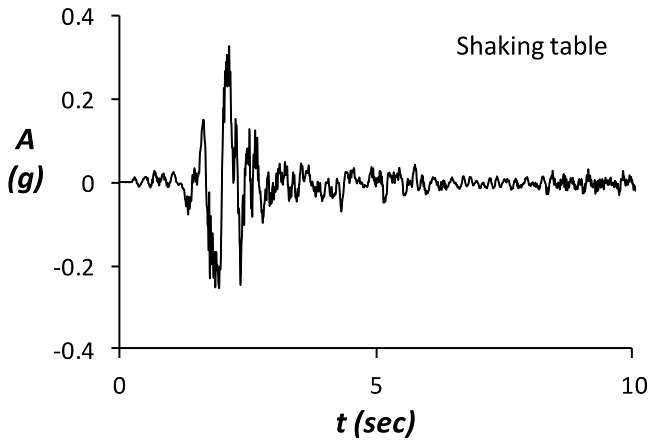

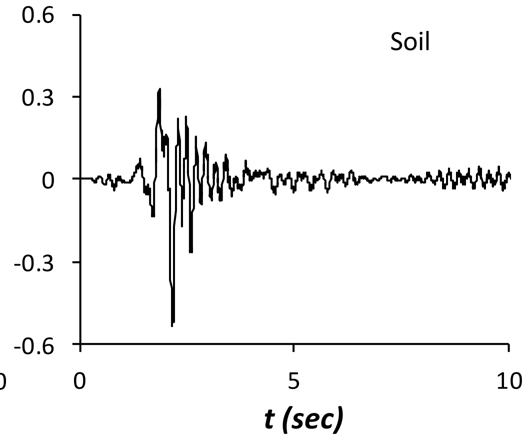

Fig.2.6 Acceleration time history imposed on the model of the original building during the experiment.

Fig.2.7 Acceleration time history imposed on the model of the original building in the Abaqus analysis.

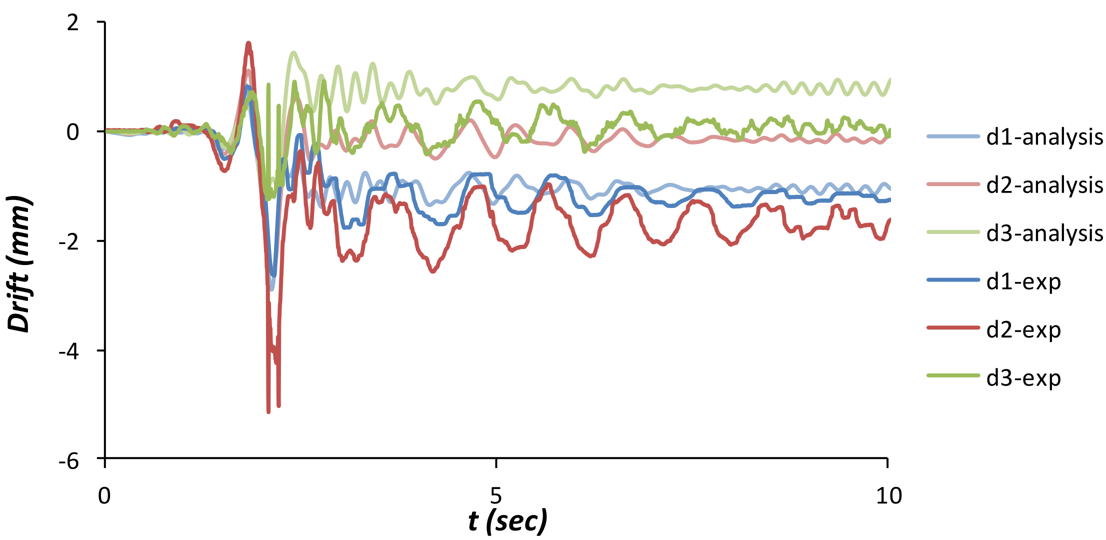

Fig.2.8 Comparison of interstorey drifts between the Abaqus analysis and the experiment results for the record of Aegion (Original building).

KALAMATA (1986)

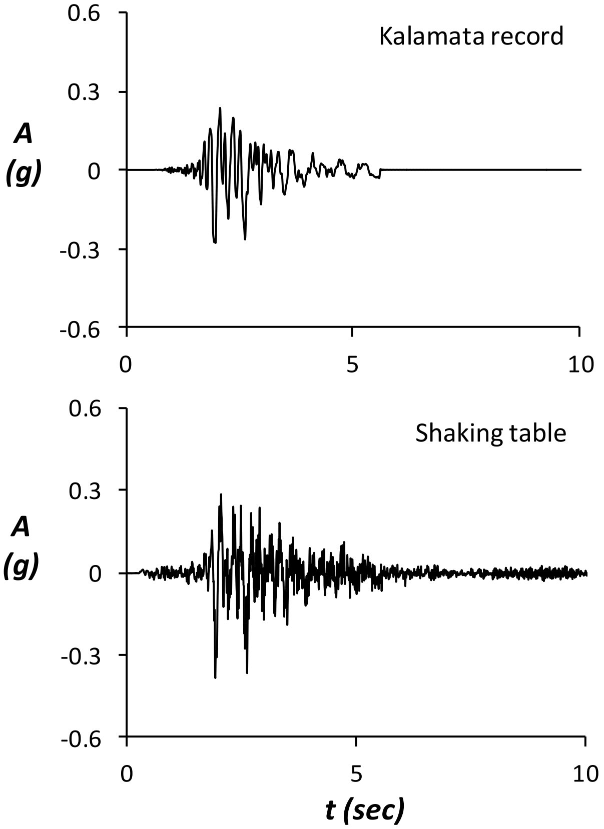

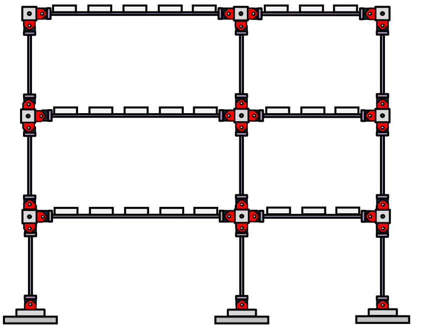

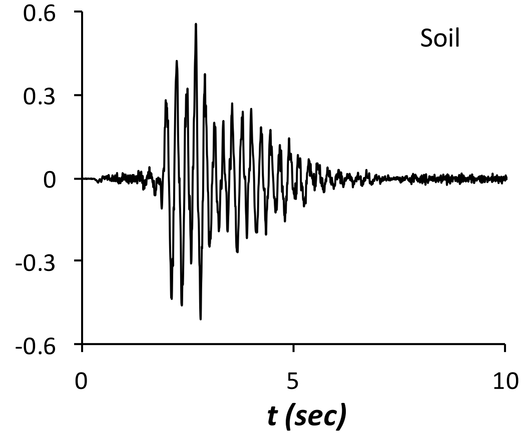

Fig.2.9 Acceleration time history imposed on the model of the original building during the experiment.

Fig.2.10 Acceleration time history imposed on the model of the original building in the Abaqus analysis.

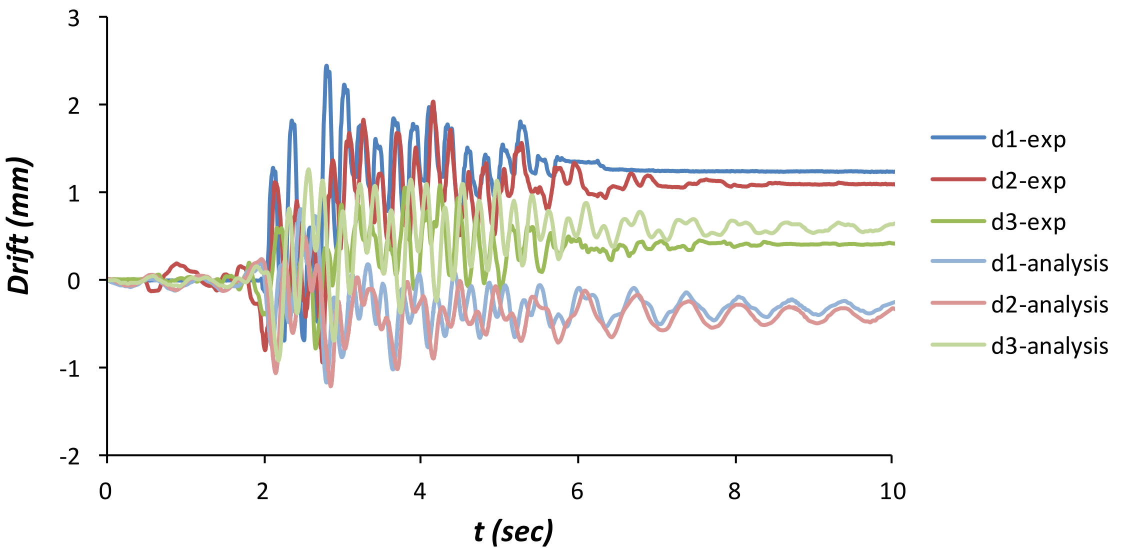

Fig.2.11 Comparison of interstorey drifts between the Abaqus analysis and the experiment results for the record of Kalamata (Original building).

LEFKADA (2003)

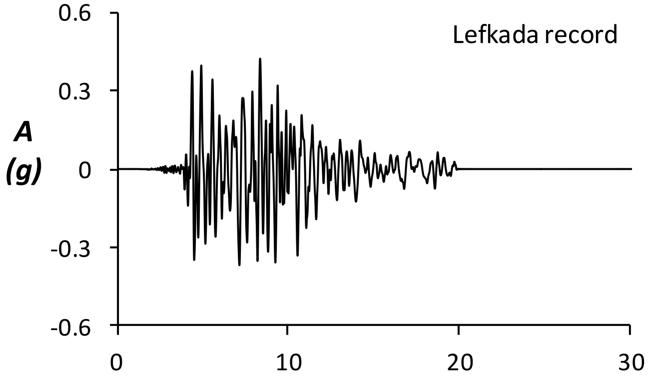

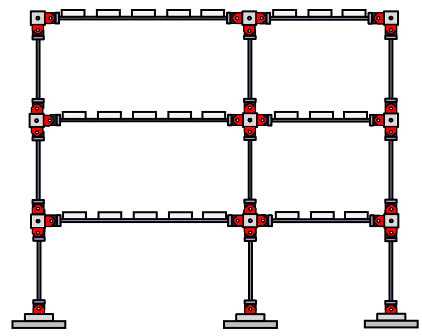

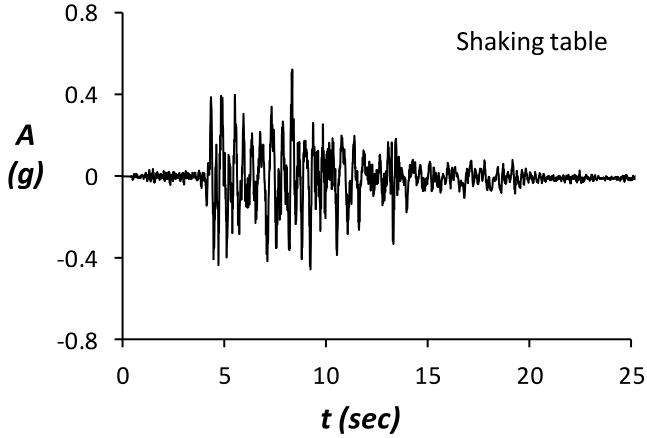

Fig.2.12 Acceleration time history imposed on the model of the original building during the experiment.

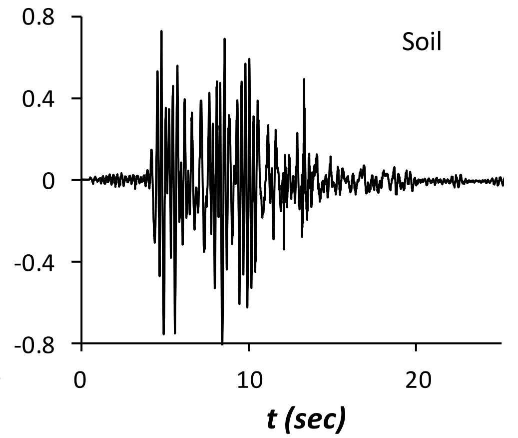

Fig.2.13 Acceleration time history imposed on the model of the original building in the Abaqus analysis.

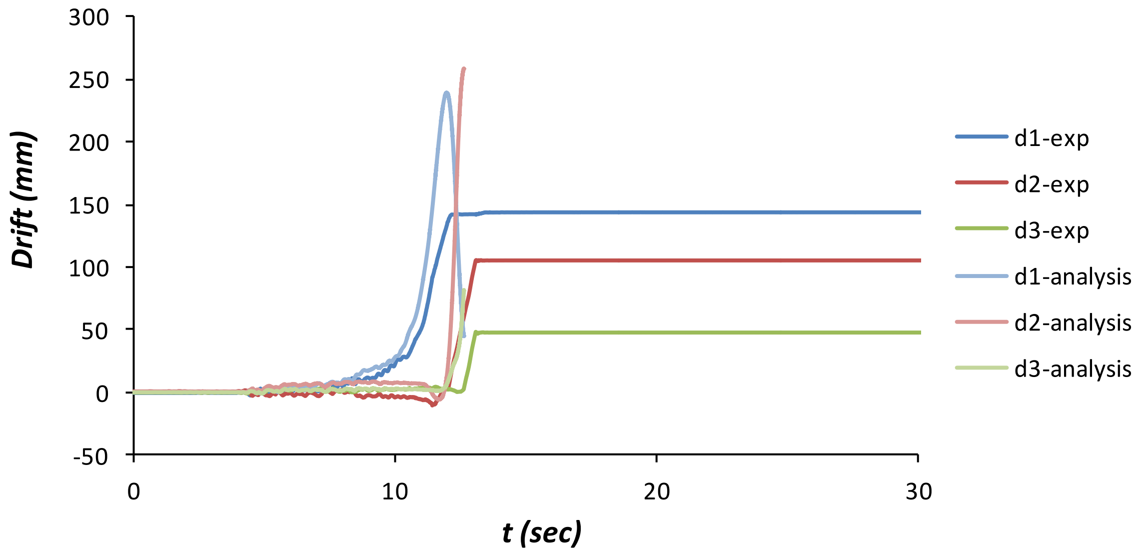

Fig.2.14 Comparison of interstorey drifts between the Abaqus analysis (fixed base) and the experiment results for the record of Lefkada (Original building).

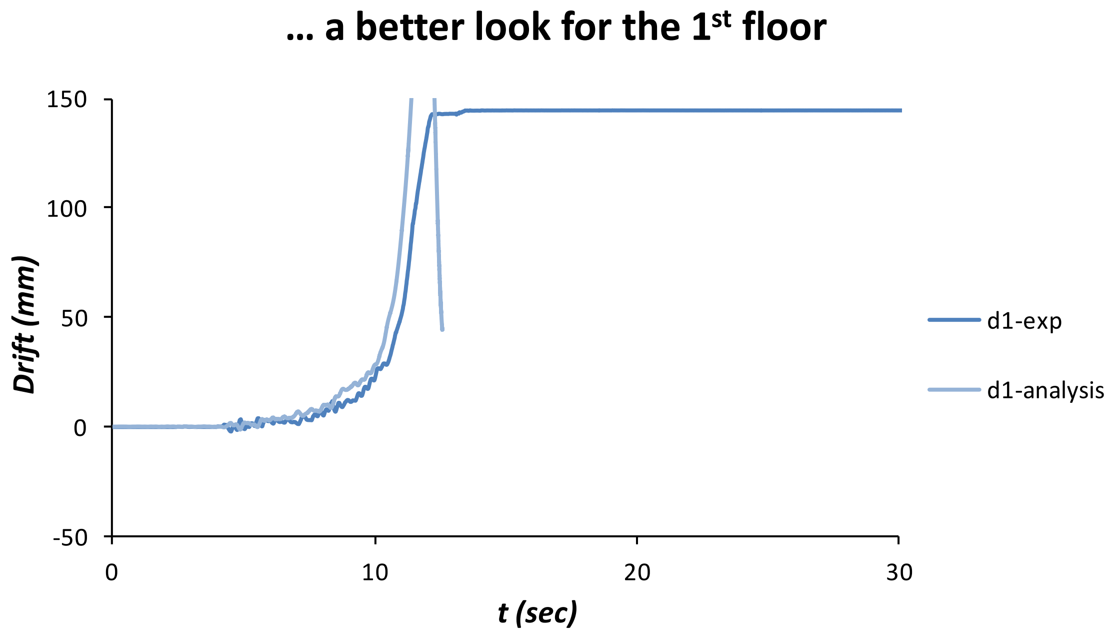

Figure 2.15 Interstorey drift for the *1st floor*, where the *soft-storey collapse mechanism* occurred - Abaqus analysis vs. experiment results for the record of Lefkada.

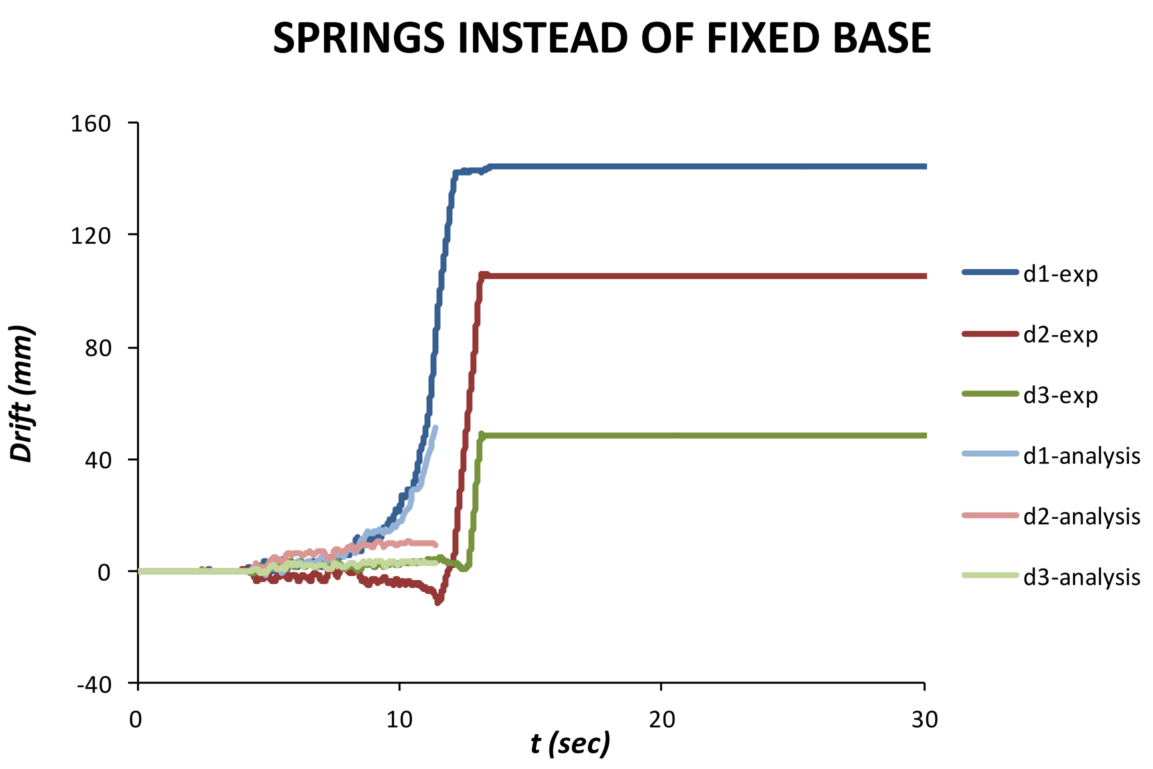

Figure 2.16 Comparison of interstorey drifts between the Abaqus analysis (base with springs) and the experiment results for the record of Lefkada .

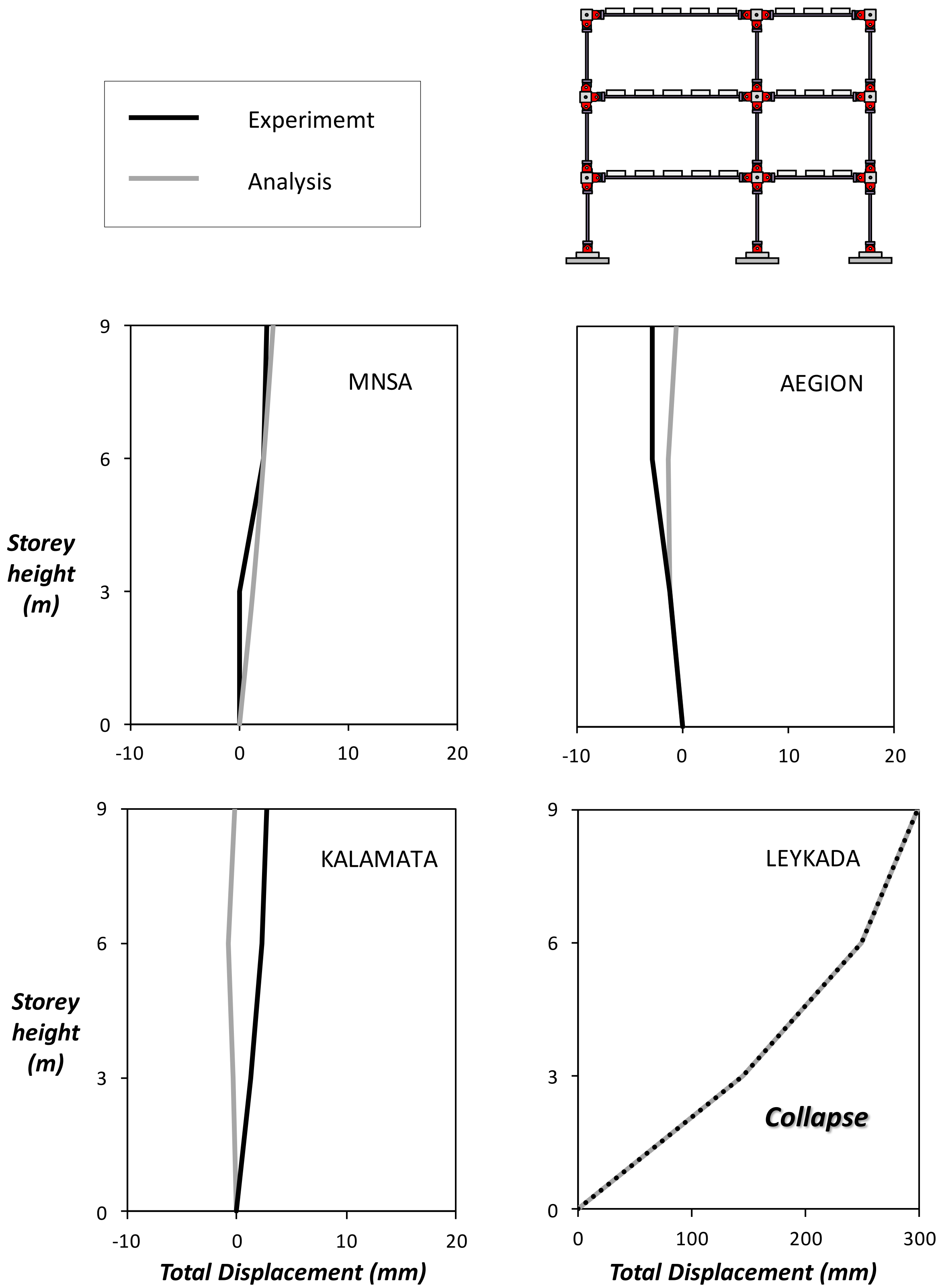

Figure 2.17 Comparison of the analysis and the experiment in terms of residual drifts.

CHAPTER A.3

RETROFITTED BUILDING VIA THE INSTED SYSTEM - COMPARISON TO THE ORIGINAL ON A NUMERICAL BASIS

3.1 Weakness of the original building and need for retrofit

The original building has already been subjected to a sequence of moderate intensity Greek seismic motions, in order to test its seismic performance. Figures 3.9 and 3.10 depict the initial and deformed shape of the structure, just before the collapse at the last record of Lefkada 2003. It is obvious that displacements are much larger in the first storey and that plastic deformation is localized in the first floor columns. Having already accumulated permanent plastic deformations from the previous seismic motions, the building fails to sustain the record of Lefkada and collapses by creating a soft – storey failure mechanism in the first floor. Hence, the original building is unable to withstand seismic records of moderate intensity and the need for reinforcement becomes a necessity. The proposed way of retrofit is via the **I**nnovative **ST**iffness and **E**nergy **D**issipation system.

Having verified the correct response of the original building's numerical model, we can move on to the addition of the INSTED system in order to test the dynamic behavior of the retrofitted model. The structure is firstly subjected to seismic records of small and moderate intensity (Mnsa, Aegion, Kalamata, Lefkada) and afterwards to motions of high intensity (Sakarya, Rinaldi, Jma, Takatori), so that the superiority of this type of retrofit is verified.

3.2 Proposal of retrofit via the INSTED system – Numerical Simulation

3.2.1 Designing the INSTED system

The INSTED system consists of two strong vertical columns, closely positioned and joined together with horizontal expandable solid rods. The columns remain elastic during seismic loading and failure is guided to the horizontal fuse elements, where energy dissipation takes place and plastic hinges are formed. The system is introduced in the center of the building's facade along the height of the middle column and towards the larger span. Its dimensions, i.e. the cross – sections required for the horizontal rods, are defined according to the considered earthquake design acceleration. The respective acceleration value is estimated according to the following formula:

$$\Phi_d\,(T) = \gamma_1\,\frac{A\;n\;\theta\;\beta o}{q} = 0.135g,$$

assuming the following parameters:

- $A = 0.16g$
- $q = 3.5$
- $\gamma_1 = 1.00$
- $\beta_o = 2.5$
- $\theta = 1.00$
- ζ=3%, n= 1.183

The *columns of the INSTED system* have to be stiff and strong, in order to remain elastic during seismic loading and guide potential failure to the expandable horizontal rods. Considering the properties of the scaled–down model (the dimension of the frame columns, materials, etc), we result to a 7.5cm x 2cm aluminum cross-section for each column (Appendix A).

The *horizontal rods* are the only structural members consisting of steel, so that no conversions – in terms of stiffness and strength – to equivalent cross-sections are made. Thus, mild steel S235 (with a yield point at f_y = 235 MPa) is selected for them. We begin by assuming a number of rods equal to 3 for each frame – thus one at the level of each storey. The inertial force imposed on the structure, according to the earthquake design acceleration, is equal to:

$$V_{ED} = \Phi_d(T) \times M = 0{,}097 \text{ (kN)},$$

since the mass of the new building is estimated ≈ 72kg.

Taking into account the first eigenmode of the 3-storey-building (*simplified spectral method*), the inertial forces at the level of each storey are calculated equal to:

$$F_1 = V_{ED} \times \frac{mi\ zi}{\Sigma\ mj\ zj} = 0.016 \text{ kN}$$

$$F_2 = V_{ED} \times \frac{mi\ zi}{\Sigma\ mj\ zj} = 0.032 \text{ kN}$$

$$F_3 = V_{ED} \times \frac{mi\ zi}{\Sigma\ mj\ zj} = 0.049 \text{ kN}$$

The required plastic moment M_{pl} and thus the required diameter for each solid rod are derived from the formula given in Eq.1. [Karydakis, 2011] and the results are presented in the following table.

$$P1 = \sum_{n=1}^{3} \left(\mathrm{Mpl} \ \frac{2\,b}{\mathrm{h}\,leff} \right)$$

- P_1 , shear force at the level of each storey
- b = 0.15 m , axial distance between the INSTED columns
- h = 0.30 m , storey height
- l_{eff} = 0.025 m , the rods' effective length

Table.1 Bending moment capacity M_{pl} and required cross-sections for the rods of each storey.

	M_{pl} (kNm)	D (cm)
1st storey	0.00243	0.40
2nd storey	0.00203	0.37
3rd storey	0.00122	0.31

For similarity reasons and ease of construction, we decided to use the same cross-section for all three rods of the INSTED system. Thus, based on the largest required diameter, we resulted in *d = 4.0 mm*.

3.2.2 Numerical simulation of the retrofitted setup

Every component of the INSTED system is simulated by 3-dimensional, 2-node linear beam elements (B31) in Abaqus software. The vertical columns are hinged to the ground, a type of connection that permits rotation. In this way, they are prevented from bending and remain elastic, while potential plastic deformation is delimited to the horizontal rods. The columns' behavior corresponds to a linear elastic constitutive law. The rods are placed centrically between the columns, thus in the middle of their axial distance (b = 0.15 m). Since they are responsible for the dissipation of seismic energy, an elastic-plastic constitutive law is assigned to them. The yield point introduced in the model is fy = 235 MPa, thus the nominal yield stress of S235 mild steel. *The* *retrofitted setup is examined according to two different elastic – plastic constitutive laws for the horizontal expandable elements,* so as to result in the most realistic approach for their behavior. These laws display the same values of yield stress, ultimate stress and yield strain. However, the first one (Constitutive Model 1) consists of a bilinear stress – strain curve for the steel, without taking into account the curve's descending branch (thus considers non - declining ultimate stress equal to fu = 360 Mpa), while the second one (Constitutive Model 2) is closer to reality, consisting of a stress – strain curve with strength degradation after the rods' plastic strain reaches the value of 20% (Figure 3.14).

In order to connect the columns' centroid with the ends of each rod, horizontal rigid beams are used in the numerical simulation (B31 elements); these beams correspond to a linear elastic constitutive model with a Young modulus 10 times greater than the aluminum one; in this way, common deformation between the column's centroid and the edge of the rod is ensured. Moreover, the connection of the INSTED system to the frame's middle columns takes place at the level of each storey, in a way that rotation is allowed. Specifically, each connection is formed by two linear springs of great stiffness - a horizontal and a vertical one – through which the building's strain is being transferred to the horizontal resistance system. For this purpose, elements of type SPRING2 are used. In addition, in order to simulate the diaphragm function of storey plates that would exist in a real structure, three horizontal laminas are placed on the INSTED system at the height of each floor, connecting its columns together. Every lamina – column connection is hinged, so that the development of bending moment at these points is prevented; thus, it is simulated by two linear stiff springs - a horizontal and a vertical one (SPRING2 elements). The addition of these bars aims to maintain the distance between the INSTED columns fixed, ensuring that they display uniform horizontal displacements. The laminas have a cross – section of 2.0 cm x 0.3 cm and a linear elastic constitutive model is assigned to them.

3.3 Pushover Testing

Before testing the retrofitted building's dynamic response, we firstly submitted the numerical model to static horizontal loading, in order to verify that the dimensioning of the retrofit corresponds to the initial design and the aiming yield acceleration. Therefore, we imposed a horizontal force on each storey of the building, according to the first triangular eigenmode.

Specifically, we imposed 1,2 & 3 kN on the first, second and third storey respectively and observed the structure's deformation. As it was expected, the structure acquired a uniform displacement towards the direction of the imposed force (Figure 3.1). The combination of total drift at the top of the building and shear resisting force at the base is depicted on Figure 3.2**.** The area where the curve's gradient changes, depicts the structure's yield point and the respective horizontal displacement at that time. This force appears to be equal to 0.26 kN, therefore the building's yield acceleration is equal to:

$$Ay = \frac{Fy}{M} = \frac{0.26\ kN}{1.44\ kN} = 0.18g$$

This acceleration is naturally greater than the one the INSTED system was designed for, but yet logical, since now both the original frame and the retrofit contribute to the total resisting force (Figure 3.3).

3.4 Dynamic Testing

3.4.1 Performance under moderate seismic shaking

The retrofitted frame is expected to display an increase in strength and ductility compared to the original one, as well as a more uniform lateral deformation. The INSTED system acts as a kinematic constraint; therefore, it should lead to a more uniform damage distribution in all three storeys and prohibit the development of a soft – storey collapse mechanism at the first floor.

In order to compare the performance of the retrofitted building with the one of the original structure (Figure 3.4), we subject it to the same sequence of seismic records (MNSA, Aegion, Kalamata, Lefkada) - Table 1 - and expect it to withstand them, without collapsing. The numerical model used for this comparison is the one including a bilinear elastic – plastic constitutive law for the rods (Constitutive Model 1), since the four Greek seismic records are of small or moderate amplitude, thus the limit of 20% in plastic strain values is not expected to be reached. Therefore, the approach is good enough.

The initial and deformed shape of the retrofitted structure, after being submitted to the record of Lefkada, is displayed in Figures 3.10 and 3.12. It is clear that the strengthened building can now sustain the imposed seismic load and that deformations along the height of the building have been homogenized. The frame basically “follows” the displacement of the INSTED system, which columns rotate like a rigid body, allowing the horizontal rods to deform and dissipate energy. Thus, the creation of a soft-storey collapse mechanism at the base storey is prevented.

More specifically, as depicted in the interstorey drift and drift ratio diagrams of Figures 3.5 – 3.7, the residual drifts for each storey of the retrofitted building after every seismic motion practically coincide. This means that the desired uniform distribution of stiffness and strength is achieved for the structure. In addition, comparison of these diagrams with the ones of the original building demonstrates that the building’s performance has been highly improved after the retrofit. Indeed, the seismic motions of MNSA, Aegion and Kalamata lead the building to a maximum drift ratio of *0.2%* for each storey. However, the actual success of the retrofit becomes apparent at the record of Lefkada, where the retrofitted structure displays an impressive performance (Figure 3.8). While the original building accumulates large deformations and finally collapses, the retrofitted one displays *negligible interstorey drifts* (Figure 3.13). Specifically, at the end of the record, it appears to have acquired a residual interstorey drift ratio of only *0.8%*. Consequently, the retrofitted structure suffers no damage from earthquakes of moderate intensity; thus, we proceed to the examination of its behavior under records of greater amplitude.

3.4.2 Performance under strong seismic shaking – Constitutive Model 1 vs. Constitutive Model 2

The retrofitted structure is subjected to a series of strong seismic motions, in order to examine the limits of its strength and ductility. The sequence of motions is displayed in Table 4.2 and the results are demonstrated in terms of interstorey drifts and drift ratios in the following diagrams (Figures 3.16 – 3.38). Both numerical setups of ***Constitutive Models 1 and 2*** are being examined here, because of the expected large values in plastic strain; in this way, we are able to compare and contrast their seismic performance.

As shown in Figure 3.39, which is derived from the numerical analyses, the system’s fuse elements undertake the imposed seismic load, leaving the rest of the structural members undamaged. Once their bending moment capacity ($M_{pl} \approx 0.0025$ kNm) is reached, they enter the plastic zone and display ductile behavior, through plastic deformation and dissipation of energy. The hysteresis loops of the moment – curvature diagrams of the rods (Figure 3.40) are quite indicative of this behavior.

One can observe that residual interstorey drifts do not exceed the value of *3.0 mm (Constitutive model 1) or 3.8mm (Constitutive model 2)* for the record of *Lefkada* (Figure 3.18), which is the strongest seismic motion implemented at the previous step of analysis. For the Greek seismic records imposed, the difference between the two *Constitutive models* in terms of interstorey drifts does not exceed the value of 0.8mm (in the record of Lefkada). Thus, it is considered negligible; the models practically behave the same. This seems logical, since motions of such moderate amplitude do not lead to the development of large plastic strain values.

The comparison becomes much more interesting, when the retrofitted building is subjected to high intensity seismic records, such as the ones of Rinaldi, JMA and Takatori. These motions display maximum accelerations that well exceed the earthquake design acceleration of the system, thus the horizontal fuse elements are expected to enter the plastic zone and develop large permanent deformations. The model corresponding to the *Constitutive Model 1* does not seem to suffer from any significant damage during these extremely severe seismic records. The interstorey drifts and drift ratios for Takatori record do not exceed the values of *6.5 mm* and *2.2%* (Figures 3.36). The respective time histories for the records of Rinaldi and Jma are even smaller (Figure 3.30, 3.33). According to this *Constitutive model* (no strength degradation), we can conclude that the proposed system displays considerable horizontal resistance and ductility under severe seismic shaking, thus preventing the building not only from collapsing, but also from significant deformations.

However, this not the case for the model to which the *Constitutive model 2* is assigned. During the records of Jma and Takatori, the retrofitted building displays significant residual interstorey drifts, with values of *10mm* and *9mm* respectively (or 3.2% and 3% in terms of interstorey drift ratio) (Figures 3.33, 3.36), whereas during the record of Rinaldi and due to the record's strong reverse pulse (between 2.5 and 3.5 sec), the building acquires residual interstorey drifts of *13mm* (Figure 3.30). Such displacement is translated into a drift ratio value of 4.3%, thus slightly bigger than the one permitted by the seismic codes (4%). Therefore, according to this numerical model, which seems more suitable for our study, **the retrofitted structure suffers from significant deformations**

during seismic motions of great amplitude, however it manages to survive without collapsing, which is very impressing.

As far as the force of the retrofitted building is concerned, we can deduce, from the respective force time histories or force - total drift curves (especially the ones regarding the three latter earthquakes), that the retrofitted structure displays significant values of shear force after yield, much higher than the ones expected according to the pushover testing, which resulted in yield force equal to ≈ 0.26 kN for the whole building. This may be partially attributed to the effect of hysteretic damping, which provides the structure with an additional horizontal resisting force ($F_{damping}$ = cu, c: damping coefficient, u: velocity). Since the proposed system is able of dissipating such large amounts of energy, with the rods being able to deform and reset their shape without failing until great values of plastic stain are reached, it is possible that this phenomenon affects the building's response to a greater extent than expected. Moreover, the rod's capability of elongating and undertaking axial forces is definitely a parameter to be taken into account for the increased values in the building's horizontal resistance. The pair of axial forces developed at the ends of each rod leads to the creation of an additional resisting moment, thus to the increase of the system's total resistance.

In terms of comparison between the two aforementioned models, the retrofitted setup of *Constitutive Model 2* appears to develop slightly smaller values of resisting force in general, compared to the one of Constitutive Model 1. The most important difference, though, lies in the shear force time histories and force – total drift curves of Rinaldi, Jma and Takatori. The *Constitutive Model 1* leads to stable resisting force during all seismic motions, while the *Constitutive Model 2* displays the realistic degradation in strength after the plastic strain exceeds the value of 20%.

At the end of Chapter A.3, cumulative displacements of the building are displayed, for all seismic motions, in order to acquire a profound insight into our system's capacity and of the difference lying among the two Constitutive models that are utilized (Figures 3.41, 3.42).

Chapter A.3

Figures

Retrofitted building (INSTED-FUSEIS system)

Numerical Analyses - Pushover Test

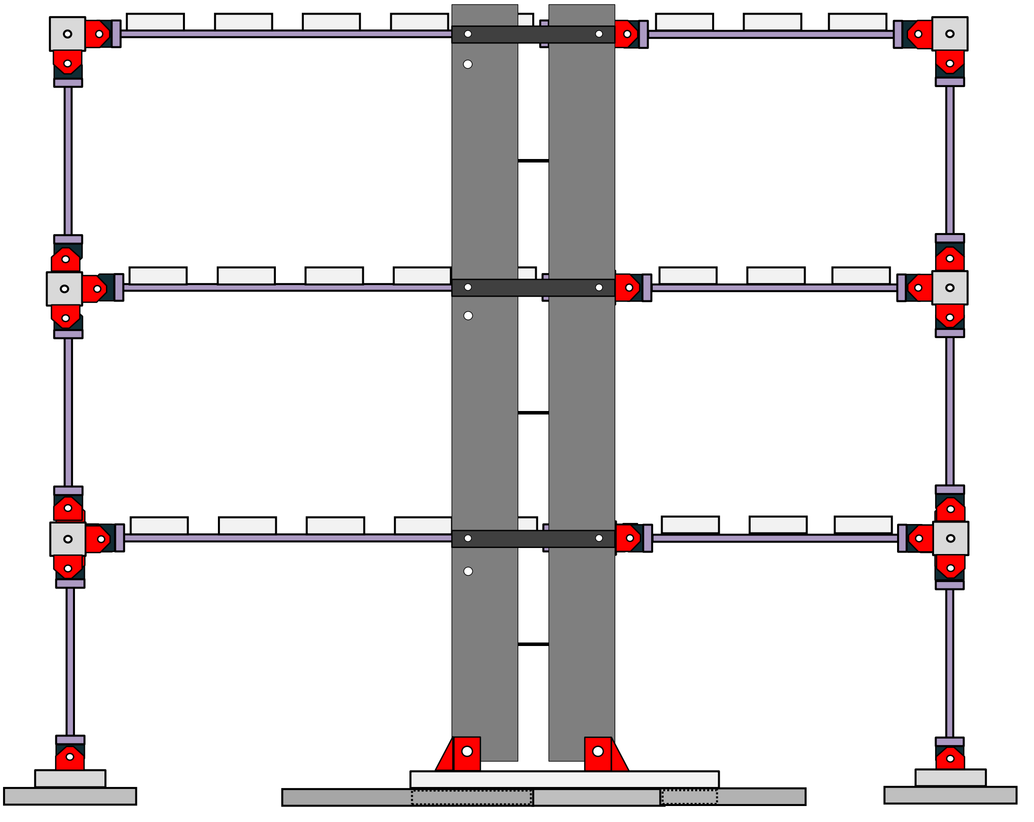

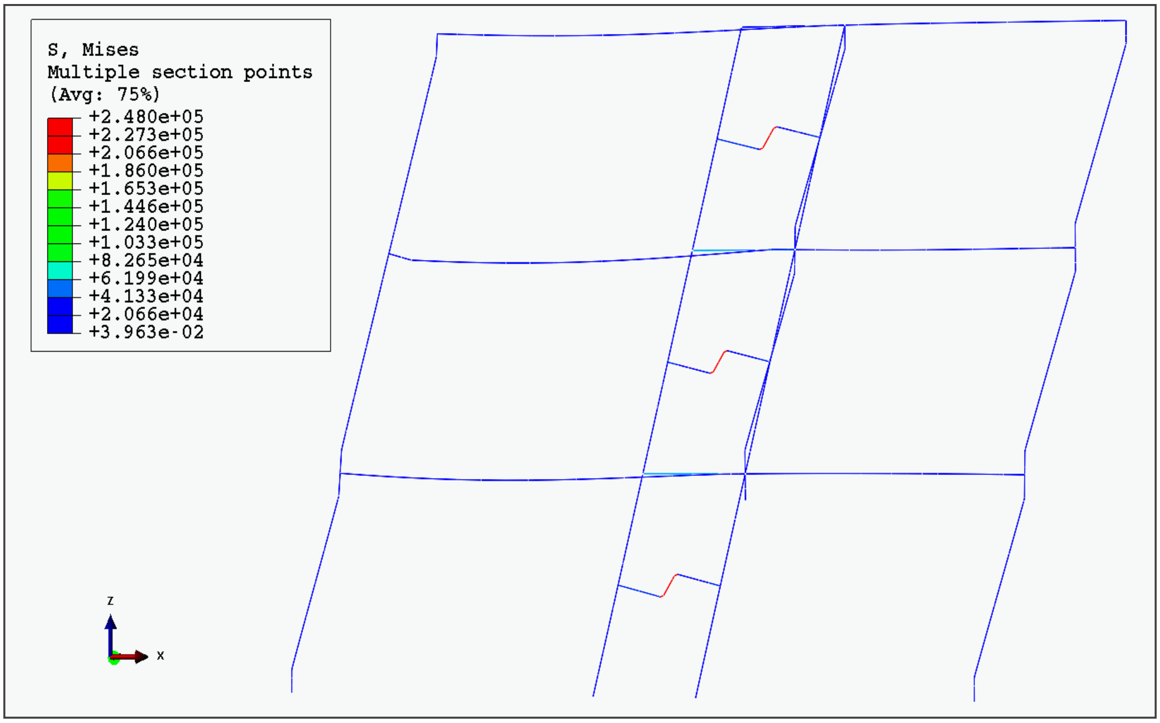

Figure 3.1 Deformed shape of the retrofitted structure after the pushover testing. Plastification at the edges of the rods is visible.

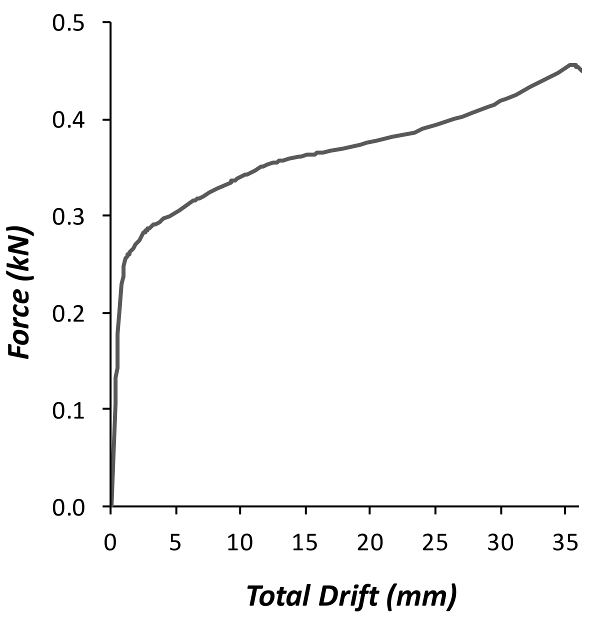

Figure 3.2 The total force of the retrofitted model (2 frames) with regard to the displacement on top of the structure.

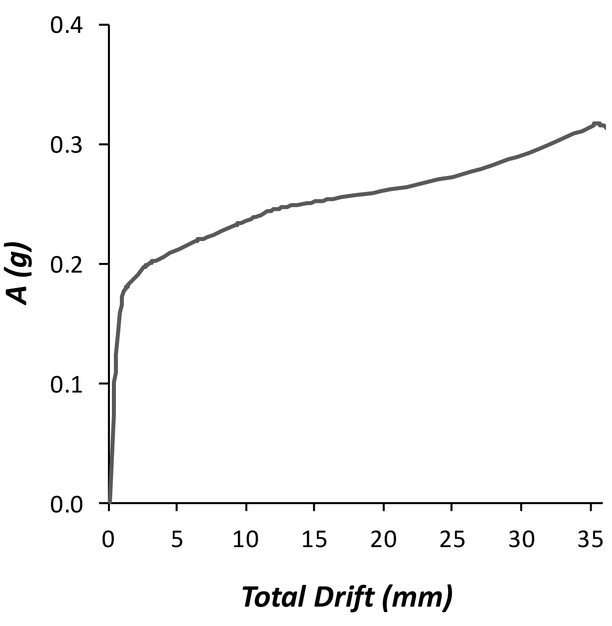

Figure 3.3 The equivalent yield acceleration of the retrofitted model with regard to the displacement on top of the structure, considering the total mass.

Retrofitted building (INSTED-FUSEIS system)
Vs Original
Numerical Analyses – Dynamic Tests

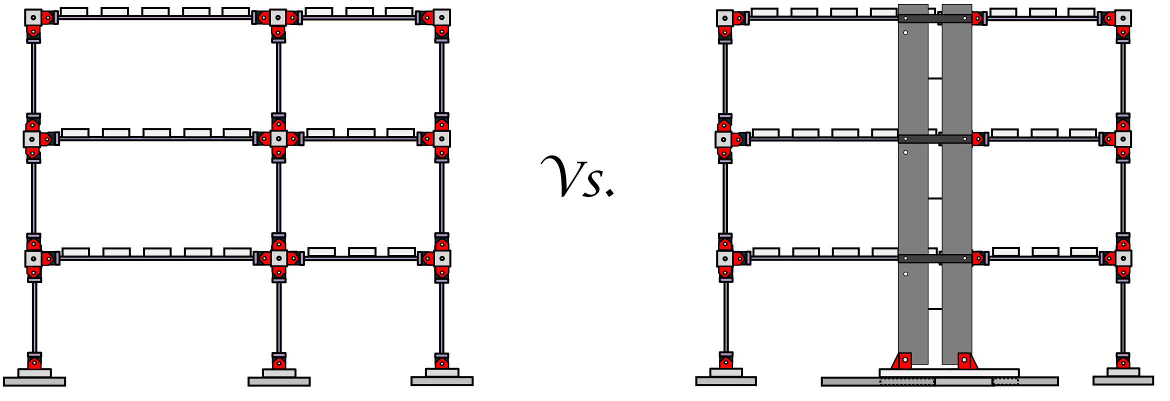

Figure 3.4 Models of the original and retrofitted buildings.

Seismic Records
<u>Moderate intensity seismic records</u> MNSA (Athens 1999) Aegion (1995) Kalamata (1986) Lefkada (2003)

Table 1 List of moderate intensity seismic records applied to the original and retrofitted building.

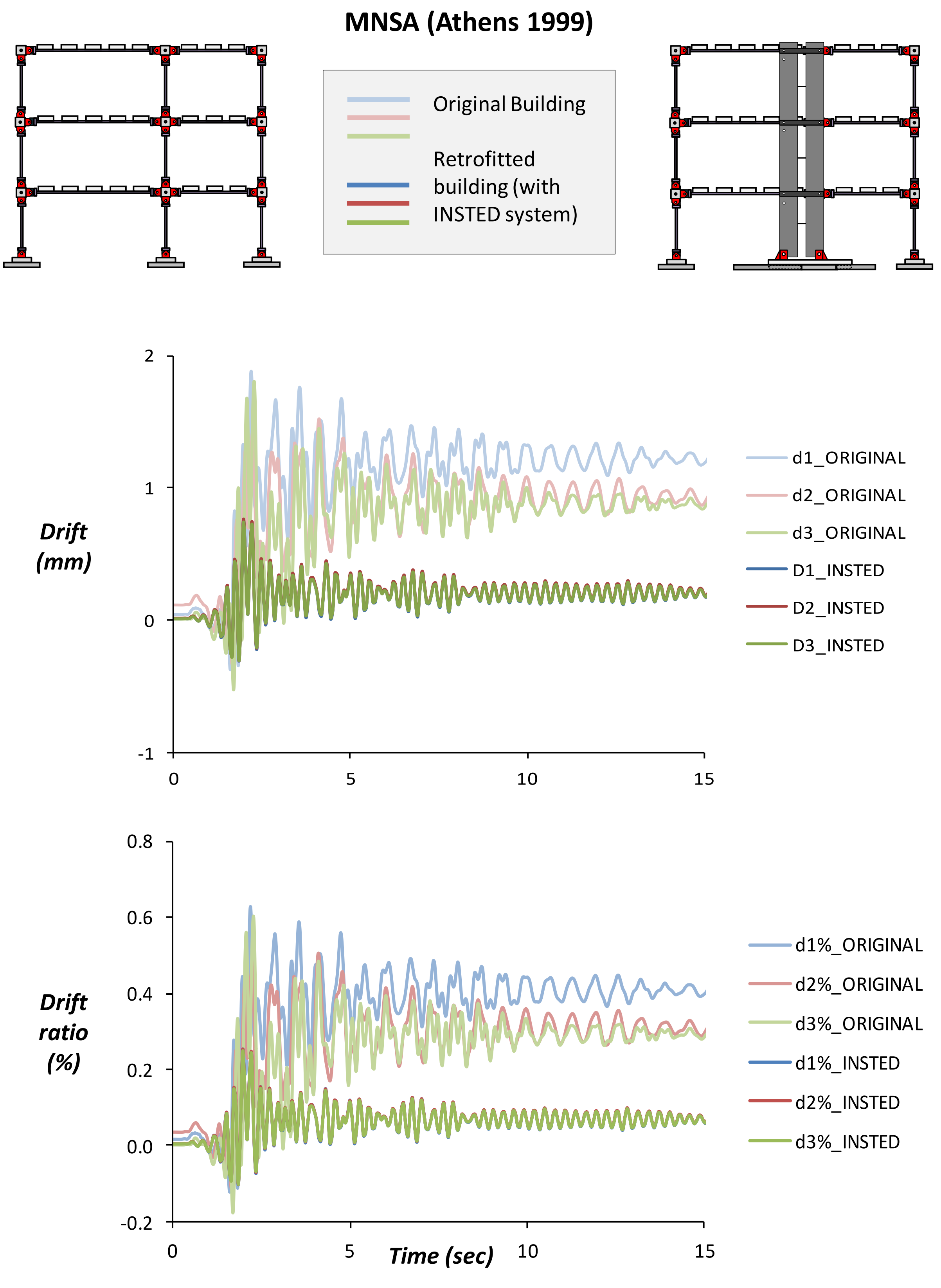

Figure 3.5 Comparison of the original and retrofitted building in terms of *interstorey drifts and drift ratios* for the MNSA record.

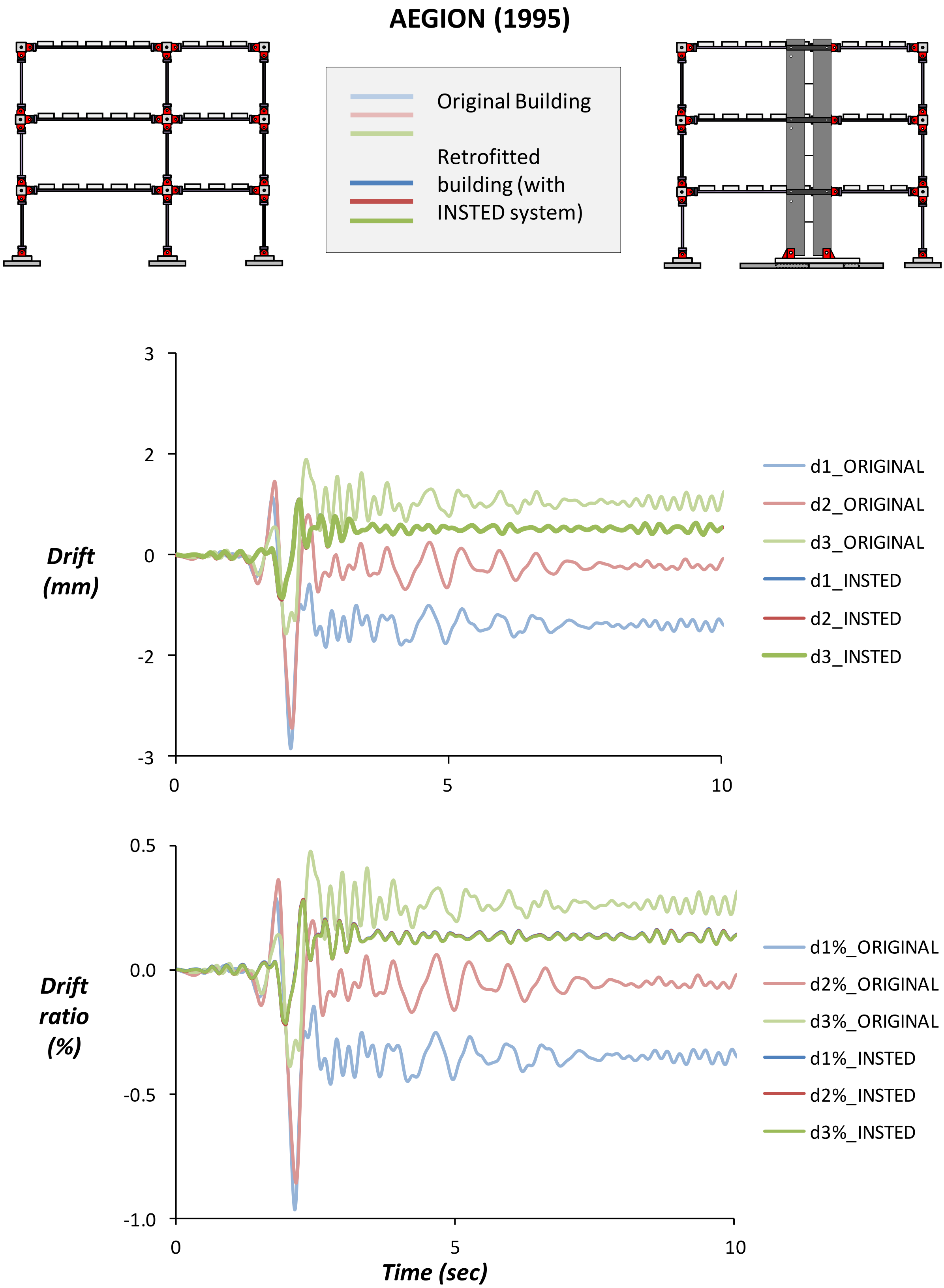

Figure 3.6 Comparison of the original and retrofitted building in terms of *interstorey drifts and drift ratios* for the Aegion record.

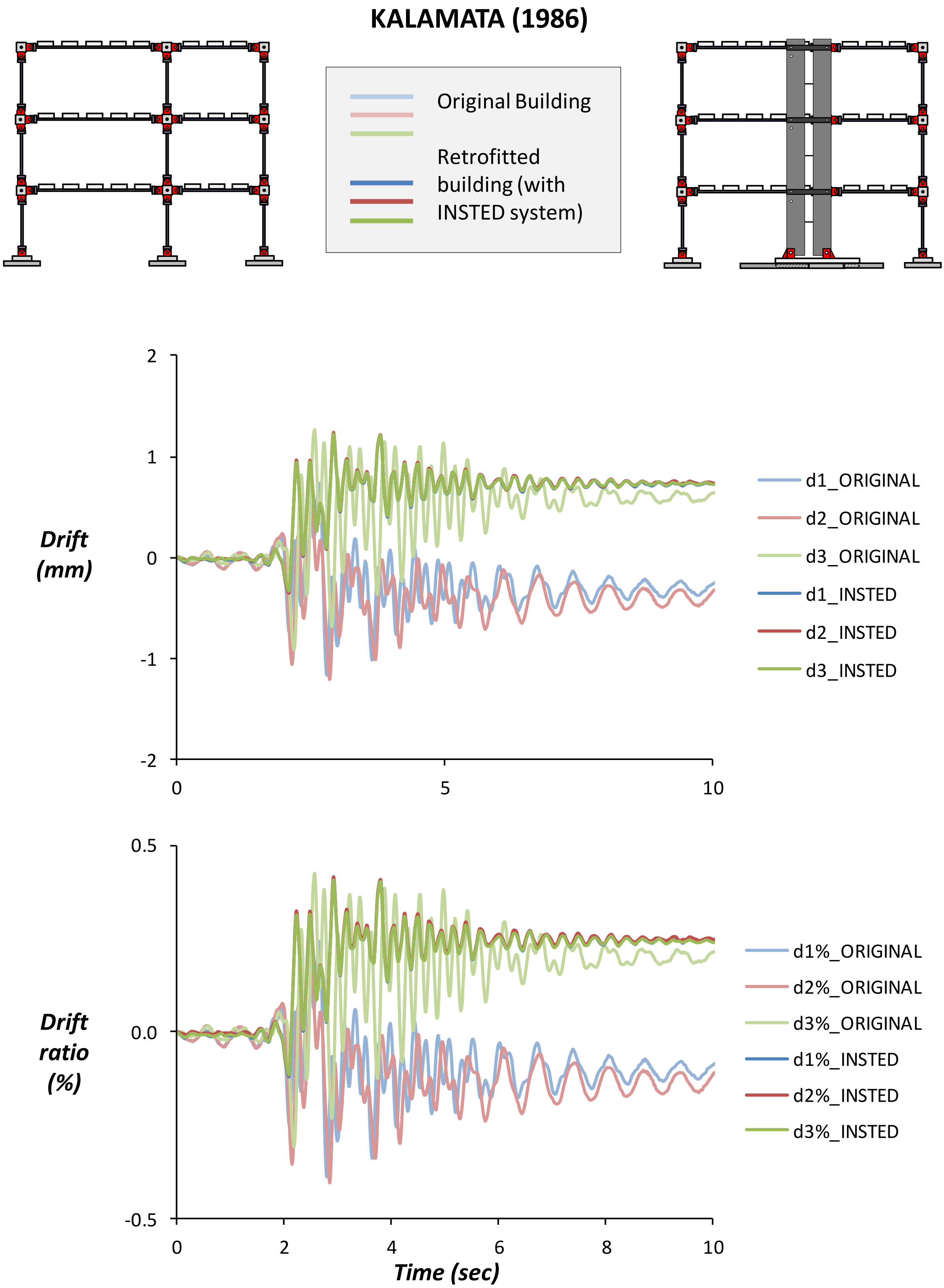

Figure 3.7 Comparison of the original and retrofitted building in terms of *interstorey drifts and drift ratios* for the Kalamata record.

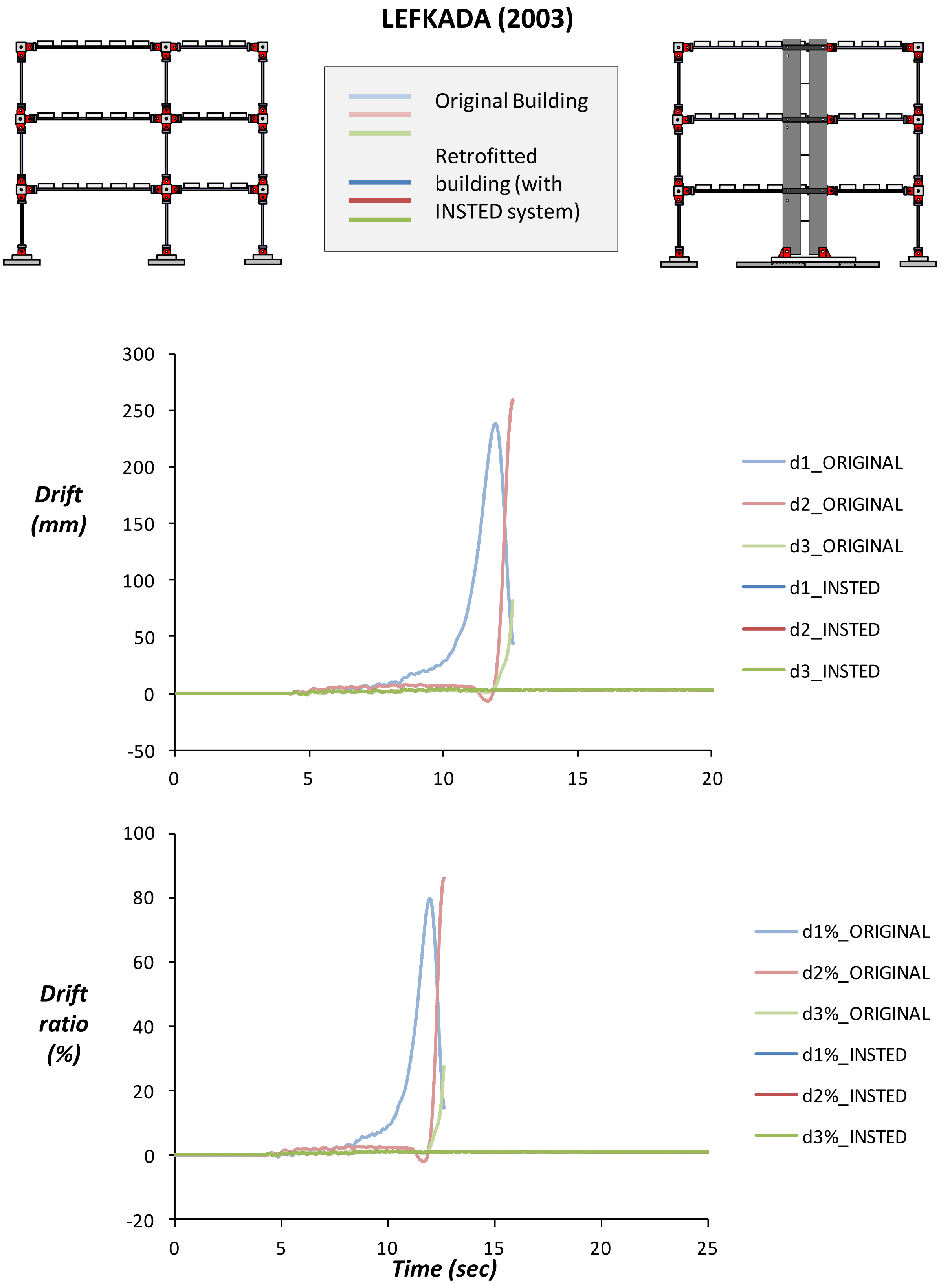

Figure 3.8 Comparison of the original and the retrofitted building in terms of *interstorey drifts and drift ratios* for the Lefkada record.

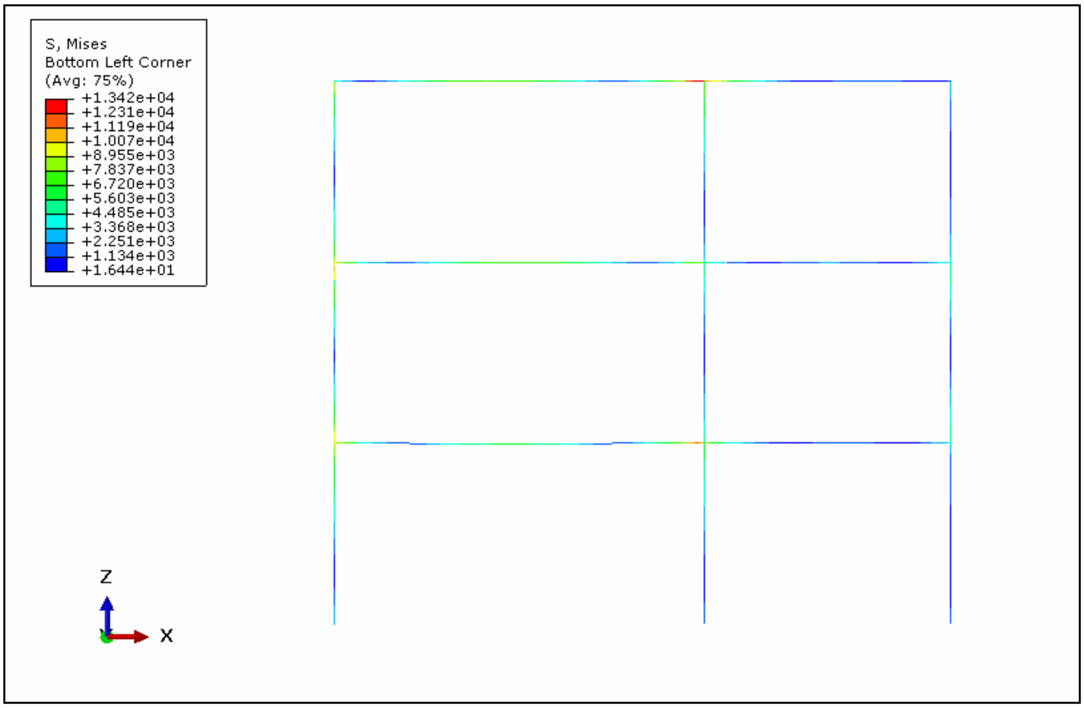

Figure 3.9 Initial shape of the original building.

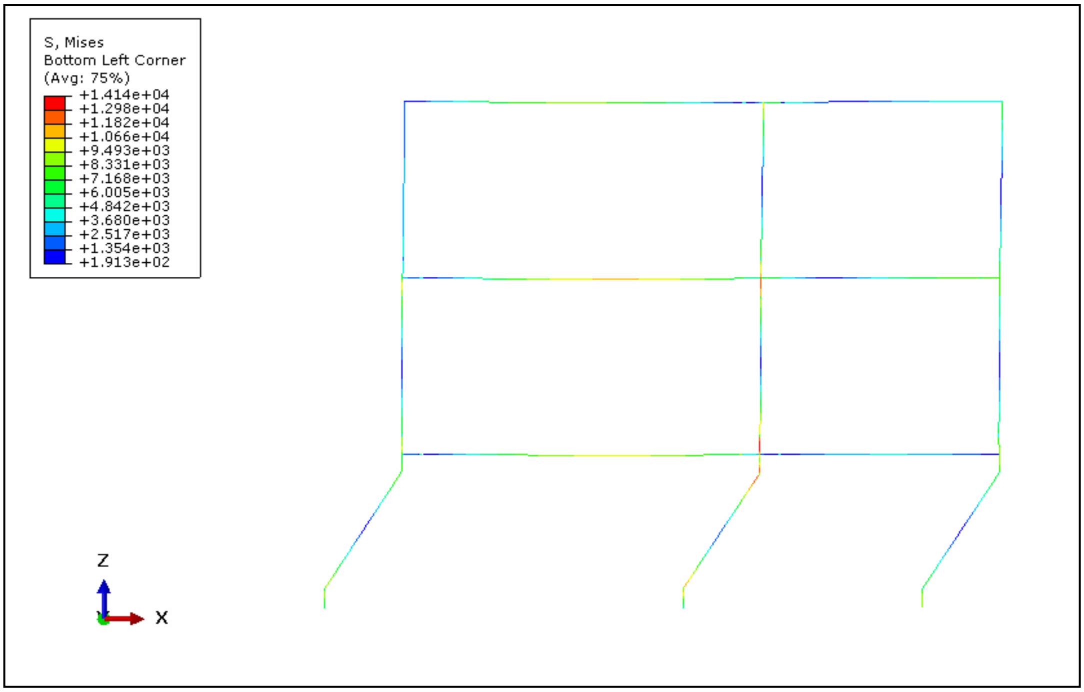

Figure 3.10 Deformed shape of the original building just before failure at the record of Lefkada.

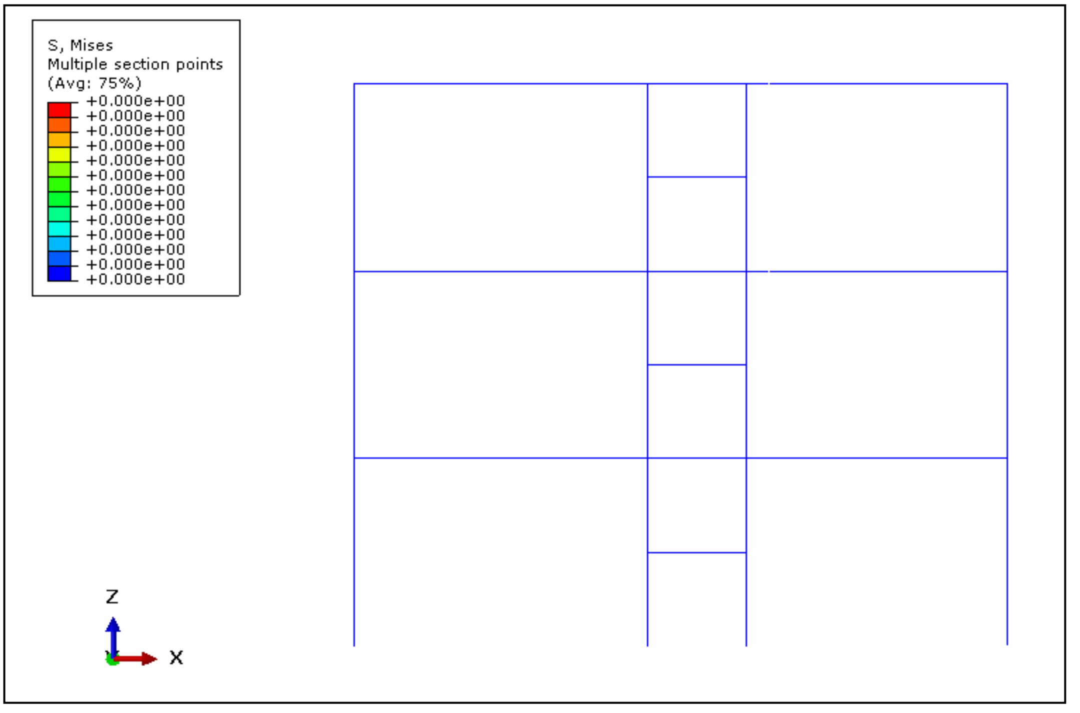

Figure 3.11 Initial shape of the retrofitted building.

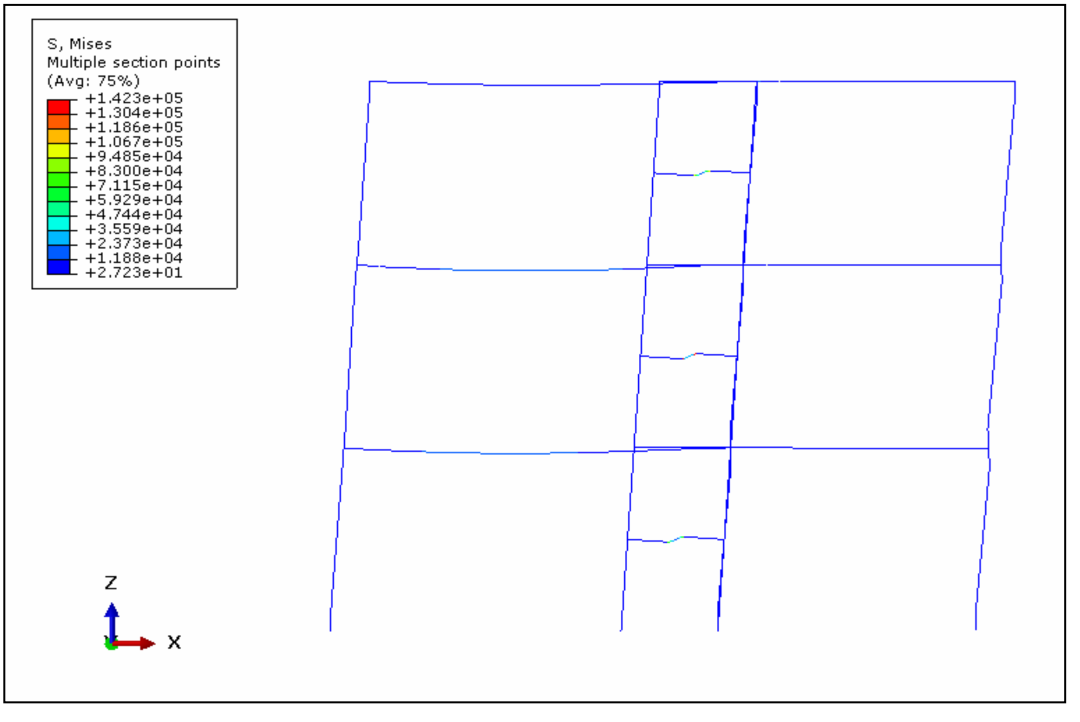

Figure 3.12 Deformed shape of the retrofitted building after the record of Lefkada. The structure did not experience any failure.

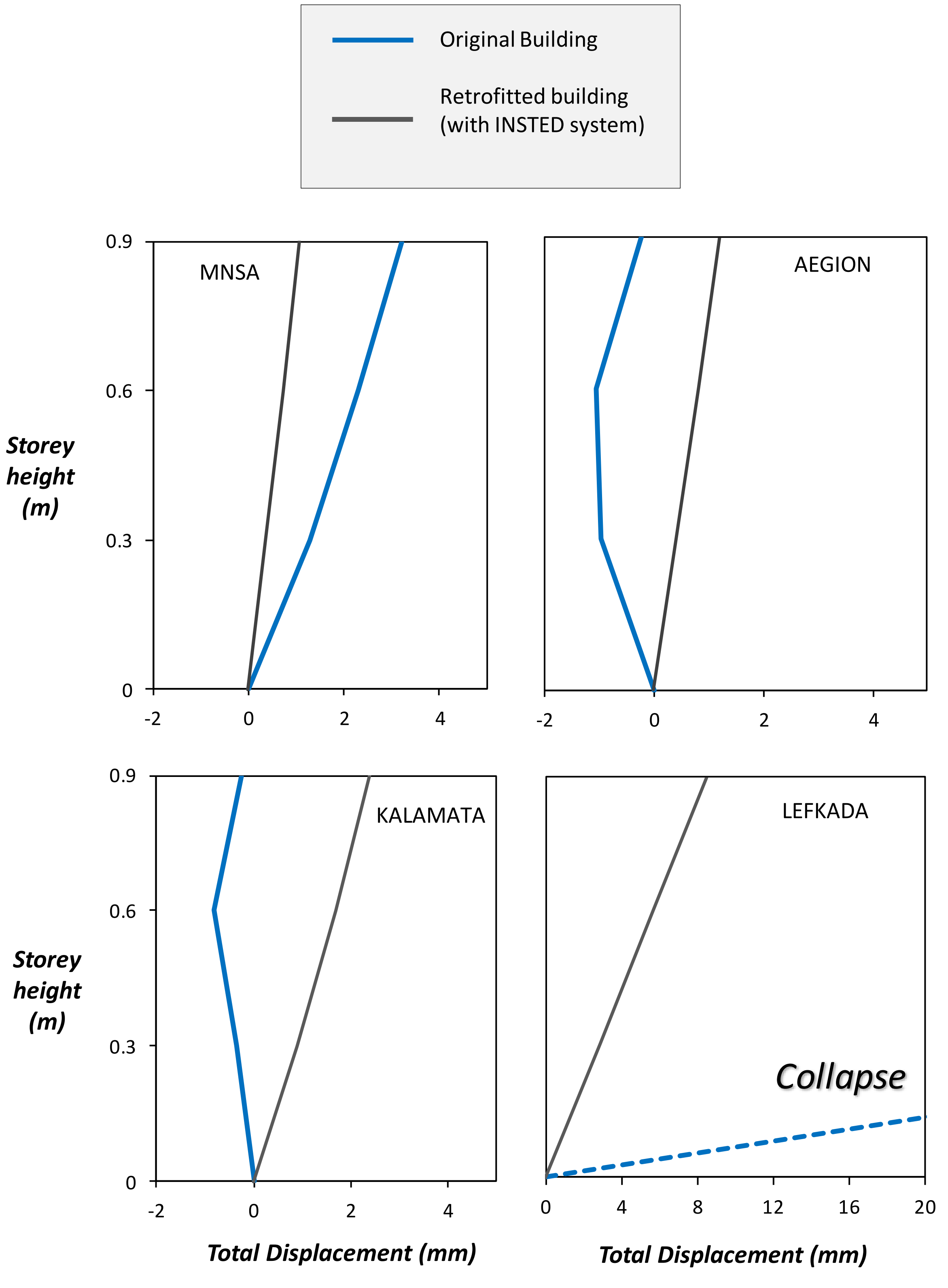

Figure 3.13 Total displacements of the original and the retrofitted building after each record, inn terms of storey height.

Retrofitted building (INSTED-FUSEIS system)
Numerical Analyses – Dynamic Tests

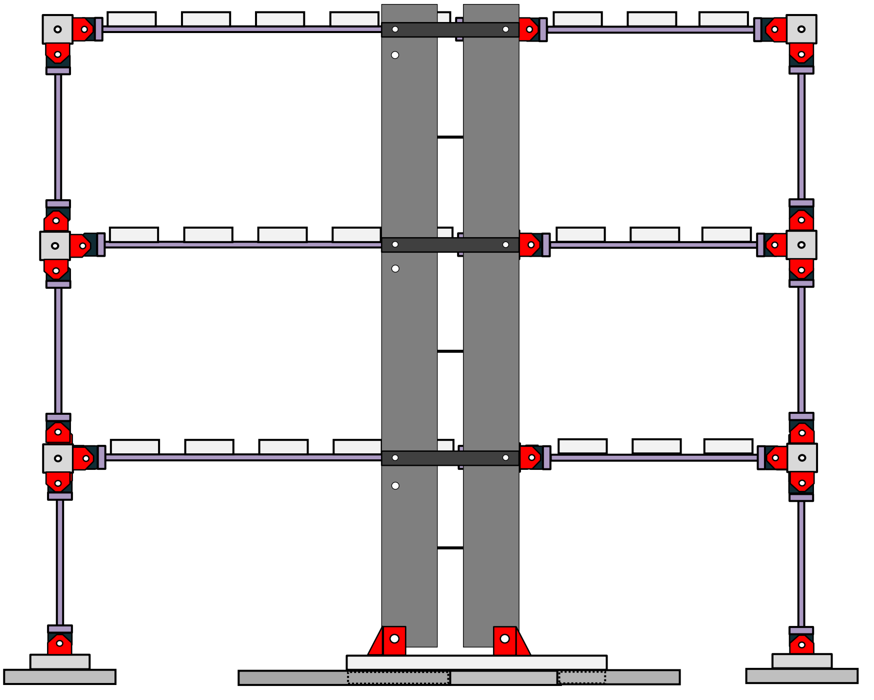

Seismic Records
Moderate intensity seismic records
MNSA (Athens 1999) Lefkada (2003) Aegion (1995) Kalamata (1986) Sakarya (Kocaeli 1999)
Strong seismic records
JMA (Kobe 1995) Rinaldi (Northridge 1994) Takatori (Kobe 1995)

Table 2 List of seismic records applied in the retrofitted building in order to examine its performance under moderate & strong seismic shaking.

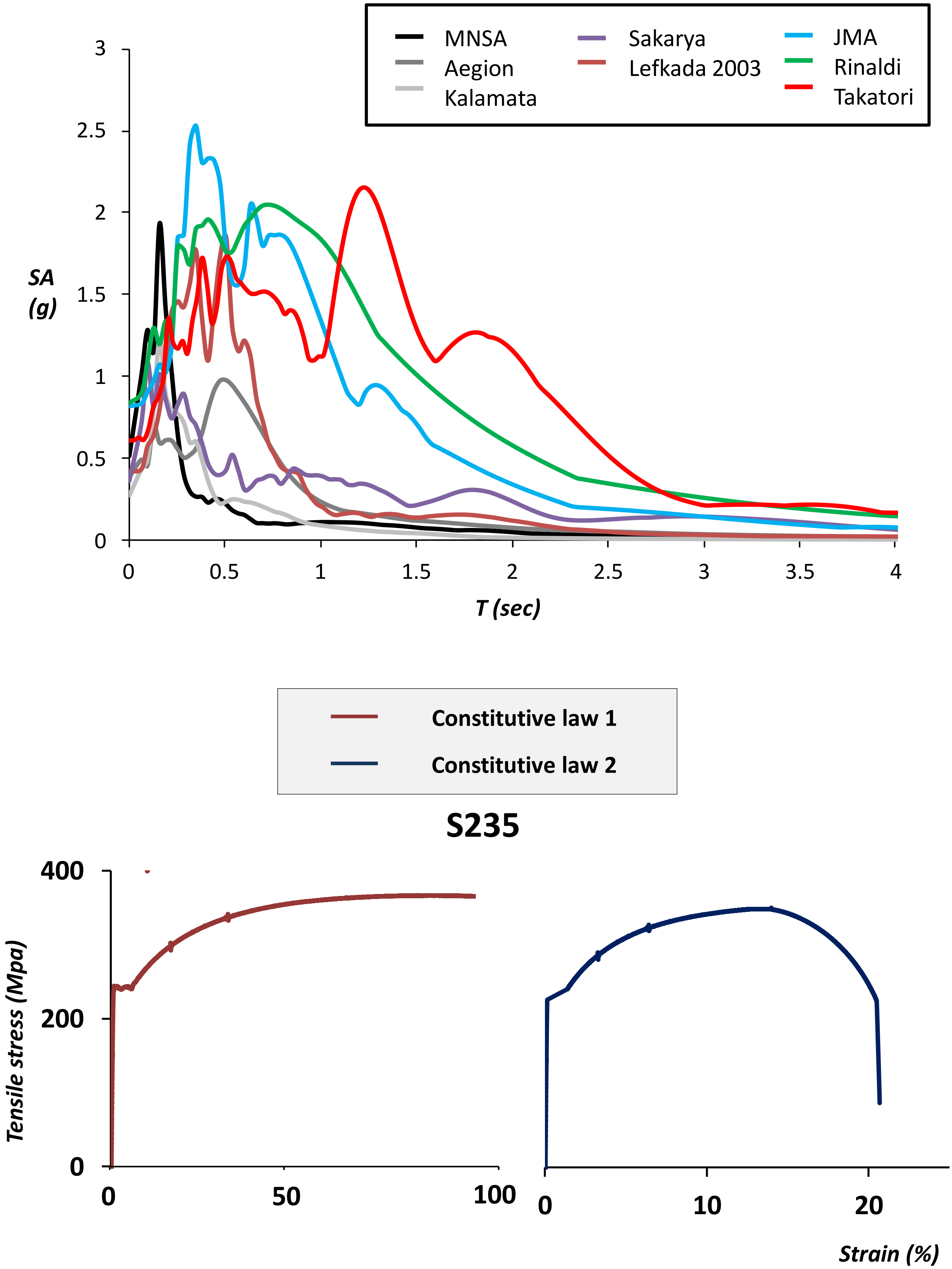

Figure 3.14 Elastic spectra of the imposed seismic excitations and the constitutive laws assigned to the fuse elements (rods) in the numerical dynamic analyses.

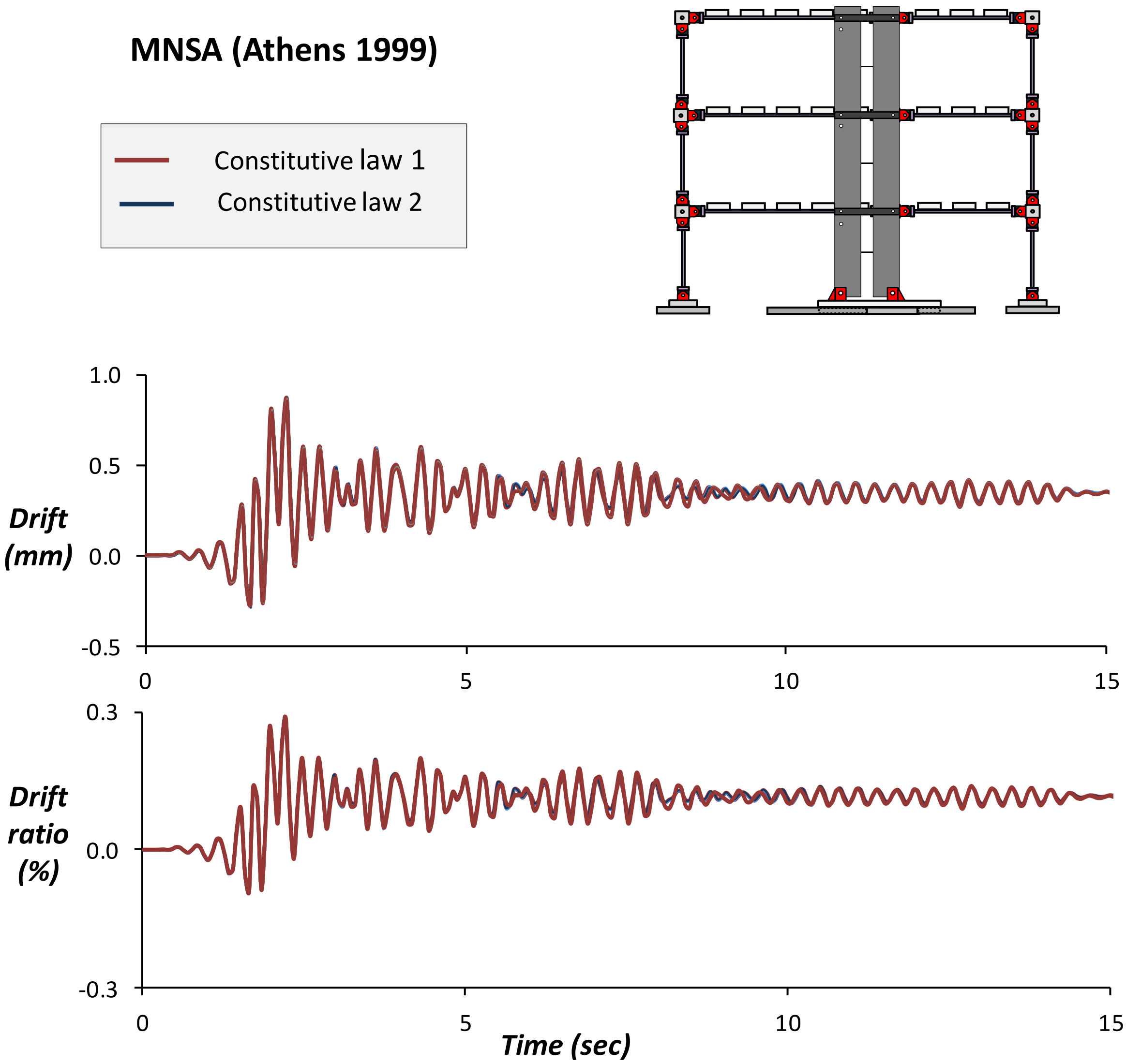

Figure 3.15 Time histories of *Interstorey drifts and drift ratios* of the retrofitted building (MNSA).

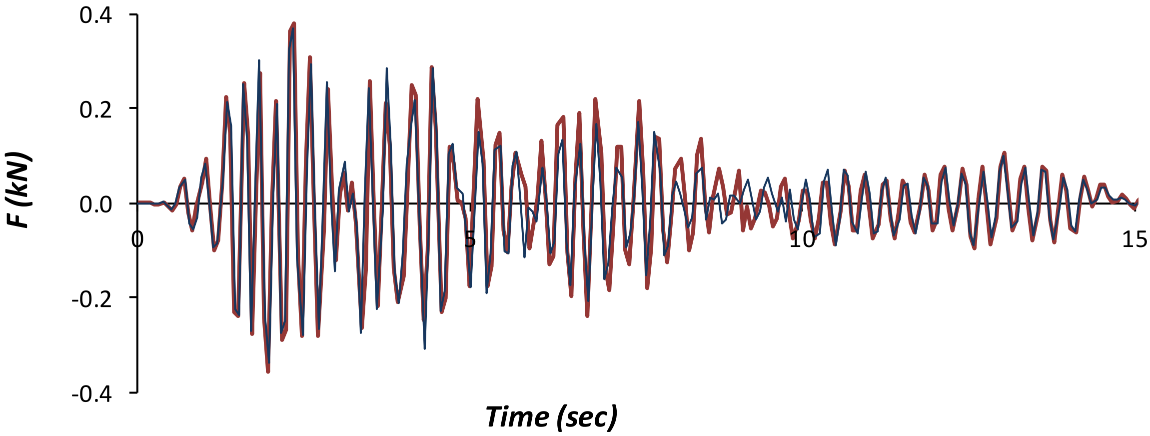

Figure 3.16 Total Resisting force's time history of the structure (MNSA).

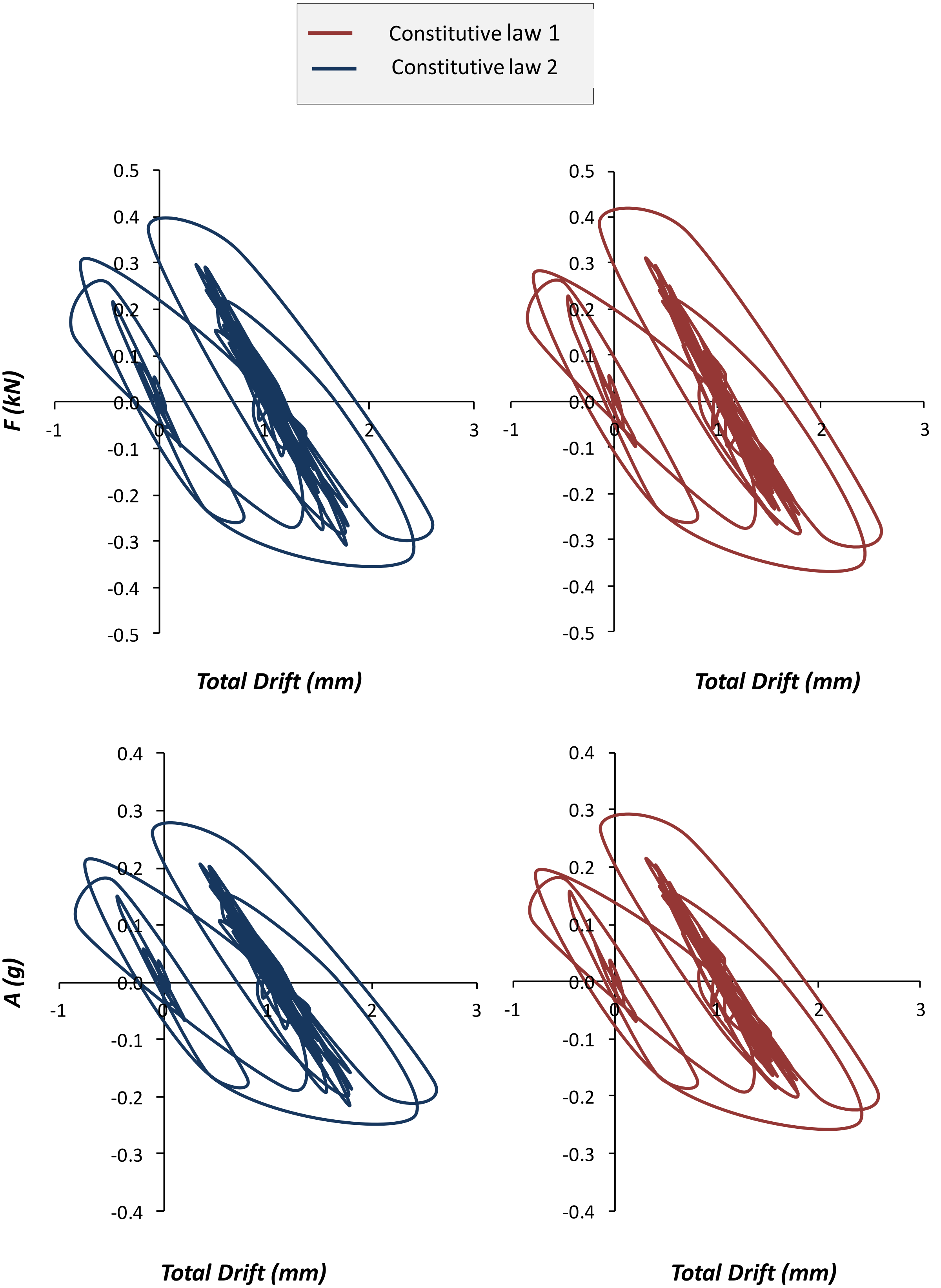

Figure 3.17 Force and acceleration with regard to the total drift of the building (MNSA).

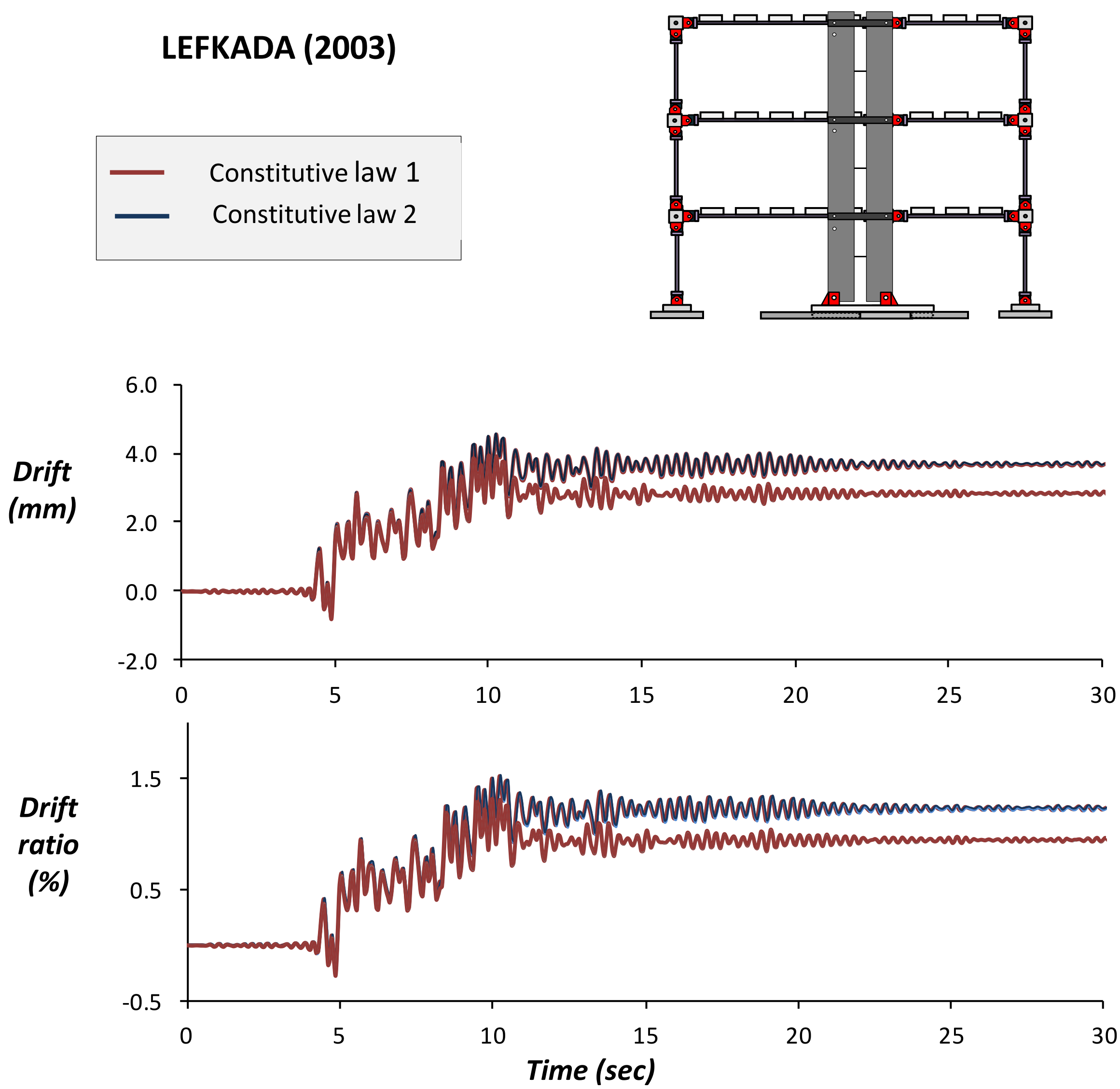

Figure 3.18 Time histories of *Interstorey drifts and drift ratios* of the retrofitted building (Lefkada).

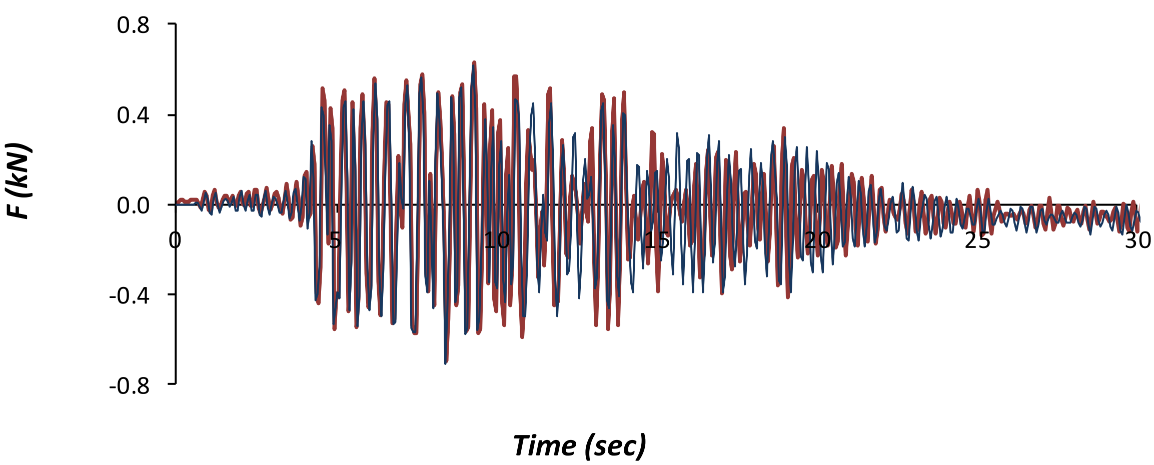

Figure 3.19 Total Resisting force’s time history of the structure (Lefkada).

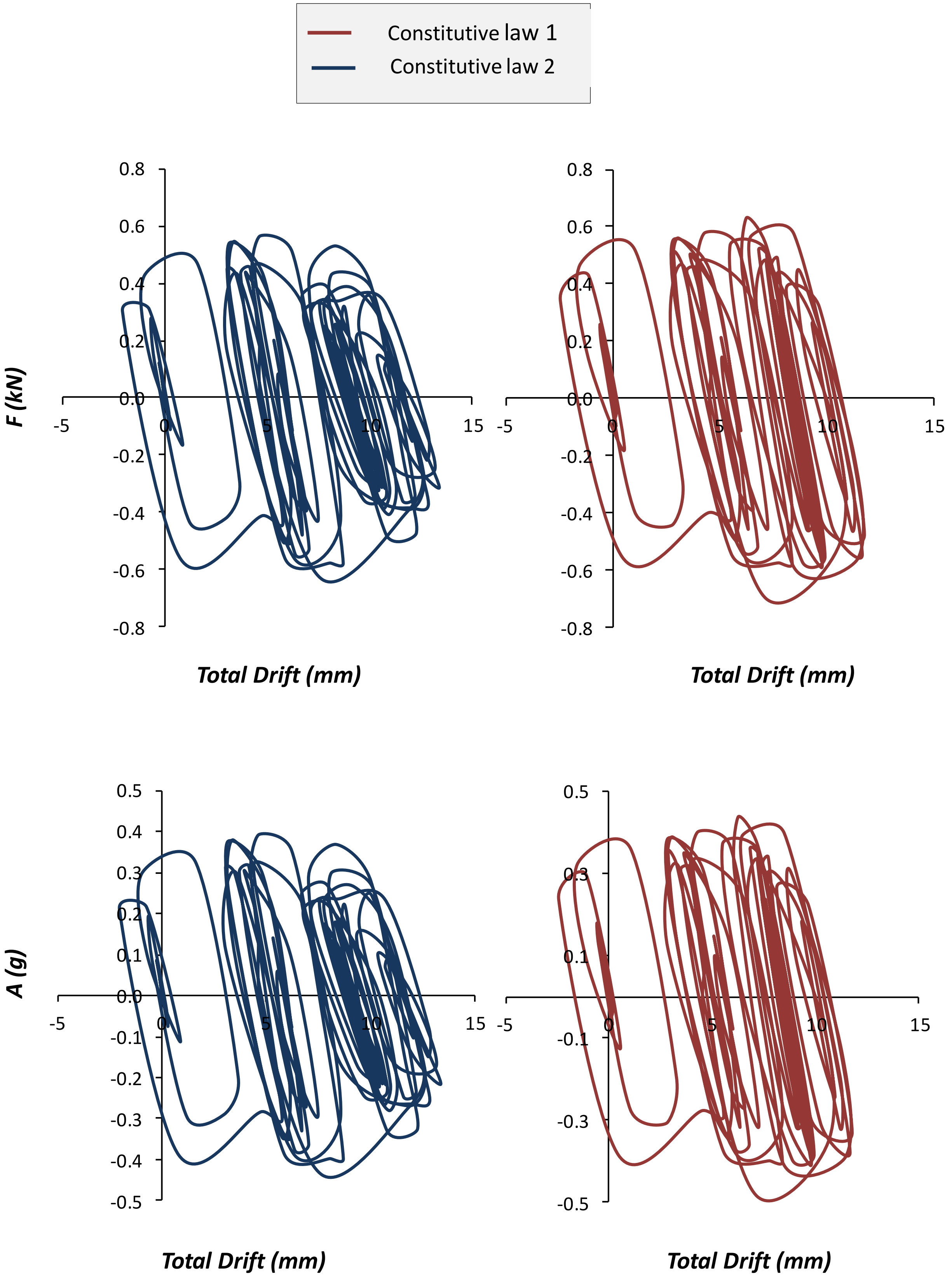

Figure 3.20 Force and acceleration with regard to the total drift of the building (Lefkada).

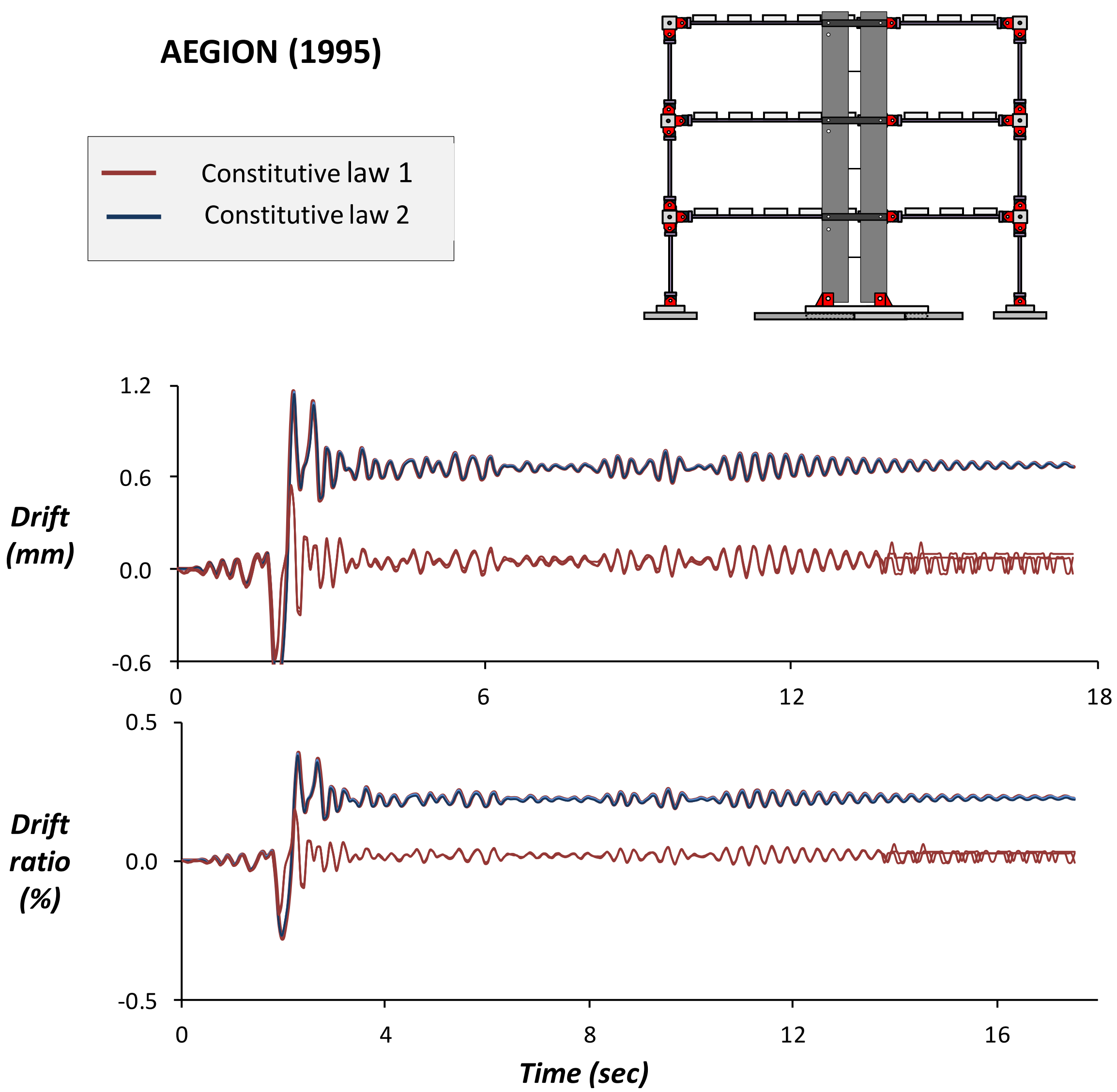

Figure 3.21 Time histories of *Interstorey drifts and drift ratios* of the retrofitted building (Aegion).

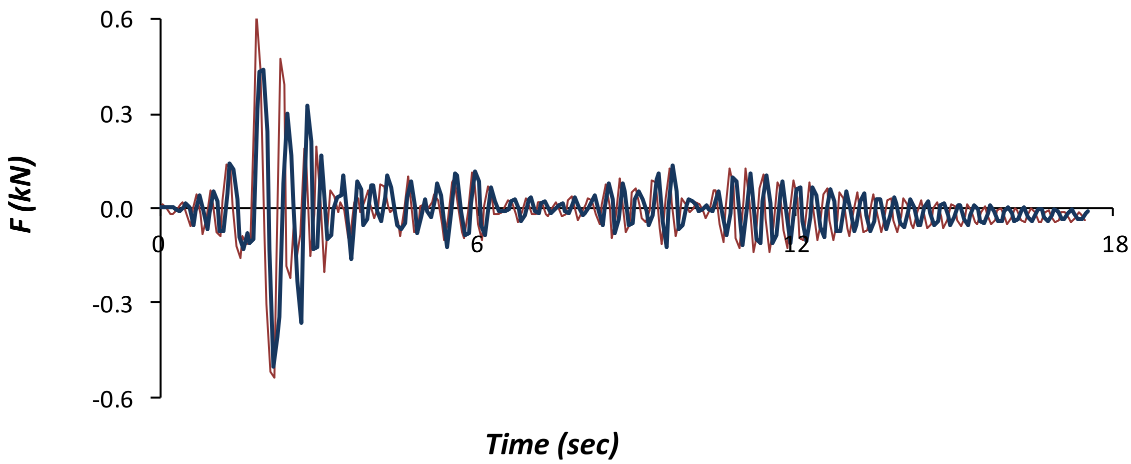

Figure 3.22 Total Resisting force's time history of the structure (Aegion).

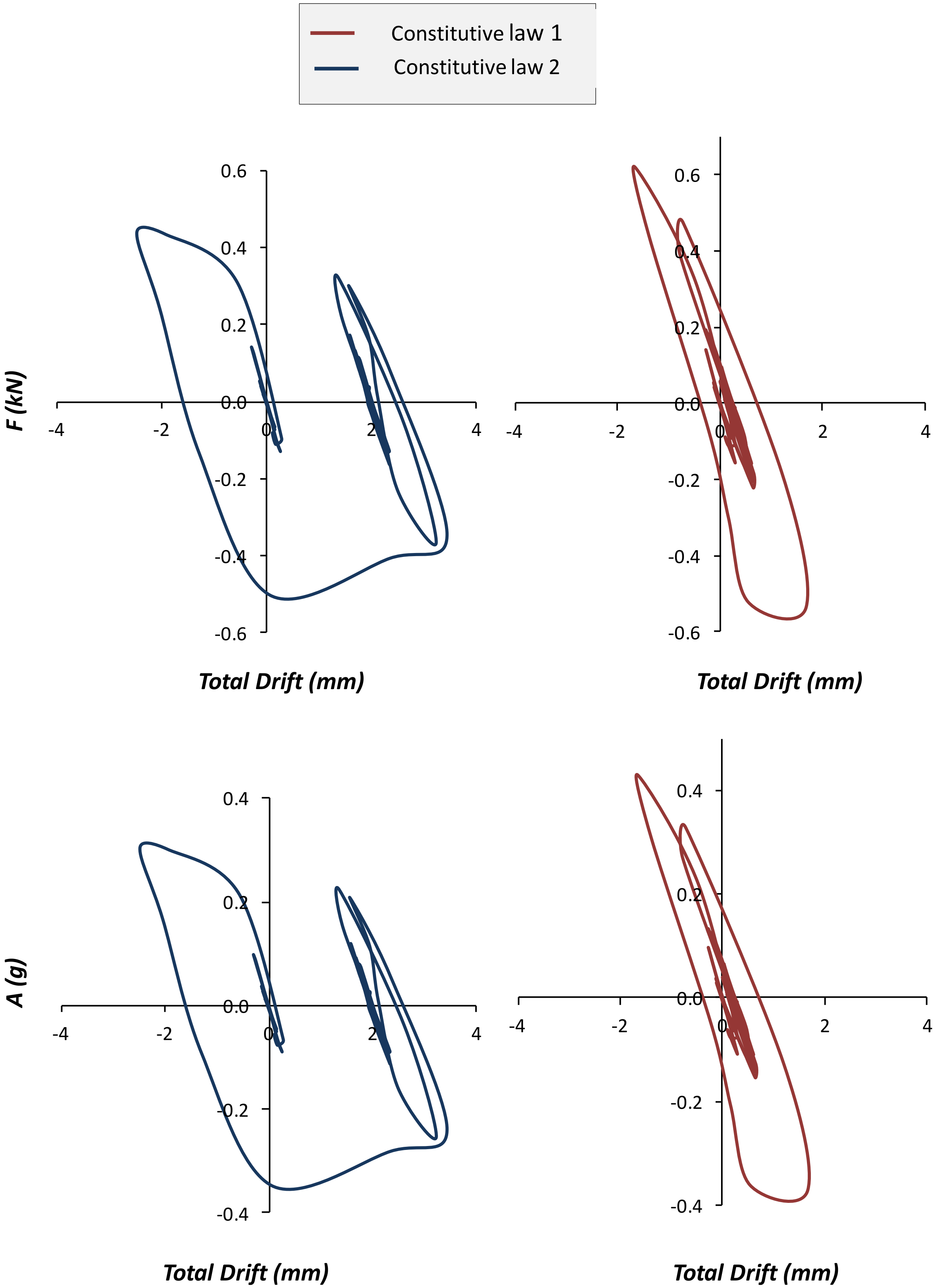

Figure 3.23 Force and acceleration with regard to the total drift of the building (Aegion).

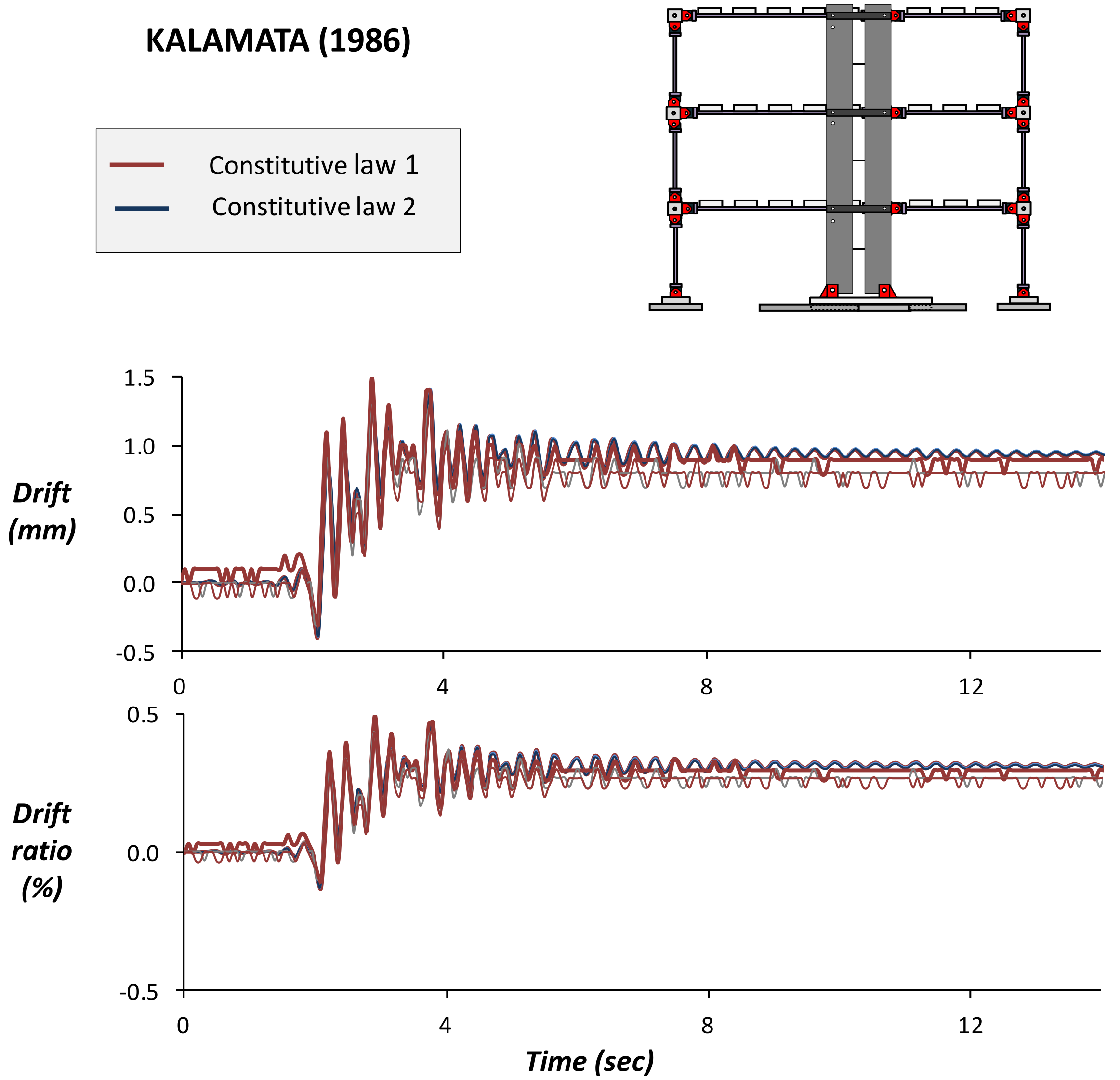

Figure 3.24 Time histories of *Interstorey drifts and drift ratios* of the retrofitted building (Kalamata).

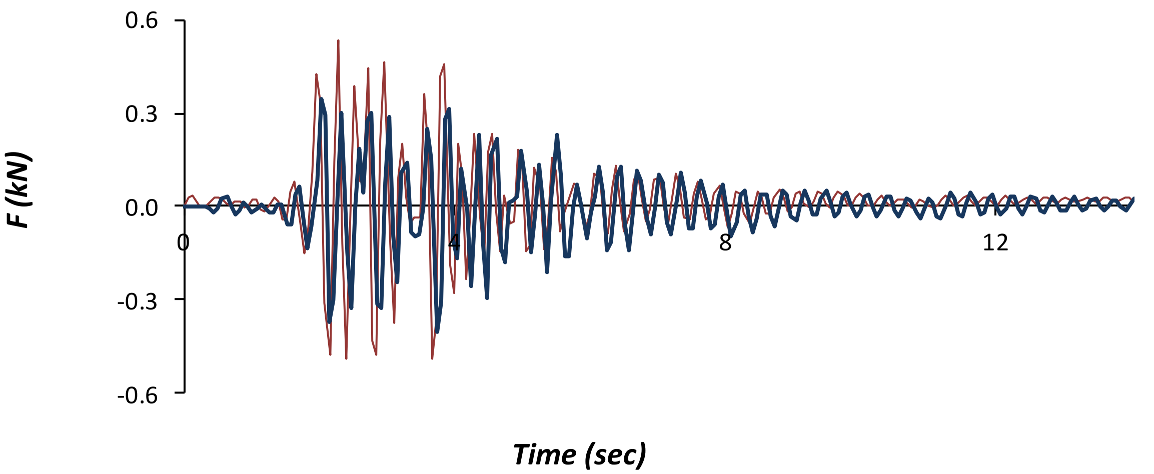

Figure 3.25 Total Resisting force's time history of the structure (Kalamata).

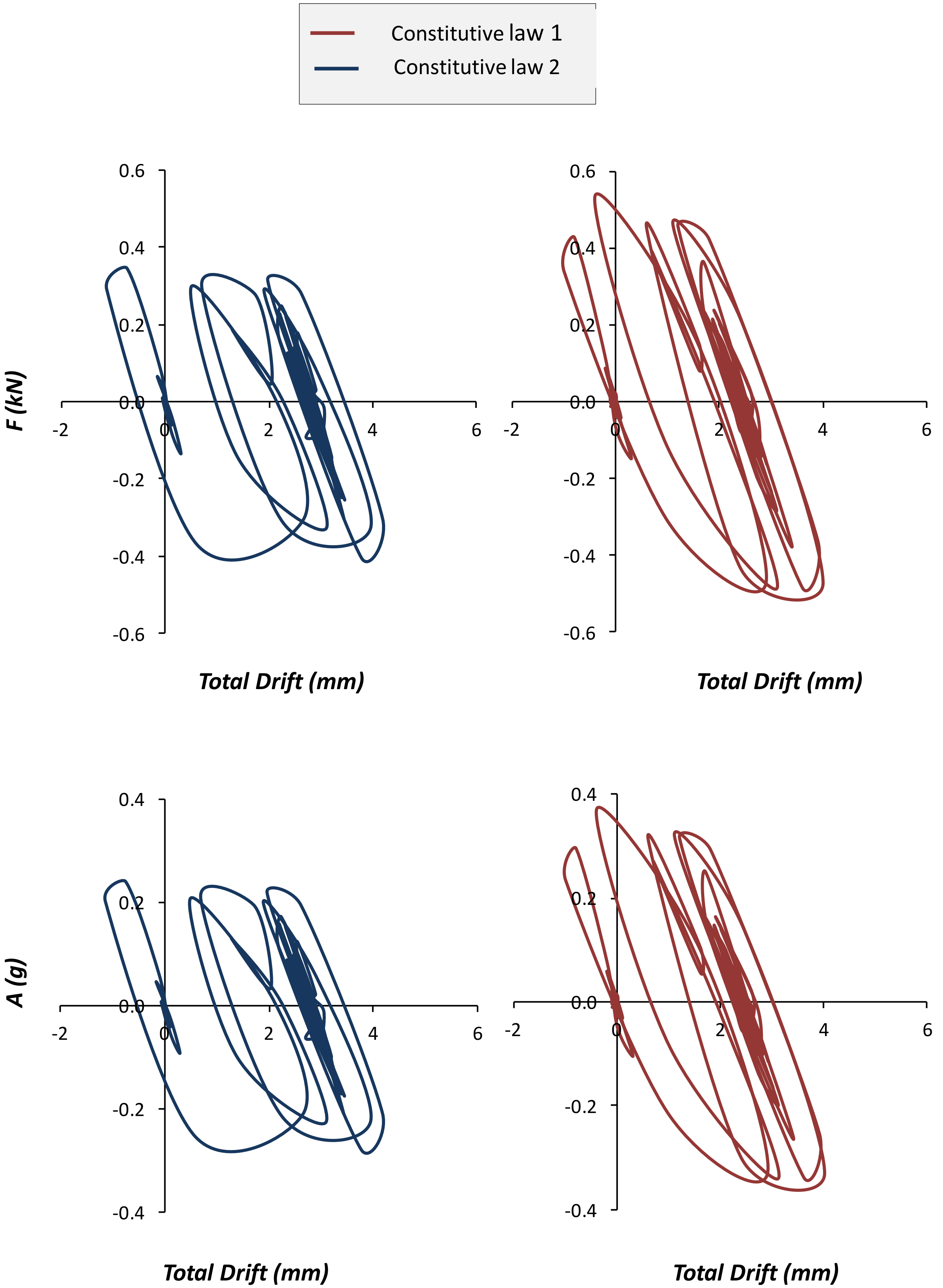

Figure 3.26 Force and acceleration with regard to the total drift of the building (Kalamata).

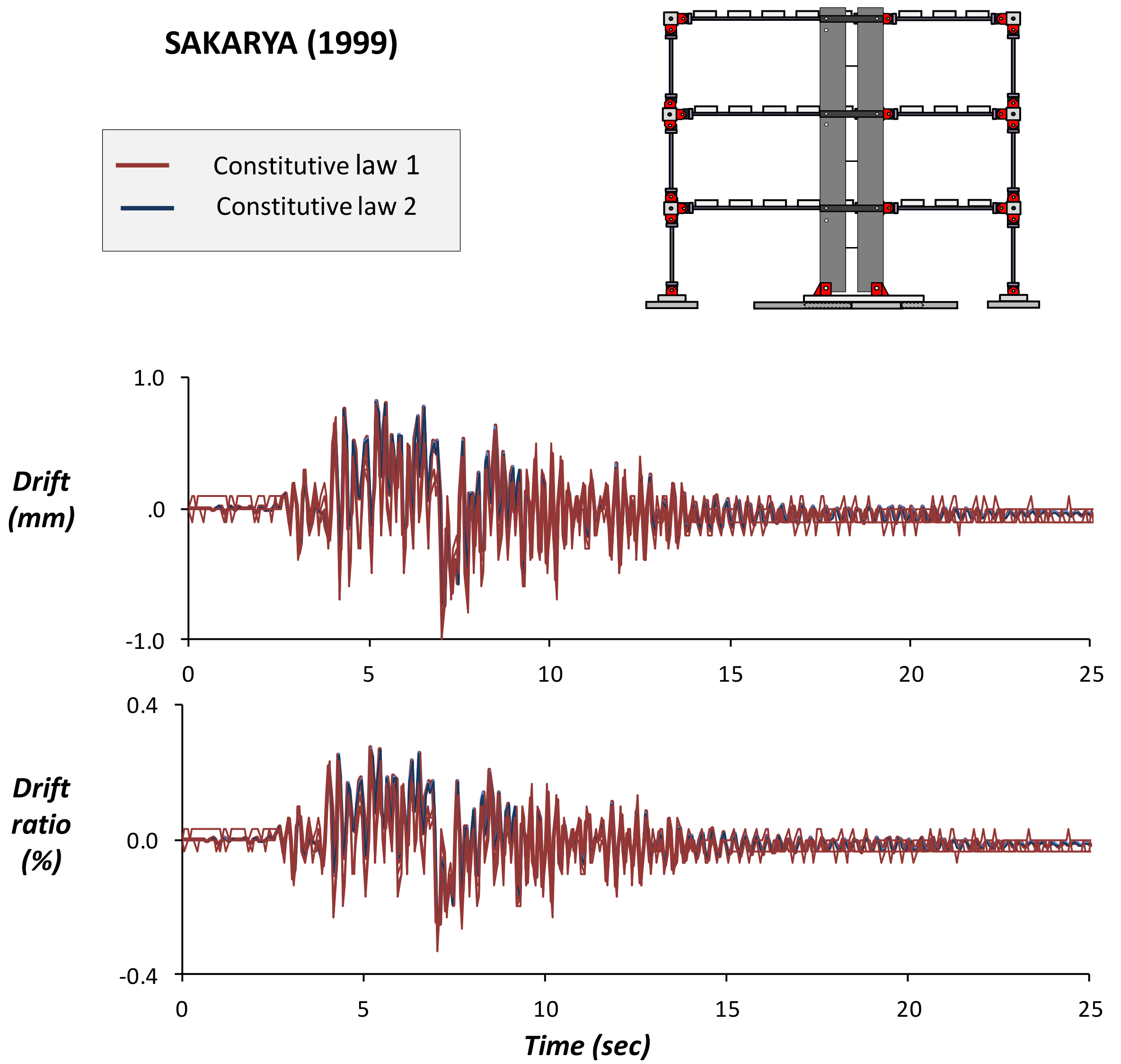

Figure 3.27 Time histories of *Interstorey drifts and drift ratios* of the retrofitted building (Sakarya).

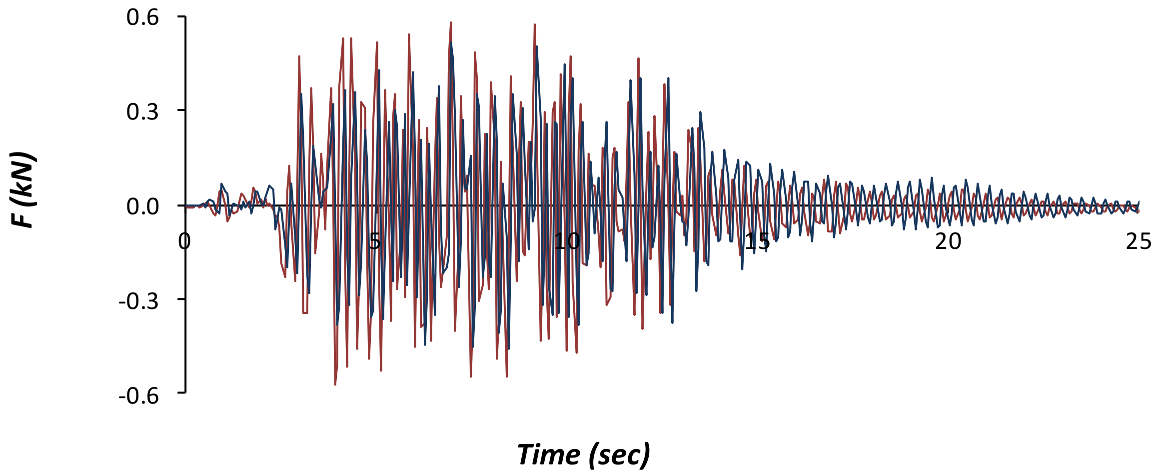

Figure 3.28 Total Resisting force's time history of the structure (Sakarya).

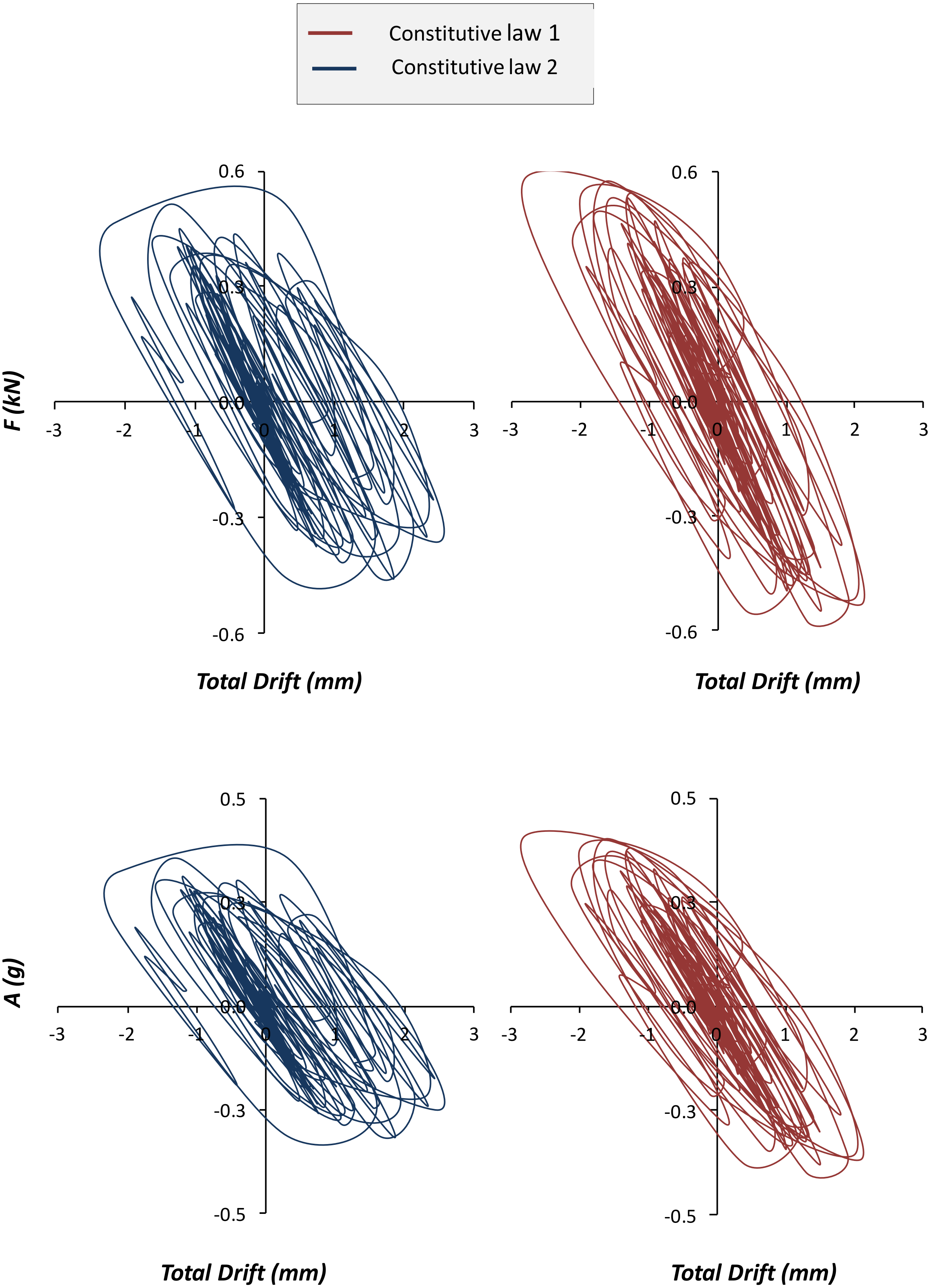

Figure 3.29 Force and acceleration with regard to the total drift of the building (Sakarya).

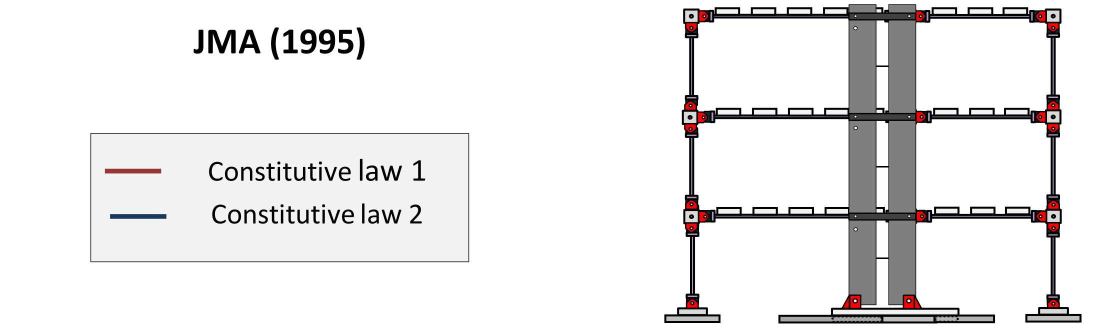

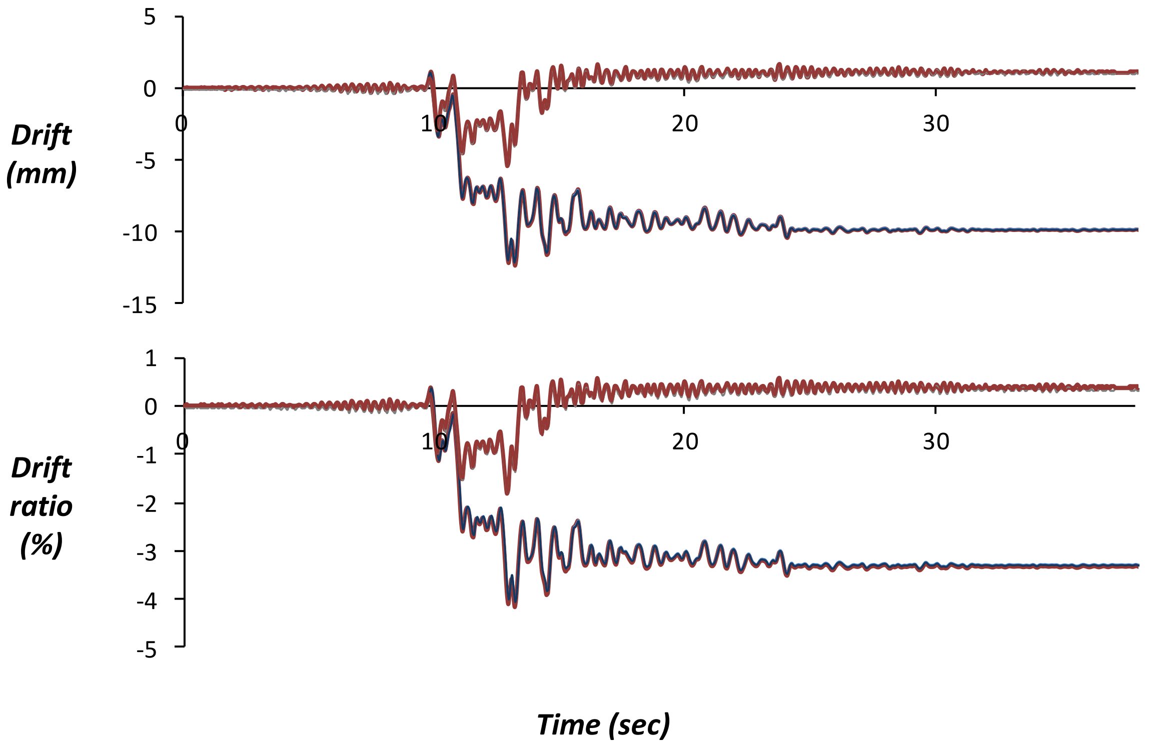

Figure 3.30 Time histories of *Interstorey drifts and drift ratios* of the retrofitted building (Jma).

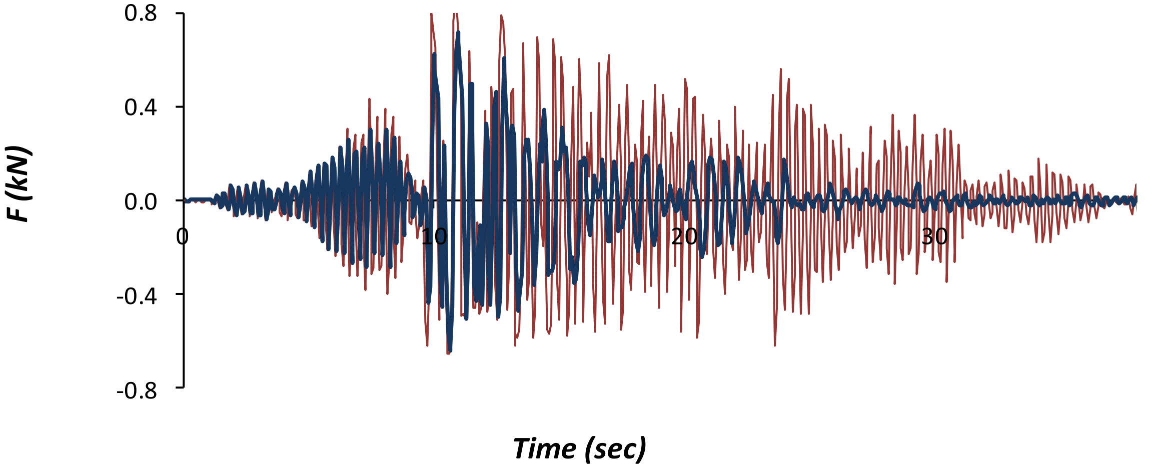

Figure 3.31 Total Resisting force's time history of the structure (Jma).

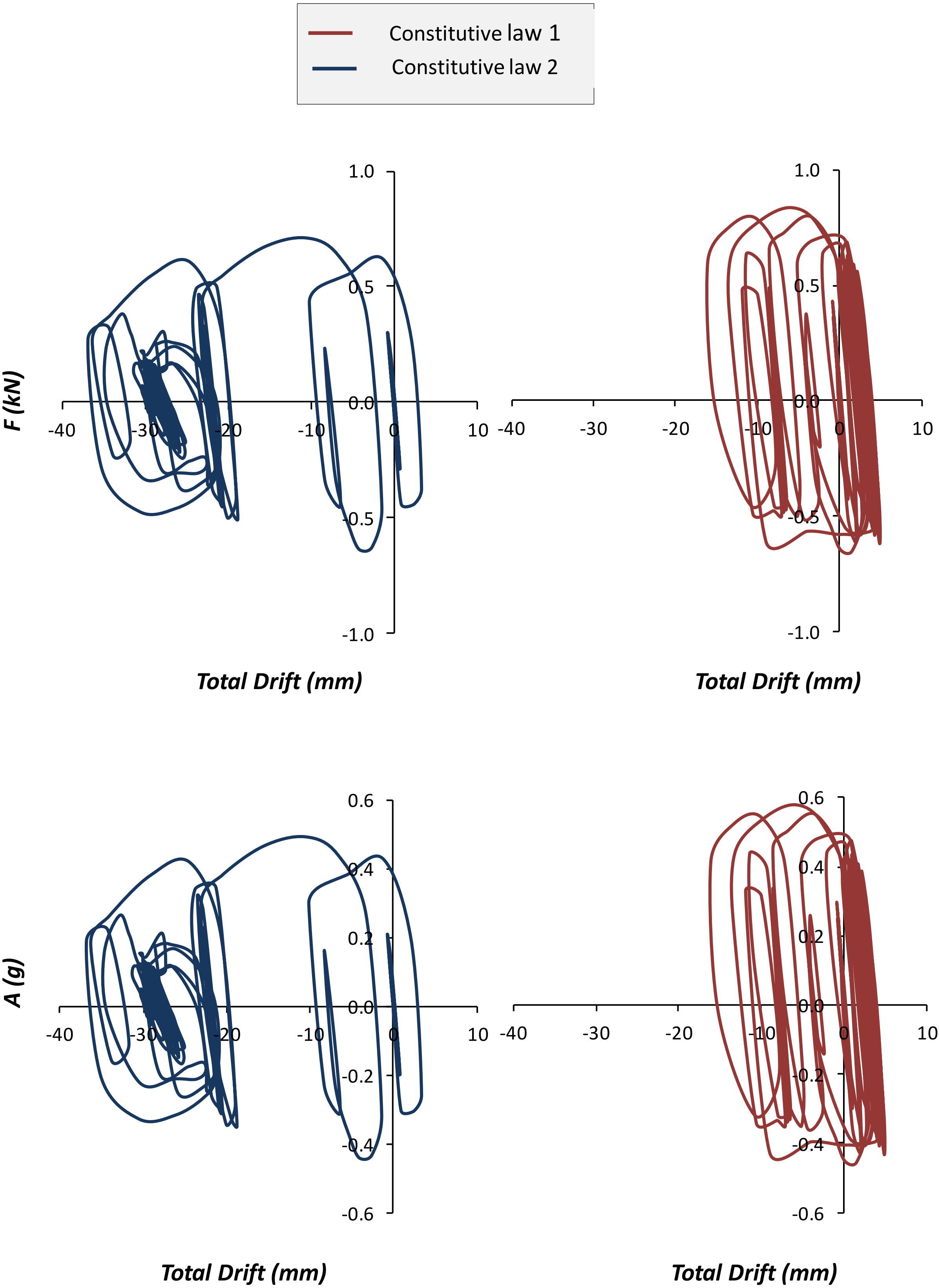

Figure 3.32 Force and acceleration with regard to the total drift of the building (Jma).

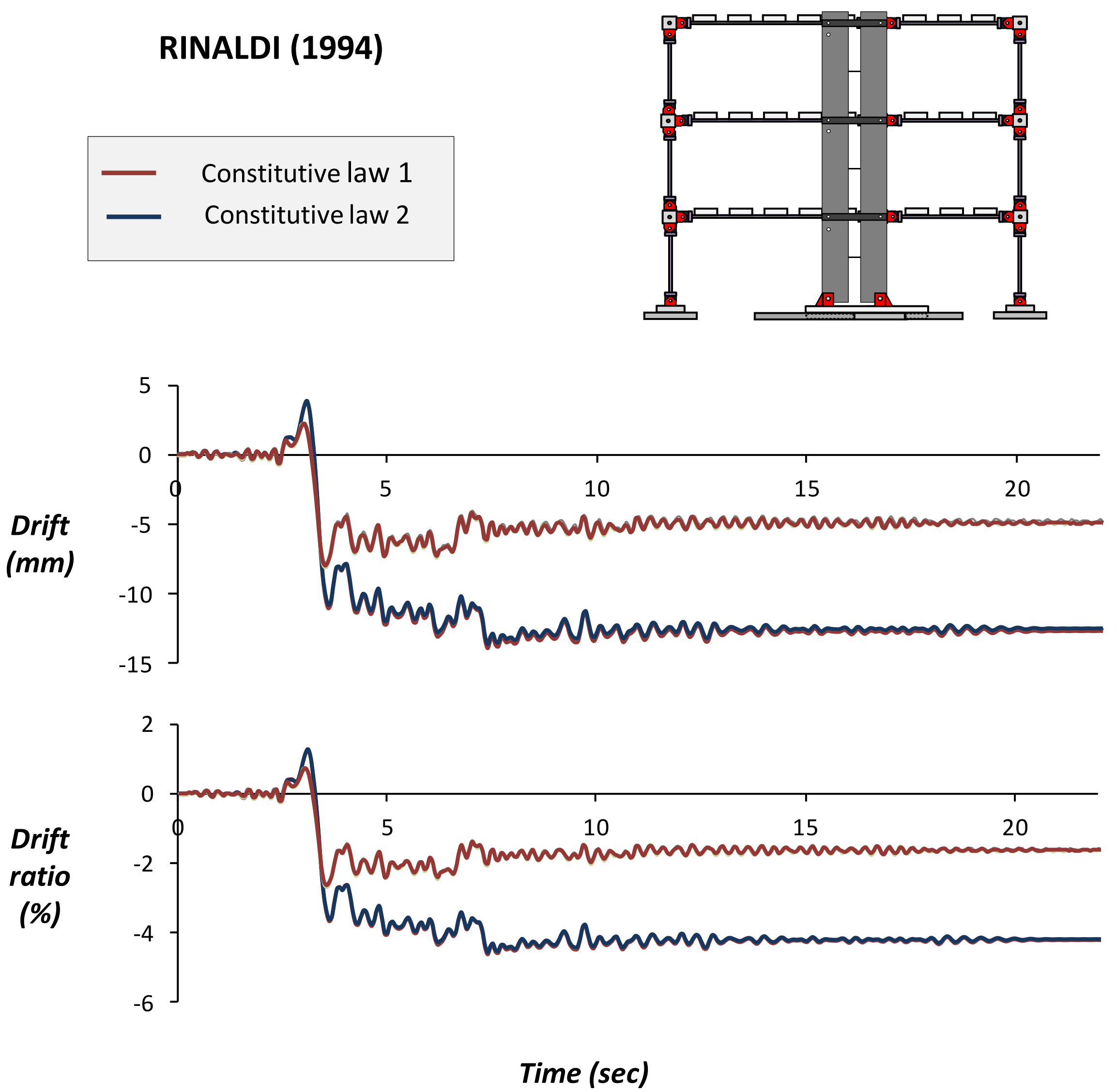

Figure 3.33 Time histories of *Interstorey drifts and drift ratio* of the retrofitted building (Rinaldi).

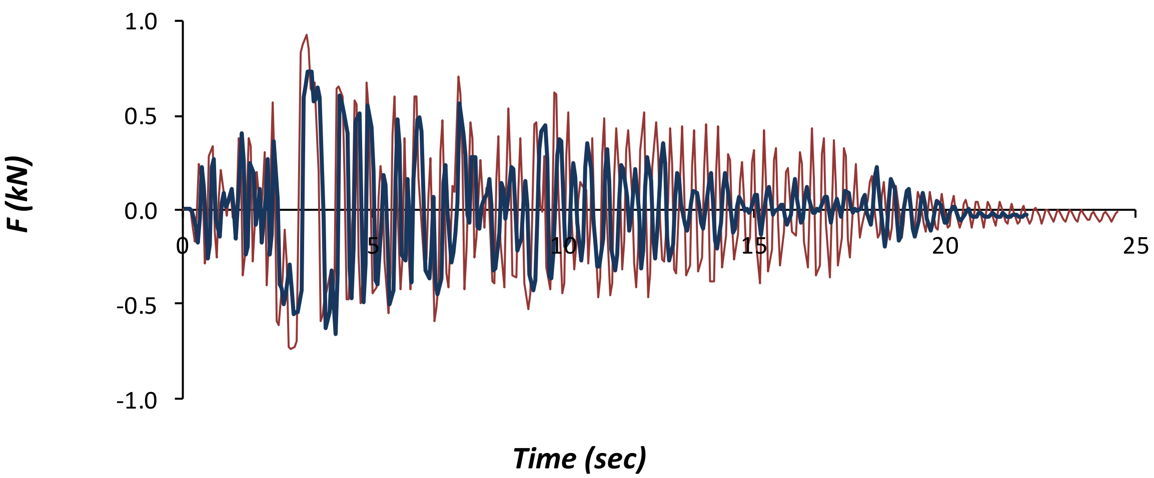

Figure 3.34 Total Resisting force's time history of the structure (Rinaldi).

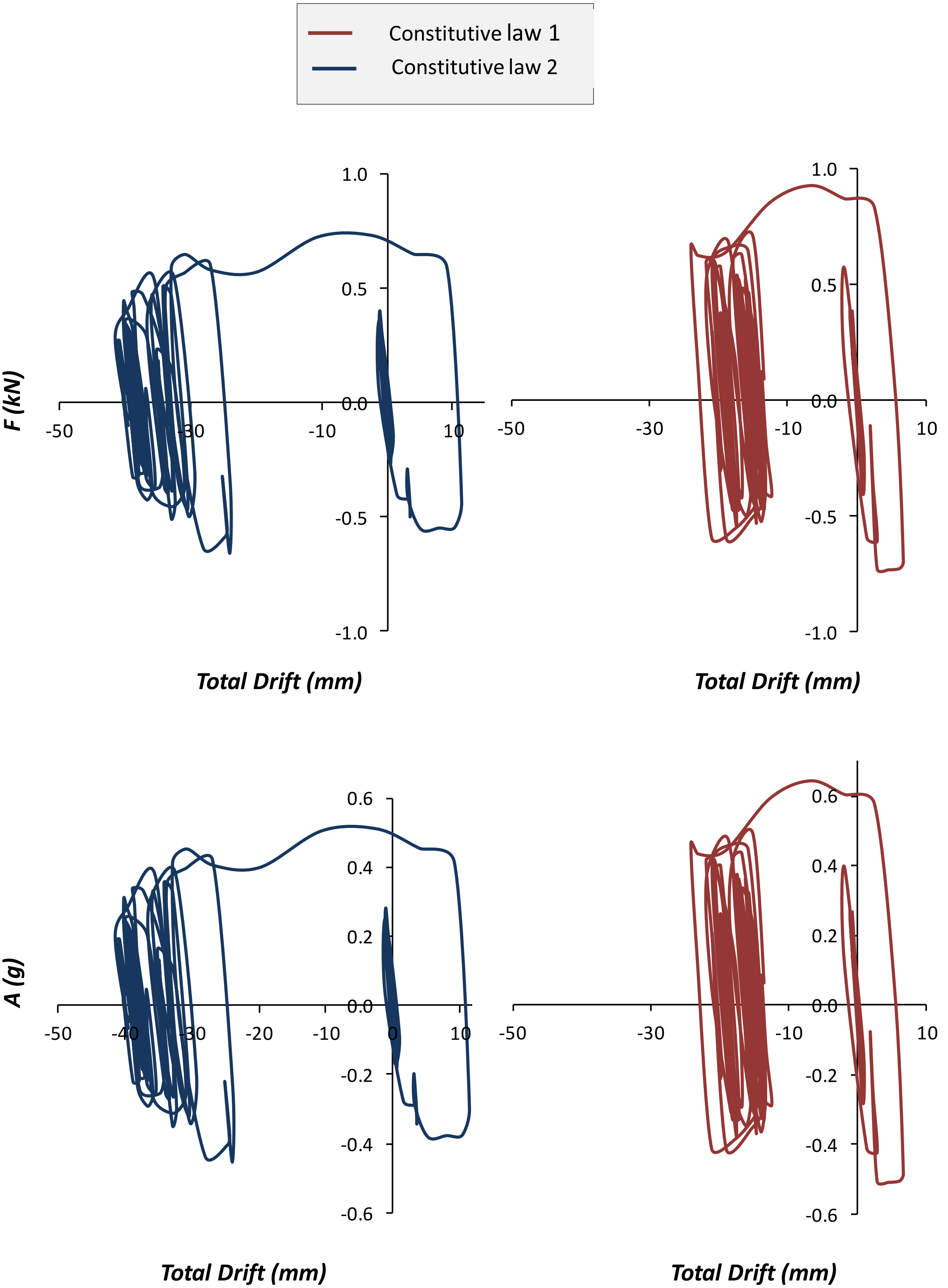

Figure 3.35 Force and acceleration with regard to the total drift of the building (Rinaldi).

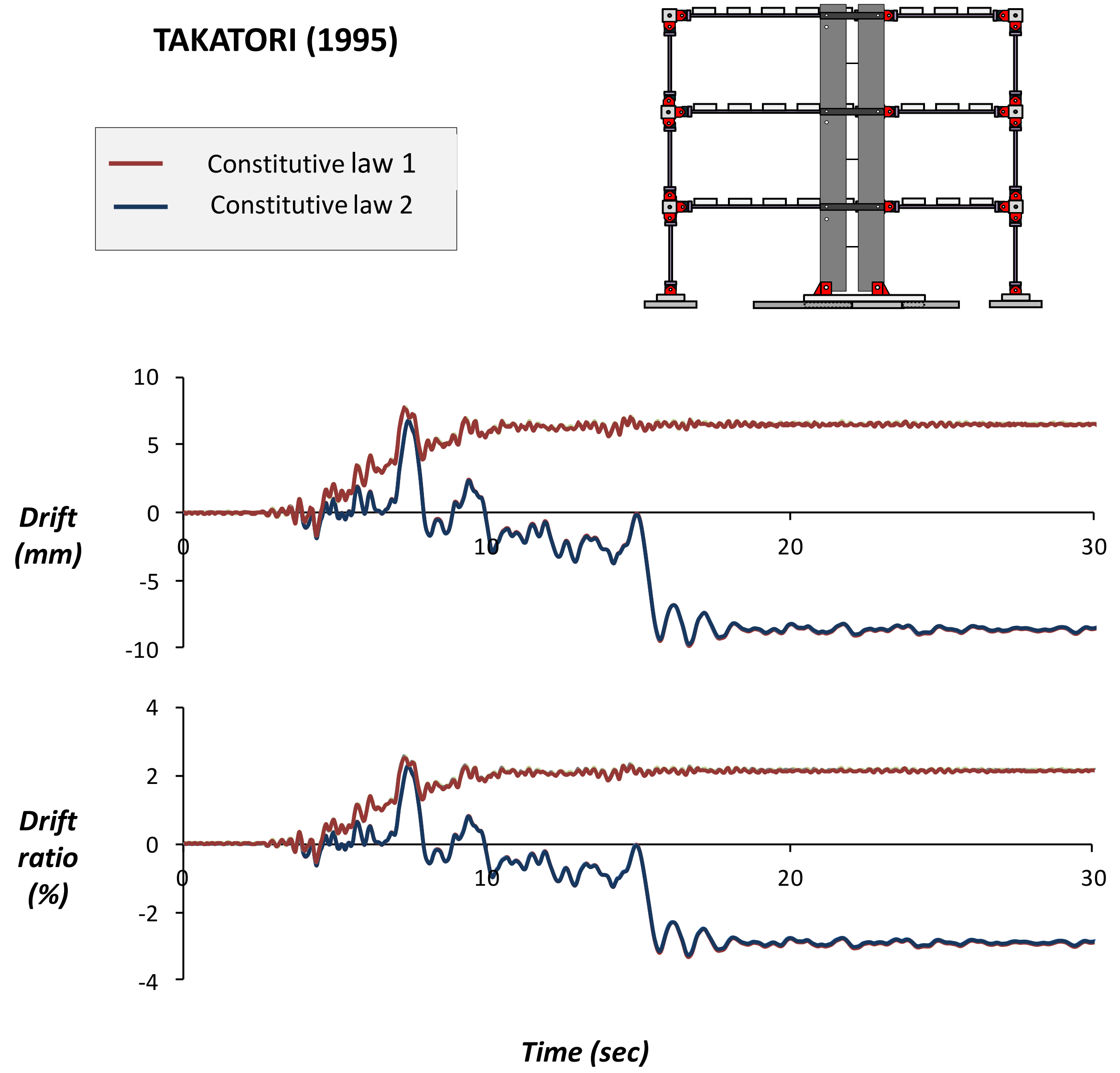

Figure 3.36 Time histories of *Interstorey drifts and drift ratios* of the retrofitted building (Takatori).

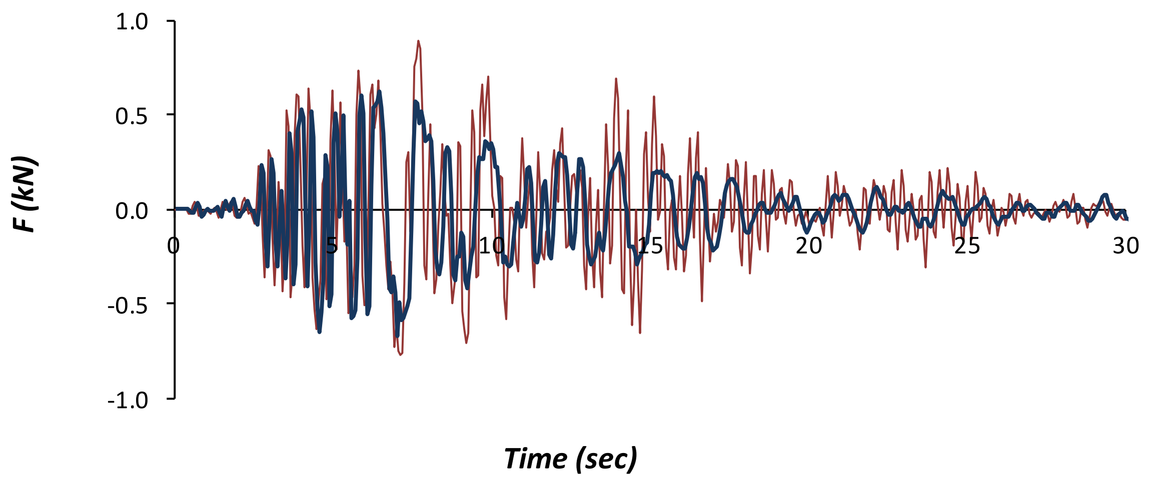

Figure 3.37 Total Resisting force's time history of the structure (Takatori).

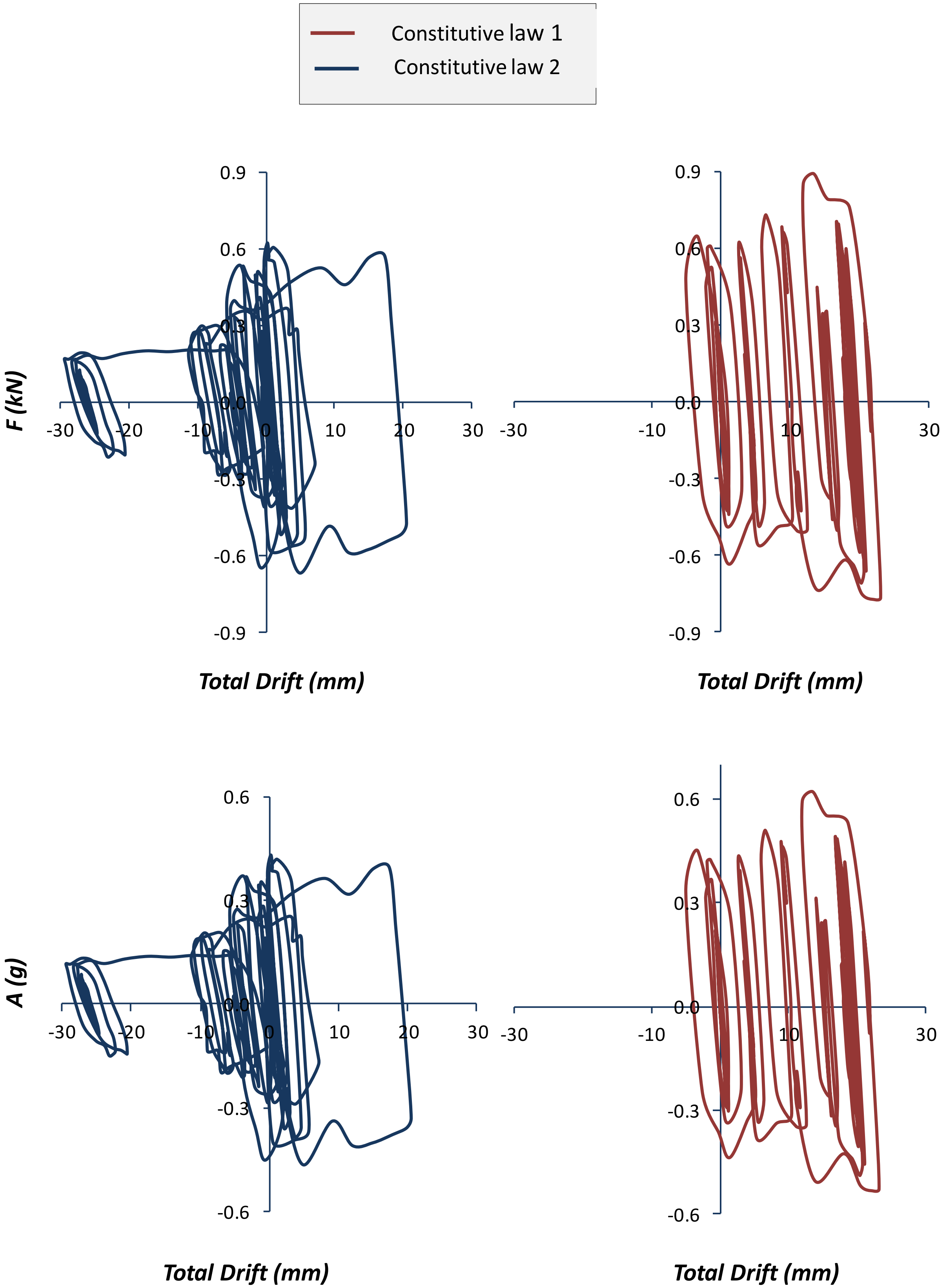

Figure 3.38 Force and acceleration with regard to the total drift of the building (Takatori).

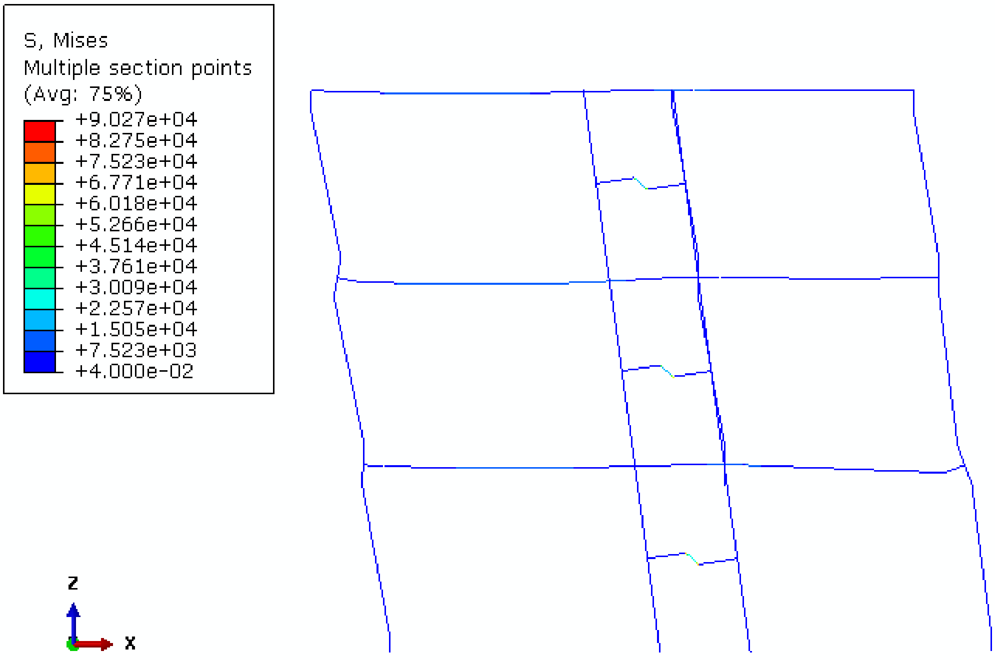

Figure 3.39 Deformed shape of the retrofitted building after the Takatori record.

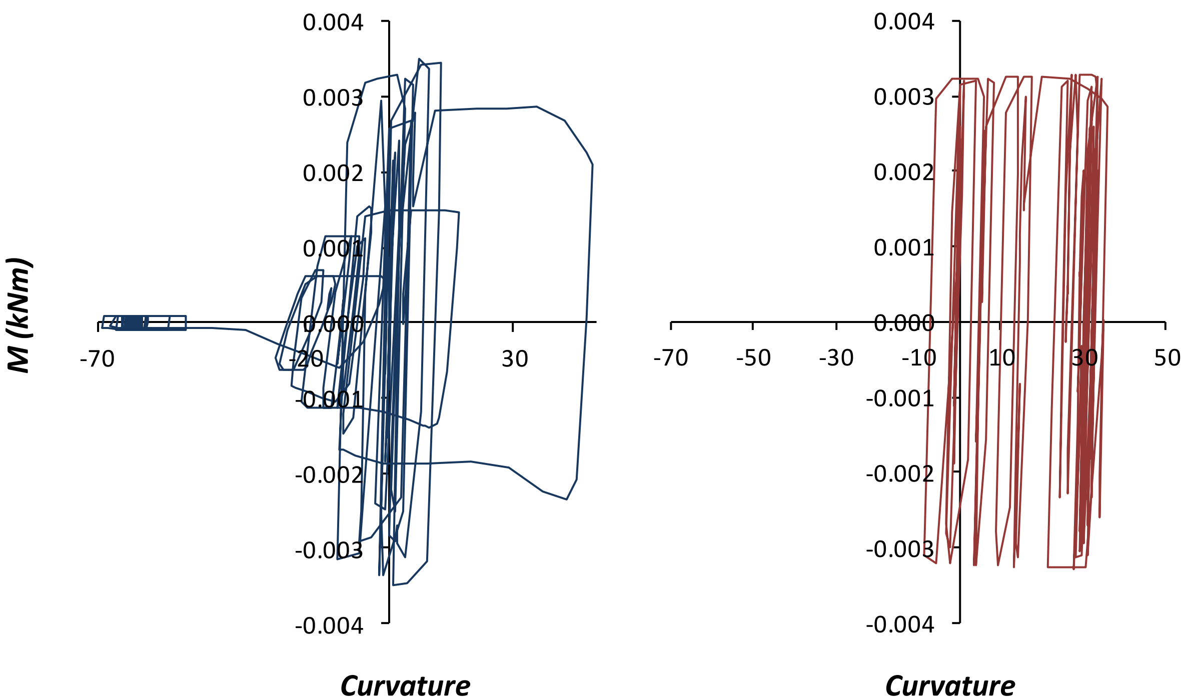

Figure 3.40 Moment - Curvature diagrams for the 1st storey' s rod after Takatori record.

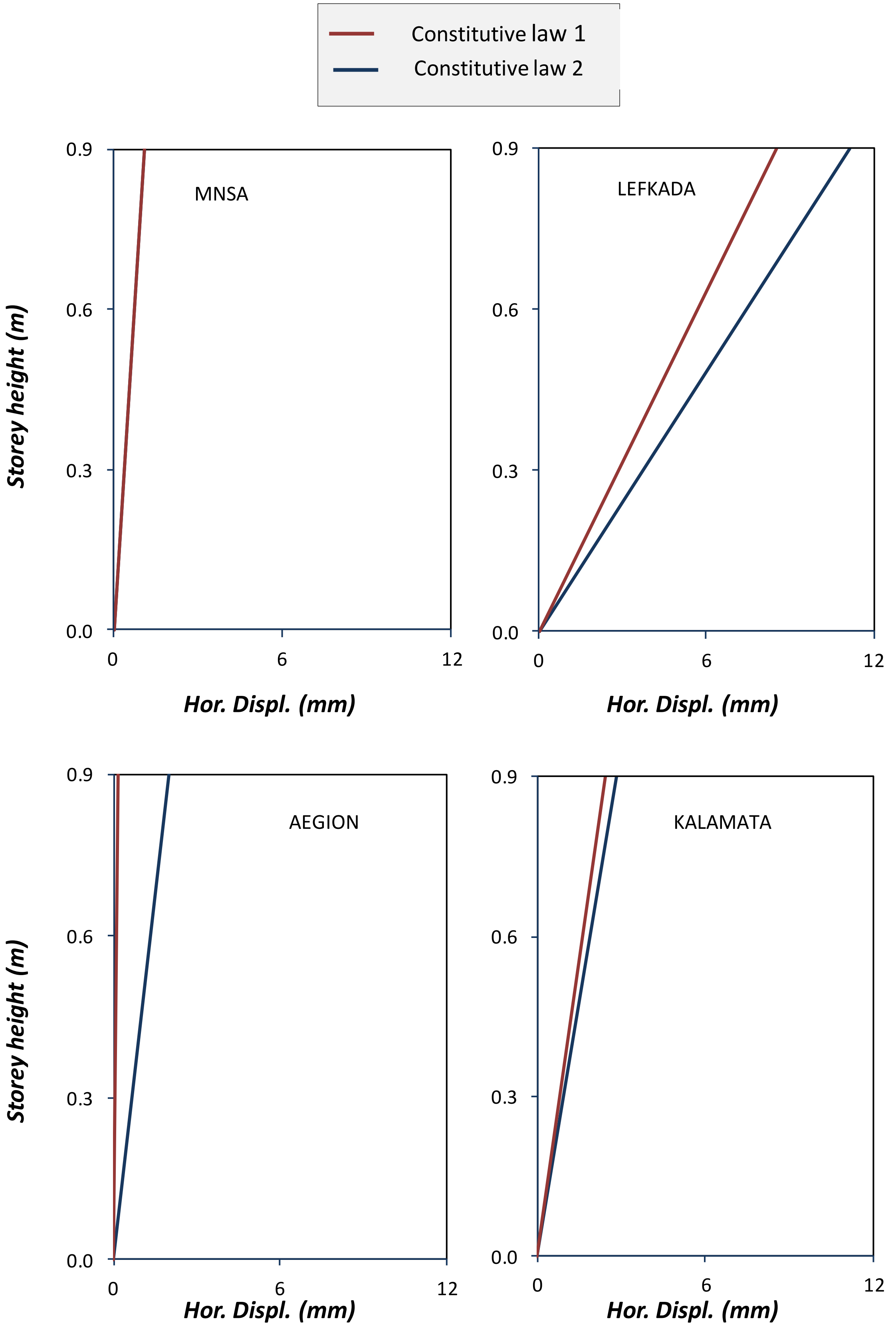

Figure 3.41 Final deformation of the retrofitted building with regard to storey height for each seismic motion.

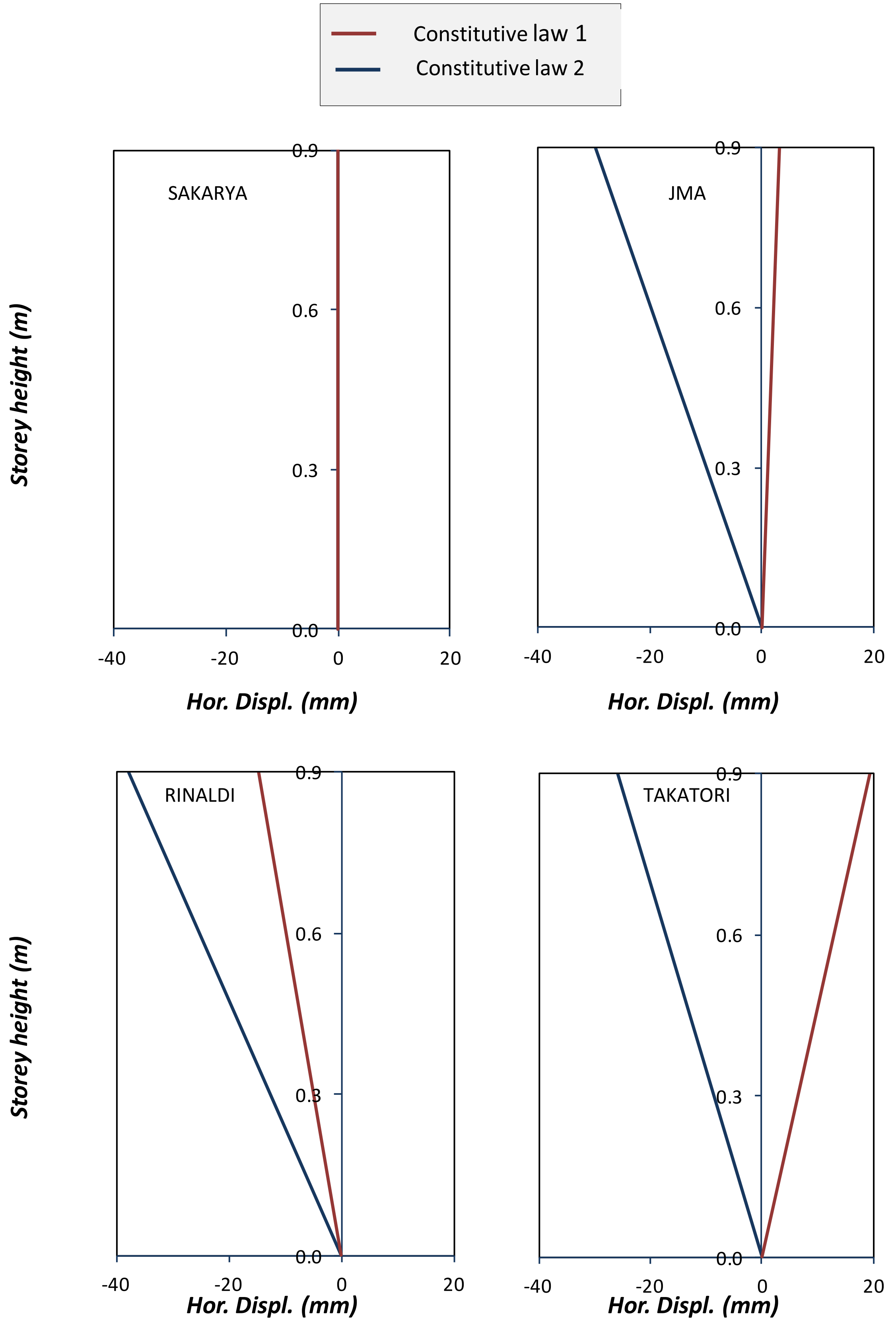

Figure 3.42 Final deformation of the retrofitted building with regard to storey height for each seismic motion.

CHAPTER A.4

RETROFITTED BUILDING VIA *RC WALL* -
NUMERICAL ANALYSES vs EXPERIMENTS

&

NUMERICAL COMPARISON:
RC WALL *vs* INSTED SYSTEM

4.1 Need for retrofit – Previous attempt with an RC shear wall

It has been shown, both numerically and experimentally, that the original structure collapses during the seismic motion of Lefkada 2003, since this record exceeds its capacity. In fact, the building has already accumulated deformations from the previously induced seismic records of Aegion and Kalamata, which encourage its later failure. Therefore, the original (un-retrofitted) structure is insufficient in terms of strength and ductility, being unable to survive even seismic motions of (relatively) moderate intensity. This conclusion is not only consistent with the SPEAR test results, confirming the equivalence of the reduced-scale model tested herein, but also compares well with reality: many such buildings experienced major damage or collapse during the aforementioned ($M \approx 6$) earthquakes in Greece. Therefore, a retrofit is considered necessary, in order to increase its seismic resistance and safety margins against collapse.

4.1.1 Experimental setup of the RC shear wall

The first kind of retrofit that was proposed was that of an RC shear wall [Nonika Antonaki, 2012]. The equivalent of this wall was designed and introduced in the experimental setup of the original building and a number of experiments followed. The shear wall had been designed according to Greek regulations (KAN.EPE.) and then scaled down to a cross-section of 0.15m x 0.20m for the experiment. It was connected to the building along the middle column with the eccentricity towards the larger span of the frame. It was modeled by a stiff aluminum plate, rigidly connected on each floor, and equipped with an artificial plastic hinge at its base. The original footing of the central column was increased to B=0.6m in width (in model scale) by rigidly connecting additional aluminum plates at both of its edges.

The way the building was placed onto the sandbox, and excited afterwards, was the same as in the case of the original. The records that were used as excitation for the retrofitted building were both those used for the original, and some stronger ones as well. The four latter records exceed substantially the design limits of the RC shear wall and were applied in order to explore the margins of safety of such a retrofit.

4.1.2 Performance under moderate and strong seismic shaking

Since the retrofit via the RC wall was supposed to have a yielding design acceleration of Φ_d=0.20g (assuming design coefficient A=0.24g and behavior factor q=3), the structure was expected to sustain seismic motions of greater magnitude by responding in a more ductile manner than the original building. Besides from the increase in strength and ductility, the addition of the shear wall would homogenize the lateral deformation of the structure (acting as a kinematic constraint), leading to a more uniform damage distribution in all three storeys and prohibiting the development of a soft-storey collapse mechanism.

Indeed, the response of the retrofitted building to the first sequence of **moderate seismic records** was really satisfactory, since the deformed shape of the building followed the displacement of the shear wall, preventing brittle soft storey collapse. Also in terms of drifts, these were significantly decreased compared to the original building. In fact, the strengthened frame not only sustains the motion that causes the original structure to collapse, but also responds with a residual value of drift ratio no more than 0.3% (in the last record of Kalamata).

Besides from the moderate seismic motions, some **high intensity seismic records** were imposed on the strengthened building, so as to investigate its durability. The first strong seismic record to be applied is the JMA record from Kobe (1995), with a maximum value of acceleration equal to 0.82g (PGA = 0.9g, as measured in a small depth). As is shown in Figure 4.21, the structure reaches a maximum residual drift of *10mm*. Therefore, it suffers from significant damage even though it does not collapse. Then the record of Rinaldi with a_{max} ≈ 0.84g (PGA = 1g) from the earthquake of Northridge (1994) is simulated and imposed on the model. The response is satisfactory (Figures 4.14 – 4.15) but the structure has already accumulated deformation and finally collapses during the very strong record of Takatori (Kobe, 1995) with a maximum acceleration of 0.61g (PGA = 0.95 g) and several cycles.

4.2 Numerical Simulation of the building retrofitted via the RC wall

The numerical model of the RC shear wall was embodied in the already existing model of the original frame. The shear wall was simulated by 3-dimensional, 2-node linear beam elements (B31), and was placed eccentrically to the middle column, as in the experimental setup. Since the wall was connected to the middle column on its right side, we had to join its centroid with the junction site by rigid beams (B31), whose Young's modulus was 10 times the aluminum one, in order to ensure that these deform alike. Subsequently the connection of these beams with the middle column was established through springs, simulating the rigidity accomplished experimentally. At last, the artificial plastic hinge formed at the bottom of the shear wall was simulated by a plastic element (likewise those of the original frame), whose vertical deformation was controlled by a vertical spring, so that it does not fall apart.

As far as the constitutive models are concerned, a linear elastic one was assigned to the shear wall and rigid beams, while a bilinear elastic-plastic law was used for the plastic element of the wall. The yield stress that was imported derived from the calibration of the wall's plastic hinge. However, it was impossible, during the pushover tests, to reach the ultimate bending moment of the real scale shear wall (M_{pl}=0.071kNm in model scale), hence a decreased one was used for both the experiment and the analysis (M_{pl}=0.05kNm in model scale). It should be mentioned here, that the final stress – strain curve assigned to the wall's plastic element does not include a descending branch after failure; thus, decrease in the wall's strength capacity won't be visible in the results of the following analyses.

At first, we imposed a pushover testing to the retrofitted numerical model, in order to test its strength and afterwards we subjected the model to dynamic loading. In all these tests, soil was not taken into account, since the fixed base simulates well enough the base of the model, considering the conventional footings and dense sand. The acceleration time-history imposed was not the shaking table's, but the one measured by the accelerometers at the soil surface, so that the amplification due to the soil is taken into account.

4.3 Comparison between numerical and experimental results

4.3.1 Pushover testing

The pushover testing was conducted in order to examine the capacity of the structure. Contrary to the original building, this one would respond in a uniform way, regardless of the point that load or displacement is applied. The original pushover experiment was conducted utilizing the pushover apparatus of the Soil Mechanics Laboratory of NTUA. This apparatus imposed displacement on the middle of the RC shear wall and the resisting force was exported. The numerical pushover test was imposed in the same way to the retrofitted frame, with the RC wall.

Figure 4.3 depicts the force of the frame in accordance to the displacement on the top of the physical model. Consequently, the acceleration amplitude that each frame could withstand is the ratio of the maximum measured resisting force to the total mass of the structure. Each frame of the building with the RC wall was found to weigh 0.72kN and have a yield force equal to 0.24kN, therefore, its yield acceleration is equal to:

$$Ay = \frac{Fy}{M} = \frac{0.24\ kN}{0.72\ kN} = 0.33g$$

4.3.2 Dynamic shaking

The comparison between the numerical and experimental results is conducted in terms of interstorey drifts, for each record imposed. The resemblance of the graphs is really satisfactory, since the greatest difference does not exceed the value of 1mm, with the exception of Lefkada record (Figure 4.9), where the deviation is a little higher. Especially in the last four records, the similarity is quite impressive. In the case of Takatori record the experimental and numerical drift time-history are almost identical until the second the physical model meets the stopper device, preventing collapse, while the numerical one continuously accumulates deformation (Figure 4.27). The above conclusions can be reached even easier if we cast an eye over the residual drifts. The basic contrast of the retrofitted structure to the original one, as appeared in both numerical and experimental results, is that the deformation of the building is homogenized, preventing formation of a plastic “side sway” storey mechanism.

Conclusively, we may infer that the simulation responds to the experimental evidence, letting us proceed with the above model of the RC wall versus the one of the INSTED system on a numerical basis.

4.4 Comparison between the RC wall and the INSTED system on a numerical basis

The comparison between these two types of retrofit is conducted in terms of strength during the pushover testing of each retrofitted structure, as well as in terms of interstorey and residual drifts during dynamic loading. Before the evaluation of results, it should be mentioned that the constitutive models assigned to the energy dissipating members of each kind of retrofit are different. The bi-linear elastic – plastic law used for the plastic element of the RC shear wall does not include a descending branch, thus no decrease in the wall's ultimate strength is expected. On the other hand, in the numerical model of the retrofitted - via the INSTED system – structure, the rods are assigned to a stress – strain curve which displays a gradual decrease in strength, after the plastic strain exceeds the value of 20%.

At first sight, we may say that both alternatives generate homogeneous interstorey drifts, since lateral deformation of the structure becomes almost uniform. However, in order to gain a better insight into what differentiates the above systems, we compare the two kinds of retrofit in terms of residual drifts, which seem to display a greater decrease in the case of the INSTED system.

Among the moderate intensity Greek seismic records, the motion of Kalamata is the only one where the INSTED system displays greater values of interstorey drifts compared to the RC wall. Still, this fact cannot be considered as representative, since the residual interstorey drifts acquired after Kalamata record are negligible for both kinds of retrofit *(≈ 0mm* for the RC wall and *≈ 1mm* for the INSTED system). Obviously, both systems' seismic performance during the Greek earthquakes is considered as very satisfactory.

The supremacy of the INSTED system becomes obvious mostly in the last three records of Rinaldi, Jma and Takatori. The proposed system is flexible and very ductile, thus able to "follow" the imposed pulses, by deforming and dissipating energy, without collapsing. In the records of Jma and Takatori, it displays residual interstorey drift values of 10mm and 9mm respectively (Figures 4.36 and 4.38), but does not exceed the value of 4% in terms of residual interstorey drift ratio (≈3.2% and 3% for Jma and Takatori respectively). During the record of Rinaldi, **the retrofitted - via the INSTED system - building suffers from significant deformation** (Figure 4.37), acquiring residual interstorey drifts of 13mm (thus, an interstorey drift ratio equal to 4.3%). This percentage surpasses the usual allowed value of 4%, **but** the building **is not led to failure**. On the other hand, **the**

retrofitted - via the RC wall - structure accumulates large deformations through these extreme seismic motions and **finally collapses during the Takatori record,** behaving in a much stiffer and less ductile manner (Figures 4.38 - 4.39).

It has to be noted that the RC wall was initially designed according to the yield design acceleration of $\boldsymbol{\Phi_d}$ **= 0.20g** and reinforced even more afterwards, according to the minimum acceptable limits that Greek regulations set. On the other hand, the INSTED system was designed according to the yield design acceleration of $\boldsymbol{\Phi_d = 0.135g}$. Of course, we kept in mind that the system's significant ductility would enable it to withstand seismic motions of much greater amplitude compared to its theoretical design acceleration, therefore we did not exceed this value. More specifically, the columns (force-controlled members) were designed to remain elastic, while the horizontal rods (deformation-controlled members) would respond in a non-linear way, providing ductility and resulting to significantly higher horizontal resistance during dynamic loading than the one the system was designed for.

Of course, the pushover tests present similar strength levels between the two types of retrofit, thus yield strength equal to 0.13kN per frame for the INSTED system and 0.24kN per frame for the RC wall. The actual superiority of the INSTED system, though, is obvious during seismic loading. Indeed, the seismic capacity of the INSTED system turns out to be greater than the one of the RC wall, explaining its sustainability during strong motions which the RC wall fails to resist, such as the record of Takatori.

Chapter A.4

Figures

1^{ST} KIND OF RETROFIT: RC SHEAR WALL

COMPARISON BETWEEN THE EXPERIMENT AND THE NUMERICAL ANALYSES

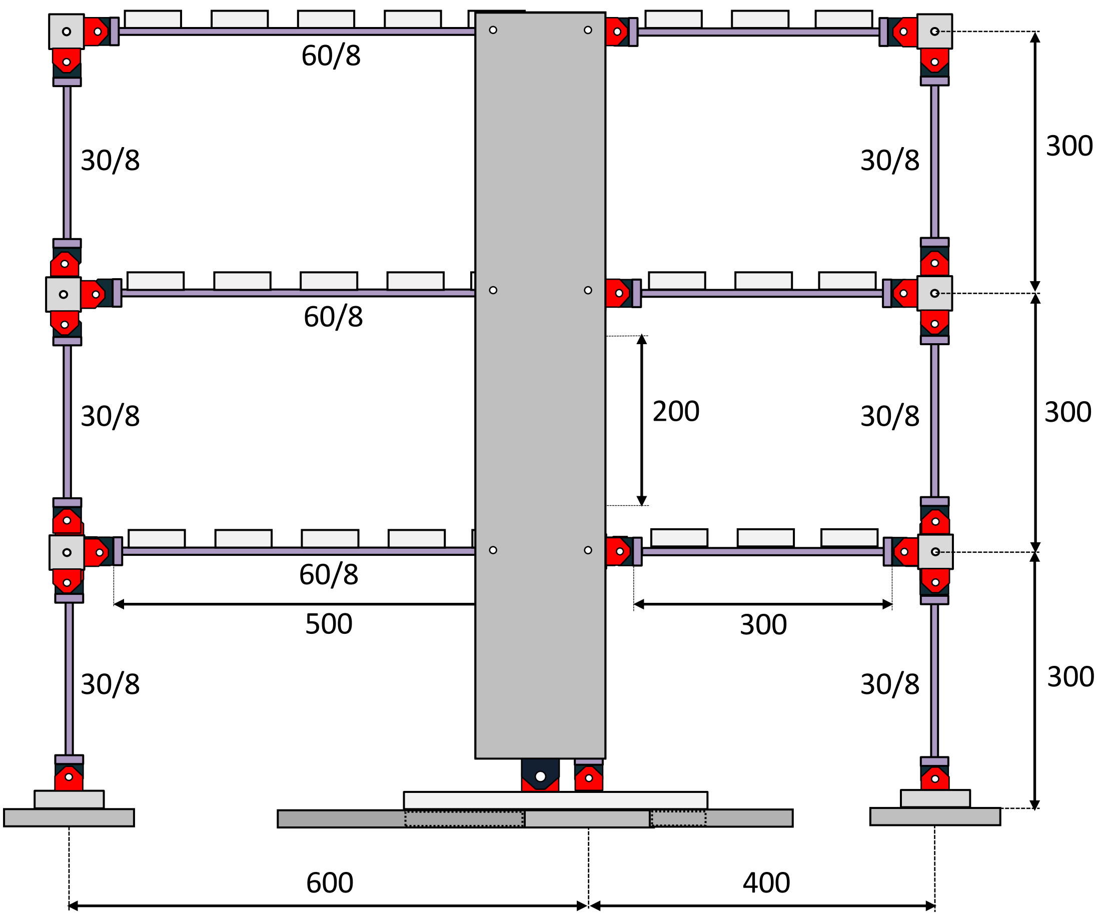

Figure 4.1 Technical drawing of the building retrofitted with the RC shear wall.

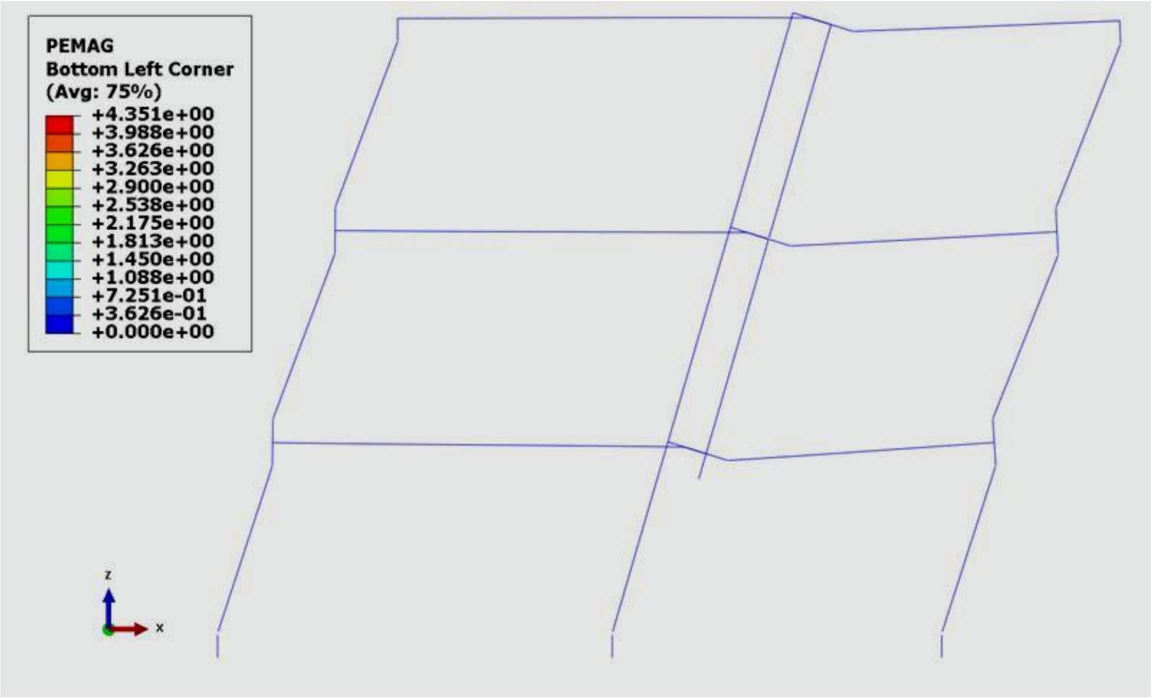

Figure 4.2 Deformed shape of the retrofitted structure after the **pushover testing**.

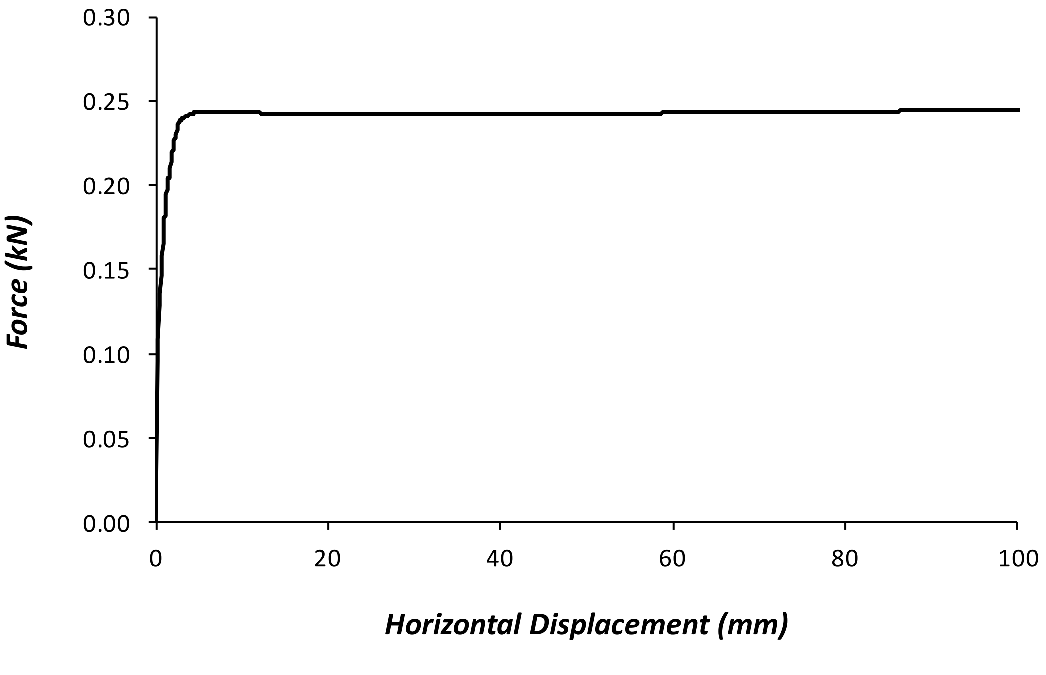

Figure 4.3 The force of the retrofitted model in accordance to the displacement on top of the structure, as derived from the pushover test in Abaqus.

MNSA (Athens 1999)

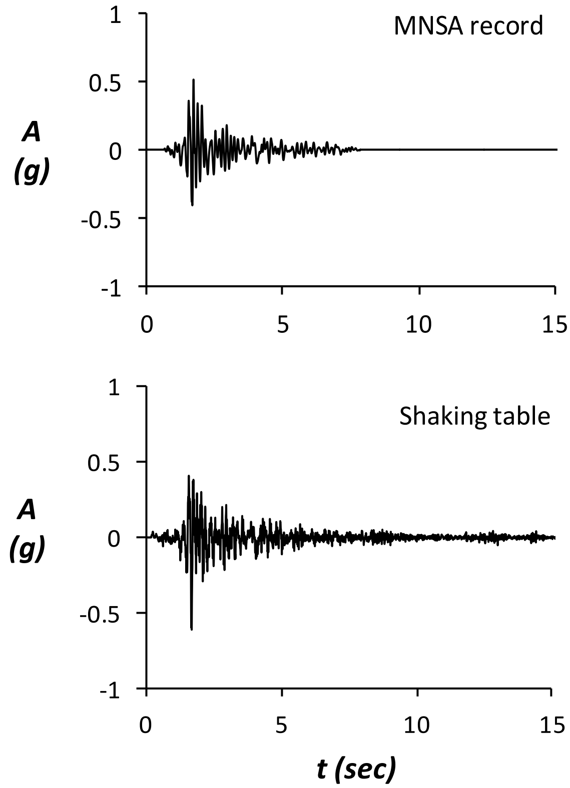

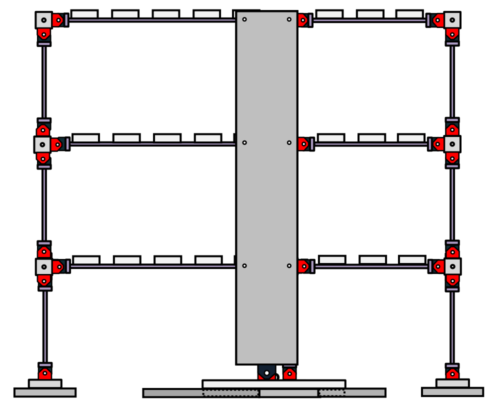

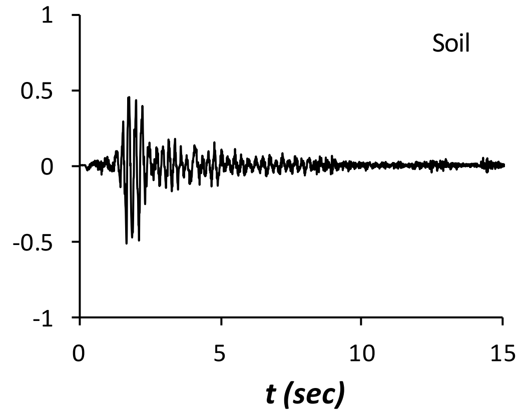

Figure 4.4 Acceleration time history imposed on the model of the original building during the experiment.

Figure 4.5 Acceleration time history imposed on the model of the original building in the Abaqus analysis.

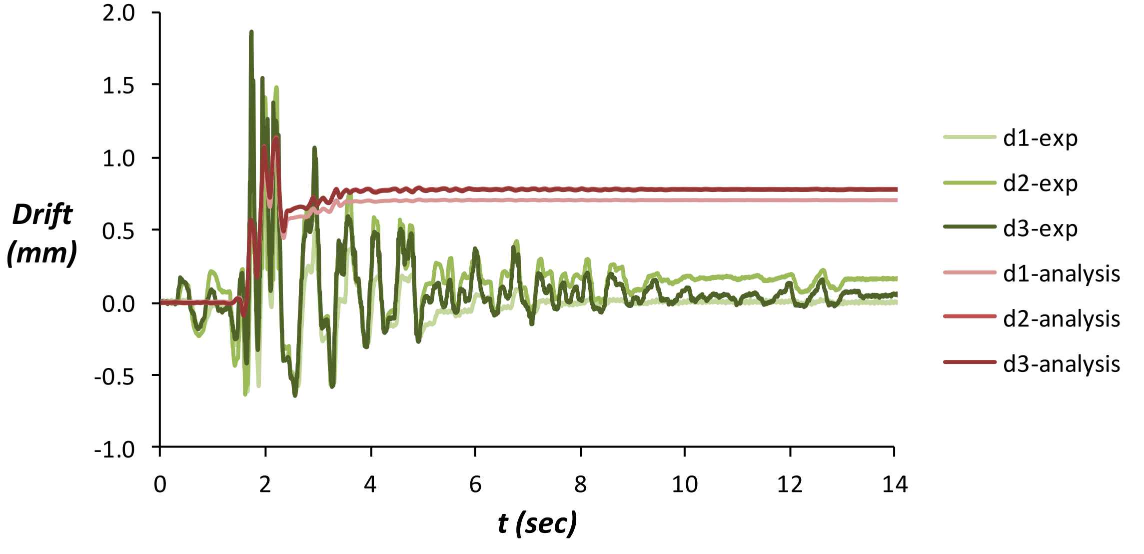

Figure 4.6 Comparison of interstorey drifts between the Abaqus analysis and the experiment results for the record of MNSA (Retrofitted building).

LEFKADA (2003)

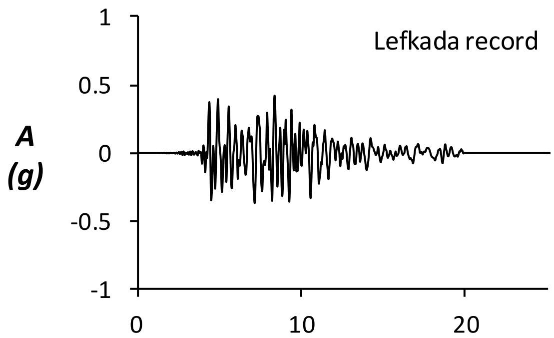

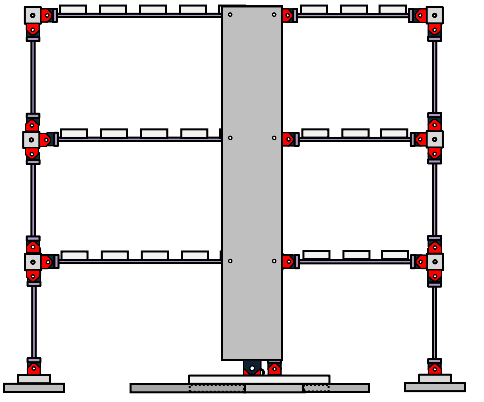

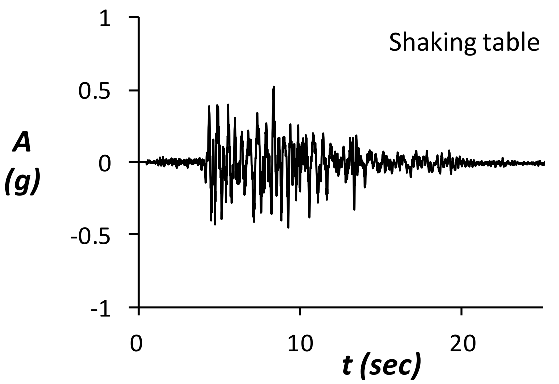

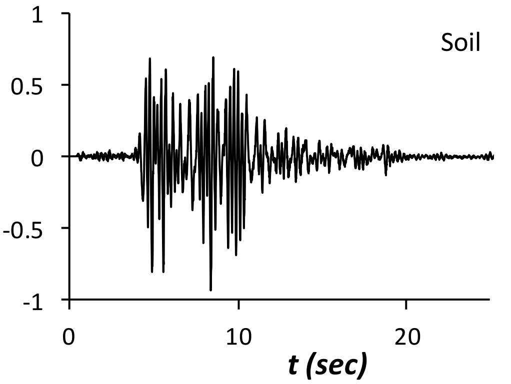

Figure 4.7 Acceleration time history imposed on the model of the original building during the experiment.

Figure 4.8 Acceleration time history imposed on the model of the original building in the Abaqus analysis.

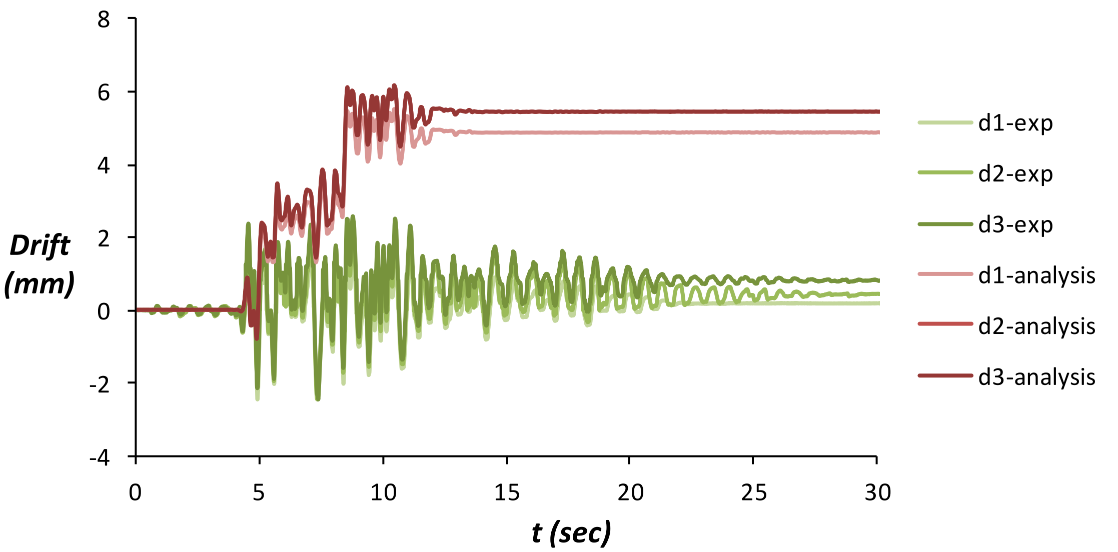

Figure 4.9 Comparison of interstorey drifts between the Abaqus analysis and the experiment results for the record of Lefkada (Retrofitted building).

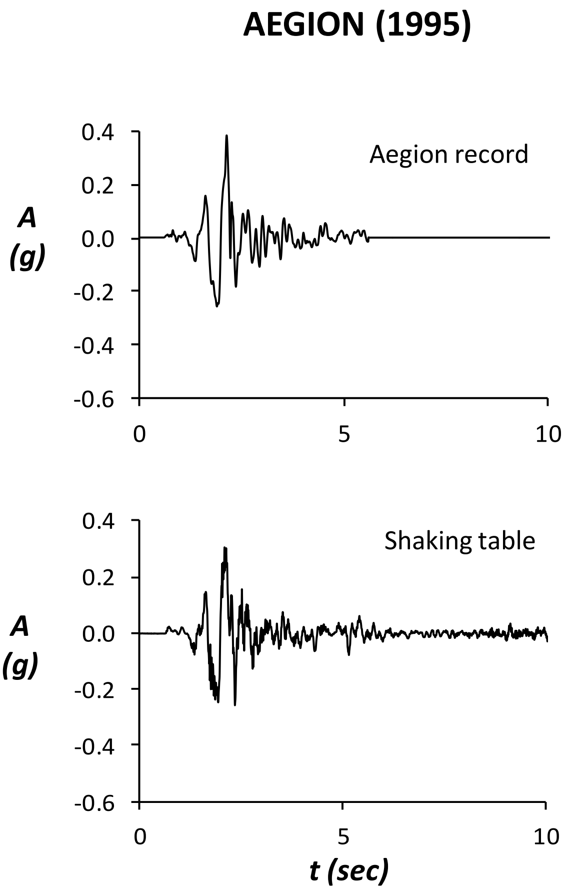

Figure 4.10 Acceleration time history imposed on the model of the original building during the experiment.

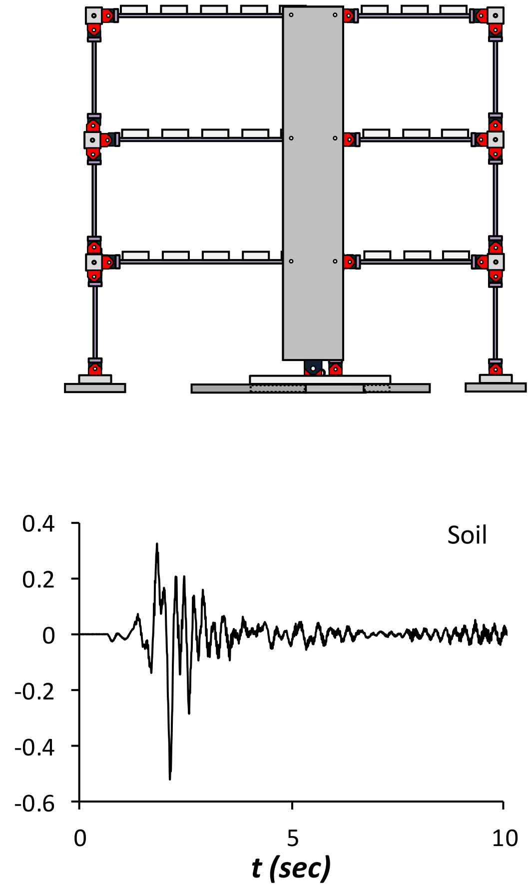

Figure 4.11 Acceleration time history imposed on the model of the original building in the Abaqus analysis.

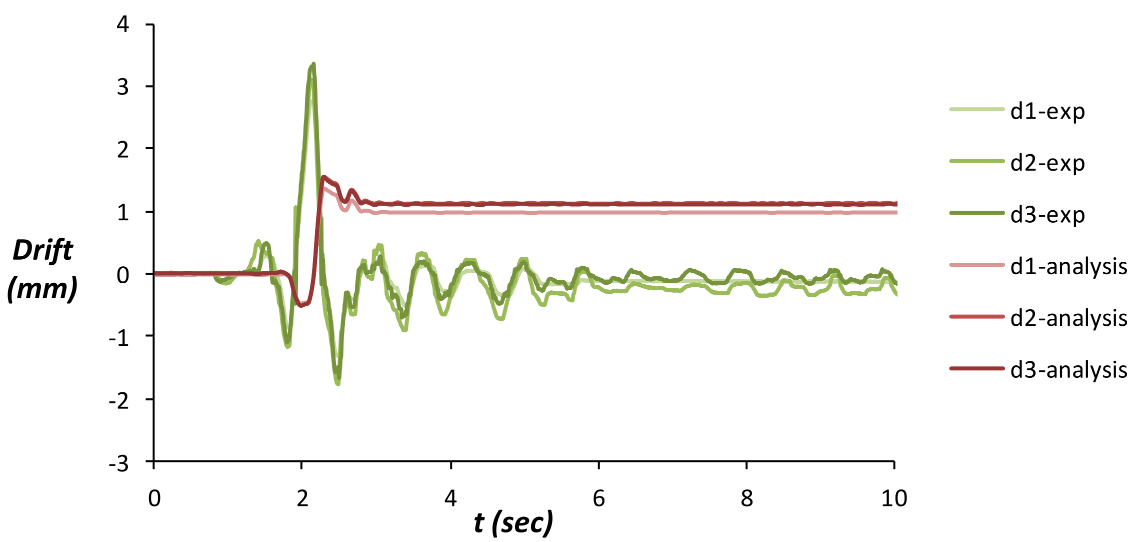

Figure 4.12 Comparison of interstorey drifts between the Abaqus analysis and the experiment results for the record of Aegion (Retrofitted building).

KALAMATA (1986)

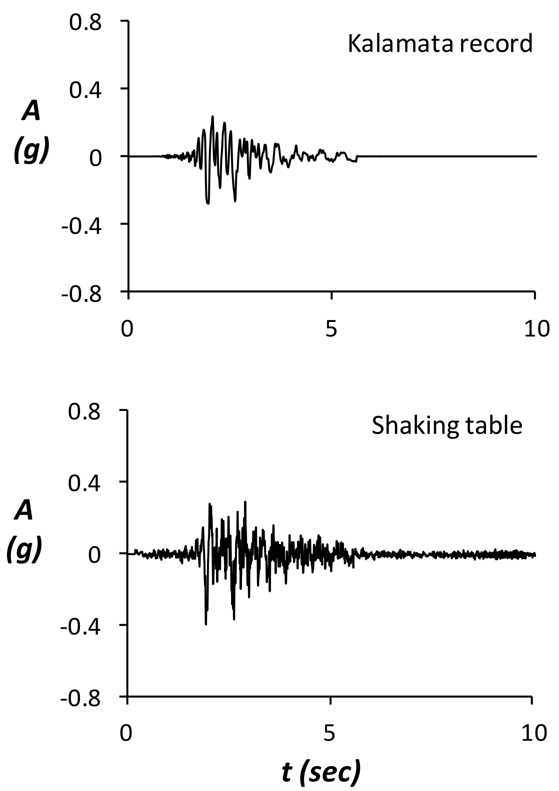

Figure 4.13 Acceleration time history imposed on the model of the original building during the experiment.

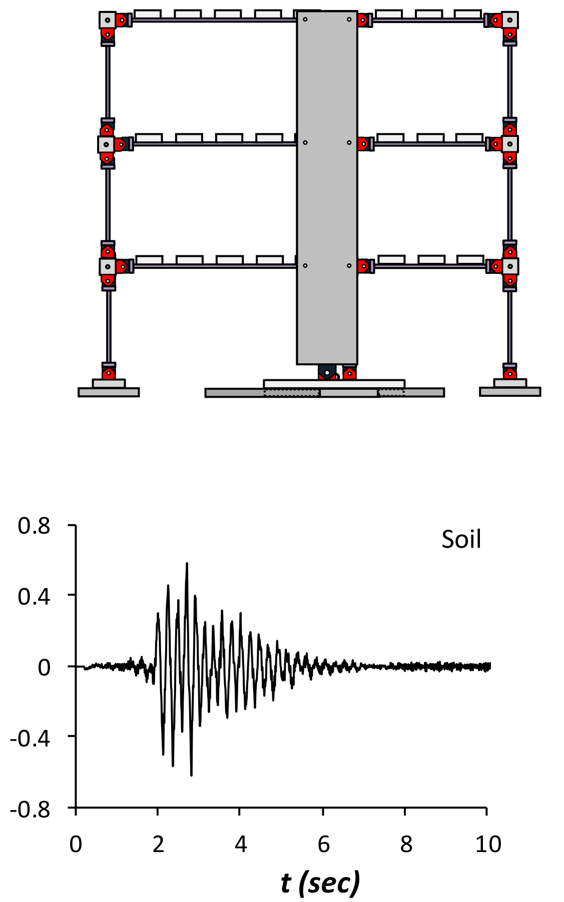

Figure 4.14 Acceleration time history imposed on the model of the original building in the Abaqus analysis.

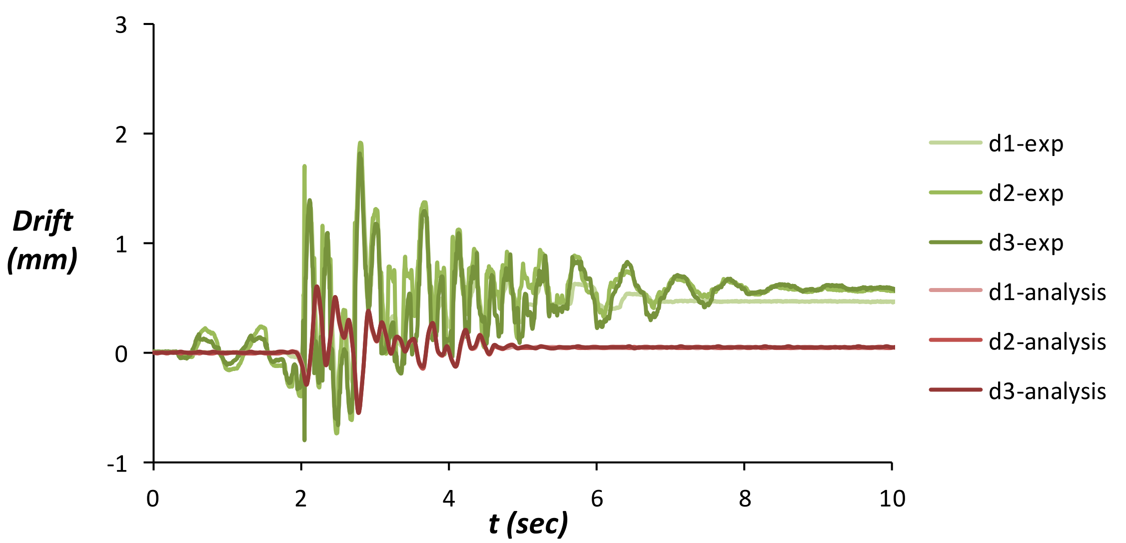

Figure 4.15 Comparison of interstorey drifts between the Abaqus analysis and the experiment results for the record of Kalamata (Retrofitted building).

SAKARYA (1999)

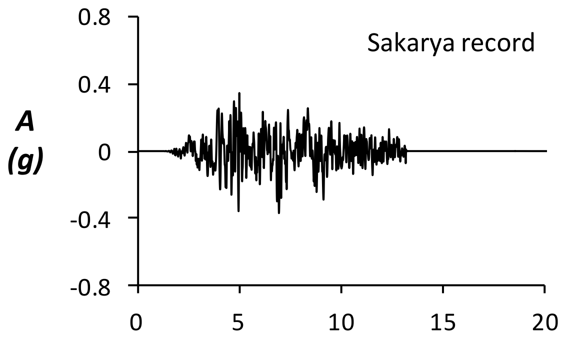

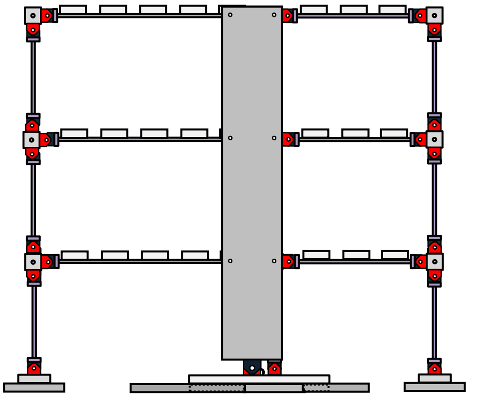

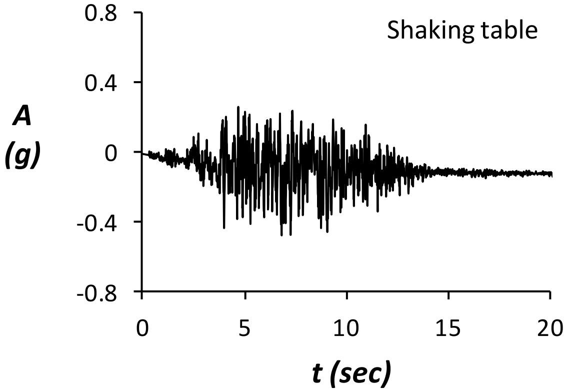

Figure 4.16 Acceleration time history imposed on the model of the original building during the experiment.

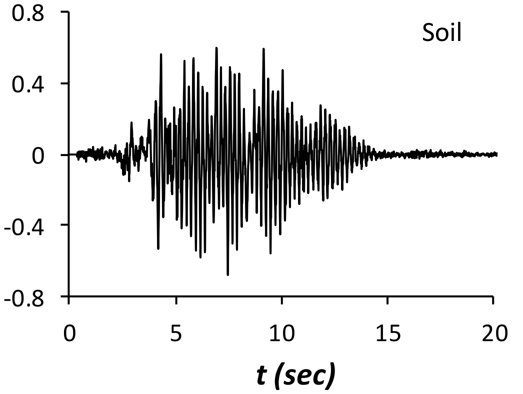

Figure 4.17 Acceleration time history imposed on the model of the original building in the Abaqus analysis.

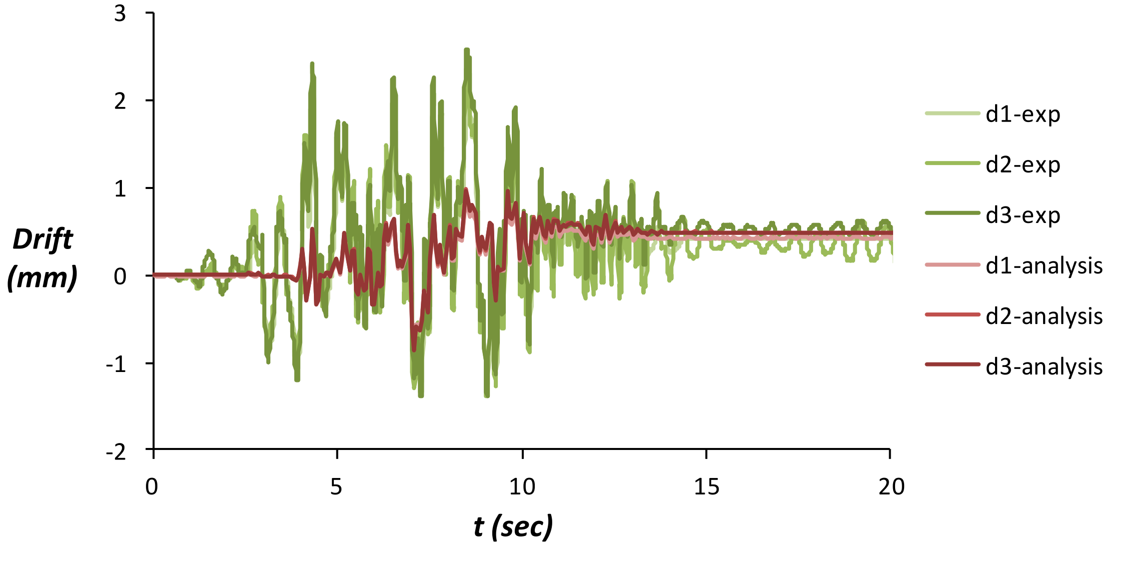

Figure 4.18 Comparison of interstorey drifts between the Abaqus analysis and the experiment results for the record of Sakarya (Retrofitted building).

JMA (1995)

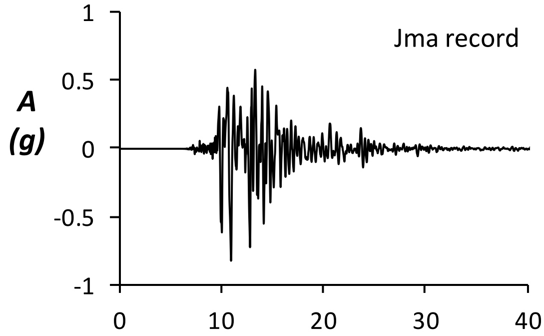

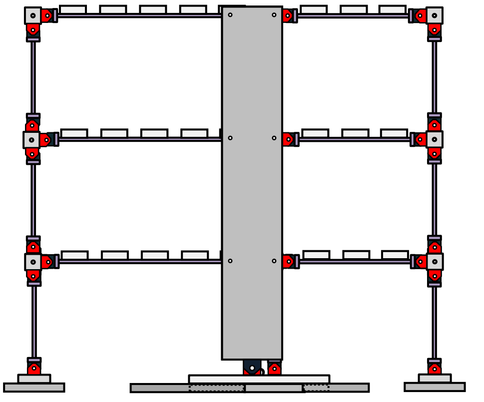

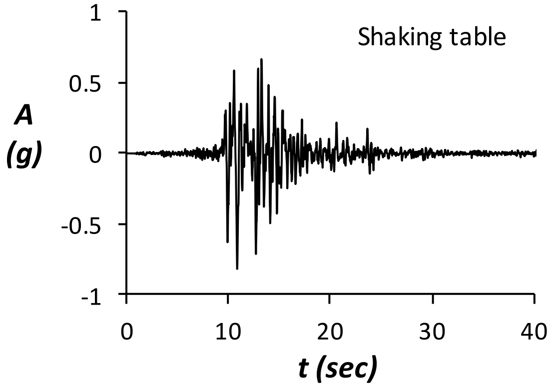

Figure 4.19 Acceleration time history imposed on the model of the original building during the experiment.

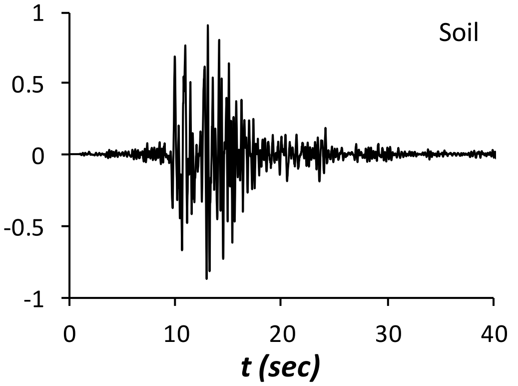

Figure 4.20 Acceleration time history imposed on the model of the original building in the Abaqus analysis.

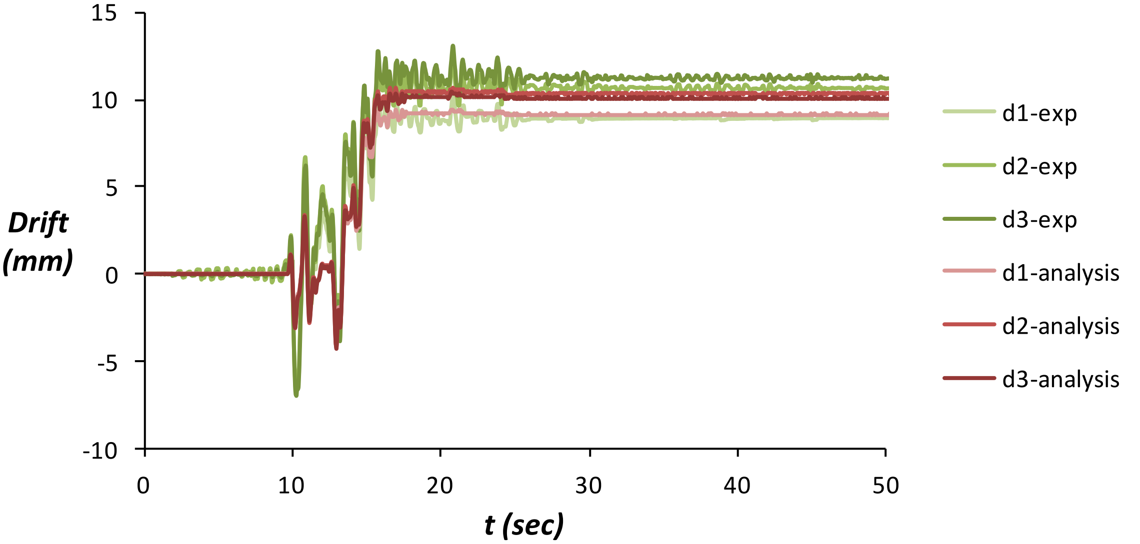

Figure 4.21 Comparison of interstorey drifts between the Abaqus analysis and the experiment results for the record of Jma (Retrofitted building).

RINALDI (1994)

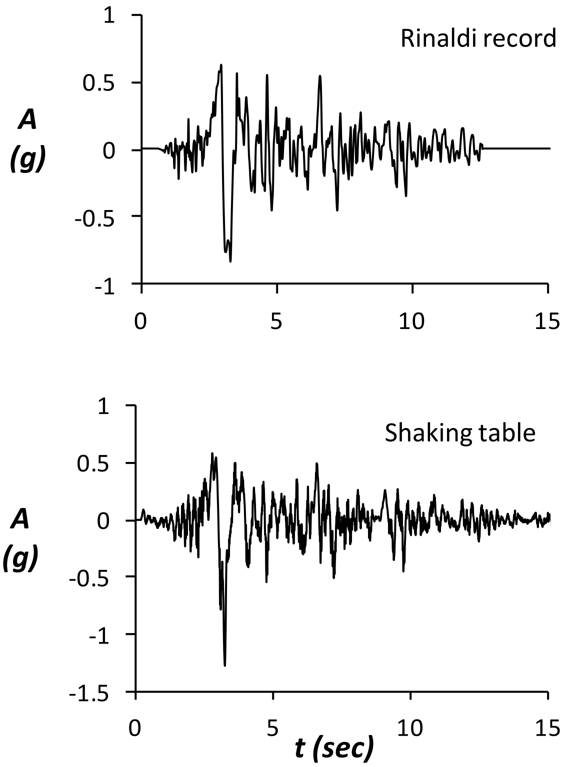

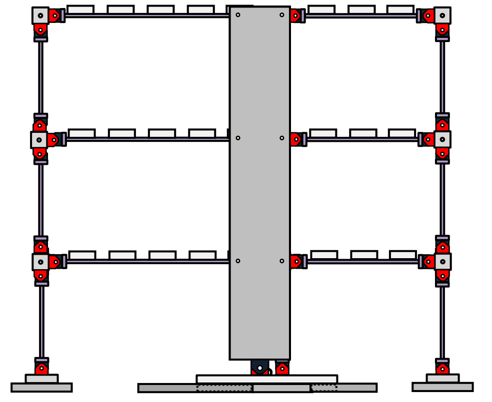

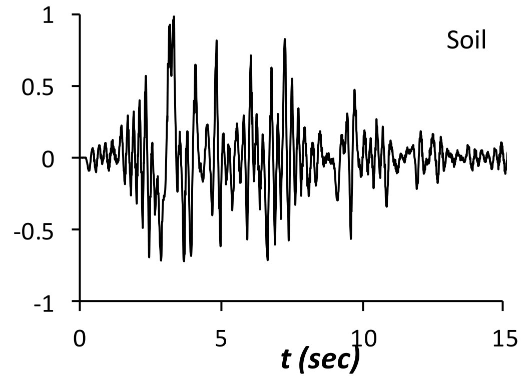

Figure 4.22 Acceleration time history imposed on the model of the original building during the experiment.

Figure 4.23 Acceleration time history imposed on the model of the original building in the Abaqus analysis.

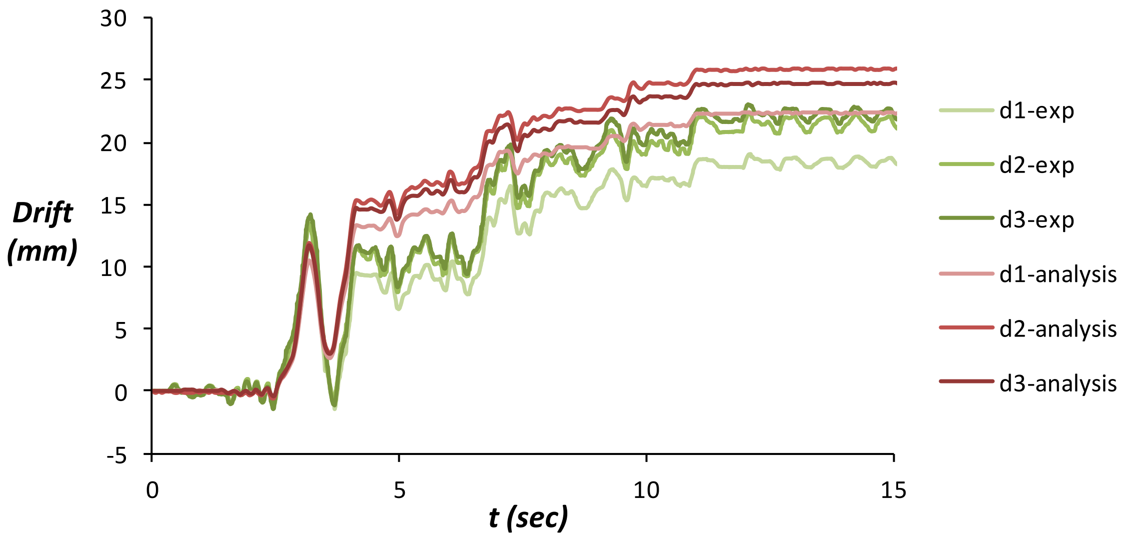

Figure 4.24 Comparison of interstorey drifts between the Abaqus analysis and the experiment results for the record of Rinaldi (Retrofitted building).

TAKATORI (1995)

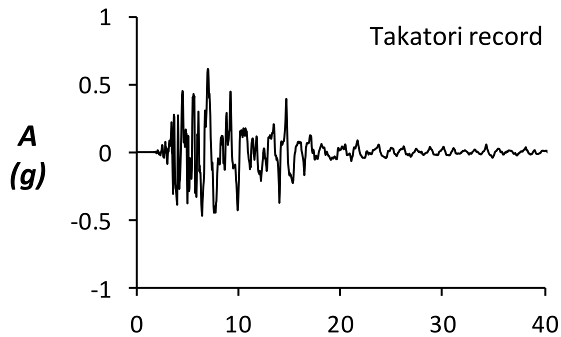

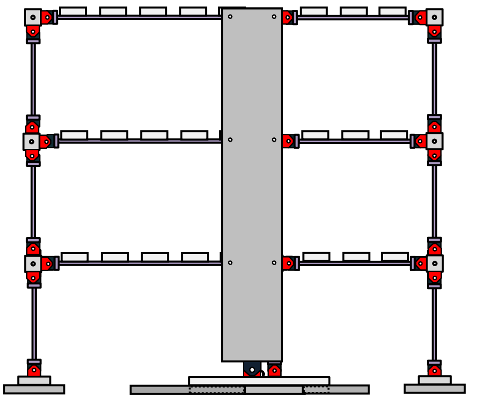

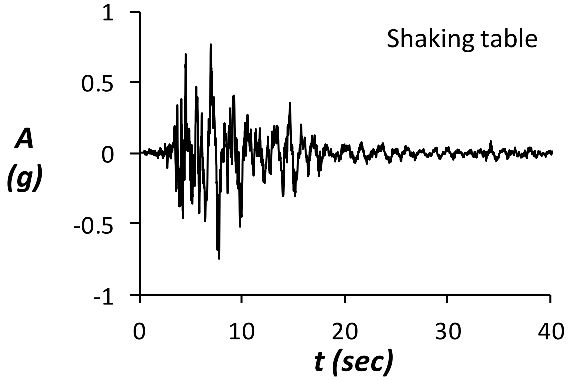

Figure 4.25 Acceleration time history imposed on the model of the original building during the experiment.

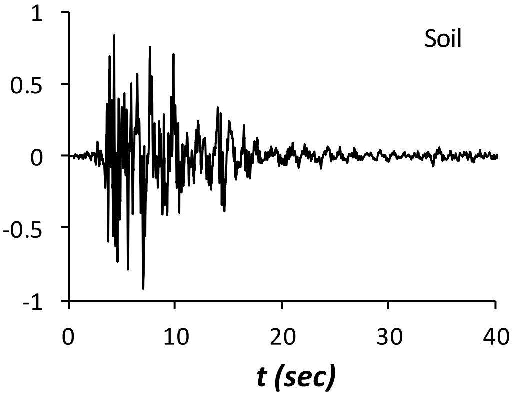

Figure 4.26 Acceleration time history imposed on the model of the original building in the Abaqus analysis.

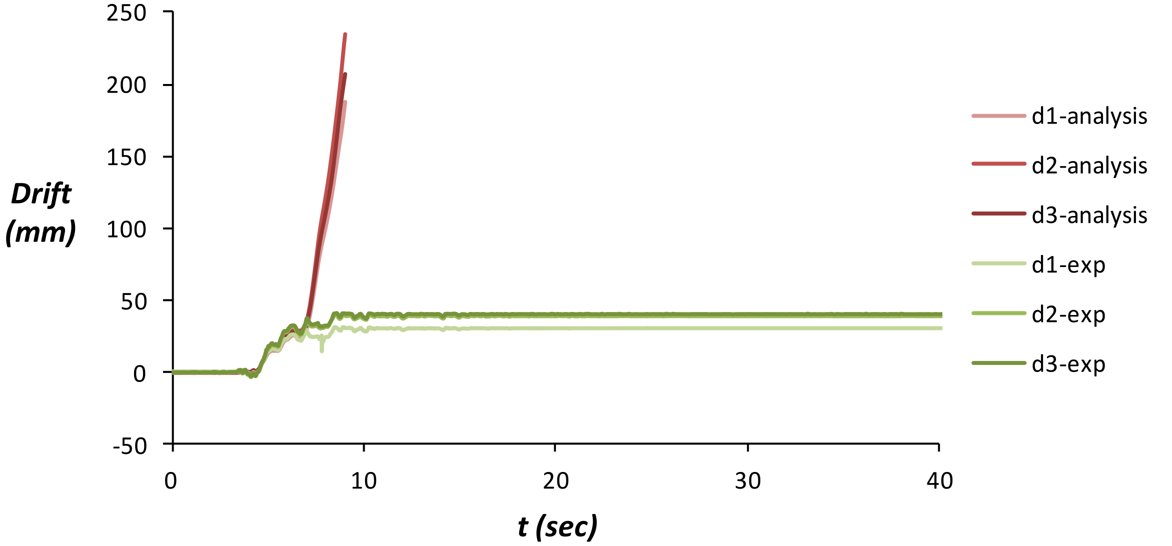

Figure 4.27 Comparison of interstorey drifts between the Abaqus analysis and the experiment results for the record of Takatori (Retrofitted building).

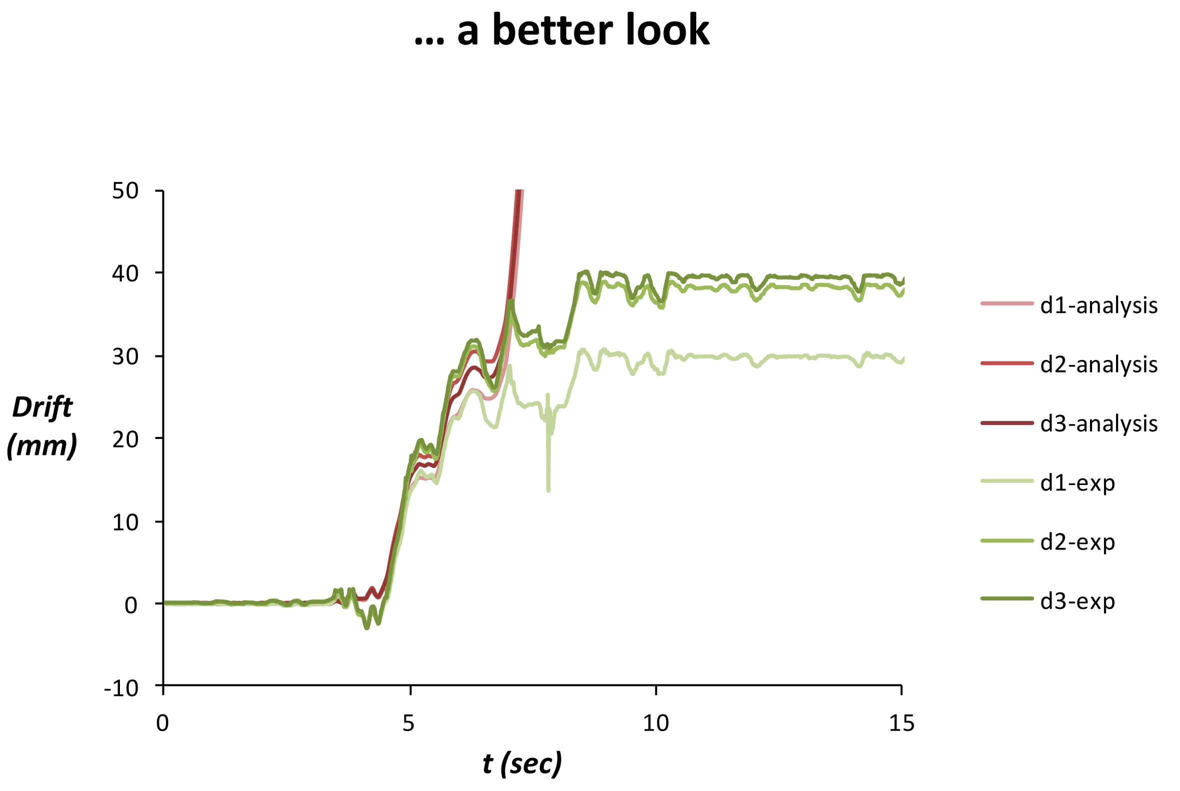

Figure 4.28 A closer look at the interstorey drifts between the Abaqus analysis and the experiment results for the record of Takatori (Retrofitted building).

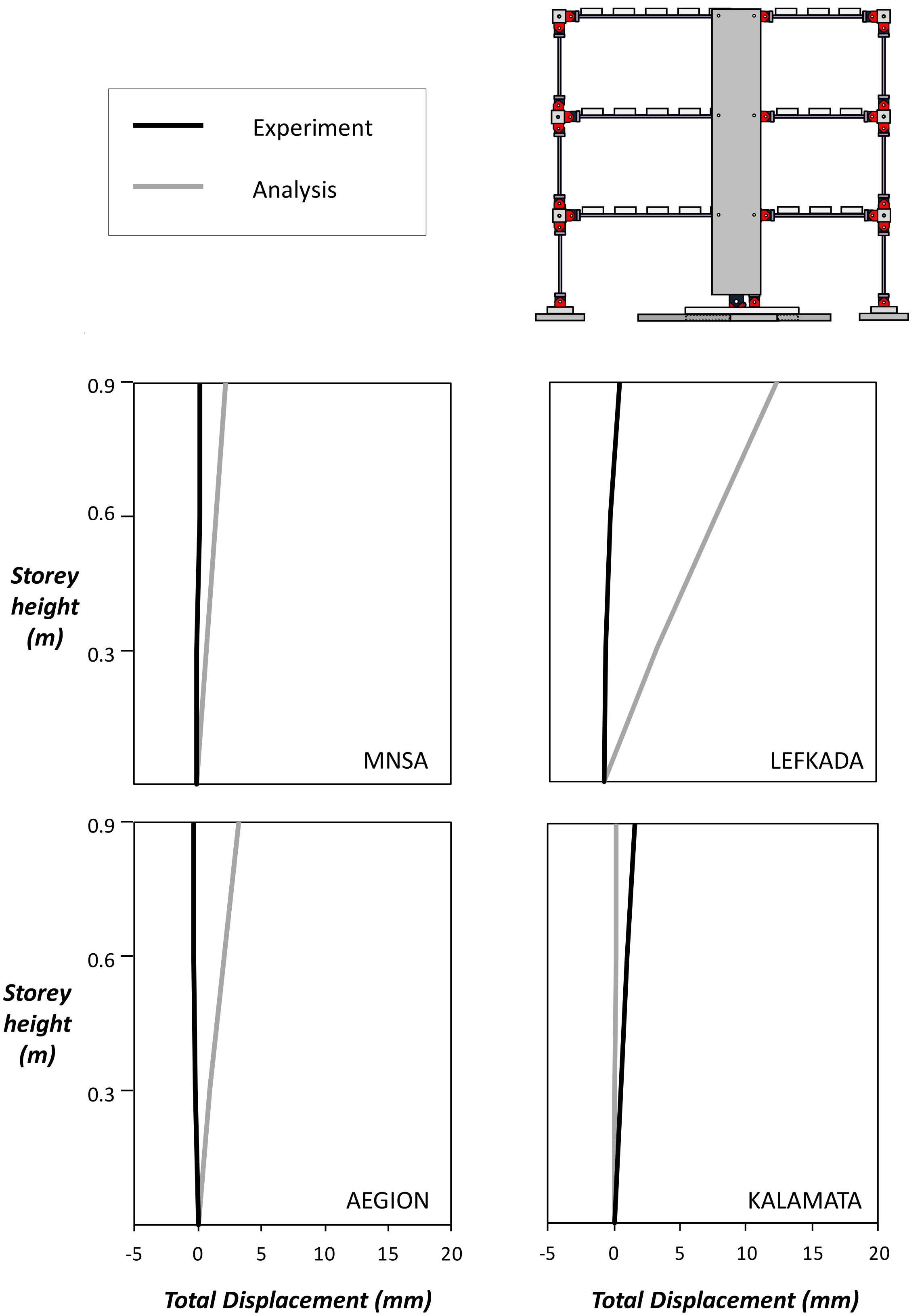

Figure 4.29 Comparison of the analysis and the experiment in terms of residual drifts.

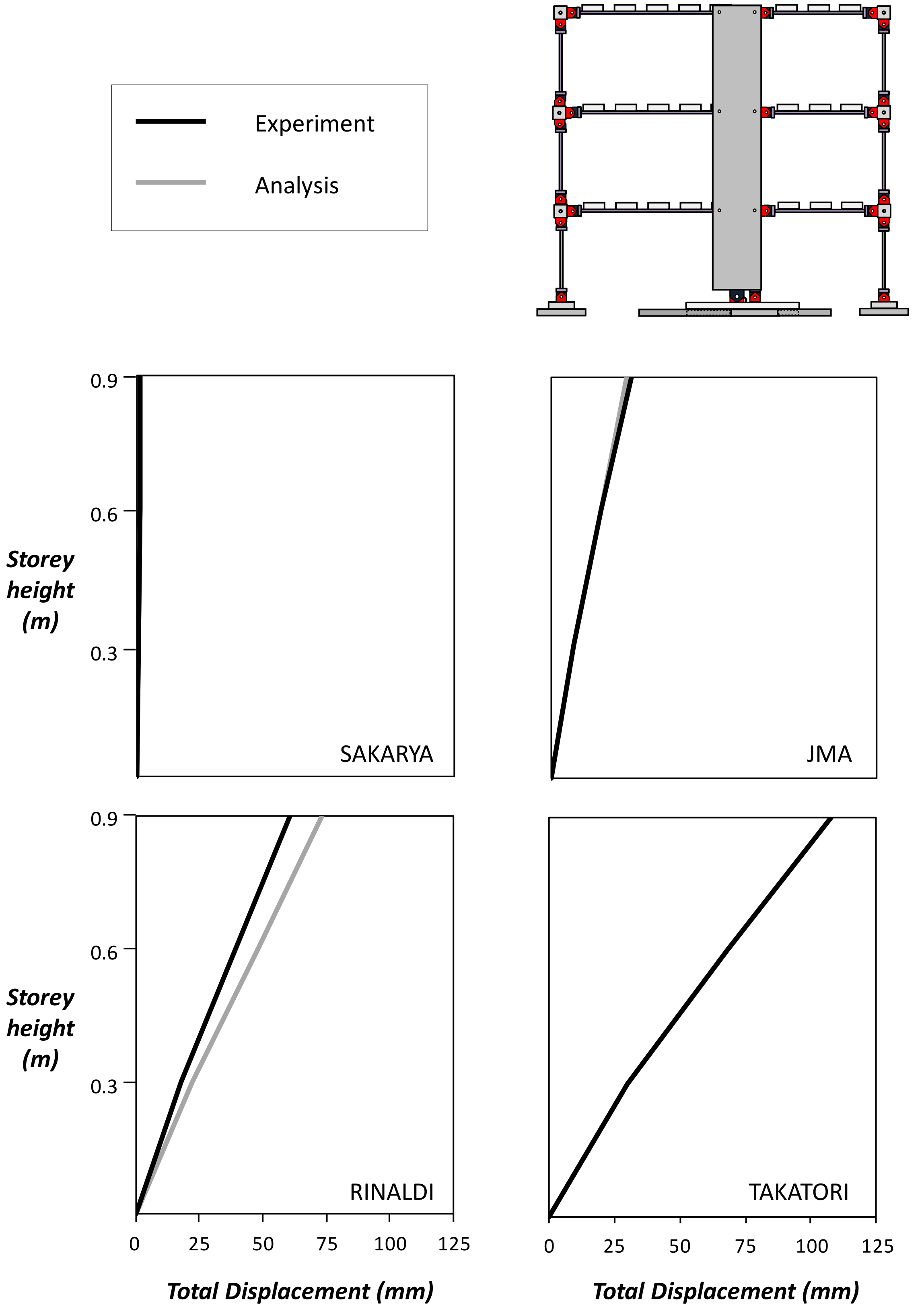

Figure 4.30 Comparison of the analysis and the experiment in terms of residual drifts.

COMPARISON BETWEEN 2 KINDS OF RETROFIT ON A NUMERICAL BASIS

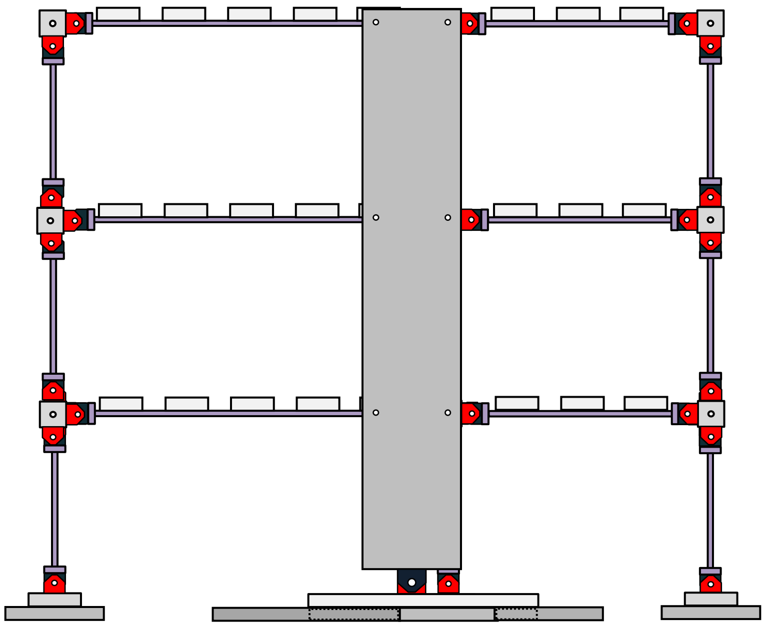

RC WALL

Vs.

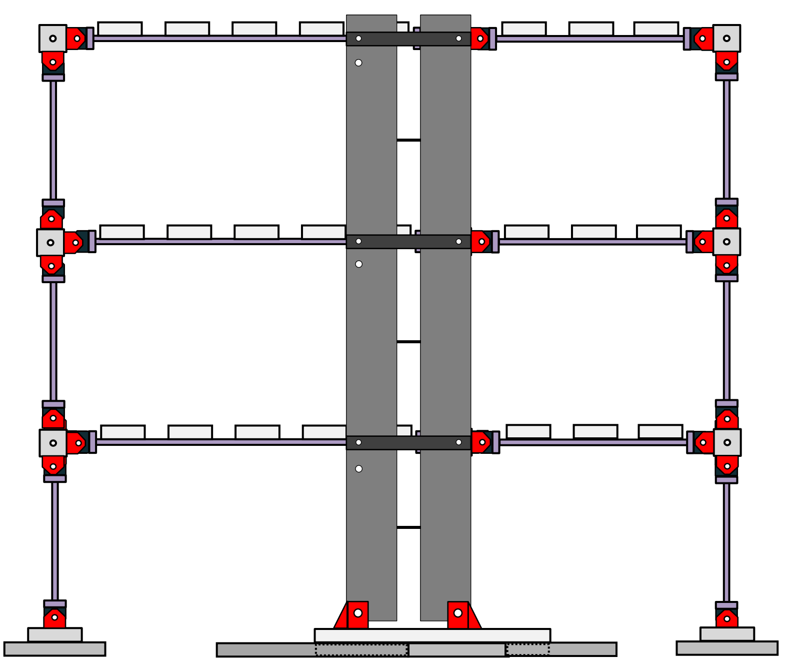

INSTED – FUSEIS system

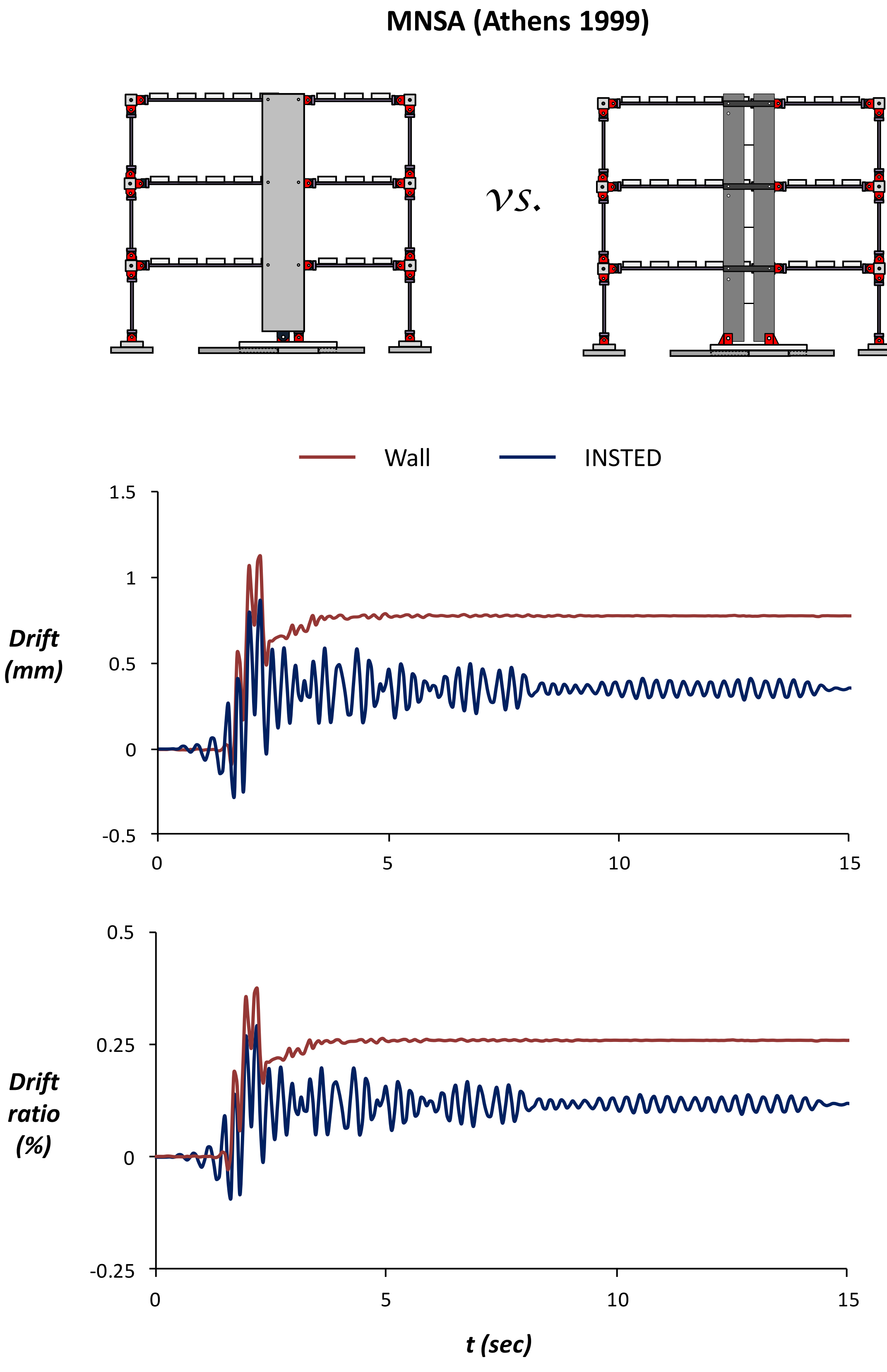

Figure 4.31 Comparison of the 3rd floor interstorey drift and drift ratio between the RC wall and the INSTED system for the record of MNSA (Numerical results).

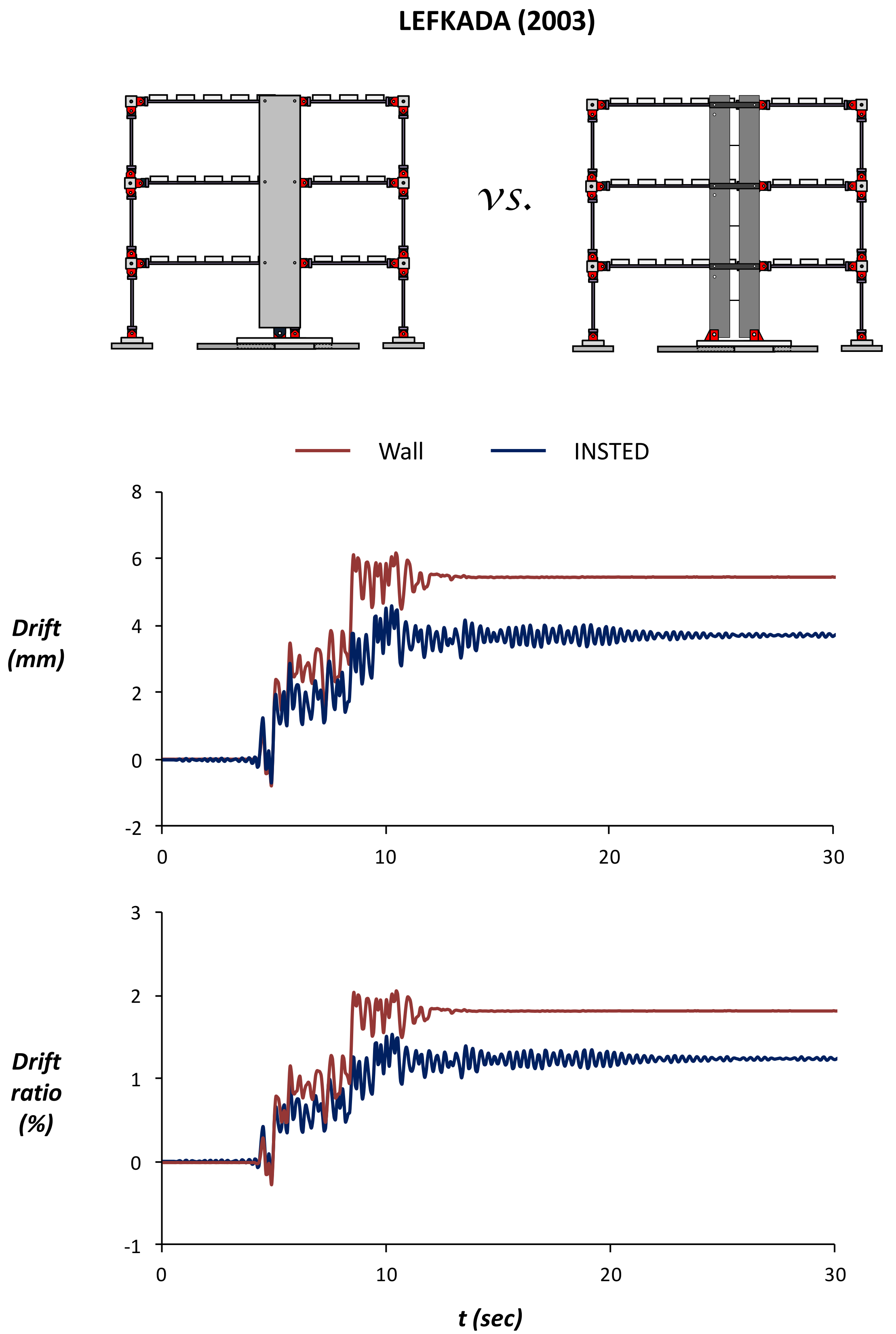

Figure 4.32 Comparison of the 3rd floor interstorey drift and drift ratio between the RC wall and the INSTED system for the record of Lefkada (Numerical results).

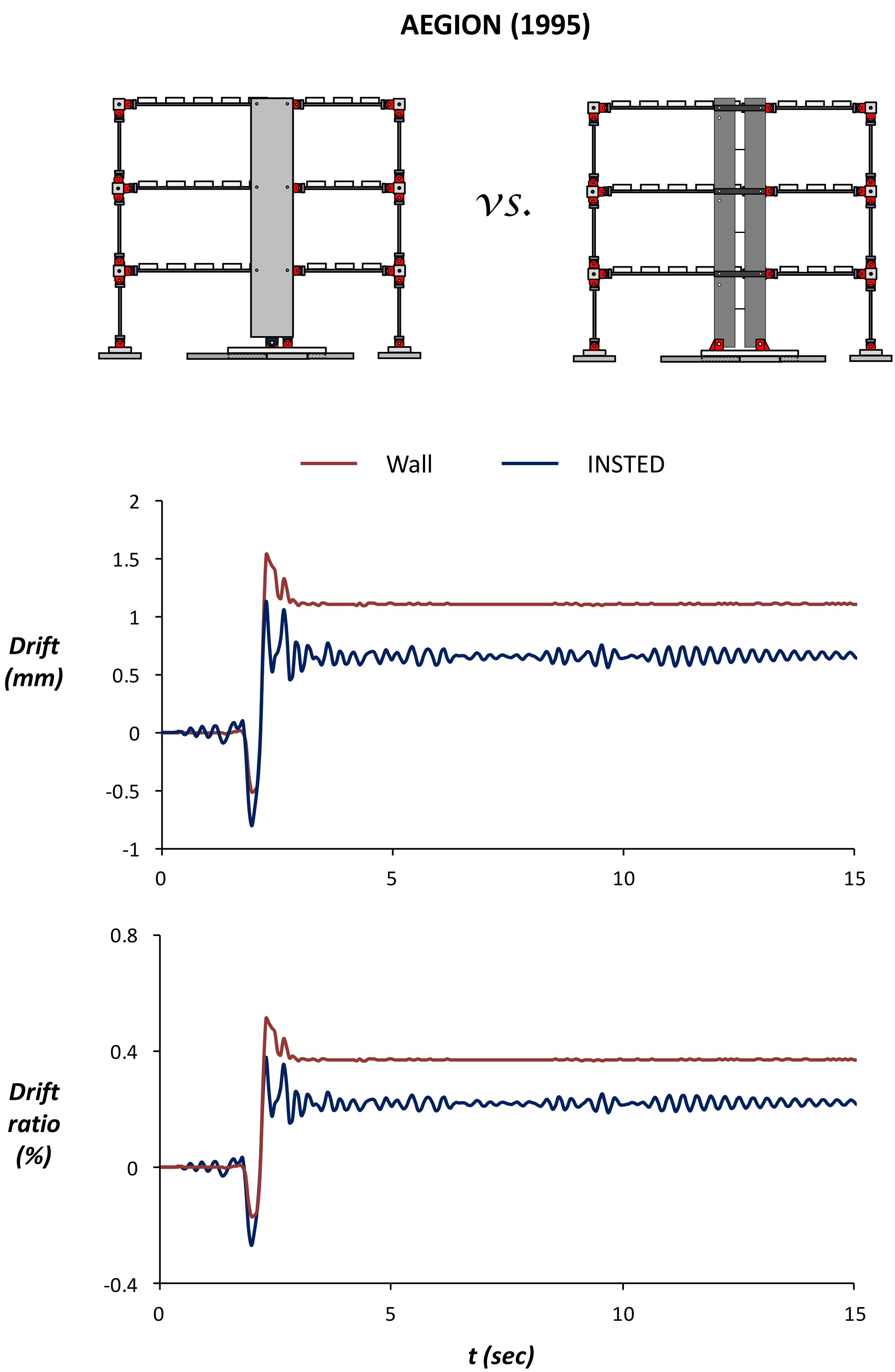

Figure 4.33 Comparison of the 3rd floor interstorey drift and drift ratio between the RC wall and the INSTED system for the record of Aegion (Numerical results).

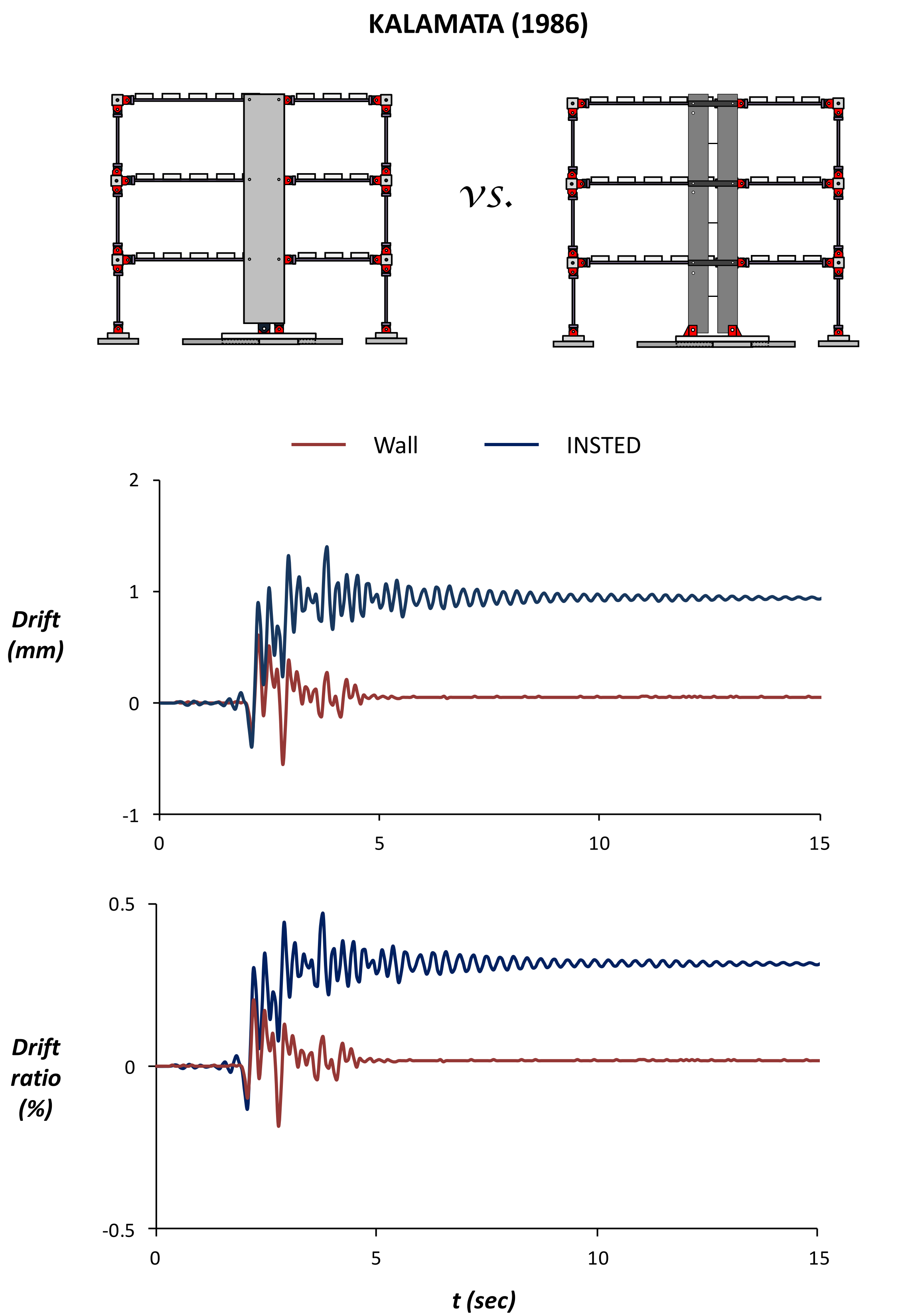

Figure 4.34 Comparison of the 3rd floor interstorey drift and drift ratio between the RC wall and the INSTED system for the record of Kalamata (Numerical results).

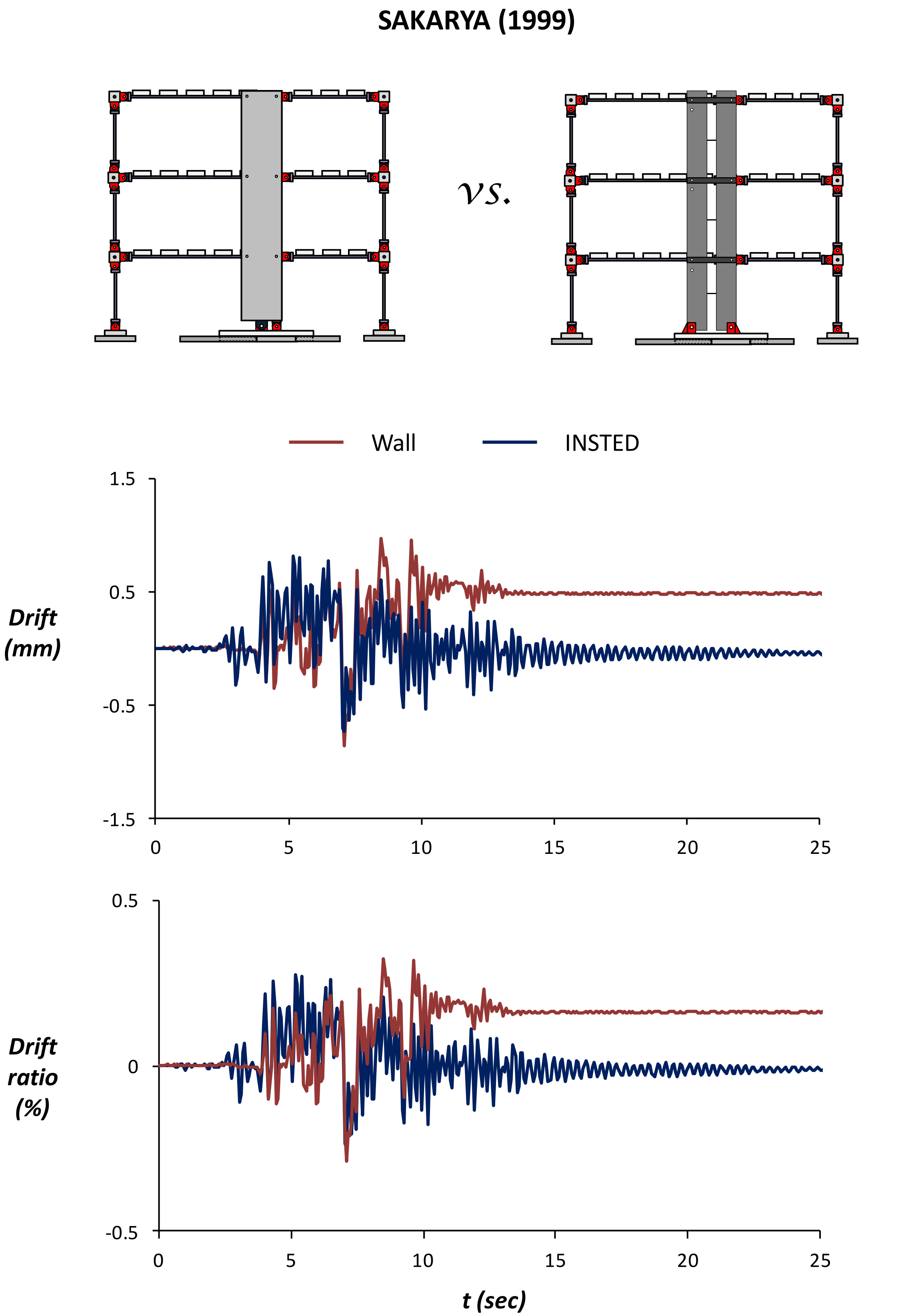

Figure 4.35 Comparison of the 3rd floor interstorey drift and drift ratio between the RC wall and the INSTED system for the record of Sakarya (Numerical results).

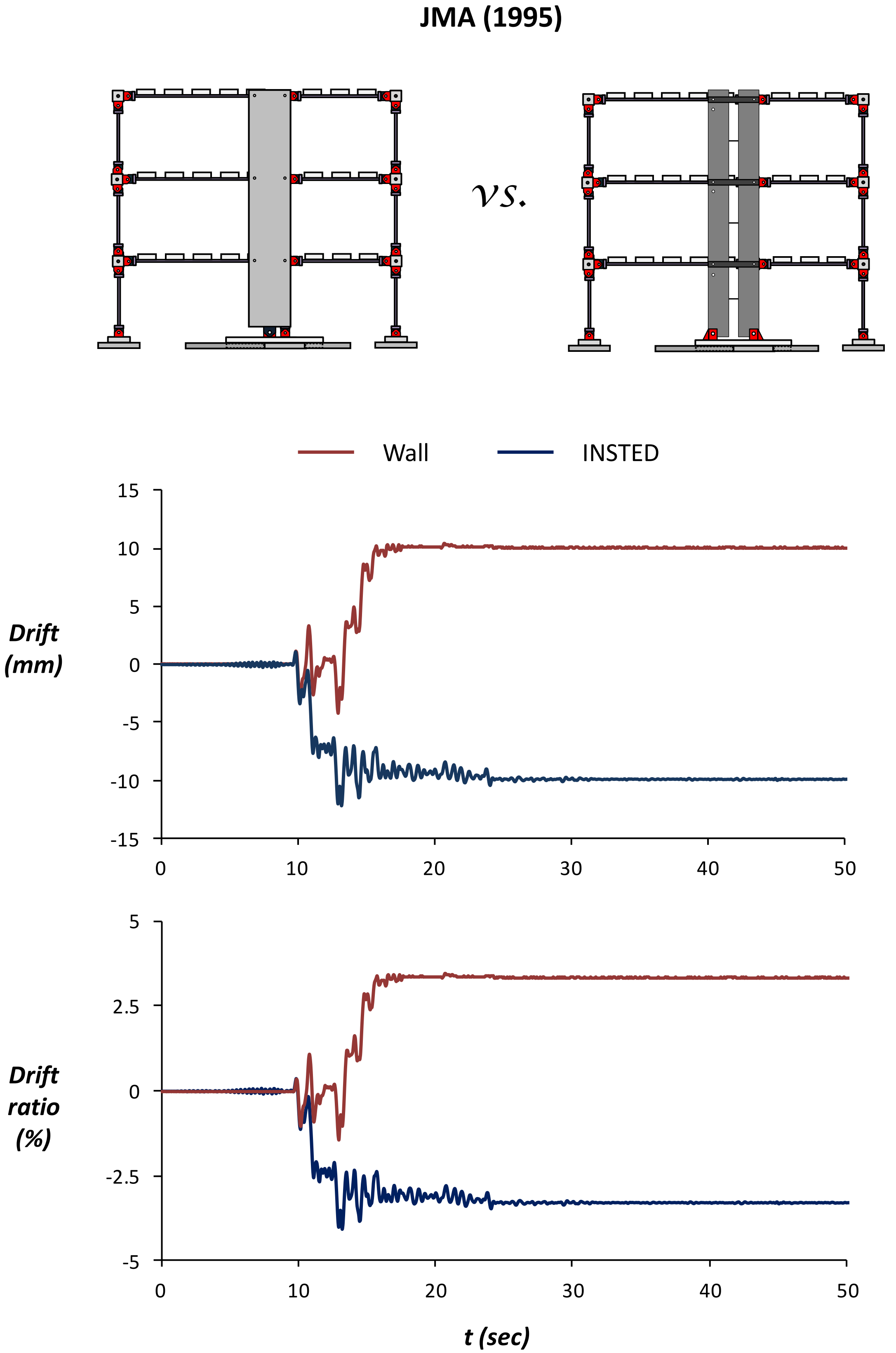

Figure 4.36 Comparison of the 3rd floor interstorey drift and drift ratio between the RC wall and the INSTED system for the record of Jma (Numerical results).

RINALDI (1994)

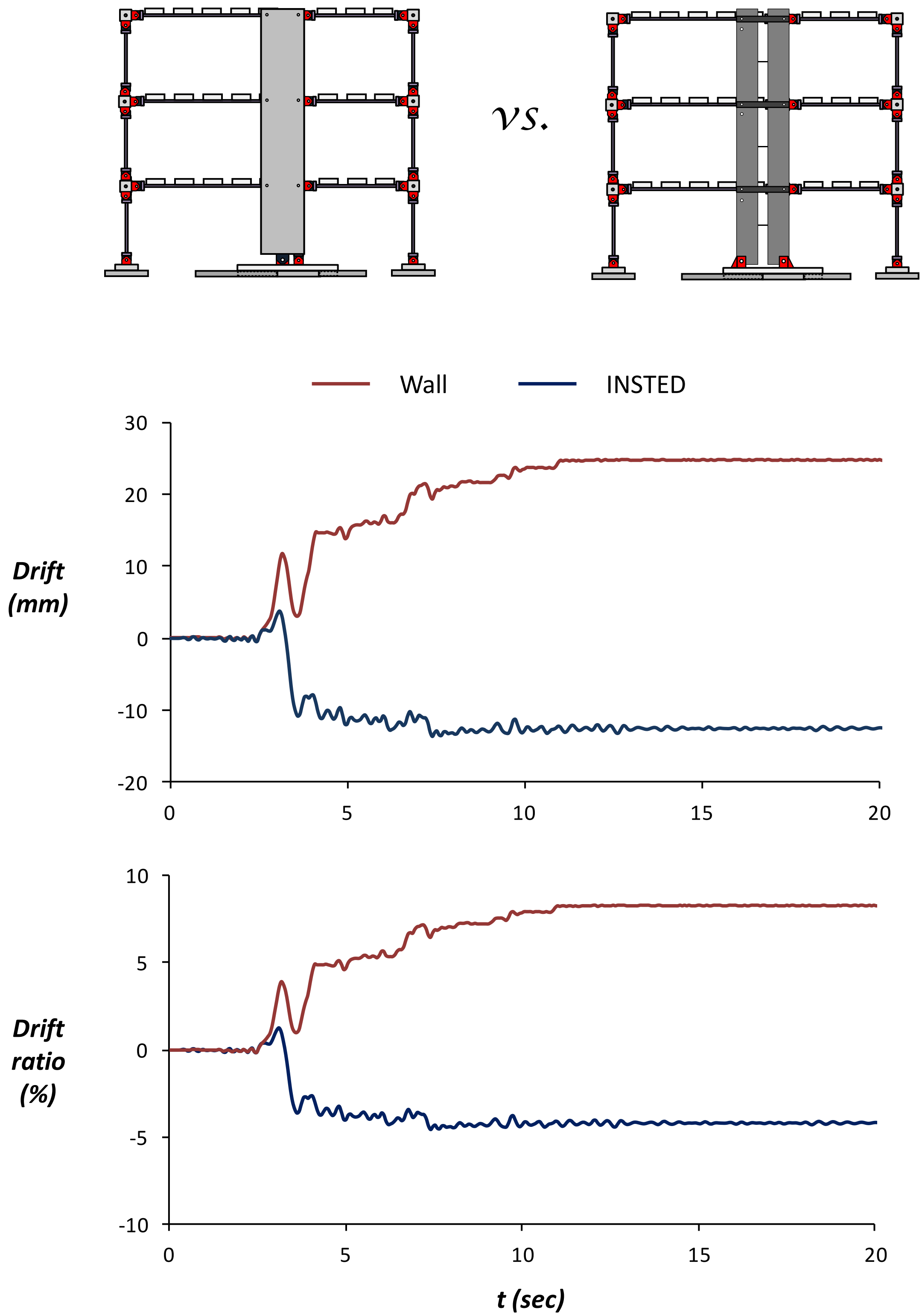

Figure 4.37 Comparison of of the 3rd floor interstorey drift and drift ratio between the RC wall and the INSTED system for the record of Rinaldi (Numerical results).

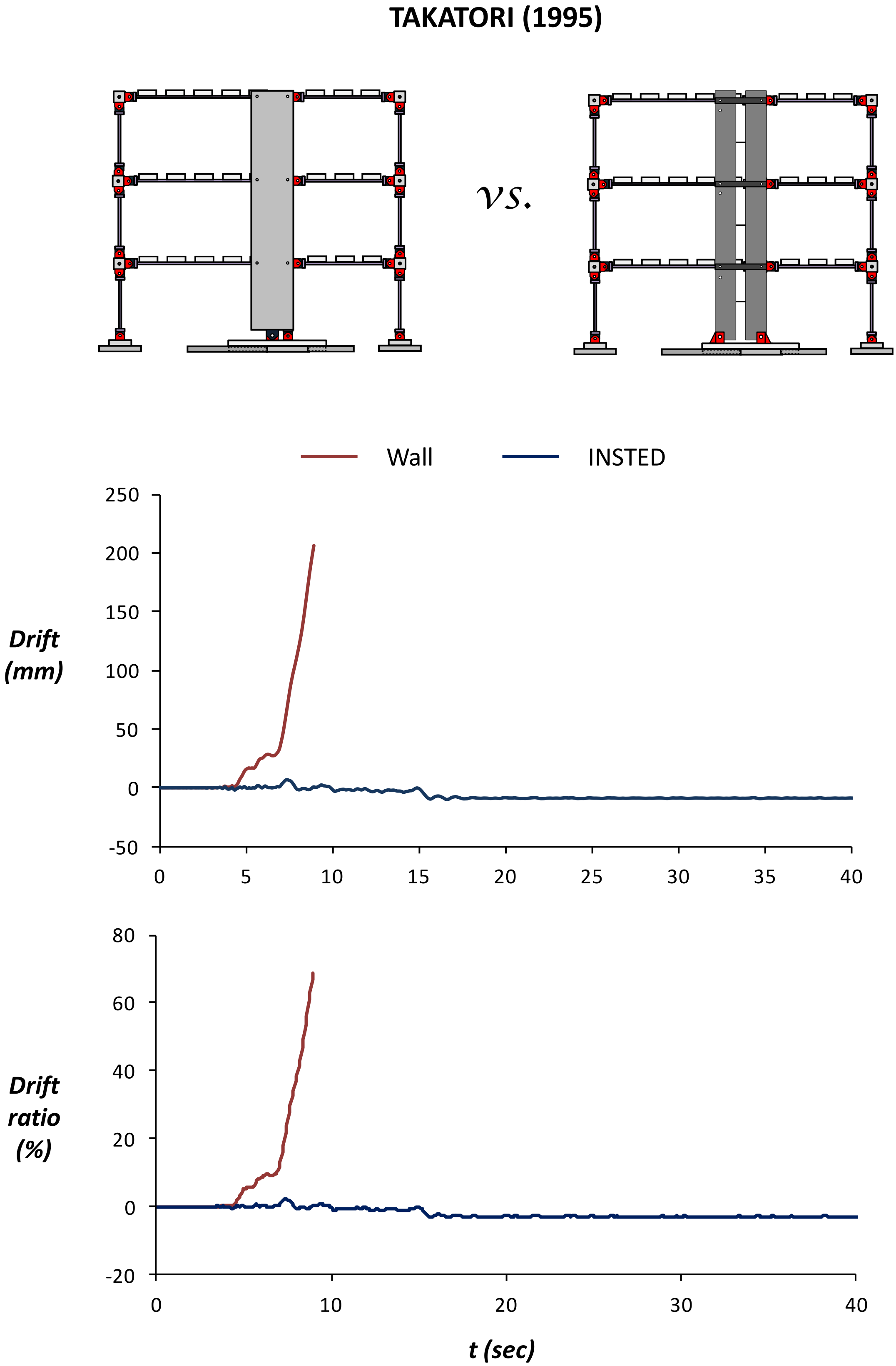

Figure 4.38 Comparison of the 3rd floor interstorey drift and drift ratio between the RC wall and the INSTED system for the record of Takatori (Numerical results).

… a more detailed look in the Takatori record

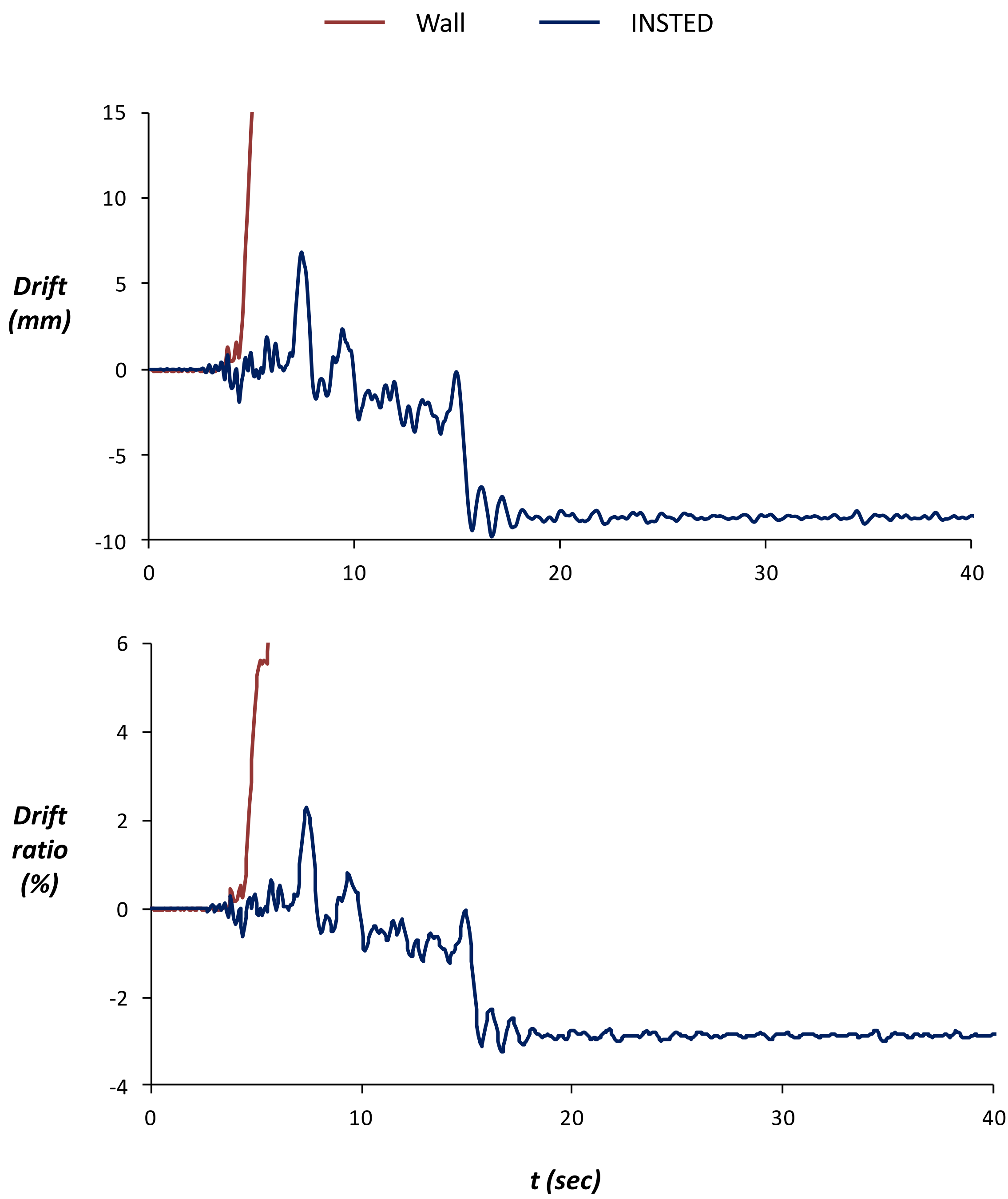

Figure 4.39 Comparison of of the 3rd floor interstorey drift and drift ratio between the RC wall and the INSTED system for the record of Takatori (Numerical results).

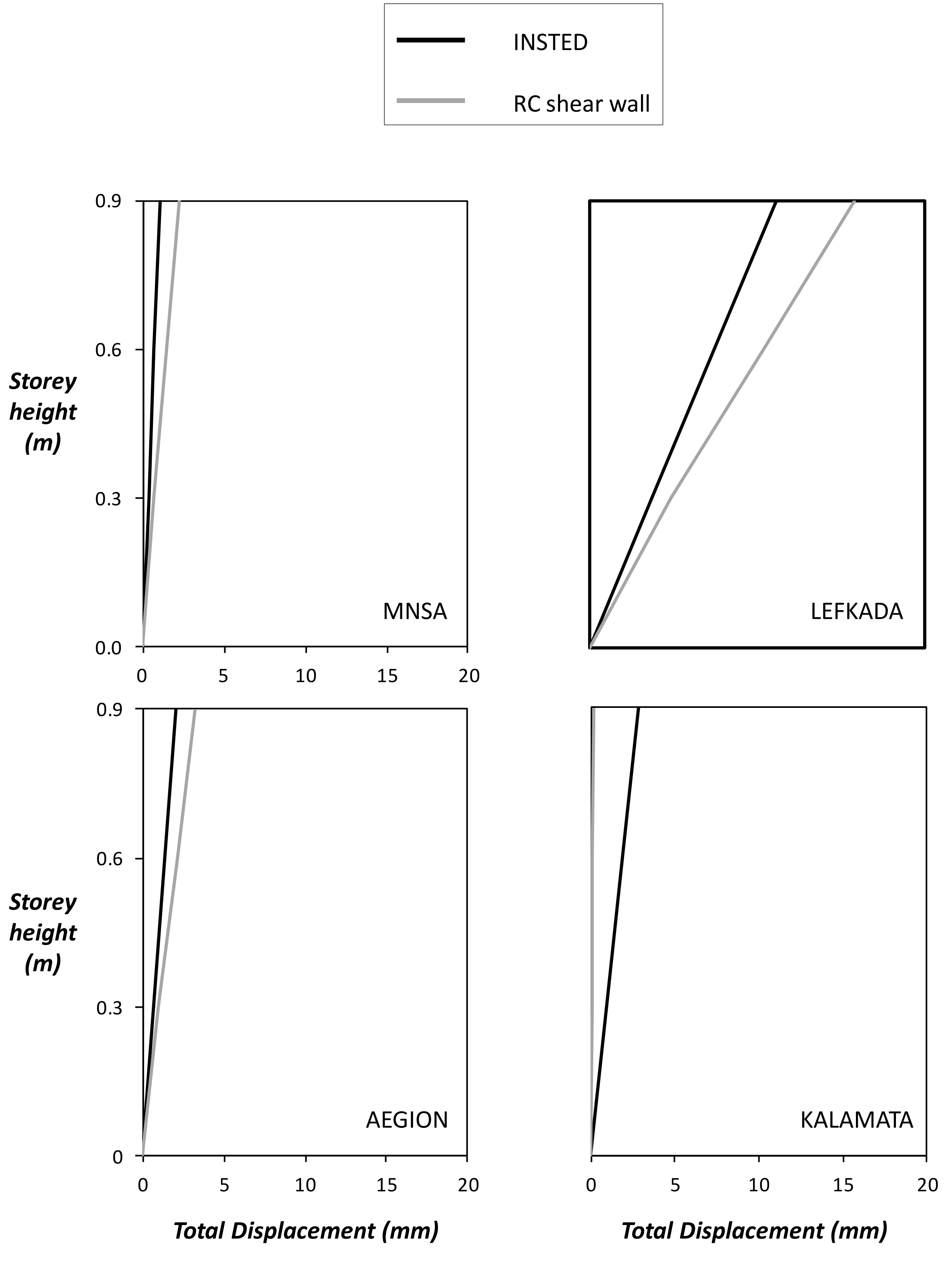

Figure 4.40 Comparison of residual drifts between the RC wall and the INSTED system. (Numerical results)

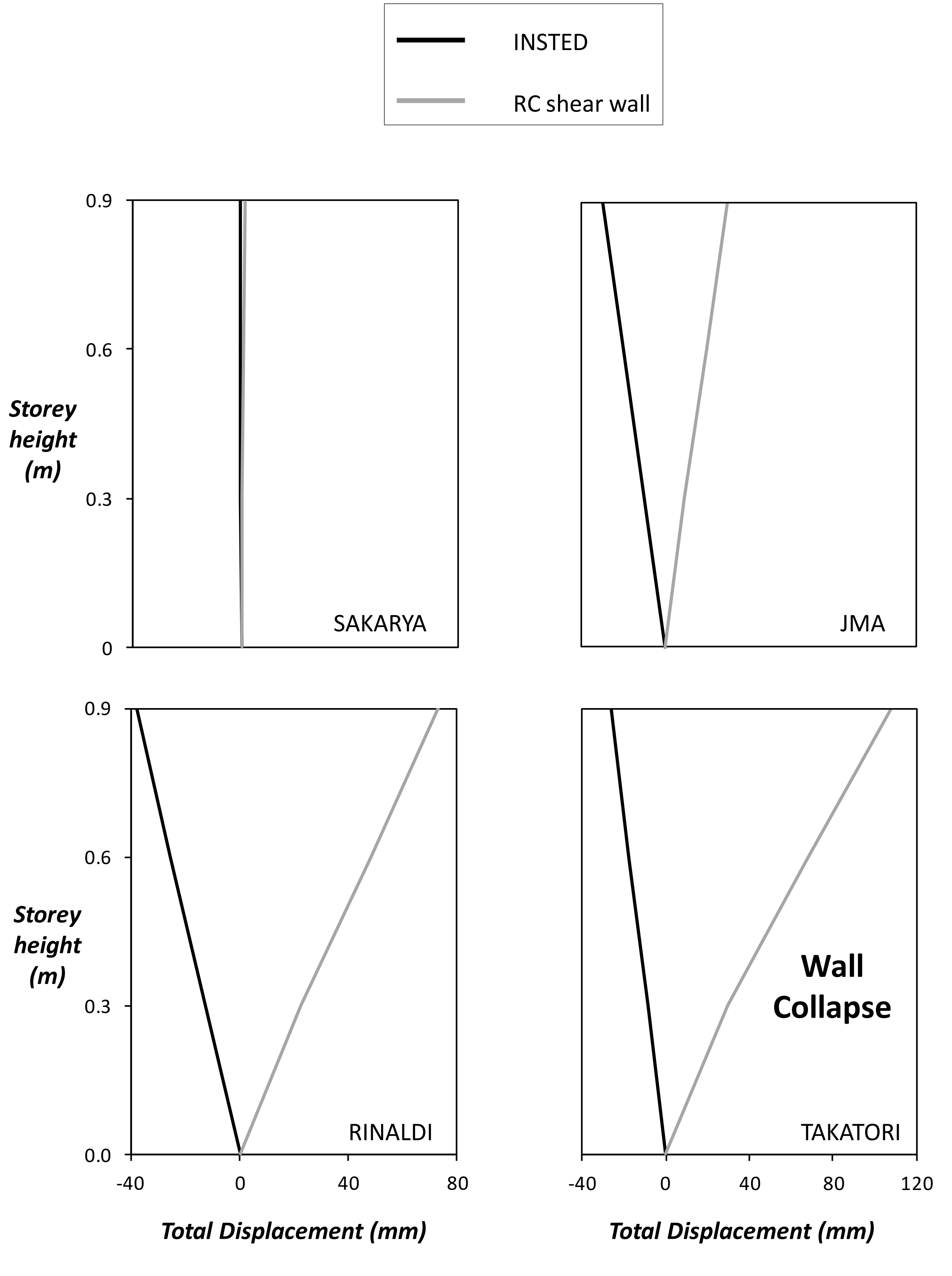

Figure 4.41 Comparison of residual drifts between the RC wall and the INSTED system.
(Numerical results)

CONCLUSIONS OF PART A

The numerical simulation of the INSTED - FUSEIS system alone, at first, and of the original building, in the next step, proved to be very satisfactory. Therefore, we proceeded to the combination of the two numerical models in order to conclude to the desired result, which is the simulation of the building with the retrofit that is proposed in this Thesis, the INSTED – FUSEIS system. The retrofitted building is subjected to horizontal pushover tests and dynamic loadng that the original had failed to withstand and subsequently compared to the original. From these tests, we are able to examine the actual dynamic performance of the INSTED system, along with the response of the structure equipped with this means of seismic retrofit. Additionally, a comparison of the INSTED – FUSEIS system with another way of retrofit - that of an RC shear wall - allows us to estimate the advantages of each system and finally result in the superiority of the first.

Original vs Retrofitted building (INSTED- FUSEIS system)

- The retrofitted building displays **uniform deformation**, due to the existence of the INSTED system, whose columns rotate like a rigid body, thus homogenizing and distributing the displacement to all stories. In this way, the formation of a soft-story collapse mechanism (brittle type of failure), which led the original building to failure, is avoided.
- The **total drifts** of the building after the retrofit (INSTED) are negligible for the seismic records of moderate intensity and quite satisfactory for the severe seismic motions of Rinaldi, Jma and Takatori. According to the results of the most realistic constitutive model utilized (the one with the descending branch), the structure displays greater deformation during the seismic record of Rinaldi, where it cumulates a total drift of 38 mm (hence 4.2%) but is not led to failure. On the contrary, the original building collapses already since the record of Lefkada, thus, no comparison is worth mentioning. The success of the INSTED system, as a means of retrofit, lies on two reasons:
  - ✓ The *strength* of the retrofitted structure is greater in comparison to the original one, therefore, it can withstand motions of greater amplitude.

- ✓ But beyond that, the most important benefit of this system is its great *ductility,* thanks to the fuse elements that are being used. These elements are made of mild steel, a material by nature displaying ductile behavior with hardening properties after yield, therefore, enabling the whole structure to deform and resist, under stable force, without collapsing. Under consecutive counter belts pulses, **the horizontal rods demonstrate an ease in deforming and resetting their shape, without reaching failure;** thus dissipation of large amounts of energy takes place while plastic hinges are formed at the rod ends. This behavior definitely gives the system an edge in dynamic motions. Of course, this is not the case for the original concrete building, which is designed out of the capacity and ductility design principles that Greek regulations now pose. Its capability of deformation after yield is negligible and, thus, fatal damage to the base floor columns seems unavoidable.

Retrofit via the INSTED system vs Retrofit via the RC shear wall

- Both types of retrofit achieved uniform deformation of the structure during horizontal loading, static or dynamic. However, the INSTED system results in much decreased **total drifts** of the building, compared to the RC shear wall. Indeed, the RC shear wall fails to withstand the motion of Takatori and finally the building collapses, whereas the alternative of the INSTED system as means of retrofit seems to be ideal, since the building's total drift after this particular record is equal to 26mm (2.9% drift ratio < 4%).
- The fact that the building retrofitted via the RC wall displays greater yield force than the one retrofitted with the INSTED system (1.8 times greater) proves to be insufficient in terms of safety against some seismic motions. The elements that make the seismic performance of the INSTED system outbalance that of the RC shear wall are the following:
  - ✓ The INSTED system displays a much more **ductile behavior** compared to the RC wall, thus, allows greater deformation before failure. This is due to the different material properties between the two kinds of retrofit; the fuse elements of the INSTED system are made of mild steel, which displays hardening after yield, whereas the shear wall is made of reinforced concrete, which has limited ductility. Thus, the rods are able to dissipate large amounts of energy, by reaching significant values of permanent deformation without failing, while the

inability of reinforced concrete to respond in a ductile manner prejudices the shear wall's earlier failure.

- ✓ Regarding the RC wall, the greatest bending moment is displayed at its base; thus, this is the point where formation of the potential plastic hinge is expected. Hence, in order for the wall to display adequate moment capacity, the dimensioning is made according to the base action moment, resulting to a cross-section of large dimensions. On the contrary, the stiff columns of the INSTED system guide the seismic force to the horizontal rods, by means of moments at their edges, which are significantly smaller than those at the base of the RC wall. This is due to the set-up adopted – the rods are placed in the middle of the system's span and equally distributed along the height of the structure. Therefore, the **moment capacity and cross-sections required are decreased**. Conclusively, the INSTED system appears to be more economical than the RC wall. Additionally, the small cross-section of the rods makes them more flexible than the RC wall, therefore, capable of altering moment values from positive to negative and reverse, which turns out to be really advantageous during cyclic loading.
- ✓ Due to fact that the potential plastic hinge of the RC shear wall is formed at the base, any visit for repair to the damaged site is practically impossible. Therefore, even if the building has survived after a strong seismic motion, it is no longer within the limits of serviceability. For the shear wall to be replaced, the structure's normal operation should be interrupted for some time. On the other hand, the **fuse elements** of the INSTED system do not participate in the dead load bearing mechanism, so they can be easily removed and **replaced or repaired** after a strong earthquake. At the same time, the columns of the INSTED system respond only elastic thus experience no damage. This is a great advantage of this system, since the structure is able of operating normally and at the same time being repaired after a strong earthquake.

PART B’

CHAPTER B.1

RETROFITTED BUILDING WITH THE INSTED SYSTEM - PUSHOVER AND DYNAMIC TESTS

1.1 Experimental Setup

1.1.1 Model

As already mentioned, the *scaled-down model building* consists of two identical 3-storey frames, connected together through evenly distributed steel plates, which are used to represent the mass of each storey (Figure 1.1). The bearing elements (columns and beams) are made of compact aluminum plates that are connected together as in a moment-resisting frame. In order to simulate the performance of the retrofitted structure, the equivalent of the INSTED system is added in the middle of each frame, along the height of the middle column (Figure 6.2).

The system's columns are modeled by two stiff aluminum plates, with a 0.75m x 0.02m cross section. Both of them are articulated at the base of the building, on an aluminum footing with a 0.60m x 0.02m cross section (Figure 1.3). The system's right column is articulately connected to the 3-storey frame at the level of each floor. The horizontal fuse elements are made of steel, with circular cross section and nominal yield stress equal to fy = 347 Mpa (Figure 1.5c). The steel's tensile stress-strain curve is determined through the conduct of tensile strength tests to a Φ8 specimen, in the Steel Structures Laboratory (Figure 1.5a &b). The rods' diameter varies between two different values (D=3.2mm and D=4mm), depending on the experiment conducted. Finally, in order to simulate the diaphragmatic function of the storey plates, three horizontal bars with a 0.02 m x 0.003m cross section are placed on the INSTED system at the level of each store (Figure 1.3b).

1.1.2 Sandbox

The sandbox, on which the model was placed for the experiments, is of internal dimensions 1.48m x 0.78m x 0.645m (Figure 1.8). The two larger sides of the box are transparent, for better observation of the experimental procedure, and they consist of a combination of Plexiglas and glass. Plexiglas is placed on the outside in order to achieve rigidity and durability, while glass is placed on the inside so as to minimize friction and simultaneously avoid scratching the Plexiglas.

1.1.3 Sand Raining System

The soil of the sandbox consists of dry "Longstone" sand, a very fine industrially-produced uniform quartz sand having a mean grain size d_{50}=0.15mm [Anastasopoulos et al, 2010]. In the series of experiments conducted, the soil deposit has a depth of about 50 cm. In order to ensure a certain sand density and its repeatability in every experiment, the Laboratory's sand raining system is used (Figure 1.7a). Through this system, it is possible to choose and audit the mechanical characteristics of the soil. This procedure is called sand pluviation. In order to achieve the desired density, the height measured from the bottom of the sandbox, the aperture of the device and the velocity of the soil hopper are defined. The suitable values for these three parameters are selected according to Figure 1.7b, which summarizes the results of an experimental series conducted to calibrate this device [Anastasopoulos et al, 2010]. Finally, it should be mentioned that for all the experiments conducted in our thesis, a dense sand of Dr=93% was used.

1.1.4 Push-over Apparatus

The push-over apparatus, used to apply horizontal displacements during the static and slow-cycling pushover tests, consists of a servomotor joined to a screw-jack actuator (Figure 1.10). The servomotor is controlled by a computer, where the desired displacement, acceleration and velocity can be selected. A device capable of measuring the applied load (load cell) is connected at the edge of the actuator.

1.1.5 Shaking table

The shaking table of the Laboratory of Soil Mechanics of NTUA is of dimensions 1.3m x 1.3m and is capable of applying any type of excitation, including actual records (Figure 1.9). It is able to shake up to 2000kg with a maximum acceleration of 1.6g and it is of one degree of freedom (longitudinal). The maximum displacement of the table is +/- 75mm and the maximum velocity > 1.2m/sec. It is connected to a data acquisition system and is controlled by an external digital system. The results of each experiment are collected and saved in the computer that controls the shaking table.

1.2 Experiment Preparation and Instrumentation

Before every experiment, the model's members are being aligned, so that the columns are vertical and the beams are horizontal. The first floor's middle column is removed before the INSTED system is added to the frame, so as not to provide unrealistic compressive or tensile strength, as the system deforms.

For the *dynamic experiments*, the shaking table is calibrated for a 1:10 scale and the sandbox is placed on it, with the sand being layered in it using the sand raining system. Afterwards, the model building is placed into the sandbox with the help of a crane bridge. In order to avoid significant deformations of the structure during this procedure, aluminum bars of small thickness are used as crosswise connectors of opposite joints. The model building is carefully installed on the soil with the use of four mechanical jacks and special care is taken during the installation, so as not to disturb the soil surface. After this, electronic spirit levels are used to ensure that the building is placed horizontally on the soil surface - without any initial inclination - and that the columns are vertical. Finally, in order to avoid possible overturn of the model during the experiments, vertical bars were placed at the larger sides of the sandbox as restraining measures.

For the *pushover experiments*, the sandbox is placed next to the pushover apparatus and the model building is again installed in it. However, in this case the soil-structure interaction does not concern us, since the purpose of these experiments is to deduce the actual strength of the retrofitted building by imposing horizontal displacement on it. Thus, the only utility of the sandbox is to operate as a base for the building, so that the building can reach the desired height. In that way, we are able to connect the screw jack actuator at the level of the second storey, where the displacements are to be imposed. Since the structure's base can be considered as fixed in these tests, the model building is not directly placed on the soil. Two aluminum bars with a 0.09m x 0.09m cross section are placed in the middle of the sandbox, parallel to its long dimension, with a certain distance between them. Each frame's footings are then rigidly connected to each one of these bars, with the use of six more aluminum beams; the beams are placed perpendicularly on the edges of each footing and connected rigidly to the aforementioned bars. In addition, the 0.09m x 0.09m aluminum bars are also rigidly connected to the smaller sides of the sandbox, in order to avoid sliding during the experiment (Figure 1.11).

In order to measure accelerations and displacements, a number of instruments are used. The horizontal in-plane acceleration is measured by accelerometers on every storey, as well as in a small depth from the soil surface. The horizontal in-plane displacements of each storey, as well as the sliding of the central footing are measured by wired displacement transducers. The horizontal displacements of the three floors are processed so as to calculate each storey's inter-storey drift, while the footing's sliding is measured in order to be deducted from the displacements of each storey. In addition, one wired displacement transducer is located on each INSTED system, in order to measure the vertical displacement of the rods. For the dynamic experiments, two wired displacement transducers are also used for each footing of the first frame to measure the vertical displacement of each side of the footing. These measurements can be processed for the calculation of the in-plane rotation and the settlement of each footing. However, in our case, the structure footings are designed conventionally, thus to remain elastic and avoid notable residual rotation or displacement after a strong earthquake. In addition, the sand in the box is of high density (Dr=93%), hence no large settlements and rotations of the footings are expected. The data from all the instruments are gathered through cables and saved in the record system of the Laboratory. Additionally, visual data are obtained using high definition cameras, recording both the response of the whole structure and the response of the horizontal rods from a closer view. The exact instrumentation for the dynamic and pushover experiments is shown in Figure 1.12 (a & b).

1.3 Loading

For our thesis, a total number of five experiments considering the retrofitted model building were conducted: two horizontal pushover tests and three dynamic tests. The whole series of experiments, along with their characteristics, are displayed in Tables 1.1 and 1.2. The type of loading imposed in both the pushover and the dynamic experiments is explained below.

1.3.1 Loading protocols of the horizontal pushover tests

Normally, the proper way of conducting a horizontal pushover to the retrofitted model building is by imposing load or displacement at the level of each storey, following the rules of triangular distribution. However, the pushover apparatus of the Laboratory is able of imposing displacement only on one point; thus, in order to achieve an equivalent result we implemented concentrated displacement at the level of the second floor, where the centroid of the triangular distribution is considered to be.

The first horizontal pushover experiment (D_{rod}=4mm) includes two types of loading: (a) a 1-cycle pushover until a total drift ratio of 5% is reached at the level of the second floor and (b) a slow – cyclic pushover with the displacement being gradually increased in every circle, until failure. For the second pushover test (D_{rod}=3.2mm), only the slow-cyclic loading protocol is used. The exact form of the loading protocols is depicted in Figure 1.14. In both experiments, displacements are being imposed with a velocity of 0.4mm/sec and the test results are gathered in the record system of the Laboratory. Due to the position of the wired displacement transducers, positive values of displacement are recorded when the setup moves towards the pushover apparatus, while negative values of displacement are recorded when it moves away from it.

1.3.2 Seismic motions

The experimental models are subjected to dynamic testing in the shaking table of the Laboratory of NTUA, using real seismic records as base excitation. Since the models' scale factor is equal to 1:10, the imposed excitations are also scaled down according to respective scaling laws. In the four dynamic tests conducted, a total number of five actual seismic records – both moderate and strong ones - are used, but the imposed sequence differs between the experiments. For moderate seismic excitation of the experimental setups, two Greek records are selected: the record of *MNSA* (from the 1999 Athens earthquake) and the only record from the *2003 Lefkada* earthquake. The record of MNSA reaches a maximum acceleration of a_{max}=0.51g, but due to its high frequency it is not considered as a severe one. The record of Lefkada, with maximum acceleration of a_{max}=0.43g, is a strong seismic shaking of long duration, consisting of several cycles with significant acceleration. For strong seismic excitation, three extremely strong seismic motions are selected, in order to examine the systems' performance over the worst possible scenarios: the record of *Rinaldi* (from the 1994 Northridge earthquake) with maximum acceleration of a_{max}=0.84g and the records of *Jma* (a_{max}=0.82g) and *Takatori* (a_{max}=0.61g), from the devastating 1995 Kobe earthquake. The last one is considered as the most severe of them all, displaying high values of acceleration in a wide range of frequencies. The five seismic records and their elastic spectral accelerations are depicted in Figure 1.15.

1.4 Description of the experiments – Results

In the ensuing, the procedure and most important results of every experiment are presented. A more detailed presentation of each experiment's results is made in APPENDIX B.

1.4.1 Experiment No. 1 (SETUP I): *Horizontal Pushover Test - D_{rod} = 4mm*

For the first experiment, the setup of the INSTED system is based on the numerical calculations and analyses that have been previously conducted in Abaqus. According to these calculations, if each INSTED system consists of three horizontal fuse elements, an earthquake design acceleration of $\Phi_d(T)$=0.135g combined with an f_y=235 Mpa steel nominal yield stress, demand *4.0mm* rod diameter. Hence, we resulted in a setup where each INSTED system consists of three rods of d=4.0mm. Hollow rods of external diameter equal to d = 8mm are placed at the edges of each d = 4mm rod, in order to lead the formation of plastic hinges away from the supports, where the developed bending moment is greater. In this way, the rod's effective length becomes equal to l_{eff} = 2.5mm. However, this setup does not ensure that local damage due to fatigue will not affect the system's performance, since at the ends of the effective length the rod's cross section displays an abrupt change.

As far as the 1-cycle pushover test is concerned, we should mention that the loading protocol was not implemented until the end, since the screw connecting the pushover apparatus' actuator to the building's second floor proved unable to sustain the constantly increasing load up to the displacement of 30mm. Thus, when the displacement reached the value of +23mm, the setup stopped working properly and the values of applied load started decreasing. At that point, the test was stopped, the screw was replaced with one of greater strength and the building was brought back to its initial position, for the slow-cyclic pushover test to follow.

Results

As one can observe from the Load – Vertical displacement curve of the 1-cycle pushover test (Figure 1.16a), the retrofitted model reaches a total strength of *1.5kN*, while yielding takes place at approximately *1.2kN (*or *0.8g* in terms of acceleration, as depicted in Figure 1.16b). The vertical displacement of the rods is measured equal to *1.5mm* at the yielding point and approximately equal to *5.2mm* at the end of the monotonic pushover test.

As far as the slow – cyclic pushover test is concerned, one can easily observe from the Load – Time curve depicted in Figure 1.18 that at the beginning of the test, thus for t = 0, the applied load does not equal to zero but instead holds a value of about 1kN; the model seems to have obtained a residual deformation from the previous monotonic pushover test, even though it was afterwards brought back to its initial position. In addition, the curve is obviously not symmetric – in terms of load - around the time axis, something that can also be attributed to this previously acquired deformation. When the building is pushed to the left, there is a gradual increase of load, until the structure reaches its total strength (equal to 1.4kN) in the 10^{th} cycle, for an imposed displacement of 20mm. On the contrary, when the building is pushed to the right, the increase in load does not follow the same pattern; the model reaches the value of 1.4kN almost immediately and continues deforming under stable load. This behavior seems rational, since the horizontal rods have already reached their yielding point in this direction from the previous monotonic test, thus very small values of displacement are now required in order to enter the plastic zone.

In Figures 1.17 (a & b), where the Load – Vertical displacement and Acceleration – Vertical displacement curves derived from the slow – cyclic pushover test are displayed, one can notice by the diagrams' loops that significant dissipation of energy is taking place, through the plastic deformation of the system's horizontal rods. During the 12^{th} and 13^{th} cycle of loading, the imposed load (corresponding to displacement values of 30mm & 40mm respectively) seems to exceed the structure's strength limits, thus *the rods are led to failure and the respective degradation in strength is visible*.

1.4.2 Experiment No. 2 (SETUP I): *Dynamic Test – D_{rod} = 4mm*

In the second experiment, SETUP I is tested on the shaking table of the Laboratory of Soil Mechanics. For the dynamic tests, the building is placed into the sandbox with its base not being fixed to the ground, thus any potential Soil – Structure Interaction is taken into account. Since the retrofitted structure developed such a significant strength in the respective pushover test, we decided to impose a sequence of strong seismic records on the model, in order to examine its behavior during extreme shaking scenarios: *Rinaldi* (Northridge 1994), *Jma* (Kobe 1995) and *Takatori* (Kobe 1995).

Results

The deformed shape of the building at the end of the test is depicted in Figure 1.22. Clearly, the INSTED system is proved strong enough to sustain the implemented seismic motions, without any significant deformation of the rods. The residual vertical displacement of rods after each motion is considered negligible; even after the record of Takatori it is practically equal to zero (Figure 1.23b). As displayed in the respective Force –vertical displacement curve of Figure 1.23c,, the system by no means reaches its yielding point (F_{yield}=1.2kN), thus the horizontal fuse elements remain elastic despite the severity of the seismic records imposed. However, the main philosophy of the INSTED system is to yield relatively quickly and then dissipate energy through the plastic deformation of its fuse elements, leaving the rest of the structure into the limits of elasticity. Elastic behavior of the rods during such strong excitations means that the retrofitting setup is over-designed, thus the value of 4.0mm for the rods' diameter is significantly larger than the one required for earthquake design acceleration of $\Phi_d(T)=0.135g$. This behavior is justified, if we consider that the actual strength of the rods turned out to be greater (f_y = 347MPa) than the one that they were initially designed for (f_y = 235MPa).

During the experiment, the INSTED system footing displays *significant sliding* (*≈ 4cm*), as depicted in Figure 1.24c for the Takatori record. However, the building's footings are not connected together with tie beams, hence, the column footings do not seem to follow the same trend. They display much smaller horizontal displacement, thus the first floor columns acquire the deformed shape depicted in Figure 1.22. The time histories of storey drifts and drift ratios that are displayed in Figures 1.24a and 1.24b surely prove that the retrofitting system actually minimized the total storey drifts, but the objective of the experiment is not achieved, since the INSTED system did not perform as desired.

1.4.3 Experiment No. 3 (SETUP II): *Horizontal Pushover Test – D_{rod} = 3.2mm*

After the previous experiments, it became clear that we needed to examine a scenario involving rods of smaller diameter. Taking into consideration the actual yield point of the steel rods used as fuse elements (measured equal to fy = 347 MPa), we resulted in SETUP II: in this setup, the INSTED system consists of three d=3.2 mm rods. The rods' cross section is equal to 8mm near the supports and weakened away from them, resulting in effective length of leff = 20mm (Figure 6.25). This format is surely more suitable for the fuse elements, since weakening from d=8mm to d=3.2mm is gradual, thus no local damage due to fatigue is expected to happen.

In this test, only one type of loading is imposed on the retrofitted building: slow – cycling horizontal pushover of 10 cycles, with maximum displacement of 20mm in the last cycle.

Results

The structure reaches a total strength of *0.90 kN*, while yielding takes place at approximately *0.7 kN*, as depicted in the Load – Vertical displacement curve of Figure 1.25a. Translating force into acceleration, the yielding and maximum pseudostatical acceleration of the retrofitted model building result in *0.49g* and *0.63g* respectively (Figure 1.25b). In addition, relative vertical displacement of the rods is measured approximately equal to *1.3mm* and *4.2mm* at yielding point and at the end of the test respectively.

1.4.4 Experiment No. 4 (SETUP II): *Dynamic Test – D_{rod} = 3.2mm*

In this experiment, SETUP II is tested on the shaking table, with the same sequence of strong seismic records that was also implemented on SETUP I: *Rinaldi* (Northridge 1994), *Jma* (Kobe 1995) and *Takatori* (Kobe 1995). Tie beams with fixed edges are now added between each frame's footings, in order to prevent differential horizontal displacement of the footings and avoid large deformation of the first floor columns that was observed in the 2nd experiment.

<u>*Results*</u>

As expected, the INSTED system acts as a kinematic constraint, homogenizing the lateral deformation of the structure and leading to more uniform damage distribution in all three storeys. Due to the retrofit, the structure now follows the displacement of the INSTED system, which is much stronger than the building's columns. The development of a soft – storey collapse mechanism in the first floor, thus the failure mechanism that the original building displays under moderate seismic records, is prevented. Again, the structure displays significant strength, even under the extremely strong shaking scenarios of Rinaldi, Jma and Takatori. As displayed in the photographs of Figures 1.29a and 1.29b, it does not seem to suffer from severe deformations after the records of Rinaldi and Takatori. Indeed, residual interstorey drifts are measured approximately equal to *5mm* (with drift ratio ≈ 2%) and *0mm* (with drift ratio = 0%) for the records of Rinaldi and Takatori respectively. The horizontal fuse elements enter the plastic zone, displaying though very small residual vertical displacement for the Rinaldi record (≈*3mm*) and practically zero (=*0mm*) for Takatori. In this experiment, the retrofitted model reaches its yield point (F_{yield}=0.7kN) and the INSTED system displays plastic behavior, but is still far away from failure. *The desired dissipation of energy takes place and is visible in the hysteresis loops of the respective Force – vertical displacement curves* of Figures 1.30c and 1.32c. Especially in the curve of Rinaldi record, plastic deformation after the record's strongest pulse (between 2.5 and 3.5 sec in the time history acceleration) is clear.

The addition of fixed tie beams at the building's footings did prevent differential horizontal displacements, as expected. The INSTED system's footing displays some sliding, though smaller than in the dynamic experiment of SETUP I, but now the column footings follow its displacement, thus no deformation of the first floor columns, due to differential displacement of footings, is observed. After the strong pulse of Rinaldi record, the central footing obtains a residual displacement of 25mm (Figure 1.31c), while in the record of Takatori, it slides up to 25mm, but then returns back to its initial position, hence displaying zero residual sliding (Figure 1.33c). On the contrary, for the dynamic test of SETUP I, residual horizontal displacement of the central footing after the record of Takatori was measured equal to 40mm.

Since the INSTED system performed so well during the imposed sequence of strong seismic motions and practically did not suffer any damage, the need to test it to the limits arose. In order to lead it to failure, the system's strength should be decreased by gradually reducing the number of fuse elements. The record of Takatori was implemented on every new weakened setup, original or amplified by the factor 1.4. The list of applied seismic motions and the description of the altered setups is displayed in Table 1.5.

As one can observe from the time history of vertical displacements and the Force – Vertical displacements curve (Figures 1.34 and 1.35 respectively), the initial retrofitted building (Setup II), when subjected to the record of Takatori, displays significantly greater strength than Setup IIa (consisting of 2 rods) and Setup IIb (consisting of 1 rod). The two latter ones, seems to behave similarly, reaching almost the same values of maximum strength and vertical rod displacement. However, none of the weakened setups is led to failure, despite the reduction of the system's strength and the considerable vertical rod displacements of Setups IIa and IIb. Hence, we moved on to examine the extreme scenario of imposing the Takatori record -amplified by a 1.4 factor- to the setup consisting of 1 rod (Setup IIb). As clearly depicted in Figure 1.36, the structure proves capable of undertaking values of shear force quite bigger than those receiving during the original Takatori record, even though the fuse element did exceed the yielding point in both motions. In fact, the total strength reached by the structure during the amplified motion of Takatori is comparable to the one measured for the initial Setup II (≈ 0.65kN), which consisted of three rods. It should be mentioned that, at the amplified record of Takatori, Setup IIb did reach failure and one can clearly see the formation of plastic hinges at the ends of the rod's effective length in Figure 1.38.

The aforementioned measurements led to the following conclusion regarding the building's performance: The addition of fixed tie beams enforced uniform displacement of the footings, thus the building's columns were bound to follow this trend. Meanwhile, the INSTED system was able to undertake great values of seismic load and rotate, with the rest of the structure following. Due to a technical defect though, the building's artificial plastic hinges were unable to rotate any further over a specific large value. With the junctions unable to rotate and the footings connected together, the building's columns were not allowed to move independently, attributing thus unrealistic stiffness and strength to the structure. This fact became obvious when the retrofitted Setup IIb, consisting of only one rod, displayed an inexplicably great strength at the amplified record of Takatori, compared to its developed resistance during the actual Takatori record (Figure 1.36). Conclusively, the addition of fixed tie beams between the footings was considered unsuccessful in the case of this experimental setup.

1.4.5 Experiment No. 5 (SETUP III): *Dynamic Test – D_{rod} = 3.2mm*

Trying to diminish the defects of the previous tests, we resulted in Setup III for Experiment No. 5: in this setup, the INSTED system consists of only one rod, in order to display stiffness and strength equivalent to the buildings seismic design requirements. The sequence of seismic motions imposed on the retrofitted structure consists of five records: two Greek moderate ones *(MNSA, Athens 1999 & Lefkada 2003)* and three strong ones *(Rinaldi 1994, Jma 1995 & Takatori 1995)*, in ascending order. The reason for imposing the Greek records to our model is to verify that the proposed retrofit behaves well under moderate seismic motions, which the original building would not withstand (such as the *Lefkada 2003* record).

Fixed tie beams are again added between the frame footings (until the record of Jma), in order to prevent deformation of the first floor columns and are removed before the last two strong motions, to ensure that jamming of junctions will be avoided.

Results

As expected, the retrofitted building displays an excellent behavior during the moderate records of MNSA and Lefkada. Not only does it not experience failure during Lefkada 2003 record, but as depicted in Figure 1.40b, its deformation is insignificant. The measured data come to verify this conclusion. The structure reaches a maximum shear force of ≈ 0.15 – 0.20 kN, while the residual vertical displacement of rods is equal to *Δv = 1mm* (Figures 1.42c and 1.42b respectively). Additionally, residual interstorey drifts do not exceed the value of *2mm* or *0.5%* in terms of interstorey drift ratio (Figures 1.43a and 1.43b). Sliding of the central footing is negligible after the record of Lefkada (≈ 0.5mm).

Moving on to the strong shaking scenario of Rinaldi, the building also demonstrates very good behavior. During the record's strong pulse (between 2.5 and 3.5 sec), the structure reaches a maximum force of *0.6 kN* (Figure 1.44c) and the horizontal rods enter the plastic zone, accumulating residual vertical displacement of *Δv = 5 mm* (Figure 1.44b). The anticipated dissipation of energy takes place, and one can observe the hysteresis loop forming in the respective Force – Vertical displacement curve of Figure 1.44c. Residual interstorey drifts are measured equal to *10mm* or *3%* in terms of drift ratio and it is obvious from Figures 1.45a and 1.45b that the INSTED system has indeed led to a uniform distribution of damage, by homogenizing drifts in all three storeys. The central footing's sliding is again insignificant (≈ 0.8mm).

Finally, the structure manages to resist failure even after the last record – the extreme seismic motion of Takatori. Despite its apparent deformation (Figure 1.41b), - which is surely exacerbated by the removal of tie beams after the record of Rinaldi - residual interstorey drifts do not exceed the value of *15mm* or *5%* in terms of drift ratio. In addition, the horizontal fuse elements do enter the plastic zone and display ductile behaviour, by obtaining a residual vertical displacement of *7mm;* clearly, though, they are not led to failure. The maximum force reached by the retrofitted setup is approximately equal to *0.5 kN* (Figure 1.46c).

Beyond doubt, the fact that Setup III resisted all of the implemented motions, without collapsing is impressive, but does not come along with the calculated predictions for the retrofitted model's total strength. Despite the removal of tie beams during the last two motions, it might be the case that the building's junctions stopped rotating freely from earlier on, leading to an increase of the system's resistance and thus, to the non-failure situation after the Takatori record.

1.4.6 SETUP II vs. SETUP III

In order to get a more complete understanding of the INSTED system's dynamic behavior, a comparison between the performance of Setup II (retrofitted by a 3-rod INSTED system) and Setup III (retrofitted by a 1-rod INSTED system) is made, for the record of *Rinaldi*. During this record, both setups are equipped with tie beams at the base and have a d = 3.2mm rod diameter, thus the comparison is made under the same terms. Also, the artificial plastic hinges have not jammed until the record of Rinaldi, therefore, the strength of the system is exclusively attributed to the design of the INSTED system, rather than to any fictitious resistance of the building.

As depicted in Figures 1.49a and 1.49b, both model structures exceed the limits of elasticity and behave in a ductile manner, displaying permanent rod deformations translated into measured relative vertical displacements. Setup II reaches a maximum force of *0.85 kN (or 0.6g in terms of acceleration)*, while Setup III reaches a maximum value of *0.6 kN (or 0.4g in terms of acceleration)*. As one can also observe in the 3rd floor acceleration time history (Figure 1.50b), Setup II develops indeed slightly greater acceleration values (of about 0.2g) compared to the ones developed by Setup III; this behavior is expected, since Setup II is a structural system of greater stiffness and horizontal resistance.

As far as the vertical rod displacement is concerned, Setup II displays a residual value of *3mm* after the record's strong pulse, while Setup III seems to respond quite more intensely: at the beginning of the pulse it displays a displacement of $\Delta v \approx 8$ mm and then acquires a residual value of *Δv ≈ 5mm* towards the opposite direction (Figure 1.50c). At this point, the horizontal fuse elements of Setup III apparently experience a more severe deformation and are challenged - to a greater extent - to behave in a ductile manner. Finally, in terms of 3rd floor interstorey drifts, Setup II reaches a residual interstorey drift ratio of *1.5 %*, while Setup III displays twice this value, thus *≈ 3%* (Figure 1.50a).

Undoubtedly, between the two Setups lies an obvious difference in strength, which is also apparent in the values of residual interstorey drifts, vertical rod displacements and accelerations. Setup III is proved weaker, leading the building and the rods to more severe deformations. However, someone would wonder whether this difference in strength is actually corresponding to the one expected. The main goal of our retrofitting proposal was to equip the original building with a horizontal resistance system that would be able to undertake the majority of seismic loading and localize the damage to its horizontal fuse elements. Thus, the building of Setup II (3 rods per frame) should be expected to display approximately 3 times greater strength than the one of Setup III (1 rod per frame). This estimation goes well with the analytical calculations of the horizontal resistance developed by the INSTED systems of each experimental setup (Table 1.) However, the assumption was not verified by the experiments, where we witnessed the retrofitted building of Setup III being able to sustain even the extreme shaking scenario of Takatori and display significant resistance values - much higher than the 1/3 of those developed by Setup II.

In order to obtain a deeper understanding of the possible defects of the experimental setups, which might have led to the aforementioned deviations from the expected results, an additional series of analyses is conducted. In these analyses, the retrofitted model building is simulated with its exact material and technical properties and then submitted to the same type of loading that was used in the experimental series. Comparison of the analytical and experimental results follows in the next chapter.

Chapter B.1

Figures

(a)

(b)

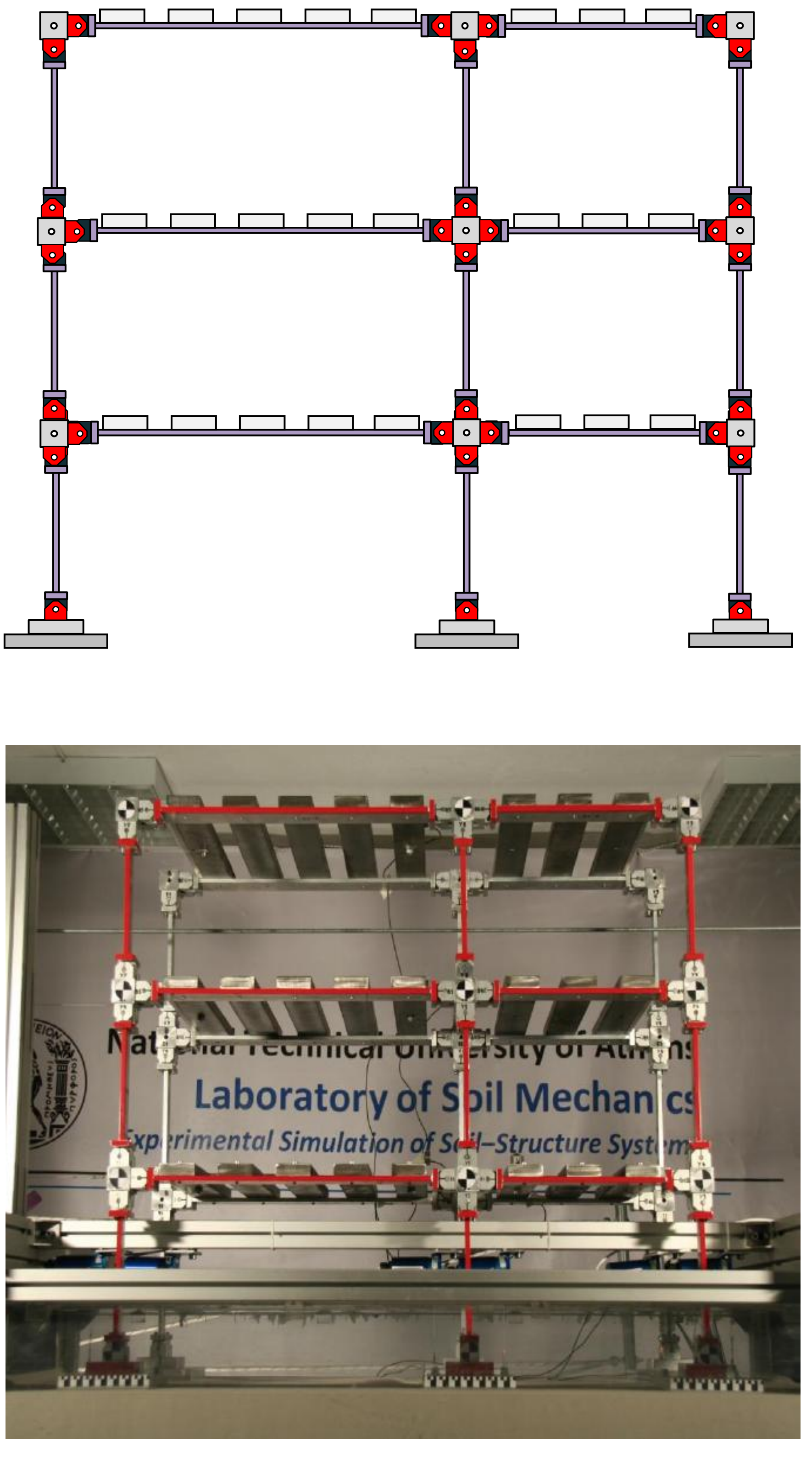

Figure 1.1 (a) Schematic illustration of the original frame and **(b)** photograph of the experimental setup of the original frame.

(a)

(b)

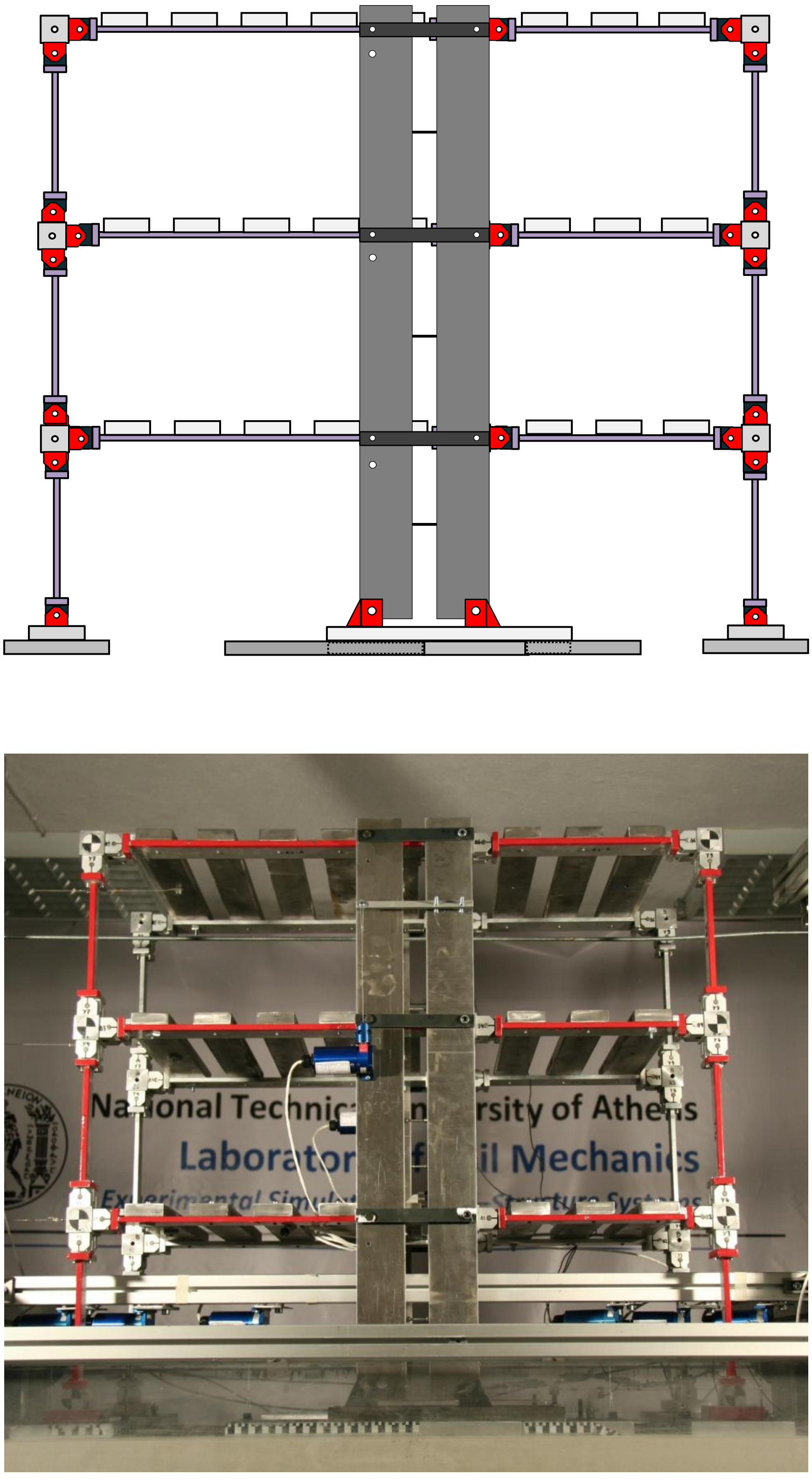

Figure 1.2 (a) Schematic illustration of the retrofitted frame and **(b)** photograph of the experimental setup of the retrofitted frame.

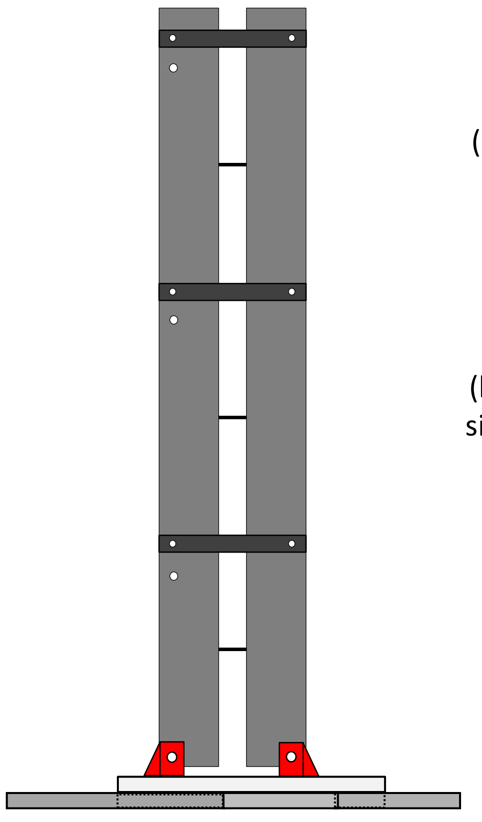

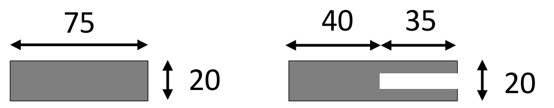

(a) Typical cross sections of the INSTED columns.

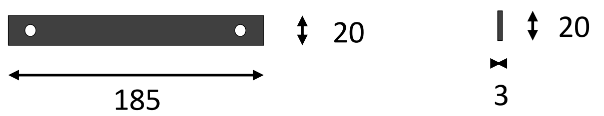

(b) Plan and typical crossection of the bars placed to simulate the diaphragmatic function of storey plates.

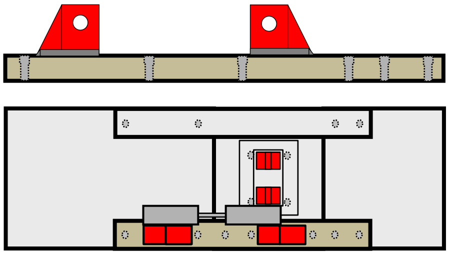

(c) Plan & facade of the INSTED foundation.

Figure 1.3 The INSTED system , its foundation & its parts as designed according to the regulations.

Figure 1.4 Typical geometry of the horizontal rods used in the experiments.

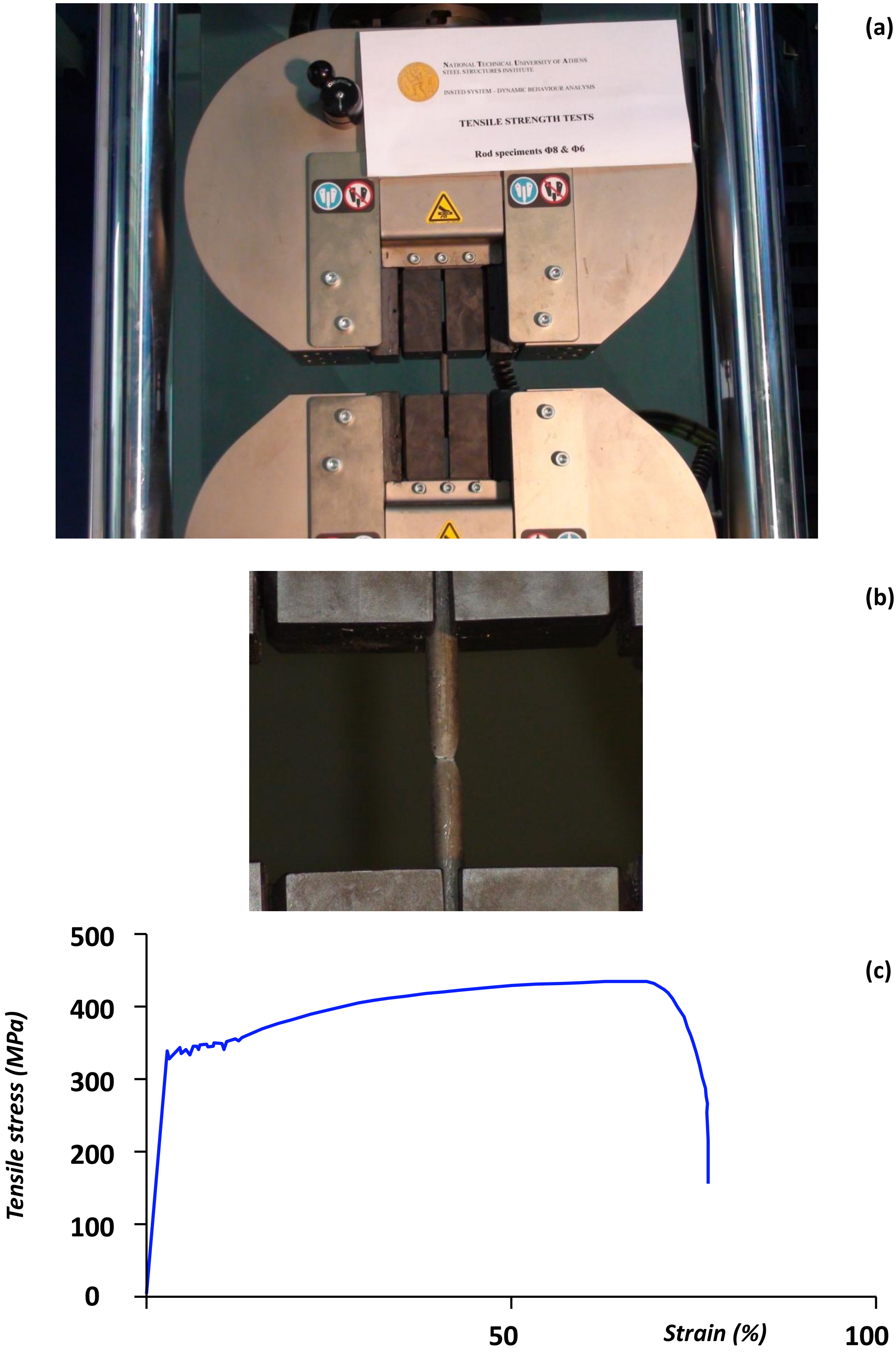

Figure 1.5 (a) & (b) Photographs of the tensile strength test of the Φ8 specimen, conducted in the Steel Structures Laboratory and **(c)** the respective tensile stress – strain curve derived from the test.

(a)

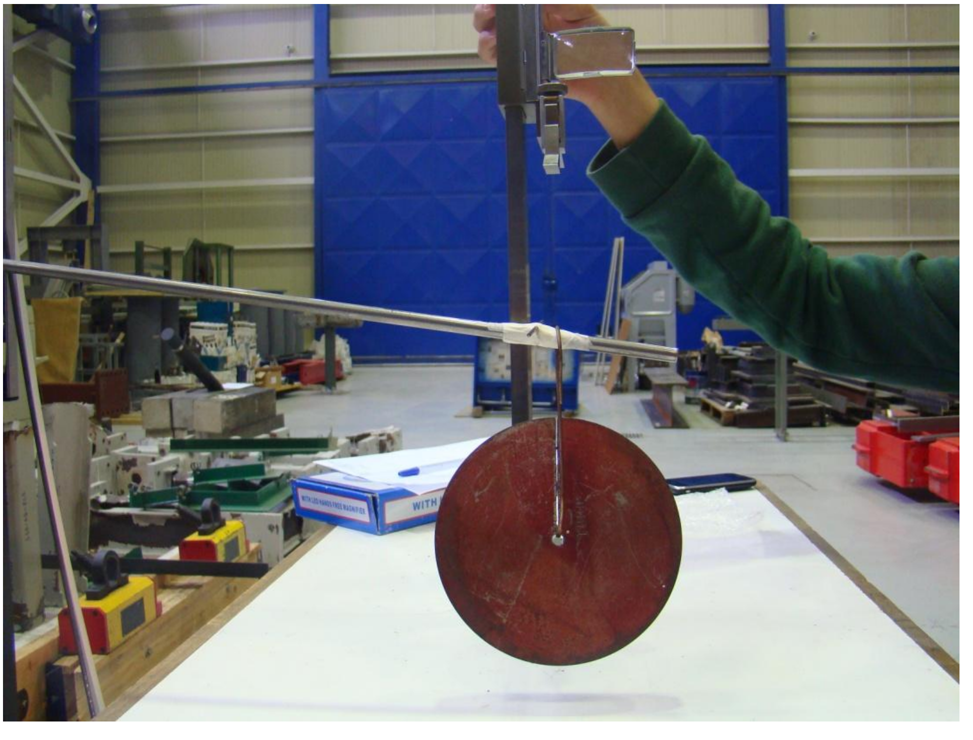

(b)

Figure 1.6 (a) & (b) Photographs of the test conducted on the Φ8 specimen, in order to determine the rod’ s actual elastic modulus.

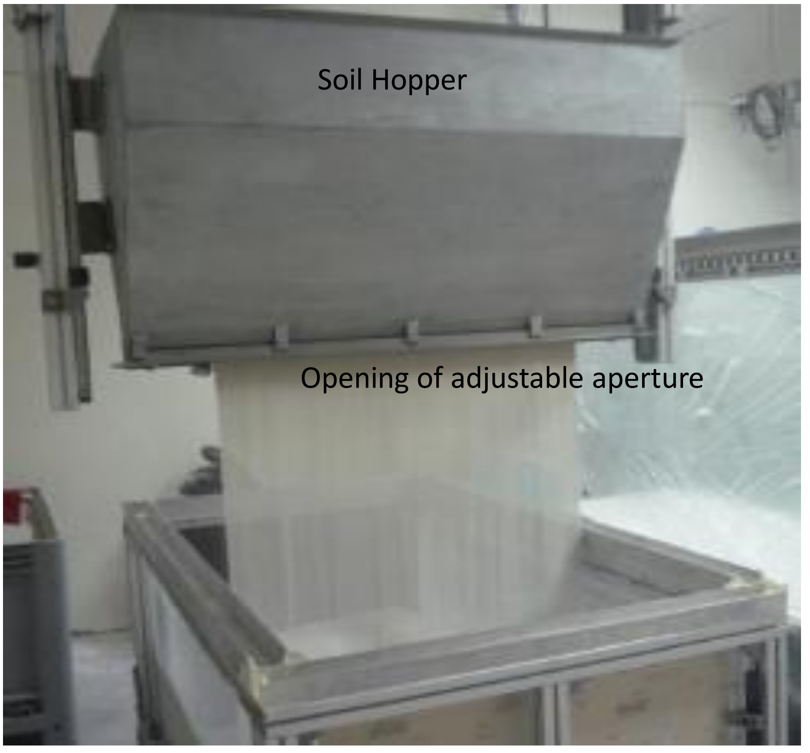

(a)

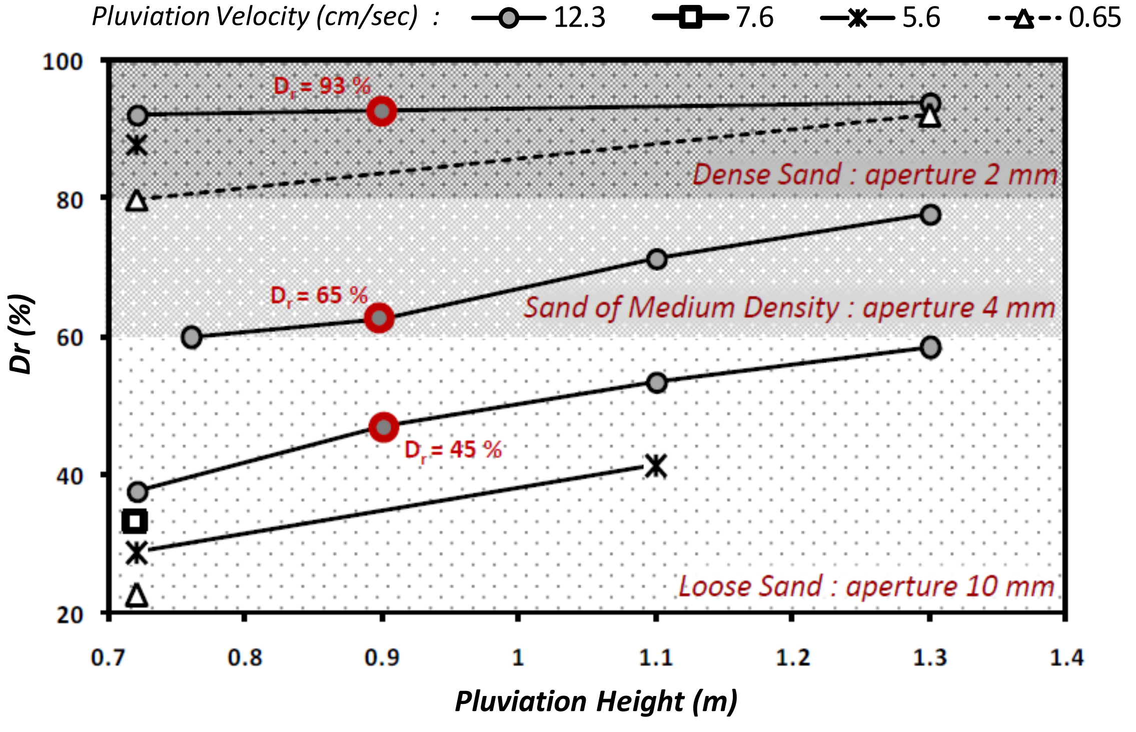

(b)

Figure 1.7 (a) Photograph of the sand raining system **(b)** Summary of pluviation results: relative density Dr versus pluviation height, raining speed and opening aperture size.

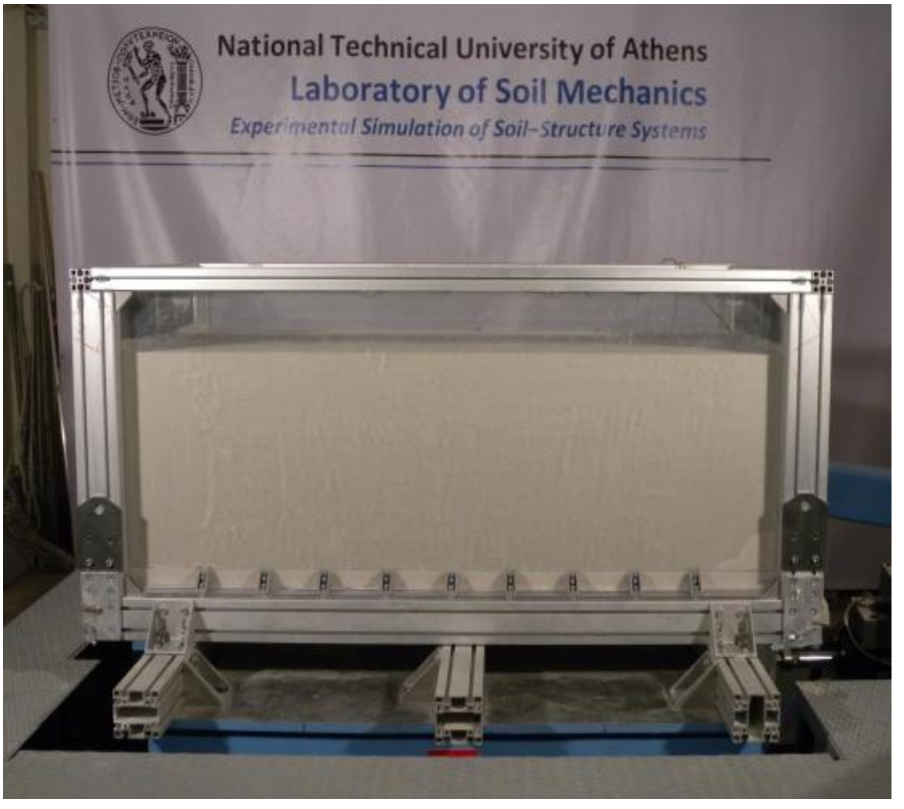

Figure 1.8 Photograph and schematic illustration of the sandbox used in the experiments.

Figure 1.9 Photograph of the Laboratory's shaking table.

Figure 1.10 Photograph of the pushover apparatus.

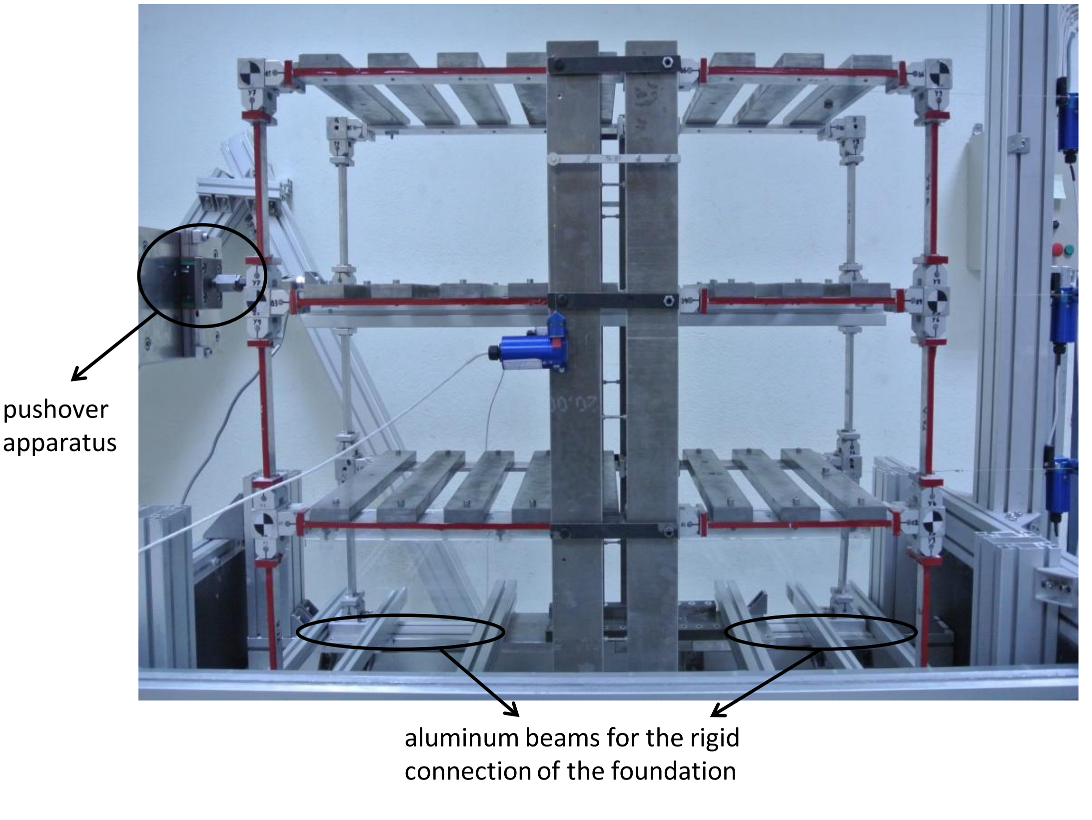

Figure 1.11 Photograph of the experimental setup for the pushover experiments.

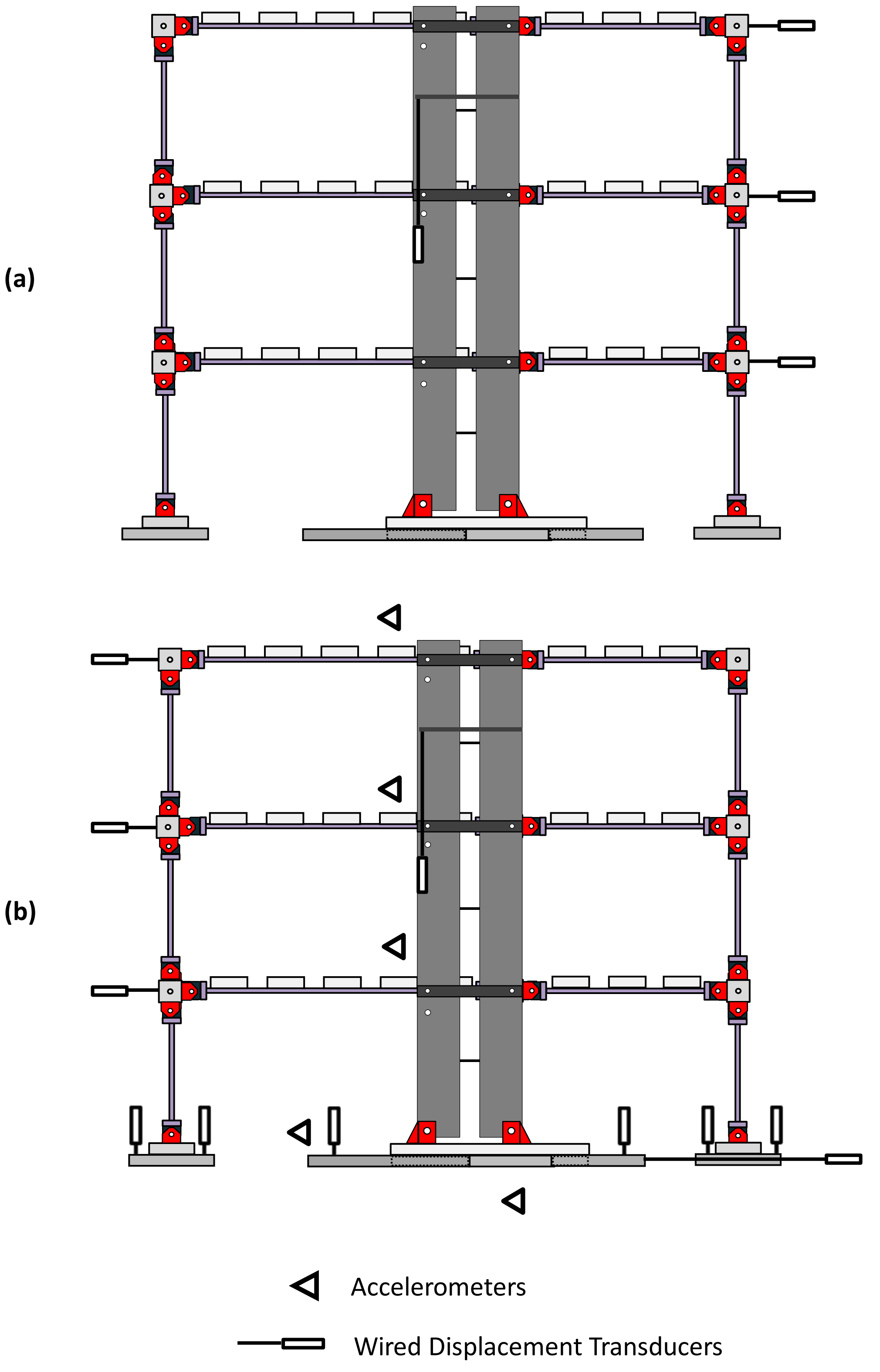

Figure 1.12 (a) Schematic illustration of the instrumentation of the model during the pushover tests **(b)** Schematic illustration of the instrumentation of the model during the dynamic experiments.

Figure 1.13 Photographs of the wired displacement transducers (up) and accelerometers (down) used in the experiments.

Table 1.1. List of Horizontal Pushover Experiments.

Description of Experiment					
Model	**Exp.**	**INSTED system**		**Soil**	**Type of Loading**
		Rods per frame	D (mm)		
Retrofitted Building (SETUP I)	1	3	4.0	-	Slow Cyclic
Retrofitted Building (SETUP II)	3	3	3.2	-	Slow Cyclic

Table 1.2. List of Dynamic Experiments.

Description of Experiment					
Model	**Exp.**	**INSTED system**		**Soil**	**Excitation**
		Rods per frame	D (mm)		
Retrofitted Building (SETUP I)	2	3	4.0	Dense Sand	Strong Seismic
Retrofitted Building (SETUP II)	4	3	3.2	Dense Sand	Strong Seismic
Retrofitted Building (SETUP III)	5	1	3.2	Dense Sand	Moderate & Strong Seismic

Horizontal Pushover Tests – Loading Protocols

1 – CYCLE PUSHOVER TEST

# Cycles	1
Δx (mm)	30
Δt (sec)	300

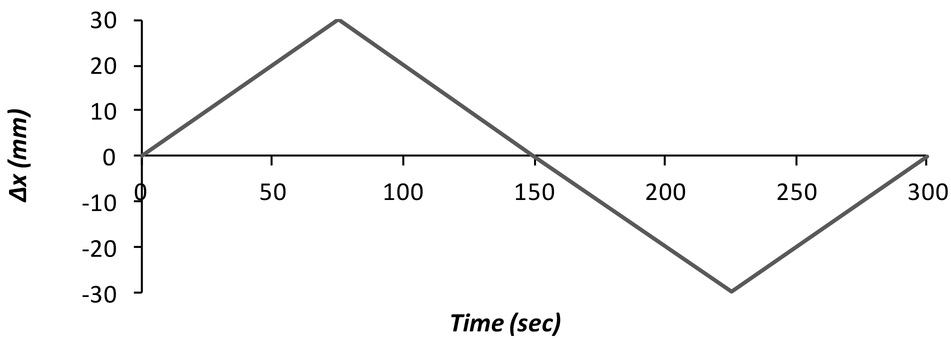

SLOW - CYCLIC PUSHOVER TEST

# Cycles	1	2	3	4	5	6	7	8	9	10	11	12	13
Δx (mm)	2	4	6	8	10	12	14	16	18	20	25	30	40
Δt (sec)	20	40	60	80	100	120	140	160	180	200	250	300	400

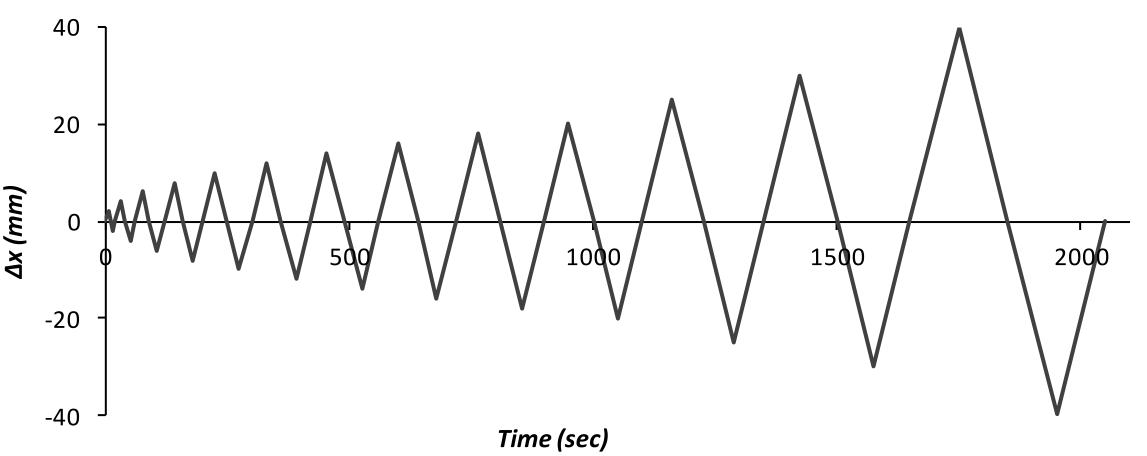

Figure 1.14 Loading protocols of the 1-cycle & slow - cycling pushover tests. In the slow-cycling pushover test of D_{rod} = 3.2mm, the loading procedure ended at cycle no. 10 (for imposed displacement equal to Δx = 20mm).

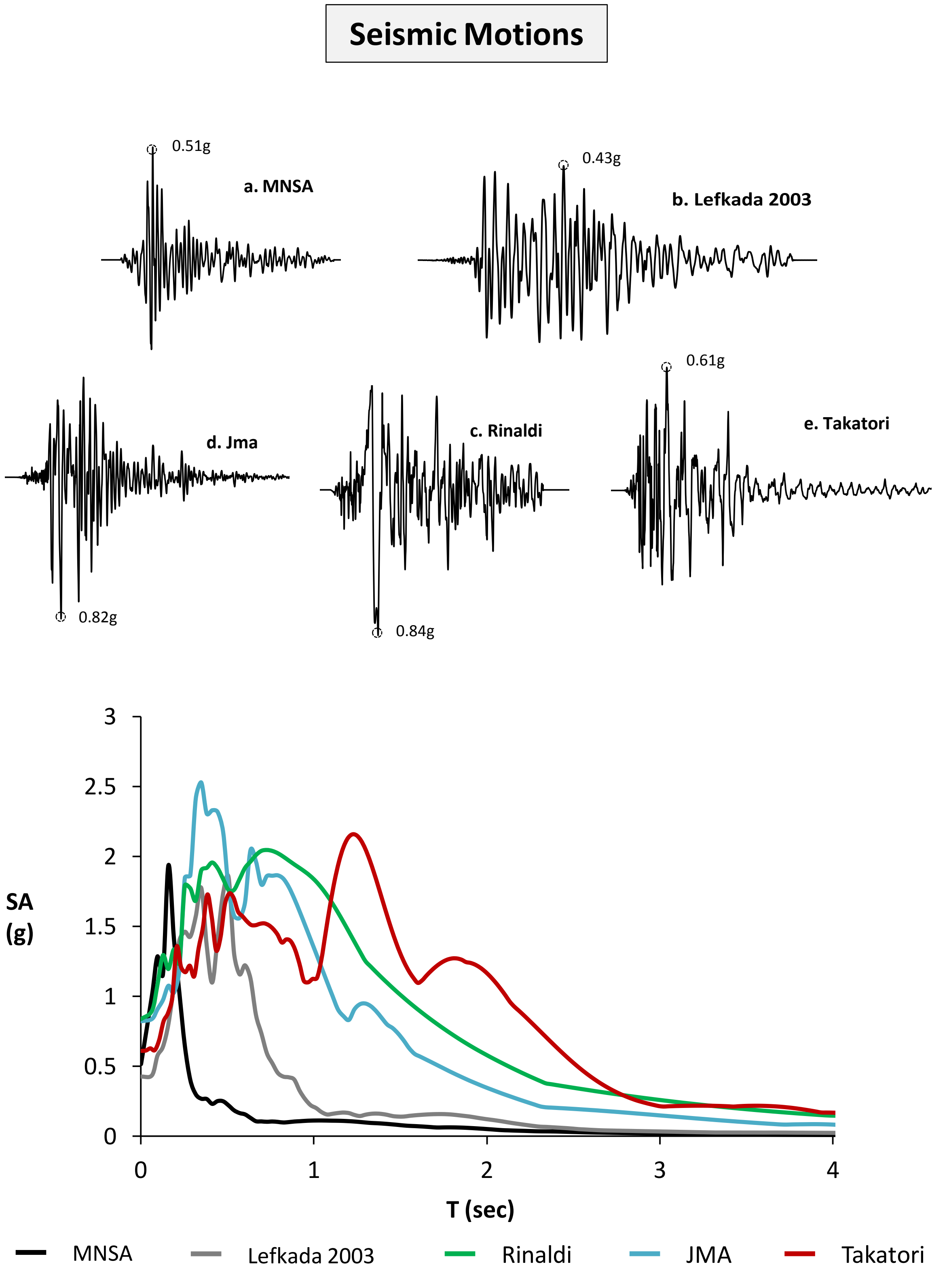

Figure 1.15 The five real seismic records used in the experimental series and their elastic spectral accelerations.

Table 1.3

Calculated horizontal shear force undertaken by ***the INSTED system*** of each experimental setup

Total shear force ▸ $$F = \sum_{n=1}^{N} Mpl \frac{2 \times b}{h \times leff}$$

Rod bending moment ▸ $$Mpl = Wpl \times fy = \frac{d^3}{6} \times fy$$

SETUP I

- L_{eff} = 2.5 cm
- N = 3 rods
- h = 30 cm
- D = 0.4 cm
- b = 15 cm
- f_y = 347 MPa

M_{pl} = 0.0037 kNm

Per frame: F = 0.44 kN

Total: F = 0.88 kN

SETUP II

- L_{eff} = 2.0 cm
- N = 3 rods
- h = 30 cm
- D = 0.32 cm
- b = 15 cm
- f_y = 347 MPa

M_{pl} = 0.0019 kNm

Per frame: F = 0.28 kN

Total: F = 0.56 kN

SETUP III

- L_{eff} = 2.0 cm
- N = 1 rod
- h = 30 cm
- D = 0.32 cm
- b = 15 cm
- f_y = 347 MPa

M_{pl} = 0.0019 kNm

Per frame: F = 0.095 kN

Total: F = 0.19 kN

EXPERIMENT No. 1
Horizontal Pushover Test
D_{rod} = 4mm

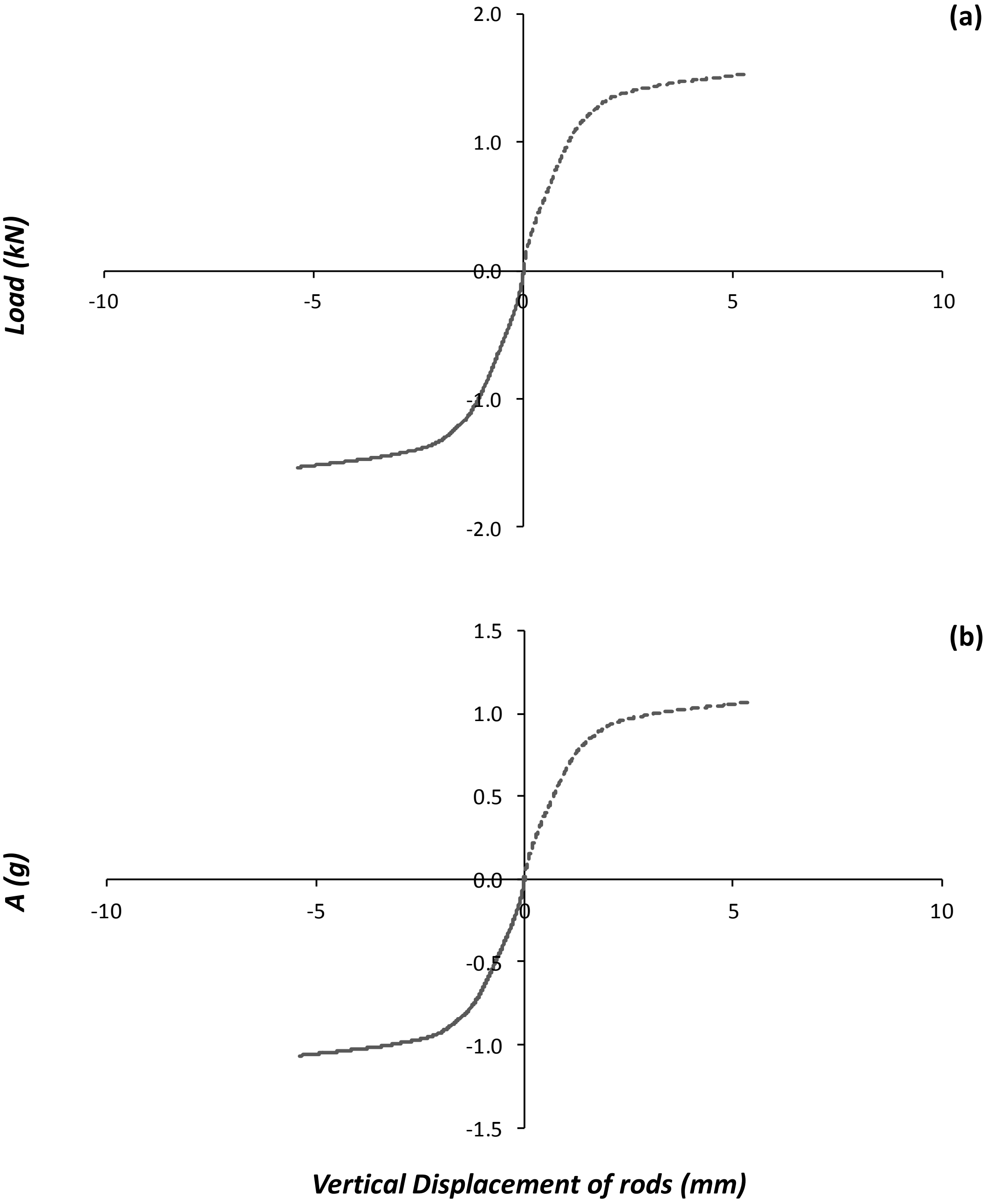

Figure 1.16 Load – vertical displacement and Acceleration – vertical displacement curves derived from the **1-cycle pushover test** of the retrofitted frame (The dashed branch is not a result of measured data, but it is formed that way because the building is considered to behave symmetrically).

EXPERIMENT No. 1

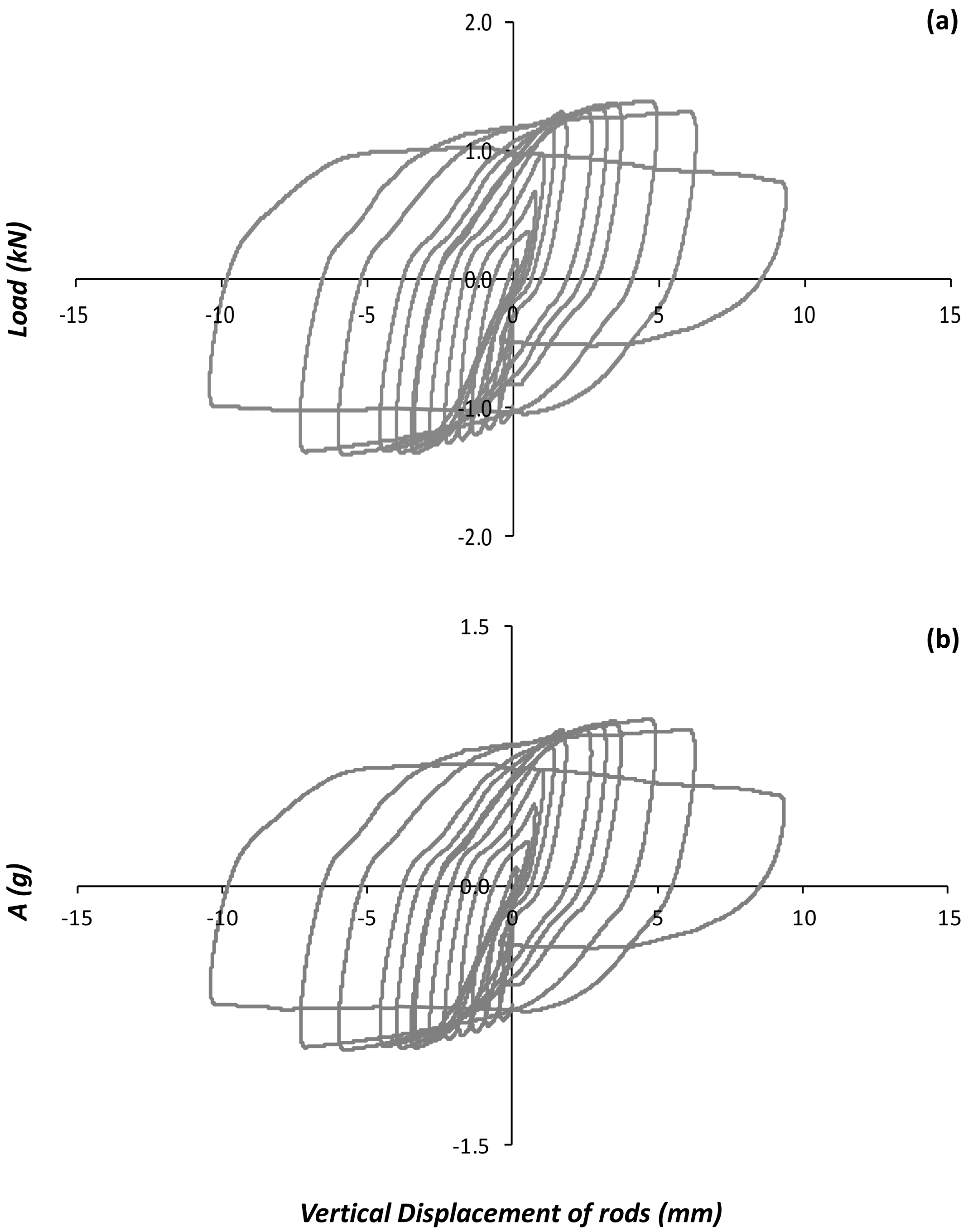

Figure 1.17 Load – vertical displacement and Acceleration – vertical displacement curves derived from the **slow-cyclic pushover test** of the retrofitted frame.

EXPERIMENT No. 1

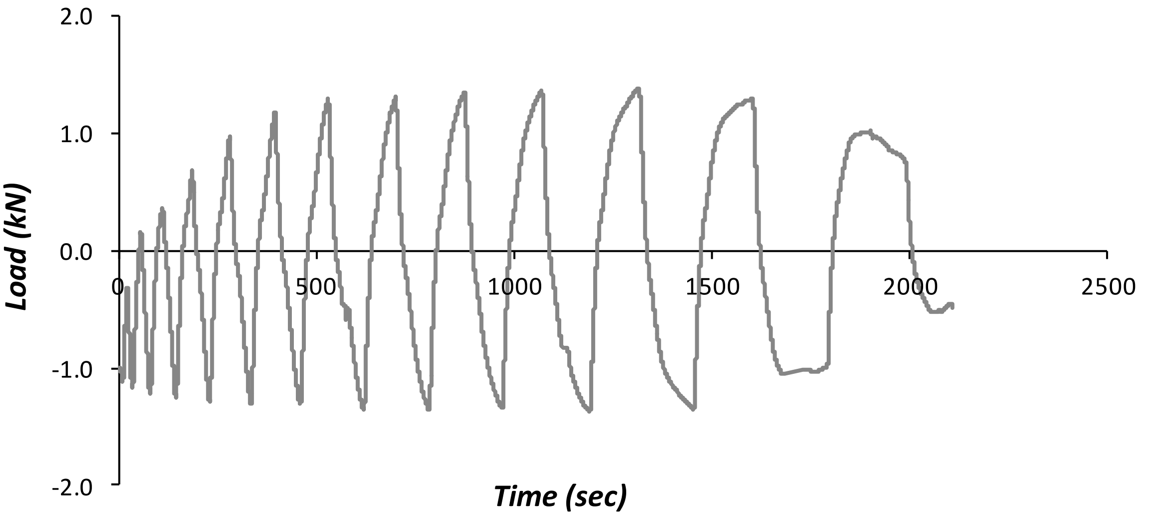

Figure 1.18 Load – Time curve derived from the slow - cyclic pushover test of the retrofitted frame.

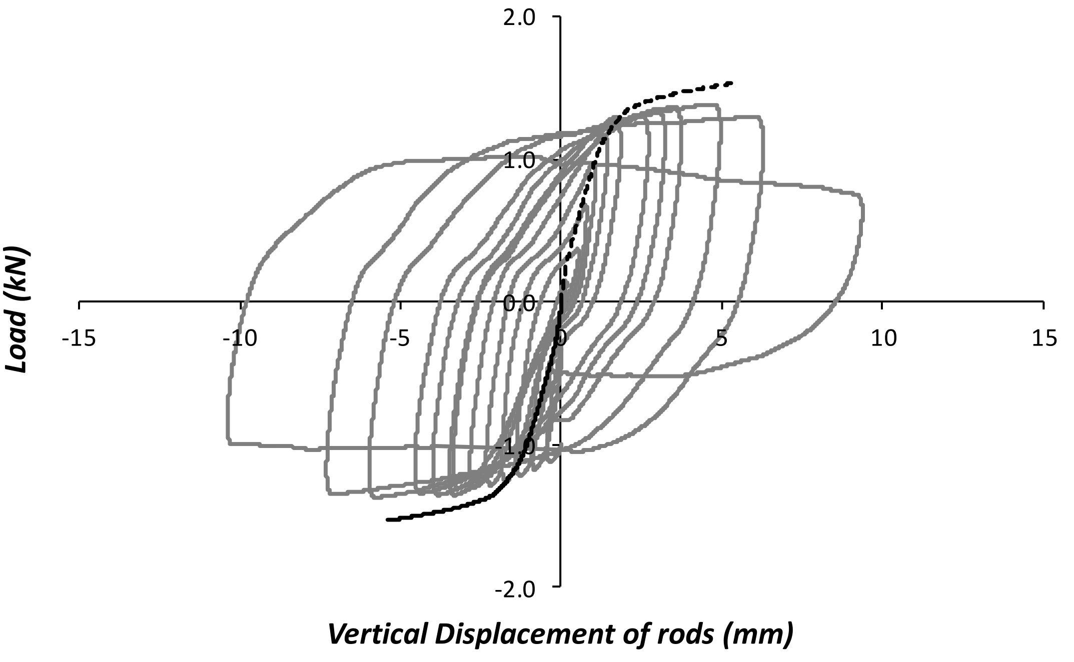

Figure 1.19 Comparison of the monotonic and slow – cyclic pushover tests in terms of strength and ductility.

	F_{yield} (kN)	F_{max} (kN)	a_{yield} (g)	a_{max} (g)
D = 4mm	1.20	1.50	0.83	1.0

Table 1.4 Results of the 1st Horizontal Pushover Test. By translating load into acceleration, an estimation of the system's pseudostatical yielding & maximum acceleration is made.

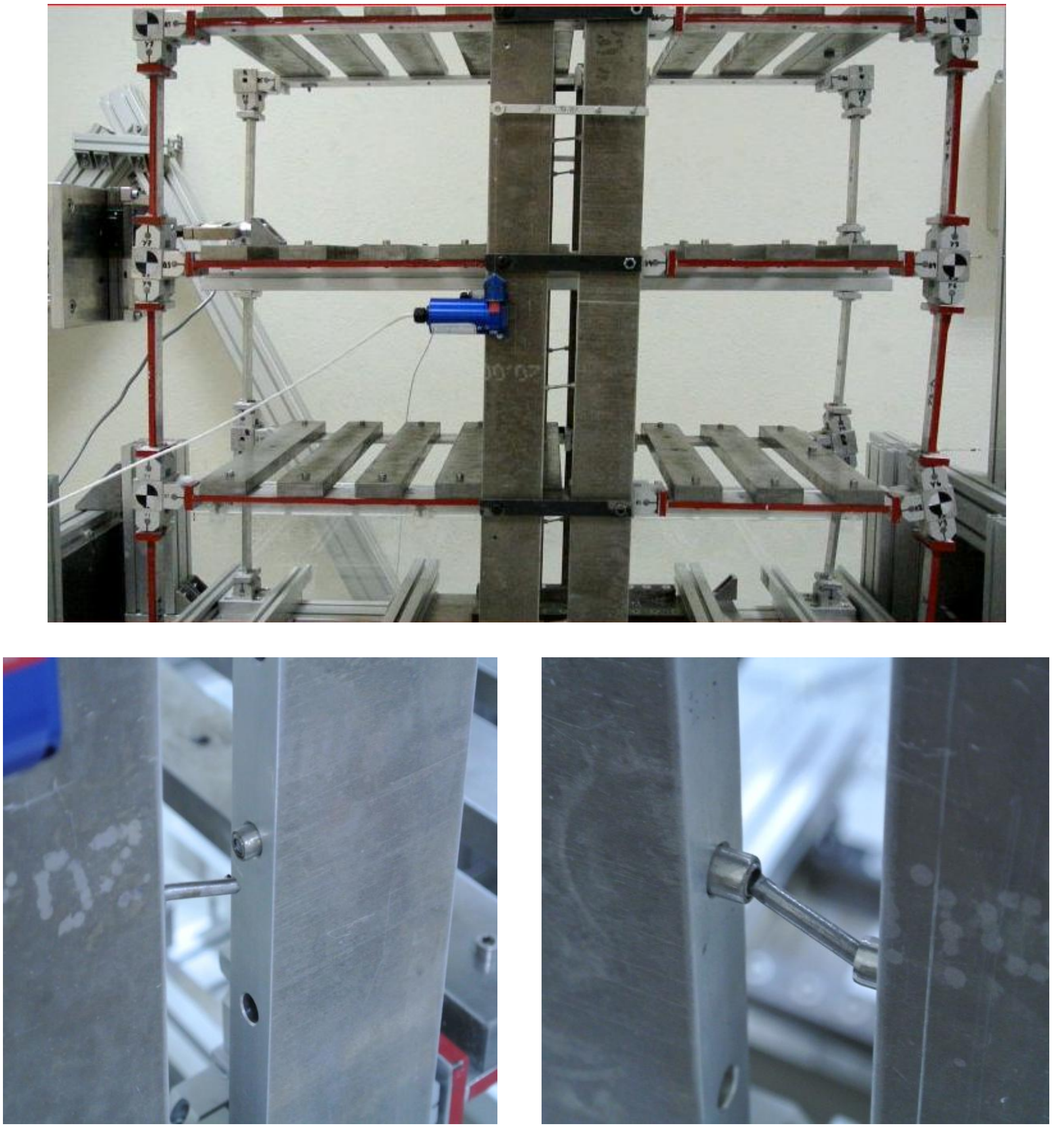

Figure 1.20 Photograph of the deformed shape of the retrofitted building at the end of the slow – cyclic pushover test and detail of the horizontal rods after their failure.

EXPERIMENT No. 2
Retrofitted building (SETUP I)
Dynamic Test

List of applied seismic records.

Strong Seismic Records
Rinaldi (Northridge 1994)
JMA (Kobe 1995)
Takatori (Kobe 1995)

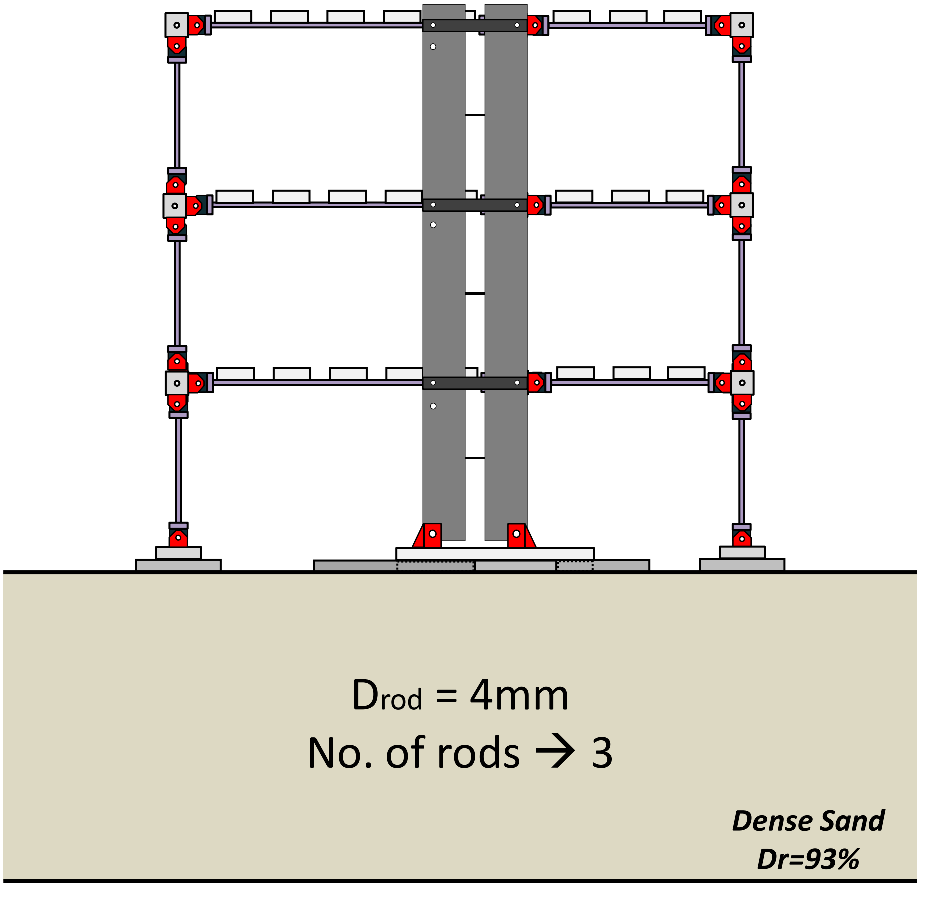

Figure 1.21 Schematic illustration of SETUP I.

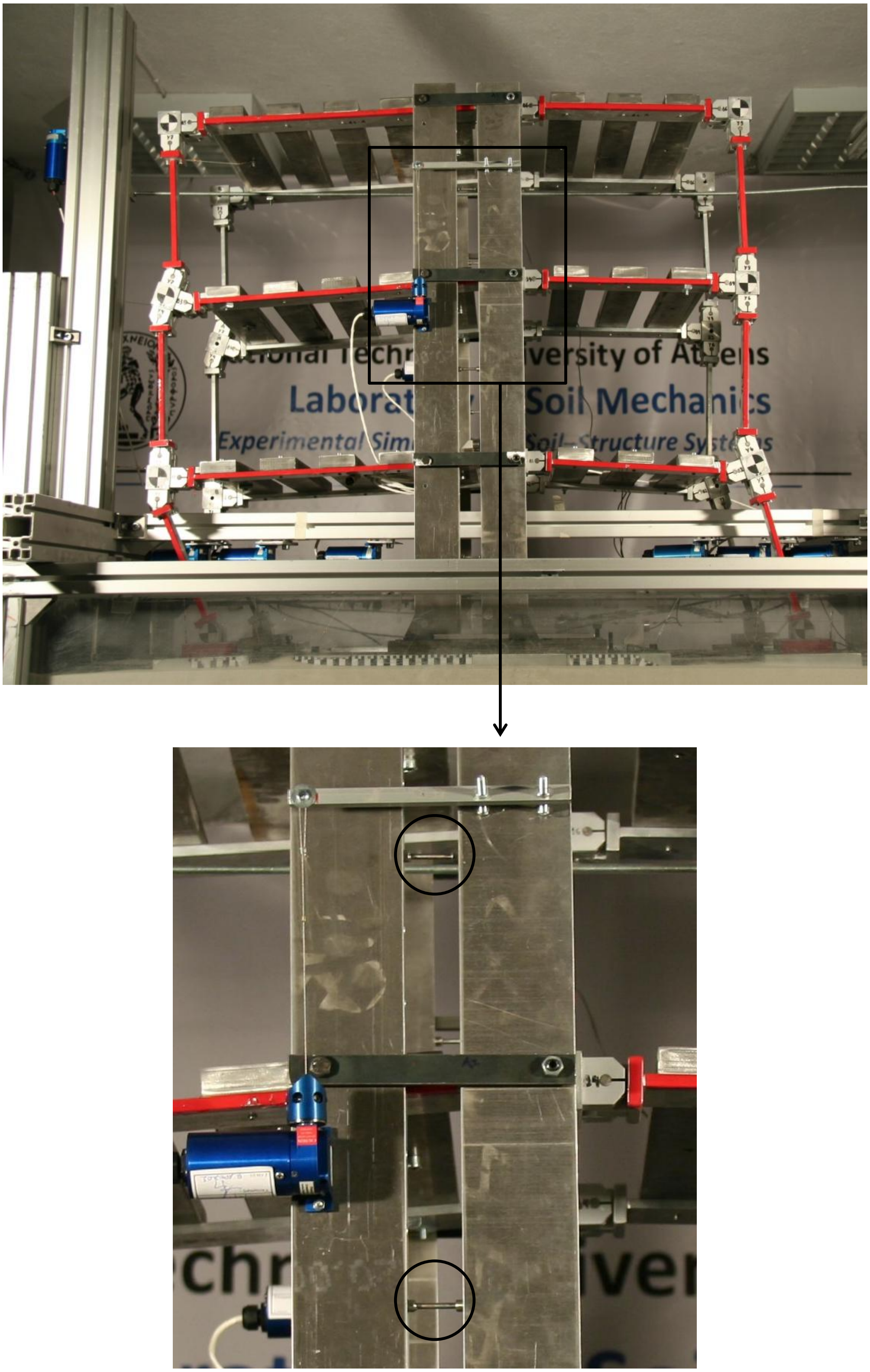

Figure 1.22 Photograph of the deformed shape of the model building after the record of Takatori – Detail of the horizontal rods.

EXPERIMENT No. 2

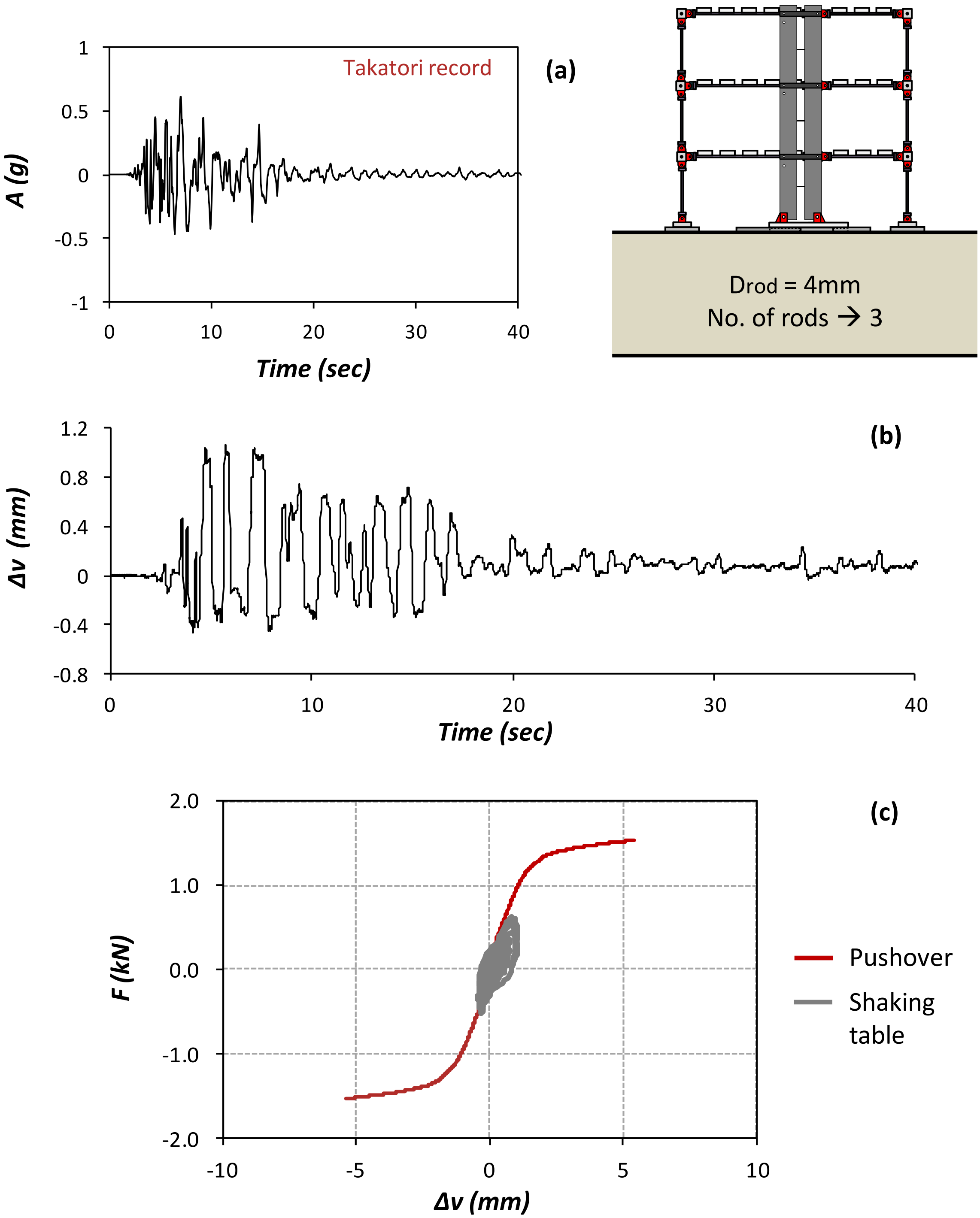

Figure 1.23 (a) Takatori record **(b)** Time history of the vertical displacement of rods and **(c)** Total shear force – vertical displacement curve for the *Takatori record*, compared with the one derived from the respective pushover test.

EXPERIMENT No. 2

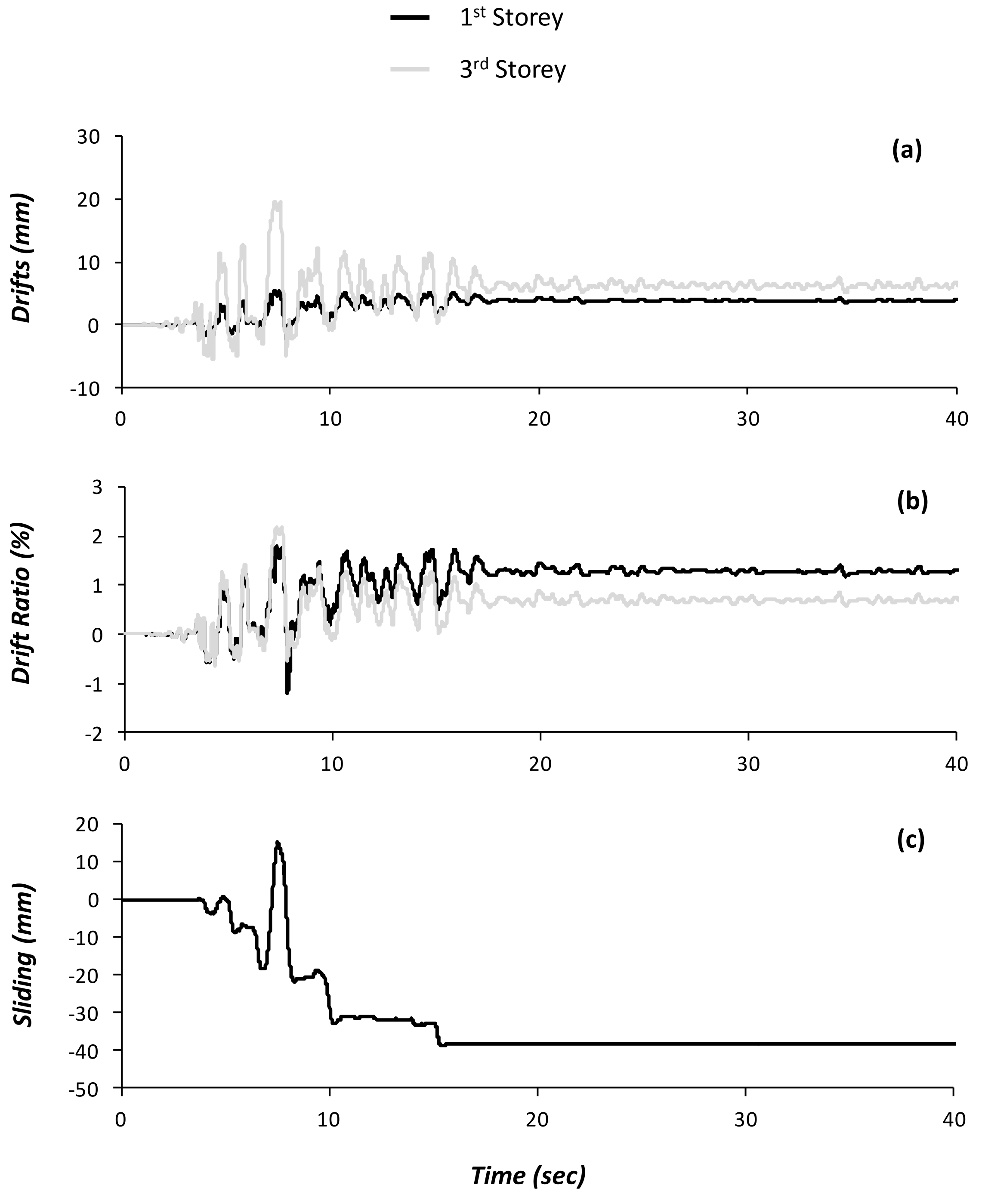

Figure 1.24 Time-histories of **(a)** the drifts at the level of the 1st and 3rd floor, **(b)** the respective drift ratios and **(c)** the sliding of the central footing, for the *Takatori record*.

EXPERIMENT No. 3
Horizontal Pushover Test
D_{rod} = 3.2mm

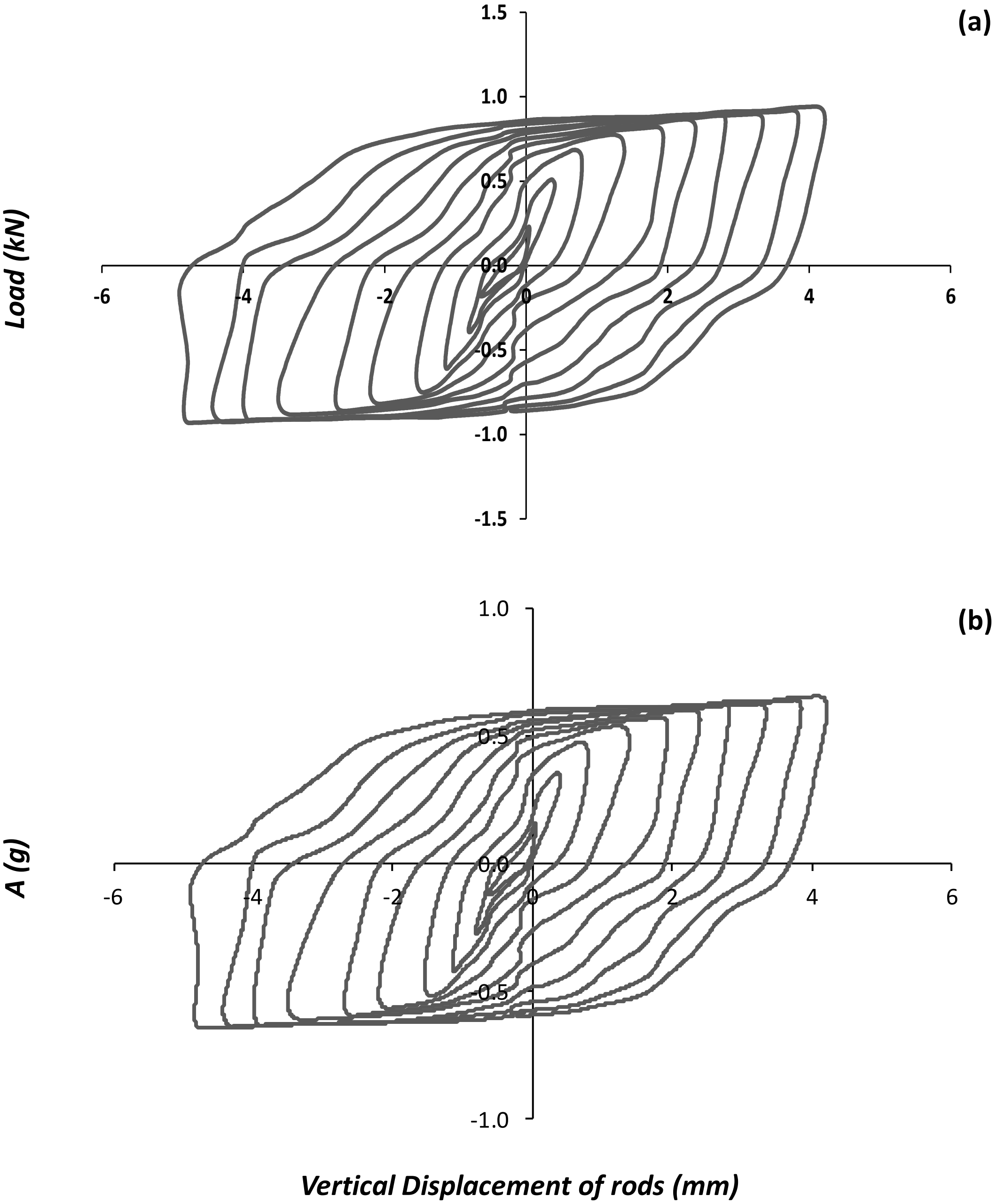

Figure 1.25 Load – vertical displacement and Acceleration – vertical displacement curves derived from the **slow - cyclic pushover test** of the retrofitted frame (SETUP II).

EXPERIMENT No. 3

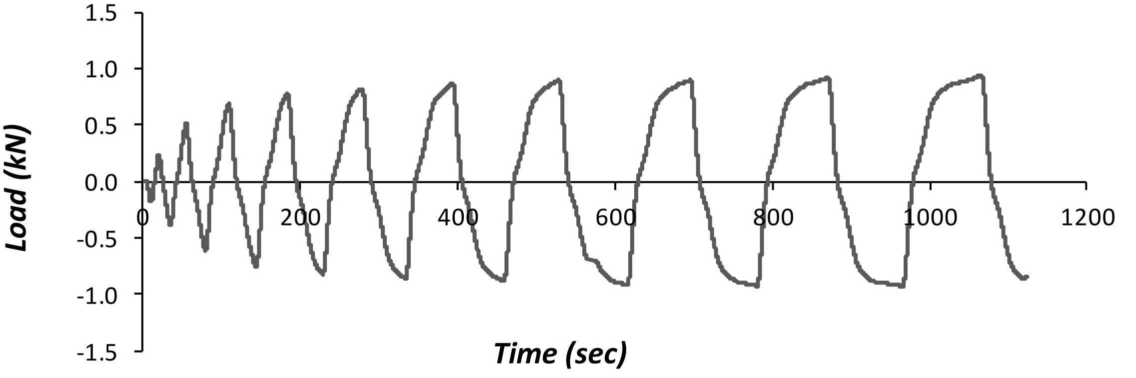

Figure 1.26 Load – Time curve derived from the slow - cyclic pushover test of the retrofitted frame (SETUP II).

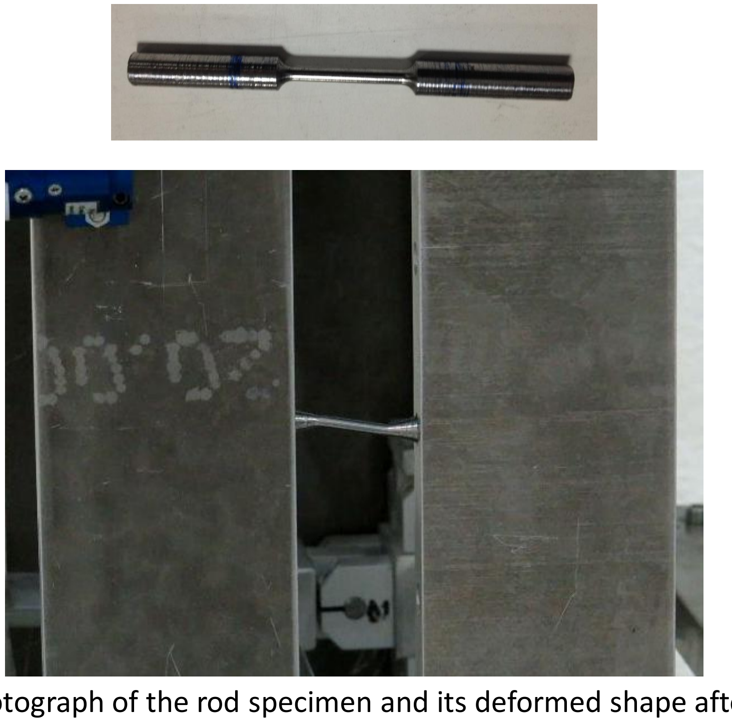

Figure 1.27 Photograph of the rod specimen and its deformed shape after loading.

Table 1.4 Results of the 2nd Horizontal Pushover Test (SETUP II).

	F_{yield} (kN)	F_{max} (kN)	a_{yield} (g)	a_{max} (g)
D = 3.2mm	0.70	0.90	0.49	0.63

EXPERIMENT No. 4
Retrofitted building (SETUP II)
Dynamic Test

List of applied seismic records.

Strong Seismic Records
Rinaldi (Northridge 1994)
JMA (Kobe 1995)
Takatori (Kobe 1995)

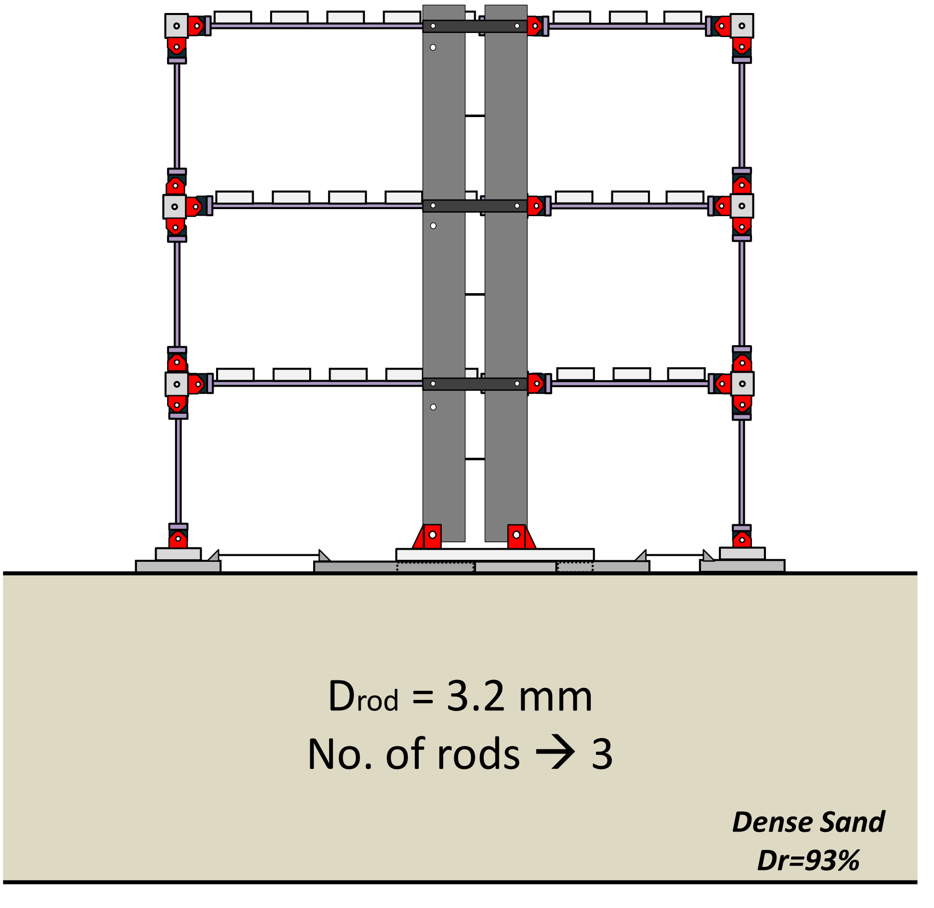

Figure 1.28 Schematic illustration of SETUP II.

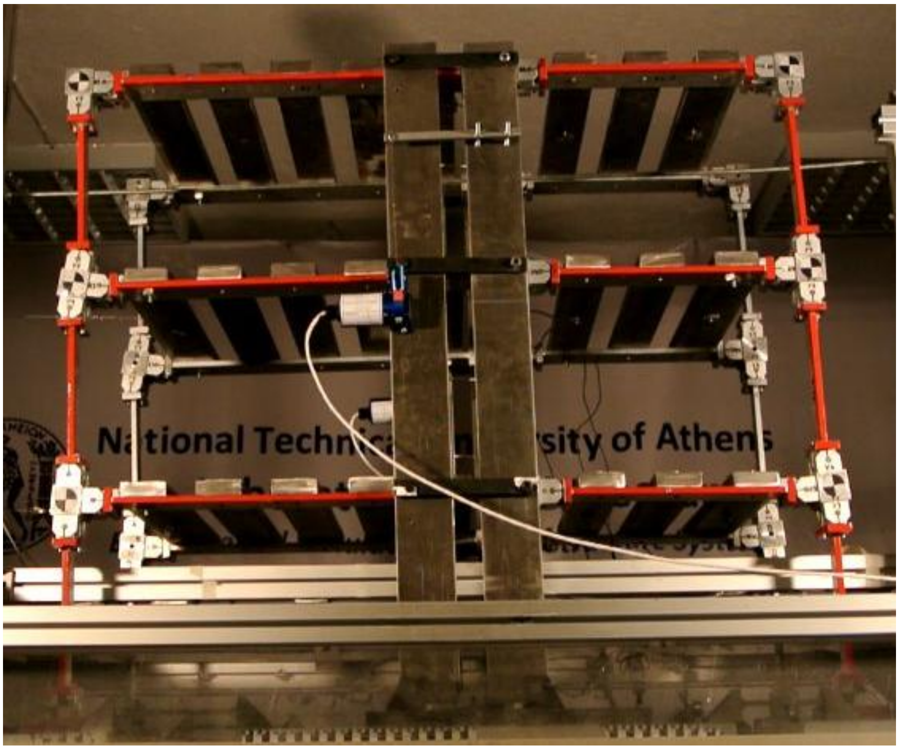

(a)

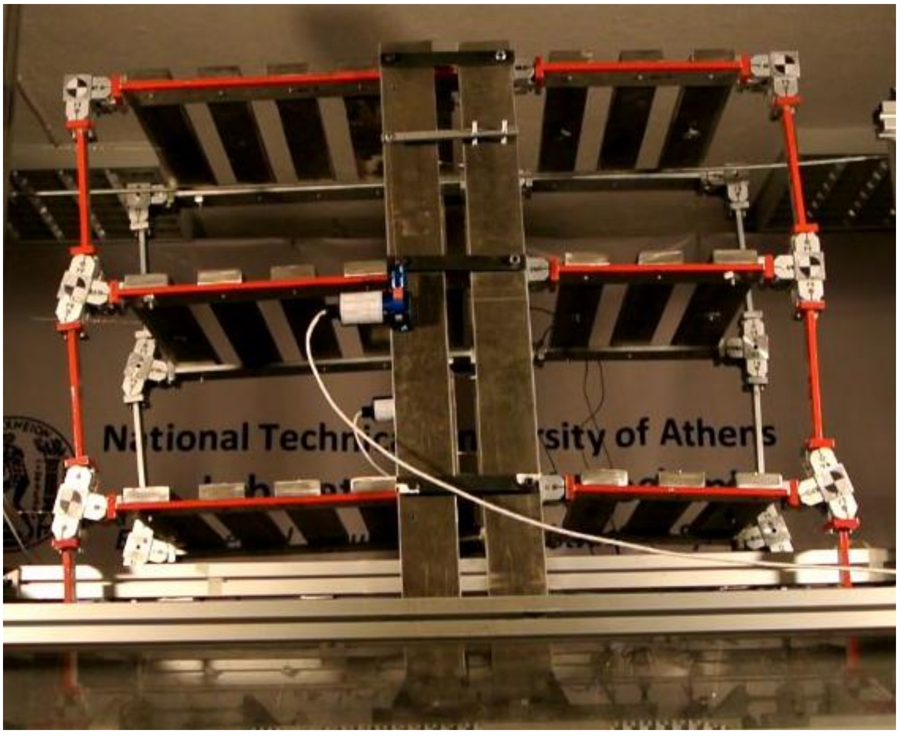

(b)

Figure 1.29 Deformed shape of the retrofitted building **(a)** after the record of *Rinaldi* and **(b)** after the record of *Takatori*.

EXPERIMENT No. 4

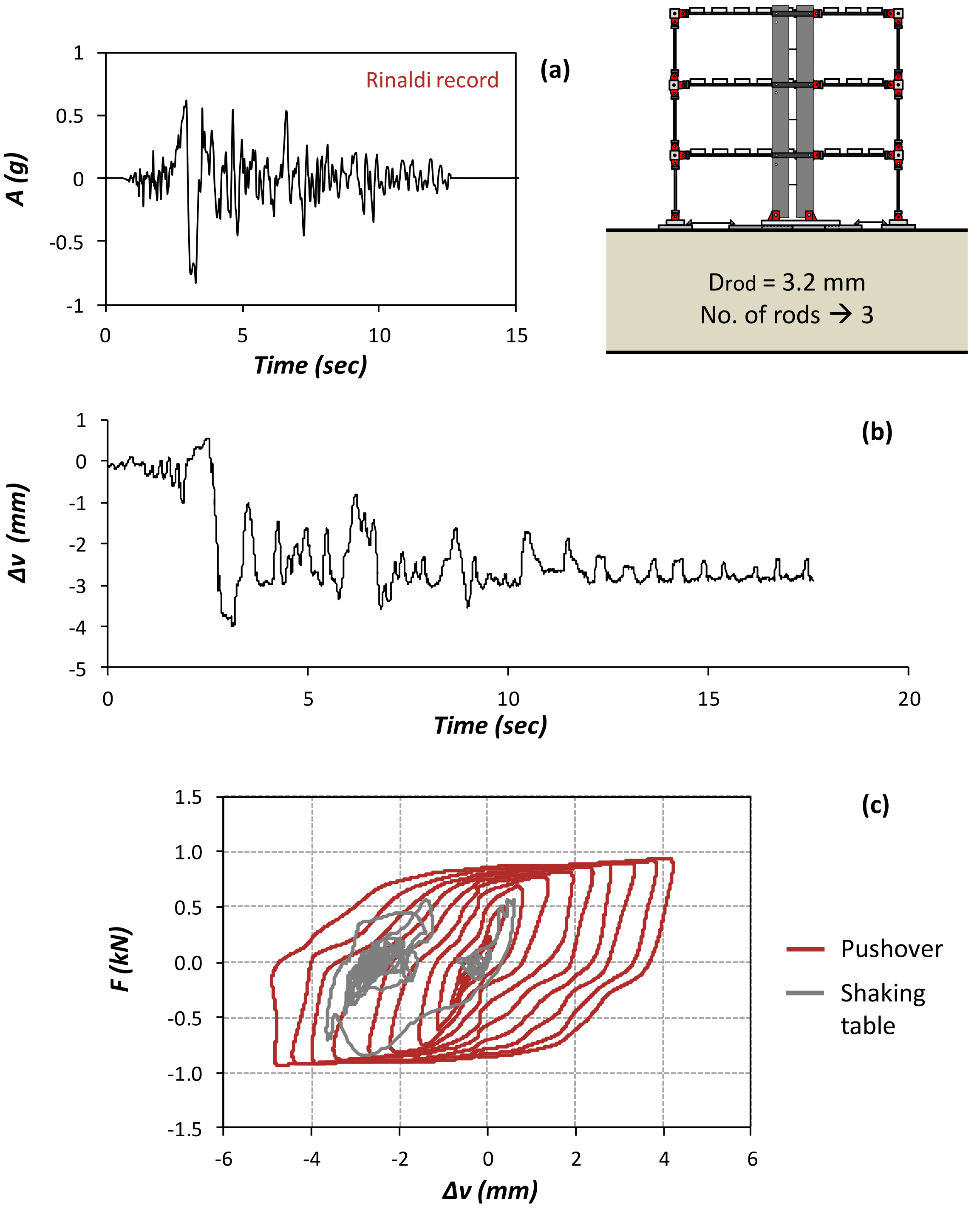

Figure 1.30 (a) Rinaldi record **(b)** Time history of the vertical displacement of rods and **(c)** Total shear force – vertical displacement curve for the *Rinaldi record*, compared with the one derived from the respective pushover test.

EXPERIMENT No. 4

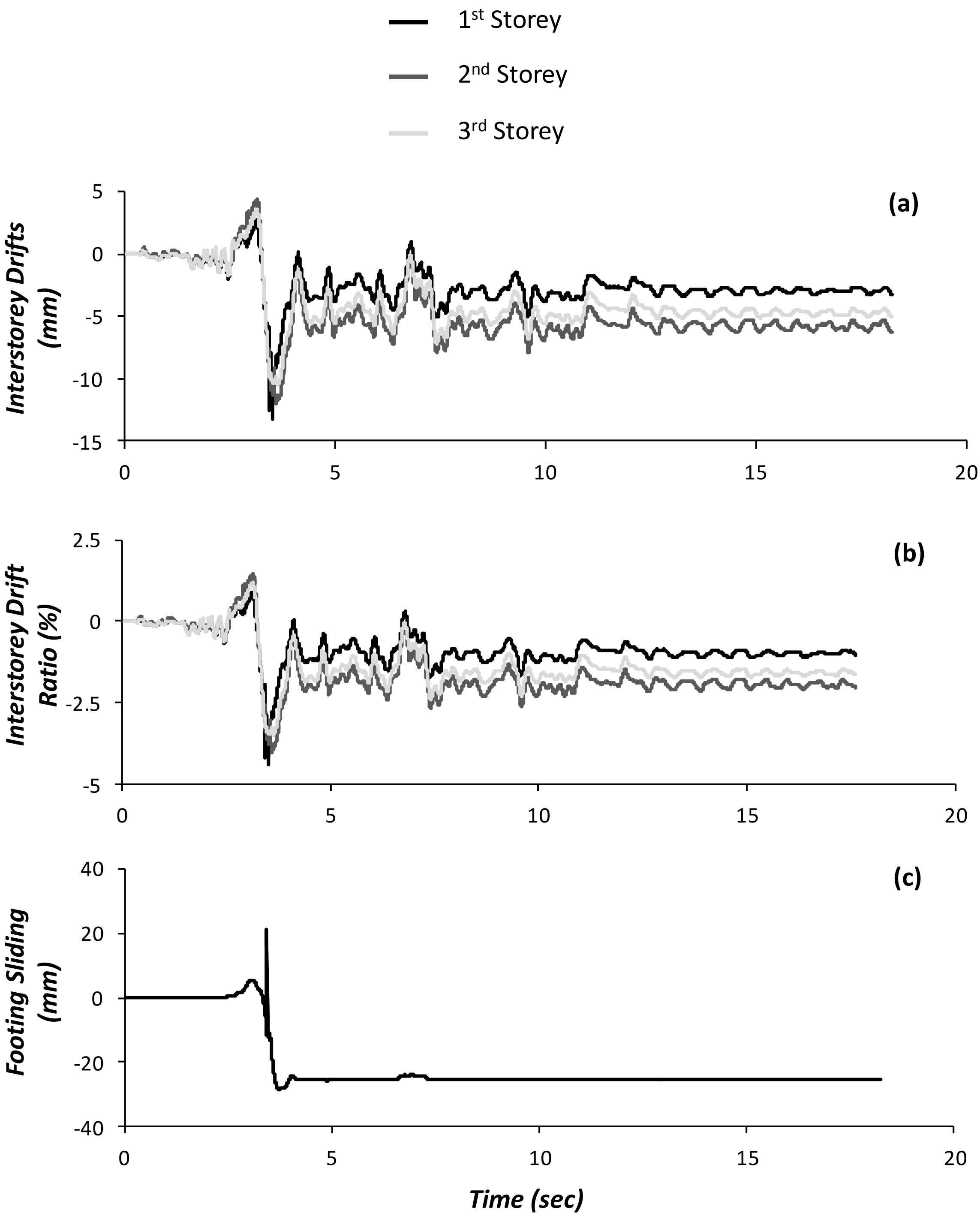

Figure 1.31 Time-histories of **(a)** the interstorey drifts at the level of each storey, **(b)** the respective drift ratios and **(c)** the sliding of the central footing, for the *Rinaldi record*.

EXPERIMENT No. 4

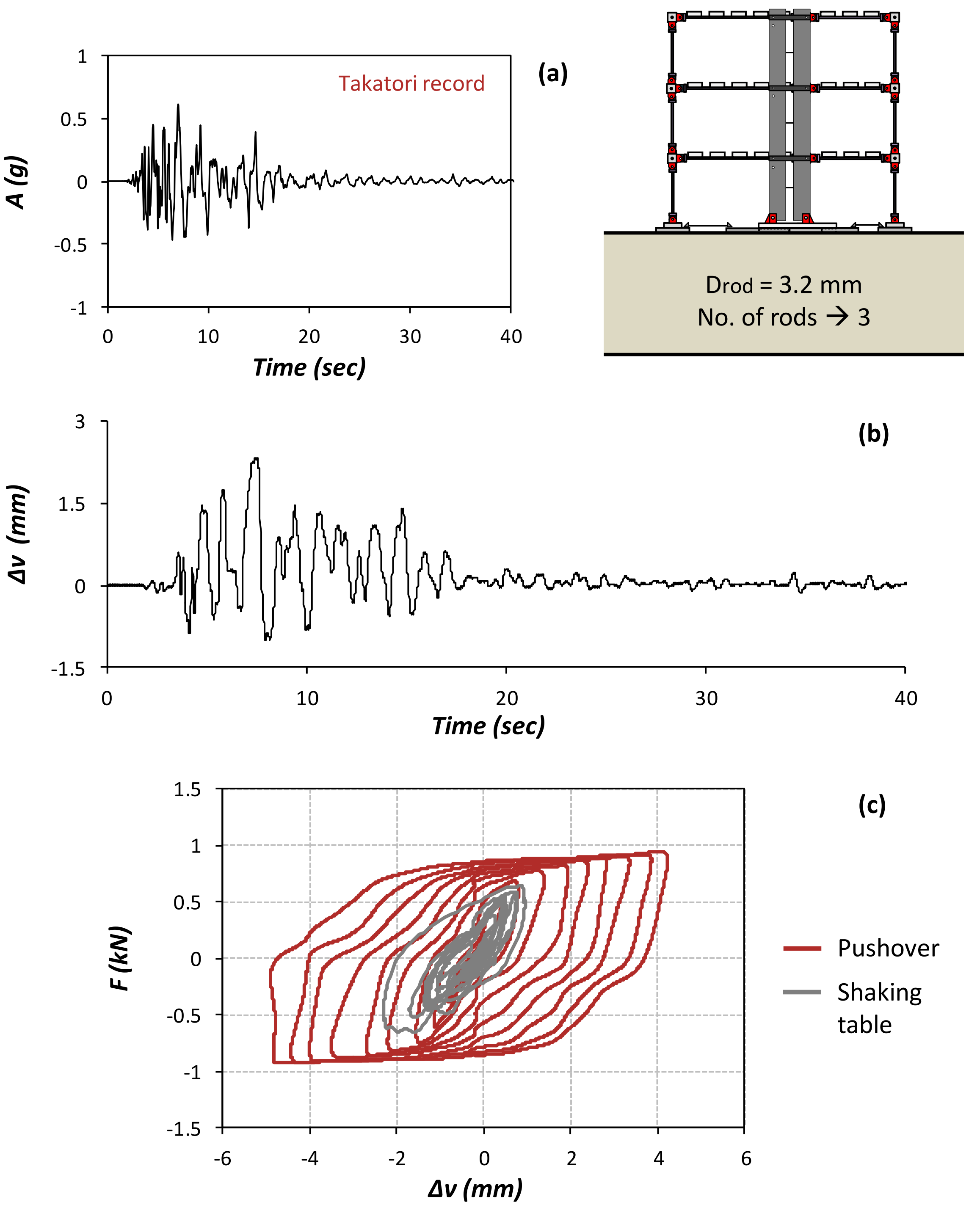

Figure 1.32 (a) Takatori record **(b)** Time history of the vertical displacement of rods and **(c)** Total shear force – vertical displacement curve for the *Takatori record*, compared with the one derived from the respective pushover test.

EXPERIMENT No. 4

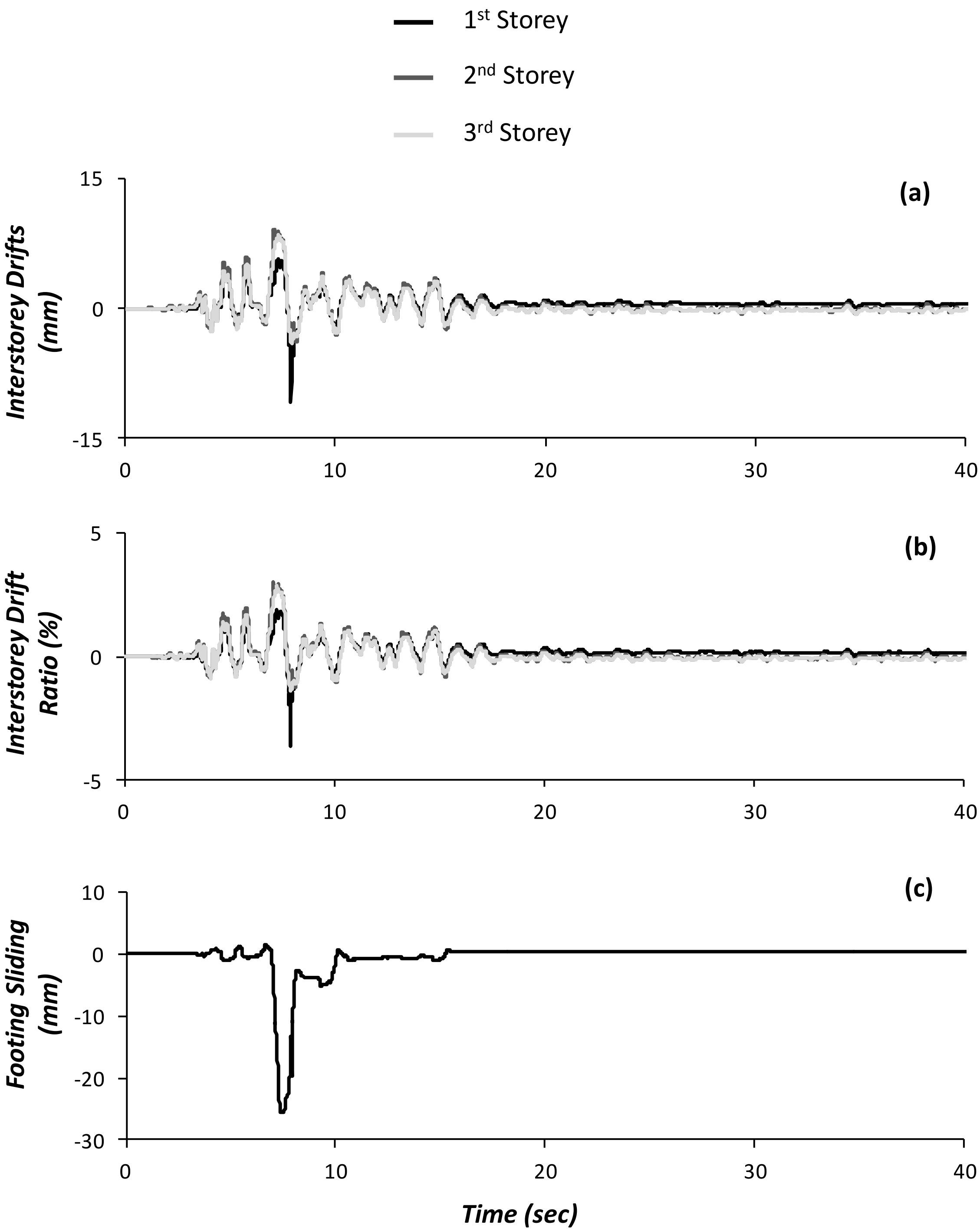

Figure 1.33 Time-histories of **(a)** the interstorey drifts at the level of each storey, **(b)** the respective drift ratios and **(c)** the sliding of the central footing, for the *Takatori record*.

EXPERIMENT No. 4

Table 1.5 List of altered models of the retrofitted SETUP II and the imposed excitations.

Description of Setup					
Model	**Exp.**	**INSTED system**		**Soil**	**Excitation**
		Rods per frame	D (mm)		
Retrofitted Building (SETUP IIa)	4	2	3.2	Dense Sand	Takatori
Retrofitted Building (SETUP IIb)	4	1	3.2	Dense Sand	Takatori
Retrofitted Building (SETUP IIb)	4	1	3.2	Dense Sand	Takatori x 1.4

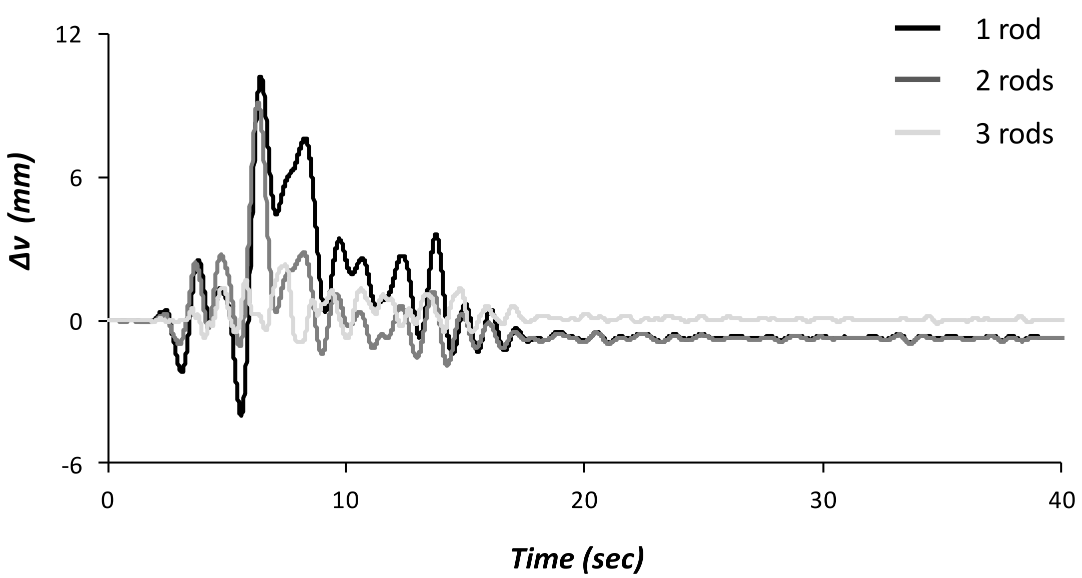

Figure 1.34 Comparison of the vertical rod displacement time histories during the Takatori record for setups II, IIa and IIb.

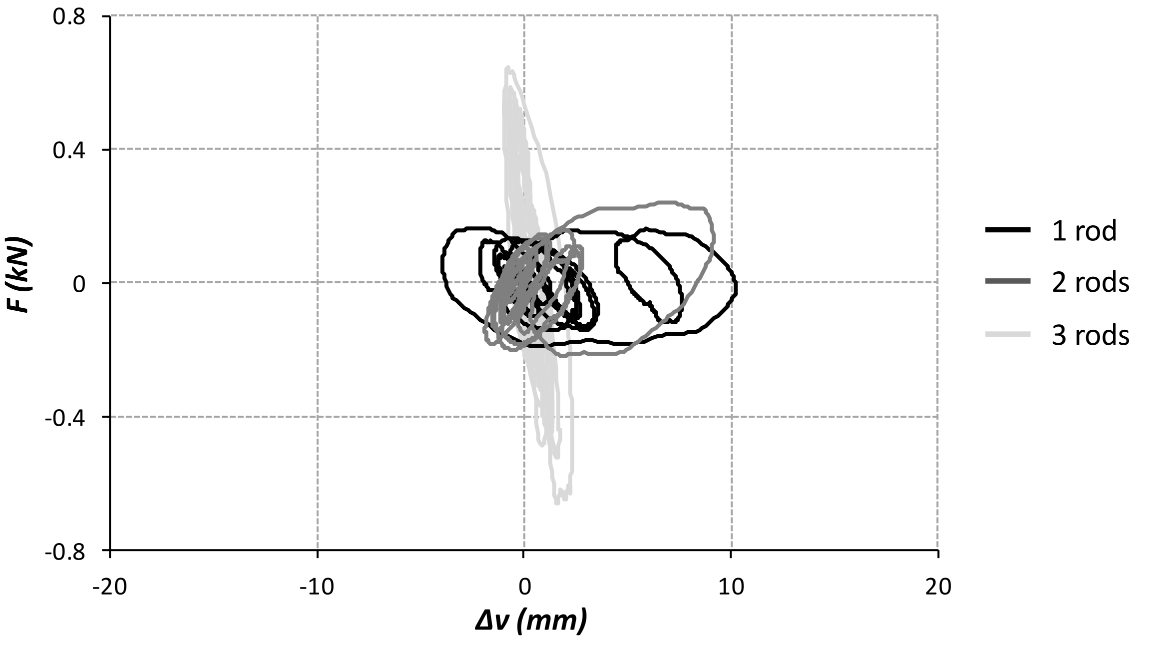

Figure 1.35 Comparison of strength in terms of Shear force – Vertical rod displacement curves for *setups II, IIa and IIb*, during the Takatori record.

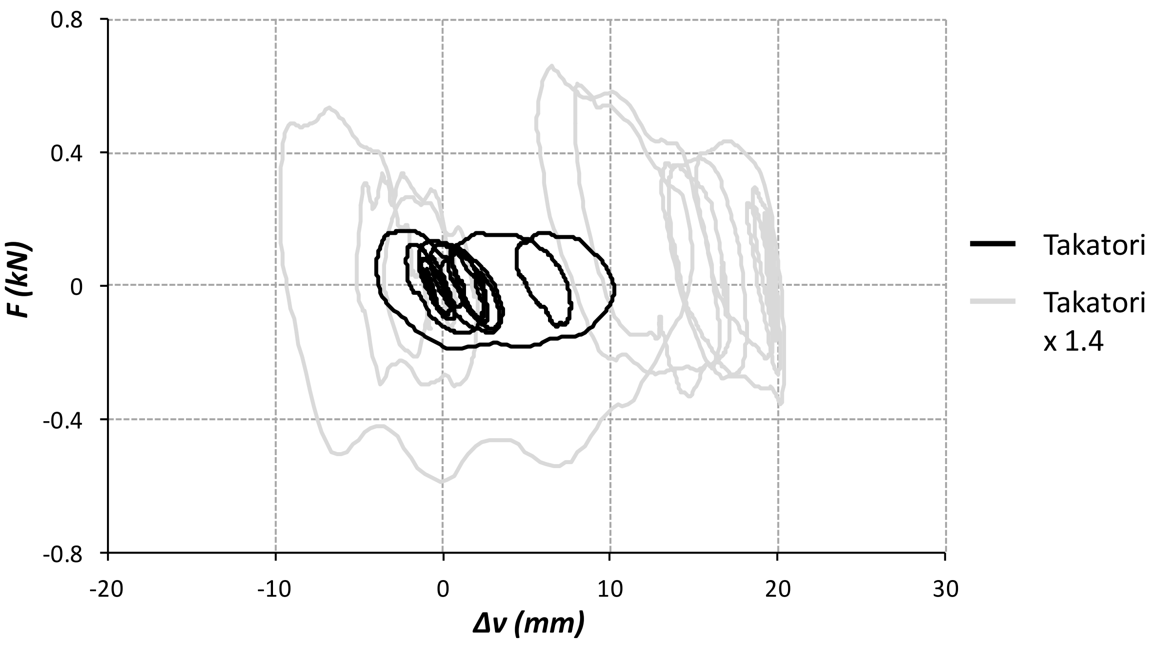

Figure 1.36 Comparison of strength for *setup IIb (1 rod)*, for two different excitations: the original Takatori record and the Takatori record amplified by a 1.4 factor.

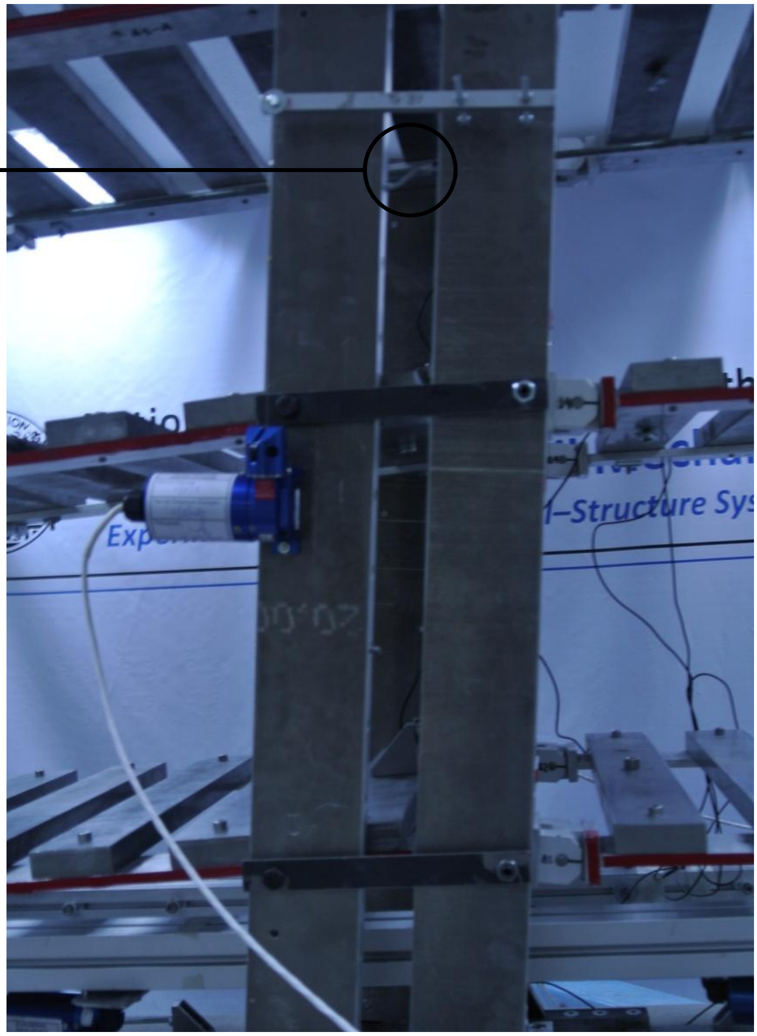

Figure 1.37 Detail of the INSTED system consisting of one rod (Setup IIb).

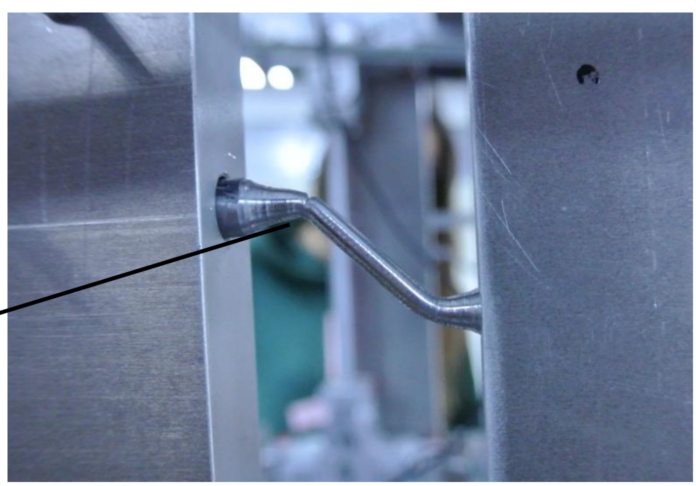

Figure 1.38 Photograph of the rod's deformed shape after Setup IIb is led to failure, during the amplified record of Takatori. The formation of plastic hinges at the end of the effective length is obvious.

EXPERIMENT No. 5
Retrofitted building (SETUP III)
Dynamic Test

List of applied seismic records.

Moderate Seismic Records
MNSA (Athens 1999)
Lefkada (2003)
Strong Seismic Records
Rinaldi (Northridge 1994)
JMA (Kobe 1995)
Takatori (Kobe 1995)

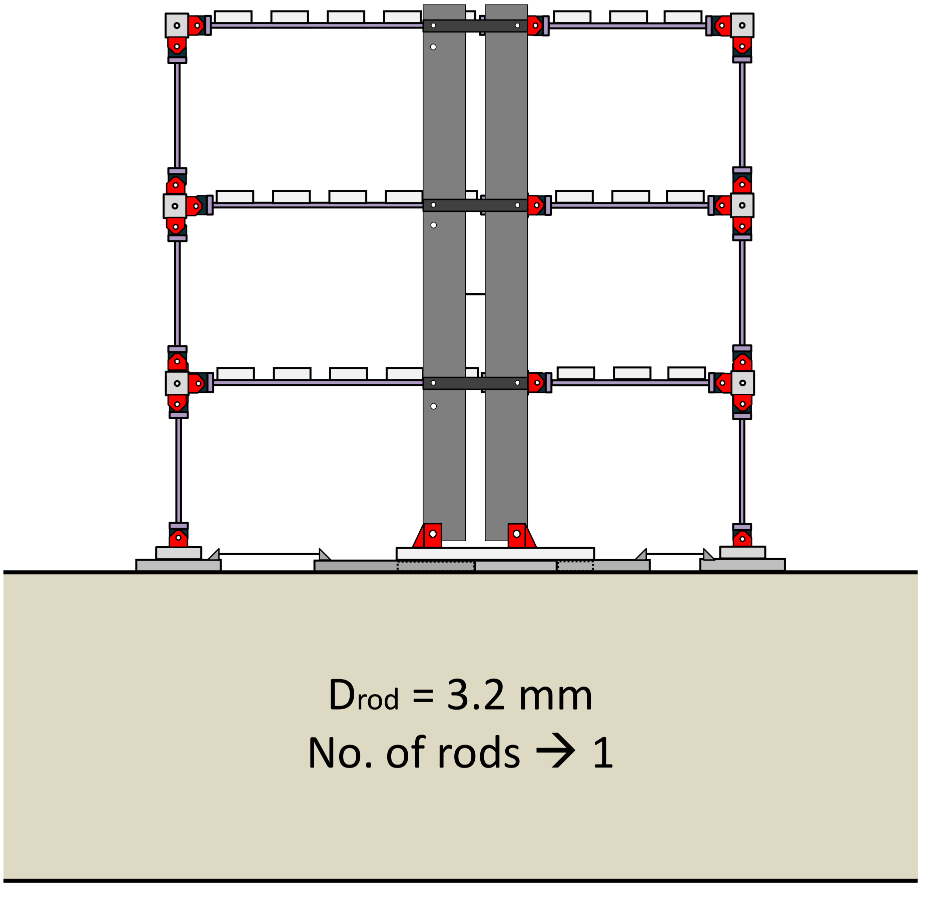

Figure 1.39 Schematic illustration of SETUP III.

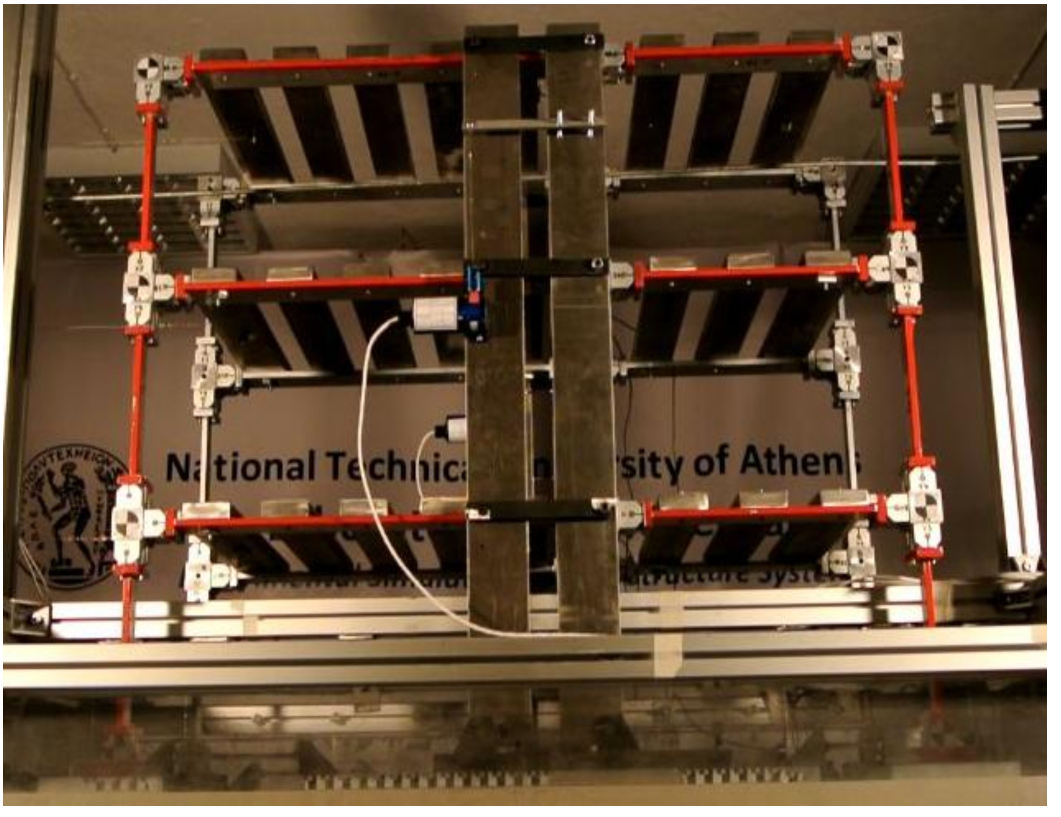

(a)

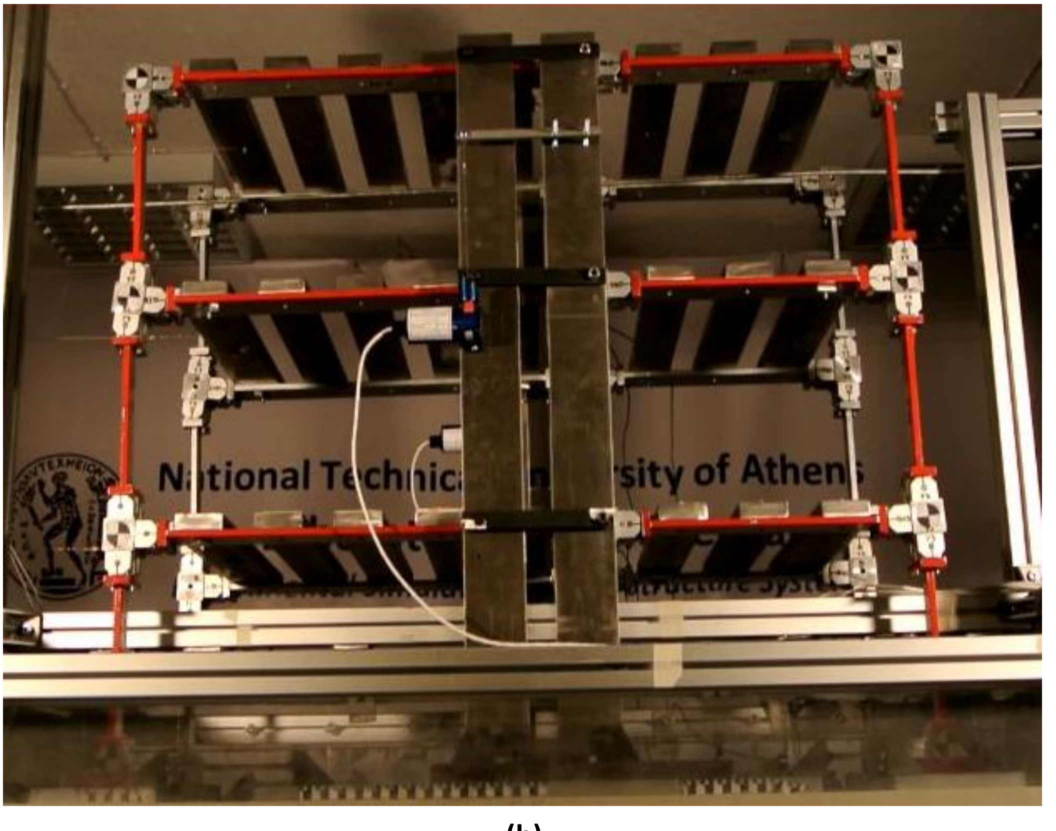

(b)

Figure 1.40 (a) Initial shape of the retrofitted building and **(b)** deformed shape of Setup III after the moderate seismic record of Lefkada.

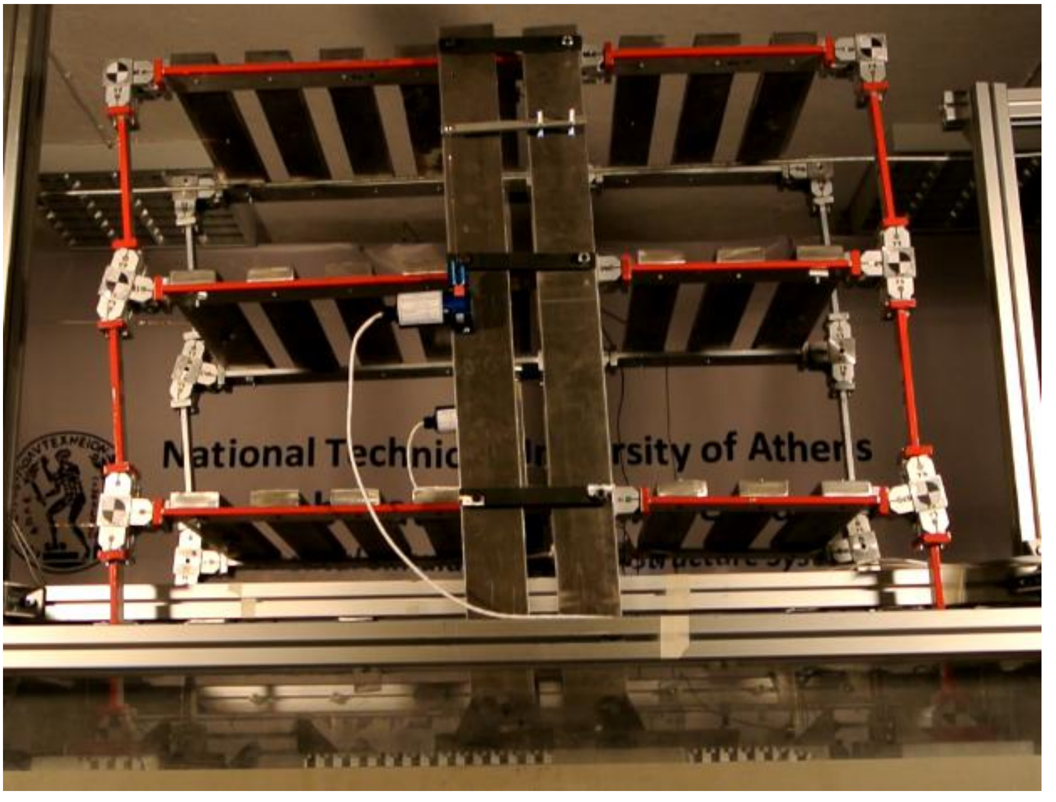

(a)

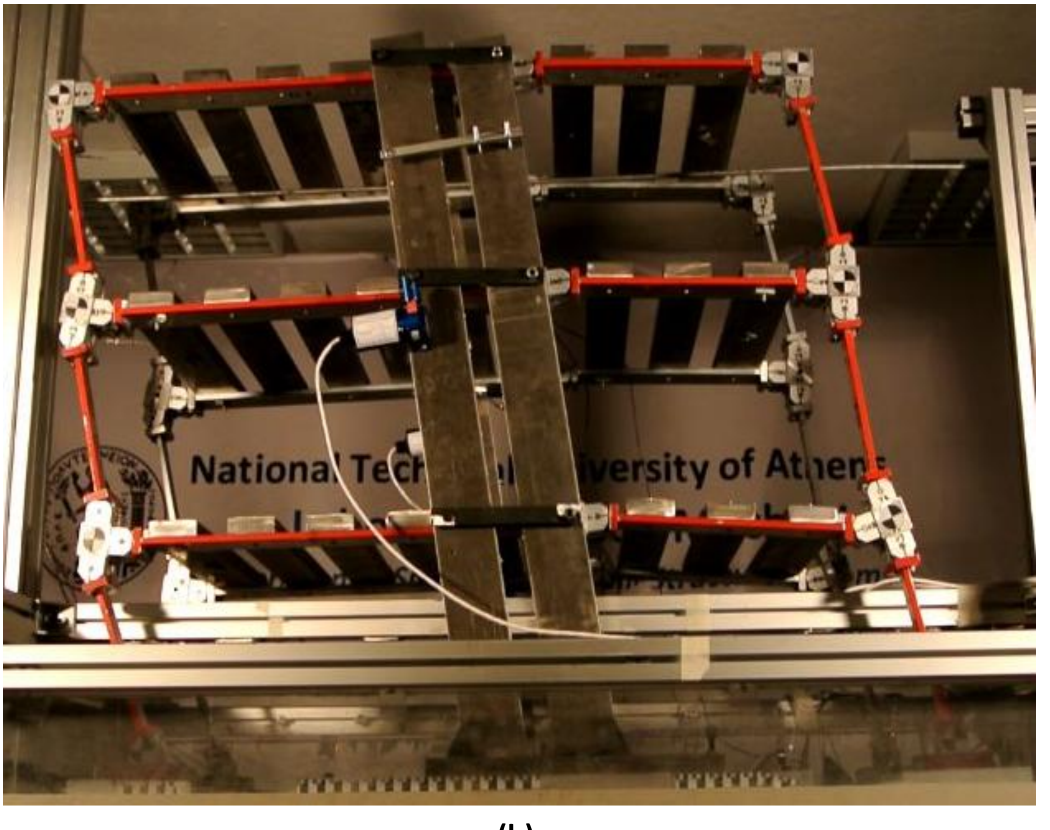

(b)

Figure 1.41 Deformed shape of the retrofitted building **(a)** after the record of *Rinaldi* and **(b)** after the high intensity record of *Takatori*.

EXPERIMENT No. 5

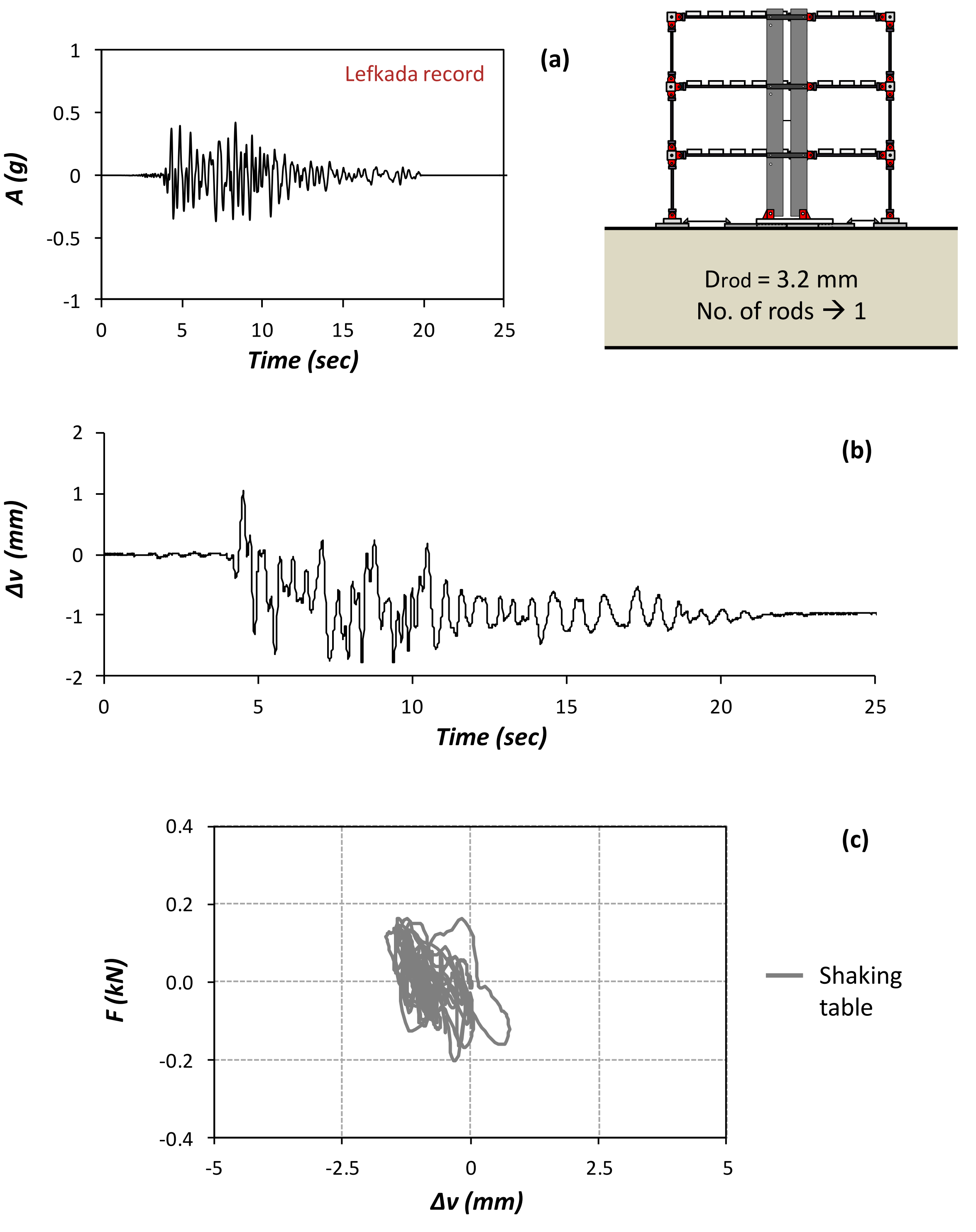

Figure 1.42 (a) Lefkada record **(b)** Time history of the vertical displacement of rods and **(c)** Total shear force – vertical displacement curve for the moderate *Lefkada 2003 record*.

EXPERIMENT No. 5

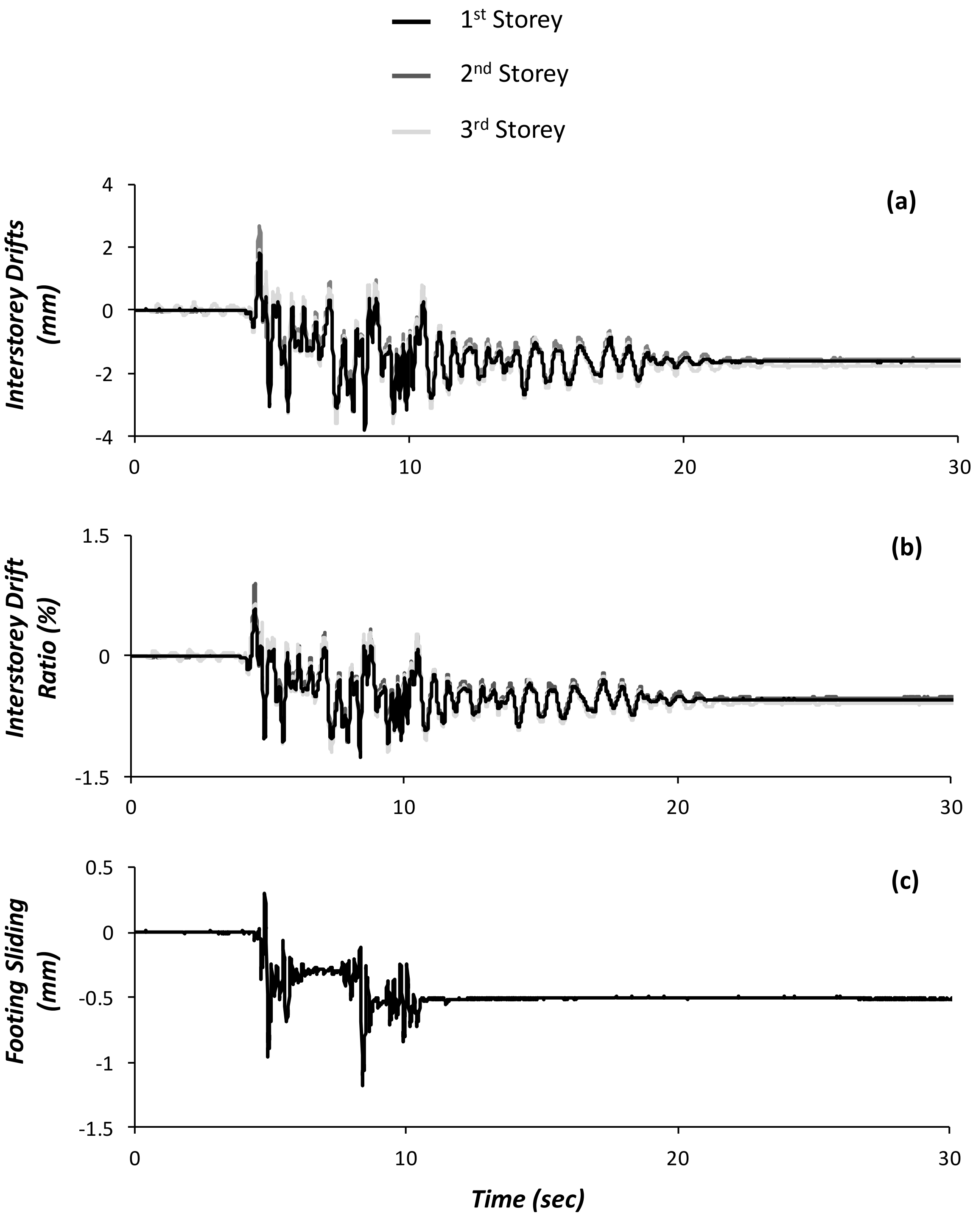

Figure 1.43 Time-histories of **(a)** the interstorey drifts at the level of each storey, **(b)** the respective drift ratios and **(c)** the sliding of the central footing, for the moderate *Lefkada 2003 record*.

EXPERIMENT No. 5

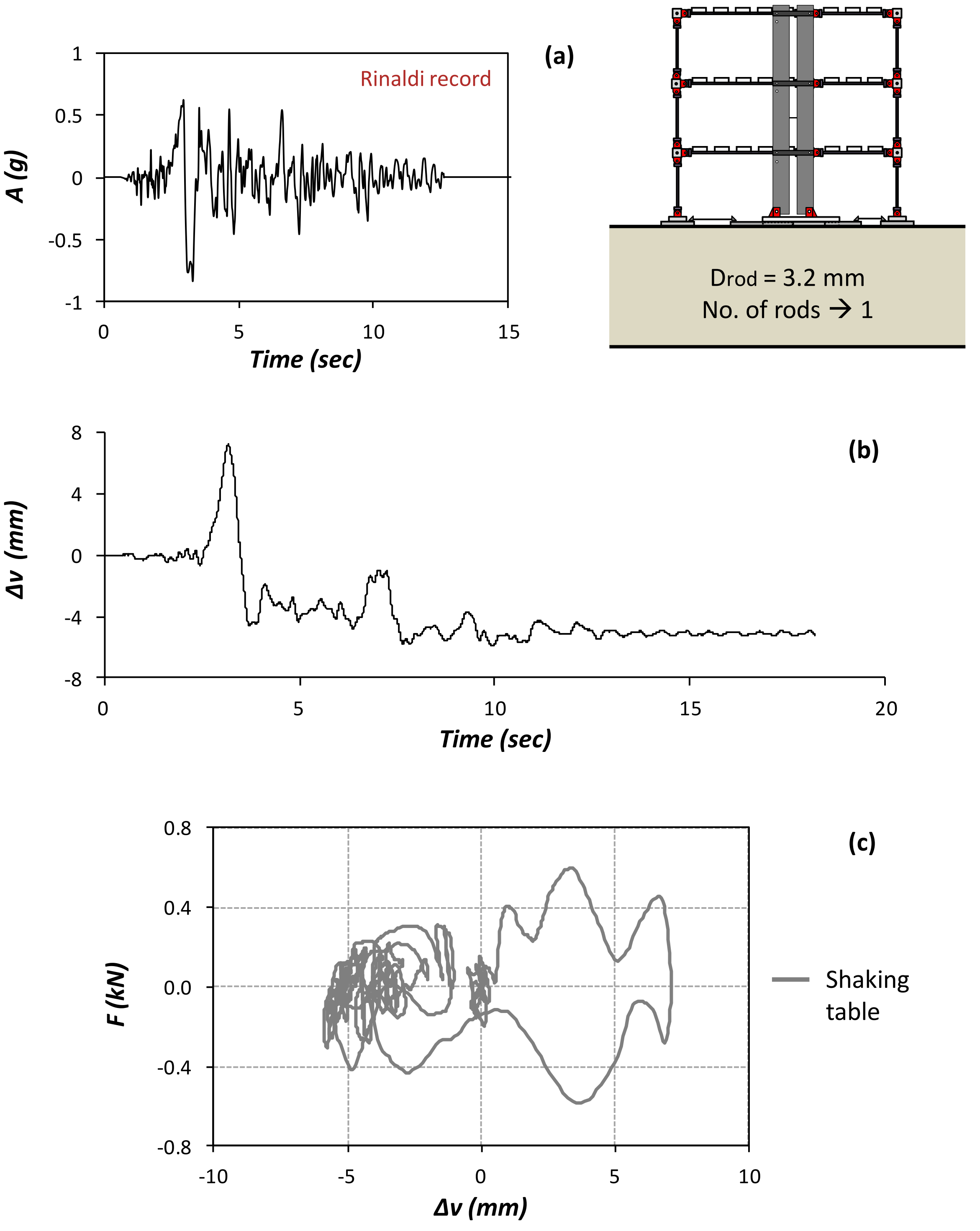

Figure 1.44 (a) Rinaldi record **(b)** Time history of the vertical displacement of rods and **(c)** Total shear force – vertical displacement curve for the *Rinaldi record*.

EXPERIMENT No. 5

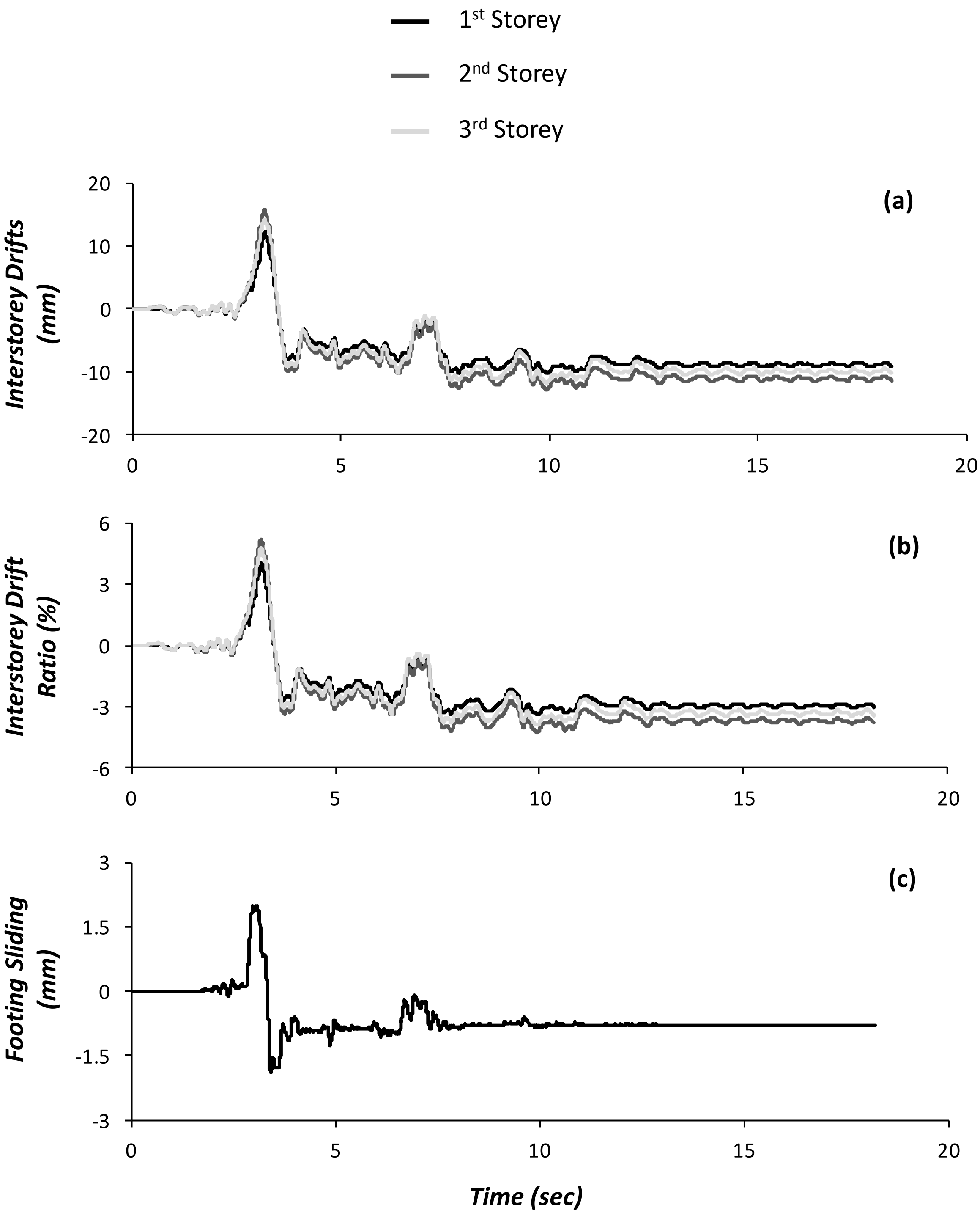

Figure 1.45 Time-histories of **(a)** the interstorey drifts at the level of each storey, **(b)** the respective drift ratios and **(c)** the sliding of the central footing, for the *Rinaldi record*.

EXPERIMENT No. 5

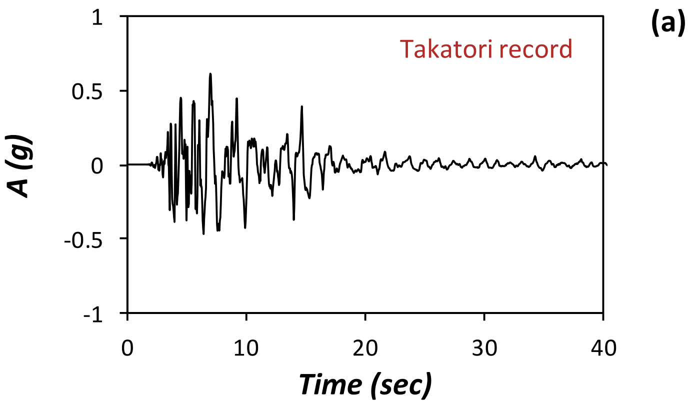

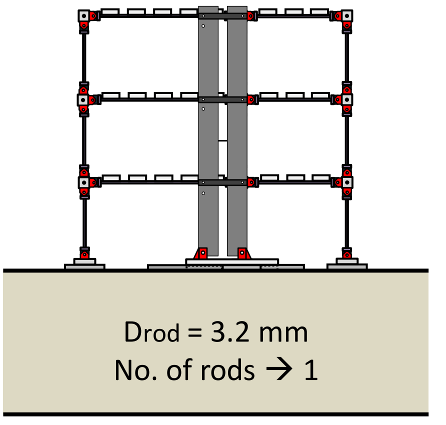

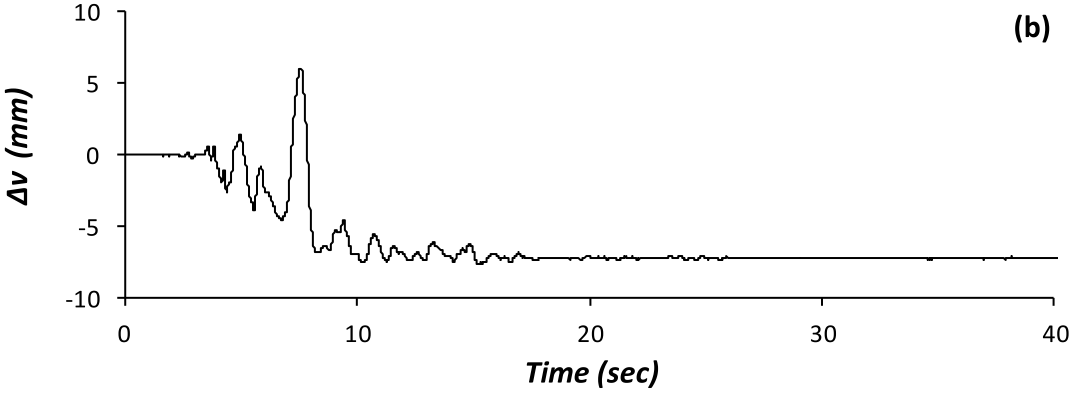

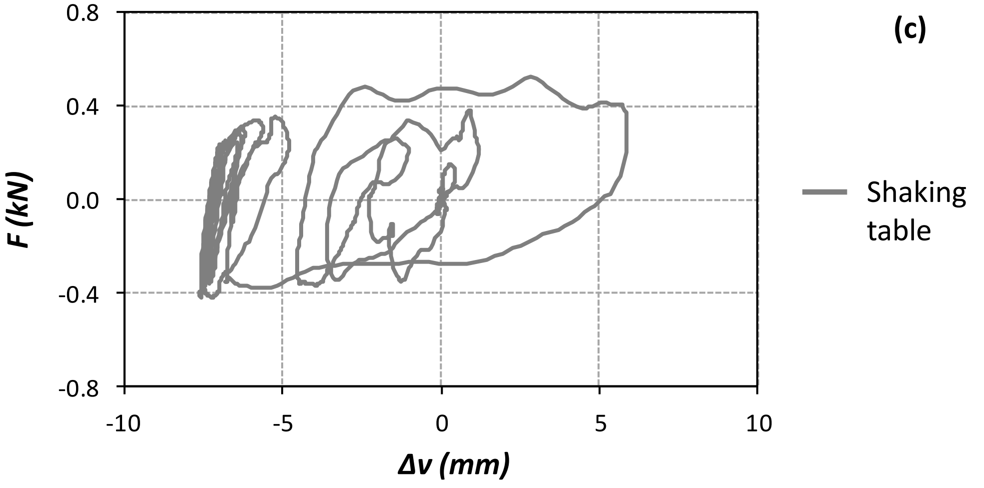

Figure 1.46 (a) Takatori record **(b)** Time history of the vertical displacement of rods and **(c)** Total shear force – vertical displacement curve for the *Takatori record*.

EXPERIMENT No. 5

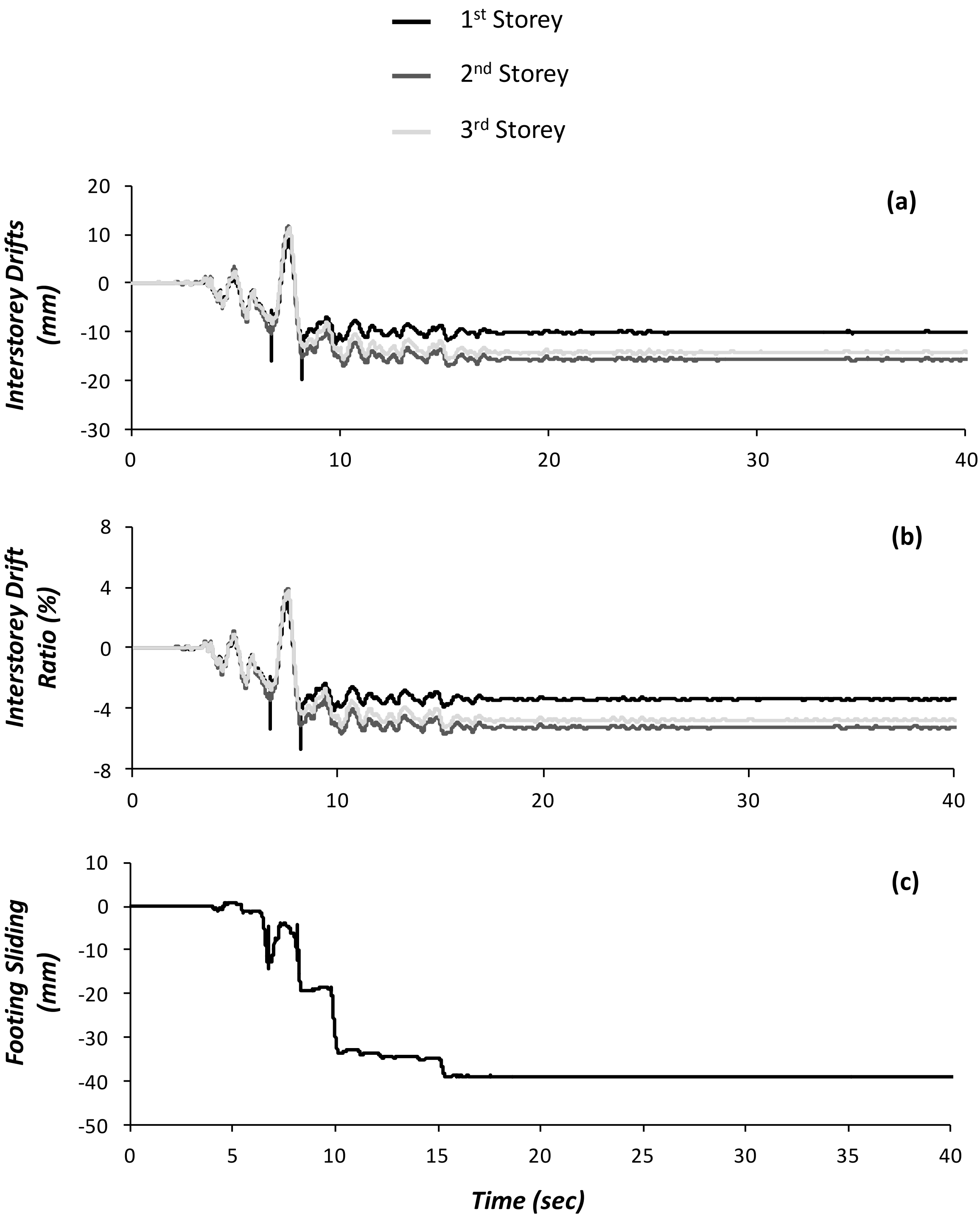

Figure 1.47 Time-histories of **(a)** the interstorey drifts at the level of each storey, **(b)** the respective drift ratios and **(c)** the sliding of the central footing, for the *Takatori record*.

Figure 1.48 Deformed shape of the rod after the record of Takatori. One can observe the residual vertical rod displacement (measured equal to Δv_{res} = 7mm) and that no formation of plastic hinges took place.

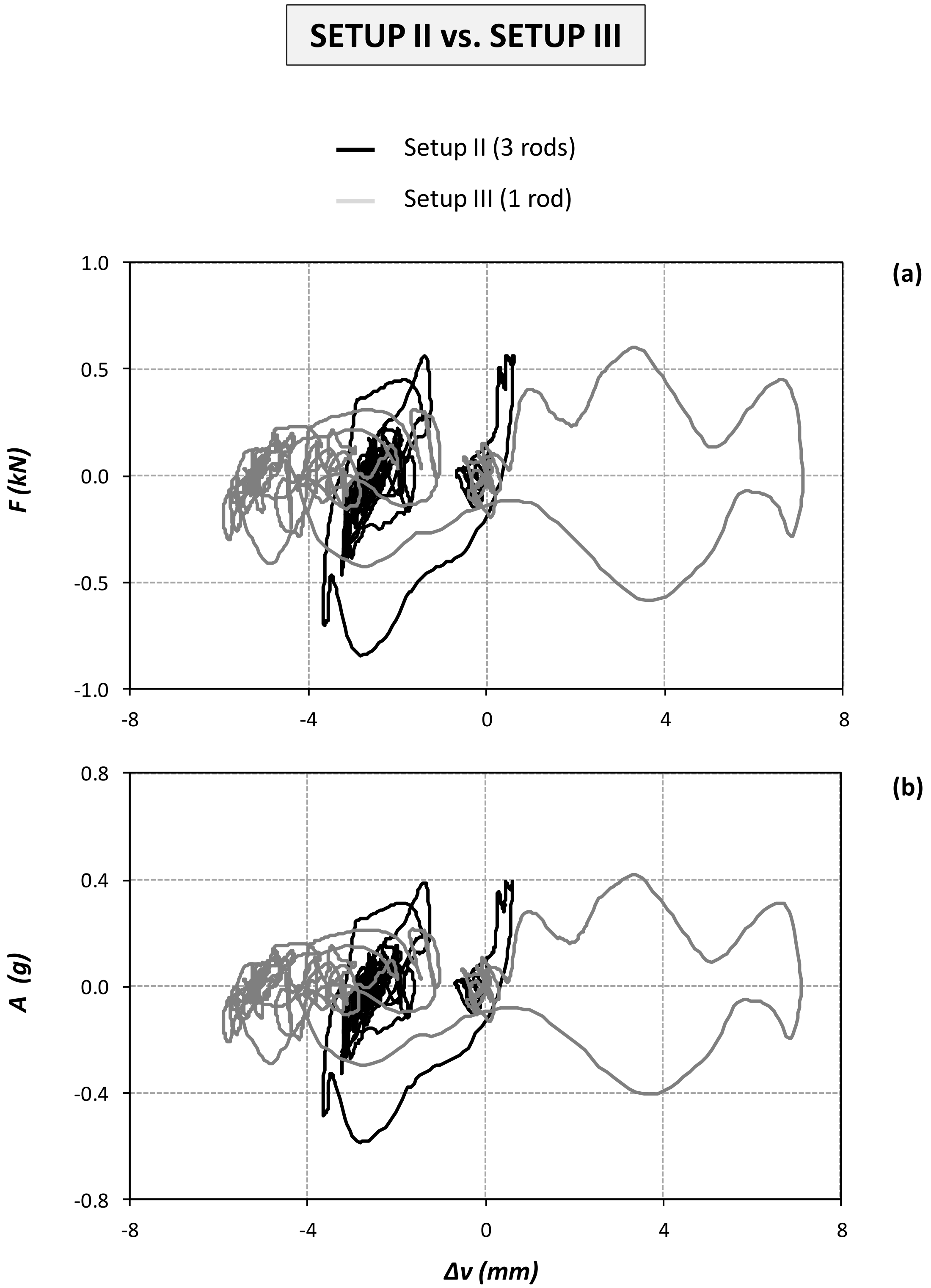

Figure 1.49 Comparison of Setup II and Setup III in terms of **(a)** Force – vertical rod displacement and **(b)** Acceleration – vertical rod displacement curves**,** for the *record of Rinaldi*.

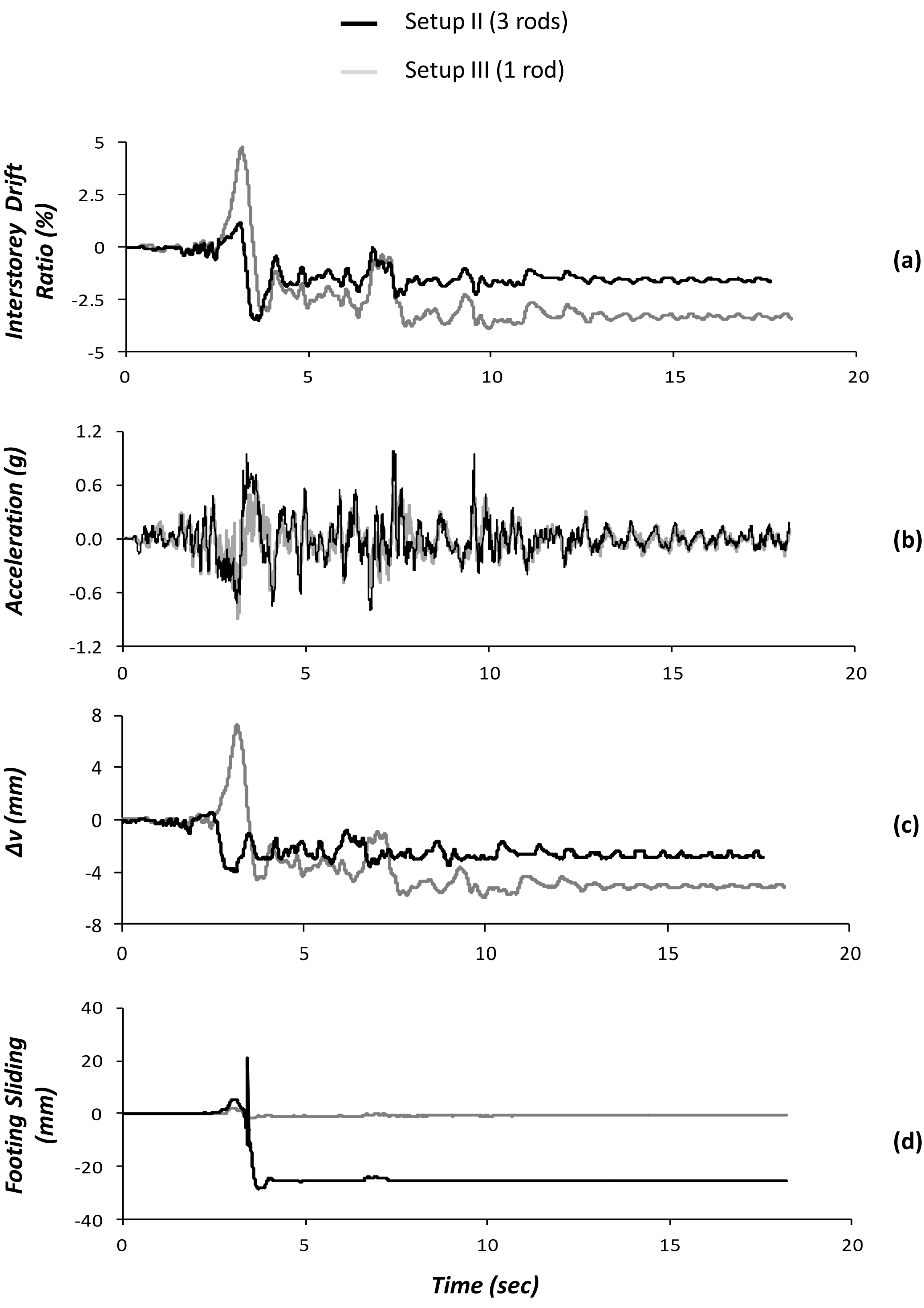

Figure 1.50 Comparison of Setup II and Setup III in terms of **(a***) 3rd storey* interstorey drift ratio **(b)** *3rd storey* acceleration **(c)** vertical rod displacement and **(d)** sliding of the central footing time histories, for the *record of Rinaldi*.

CHAPTER B.2

RETROFITTED BUILDING WITH THE INSTED SYSTEM - NUMERICAL ANALYSES vs EXPERIMENTS

2.1 Numerical Simulation of the Retrofitted Building

After having completed the experiments, we moved on to the numerical simulation of the retrofitted building, with the INSTED system. The ultimate goal is to create a numerical model that would respond just like the experimental physical one.

The initial idea of the model remains the same, as far as the design methodology is concerned. The original frame, indeed, is the same that was used in former analyses. The elements that were changed were the ones referring to the INSTED system, since the experimental materials differed in some way from those originally applied in the analyses. For example, the steel properties of the rods that were used in the experimental setup were not the nominal ones. In order to introduce the real constitutive law of these elements in the numerical analyses, we conducted a series of tensile strength tests. The stress-strain curve that was exported from these tests appears in Chapter B.1. Also the effective length as well as the diameter of the rods varied in each experiment, since the procedure of reducing its diameter encases imperfections and uncertainties. Therefore, each numerical analysis included the corresponding properties of the rods.

During the experimental procedure, it was noticed that the retrofitted model building (including all three Setups) displayed significantly greater strength compared to the one expected – even though the calculation of the system's horizontal resistance was made using the rods' actual properties. Knowing that the spigots used to form the hinges at the base of the INSTED system were placed in a very tight arrangement, we were led to the conclusion that the hinges might not have responded in the desired way; they did not allow free rotation of the system, on the contrary, they displayed moment resistance until a certain value of rotation. For this reason, we altered the existing numerical model of the retrofitted building in Abaqus, by adding three springs at the base of each INSTED system's columns: a horizontal, a vertical and a rotational one (simulated by elements of type SPRING2). The first two springs were designed as linear, elastic and very stiff in order to prohibit vertical and horizontal displacements, while the rotational was designed as non-linear. Specifically, a moment - rotation curve was introduced in order to determine the ultimate bending capacity of the rotational spring. This curve differed in accordance to the strength of the structure, since a greater force was needed for the columns to bend, when the structure appeared greater resistance.

2.2 Pushover Tests to the Retrofitted Building

2.2.1 Setup I

The first pushover test included rods, which had a diameter of 4mm and an effective length of 25mm (effective length is the distance between the predefined plastic hinges, according to the reduction of its cross-section). The curve, depicting the relation between the strength and the displacement of the structure, which derived from the pushover test, appears in Figure 2.1. This is also compared to the one exported from the cyclic pushover testing of the experiment. The two curves resemble in terms of strength, however, the stiffness is significantly different.

This deviation can be explained by the fact that the connections of the experimental setup are less rigid than in the analyses; on the contrary, they include gaps, which may justify the reduced stiffness of the model. Indeed, as the displacement increases, the experimental curve becomes stiffer, indicating that the connections attach to each other, leaving no more free space between them, therefore resembling more to the numerical curve. Also, the experimental pushover test was conducted in a way that the setup was not rigidly fixed on base. The connections of the aluminum bars, which were used as base for the building (Chapter 6.2 Experiment Preparation and Instrumentation), encased also gaps, which reduced the actual initial stiffness of the structure. Additionally, the fact that these bars were placed upon the sandbox, instead of a rigid base, a minor rotation of the setup was allowed, making the system more flexible than it was actually.

Taking all the above into consideration, we may infer that the numerical model on a -totally- fixed base represents sufficiently the experimental one, allowing us to continue with the seismic excitation of it, so as to compare with the Experiment No 2.

2.2.2 Setup II

The second pushover test included rods with a diameter of 3.2mm and an effective length of 2mm. The constitutive law and dimensions of these fuse elements were introduced in the numerical analyses and the pushover horizontal loading was imposed. The curve, depicting the relation between the strength and the displacement of the structure, which derived from the pushover test, appears in Figure 2.1.

This is also compared to the one exported from the cyclic pushover testing of the experiment. The two curves much resemble in terms of strength, however, a satisfactory approach of the system's stiffness is not achieved. The explanation for this deviation follows the same pattern as the one given above for Setup I. Consequently, we may proceed to the dynamic loading of this setup, as well, on a numerical basis, so as to compare it with Experiment No 3.

2.2.2.1 Setup II – Analysis with Soil

In our endeavor to simulate the system's actual stiffness, as exported from the experimental pushover test of Setup II, we conducted a number of analyses, where the structure was placed upon soil. We simulated the half of the sandbox, utilizing the properties of the dense sand that was used in the experiments. Generally the soil was finely-meshed, using the finer discretization for the upper layer of the soil (the upper 15cm, 30% of the total height). The elements of this discretization were square C3D8 (defined by 8 nodes) with a cross-section of 1.5x1.5cm (Figure 2.2.).

The constitutive law that we utilized for the soil was the hardening one. The curve that depicts the elastic modulus in relation to the depth is shown in Figure 2.3. The friction angle that we imported to this curve was $\phi=45^{o}$. Afterwards, we defined the boundaries of the sandbox, restricting the sides parallel to the building from moving towards the out-of-plane direction, the lateral ones from moving towards the direction of the pushover and considering the box's base as fixed. The footings were connected with some rigid elements, simulating their 'fixed' connection during the experiment. The springs that were utilized in the former analyses (fixed base), simulating the bending capacity of the base of the INSTED, were replaced with a plastic hinge, whose strength was calibrated in a way that would resemble that of the rotational spring.

The pushover loading (Figure 2.4) was imposed in all three stories considering a triangular eigenmode. The curve that derived from the pushover testing, depicting the relation between the resisting force of the structure and the total horizontal drift of the building, appears in Figure 2.5. This is also compared to the one exported from the cyclic pushover testing of the experiment. As we can see, the stiffness of the structure which is placed on soil resembles the experiment in a better way. On the other hand, the strength of the structure is not managed. The greater strength that the experimental setup displays can be justified from the fact that the structure's base was not allowed to move horizontally during the experiment, while the numerical model appeared to slide.

Concluding, we may infer that the real stiffness of the experimental setup, according to the pushover test, is managed when the model is placed on dense sand, which is considered very dense and its strength is managed when the footings cannot slide, that is when the building's base is fixed (Figure 2.6).

2.3 Dynamic Tests to the Retrofitted Building

The methodology that we utilized in our numerical analyses for seismic motions differed from the one used in the pushover static analyses. The reason, of course, was the fact that the experimental seismic motions were imposed on the soil-foundation-structure system, while the pushover tests were imposed on the fixed structure. Therefore, we had to take the non-linear behavior of the soil into account. At first step, we did not simulate the sandbox numerically, however, we did simulate the sliding of the footings that took place during the seismic loading. The fixed base would not correspond to a realistic response of the structure during the seismic records imposed.

The original design of the superstructure, including the INSTED system, remains the same as before. As far as the base is concerned, this is no longer fixed, due to the above reason. Instead, three extra nodes are defined, in the same place where the base nodes existed, and connected to the old ones with gap elements (GAPUNI), which allow sliding of the superstructure, relative to the friction coefficient. This coefficient is not the same for all base nodes, but each one is assigned with a different one, since the sliding that took place does not refer to the soil properties, rather, to an equivalent one that simulates the shear failure of each footing. The shear capacity of each footing is calibrated according to some vertical pushdown and horizontal pushover tests that had been previously conducted in the Soil Mechanics Laboratory (Papadopoulos Efthymios, 2011 & Nonika Antonaki, 2011) and to some theoretical values (Loli Marianna, 2012), which had derived from the Meyerhof equation and the Butterfield & Gottardi envelope.

Side Footings (B=0.15m, L=0.15m)

At first, the vertical bearing capacity of these footings is calculated, according to the equation of *Meyerhof's* formula for the bearing capacity of rectangular footings.:

$$N_q = e^{\pi \times \tan\varphi} \times \frac{1 + \sin\varphi}{1 - \sin\ \varphi}$$

$$N_c = \frac{N_q - 1}{\tan\varphi}$$

$$N_g = (N_q - 1) \times \tan 1.4\varphi$$

$$s_c = 1 + 0.3 \times {}^{B}/_{L}$$

$$s_q = 1$$

$$s_g = 1 - 0.2 \times {}^{B}/_{L}$$

$$\sigma_{uv} = c \times N_c \times s_c + \gamma \times D_{emb} \times N_q \times s_q + 0.5 \times \gamma \times N_g \times B \times s_g$$

where γ=1.6kN/m^3, c equals zero for sand and ϕ is approximately equal to 44^o in this case [Anastasopoulos, Kokkali, Tsatsis, 2011]. The vertical load of the left and right footing, when they are part of the structure, considering the one frame, is equal to 0.20 and 0.10kN respectively. Therefore, the vertical factor of safety for these footings can be calculated as the ratio:

$$FS_v = \frac{N_u}{N}$$

The *Butterfield & Gottardi envelope* provide graphs relating the moment and horizontal load, in terms of several safety factors. According to those derived for the two side footings we can find that the ultimate moment is M_{ult} = 0.067kNm and M_{ult} = 0.042kNm for the left and right footing respectively.

Since the side columns of the building deform like a cantilever, thus its hinge is formed on half of the 1st story height, therefore the ultimate horizontal load would be equal to:

$$Q_u = \frac{M_u}{h/2}$$

Taking all the above into account, we are now able to find the theoretical ultimate horizontal load for each footing, in the case of combined moment and horizontal push, as it is actually in the case of a seismic motion. The box below summarizes the values that have derived from the above procedure.

B x B = (15 x 15 cm)		
(kN/kNm)	left	right
N	0.20	0.10
Nu (ϕ = 44)	4.6	4.6
Mu	0.01	0.0063
Qu	0.067	0.042

Central Footing (B=0.15m, L=0.60m)

As regards this bigger footing, the experiments that have been conducted in the Soil Mechanics Laboratory, in the case of the RC shear wall, provide sufficient results. The wall was assumed to bear approximately 50% of total mass of the structure, which is 0.33kN for the one frame. The percentage is similar to the one that the central footing is bearing in the case of the INSTED system (0.4 out of 0.72kN – 55%), therefore, the ultimate horizontal load can be utilized for our case as well.

Like before, the vertical bearing capacity of this footing is calculated from the *Meyerhof* equation (N_u=18.27kN) and its vertical factor of safety is calculated equal to FS_v=55. In this case, however, the ultimate horizontal load was measured experimentally (Nonika Antonaki, 2012). The system that was tested consisted of both retrofitting walls for balancing purposes. The mass - inducing steel plates were evenly distributed between the three storeys. The walls were rigidly connected with the steel plates and the artificial plastic hinges at the base of the walls were prevented from rotating, thus creating a rigid block. The model was placed on dense sand as previously described. The horizontal displacement was applied by the pushover apparatus close to the center of mass of the model, below the second storey. Six wired displacement transducers were used to measure the displacement that was imposed, the settlements of both footings and the sliding of the system. A load cell was attached to the pushover apparatus and measured the reaction force throughout the test (Figure 2.7).

Due to the large bending capacity of the soil – foundation system, it developed a failure mechanism through sliding long before reaching soil failure. The Figure 2.8 depicts the measured horizontal load with regard to the horizontal displacement on top and Figure 2.9 depicts the calculated bending moment, at the base of the footing, with regard to the rotation angle of the footing, considering M=Qh (h=0.62m). The ultimate force is Q_u=0.27kN for both frames. For all cases, the friction coefficient is equal to:

$$\mu = \frac{Q_u}{N}$$

The box below depicts the friction coefficients for all footings, with regard to its own way of calculation:

	left	central	right
μ	0.34	0.34	0.42

2.3.1 Setup I, II & III

The numerical model of the retrofitted building is excited by some representative seismic records that were used in the relative experiments in order to examine the correspondence of the numerical analyses to the experiments. The results exported from the analyses are in terms of acceleration time histories on each story level as well as in terms of the total force and total horizontal drift time histories (Figures 2.10 - 2.30). All these graphs are compared to those measured from the experiments, as shown in the figures at the end of chapter 7. Also, the force of the system with regard to the horizontal displacement depicts the ductility of the system, as well as the capacity of it to dissipate large amounts of energy.

It is obvious that the time histories of accelerations and resisting force of the system resemble a lot those exported from the experiments. Naturally, the total drift time histories are not identical, due to the uncertainties and flaws of the experiment, as they are concluded in the end of Part B. However, the residual drift that the numerical model displays, in most seismic motions, are very satisfactory when compared to those measured in the experiments. Therefore, we may conclude that the numerical model is correct, since it responds similarly to the experiments.

Chapter B.2

Figures

Retrofitted building - SETUP I & II
Pushover Tests

Experiments

Vs.

Analyses

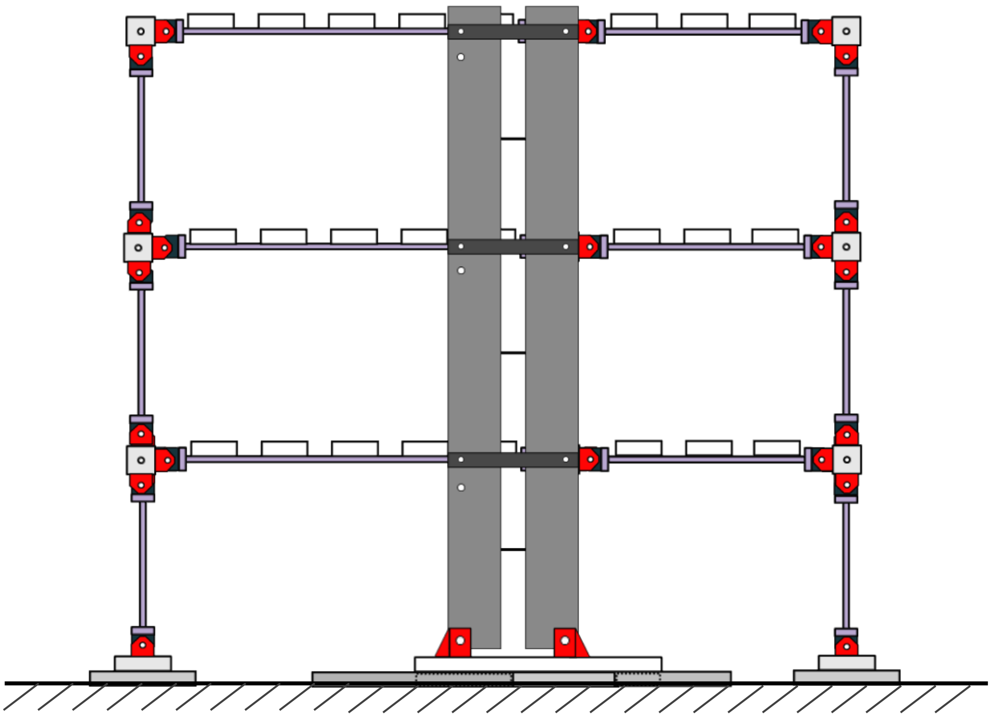

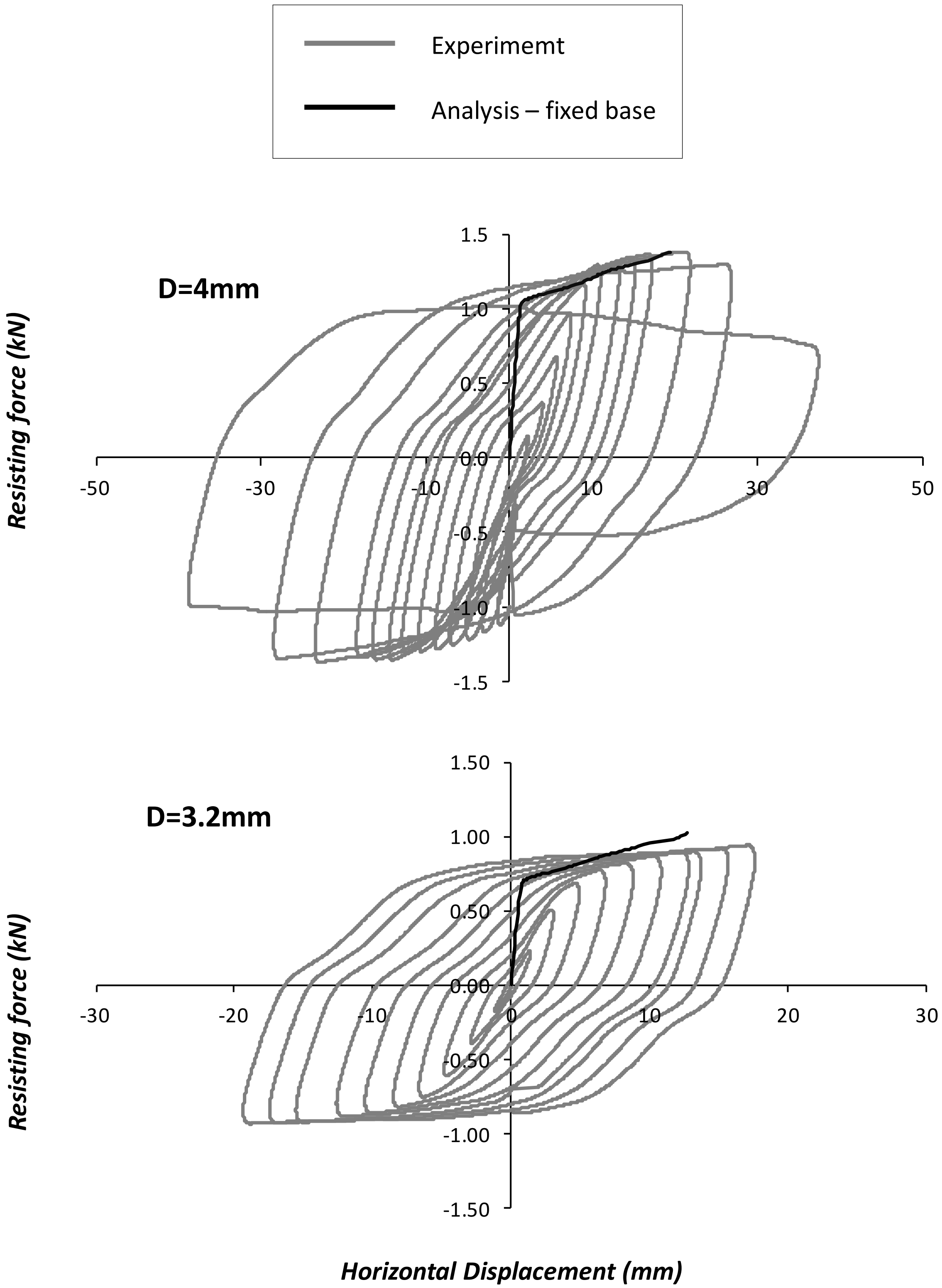

Figure 2.1 The resisting force according to the total horizontal displacement on top of the structure for both Setups (I & II).

Pushover Test with soil – Setup II

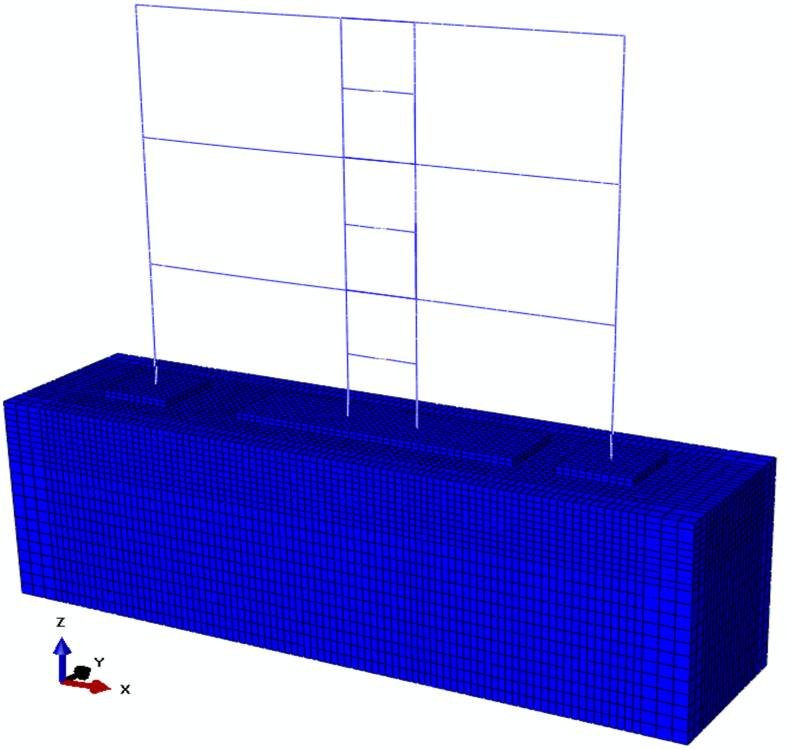

Figure 2.2. Photo from Abaqus of the numerical model (Setup II).

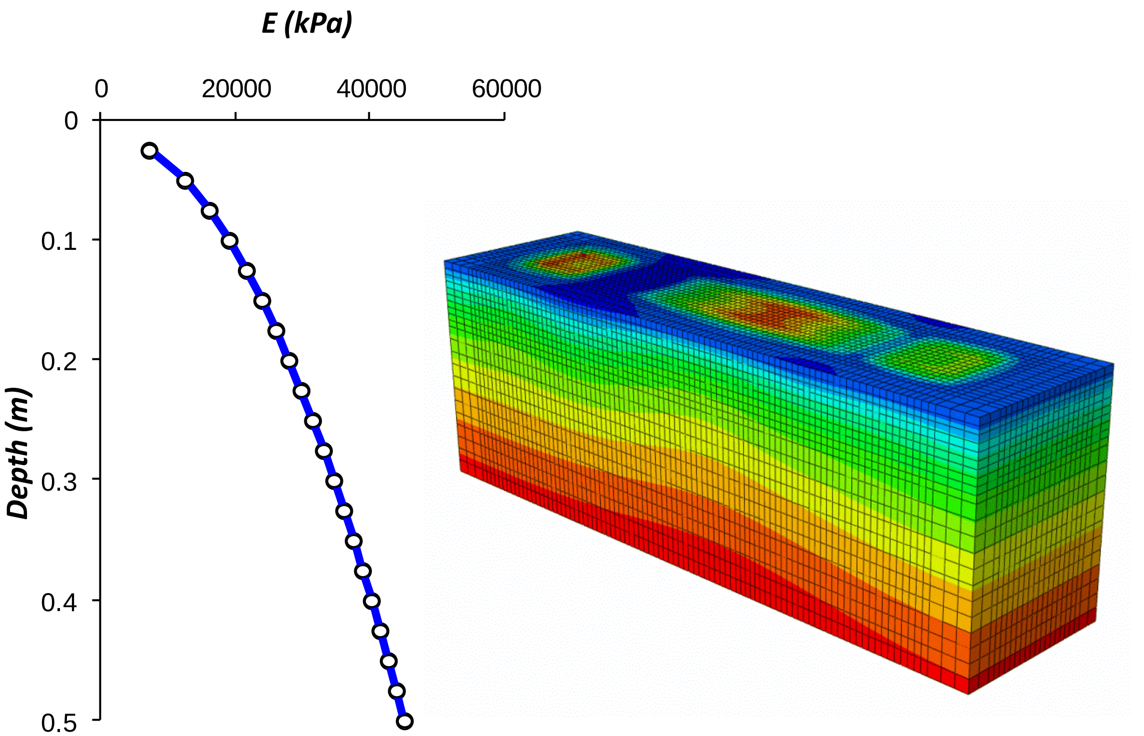

Figure 2.3 The constitutive law used for the sand and a photo from Abaqus depicting the stresses on soil.

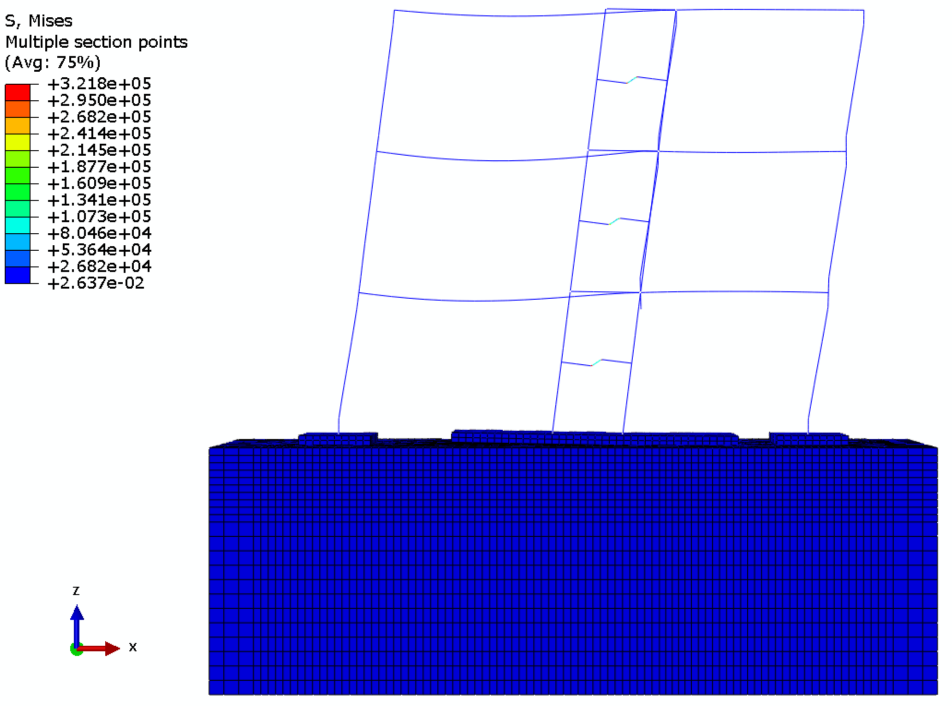

Figure 2.4 Photo from Abaqus after the pushover test.

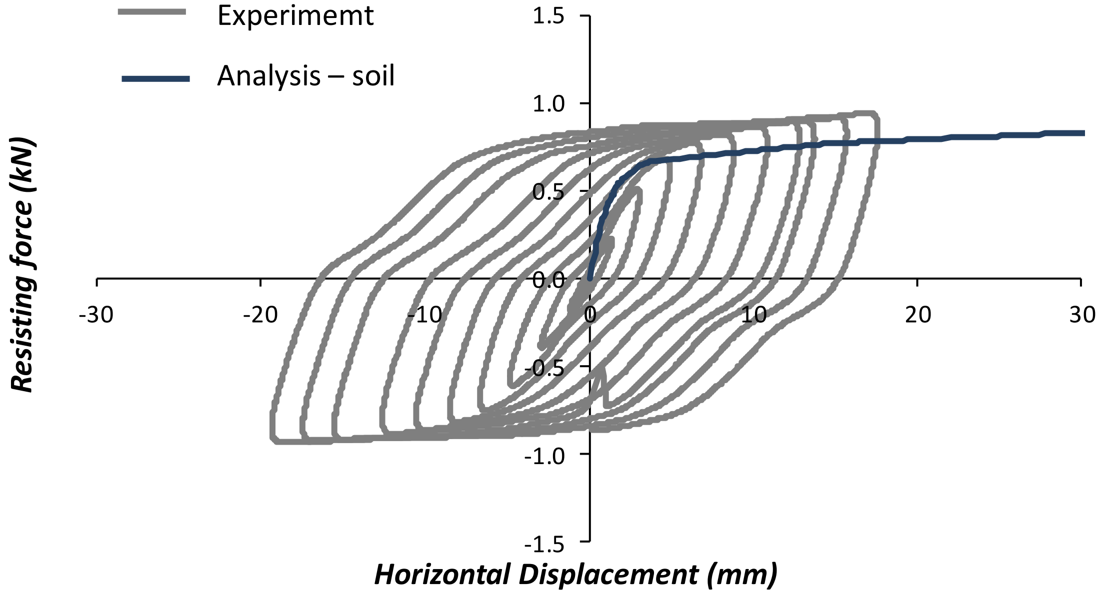

Figure 2.5 The resisting force according to the total horizontal displacement on top of the structure according to the numerical analysis with soil.

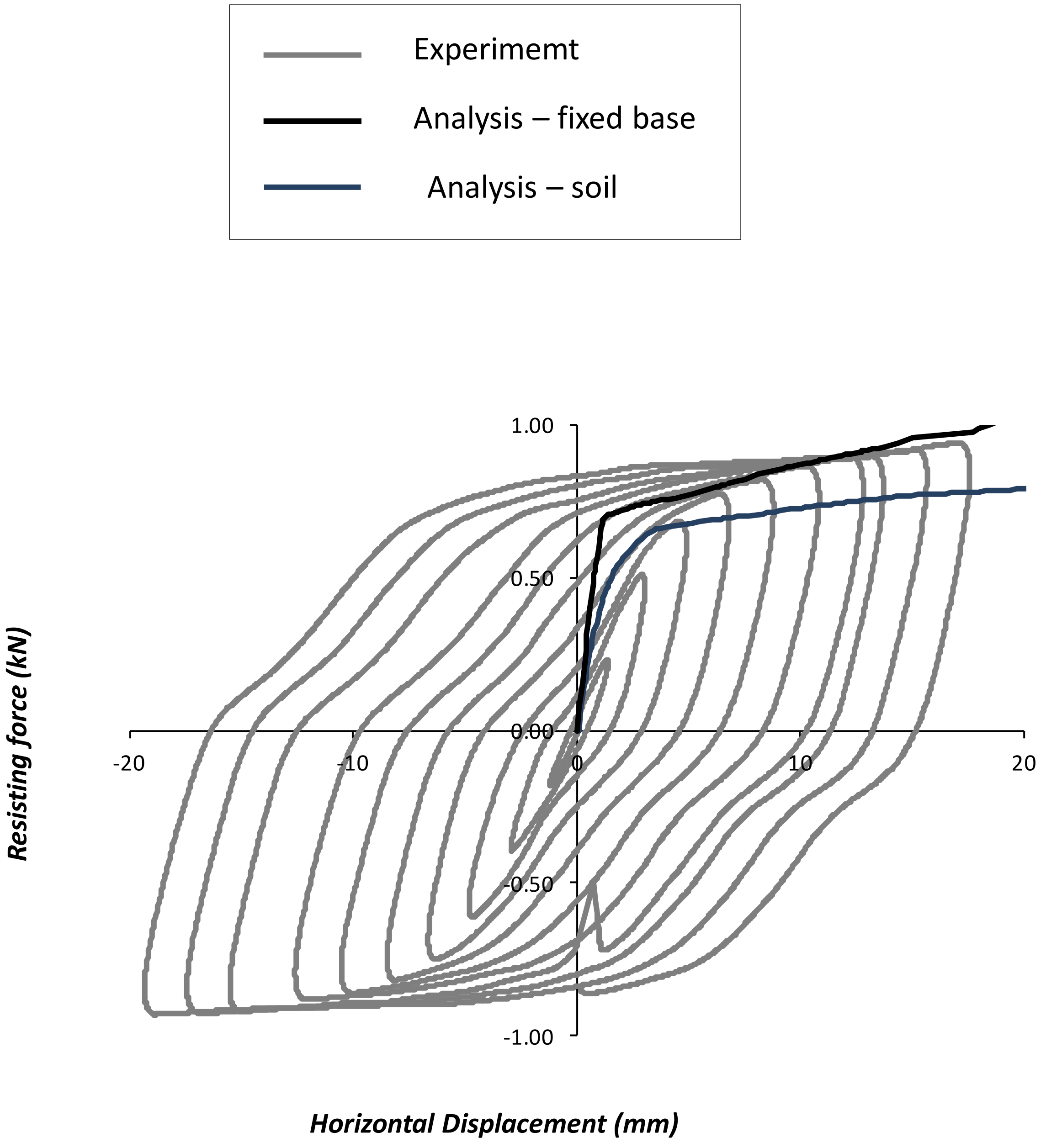

Figure 2.6 The resisting force according to the total horizontal displacement on top of the structure for Setup II as exported from the numerical analysis with soil, in comparison with the experimental curve and the previous analysis.

Retrofitted building - SETUP I
Dynamic Test

Experiments

Vs.

Analyses

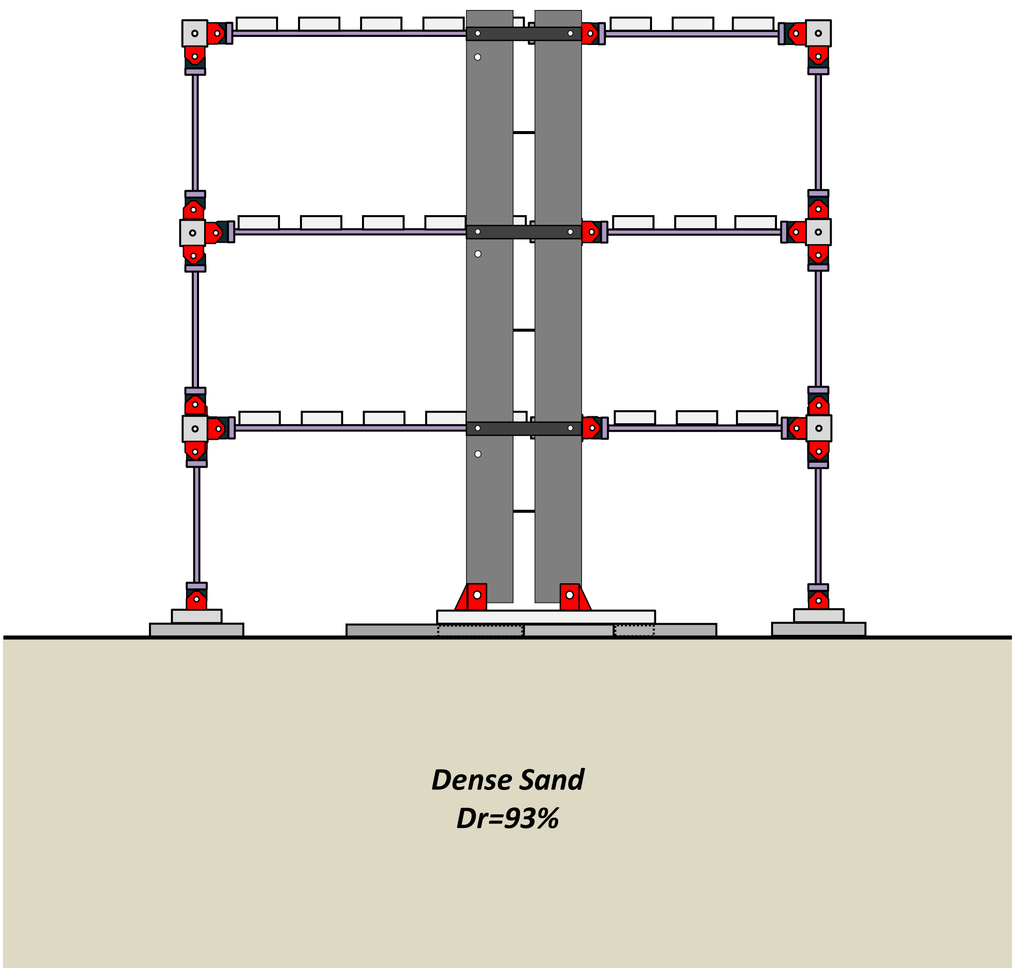

No. of rods per frame → 3
D = 4mm

Central footing bearing capacity

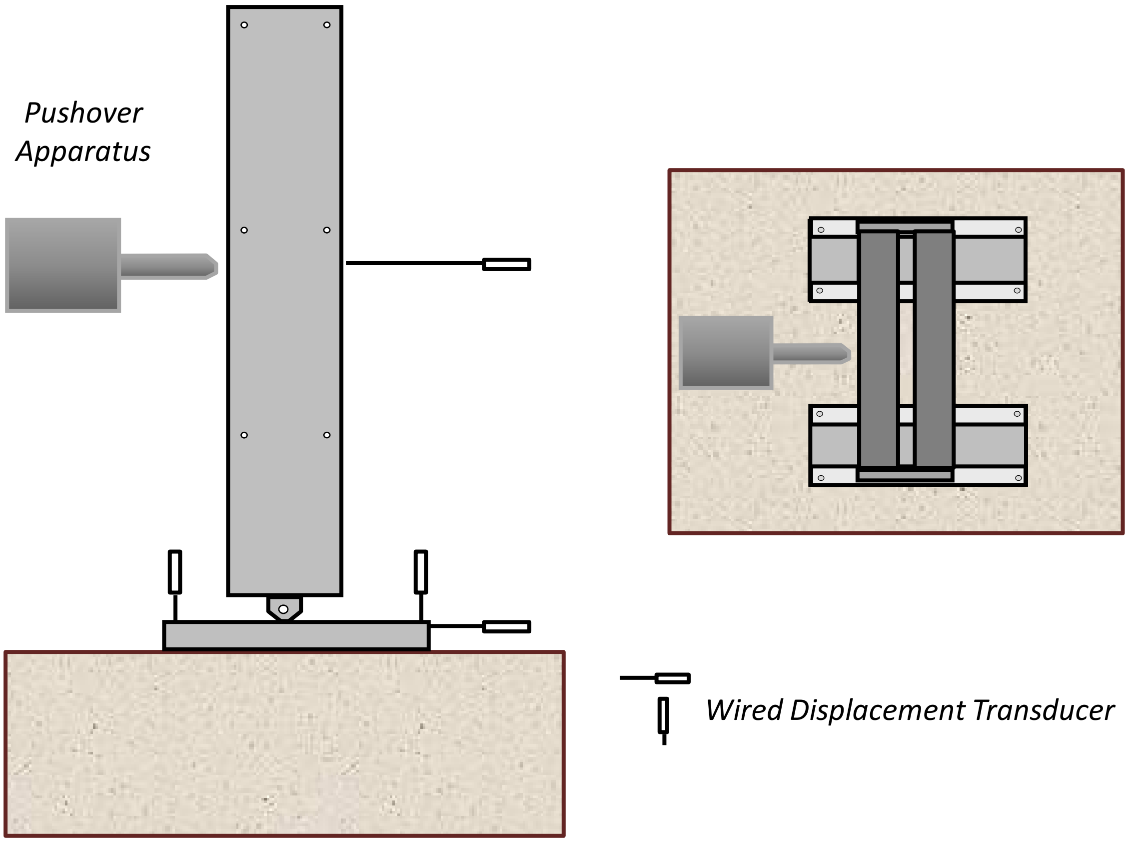

Figure 2.7 Schematic illustration of the footing pushover test and the instrumentation.

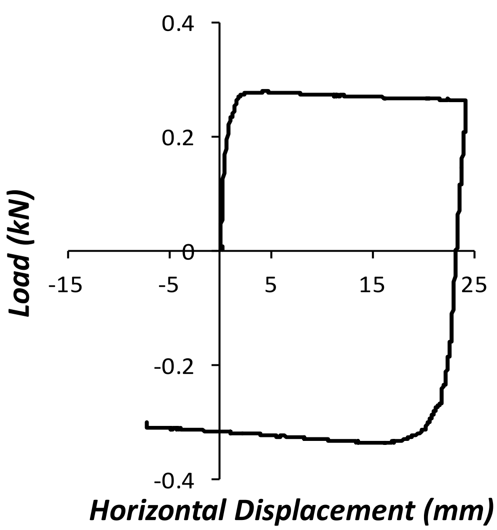

Figure 2.8 Horizontal load with regard to the horizontal displacement on top of the wall.

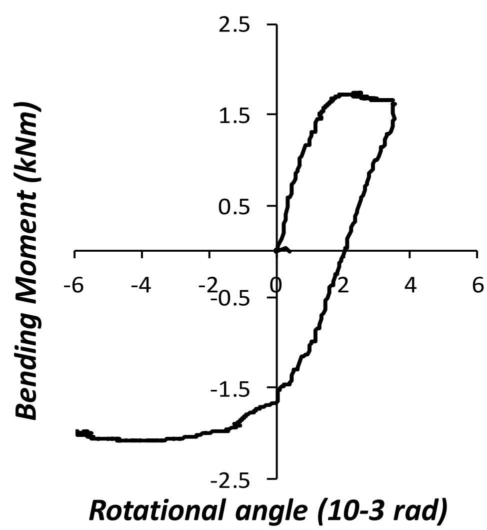

Figure 2.9 Bending moment on base with regard to the rotational angle of the wall.

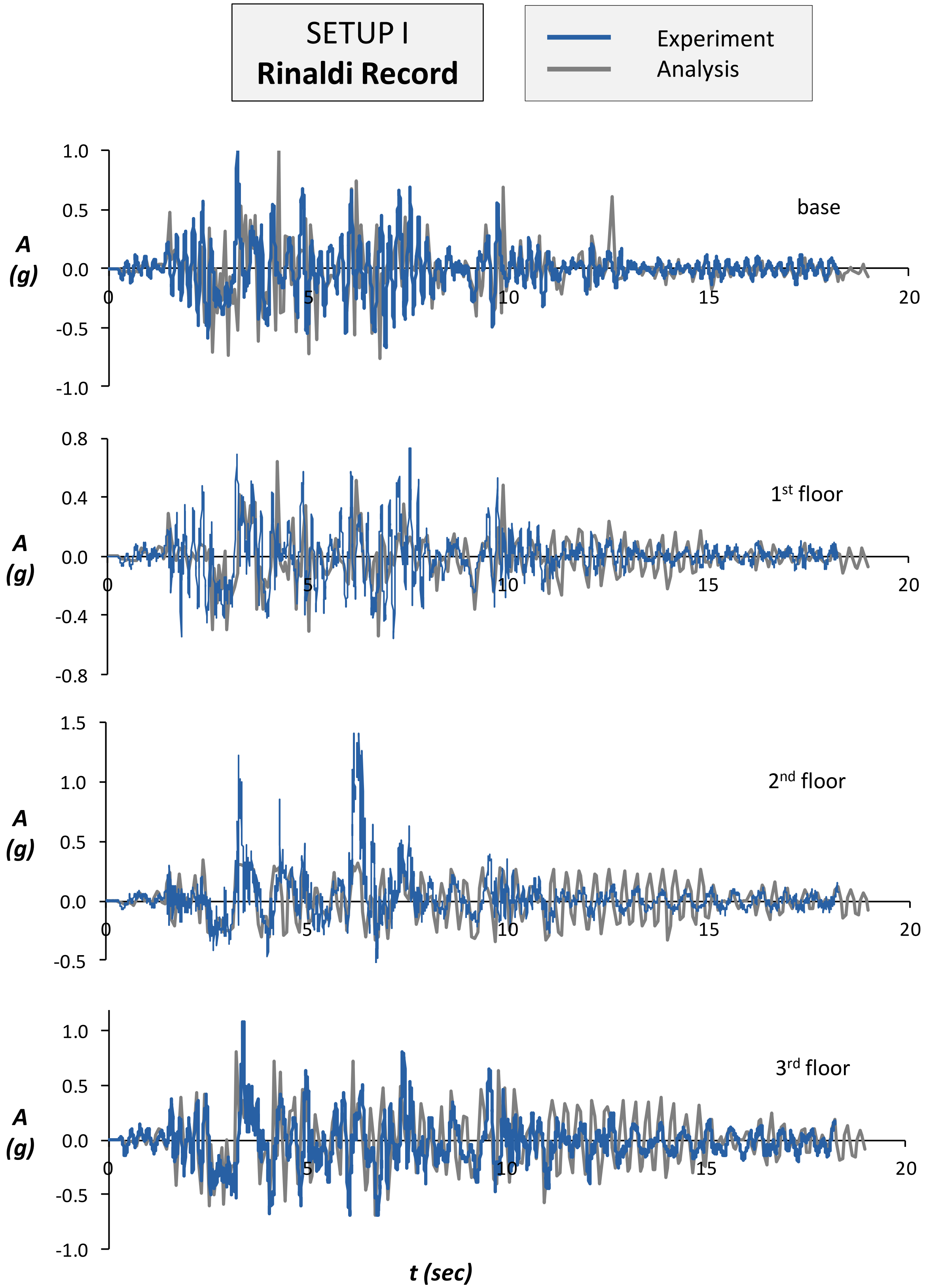

Figure 2.10 Acceleration time histories on the base and on each storey.

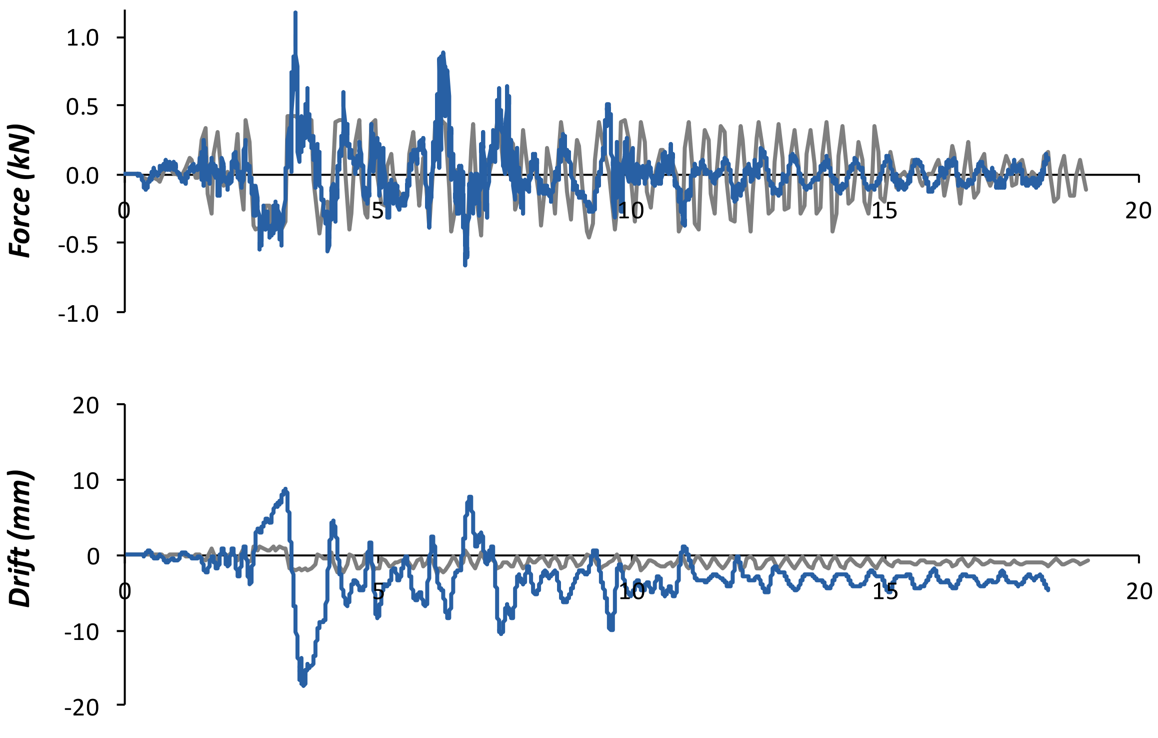

Figure 2.11 Time histories of **(a)** the force and **(b)** the total drift of the building.

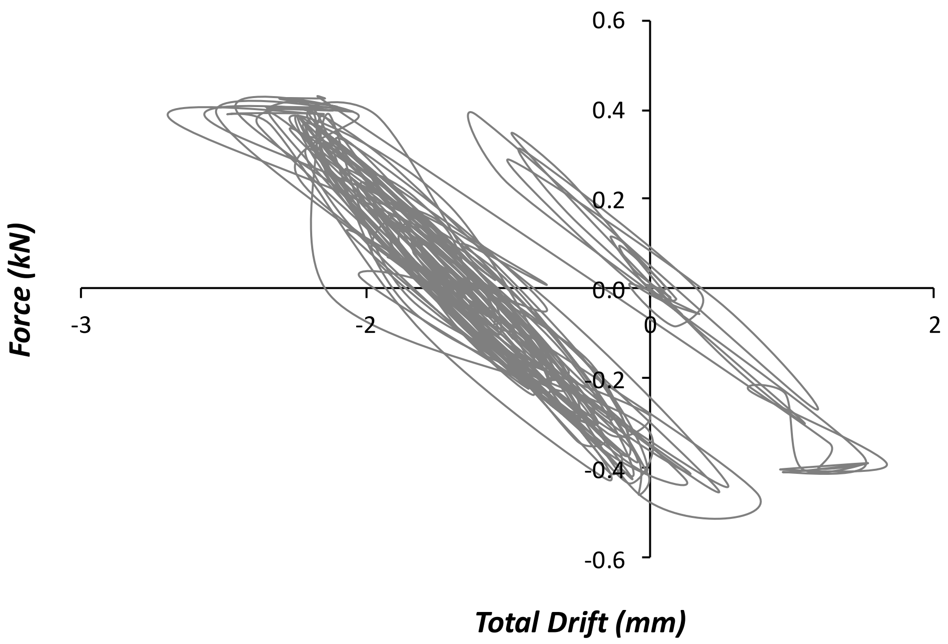

Figure 2.12 Force with regard to the total drift of the building on a ***numerical basis***.

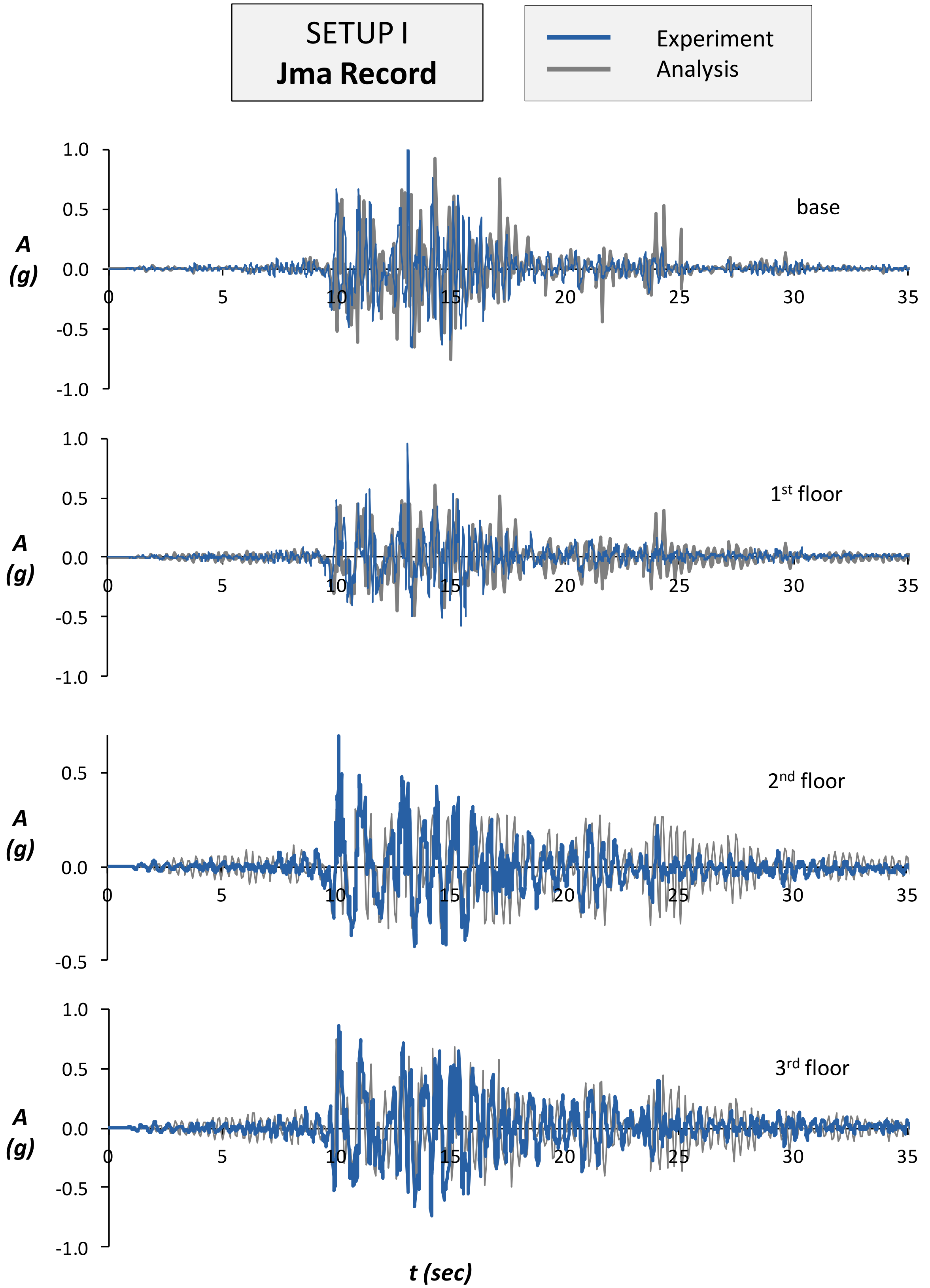

Figure 2.13 Acceleration time histories on the base and on each storey.

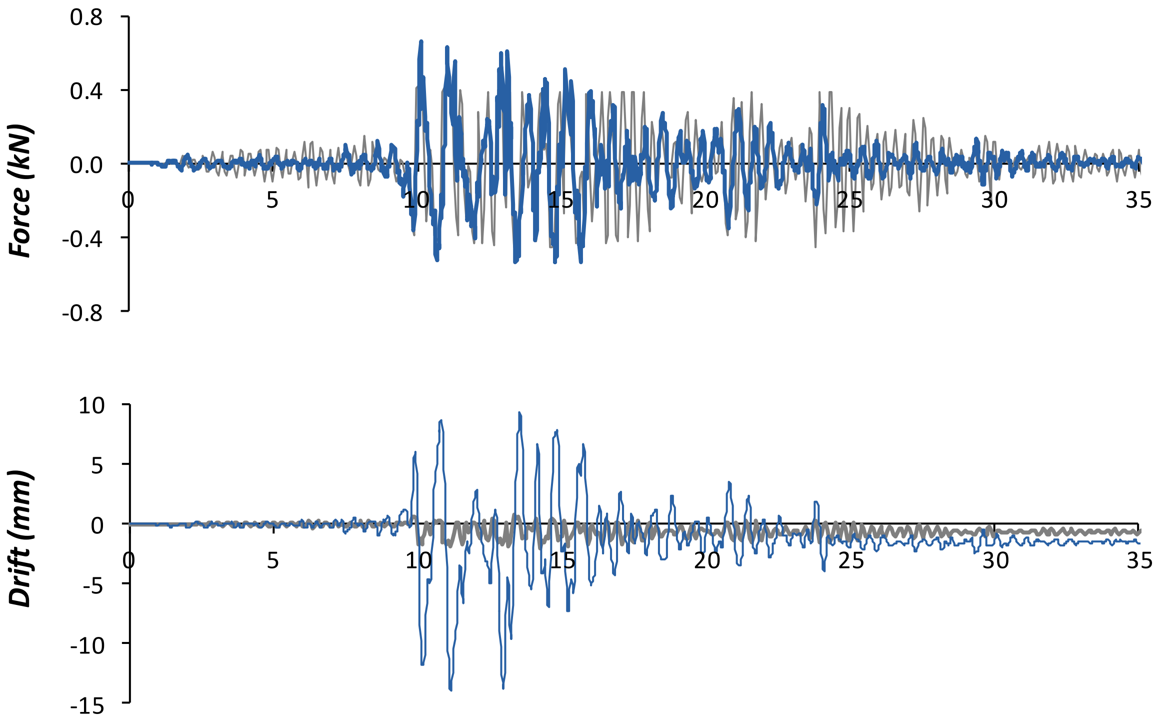

Figure 2.14 Time histories of **(a)** the force and **(b)** the total drift of the building.

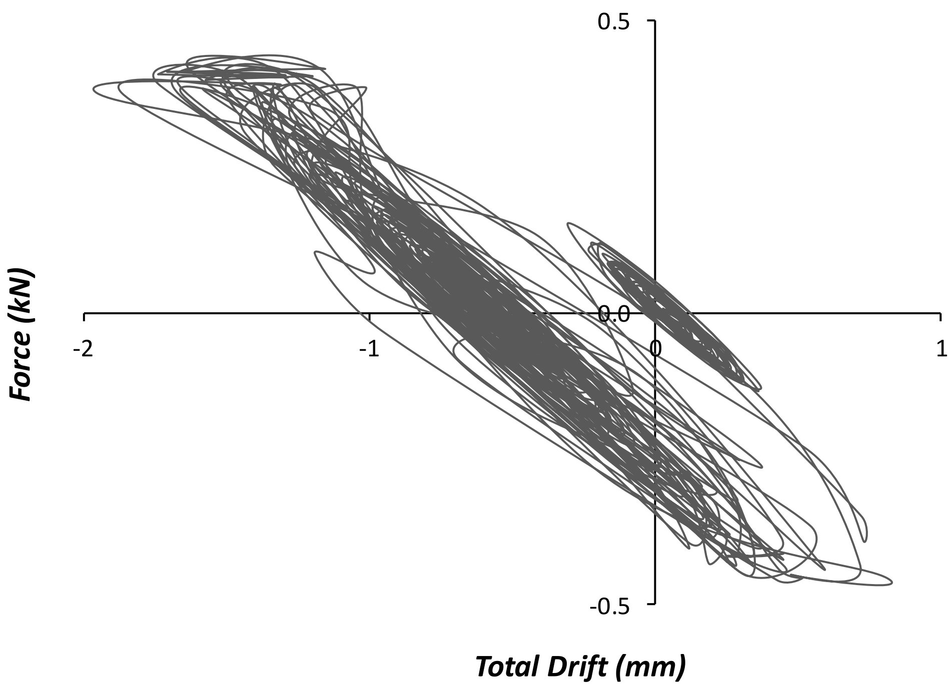

Figure 2.15 Force with regard to the total drift of the building on a ***numerical basis***.

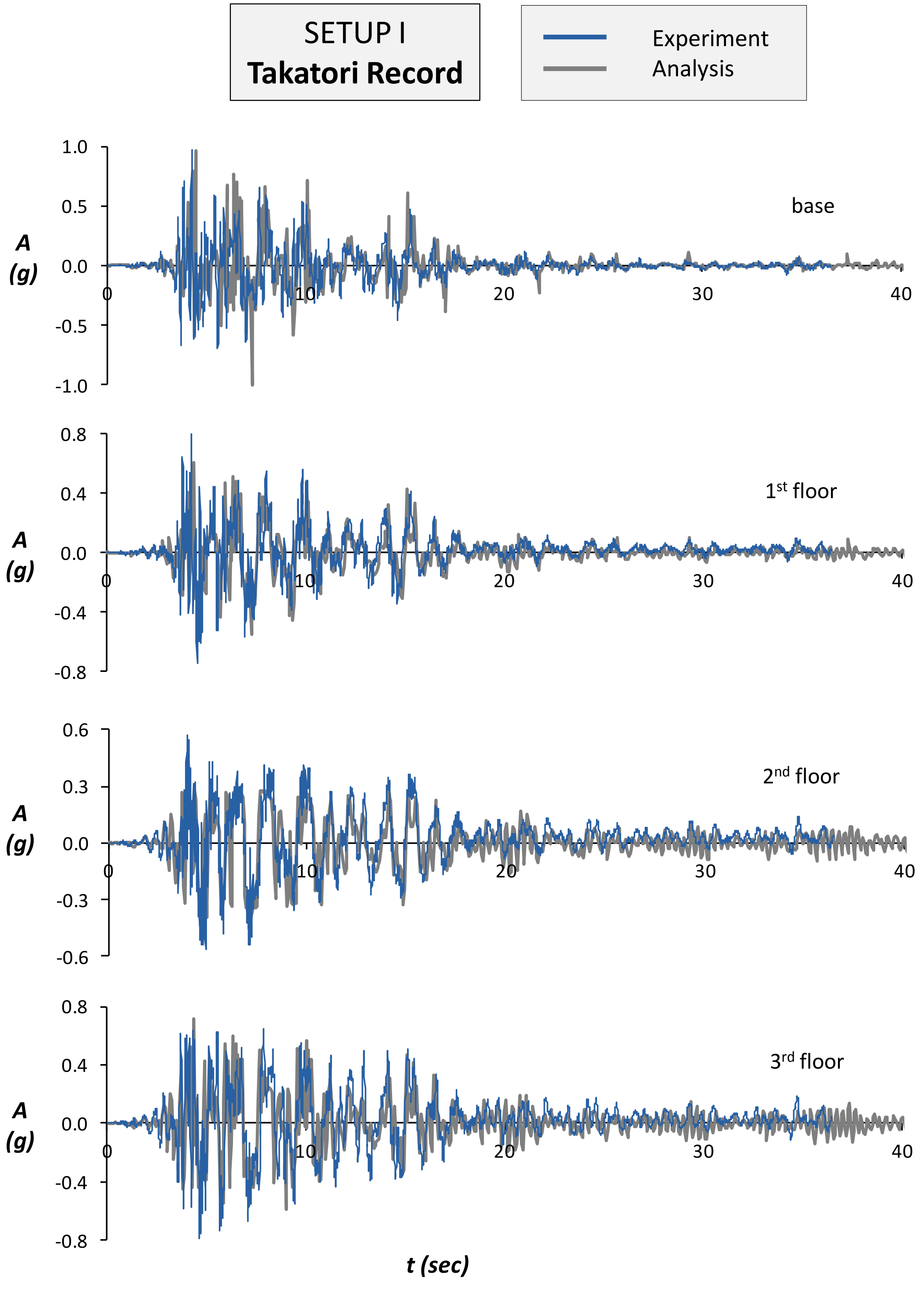

Figure 2.16 Acceleration time histories on the base and on each storey.

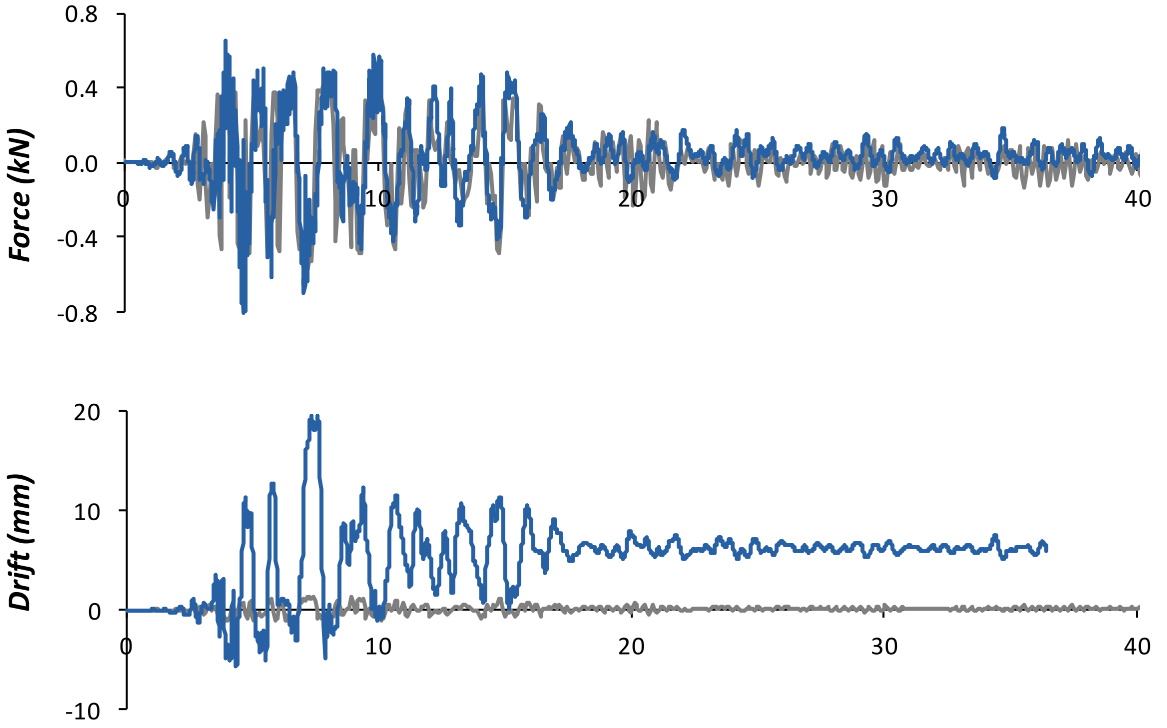

Figure 2.17 Time histories of **(a)** the force and **(b)** the total drift of the building.

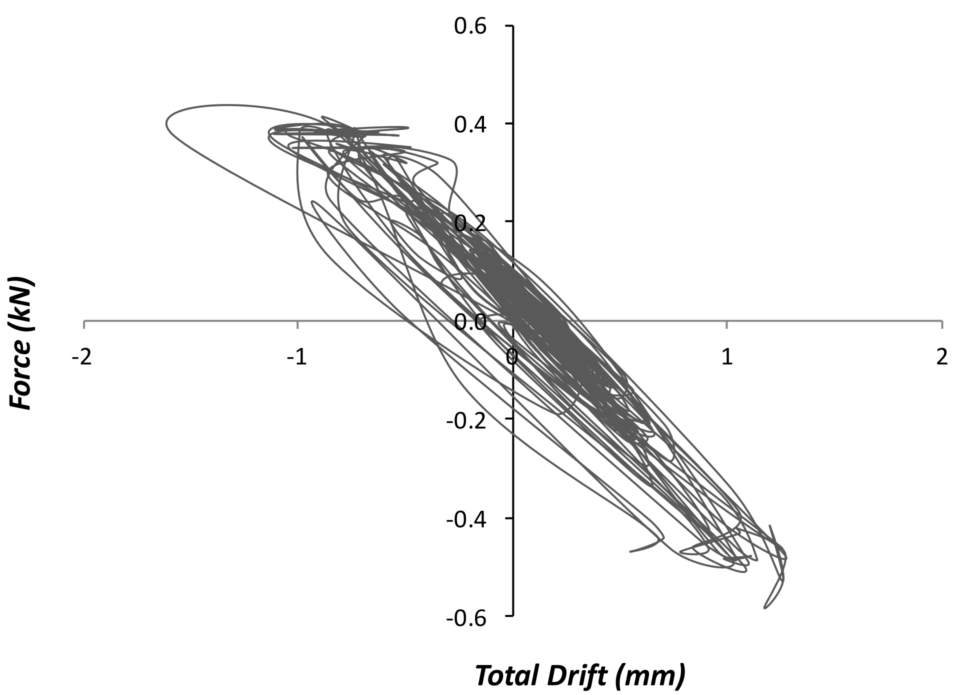

Figure 2.18 Force with regard to the total drift of the building on a ***numerical basis***.

Retrofitted building - SETUP II
Dynamic Test

Experiments

Vs.

Analyses

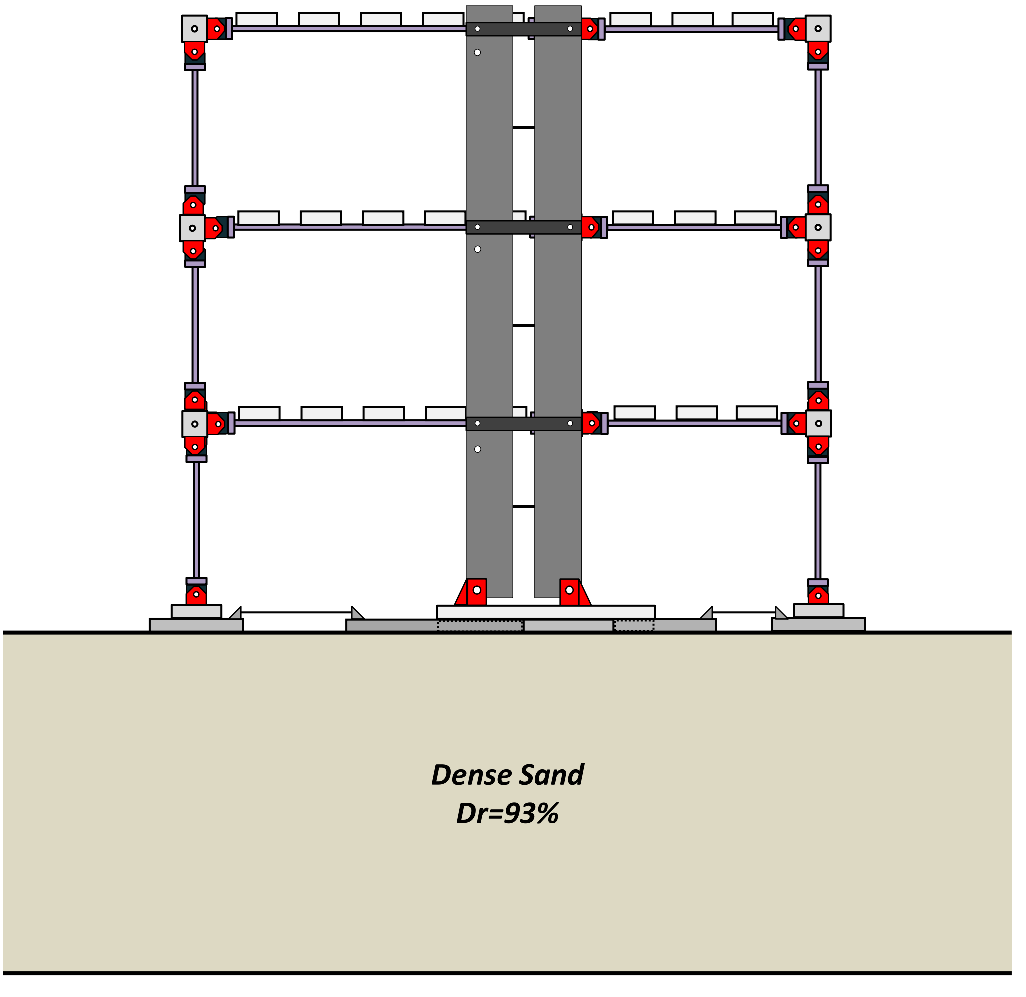

No. of rods per frame → 3

D = 3.2 mm

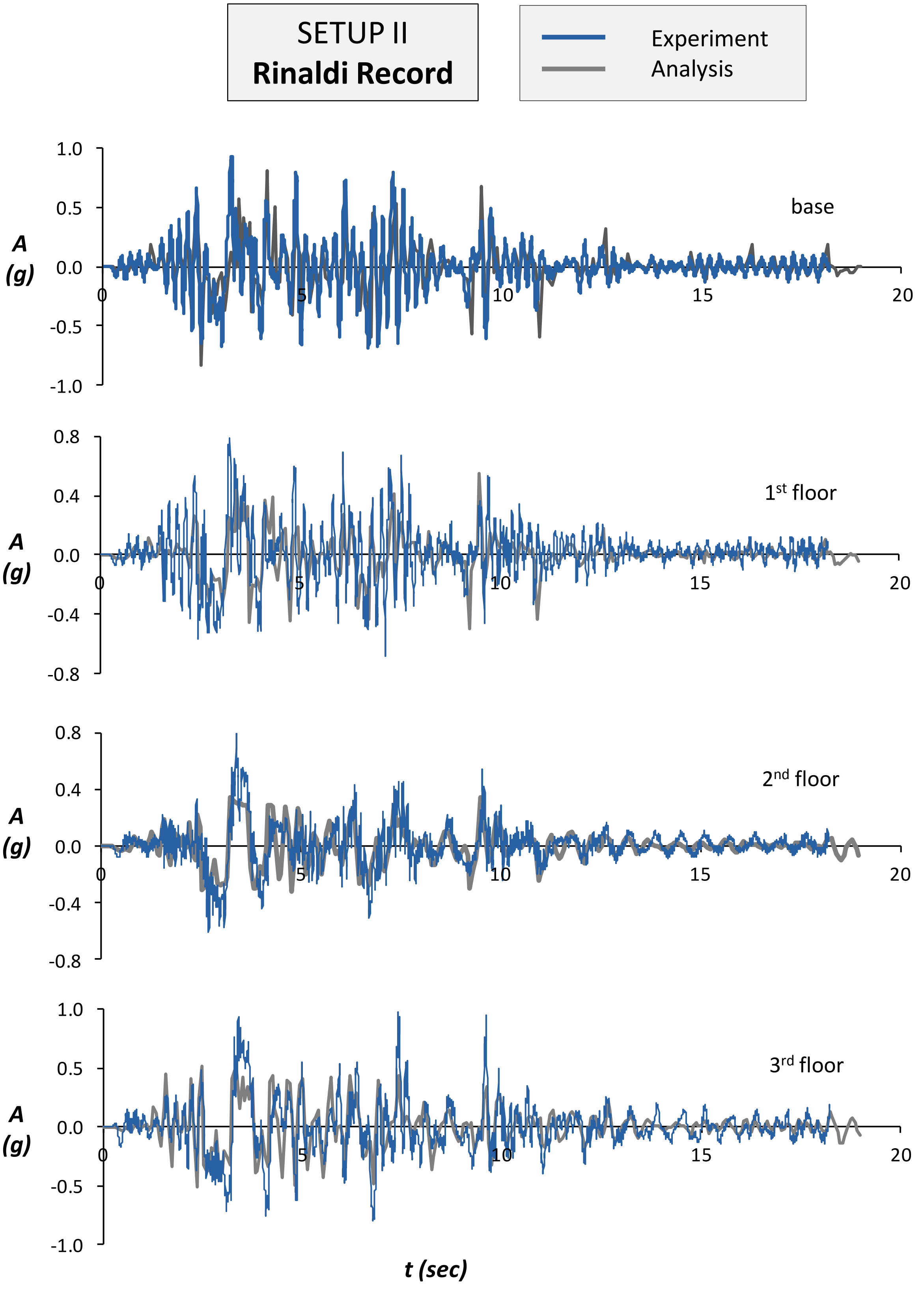

Figure 2.19 Acceleration time histories on the base and on each storey.

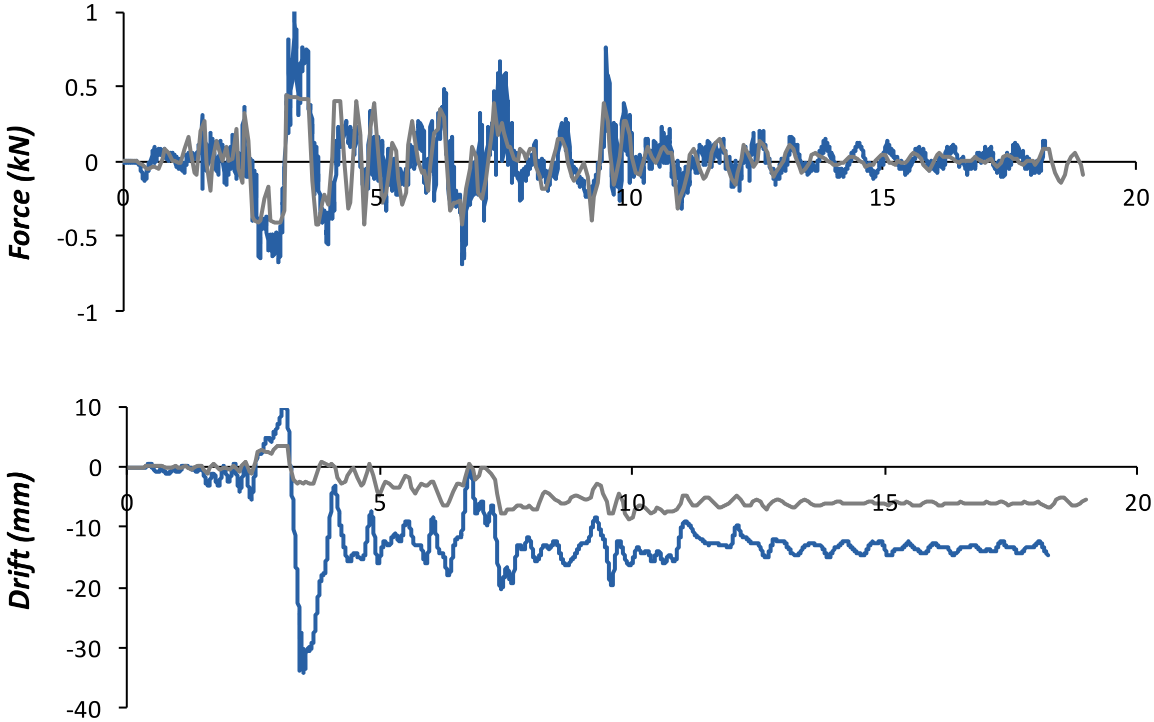

Figure 2.20 Time histories of **(a)** the force and **(b)** the total drift of the building.

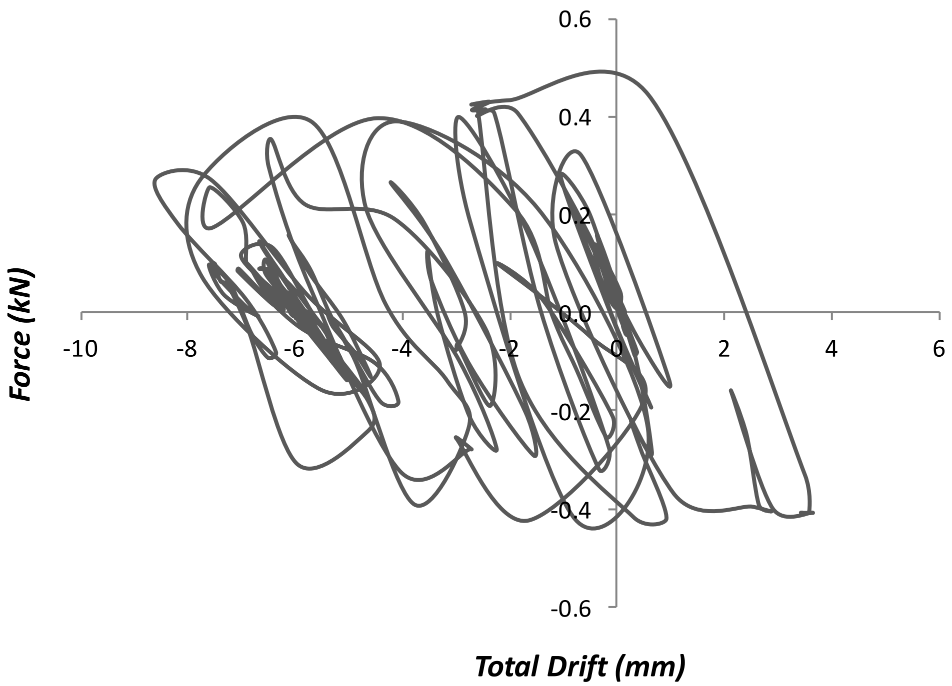

Figure 2.21 Force with regard to the total drift of the building on a ***numerical basis***.

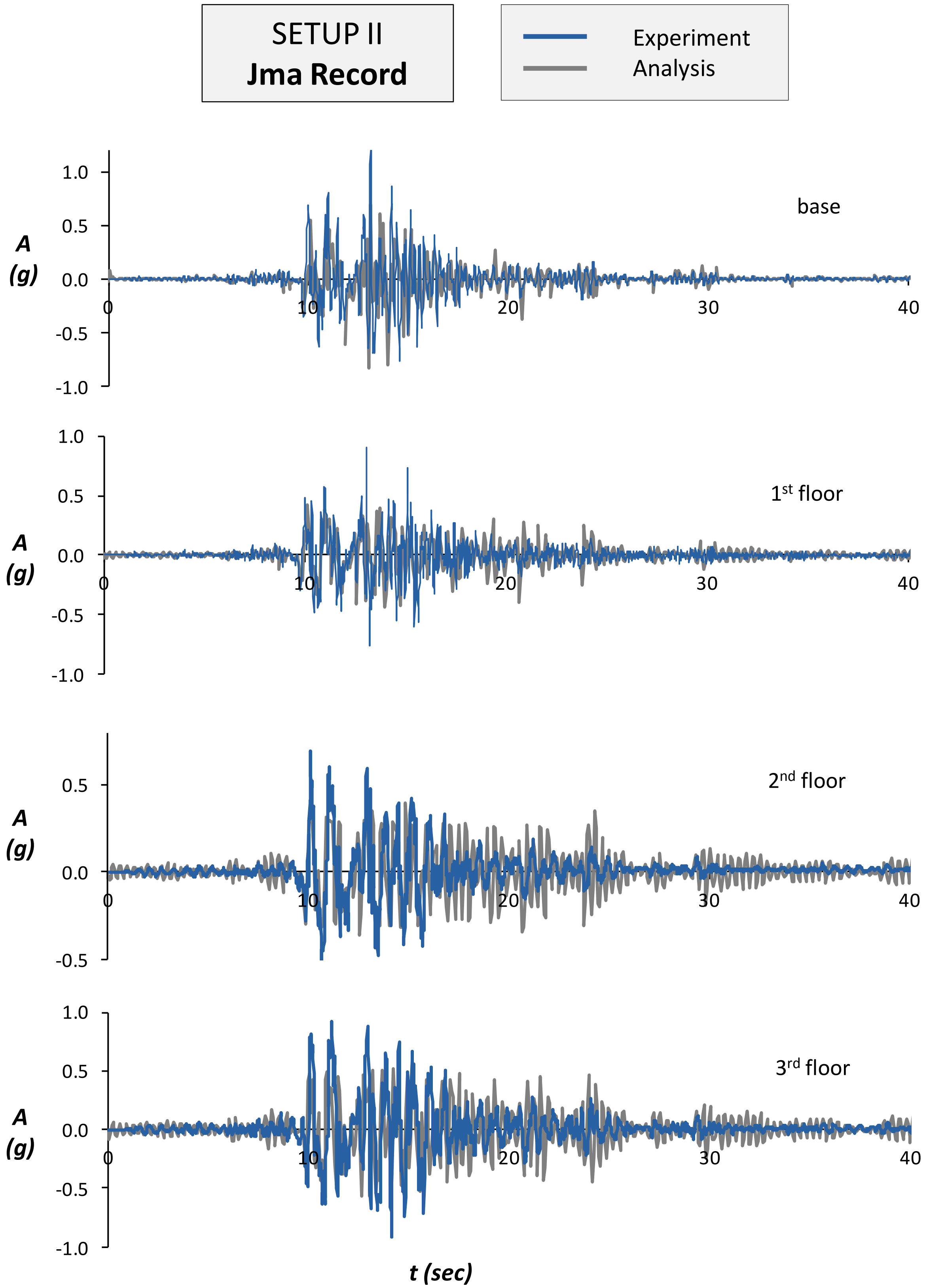

Figure 2.22 Acceleration time histories on the base and on each storey.

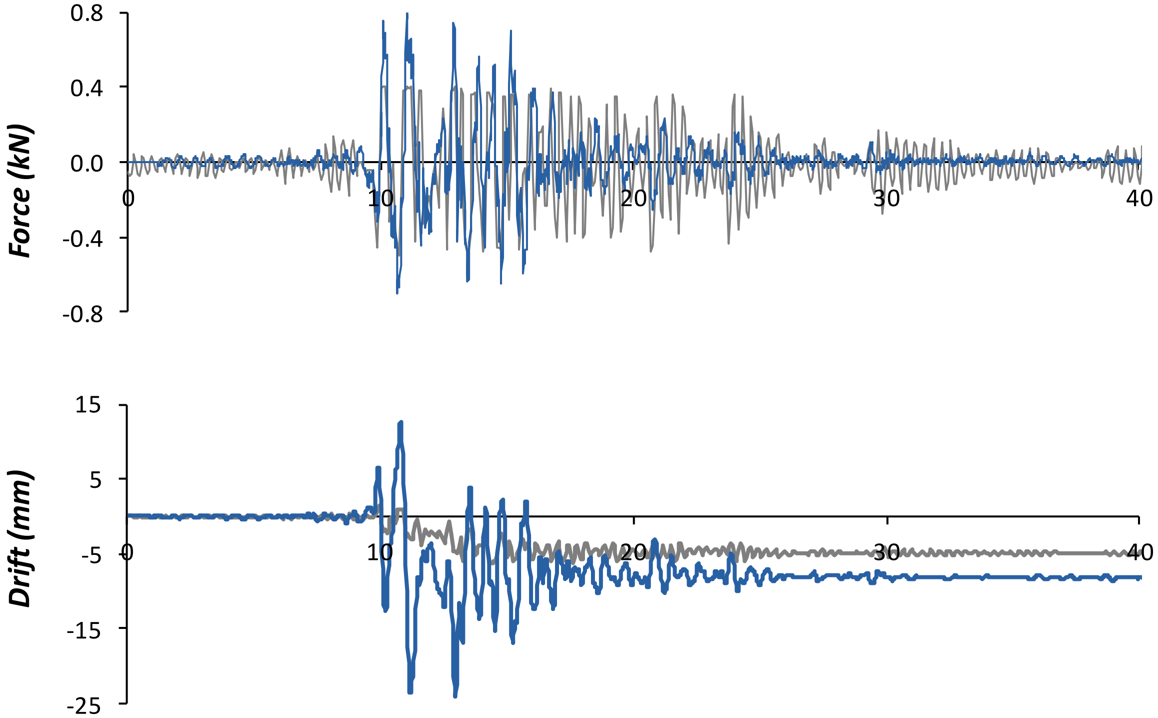

Figure 2.23 Time histories of **(a)** the force and **(b)** the total drift of the building.

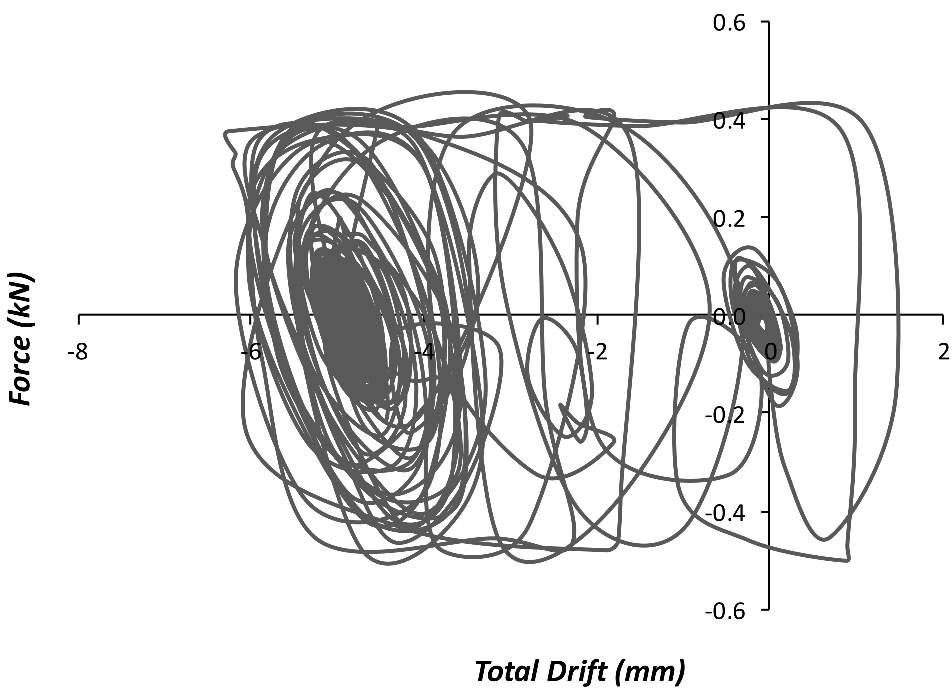

Figure 2.24 Force with regard to the total drift of the building on a ***numerical basis***.

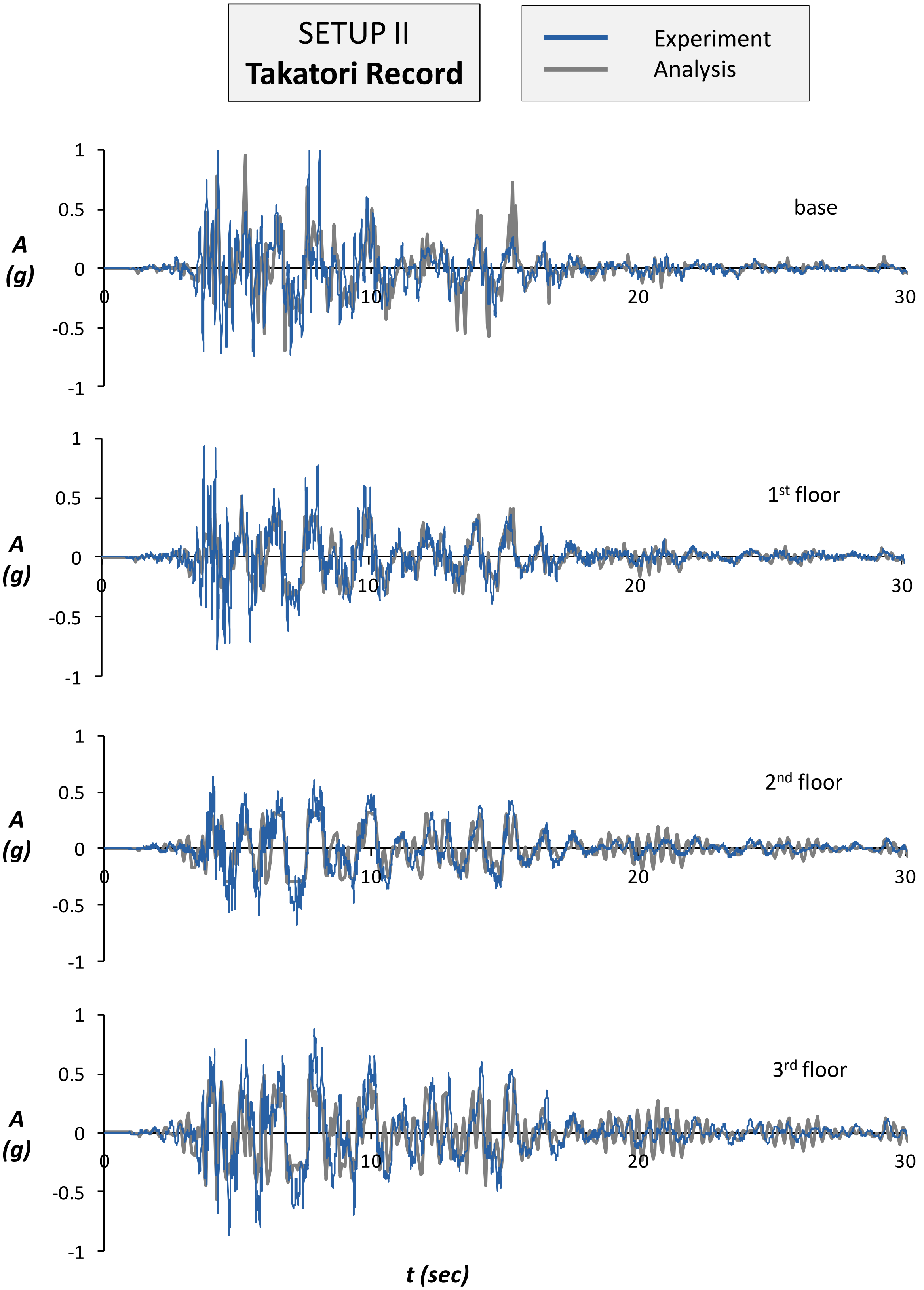

Figure 2.25 Acceleration time histories on the base and on each storey.

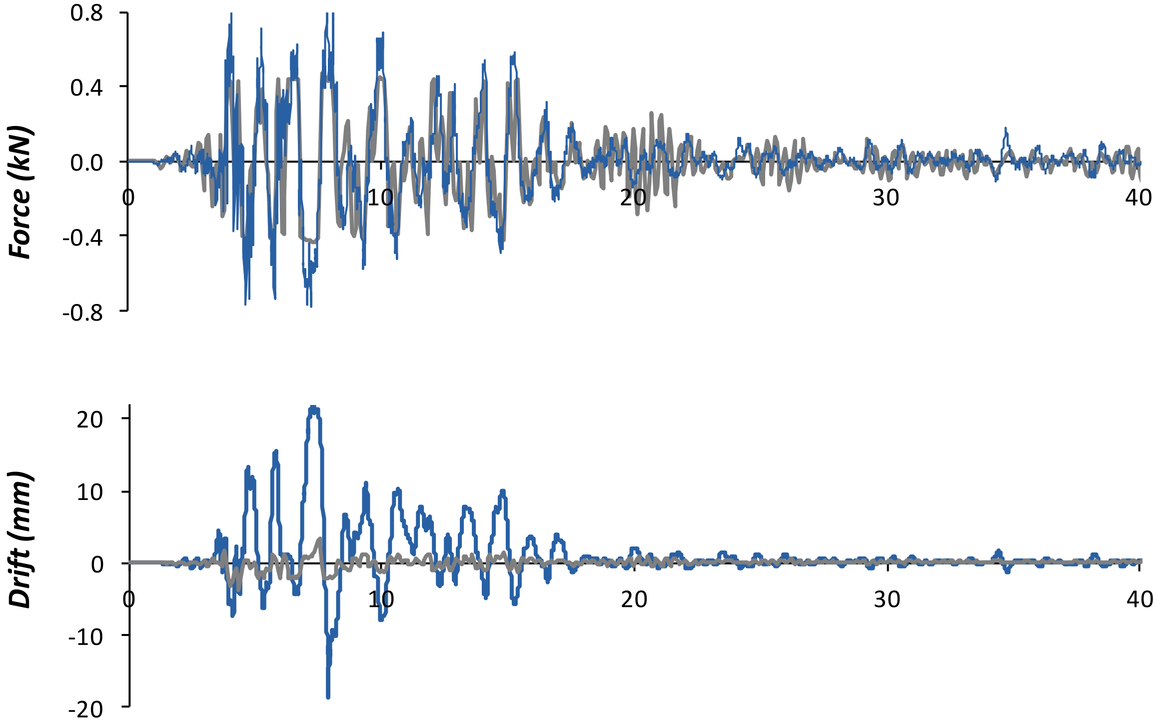

Figure 2.26 Time histories of **(a)** the force and **(b)** the total drift of the building.

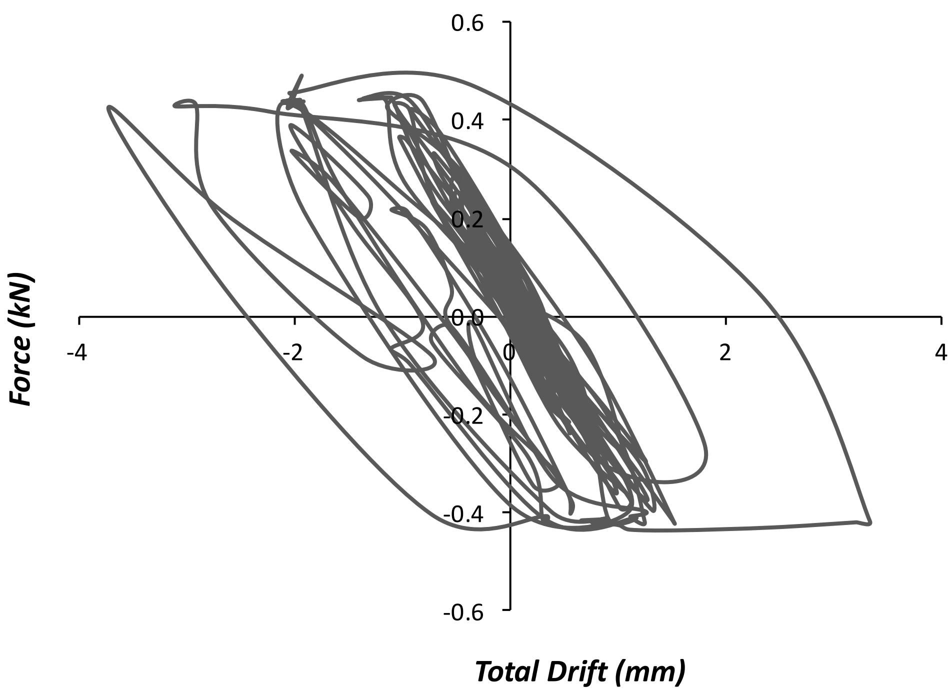

Figure 2.27 Force with regard to the total drift of the building on a ***numerical basis***.

Retrofitted building - SETUP III
Dynamic Test

Experiments

Vs.

Analyses

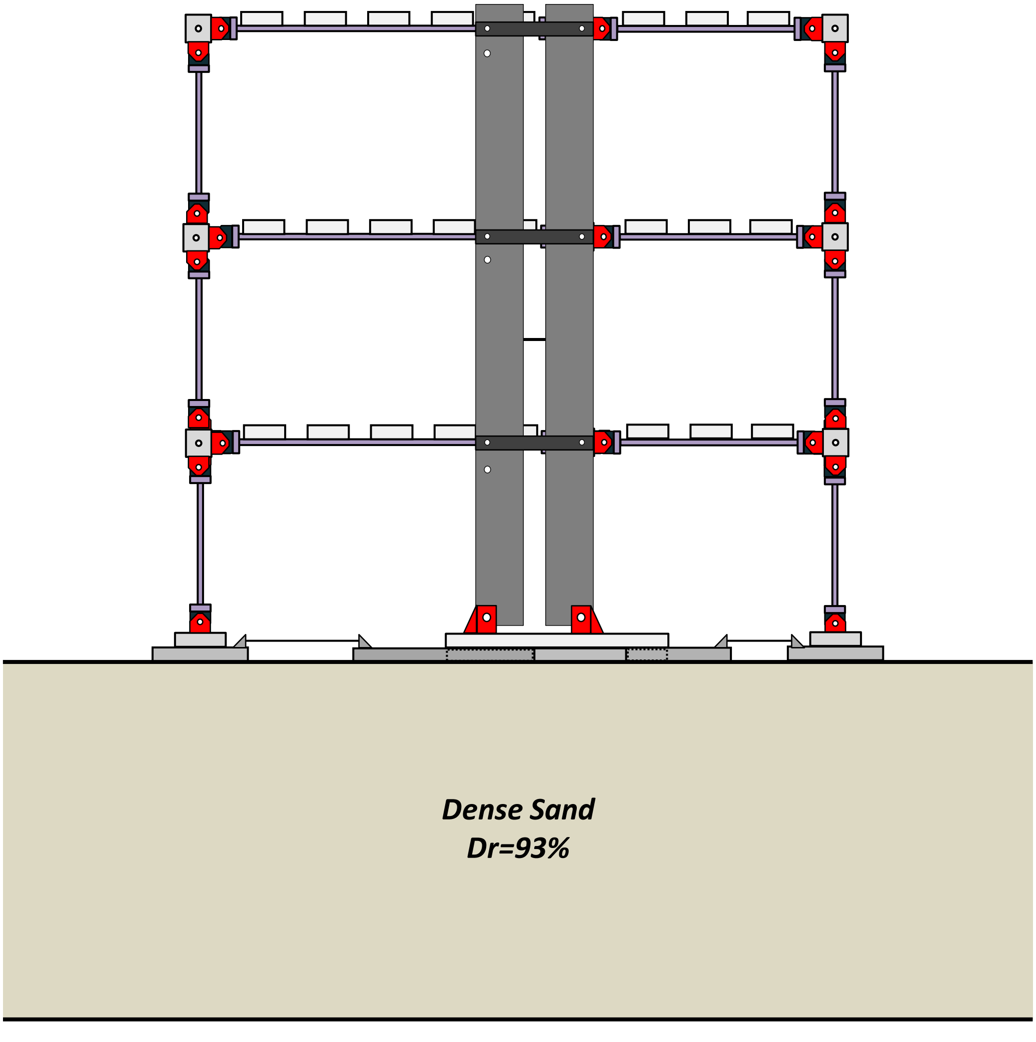

No. of rods per frame → 1
D = 3.2 mm

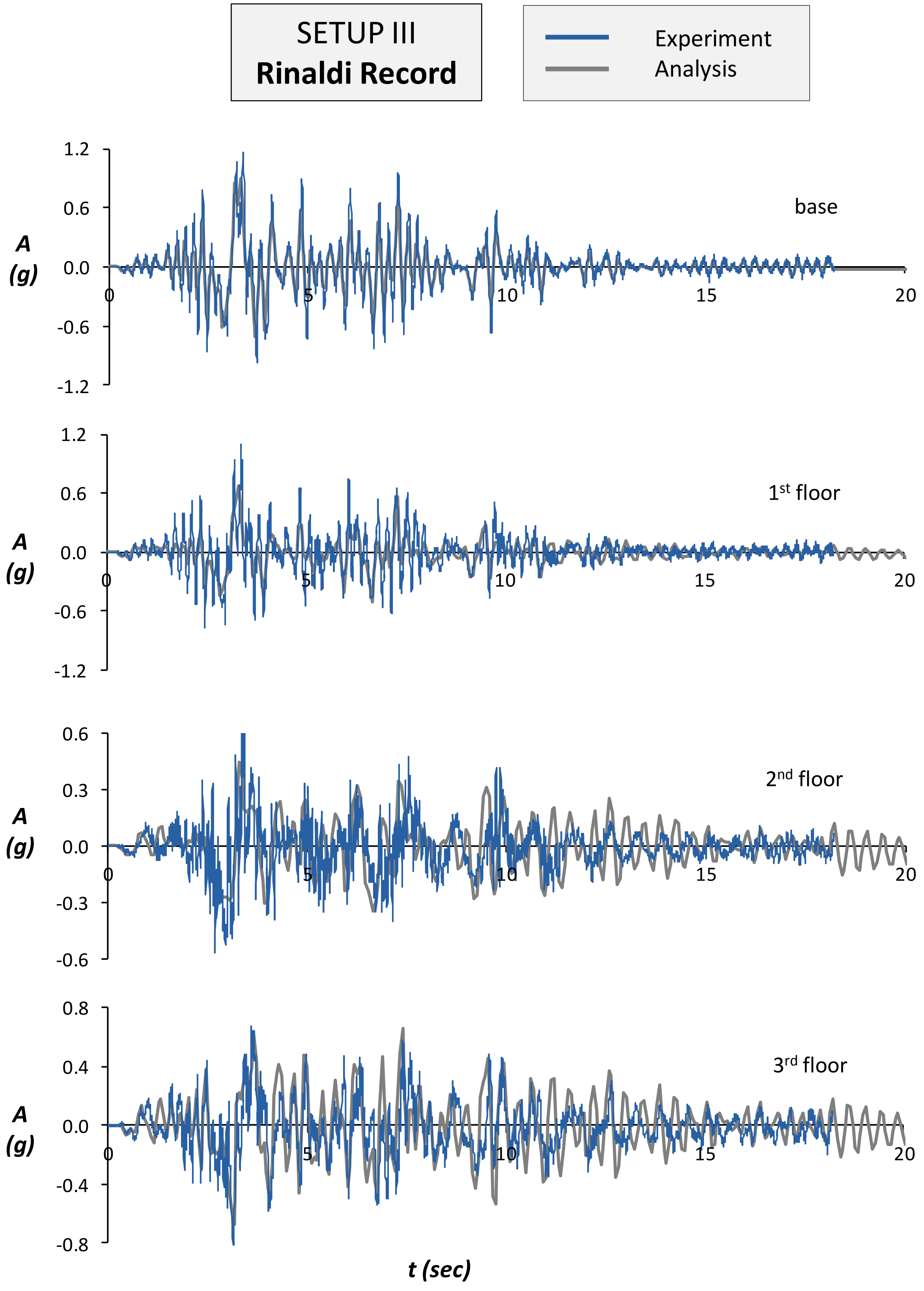

Figure 2.28 Acceleration time histories on the base and on each storey.

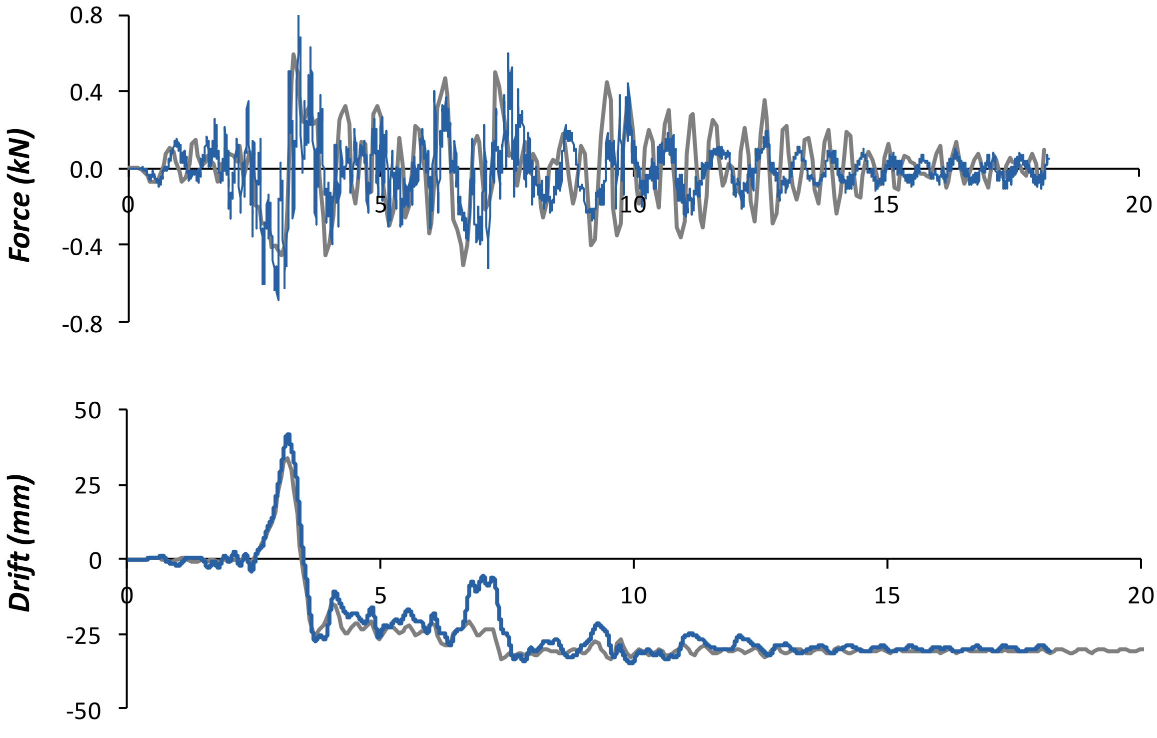

Figure 2.29 Time histories of **(a)** the force and **(b)** the total drift of the building.

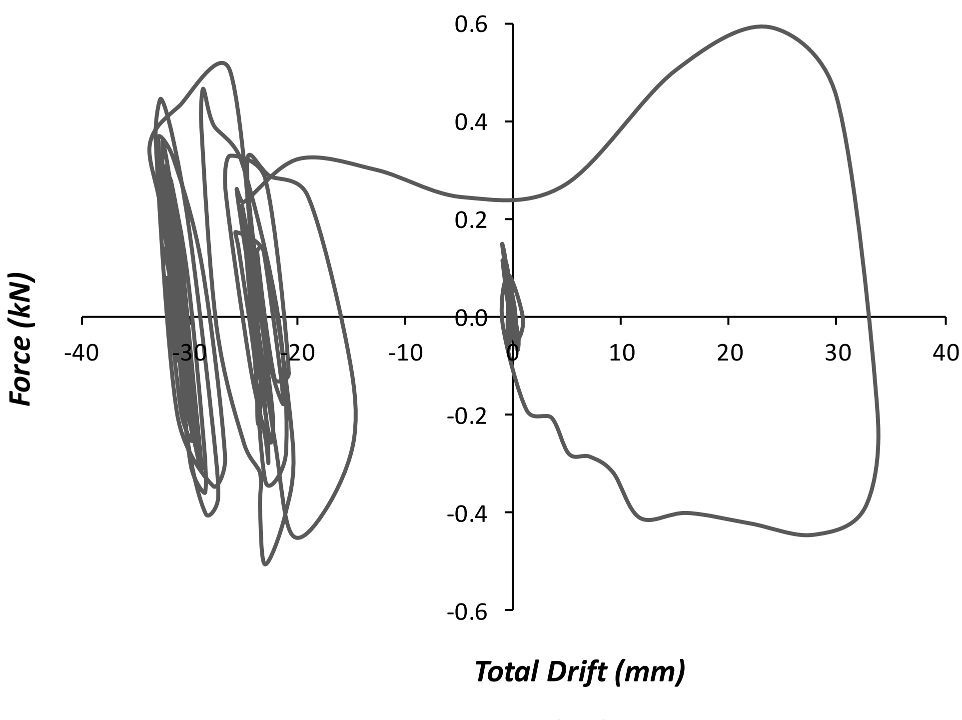

Figure 2.30 Force with regard to the total drift of the building on a ***numerical basis***.

CHAPTER B.3

SEISMIC RESPONSE OF A 1-DOF MODEL STRUCTURE CONSISTING OF THE INSTED SYSTEM

3.1 Introduction

The series of experiments, regarding the retrofitted model building, encased drawbacks that did not allow complete understanding of the INSTED system's dynamic performance. The original model building, due to its properties and the way it was manufactured, displayed certain incompatibilities respecting the design requirements of our retrofitting system. The inability of the artificial hinges to rotate limitlessly, for example, was a problem that could not be solved. Thus, the need arose to examine the seismic response of the INSTED system alone, free of any interference with the building's behavior and properties or any potential soil - structure interaction (Figure 3.1).

3.2 Experimental Setup

The adopted model is a *1-DOF structure system* consisting of the INSTED system, loaded on top with concentrated mass of m = 185 kg (Figure 3.2). In real scale, the model structure simulates a 1-storey structure of 4.5 m height and m = 23 tn at the storey level, thus a scale of 1:5 is considered for the experiment (Table 3.2).

The exact experimental setup includes two horizontal resistance systems (the ones utilized as a retrofit for the 3-storey model building), placed in opposite position and connected together with two Φ14 steel rods. The loading mass consists of two 45,3cm x 40,1cm steel plates, supported regionally by four UPN 140 beams. Anti-diagonal bracings made of steel tape are used in the out-of-plane direction, in order to ensure that buckling in this direction will be prevented. The system's columns are connected through hinges with the footing, which is made of aluminum and has dimensions of 0.60m x 0.15m x 0.02m. In this experiment, the Φ12 spigots used to form the hinge at the base of the INSTED columns are replaced with M12 screws, in order to achieve a less tight arrangement and avoid the creation of a moment resisting connection; in this way one of the main problems of the previously conducted tests is solved. Finally, in accordance to the mass and geometry of the model structure, each INSTED system is equipped with one d = 6mm rod, placed in the middle of its height (Table 3.3)

3.3 Experiment preparation and Instrumentation

Before the experiment, the shaking table is calibrated for a 1:5 scale. The sandbox is not placed on the shaking table, since the structure's base is considered as fixed for this test. Thus, the effects of soil – structure interaction are not taken into consideration and the interest focuses on the seismic performance of the superstructure. The model's footings are placed in opposite positions on the shaking table and are connected rigidly with it. With the help of the crane bridge, the concentrated mass is moved upon the shaking table and along with the system's columns is being installed into the right position. After that, spirit levels are used to ensure that the columns are vertical and the mass horizontal.

In order to measure the horizontal in-plane displacement at the mass level, as well as the relative vertical displacement of rods, three wired displacement transducers are being used. For the placement of the transducer measuring horizontal displacements, a frame consisting of three aluminum bars was installed around the model structure. Additionally, the horizontal in-plane acceleration is measured by two accelerometers at the mass level, one placed in the middle and one at the right back corner of the mass component. The exact instrumentation for the experiment is shown in Figure 3.3.

3.4 Imposed Seismic Motions

Similarly to the previous dynamic experiments, the imposed seismic motions are real records, scaled-down according to the respective scaling laws, so as to correspond to the model's 1:5 scaling factor (Table 3.1). In order to have a more complete picture, we subjected the model structure to both moderate and strong seismic shaking, thus we resulted in this familiar motion sequence: *MNSA – Athens 1999, Lefkada 2003, Rinaldi – Northridge 1994, Jma – Kobe 1995 and Takatori - Kobe 1995*.

3.5 Results

3.5.1. Performance under moderate seismic shaking

The 1-DOF model structure demonstrates excellent behavior during the moderate intensity Greek seismic motions, displaying negligible residual drifts. As depicted in Figures 3.5 (a &b) and 3.6

(a&b), practically zero (≈0) residual horizontal displacement is measured at the top of the structure for the record of MNSA, while only *5mm* are recorded for Lefkada 2003 (0% and 0.6% respectively in terms of storey drift ratio) (Figure 3.8b). The INSTED system does not appear to suffer from significant strain, since the relative vertical displacement measured on the rods is also very small; equal to *0mm* and *1mm* for the records of MNSA (Figure 3.6c) and Lefkada (Figure 3.8c) respectively. The maximum acceleration the 1 – DOF structure reaches during these motions is measured equal to 0.28g, in the record of Lefkada.

3.5.2. Performance under strong seismic shaking

Since the structure performed so well during moderate seismic shaking, it is afterwards challenged to demonstrate its sustainability during the extremely strong seismic records of Rinaldi, Jma and Takatori (Figure 3.4).

The first motion applied to the 1 DOF system is that of Rinaldi (with a_{max} = 0.84g). The model withstands the imposed record, displaying though significant deformation and acquiring a residual drift equal to *40mm* (or *4%* in terms of drift ratio) (Figure 3.10a). The residual vertical rod displacement is measured equal to *6.5mm* (Figure 3.10c), proving that the fuse elements of the INSTED system entered the plastic zone, in order to dissipate the required amounts of seismic energy. As depicted in Figure 3.9 (b), during the record's strong pulse the structure reaches an acceleration of about 0.85g at the mass level. Then, the structure is submitted to the record of Jma (with a_{max} = 0.82g), which also manages to sustain; again large values of residual drift (30mm) and vertical rod displacement are developed (5.5mm) and the maximum measured acceleration value at the mass level is equal to 0.7g. (Figures 3.11 -3.12 (a,b,c)) However, its response is considered quite satisfactory, considering the severity of the record imposed. Finally, the 1 – DOF model structure is subjected to the Takatori record, with a_{max} = 0.61g. Having accumulated significant permanent deformation from the previous records, the system collapses during this motion, displaying a residual vertical rod displacement equal to *23.5mm* (Figure 3.14 c, Figure 3.15). The maximum value of acceleration measured on top was almost 1g (Figure 3.13 c). One can easily observe, from the photo displayed in Figure 3.16, that the right column of the INSTED system has reached the critical value of rotation at the base (ϕ_{crit} = 8 degrees) and cannot rotate any further. The value of ϕ_{crit} corresponds to a storey drift equal to 140mm at the top of the structure (or 14% in terms of interstorey drift), hence the system is considered to have experienced failure.

Chapter B.3

Figures

1-DOF MODEL STRUCTURE Dynamic Test

Table 3.1 List of applied seismic records.

Moderate Seismic Records
MNSA (Athens 1999) Lefkada (2003)
Strong Seismic Records
Rinaldi (Northridge 1994) JMA (Kobe 1995) Takatori (Kobe 1995)

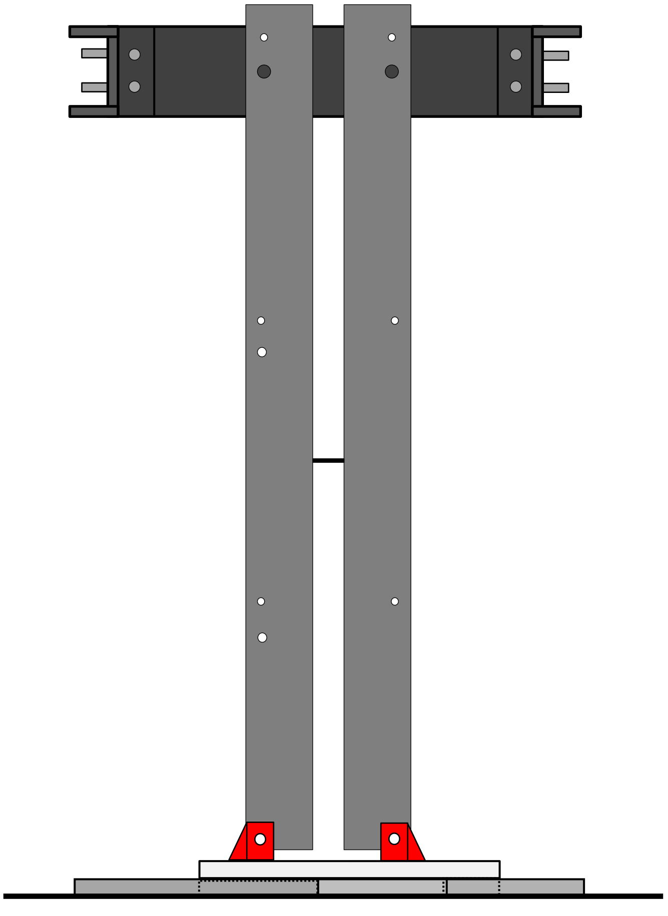

Figure 3.1 Schematic illustration of the 1-DOF structural system.

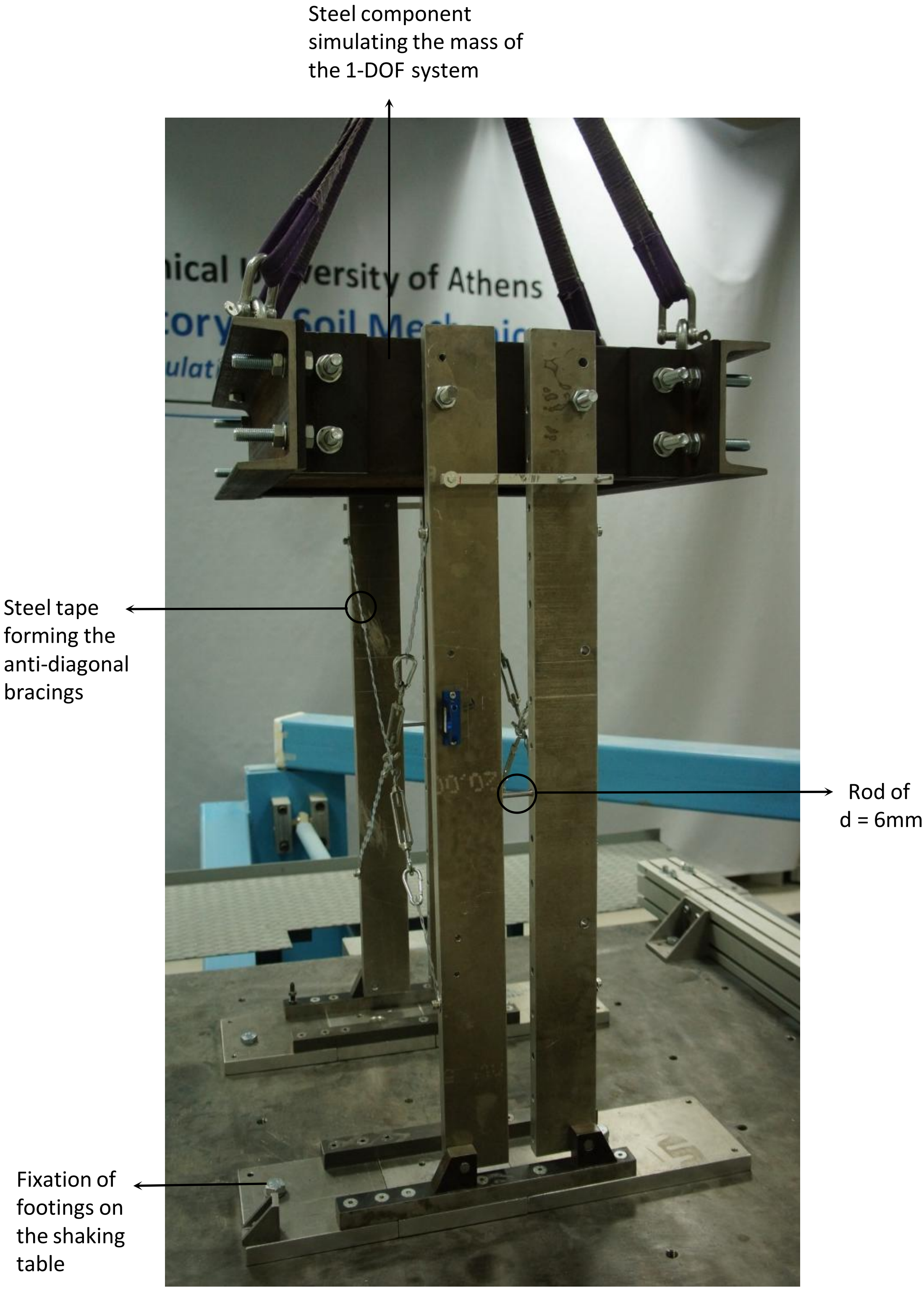

Figure 3.2 Photograph the 1 – DOF model structure.

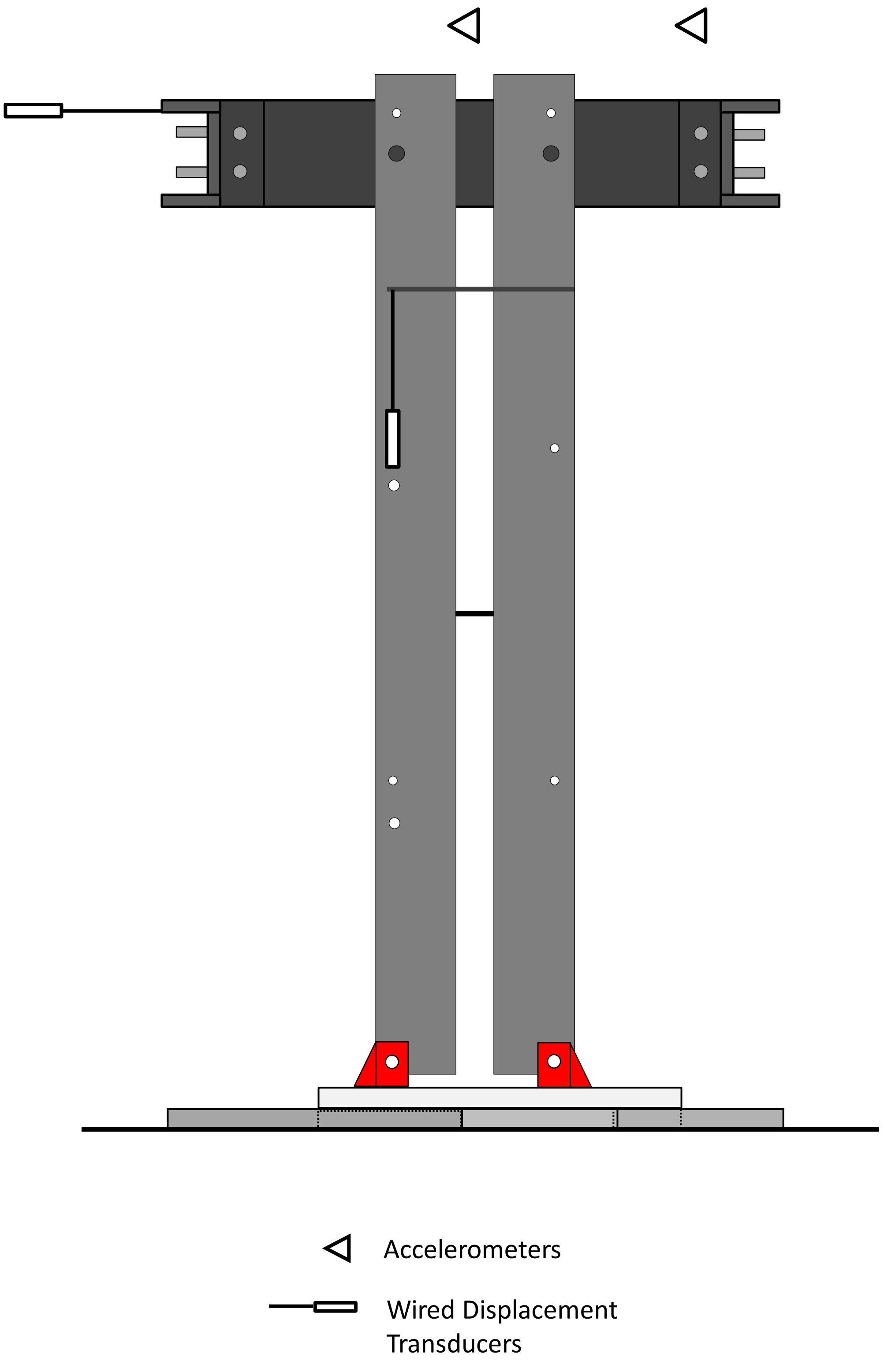

Figure 3.3 Schematic illustration of the model structure's instrumentation.

Quantity to be scaled	1g scaling factor prototype to model ratio	Centrifuge scaling factor prototype to model ratio
Displacement	N	N
Time (dynamic)	$N^{0.5}$	N
Velocity	$N^{0.5}$	1
Acceleration	1	N^{-1}
Force	$\rho*N^{3}$	N^{2}
Energy, moment	$\rho*N^{4}$	N^{3}
Moment of inertia	N^{5}	N^{4}
Frequency	$N^{-0.5}$	N^{-1}

Table 3.2 Scaling factors for 1g and centrifuge modeling.

Calculated horizontal shear force undertaken by the 1 – DOF model structure		
Horizontal yield force per system	▶	$$F = \sum_{n=1}^{N} Mpl \frac{2 \times b}{h \times leff}$$
Rod moment capacity	▶	$$Mpl = Wpl \times fy = \frac{d^3}{6} \times fy$$

- Leff = 3.0 cm
- N = 1 rod
- h = 90 cm
- D = 0.6 cm
- b = 15 cm
- fy = 347 MPa

Mpl = 0.0125 kNm

Force per system: F = 0.14 kN

Total yield force: ***F = 0.28 kN***

Total yield acceleration: ***Ay = 0.14g***

Table 3.3

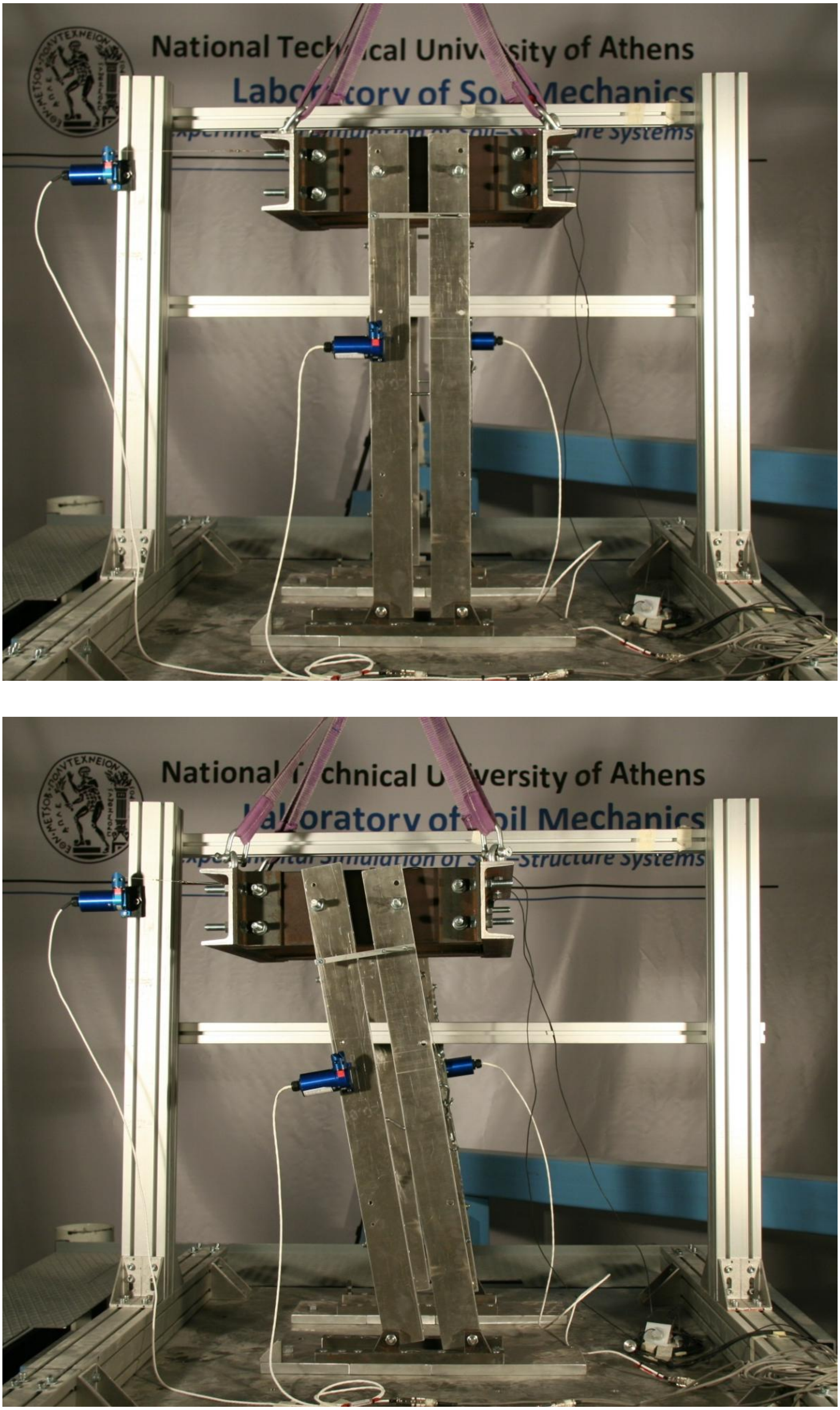

Figure 3.4 Initial and deformed shape of the 1-DOF structure system after the record of Takatori.

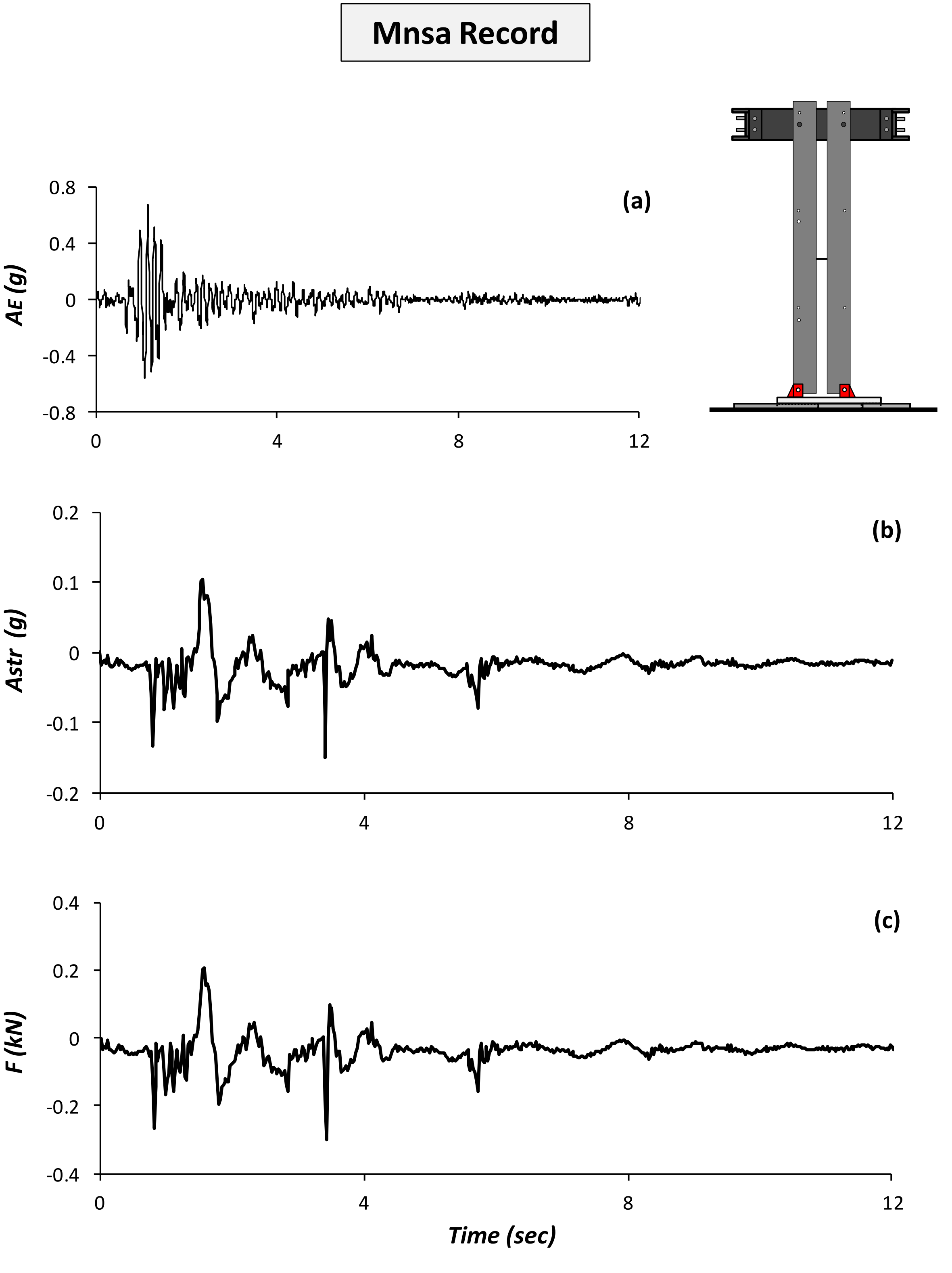

Figure 3.5 Time histories of **(a)** the acceleration used as base excitation, **(b)** the acceleration measured at the mass level and **(c)** the structure's horizontal resistance.

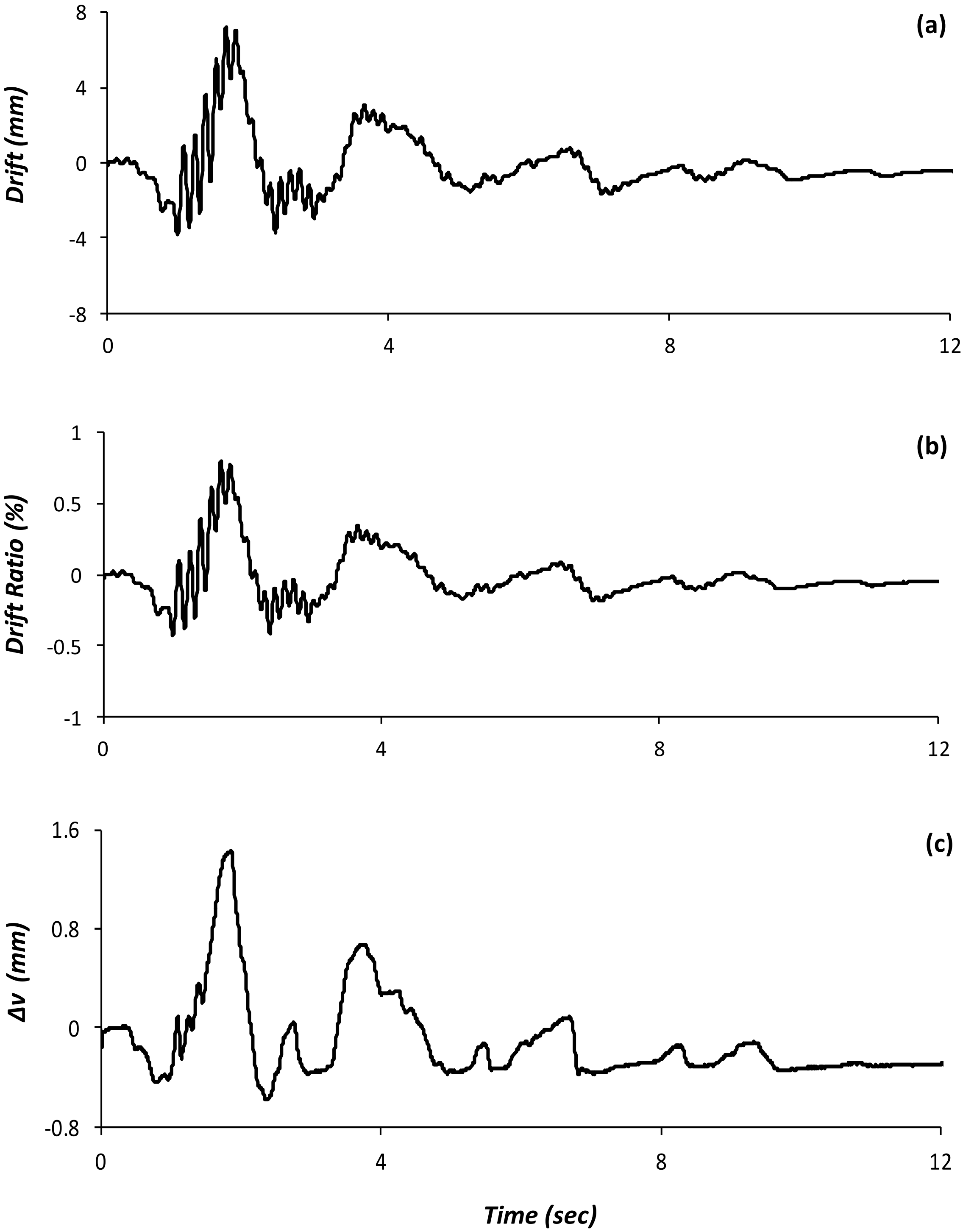

Figure 3.6 (a) Time history of the structure's total drift, **(b)** the respective drift ratio and **(c)** the relative vertical displacement of the rod for the *Mnsa record*.

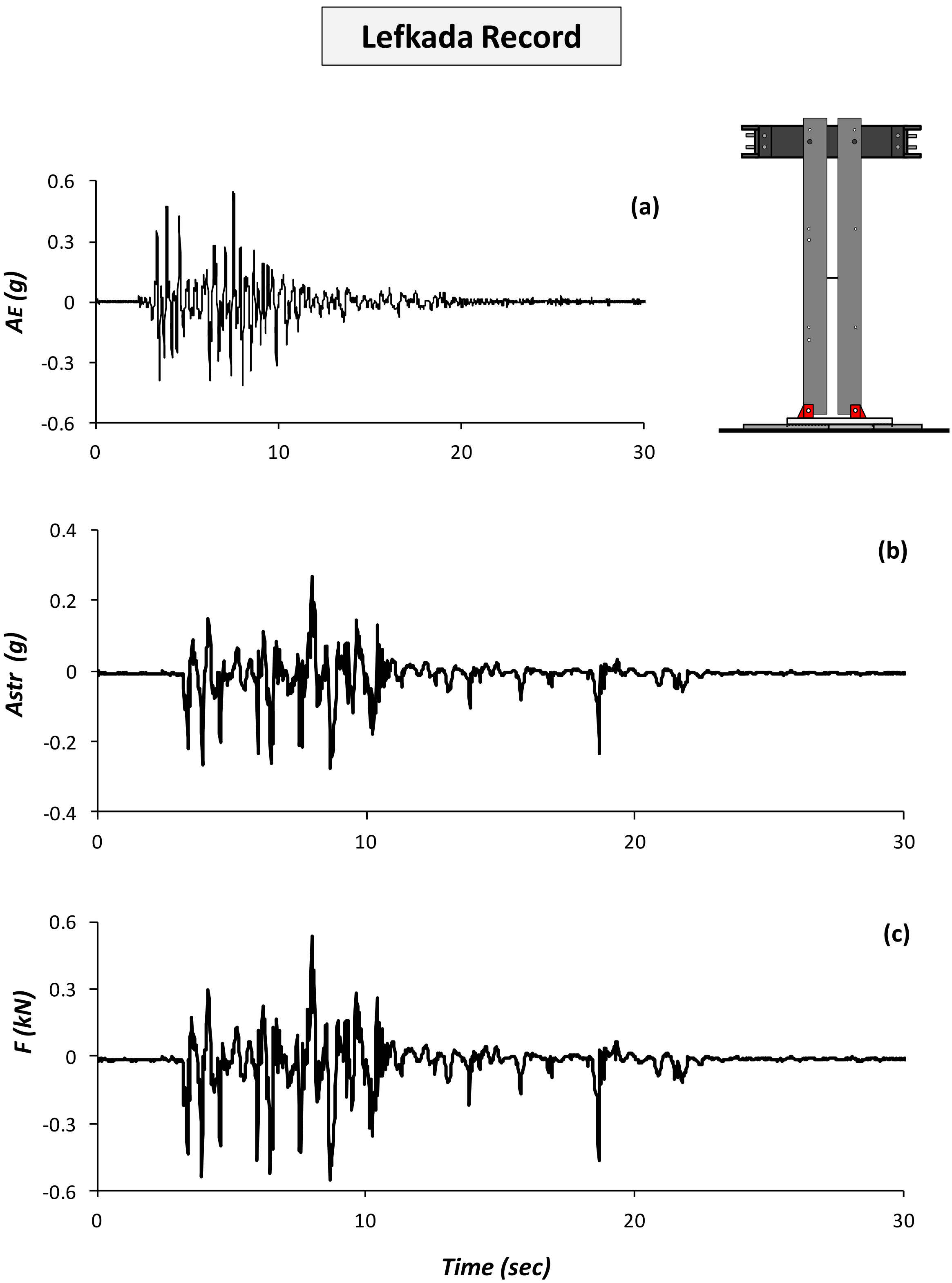

Figure 3.7 Time histories of **(a)** the acceleration used as base excitation, **(b)** the acceleration measured at the mass level and **(c)** the structure's horizontal resistance.

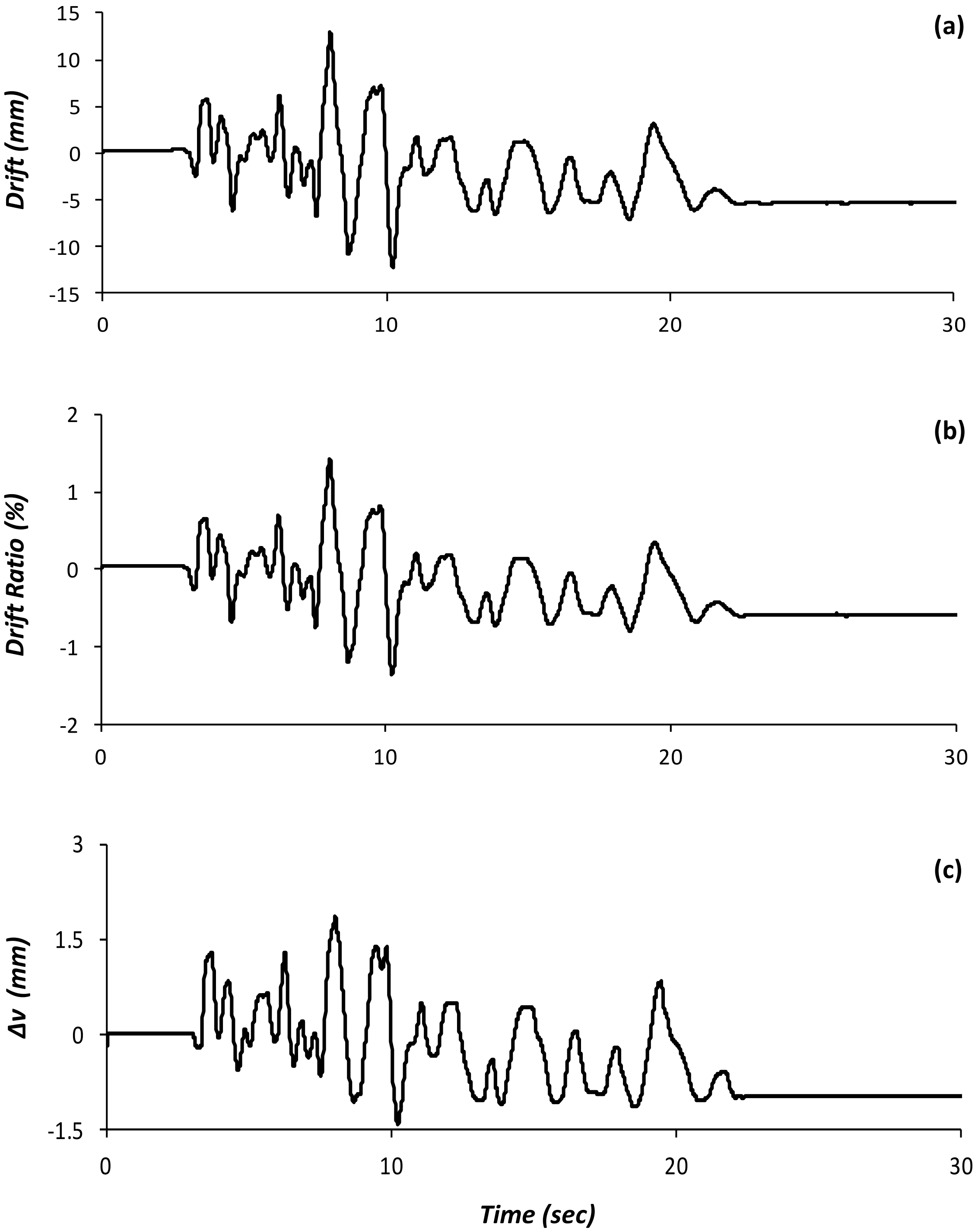

Figure 3.8 (a) Time history of the structure's total drift, **(b)** the respective drift ratio and **(c)** the relative vertical displacement of the rod for the *Lefkada record*.

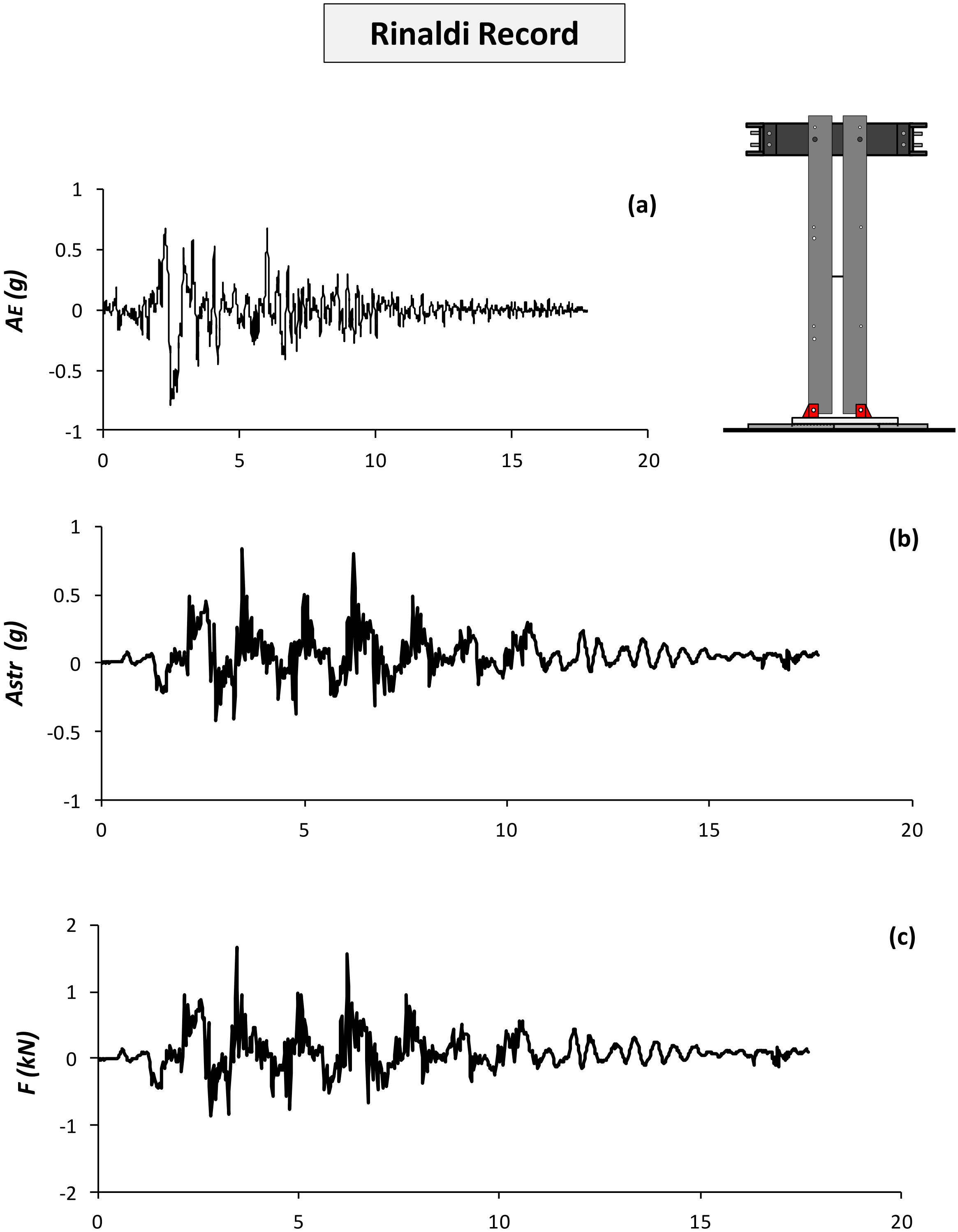

Figure 3.9 Time histories of **(a)** the acceleration used as base excitation, **(b)** the acceleration measured at the mass level and **(c)** the structure's horizontal resistance.

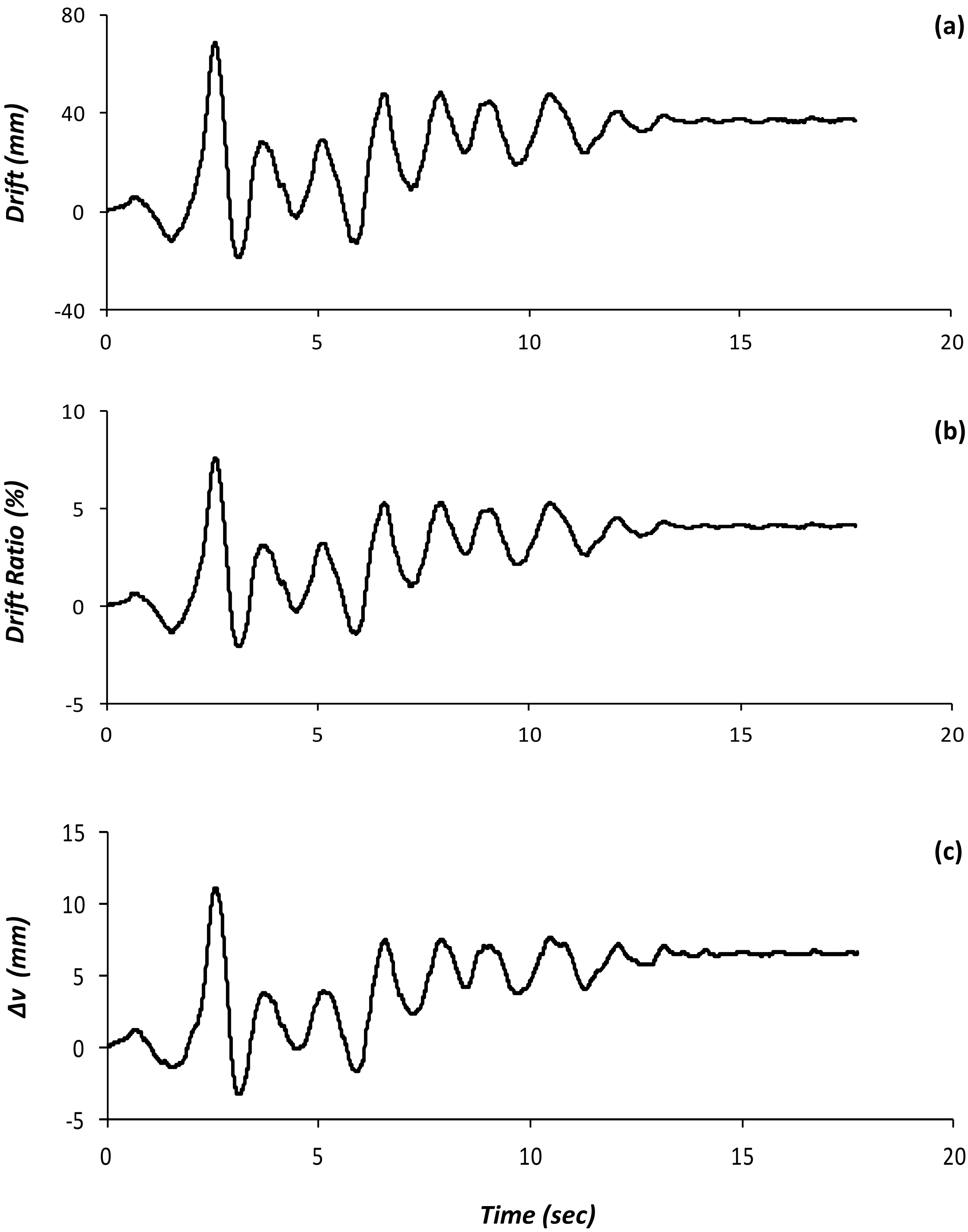

Figure 3.10 (a) Time history of the structure's total drift, **(b)** the respective drift ratio and **(c)** the relative vertical displacement of the rod for the *Rinaldi record*.

Jma Record

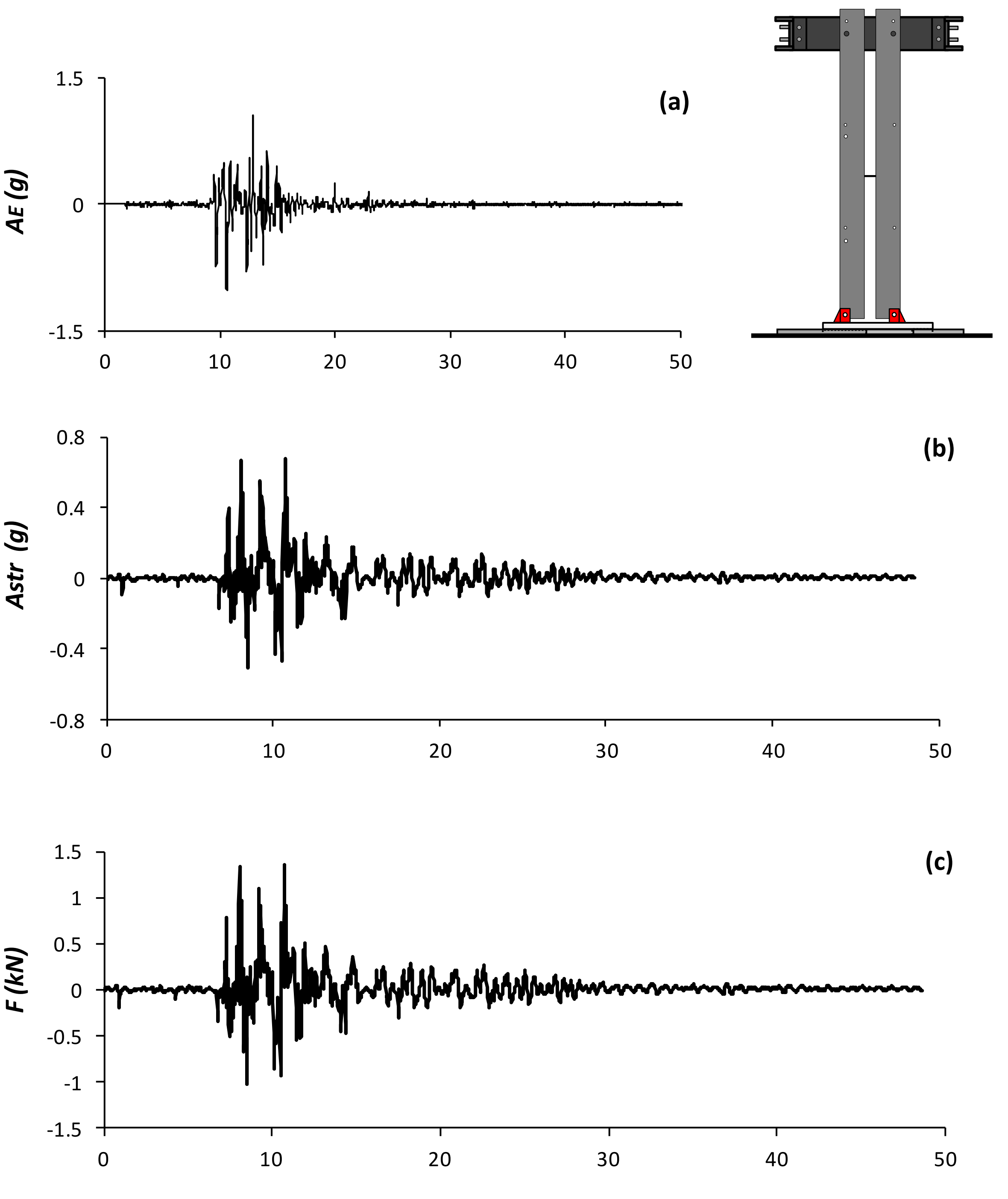

Figure 3.11 Time histories of **(a)** the acceleration used as base excitation, **(b)** the acceleration measured at the mass level and **(c)** the structure’s horizontal resistance.

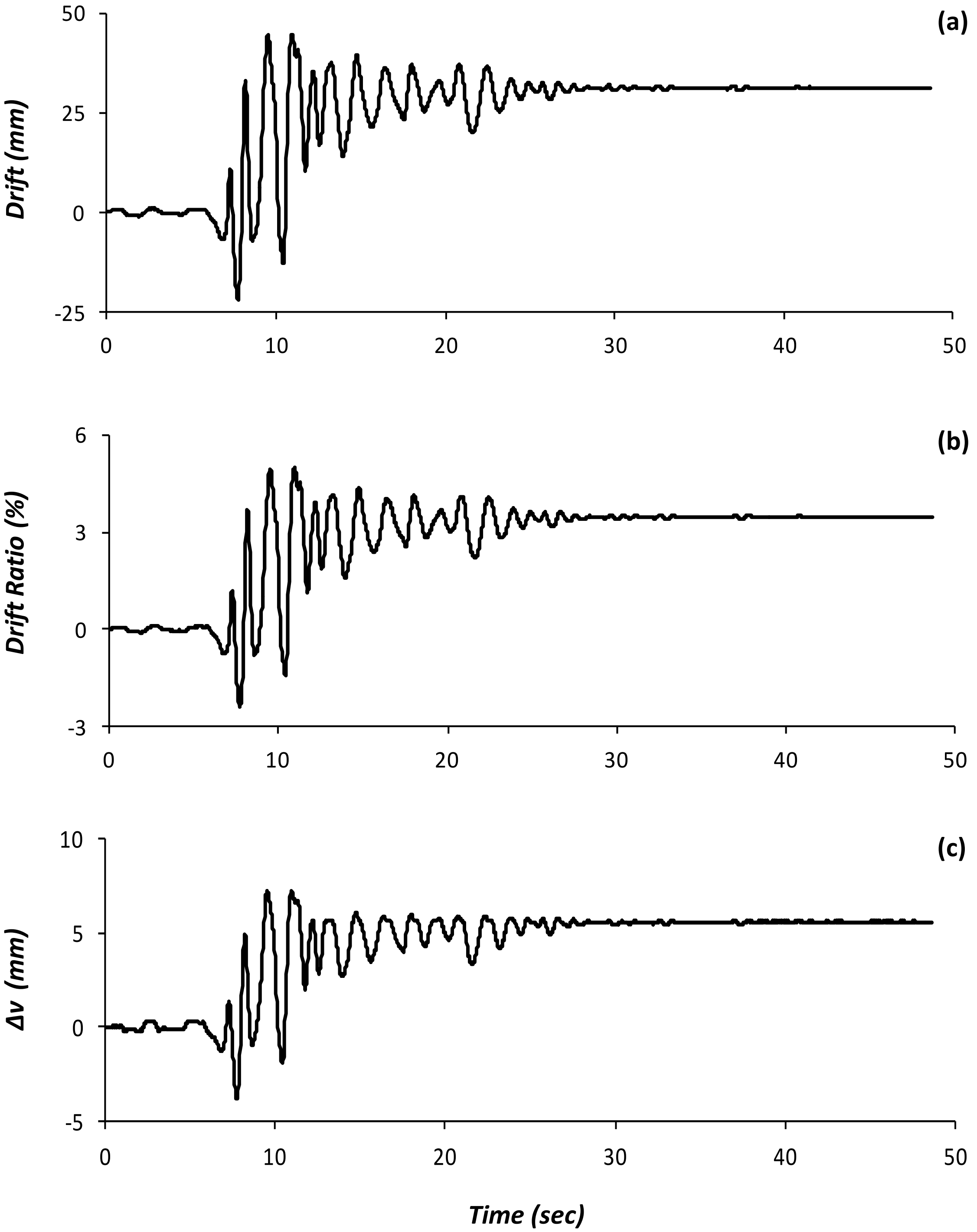

Figure 3.12 (a) Time history of the structure's total drift, **(b)** the respective drift ratio and **(c)** the relative vertical displacement of the rod for the *Jma record*.

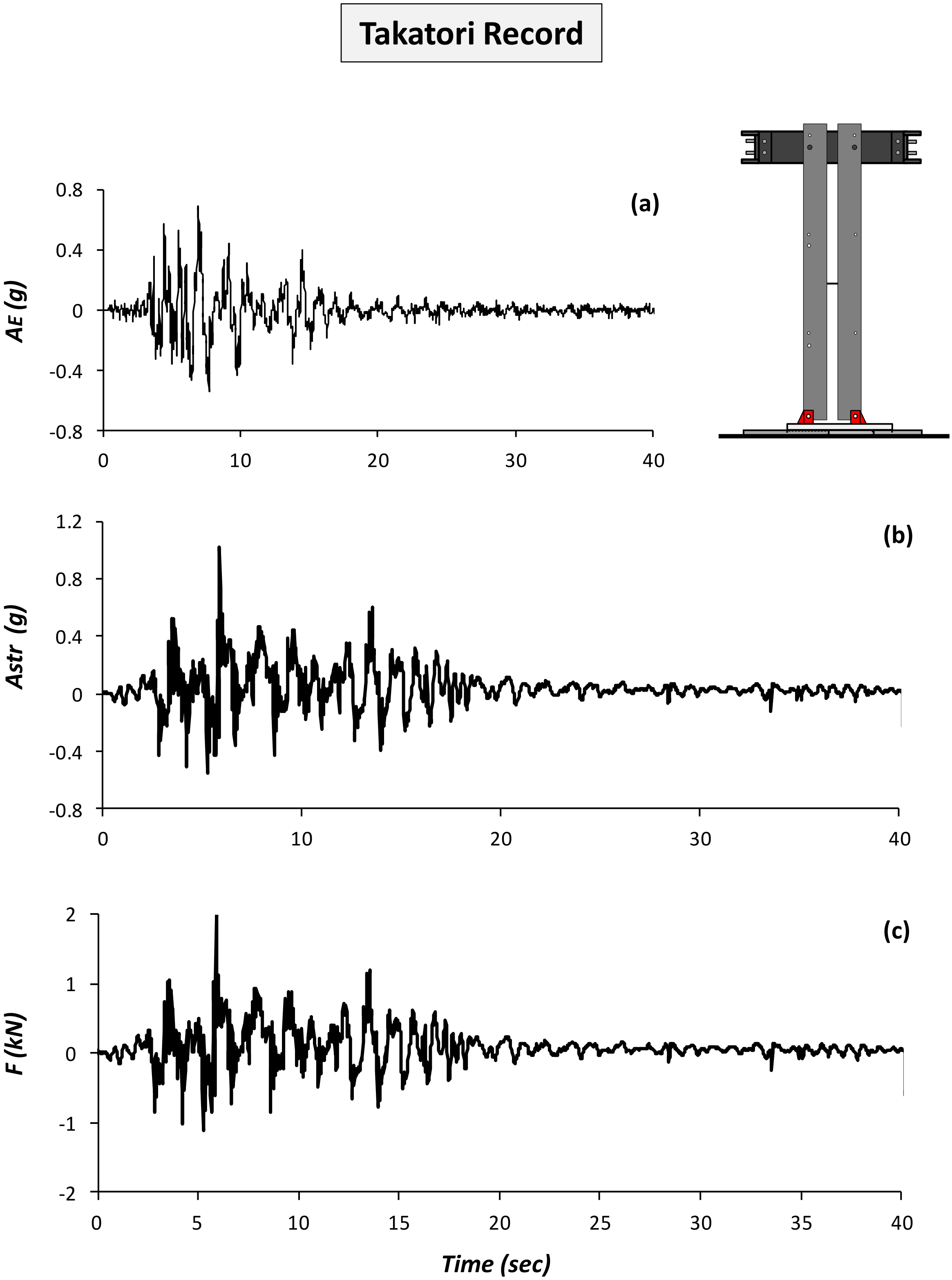

Figure 3.13 Time histories of **(a)** the acceleration used as base excitation, **(b)** the acceleration measured at the mass level and **(c)** the structure's horizontal resistance.

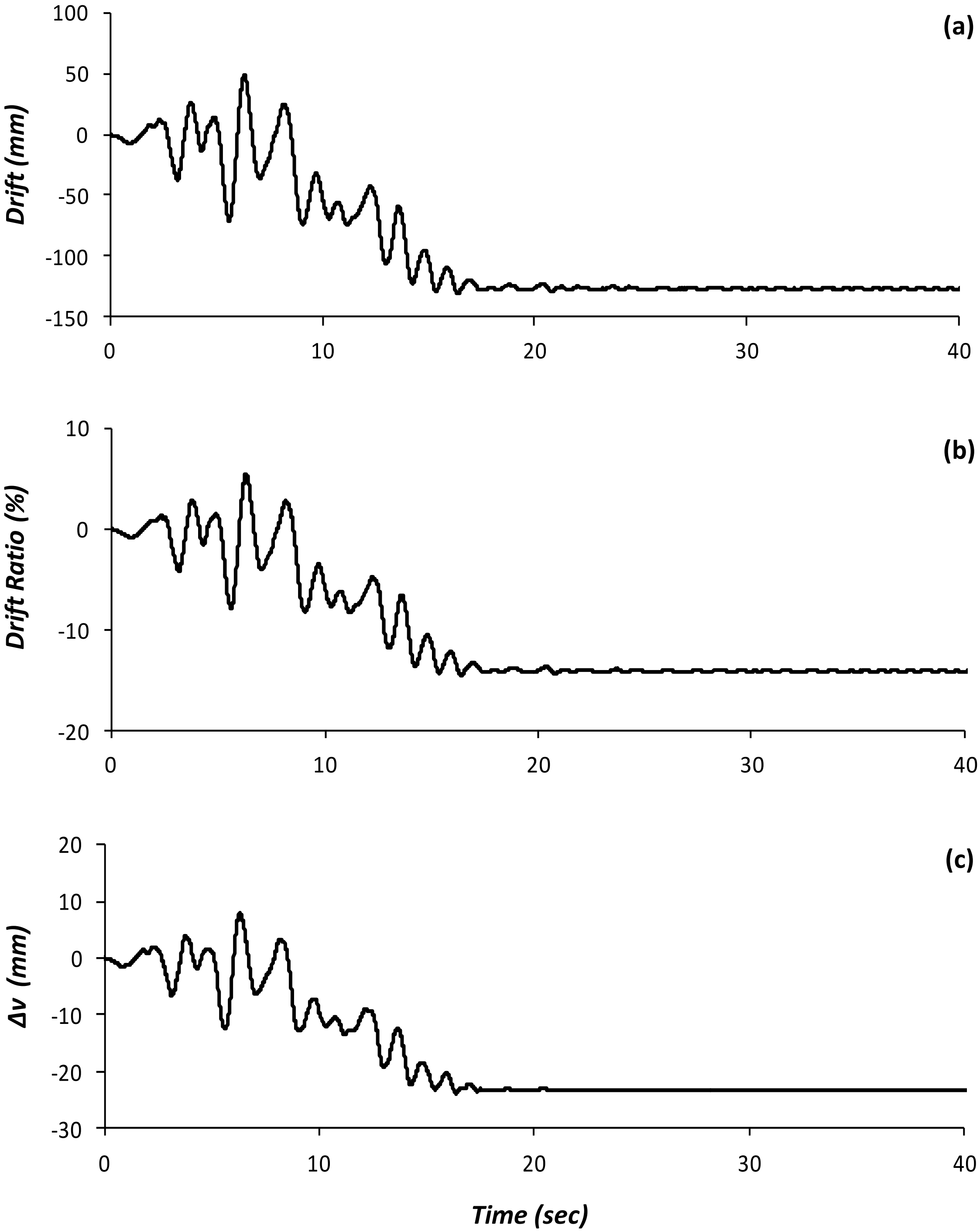

Figure 3.14 (a) Time history of the structure's total drift, **(b)** the respective drift ratio and **(c)** the relative vertical displacement of the rod for the *Takatori record*.

Figure 3.15 Photograph of the deformed shape of the horizontal rod after the Takatori record. The rods did not experience fracture; however, there are signs that plastic hinge formation is about to begin at their ends.

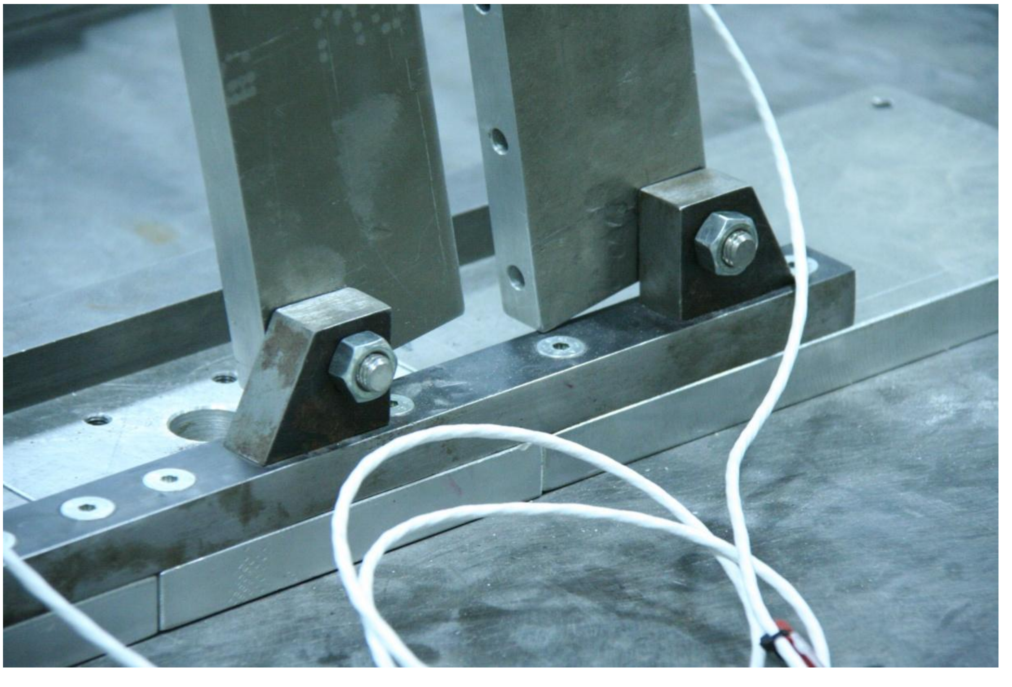

Figure 3.16 Photograph of the INSTED system columns reaching the critical rotation value (ϕ_{crit}= 8 degrees), during the record of Takatori. The 1-DOF structure did not withstand the severity of this motion.

CONCLUSIONS OF PART B

Experimental model of the building retrofitted with the INSTED – FUSEIS system

The aim of this experimental program is to examine the performance of the INSTED - FUSEIS system as means of retrofit to an existing concrete structure. The fact that the proposed system was for the first time tested experimentally in combination with a stiff, concrete structure made things quite complicated. Therefore, our study faced several practical problems and modeling defects. The main **technical problems** faced during the experimental series are the following:

- The hinges at the base of the INSTED - FUSEIS system did not perform as desired; they displayed significant moment resistance until a certain value of rotation, thus preventing initial free rotation of the system and resulting to unrealistic increase of the system's stiffness and strength. The problem stemmed from the fact that the Φ12 spigots used to form the hinges were not manufactured with the required tolerances, resulting to a very tight arrangement.
- Due to their shape, the column – beam connections of the original building were unable to rotate limitlessly; over a specific large value they prevented rotation of the building's members, attributing "fictitious" resistance to the structure. This is the reason why the building responded with such a great resistance during the 3rd Experiment (Setup II - 1rod of D=3.2mm), even though 2 of the rods had been removed.
- Since the aim of the INSTED system is to localize strain and failure at the expandable horizontal elements, mild steel (S235) is preferred for the rods. Thus, initial calculations for the design of the experimental model were made according to the nominal yield stress of S235 steel. However, due to the scaling factor (1:10) of the experimental setups, the required rod diameter was really small and it was hard to find such dimensions made of mild steel in the market. Indeed, the Φ8 rods selected to form the fuse elements of the experiments, although prescribed as S235, they displayed - after tensile testing – a yield point at f_y = 347 MPa and ultimate strength equal to f_u = 436 Mpa. In addition, the rods' cross section, due to technical problems, could not be weakened to values smaller than 3mm. Thus, in order to achieve an equivalent design, the initial diameter that had been

decided equal to 4mm considering fy = 235Mpa, resulted to be smaller (3.2mm), taking account of the increased yield stress of our specimens (fy = 347MPa).

Despite the aforementioned modeling imperfections, the results of this experimental study led to useful **conclusions**. In general:

- ✓ As observed from previously conducted experiments [N. Antonaki, 2012], but also from the numerical analyses conducted in the first part of this dissertation, the original building cannot withstand motions of moderate intensity and displays a soft–storey collapse mechanism when subjected to the record of Lefkada 2003. The addition of the INSTED – FUSEIS system to the building apparently increases the structure's strength and ductility, since *the retrofitted model is capable of sustaining very strong seismic records (such as those of Rinaldi, Jma and Takatori) without collapsing*. The system acts as a kinematic constraint, homogenizing interstorey drifts and leading to a more uniform damage distribution to all three storeys. The seismic energy undertaken by the system is being dissipated as expected, through plastic deformation of the horizontal rods, which display very ductile behavior.

- ✓ The addition of fixed tie beams at the foundation is considered necessary, in order to avoid differential displacement of footings and consequently the severe deformation of the first floor columns that was observed during Experiment No.2. However, in the case of our experimental model, the addition of tie beams led to misleading results, due to the technical defect of the column–beam connections. During strong seismic records, when the retrofitted model concentrates great values of shear force, the uniform displacement of footings, combined with the unavoidable jamming of the artificial plastic hinges, caused the development of unrealistically great values of stiffness and strength to the structure.

- ✓ Until now, the INSTED – FUSEIS system was considered as an innovative alternative towards conventional horizontal resistance systems for the seismic design of newly built steel structures but had never been used as additional reinforcement to an old structure. The original model building used in this experimental study, simulates a real – scale concrete structure, designed in the 70's according to obsolete seismic codes. Hence, it has great stiffness but quite small strength. Such design indicates that, even during a moderate seismic motion, the building's members will attract significant amount of shear force and easily yield, thus accumulate serious permanent deformations. This kind of behavior certainly rises questioning about ***the design procedure that should be followed when the INSTED - FUSEIS system is combined with such stiff structures, in order to achieve good performance under seismic shaking***. Ideally, the proposed system should be a lot stiffer than the rest of the structure, so as to undertake the whole amount of the imposed seismic loading and delimit potential failure to its fuse elements, leaving the other structural members within the limits of elasticity. Meanwhile, the horizontal rods should be able to reach the yield point rather quickly, so as to dissipate the desired amounts of seismic energy. When the INSTED – FUSEIS system is used as seismic reinforcement for steel structures, the flexibility of this kind of structures as well as the material homogeneity between the system and the rest of the structural members, make determination of the system's proper stiffness and strength simpler.

However, when the proposed system is combined with stiff, concrete structures, a **much more careful design is needed**. The system and the retrofitted structure should, by no means, undertake the same values of seismic force. *The INSTED – FUSEIS system should be stiffer than the rest of the structure, in order to undertake the majority of seismic load, but at the same time should not display unreasonably high values of strength, so as to ensure that the fuse elements will reach their yield point before the other structural members do*. Taking into account that both the strength and stiffness of the system depend on its fuse elements, optimum design requires careful calculation of the system's horizontal rods: proper number and rod diameter should be selected, so that the system results in the correct combination of stiffness and strength. Certainly, *the choice of mild steel fuse elements would help towards the right direction, since it would not affect the system's stiffness but would guarantee quicker plastification of the rods.*

Experimental model of the INSTED – FUSEIS (1-DOF) system

The examination of the INSTED – FUSEIS system as part of a 1–DOF system led to more unambiguous results for the system's dynamic performance, as this experiment was free of the previous technical defects. The system displayed excellent behavior during motions of moderate intensity (MNSA and Lefkada 2003), as expected. However, the most impressive fact is that it managed to sustain the severe records of Rinaldi and Jma without collapsing, although it suffered from significant deformations. The system's horizontal rods resisted the imposed seismic loading, through plastic deformation and dissipation of large amounts of energy, before failure at the record of Takatori. The dynamic performance of the system during this experiment is clearly indicative of the importance of ductile behavior in seismic design.

References

I. Anastasopoulos, V. Drosos, N. Antonaki, A. Rontogianni (2012). The Role of Soil–Foundation Structure Interaction on the Seismic Performance of a n Existing 3-storey Building : Numerical Simulation and Shaking Table Testing, *15 WCEE, Lisboa 2012.*

Anastasopoulos I., Gelagoti F., Kourkoulis R., Gazetas G. (2011), Simplified Constitutive model for Simulation of Cyclic Response of Shallow Foundations: Validation against Laboratory Tests, *Journal of Geotechnical and Geoenvironmental Engineering,* ASCE, Vol. 137, No. 12, pp. 1154–1168.

Anastasopoulos I., Kokkali P., Tsatsis A. (2011). Experimental Investigation of Vertical Load Capacity of Surface Footings.

Anastasopoulos I., Kokkali P., Tsatsis A. (2011). 1-dof System Lying on Square Foundation: Monotonic and Cyclic Loading.

Antonaki N. (2012). Experimental study of rocking isolation: Application to the retrofit of an existing building. Diploma Thesis, NTUA.

ATC – 40: *Seismic Evaluation and Retrofit of Conctrete Buildings* (1996), Applied Technology Council, 1997.

Chopra A. K. (1995): *Dynamics of structures – Theory and applications to earthquake engineering*, Prentice-Hall Inc.

Drosos V., Georgarakos T., Loli M., Anastasopoulos I.**,** Zarzouras O., and Gazetas G. (2012), Soil–Foundation–Structure Interaction with Mobilization of Bearing Capacity : An Experimental Study on Sand, *Journal of Geotechnical and Geoenvironmental Engineering,* ASCE (*in press*).

European Convention for Constructional Steelwork (ECCS): *Recommended testing procedure for assessing the behaviour of structural steel elements under cyclic loads*, ECCS Publ. No 45, Rotterdam, The Netherlands, 1986.

EN1993-1-1, Eurocode 3: *Design of steel structures – Part 1 -1: General rules and rules for buildings, CEN, 2003*

EN1998-1-1, Eurocode 8: *Design of structures for earthquake resistance – Part 1 -1: General rules, seismic actions and rules for buildings, CEN, 2003*

Fardis M.N. (2002). *Design of an irregular building for the SPEAR project—description of the 3-storey structure*. Research report University of Patras, Greece.

Fardis M.N., Negro P. (2006). SPEAR—seismic performance assessment and rehabilitation of existing buildings. *Proceedings of the international workshop on the SPEAR project*, 4-5 April, Ispra, Italy.

Gourvenec S. (2007). Shape effects on the capacity of rectangular footings under general loading, *Geotechnique 57, No. 8, pp. 637–646.*

Jafarzadeh F, Faghihi D. and Ehsani M. (2008). Numerical simulation of shaking table tests on dynamic response of dry sand. *The 14th World Conference on Earthquake Engineering, October 12-17, 2008, Beijing, China.*

Karydakis Ph. (2011). INSTED: Innovative Stiffness and Energy Dissipation system for multi-storey steel buildings. PhD Thesis, NTUA.

Karydakis Ph. S., Vagias I., Ioannidis G. (2011). INSTED: Innovative Stiffness and Energy Dissipation System, Final Report. *Proceedings of the 4th Japan – Greece Workshop: Seismic Design of Foundations, Innovations in Seismic Design and Protection of Cultural Heritage, Vol.2, pp.271-277, October 6-7, Kobe, Japan.*

KAN.EPE. (2009). *Regulation for Strengthening and Rehabilitation*. OASP, Athens-Greece.

Kokkali P. (2010). Metaplastic Rocking Response of 1 – DOF system: Dimensional analysis. Diploma Thesis, NTUA.

Rontogianni A. (2011). Seismic Rehabilitation of an Existing 3 – storey Building : Conventional Design and Rocking Isolation System. Diploma Thesis, NTUA.

Sideri E., Spyridaki A. (2011). Inelastic Rocking of Asymmetric Frame. Diploma Thesis, NTUA.

Vayas I. and Thanopoulos P. (2005). Innovative dissipative (INERD) pin connections for seismic resistant braced frames, *International journal of steel structures, vol. 5, no. 5, pp. 453-463.*

APPENDIX A

I. Model components of the original building

II. Model components of the INSTED system

I. Model components of the original building

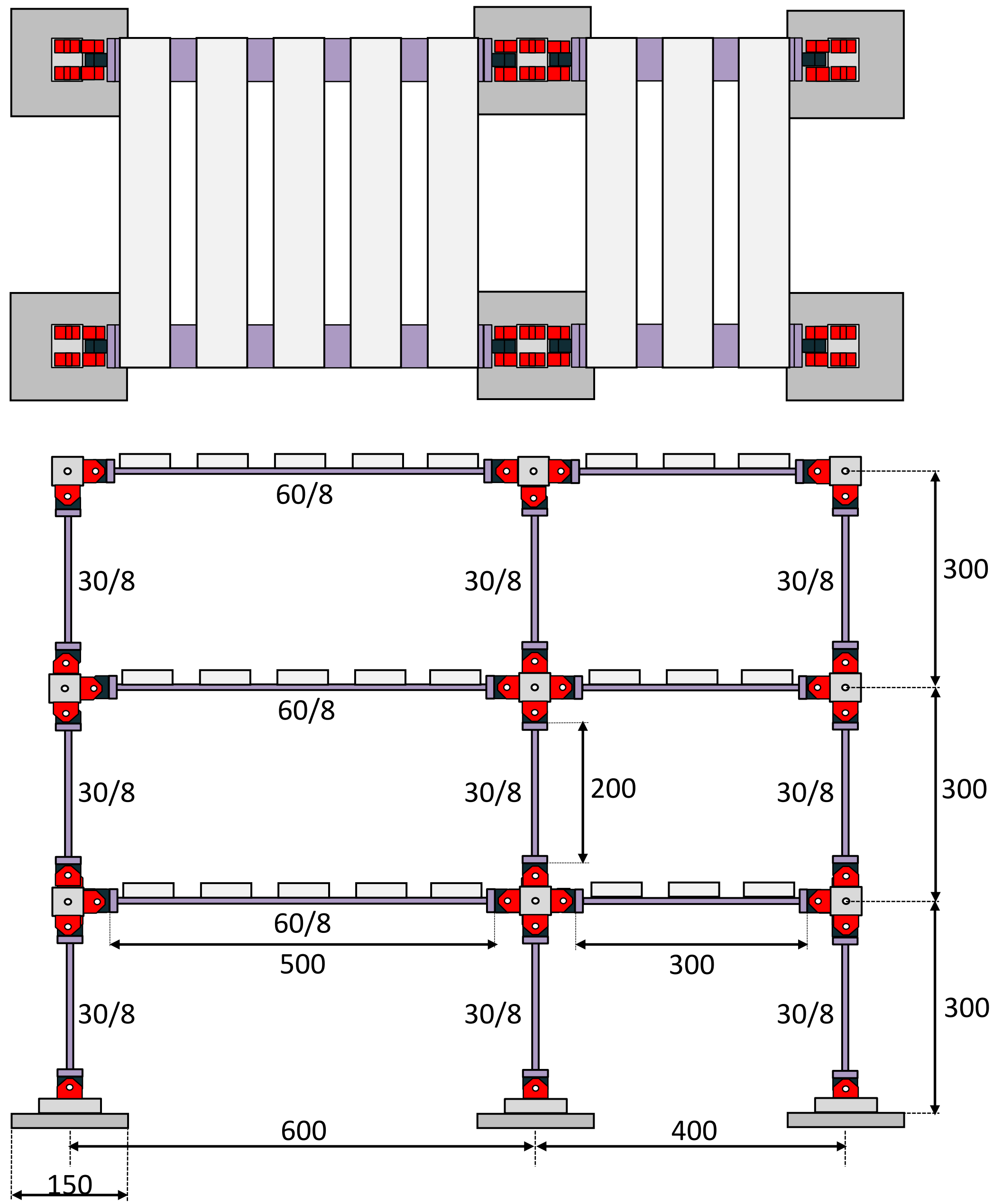

Figure 1. Technical drawing of original model building.

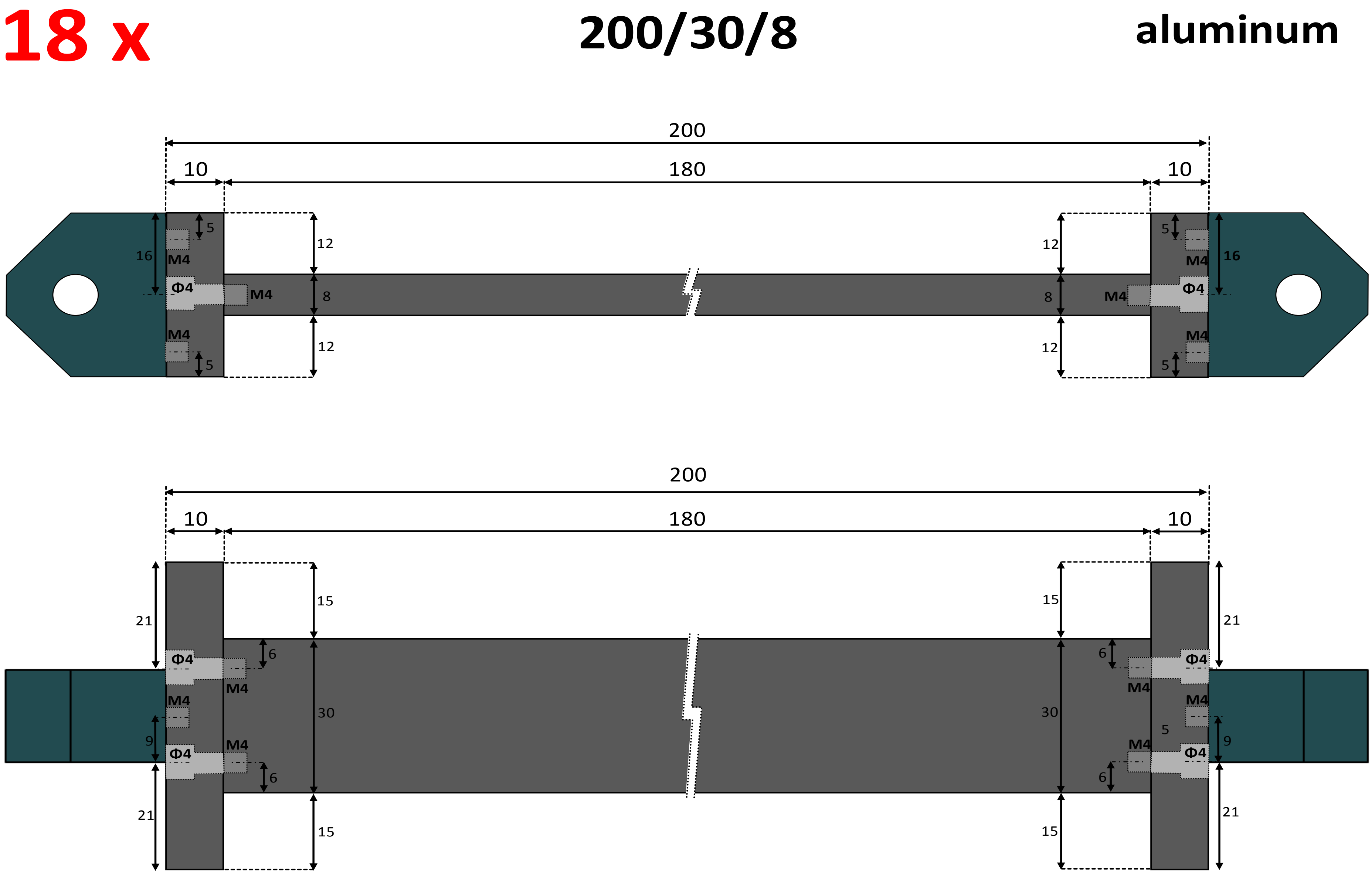

Figure 2. Technical drawing of model columns.

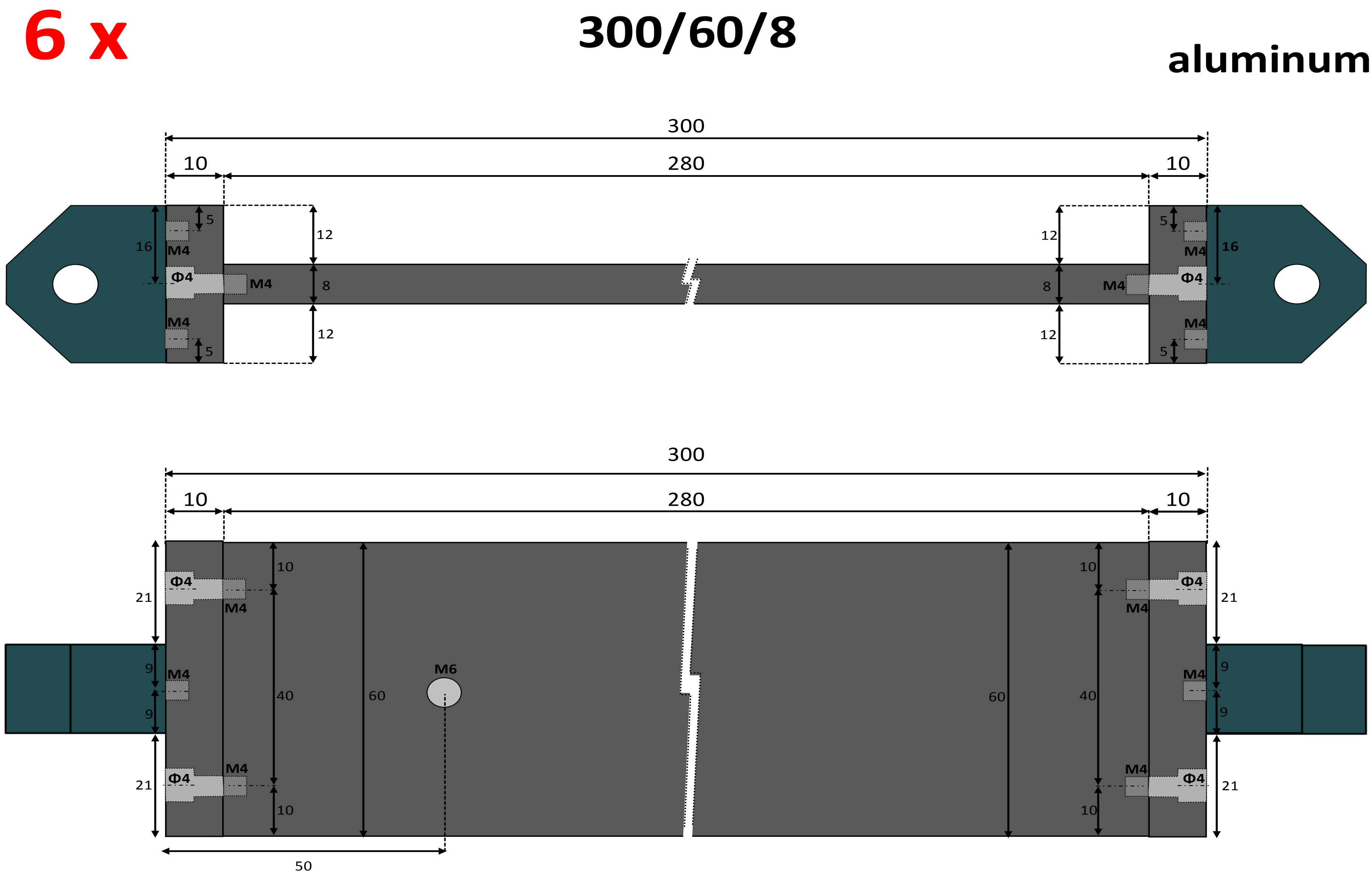

Figure 3. Technical drawing of model beams.

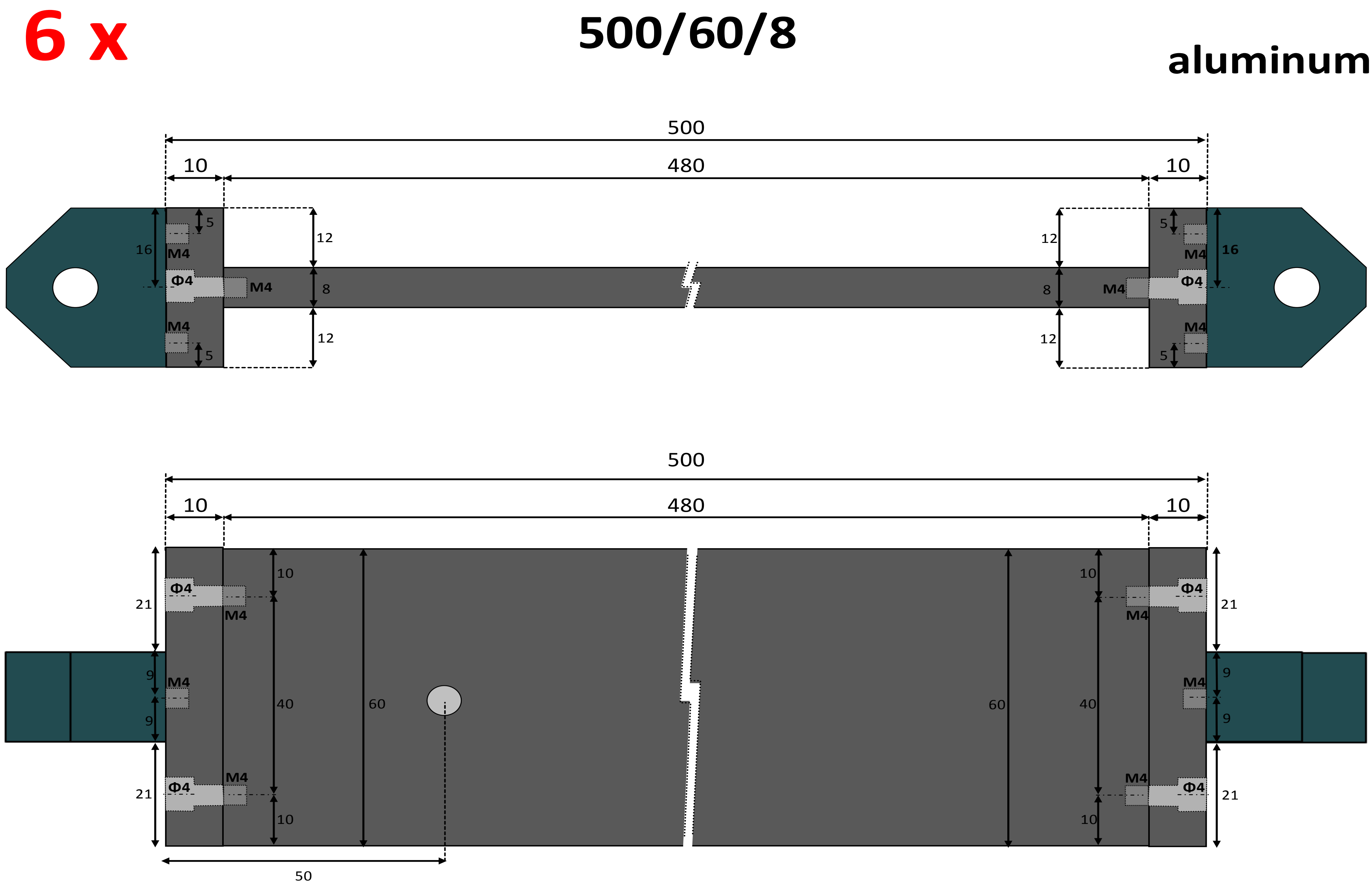

Figure 4. Technical drawing of model beams.

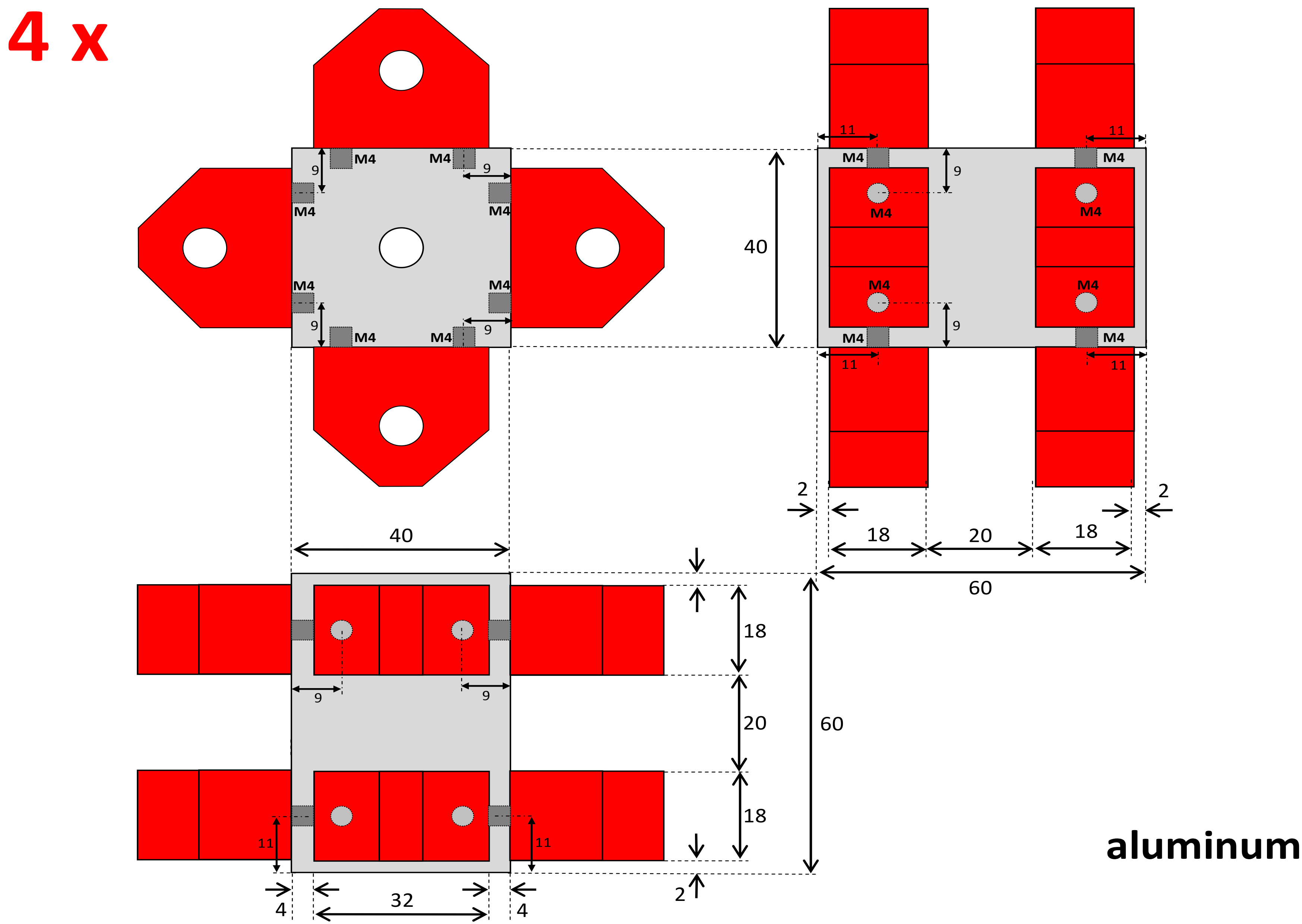

Figure 5. Technical drawing of beam – column connection.

10 x

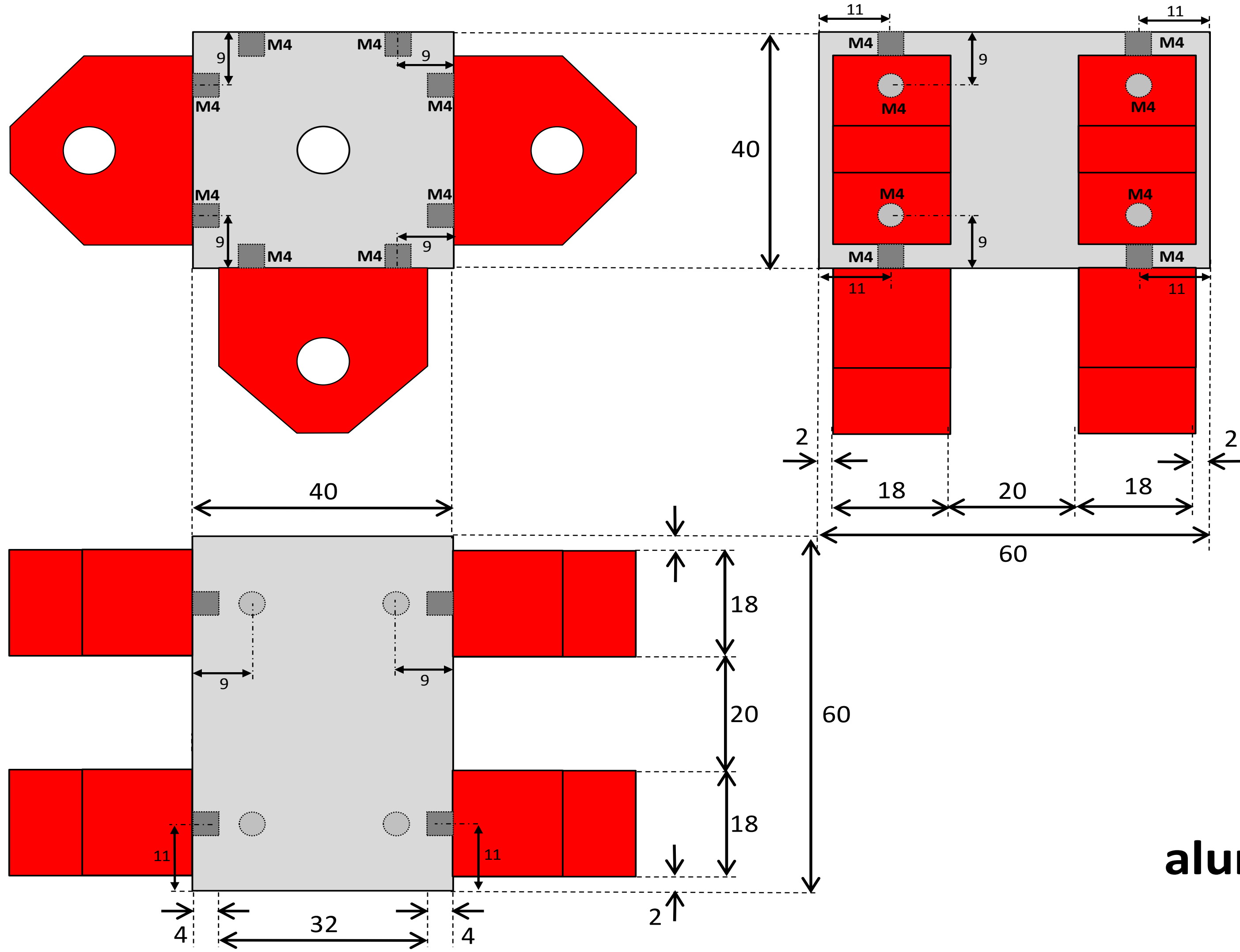

aluminum

Figure 6. Technical drawing of beam – column connection.

4 x

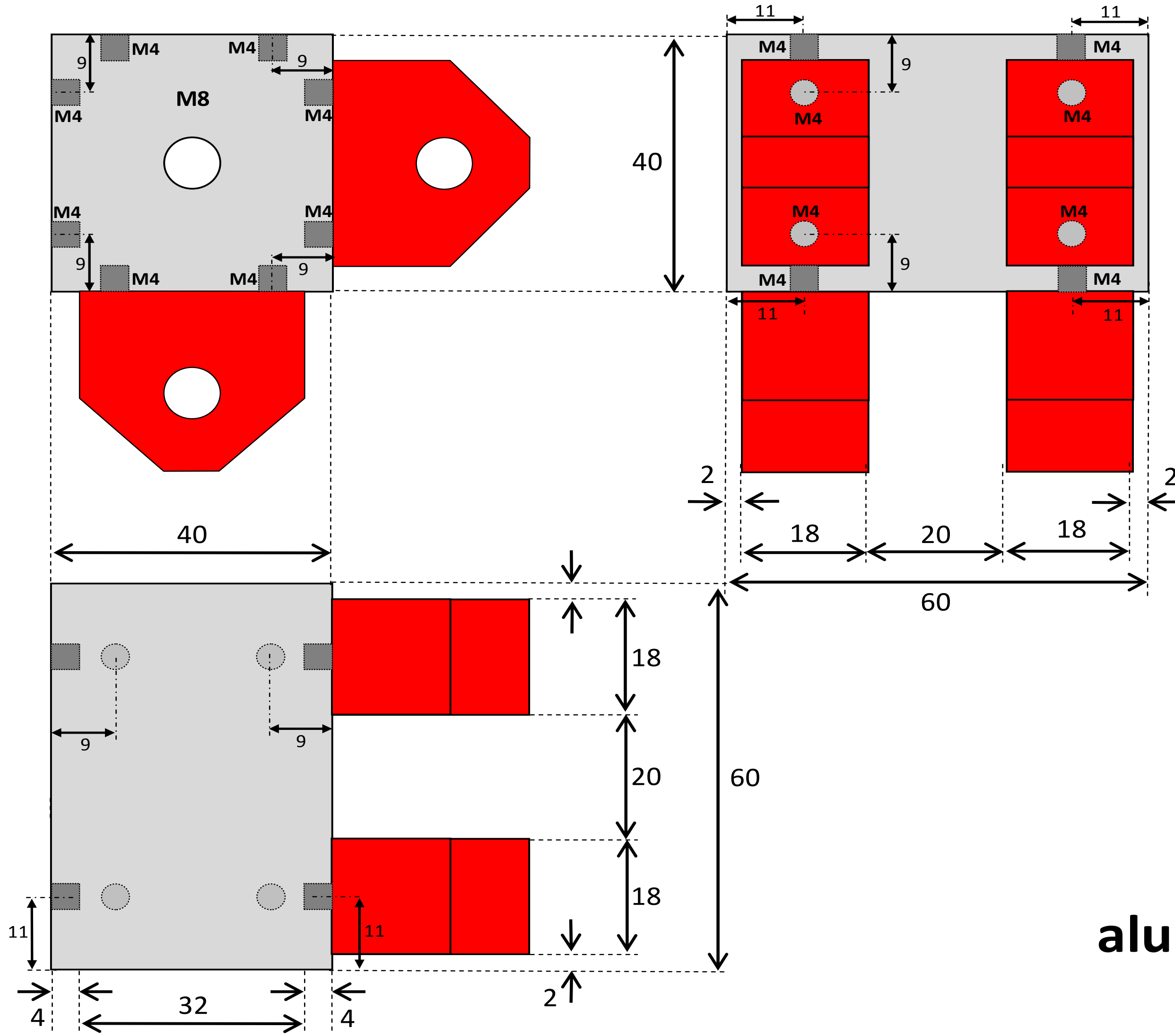

aluminum

Figure 7. Technical drawing of beam – column connection.

6 x

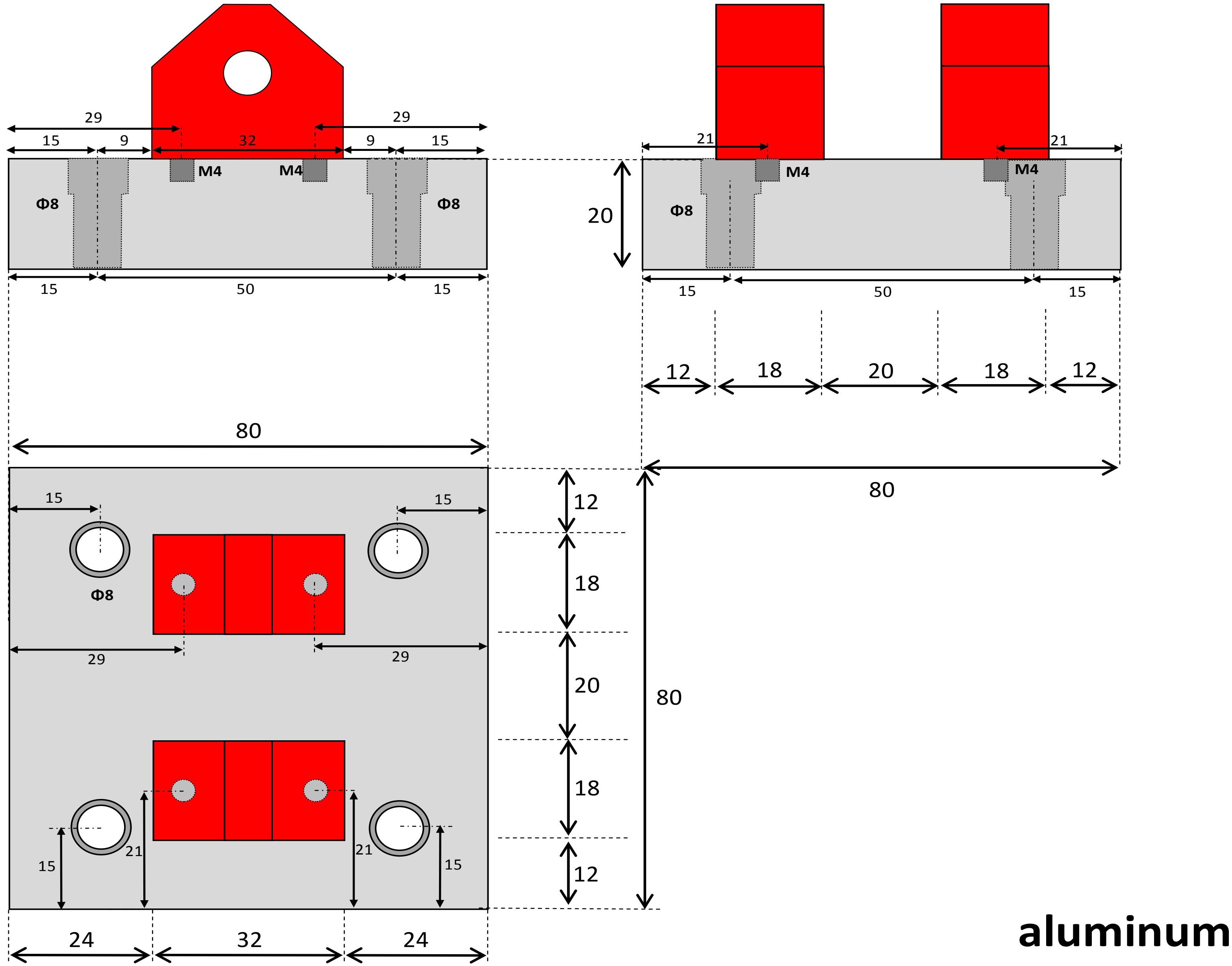

Figure 8. Technical drawing of column – footing connection.

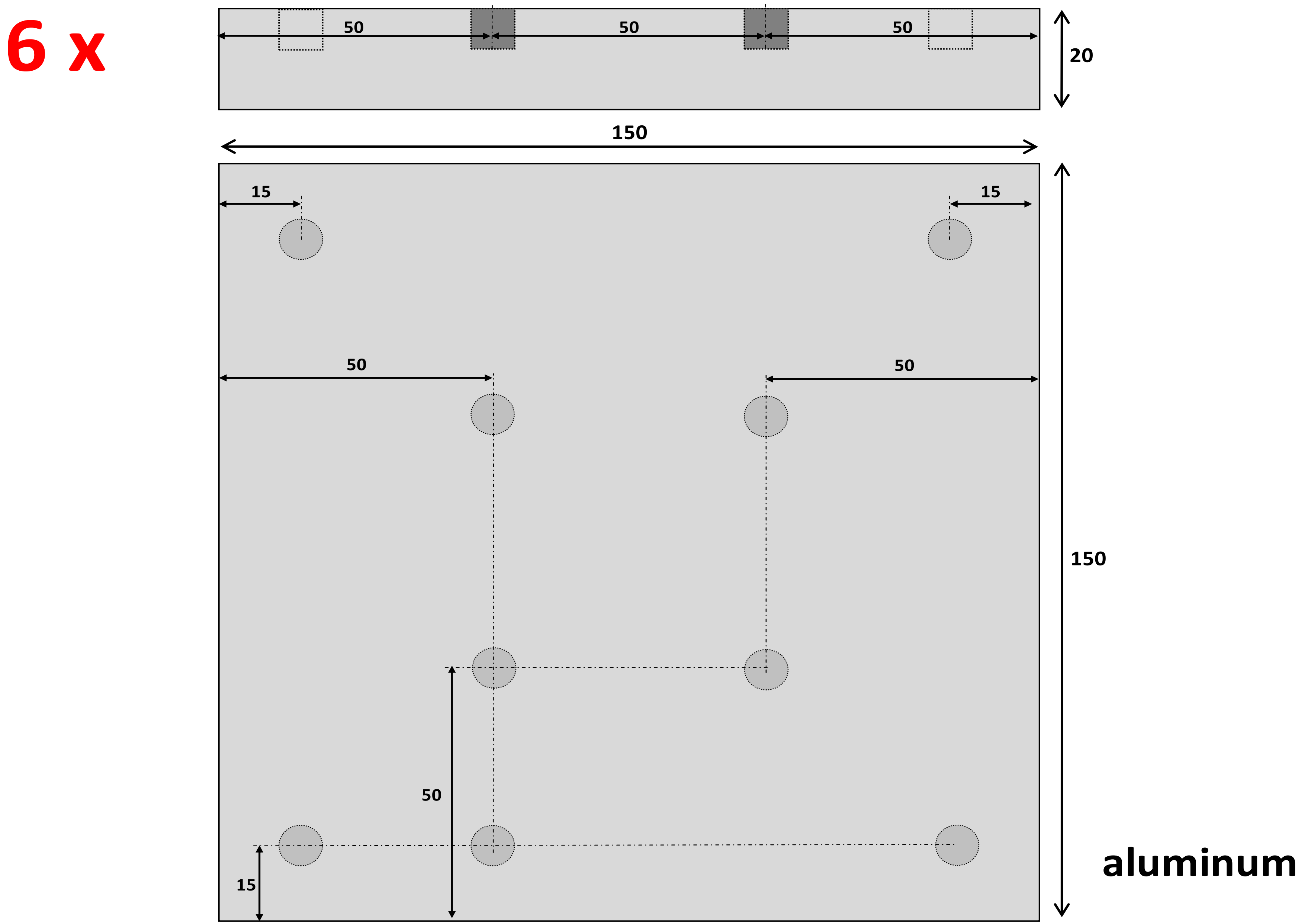

Figure 9. Technical drawing of column footing.

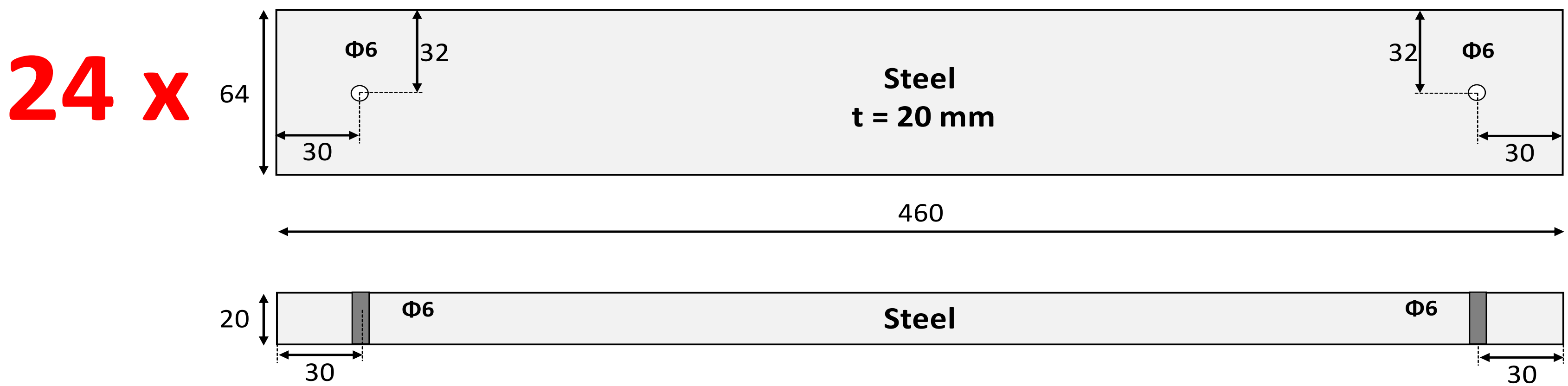

Figure 10. Technical drawing of mass - inducing steel plates.

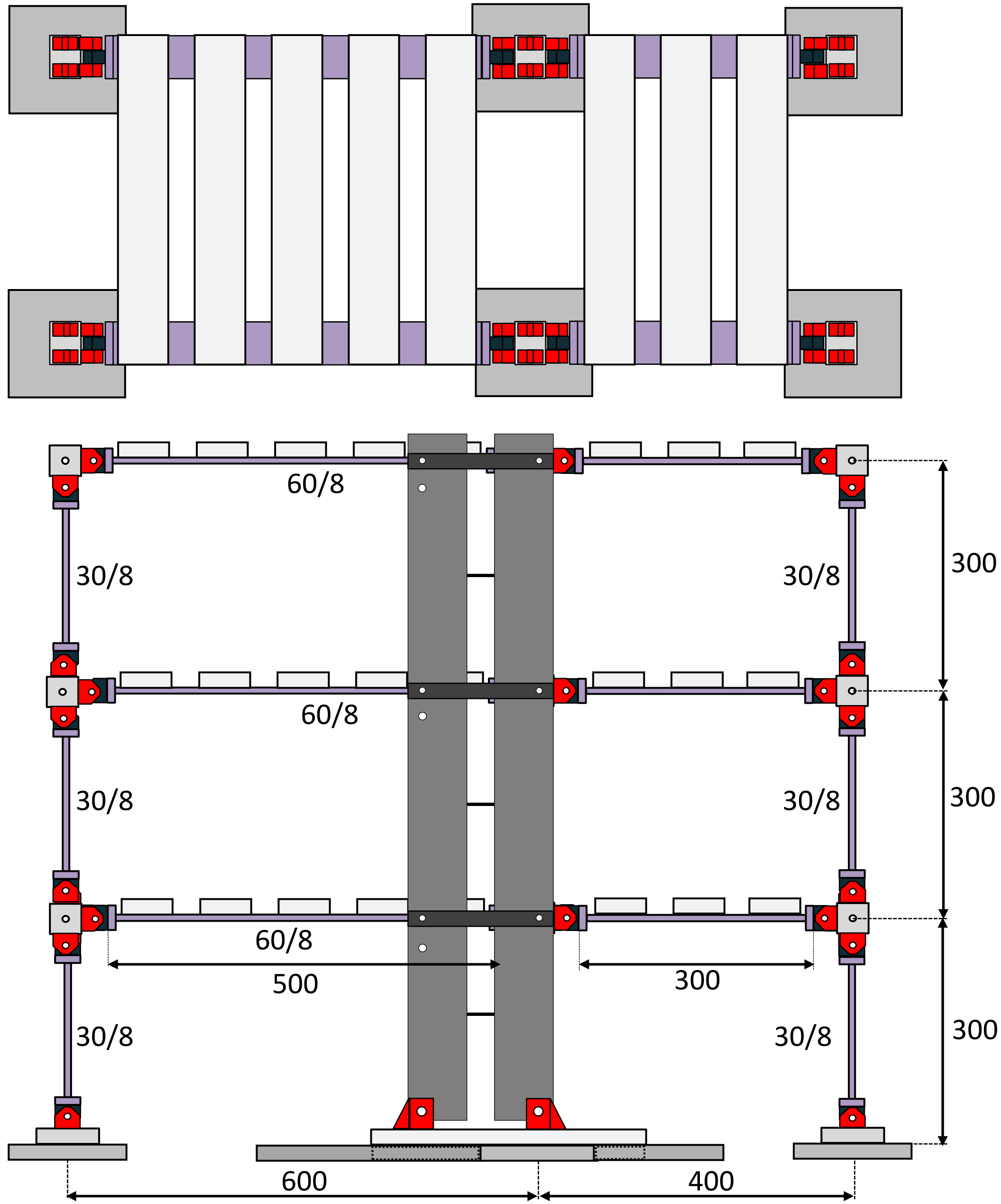

Figure 11. Technical drawing of retrofitted model building.

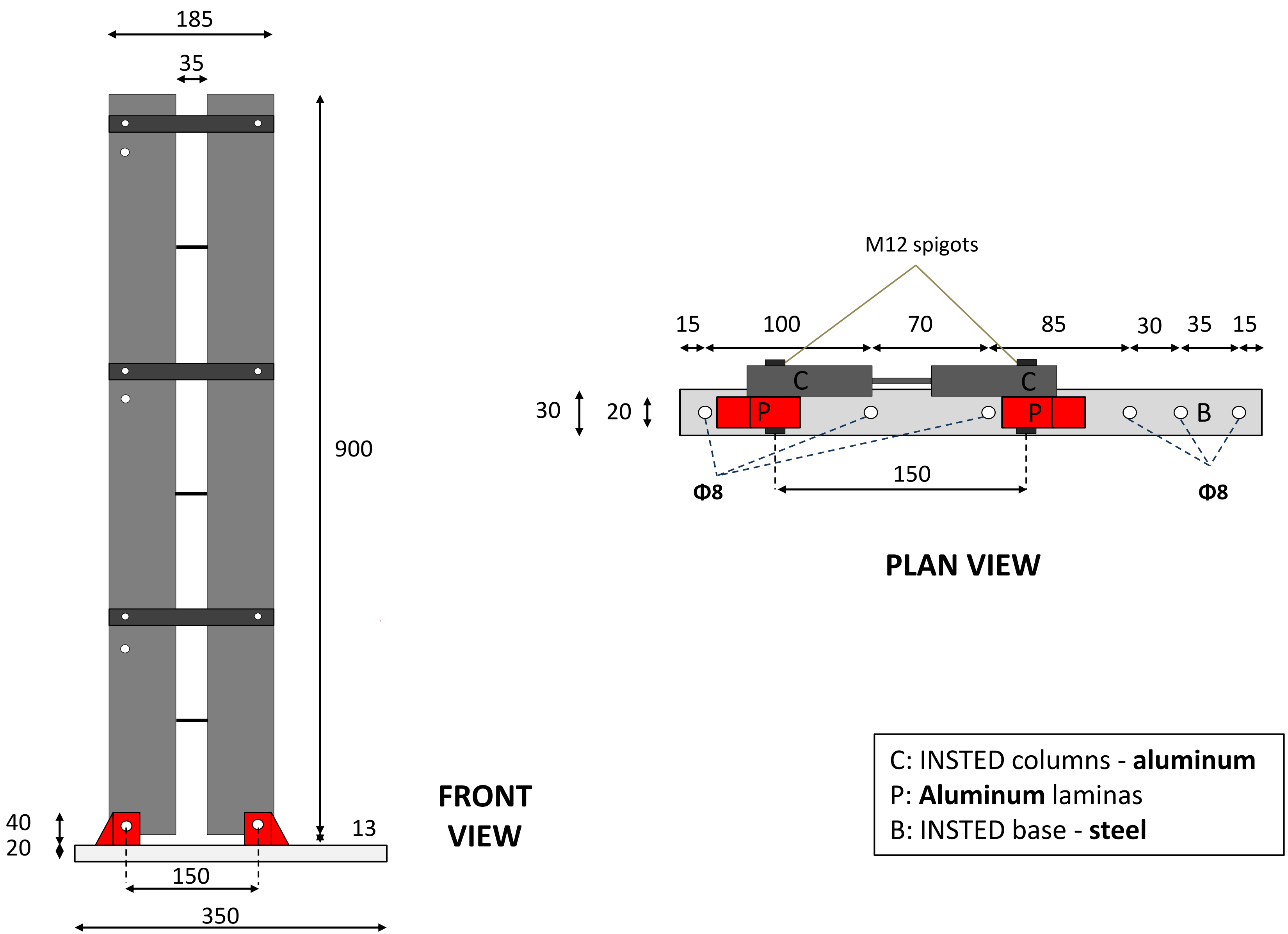

Figure 12. Technical drawing of the INSTED system.

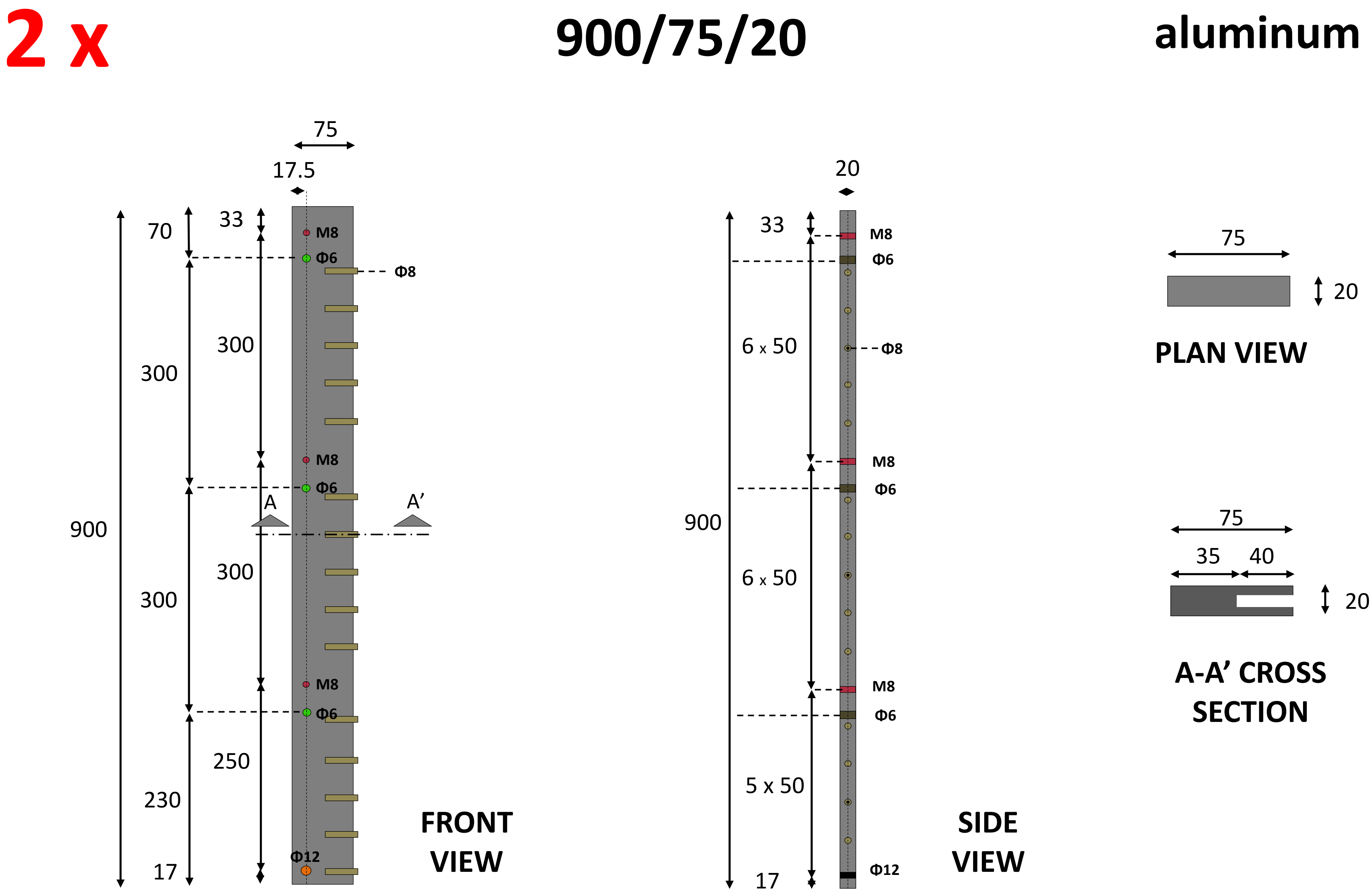

Figure 13. Technical drawing of the INSTED left column.

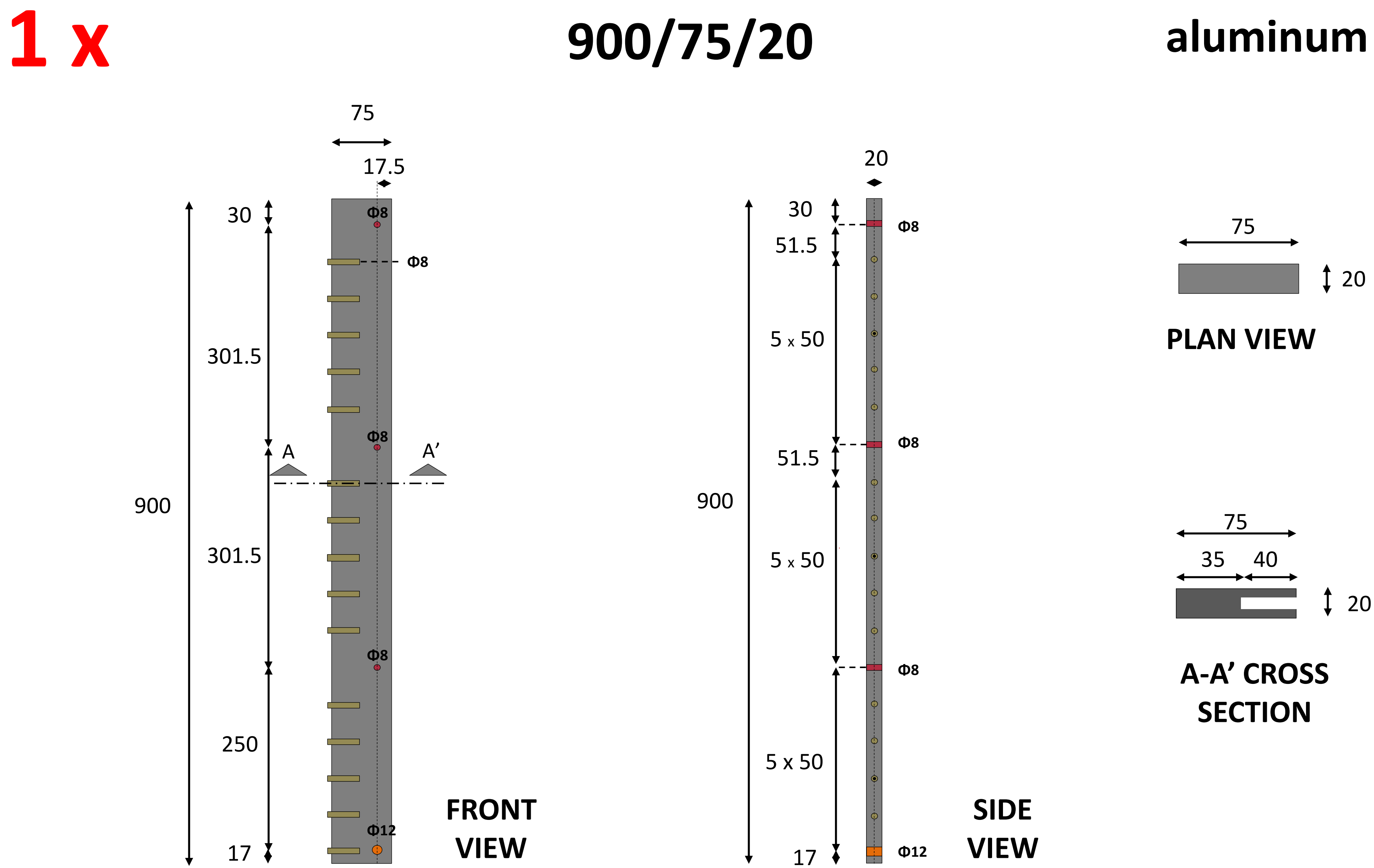

Figure 14. Technical drawing of the INSTED right column (Frame A).

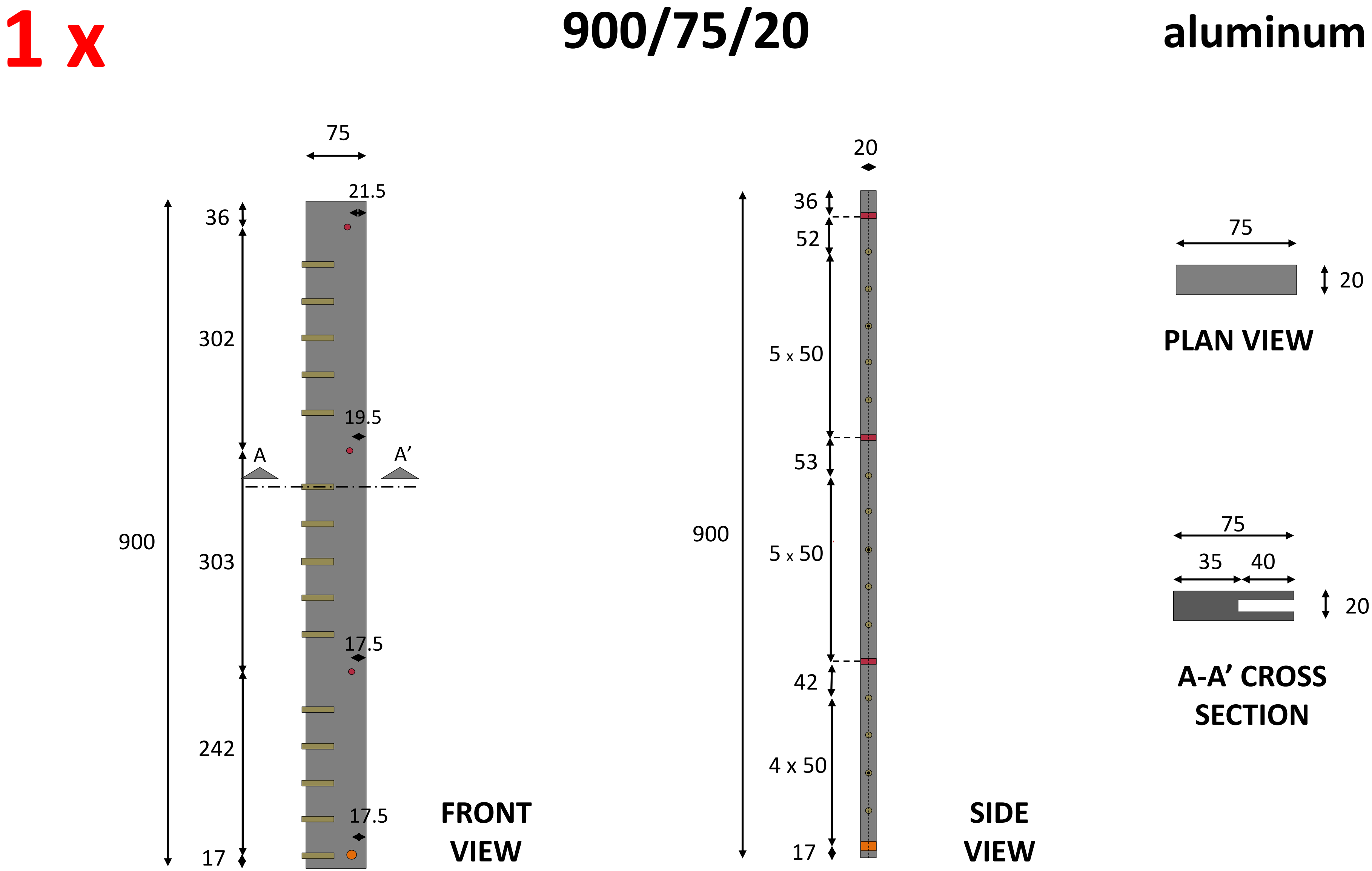

Figure 16. Technical drawing of the INSTED right column (Frame B).

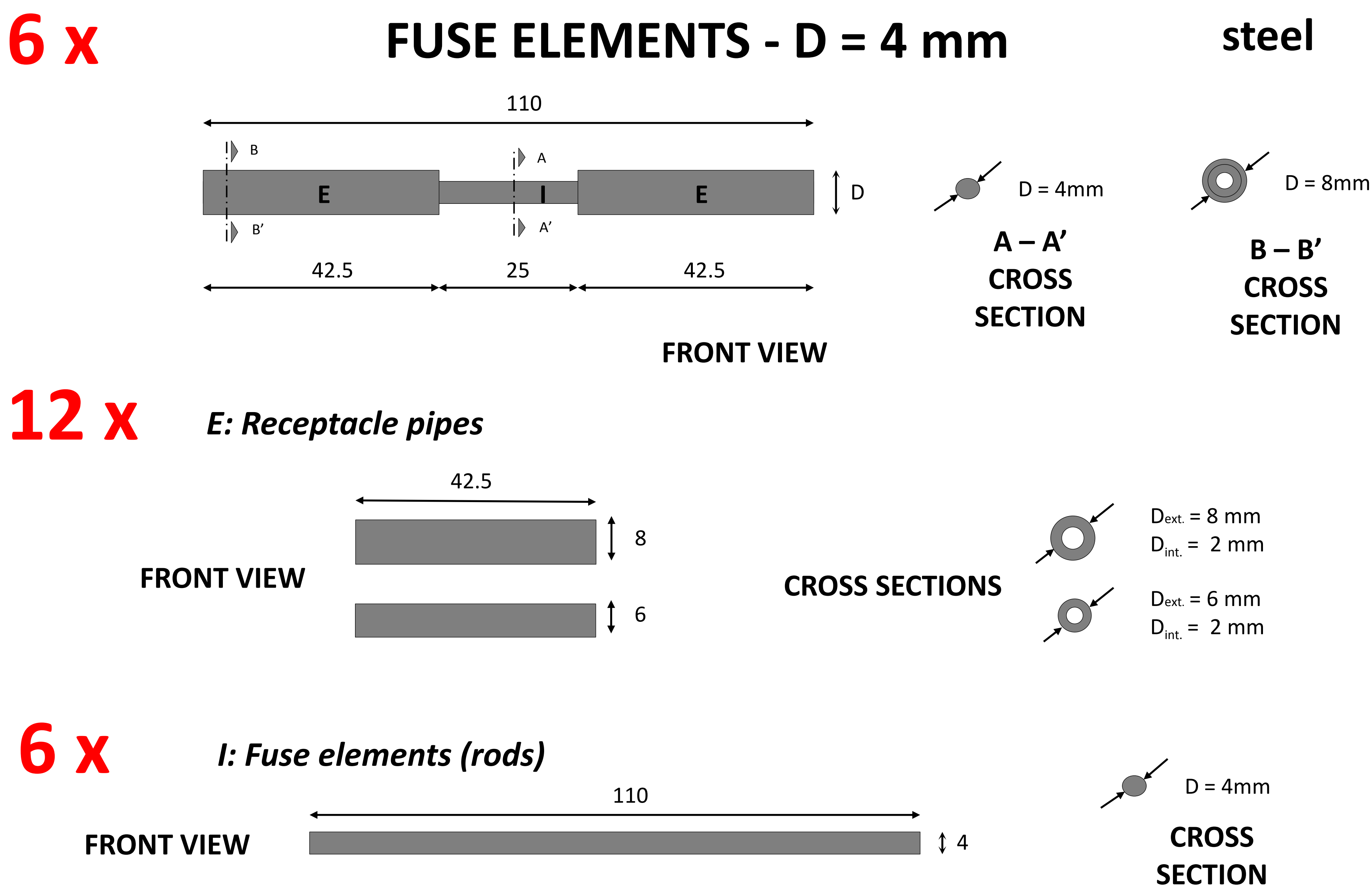

Figure 17. Technical drawing of d = 4 mm rods.

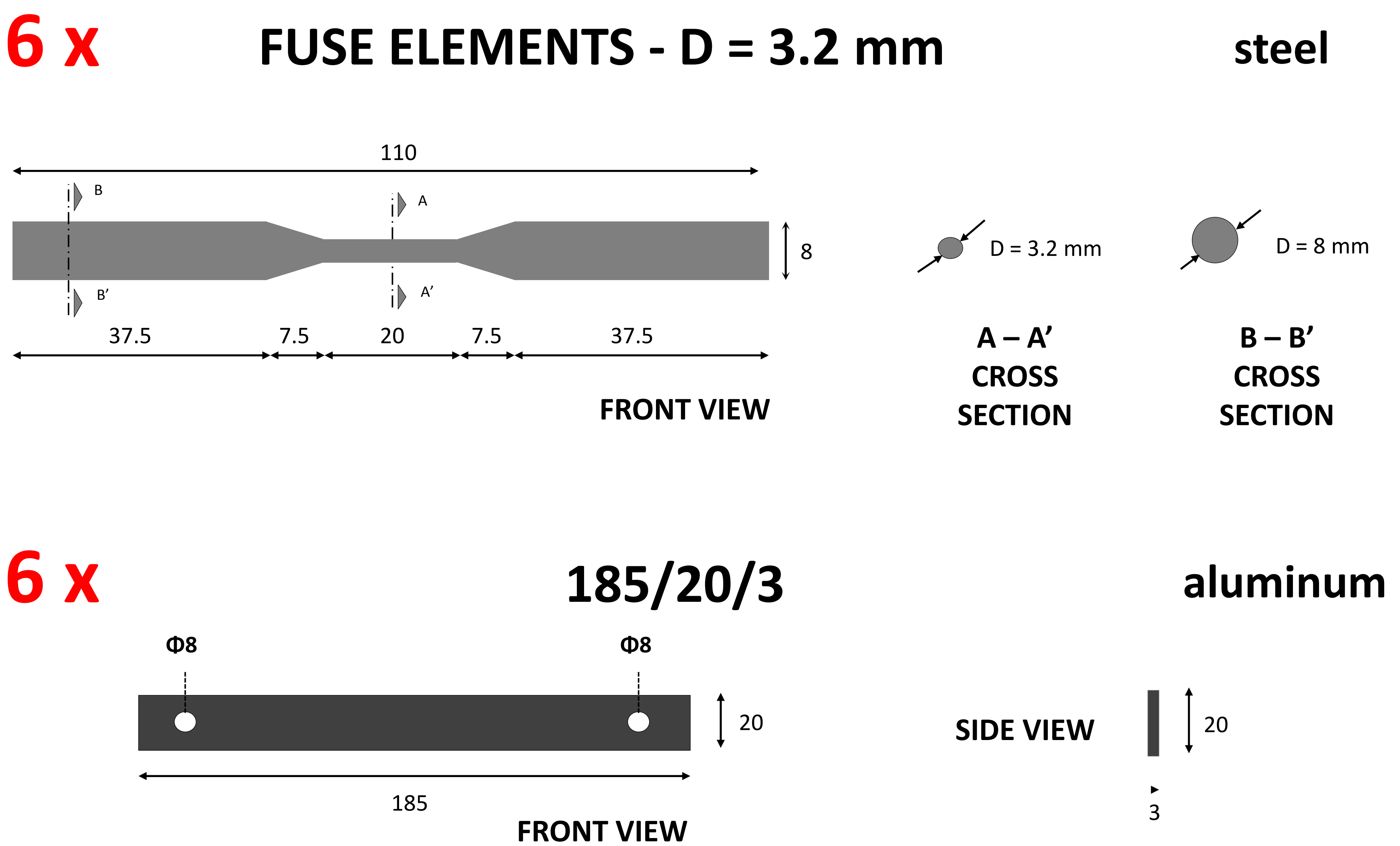

Figure 18. Technical drawing of the d = 3.2 mm rods and the aluminum bars simulating the stores' diaphragmatic function .

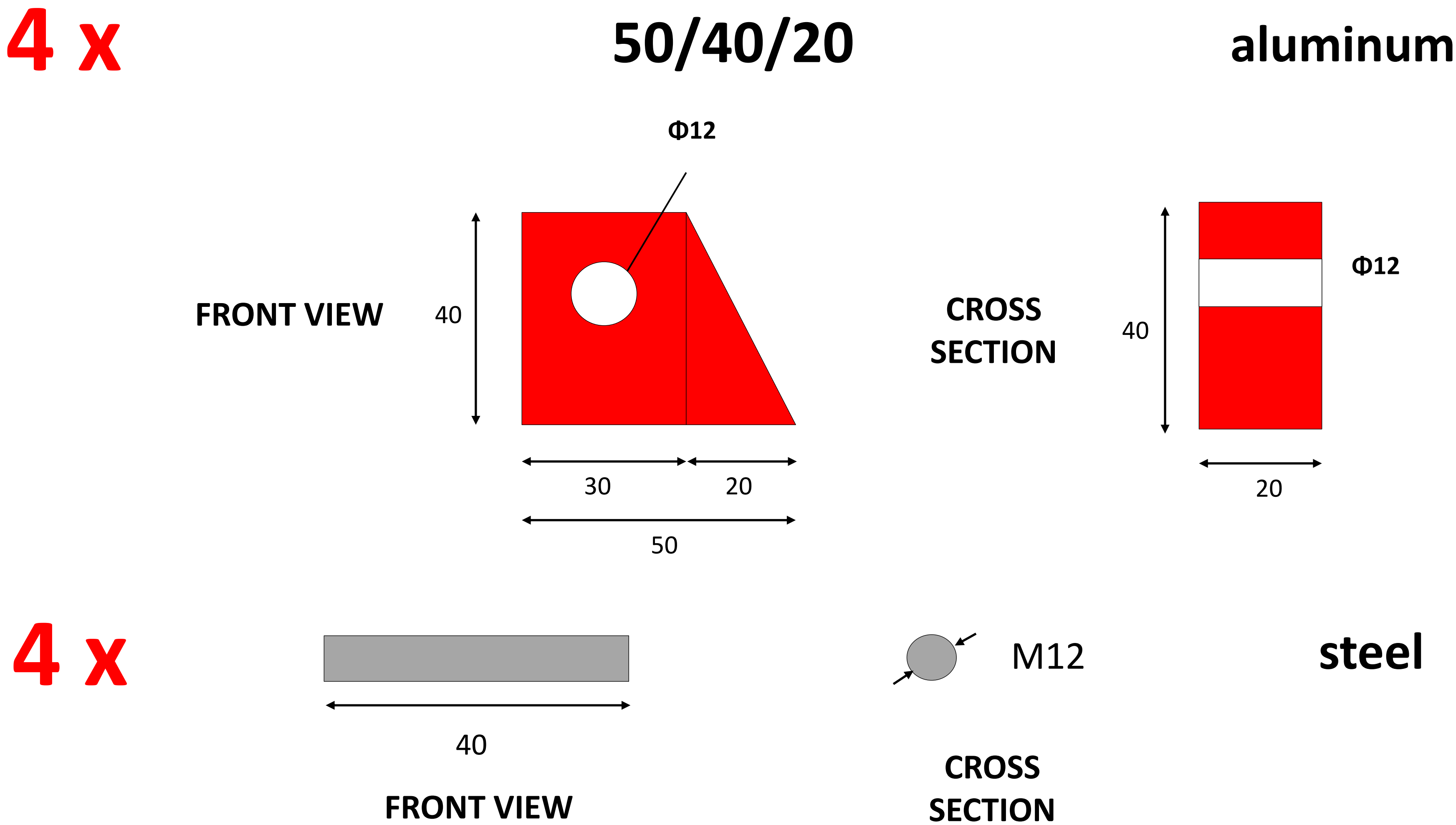

Figure 19. Technical drawing of the INSTED columns – base connection laminas and the spigots utilized for this connection.

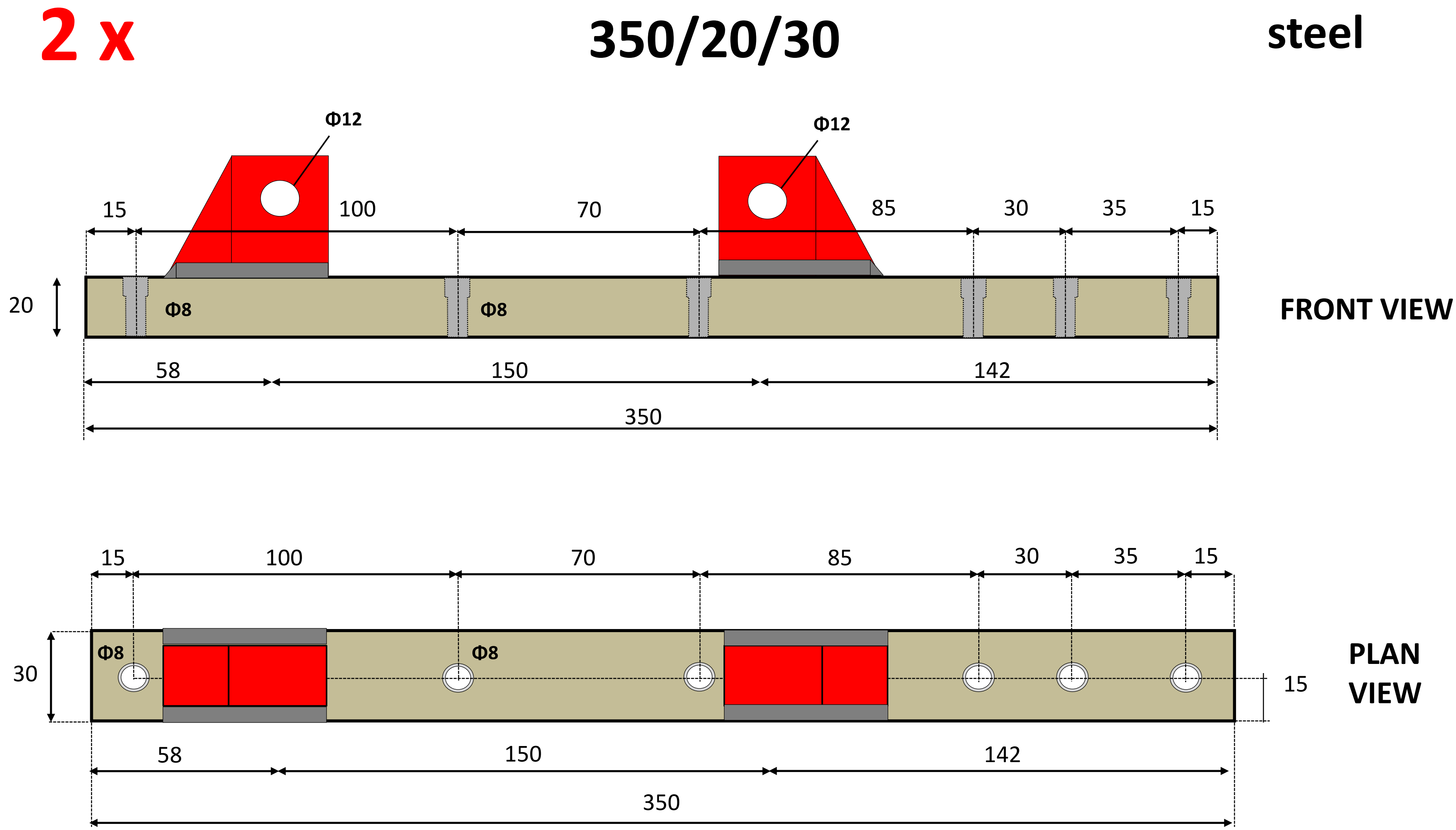

Figure 20. Technical drawing of the INSTED system base.

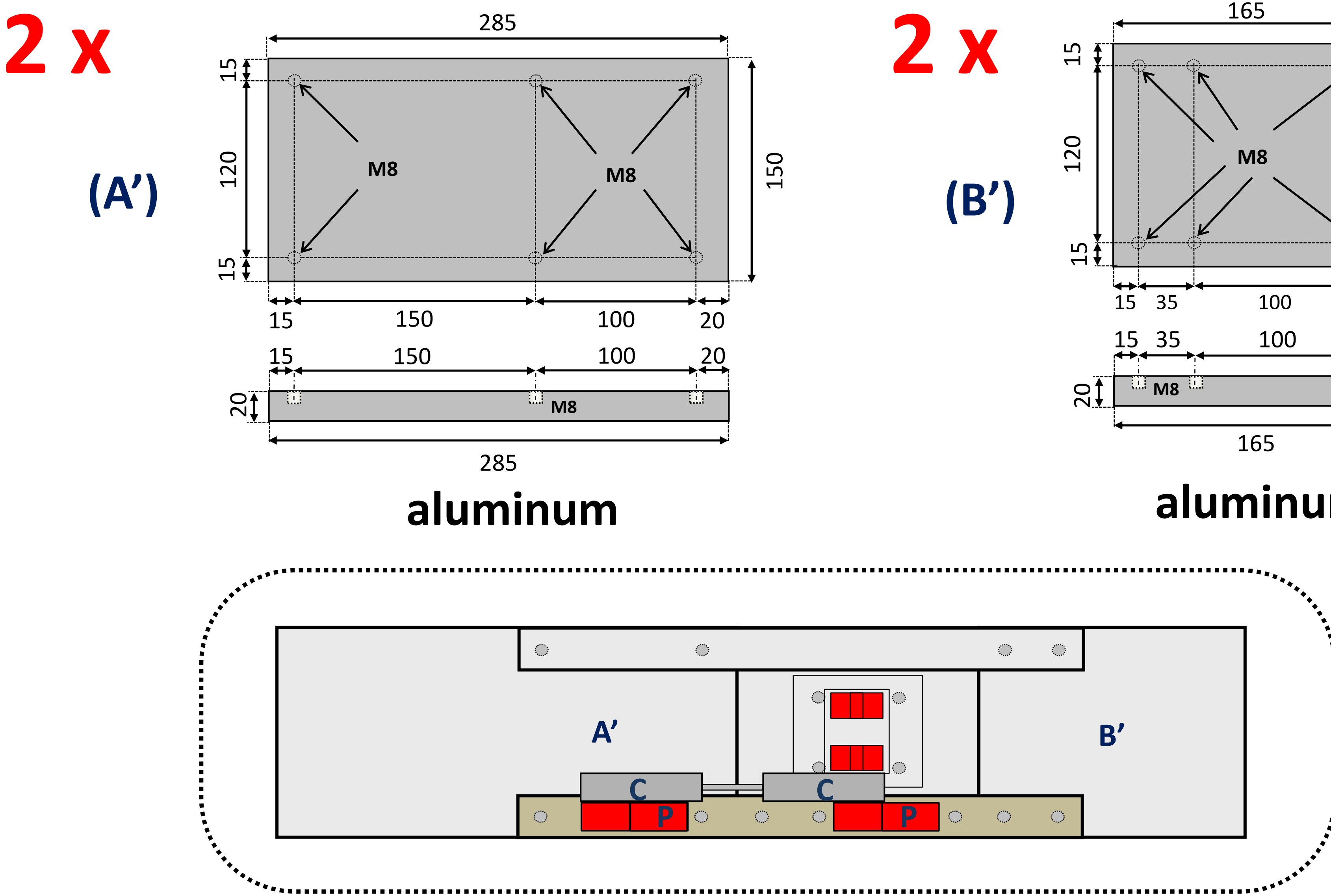

Figure 21. Technical drawing of the INSTED system footings.

APPENDIX B

I. Horizontal Pushover Tests

II. Dynamic Tests

I. Horizontal Pushover Tests

1st HORIZONTAL PUSHOVER TEST
Drod=4mm

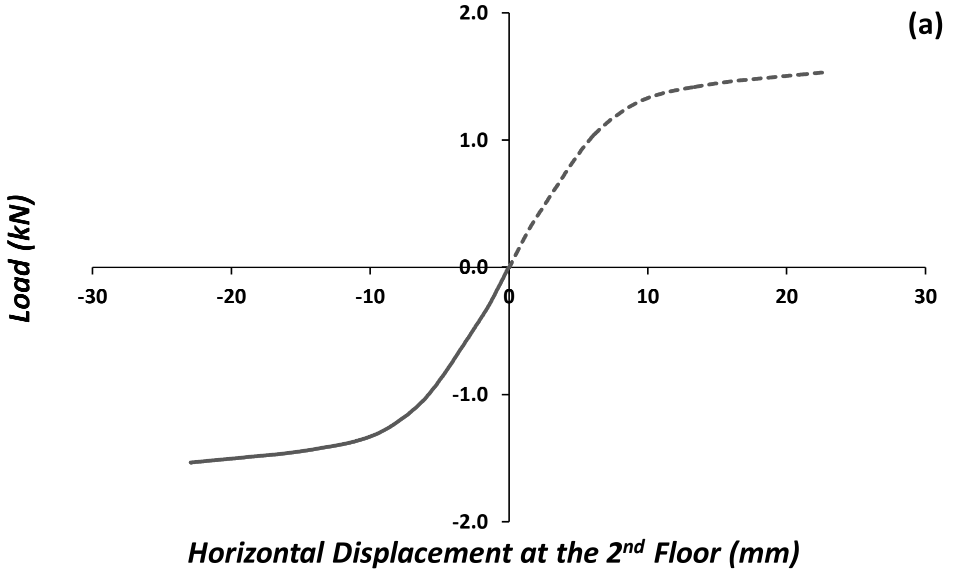

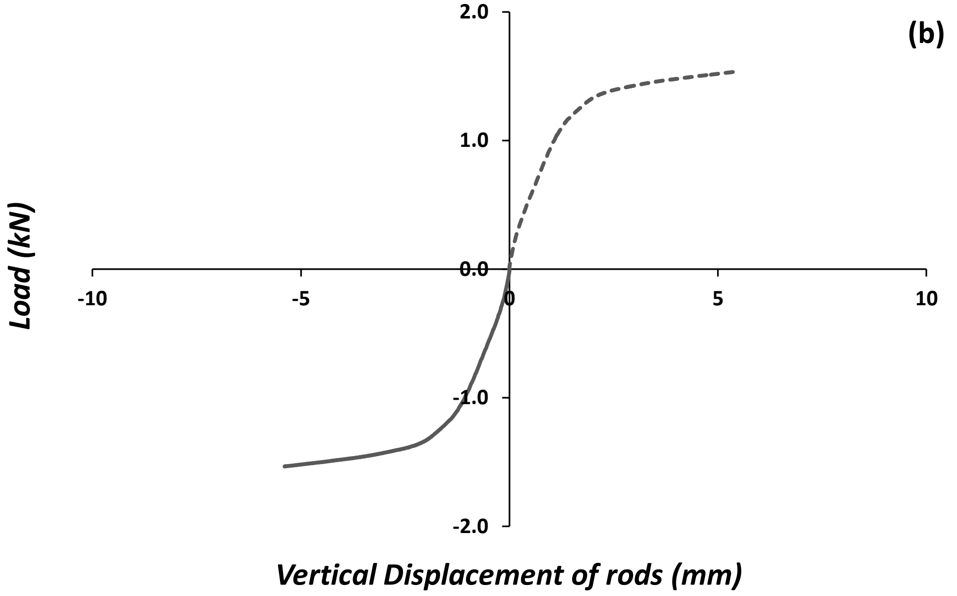

Figure 1. Load – Displacement curves derived from the ***monotonic pushover test*** of the retrofitted frame (The dashed branch is not a result of measured data; it is considered to be identical with the measured curve though, due to the building's symmetric behavior).

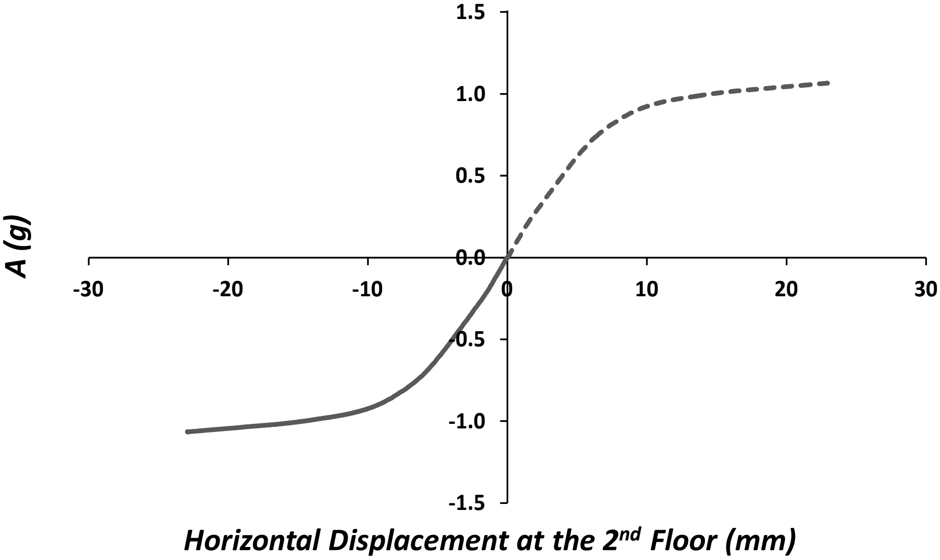

Figure 2. Acceleration – Displacement curve derived from the ***monotonic pushover test*** of the retrofitted frame.

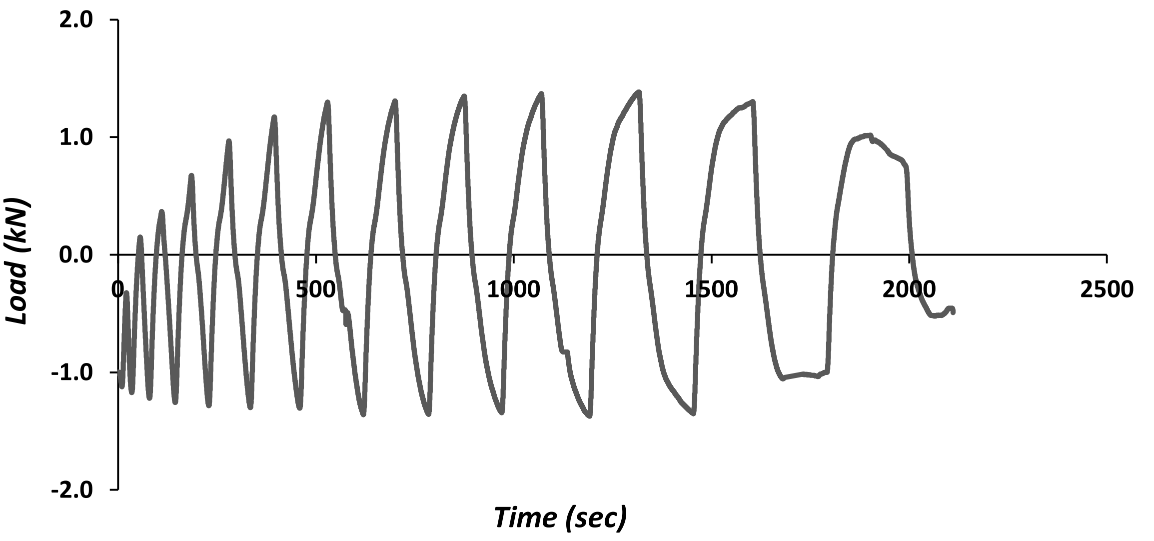

Figure 3. Load – Time curve derived from the ***slow - cyclic pushover test*** of the retrofitted frame.

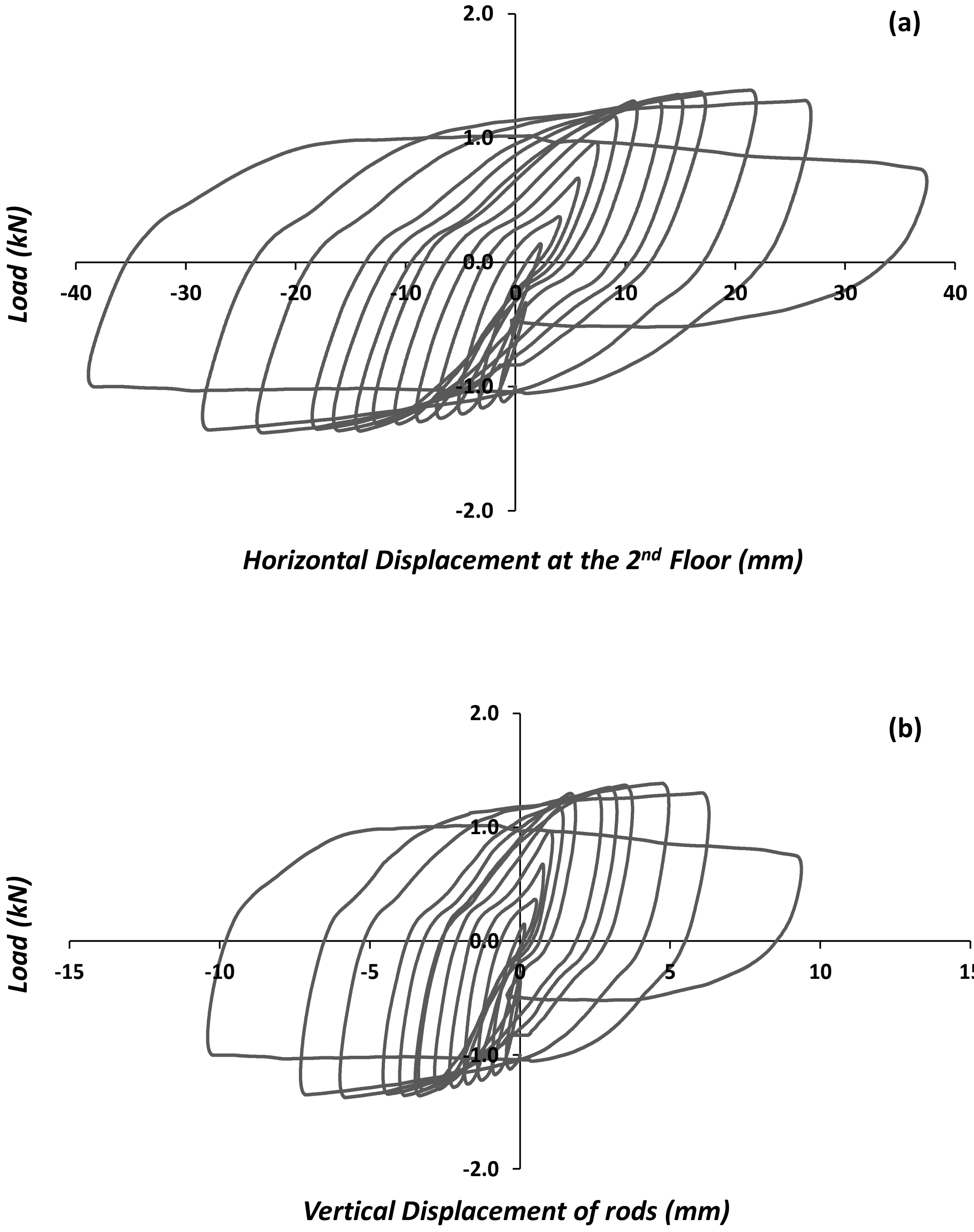

Figure 4. Load – Displacement curves derived from *the* ***slow - cyclic pushover test*** of the retrofitted frame.

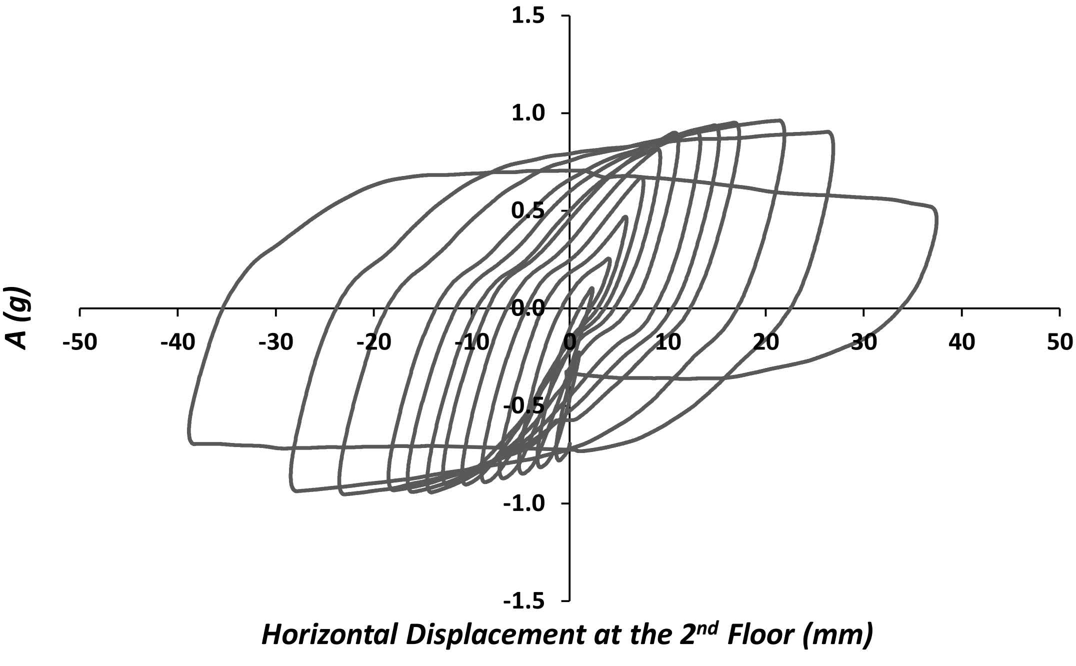

Figure 5. Acceleration – Displacement curve derived from the ***slow-cyclic pushover test*** of the retrofitted frame.

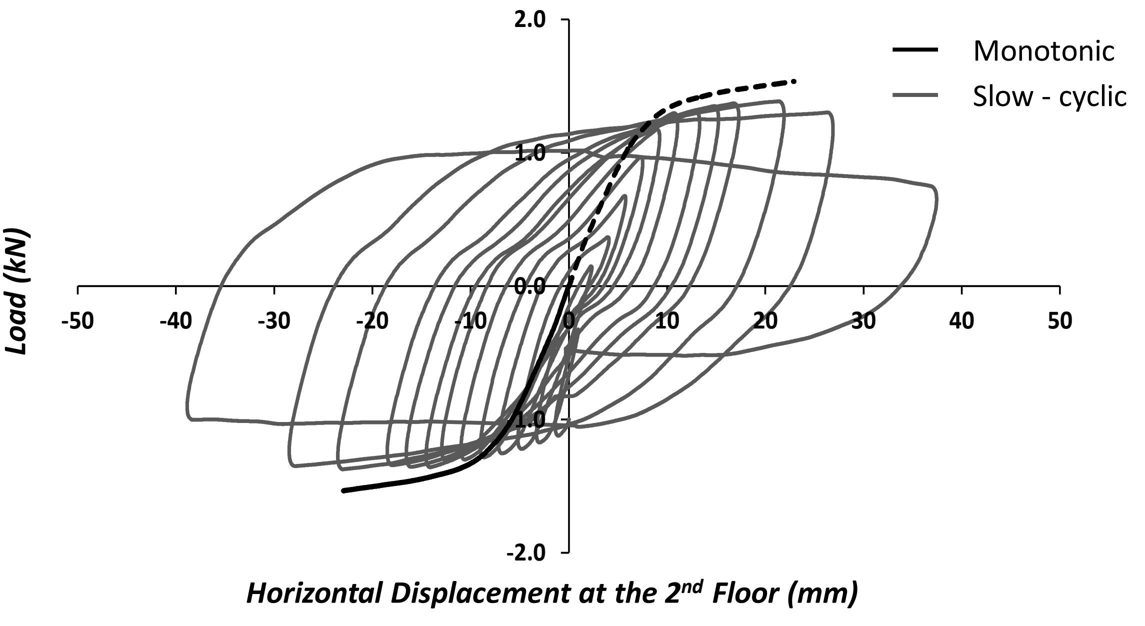

Figure 6. *Comparison* of the ***monotonic and slow – cyclic pushover tests*** in terms of strength and ductility.

2^{nd} HORIZONTAL PUSHOVER TEST
D_{rod}=3.2mm

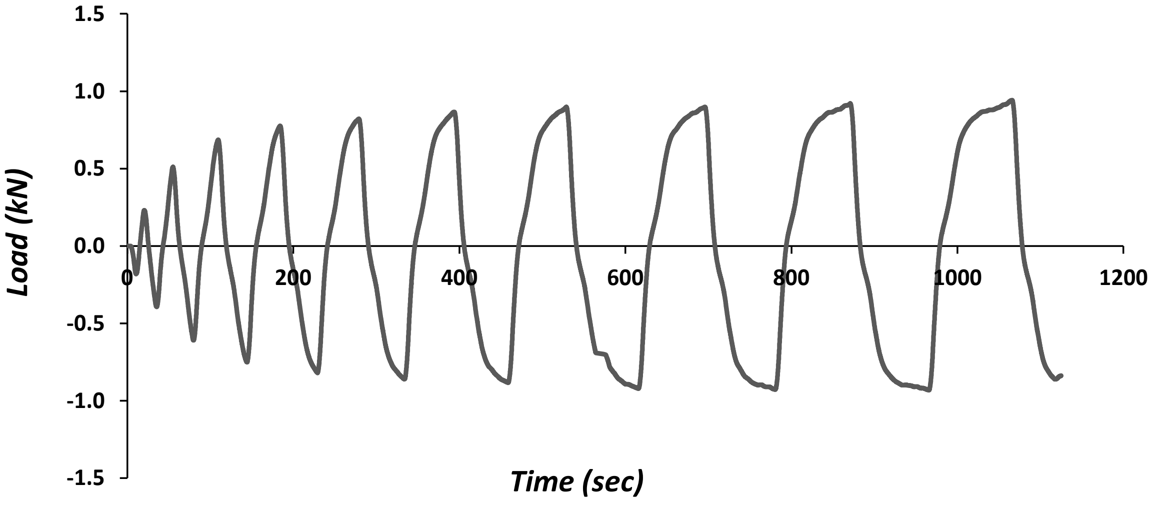

Figure 7. Load – Time curve derived from *the* ***slow - cyclic pushover test*** of the retrofitted frame.

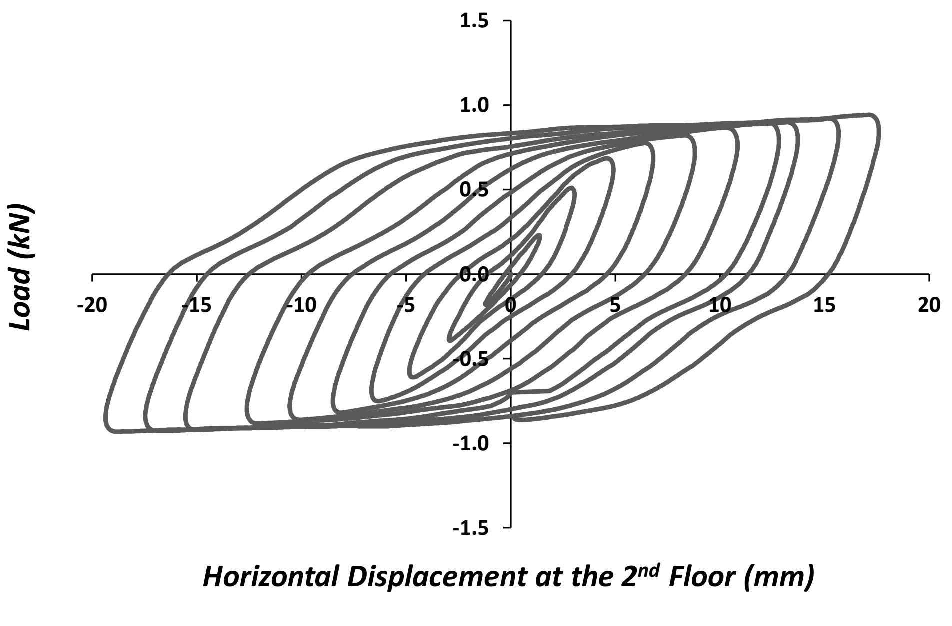

Figure 8. Load – Displacement curve derived from *the* ***slow - cyclic pushover test*** of the retrofitted frame.

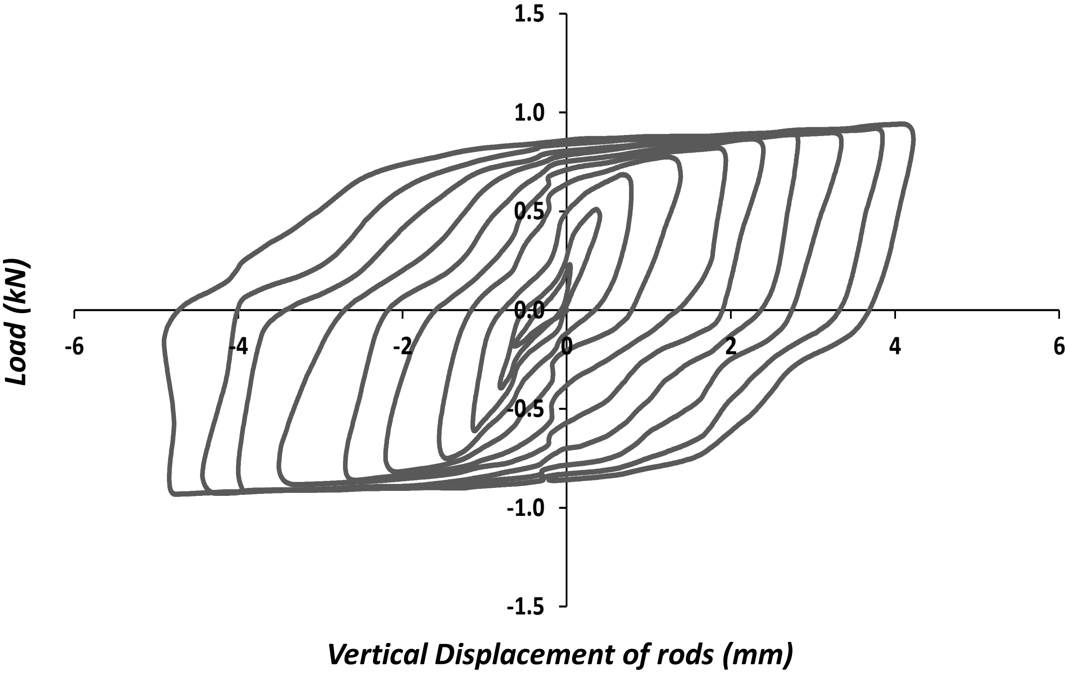

Figure 9. Load – Vertical Displacement derived from *the* ***slow - cyclic pushover test*** of the retrofitted frame.

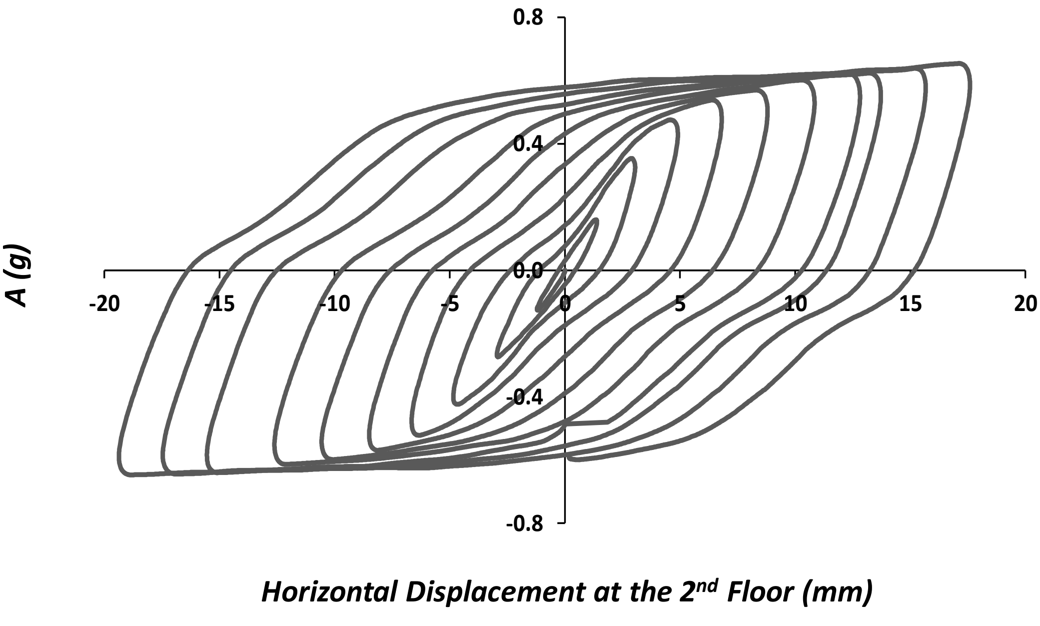

Figure 10. Acceleration – Displacement curve derived from the ***slow-cyclic pushover test*** of the retrofitted frame.

	F_{yield} (kN)	F_{max} (kN)	a_{yield} (g)	a_{max} (g)
D = 4mm	1.20	1.50	0.80	0.97
D = 3.2mm	0.70	0.90	0.49	0.63

Figure 11. Results of the Horizontal Pushover Tests conducted for the retrofitted model. By translating the yielding force and maximum strength into acceleration, an estimation of the system's pseudostatical yielding & maximum acceleration is made.

II. Dynamic Tests

Retrofitted building - SETUP I
Dynamic Test

List of applied seismic records.

Strong Seismic Records
Rinaldi (Northridge 1994)
JMA (Kobe 1995)
Takatori (Kobe 1995)

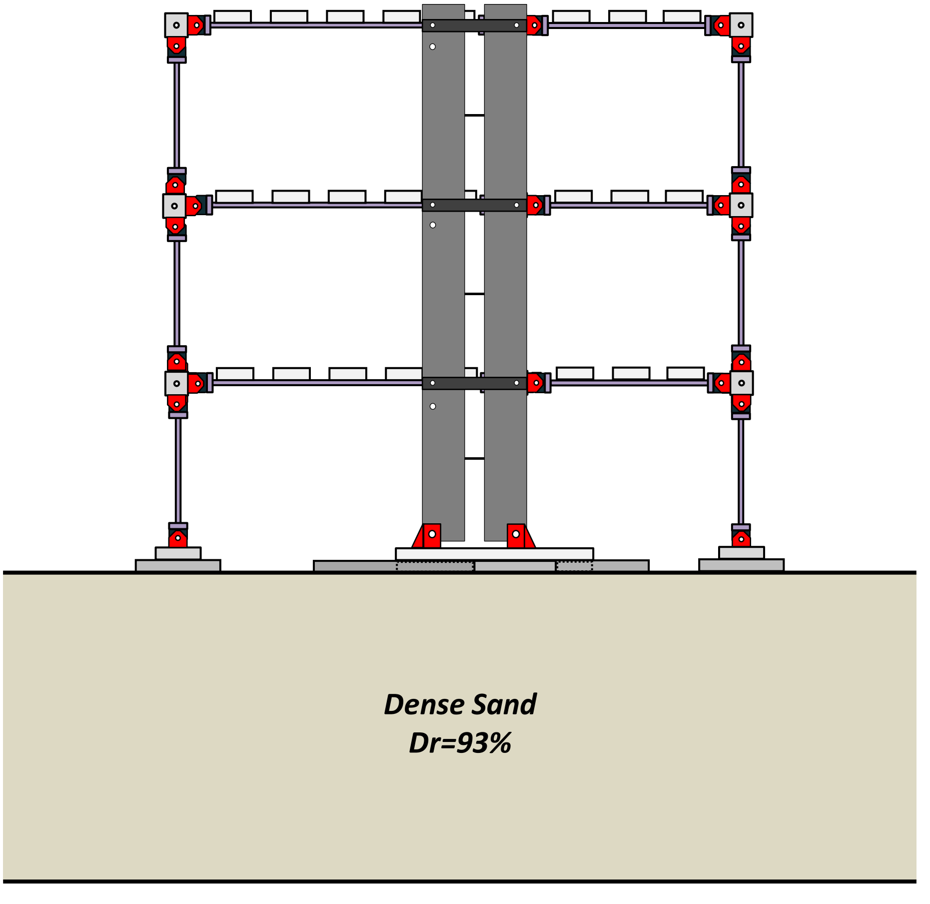

No. of rods per frame → 3
D = 4mm

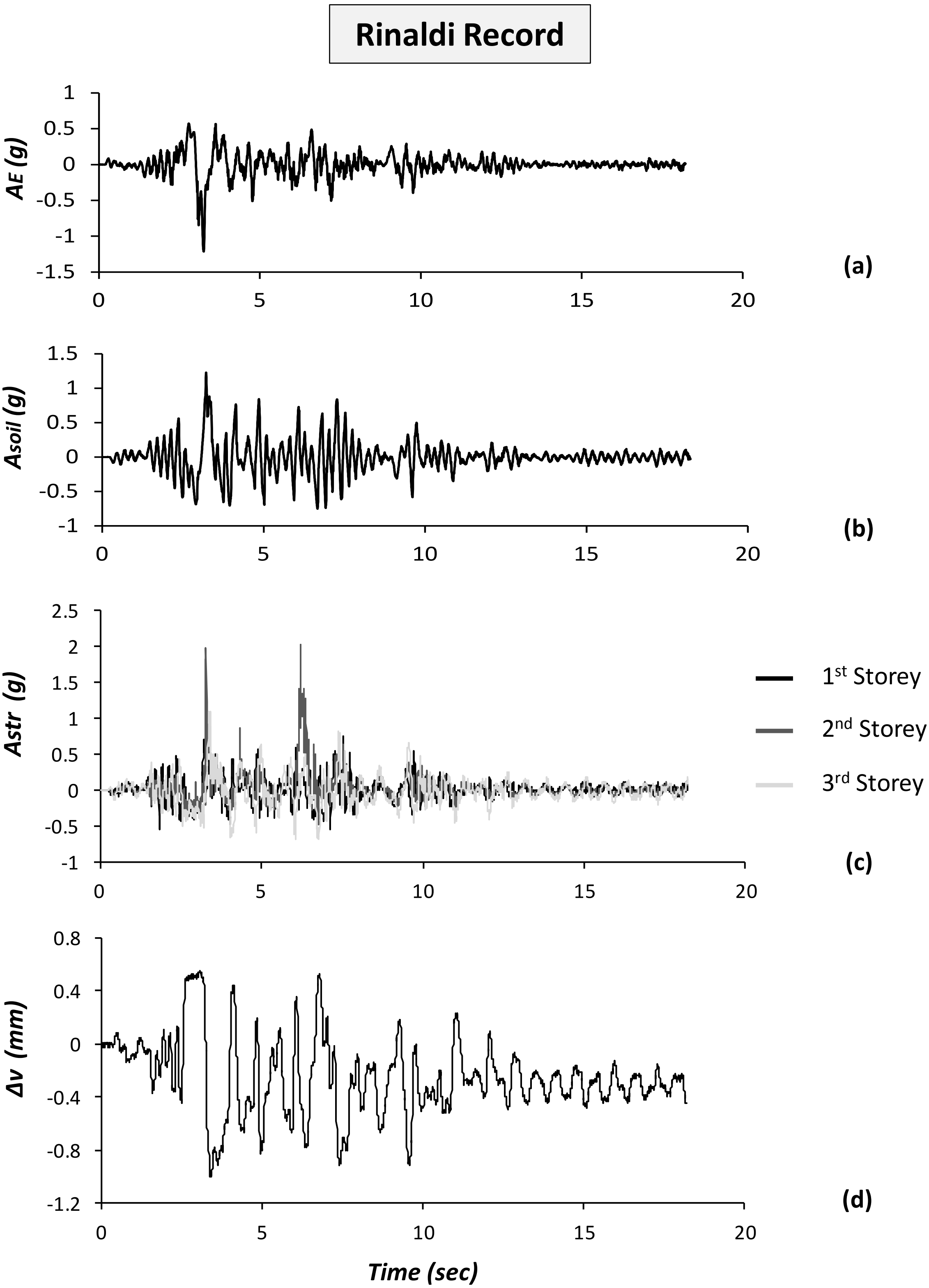

Figure 12. Time histories of **(a)** the acceleration used as bedrock excitation, **(b)** the acceleration measured in a small depth from the soil surface, **(c)** the accelerations measured at storey levels and **(d)** the vertical displacement of the rods.

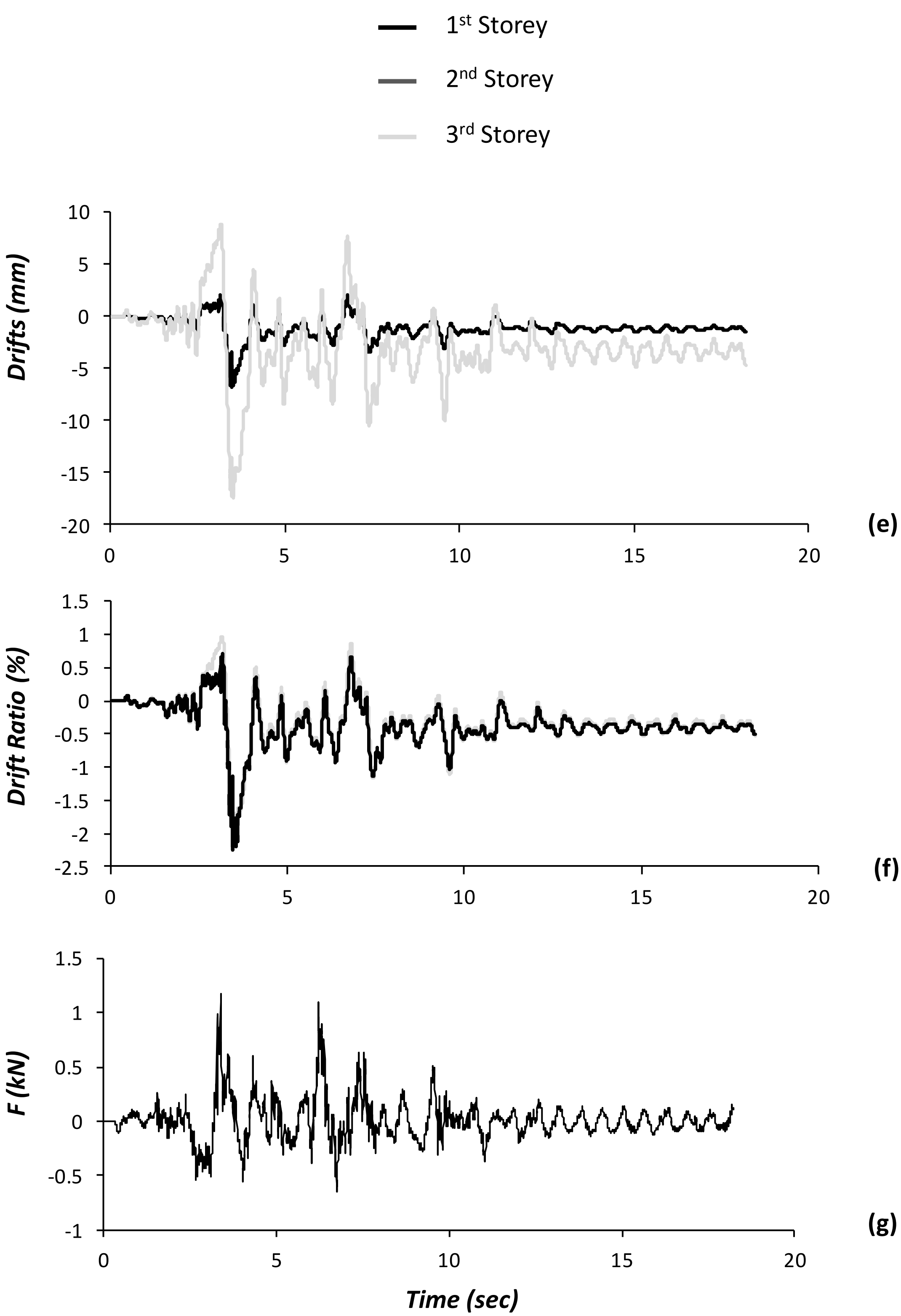

Figure 13. Time histories of **(e)** the drifts at the level of the 1st and 3rd storey, **(f)** the respective drift ratios and **(g)** the total shear force the retrofitted structure receives .

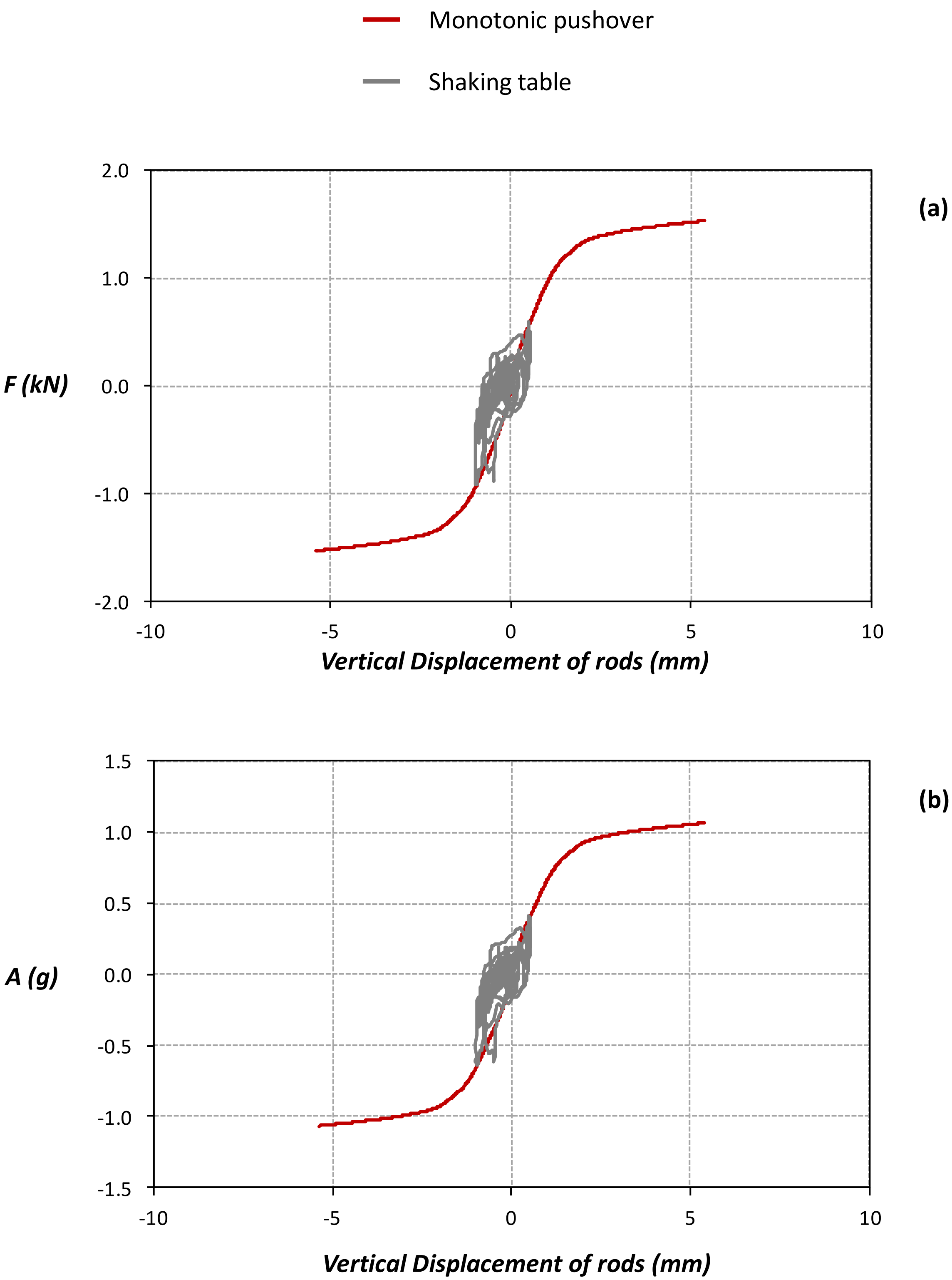

Figure 14. (a) Total shear force – relative vertical displacement of rods and **(b)** acceleration – vertical displacement curves compared to the respective monotonic curves derived from the 1st horizontal pushover test.

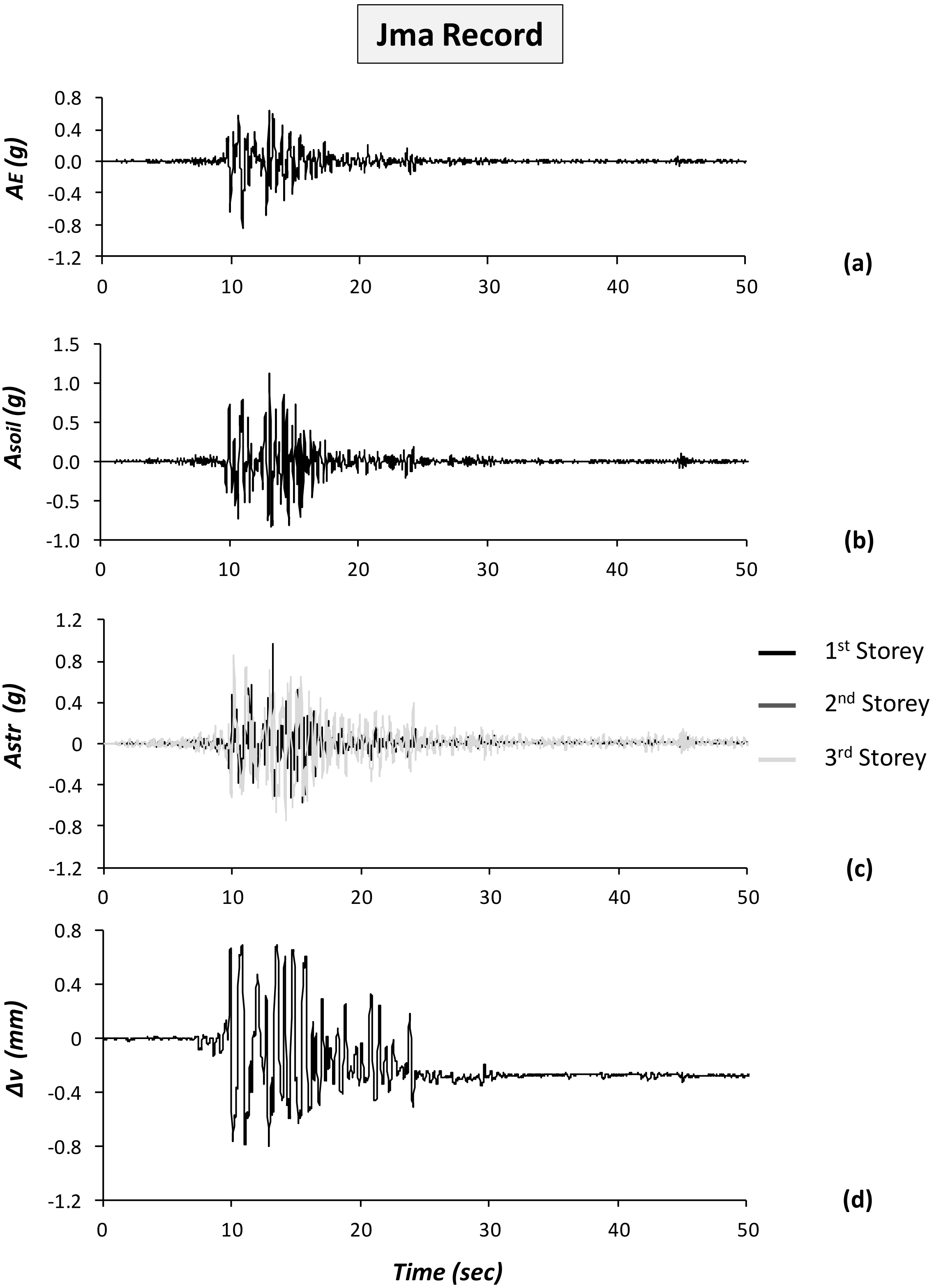

Figure 15. Time histories of **(a)** the acceleration used as bedrock excitation, **(b)** the acceleration measured in a small depth from the soil surface, **(c)** the accelerations measured at storey levels and **(d)** the vertical displacement of the rods.

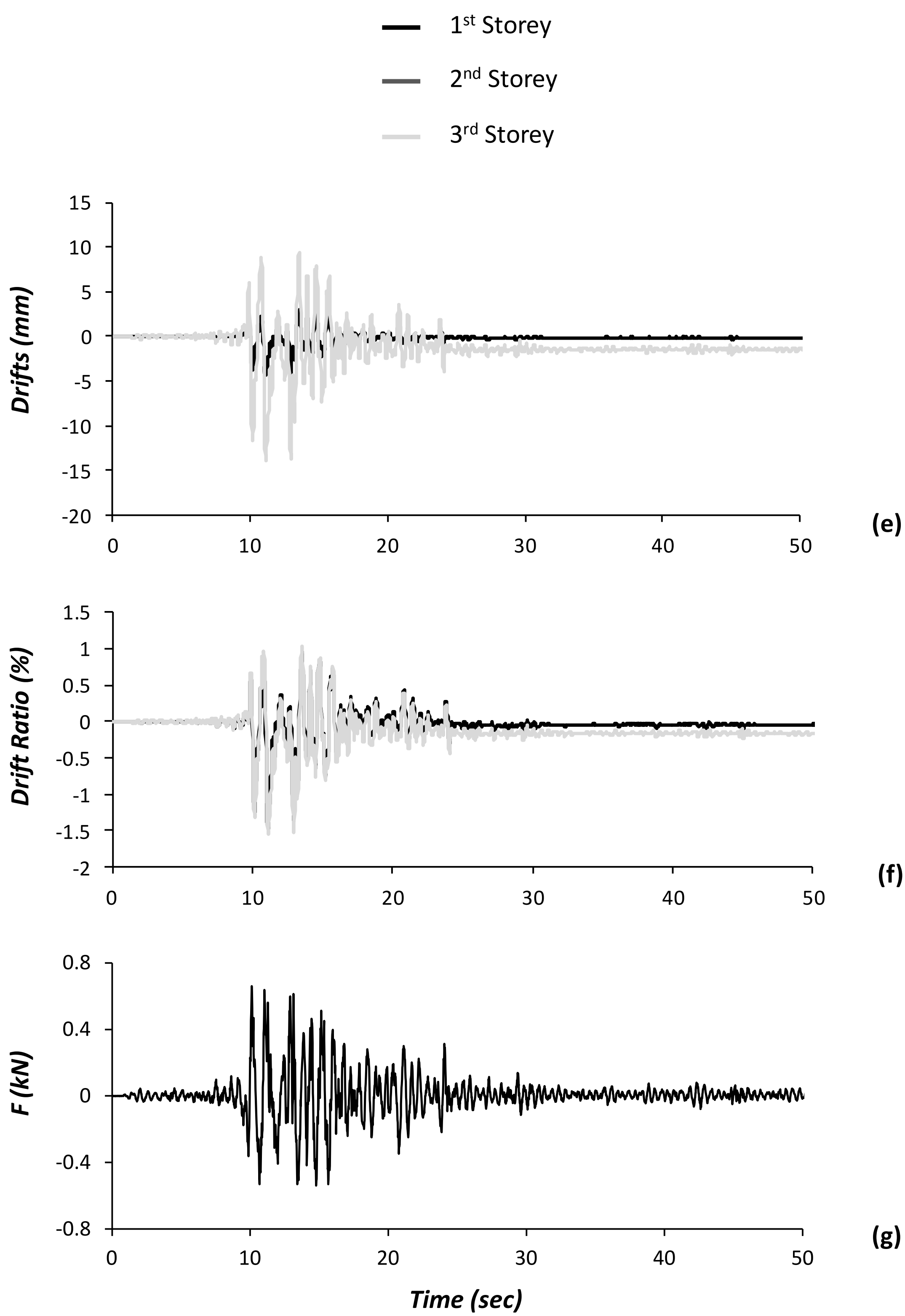

Figure 16. Time histories of **(e)** the drifts at the level of the 1st and 3rd storey, **(f)** the respective drift ratios and **(g)** the total shear force the retrofitted structure receives .

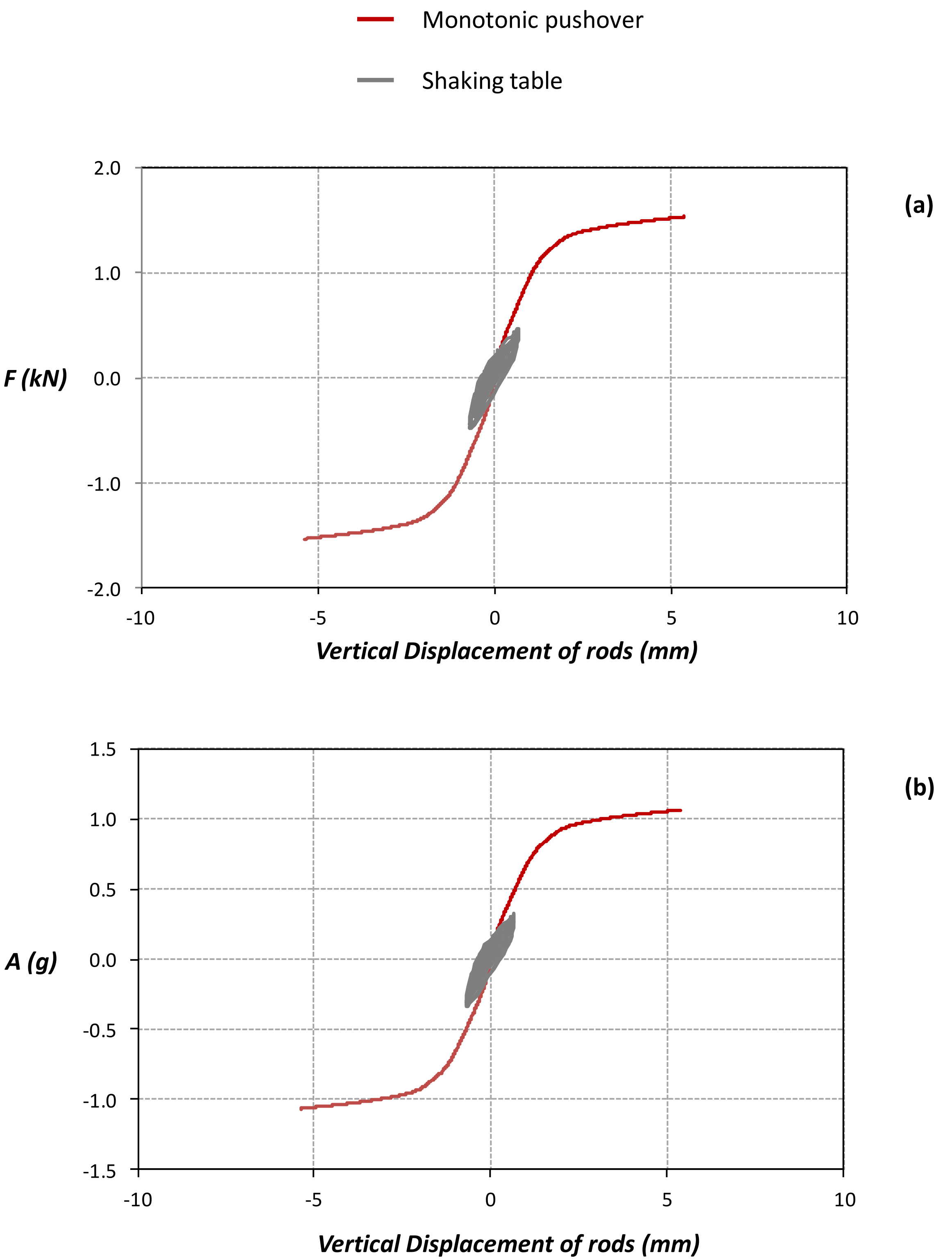

Figure 17. (a) Total shear force – relative vertical displacement of rods and **(b)** acceleration – vertical displacement curves compared to the respective monotonic curves derived from the 1st horizontal pushover test.

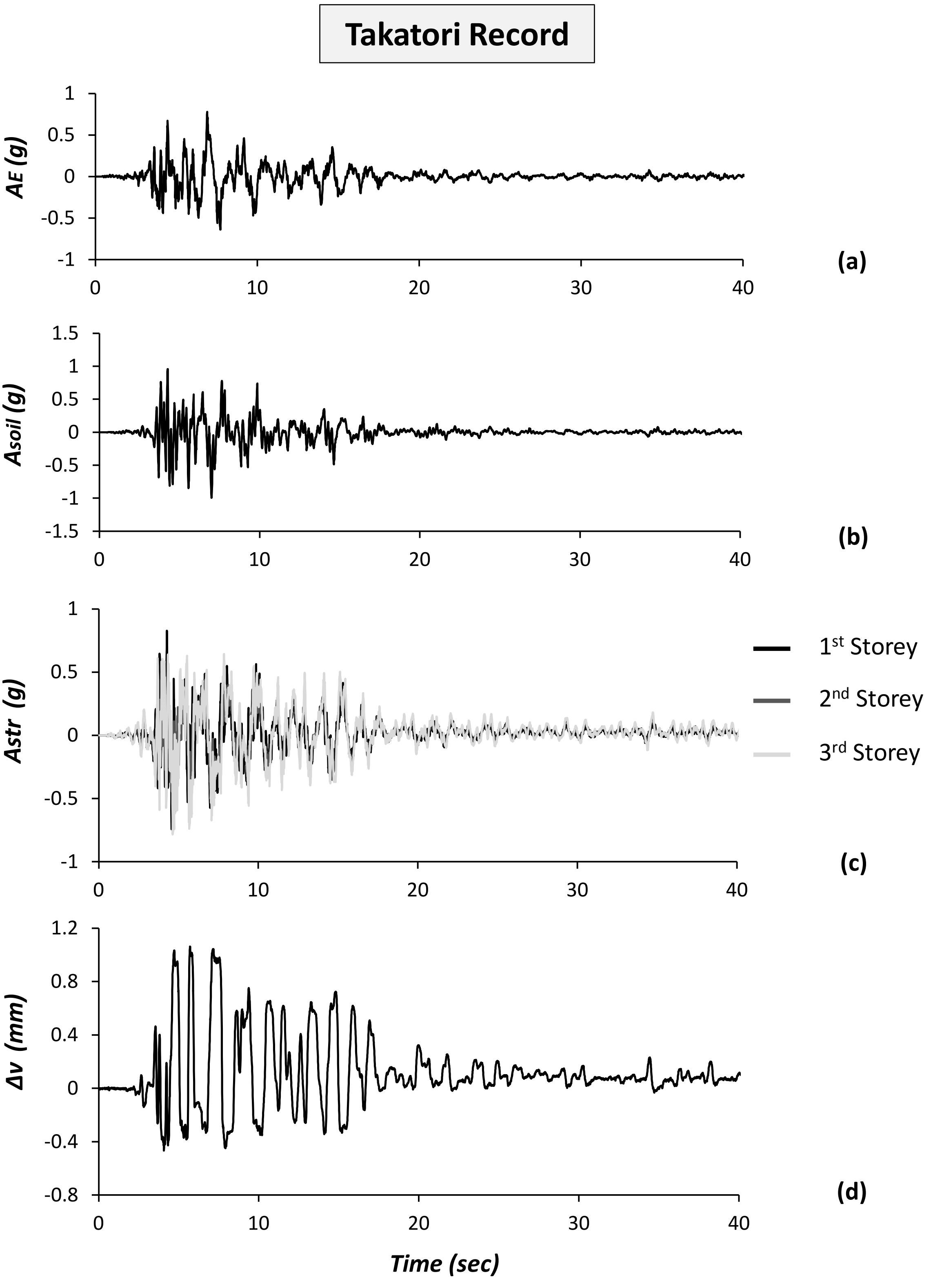

Figure 18. Time histories of **(a)** the acceleration used as bedrock excitation, **(b)** the acceleration measured in a small depth from the soil surface, **(c)** the accelerations measured at storey levels and **(d)** the vertical displacement of the rods.

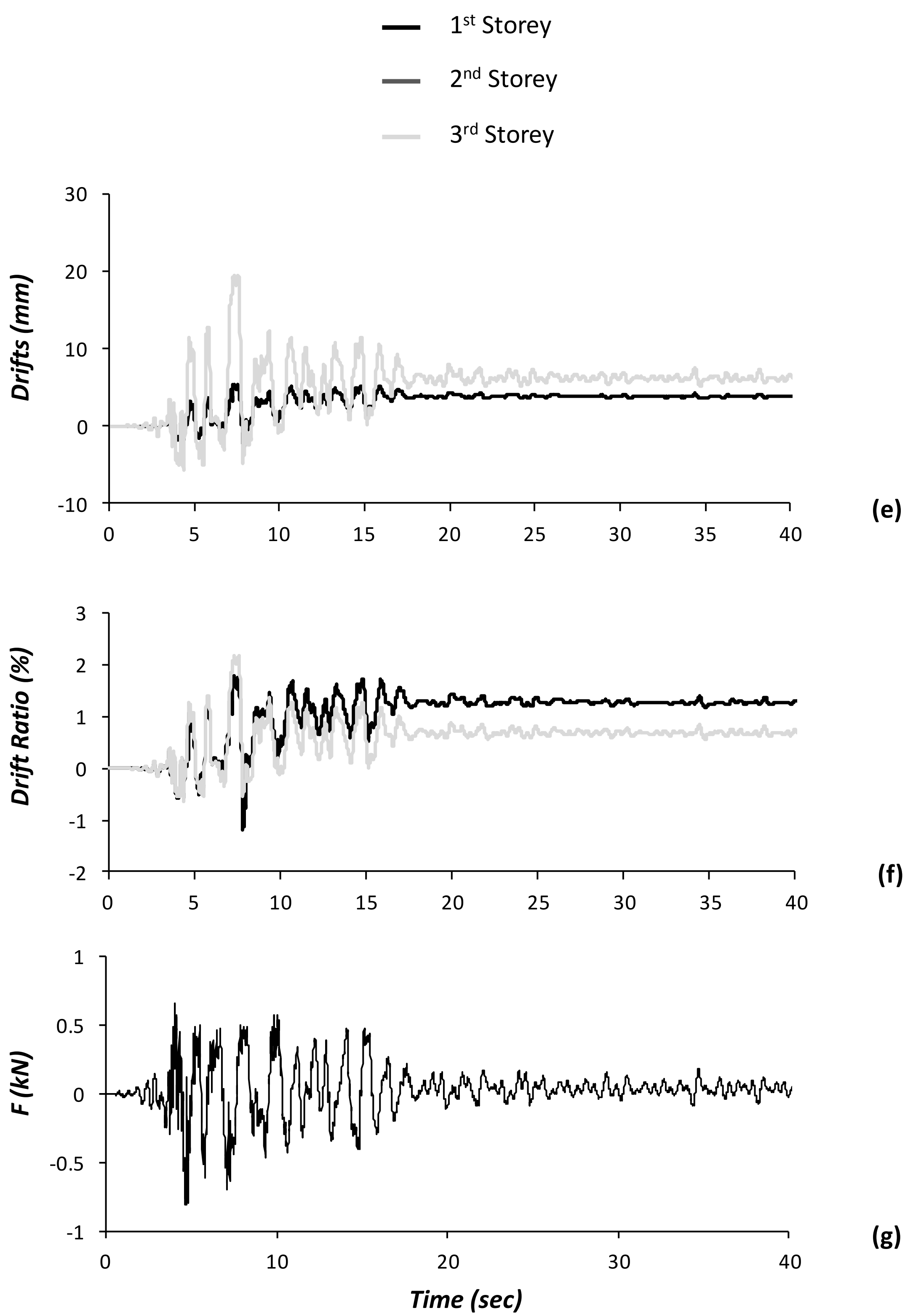

Figure 19. Time histories of **(e)** the drifts at the level of the 1st and 3rd storey, **(f)** the respective drift ratios and **(g)** the total shear force the retrofitted structure receives .

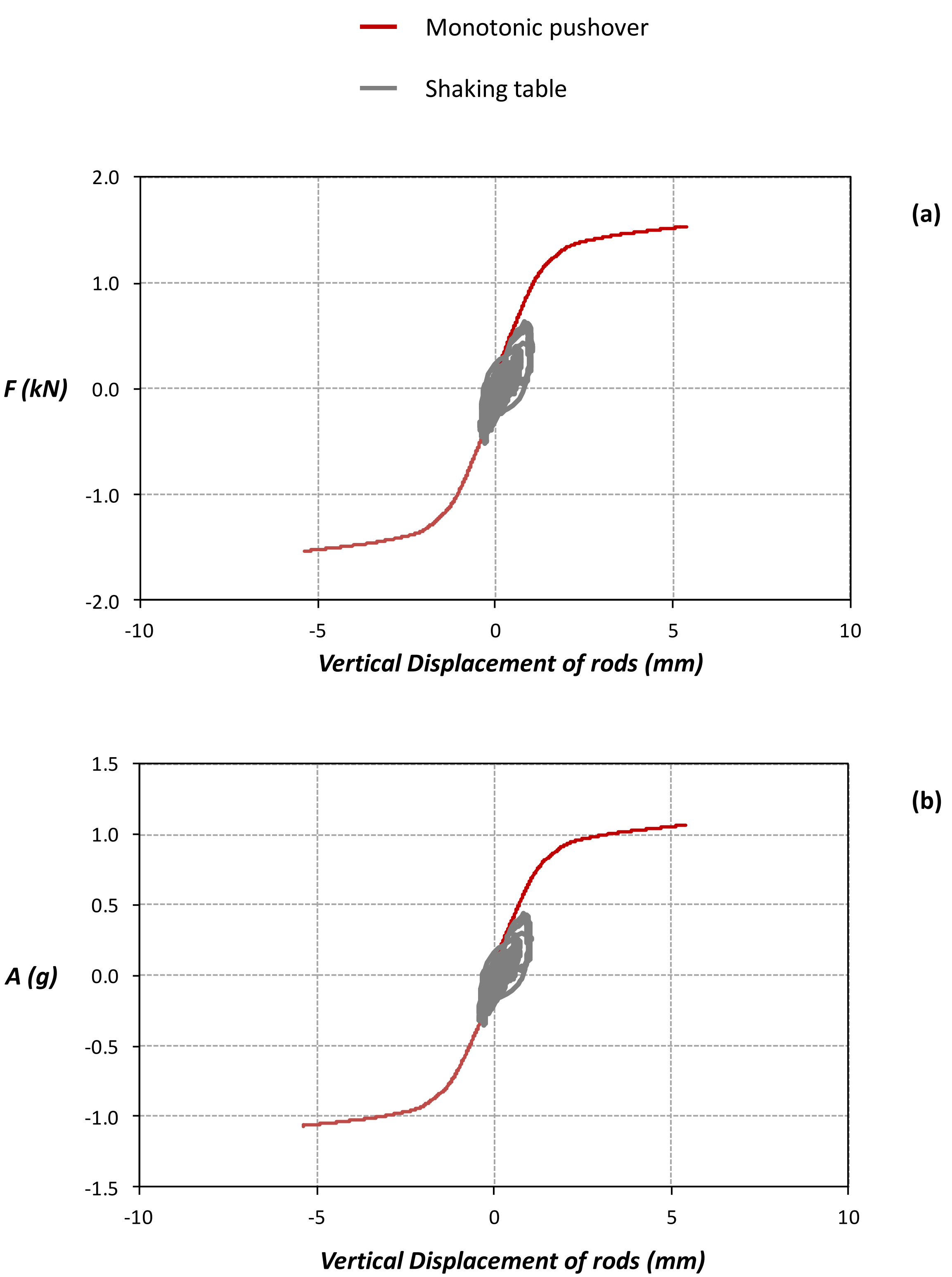

Figure 20. (a) Total shear force – relative vertical displacement of rods and **(b)** acceleration – vertical displacement curves compared to the respective monotonic curves derived from the 1st horizontal pushover test.

Retrofitted building - SETUP II
Dynamic Test

List of applied seismic records.

Strong Seismic Records
Rinaldi (Northridge 1994)
JMA (Kobe 1995)
Takatori (Kobe 1995)

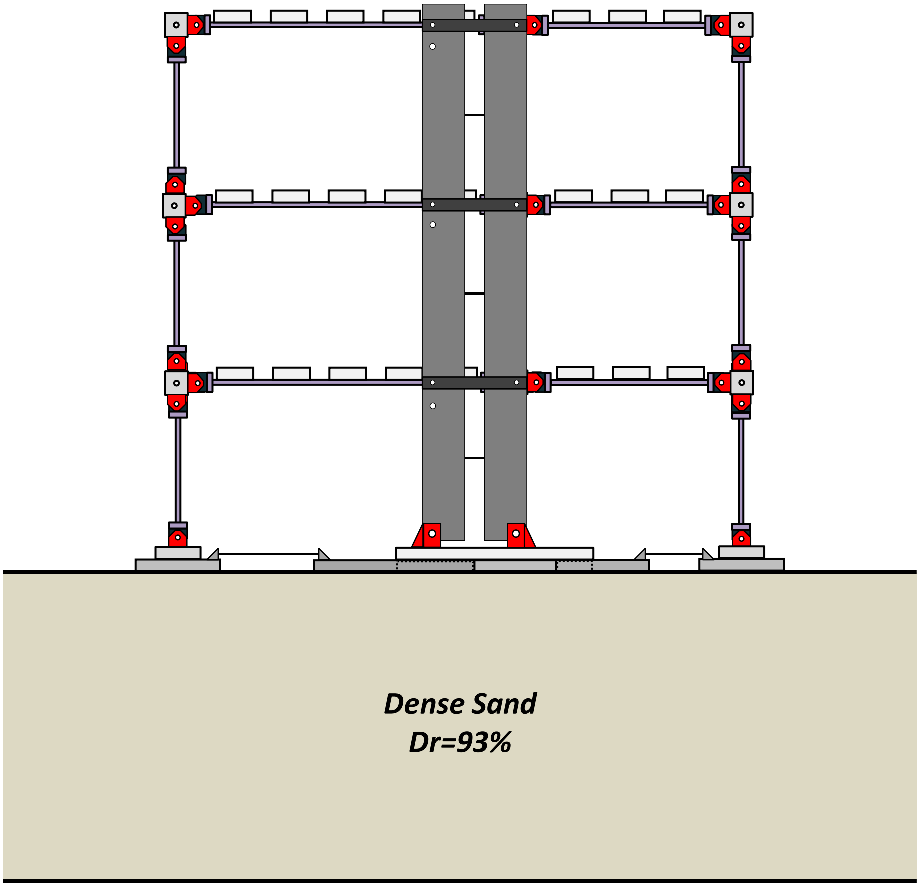

No. of rods per frame → 3
D = 3.2 mm

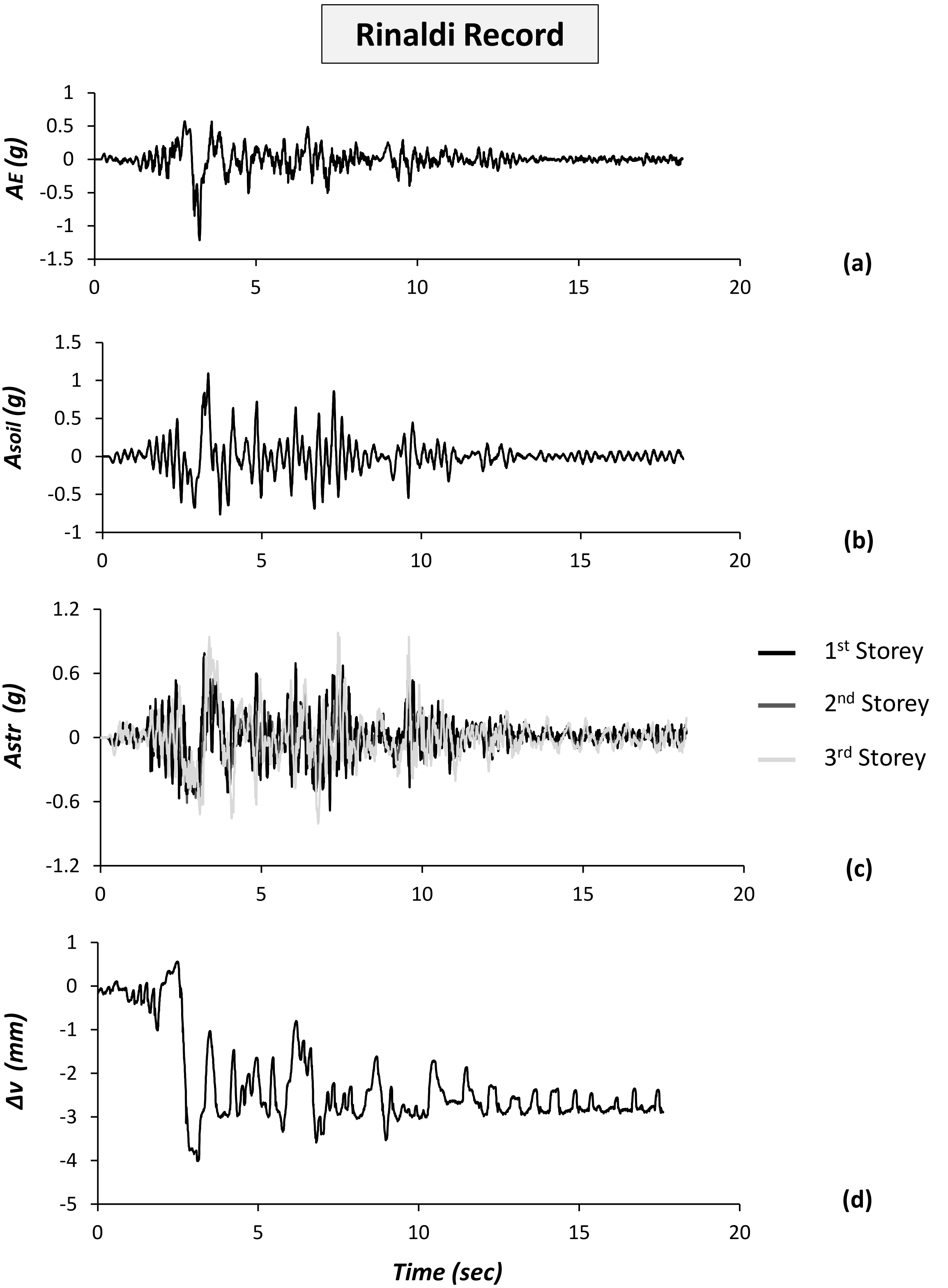

Figure 21. Time histories of **(a)** the acceleration used as bedrock excitation, **(b)** the acceleration measured in a small depth from the soil surface, **(c)** the accelerations measured at storey levels and **(d)** the vertical displacement of the rods.

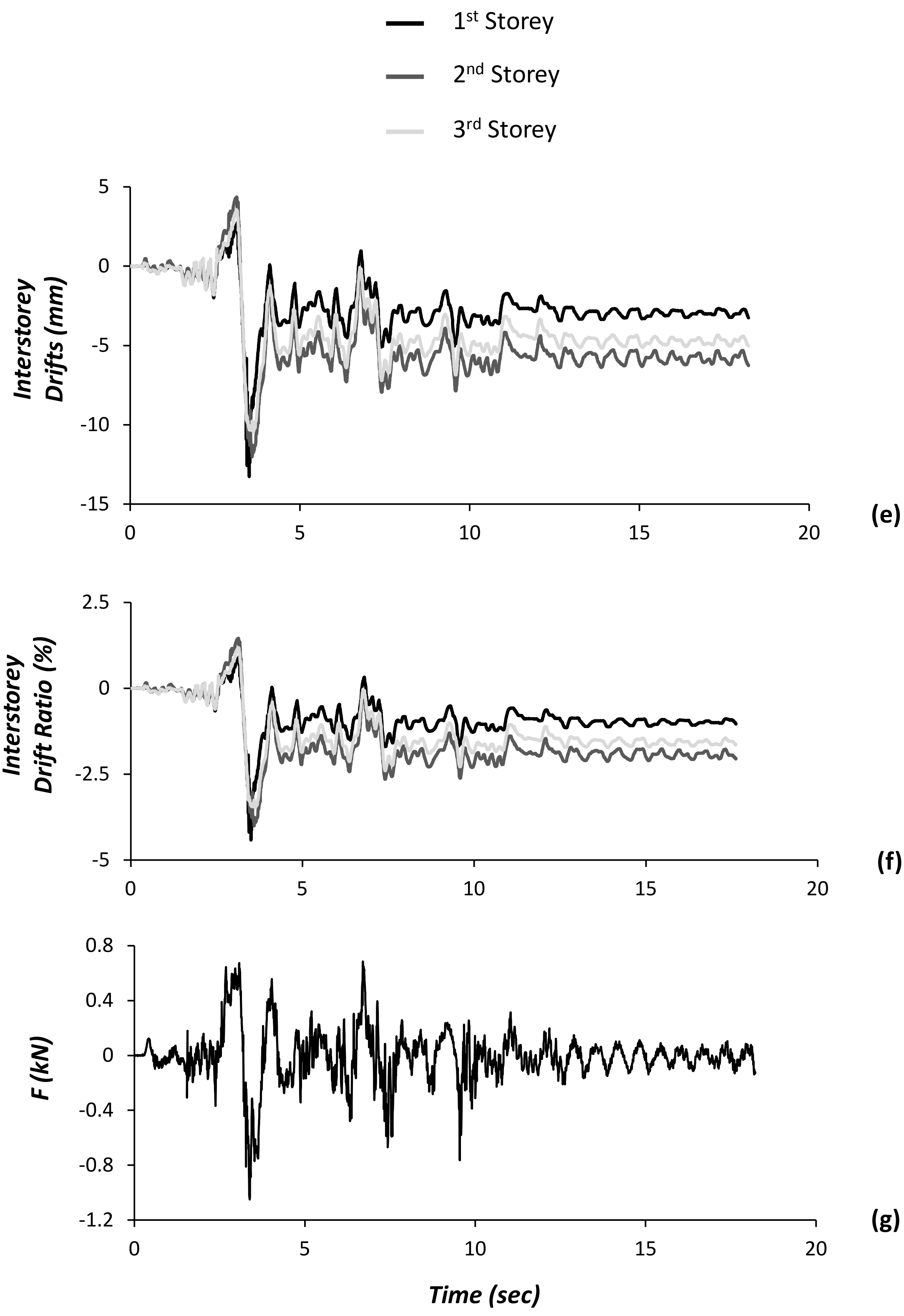

Figure 22. Time histories of **(e)** interstorey drifts at the level of each storey, **(f)** the respective drift ratios and **(g)** the total shear force the retrofitted structure receives .

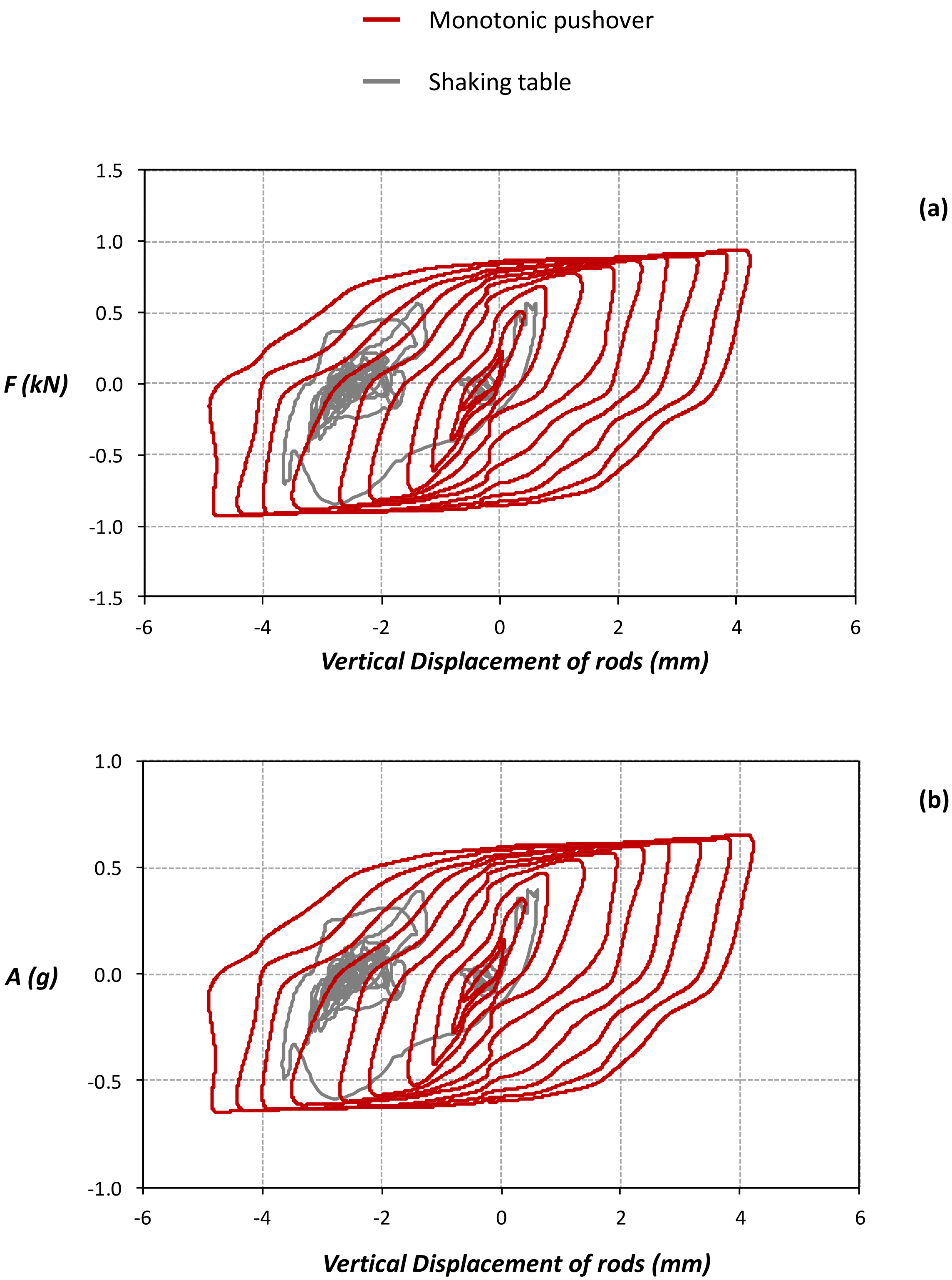

Figure 23. **(a)** Total shear force – relative vertical displacement of rods and **(b)** acceleration – vertical displacement curves compared to the respective curves derived from the 2nd horizontal pushover test.

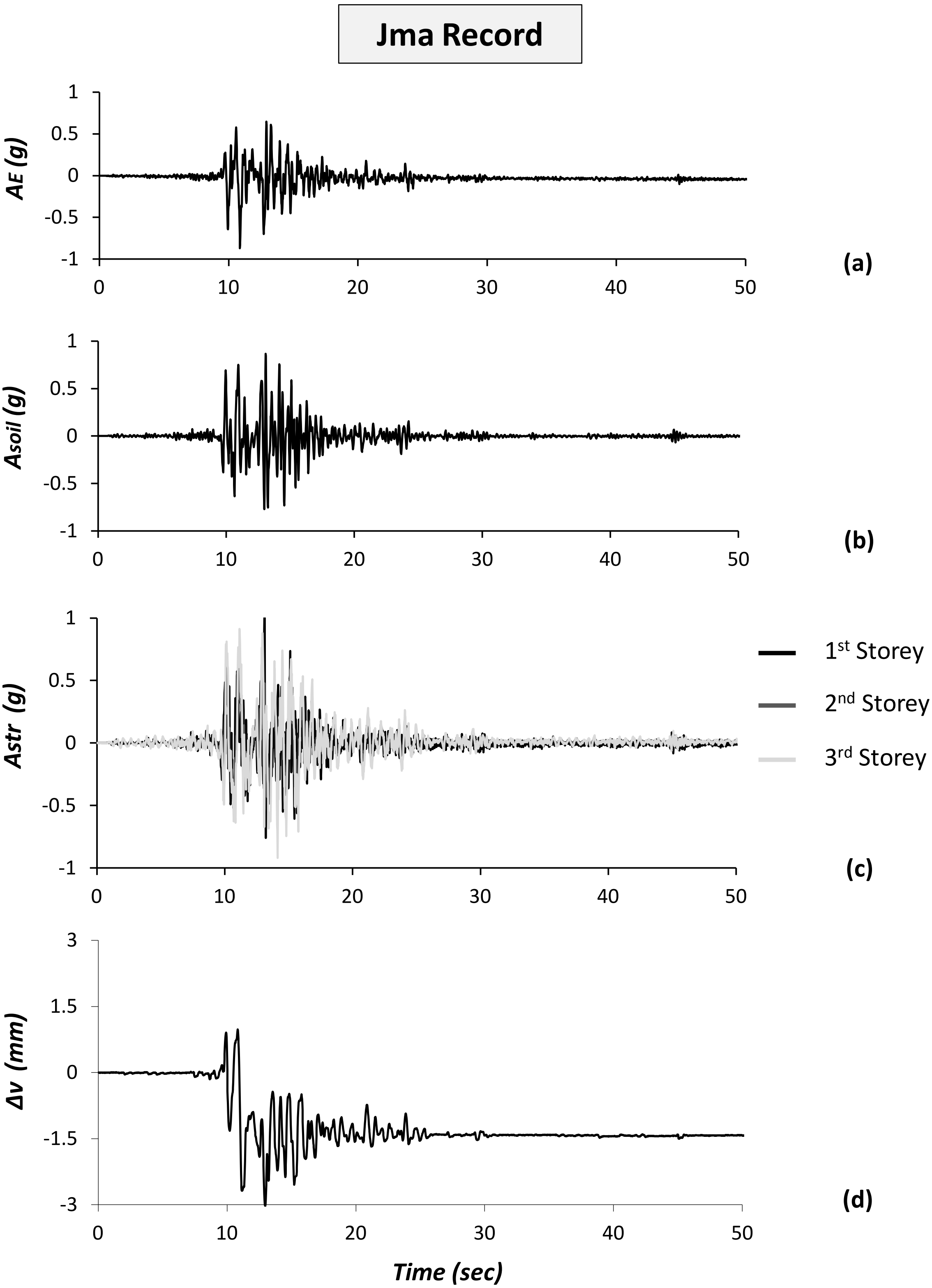

Figure 24. Time histories of **(a)** the acceleration used as bedrock excitation, **(b)** the acceleration measured in a small depth from the soil surface, **(c)** the accelerations measured at storey levels and **(d)** the vertical displacement of the rods.

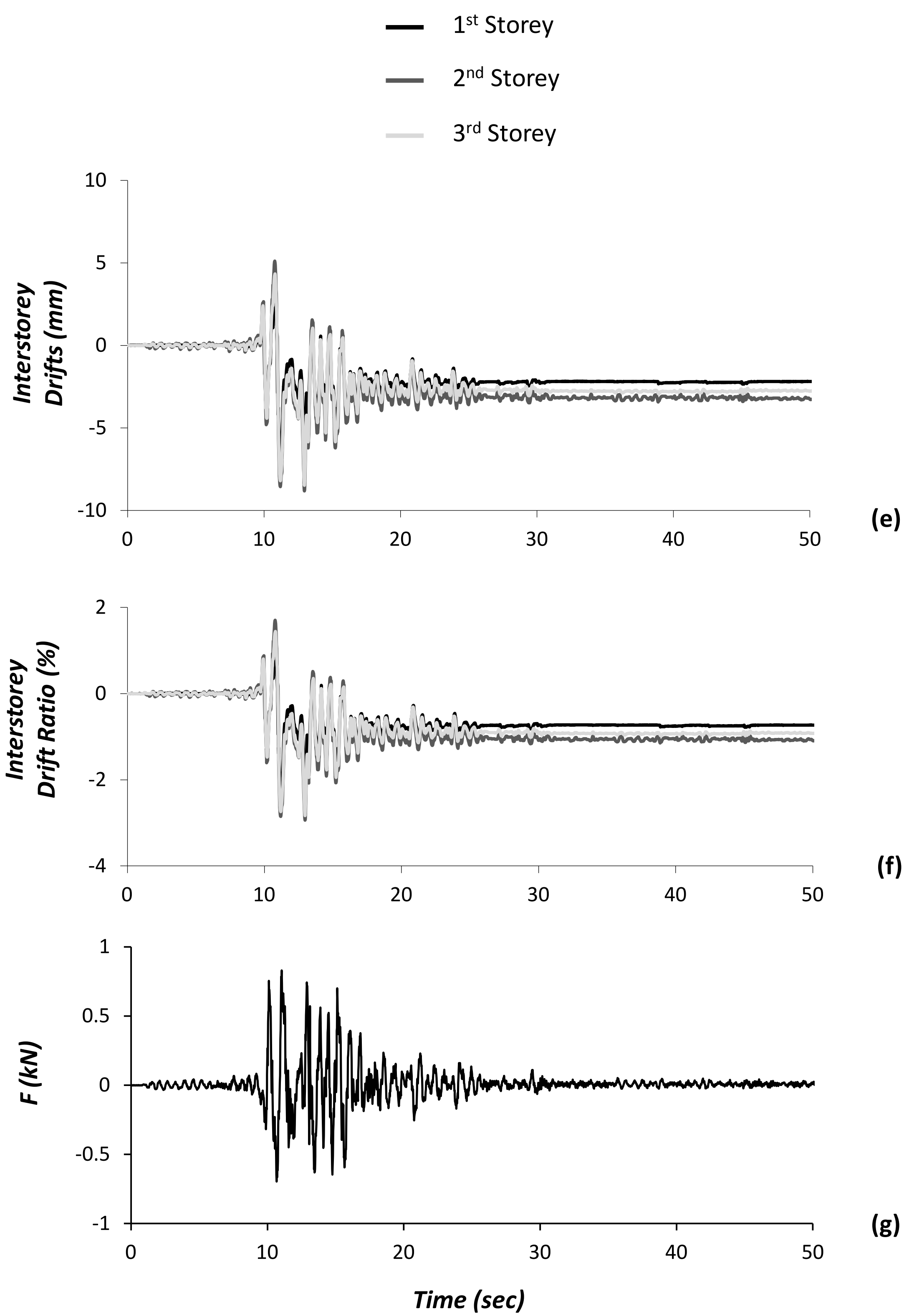

Figure 25. Time histories of **(e)** interstorey drifts at the level of each storey, **(f)** the respective drift ratios and **(g)** the total shear force the retrofitted structure receives .

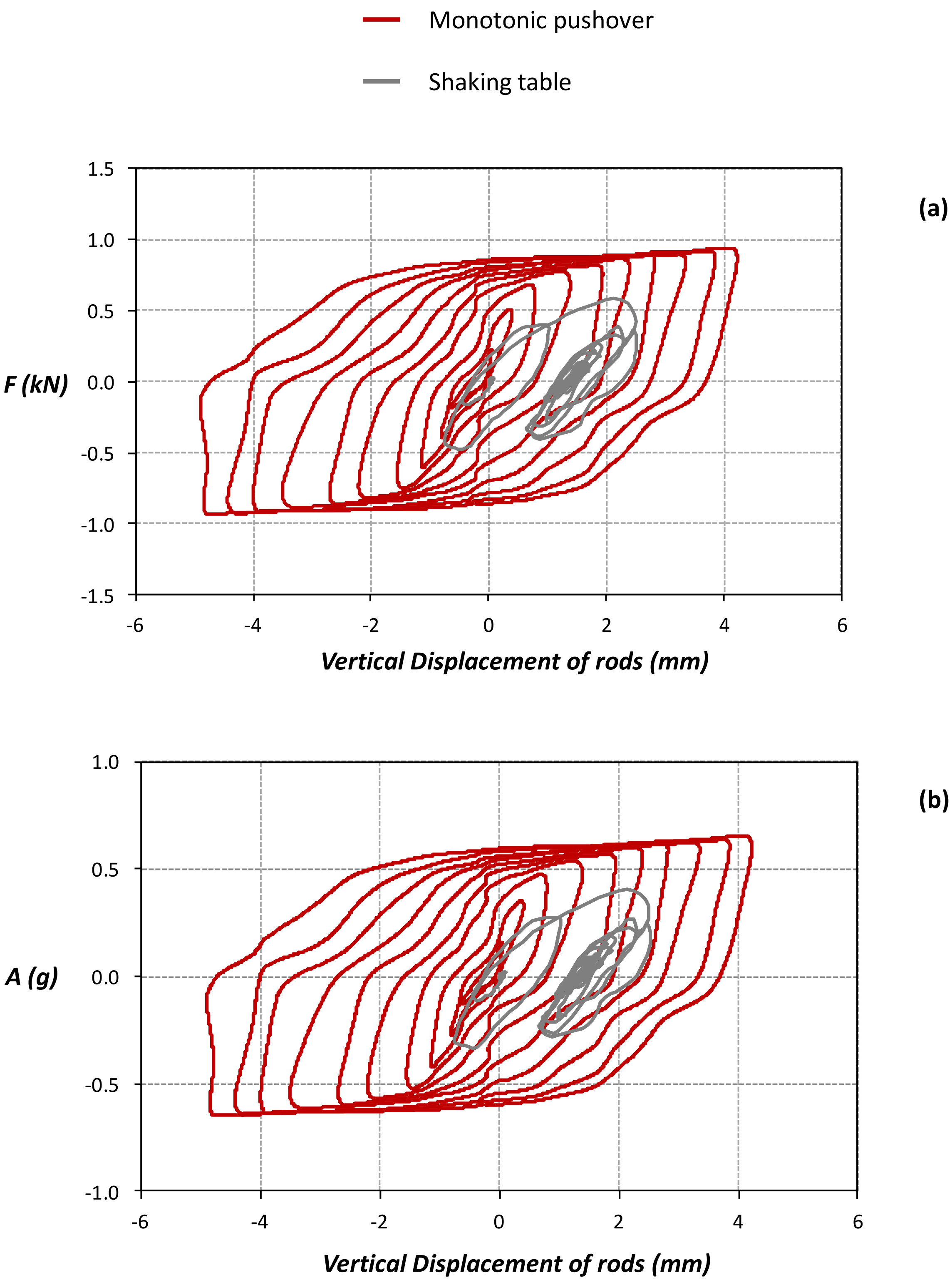

Figure 26. (a) Total shear force – relative vertical displacement of rods and **(b)** acceleration – vertical displacement curves compared to the respective curves derived from the 2nd horizontal pushover test.

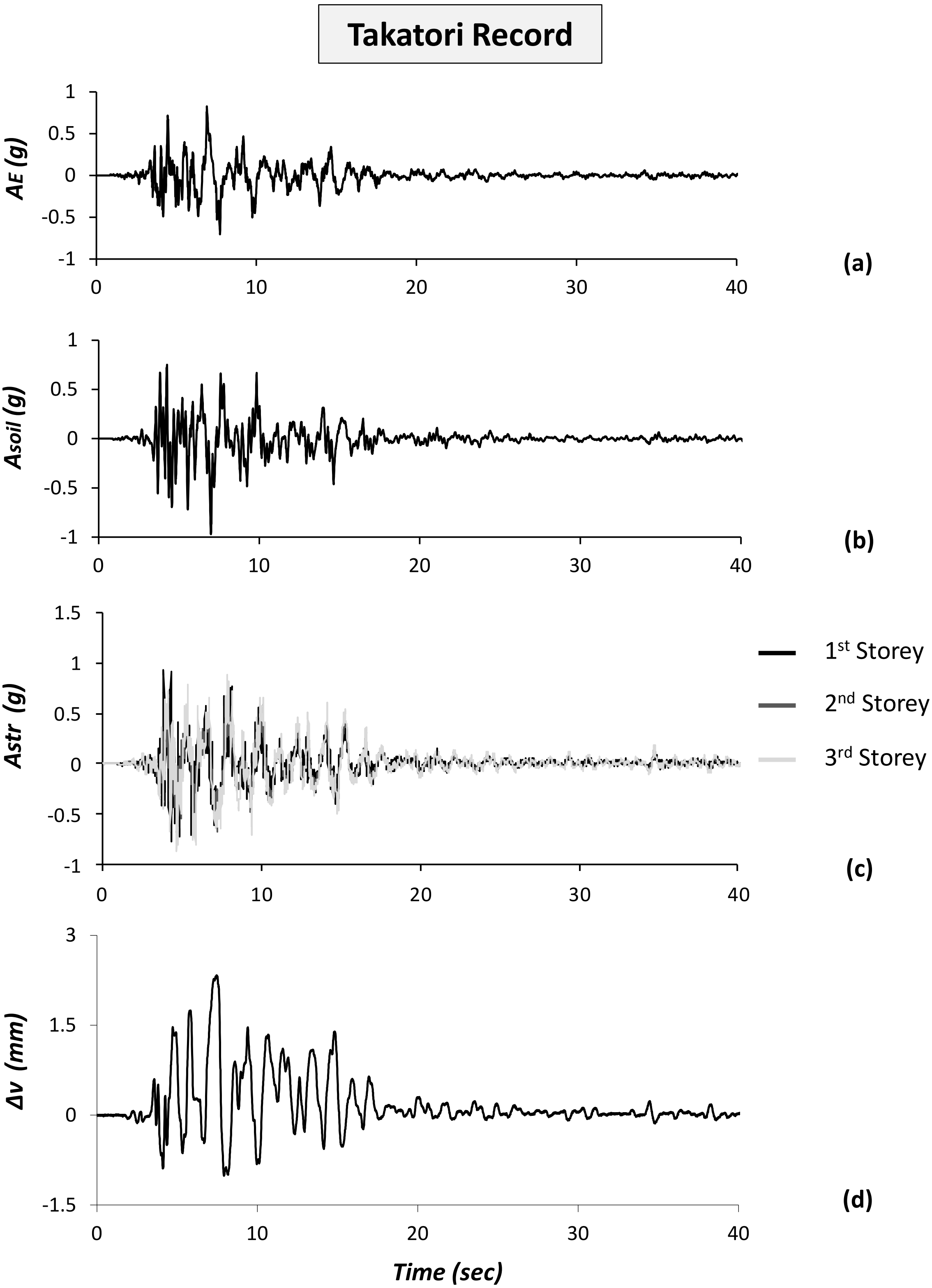

Figure 27. Time histories of **(a)** the acceleration used as bedrock excitation, **(b)** the acceleration measured in a small depth from the soil surface, **(c)** the accelerations measured at storey levels and **(d)** the vertical displacement of the rods.

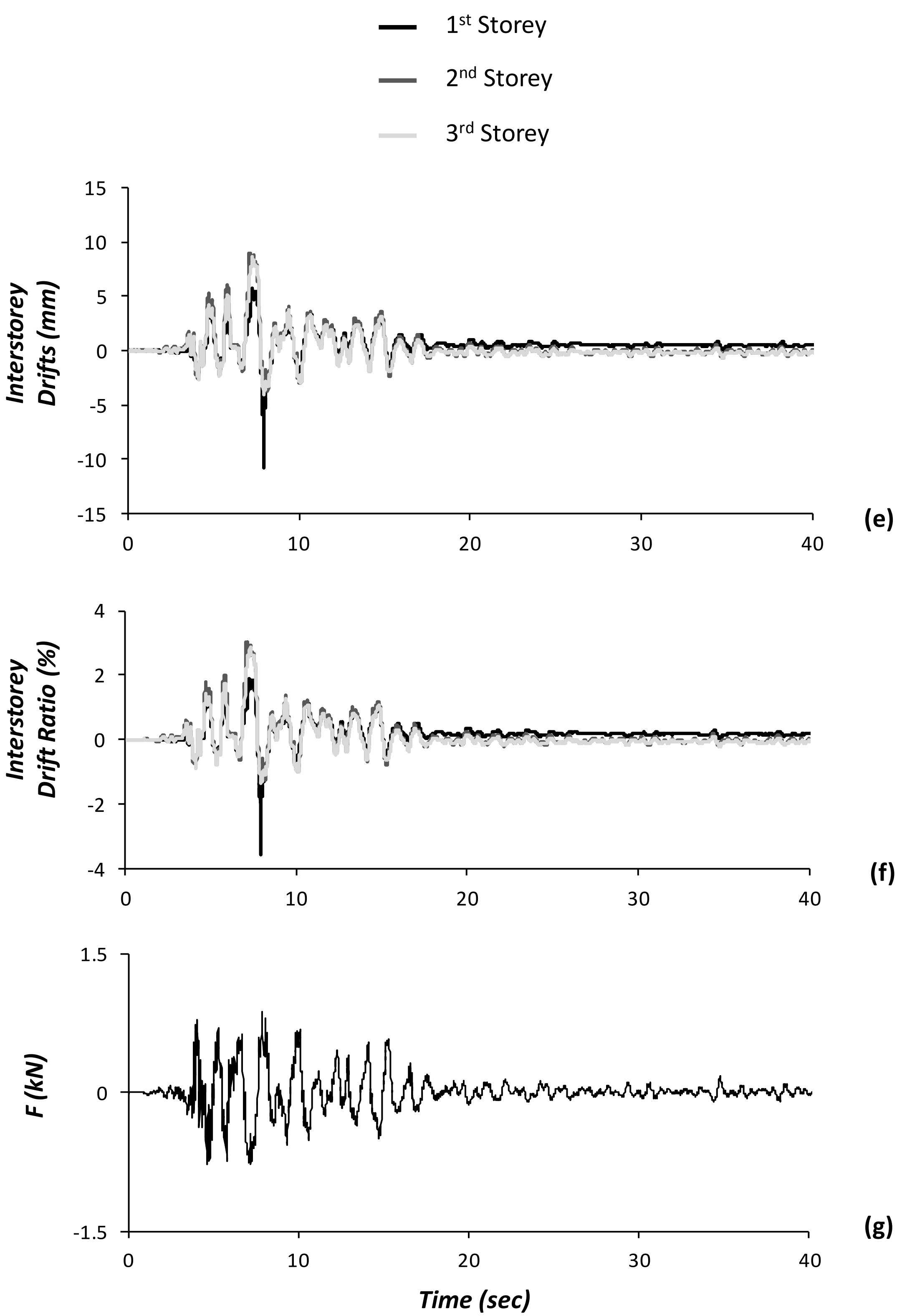

Figure 28. Time histories of **(e)** interstorey drifts at the level of each storey, **(f)** the respective drift ratios and **(g)** the total shear force the retrofitted structure receives .

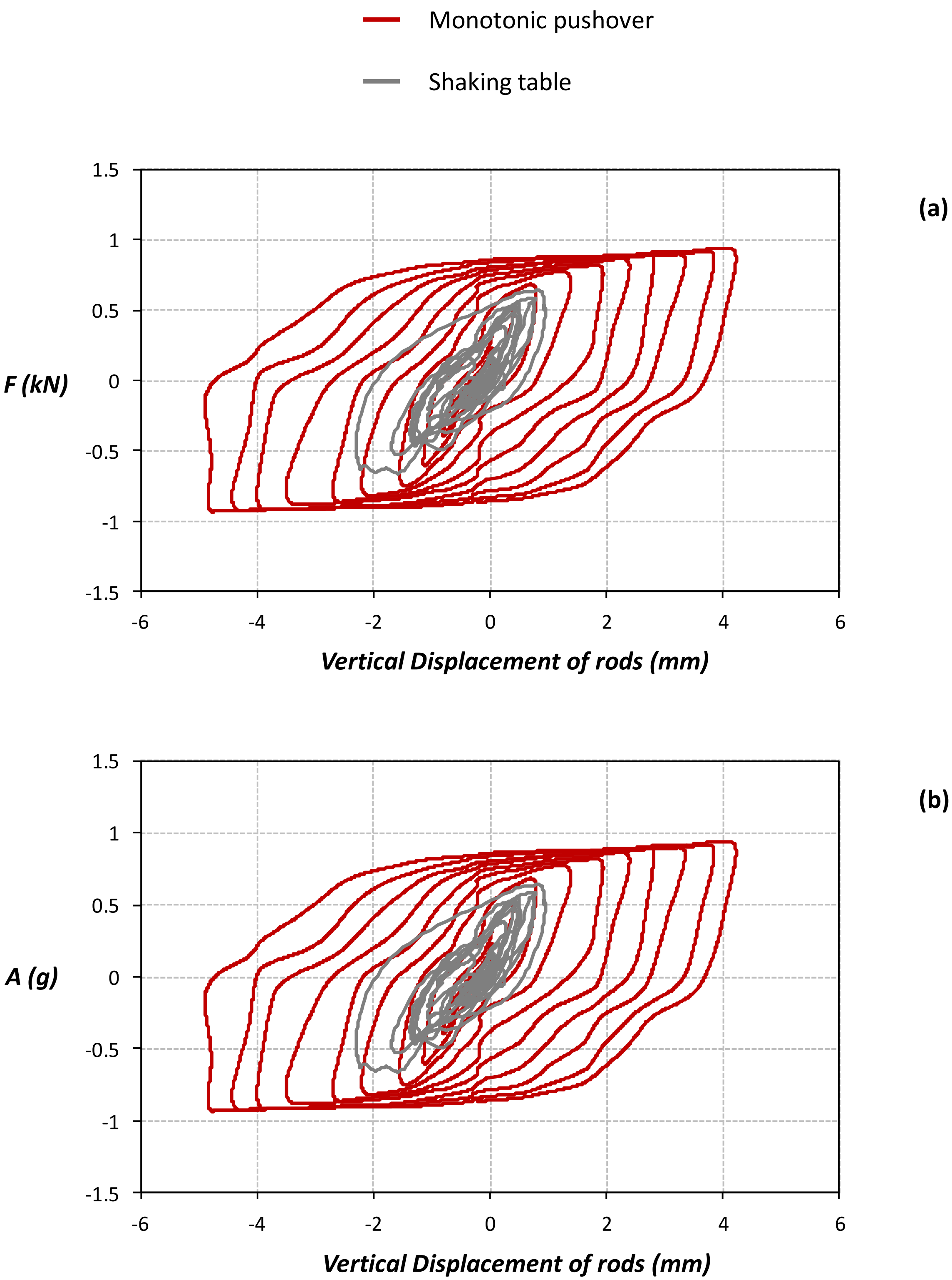

Figure 29. (a) Total shear force – relative vertical displacement of rods and **(b)** acceleration – vertical displacement curves compared to the respective curves derived from the 2nd horizontal pushover test.

Retrofitted building - SETUP III
Dynamic Test

List of applied seismic records.

Moderate Seismic Records
MNSA (Athens 1999) Lefkada (2003)
Strong Seismic Records
Rinaldi (Northridge 1994) JMA (Kobe 1995) Takatori (Kobe 1995)

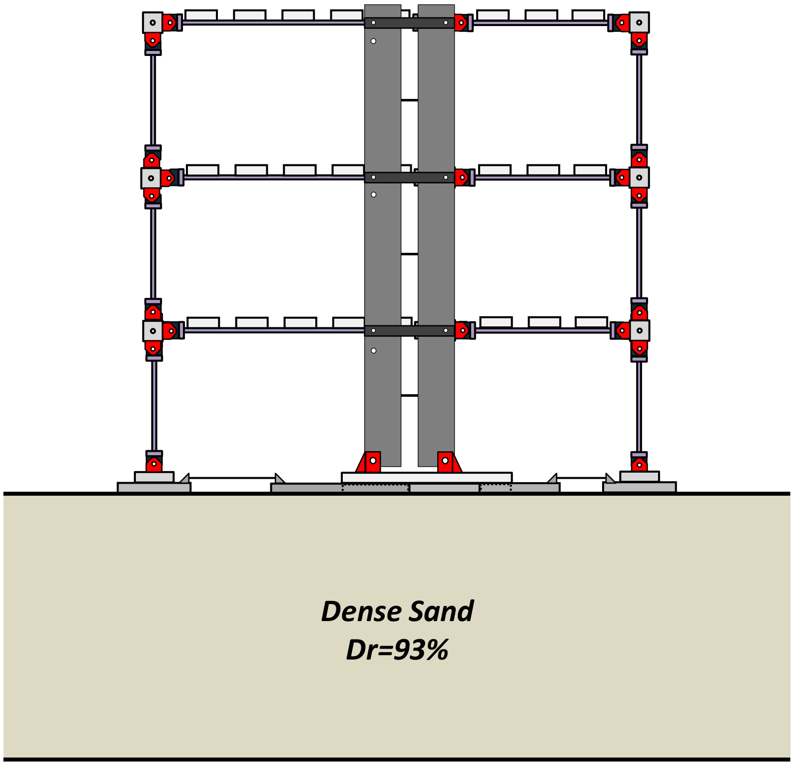

No. of rods per frame → 1
D = 3.2 mm

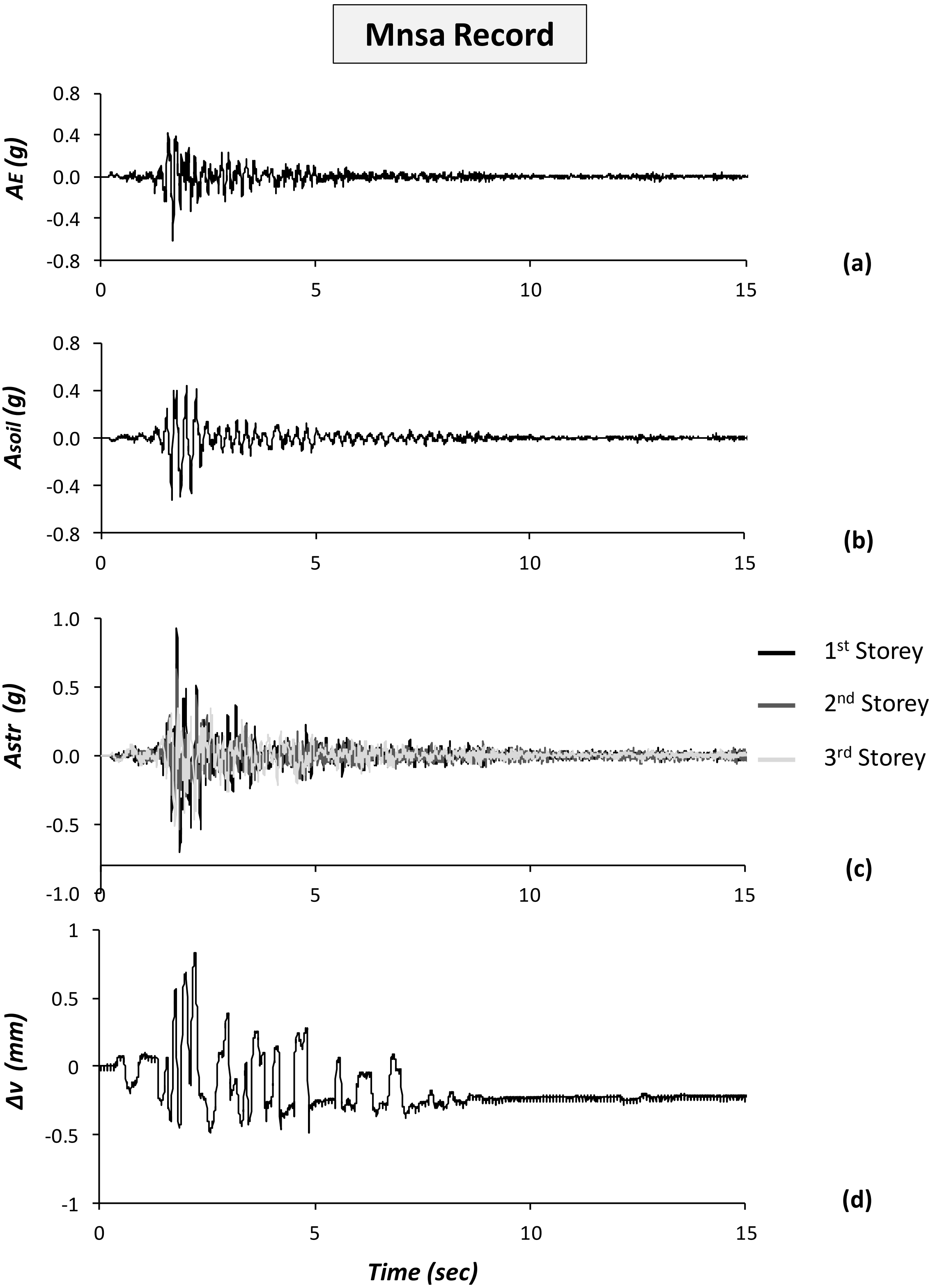

Figure 30. Time histories of **(a)** the acceleration used as bedrock excitation, **(b)** the acceleration measured in a small depth from the soil surface, **(c)** the accelerations measured at storey levels and **(d)** the vertical displacement of the rods.

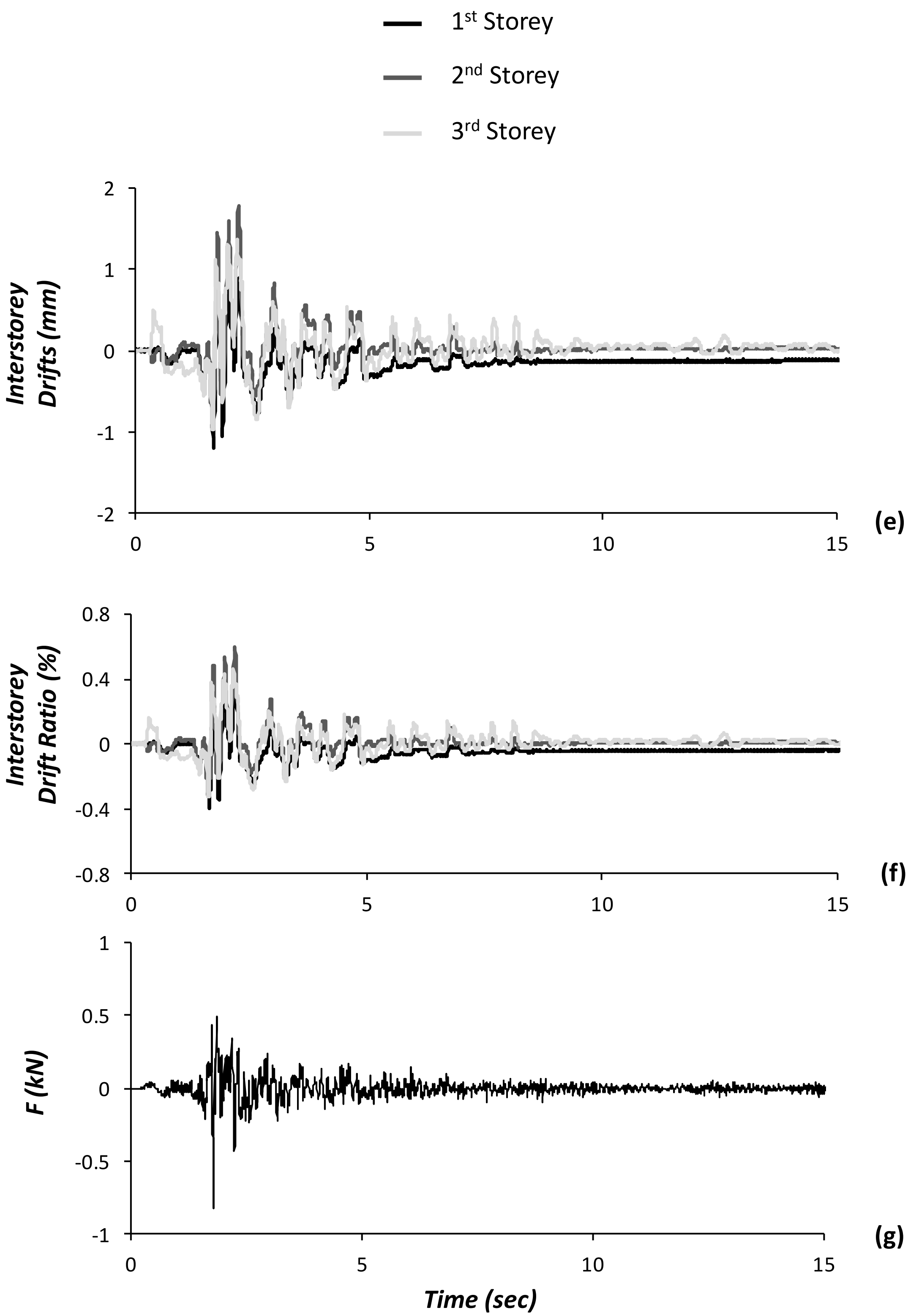

Figure 31. Time histories of **(e)** interstorey drifts at the level of each storey, **(f)** the respective drift ratios and **(g)** the total shear force the retrofitted structure receives .

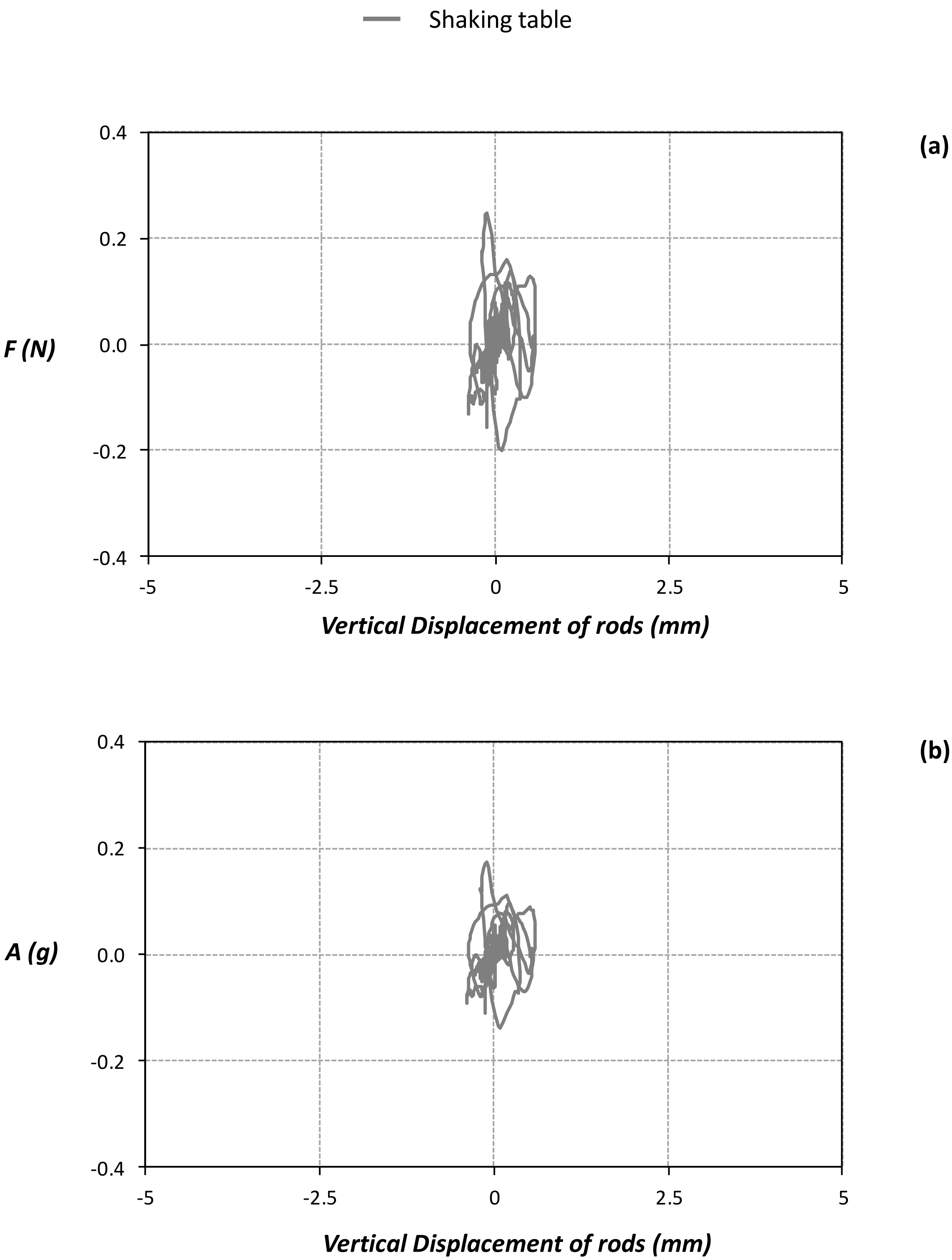

Figure 32. (a) Total shear force – relative vertical displacement of rods and **(b)** acceleration – vertical rod displacement curves.

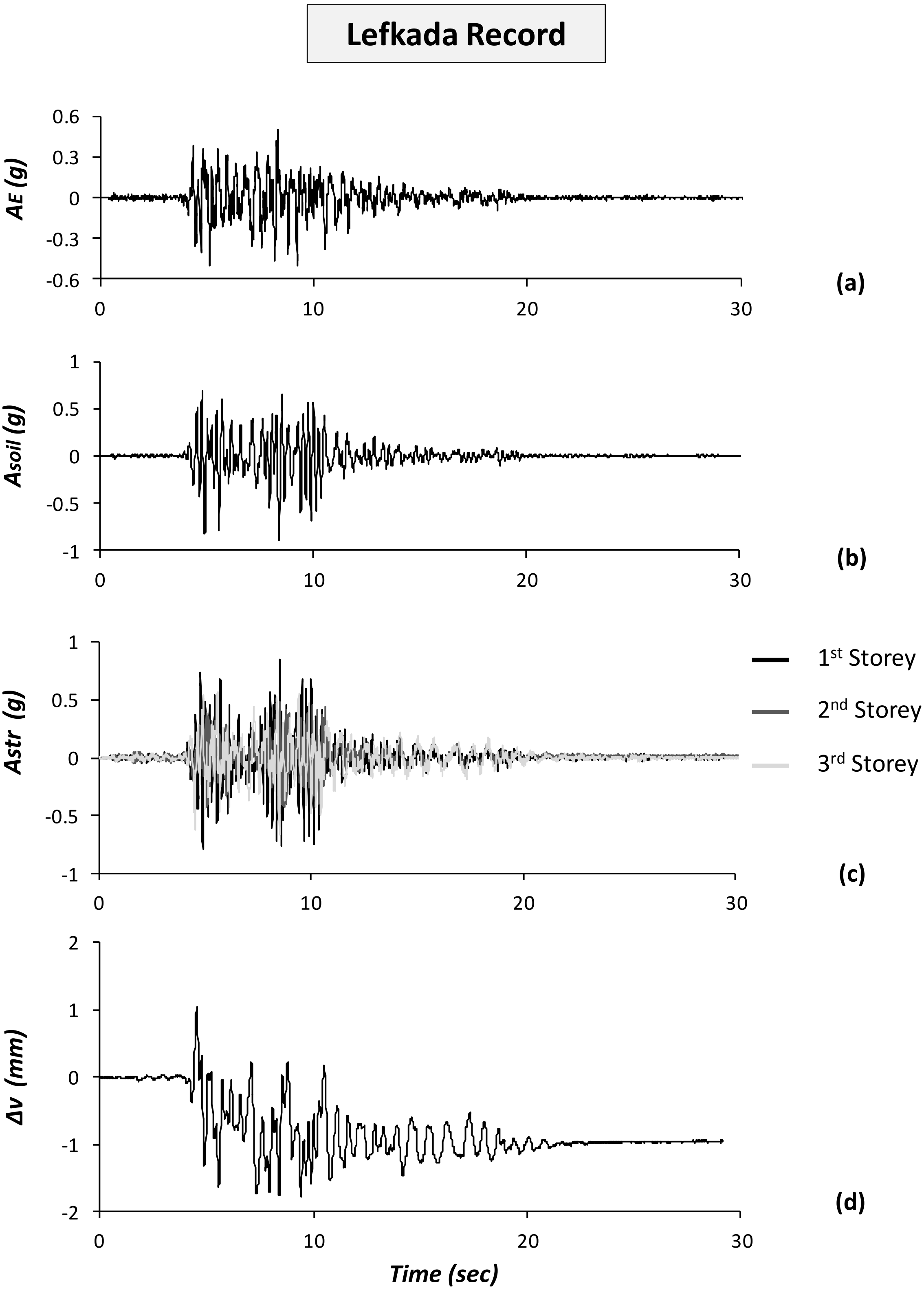

Figure 33. Time histories of **(a)** the acceleration used as bedrock excitation, **(b)** the acceleration measured in a small depth from the soil surface, **(c)** the accelerations measured at storey levels and **(d)** the vertical displacement of the rods.

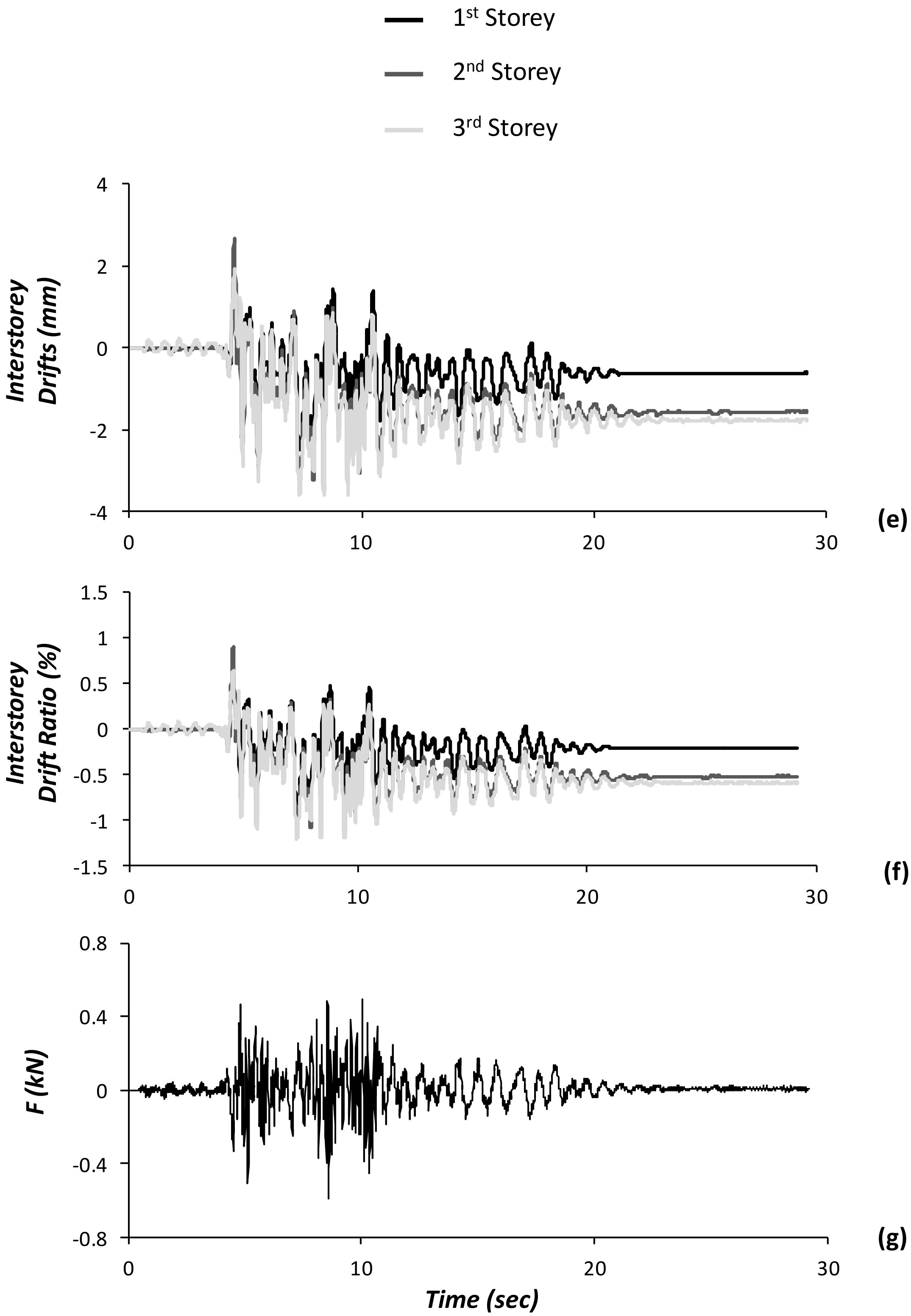

Figure 34. Time histories of **(e)** interstorey drifts at the level of each storey, **(f)** the respective drift ratios and **(g)** the total shear force the retrofitted structure receives .

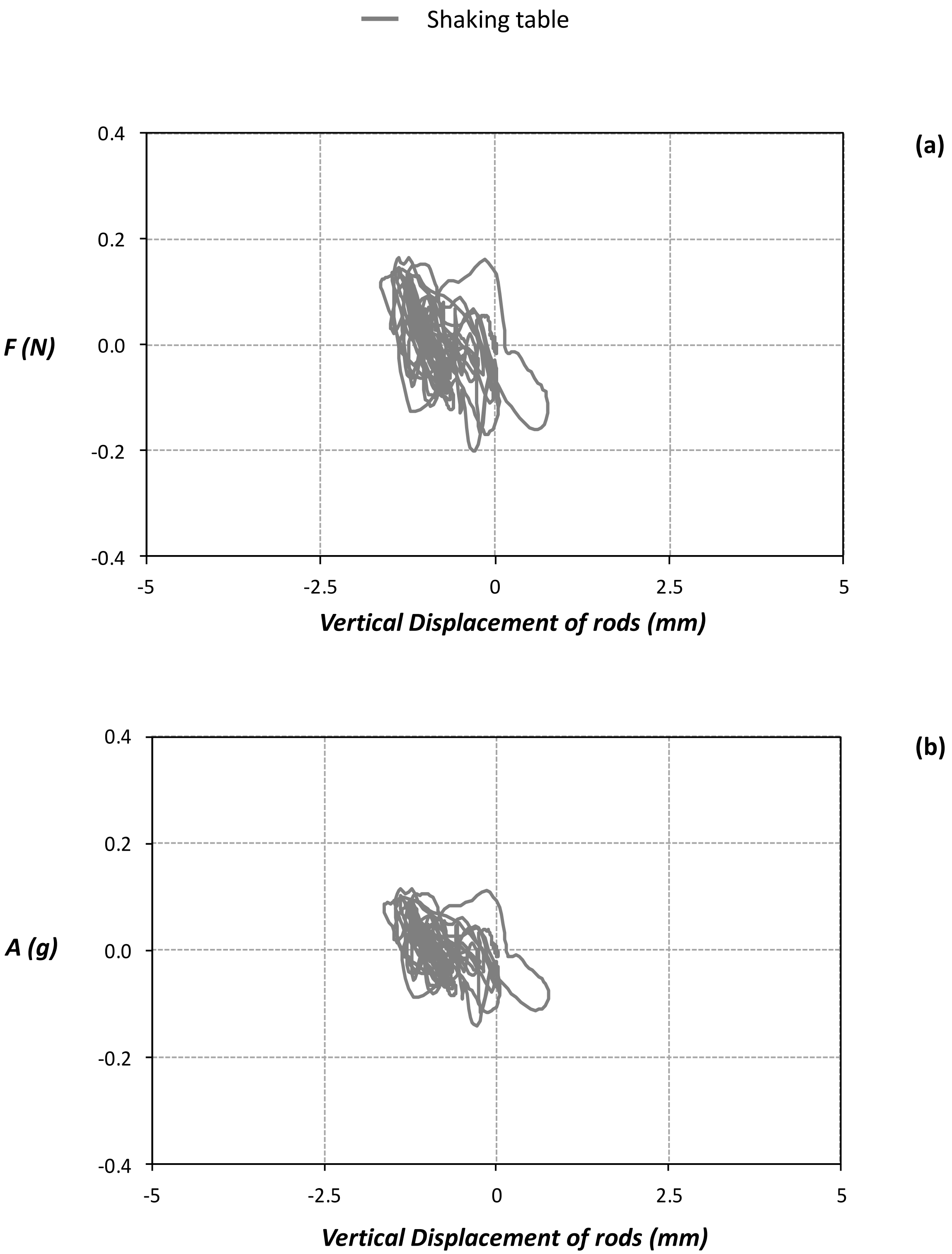

Figure 35. (a) Total shear force – relative vertical displacement of rods and **(b)** acceleration – vertical rod displacement curves.

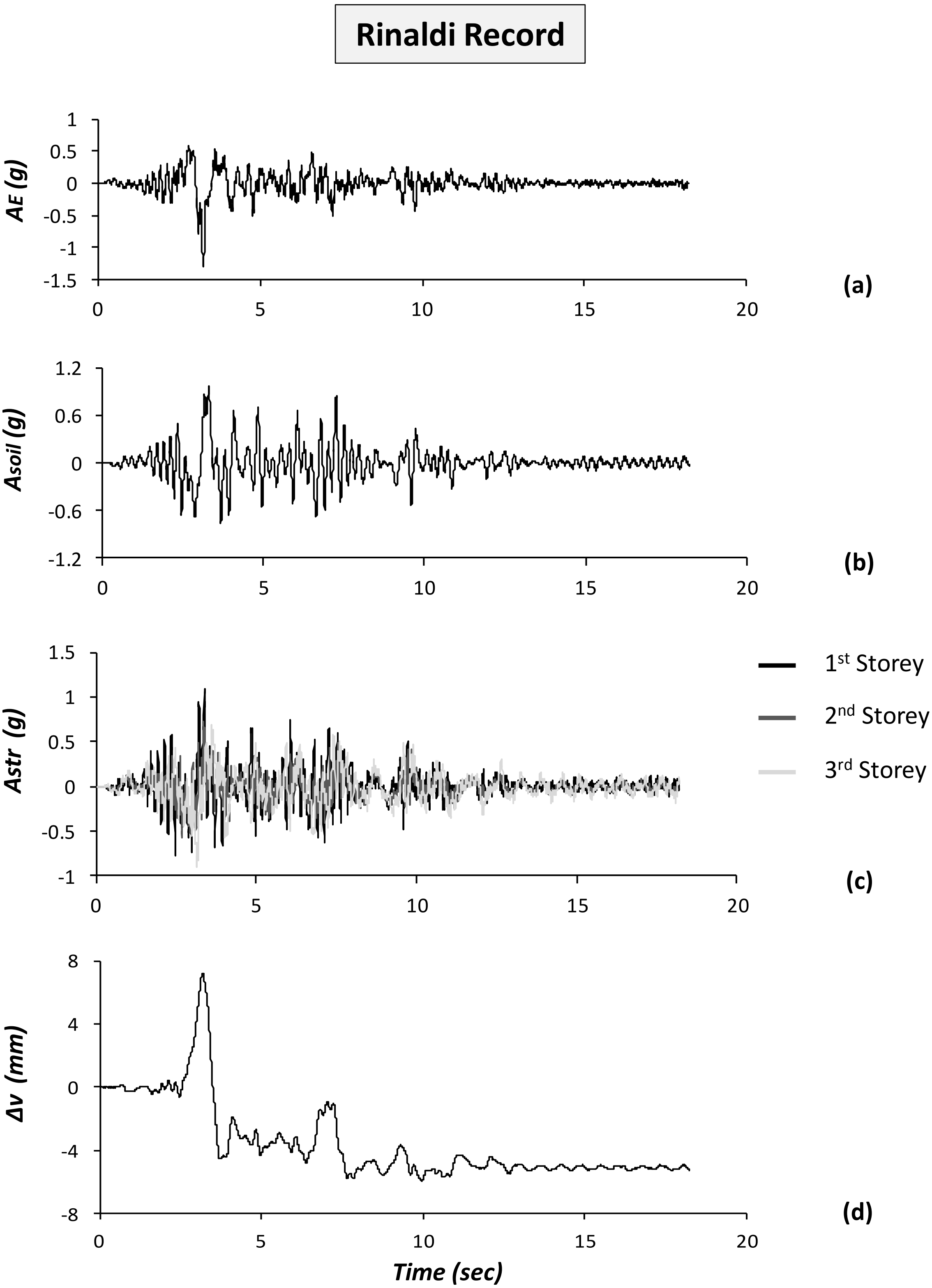

Figure 36. Time histories of **(a)** the acceleration used as bedrock excitation, **(b)** the acceleration measured in a small depth from the soil surface, **(c)** the accelerations measured at storey levels and **(d)** the vertical displacement of the rods.

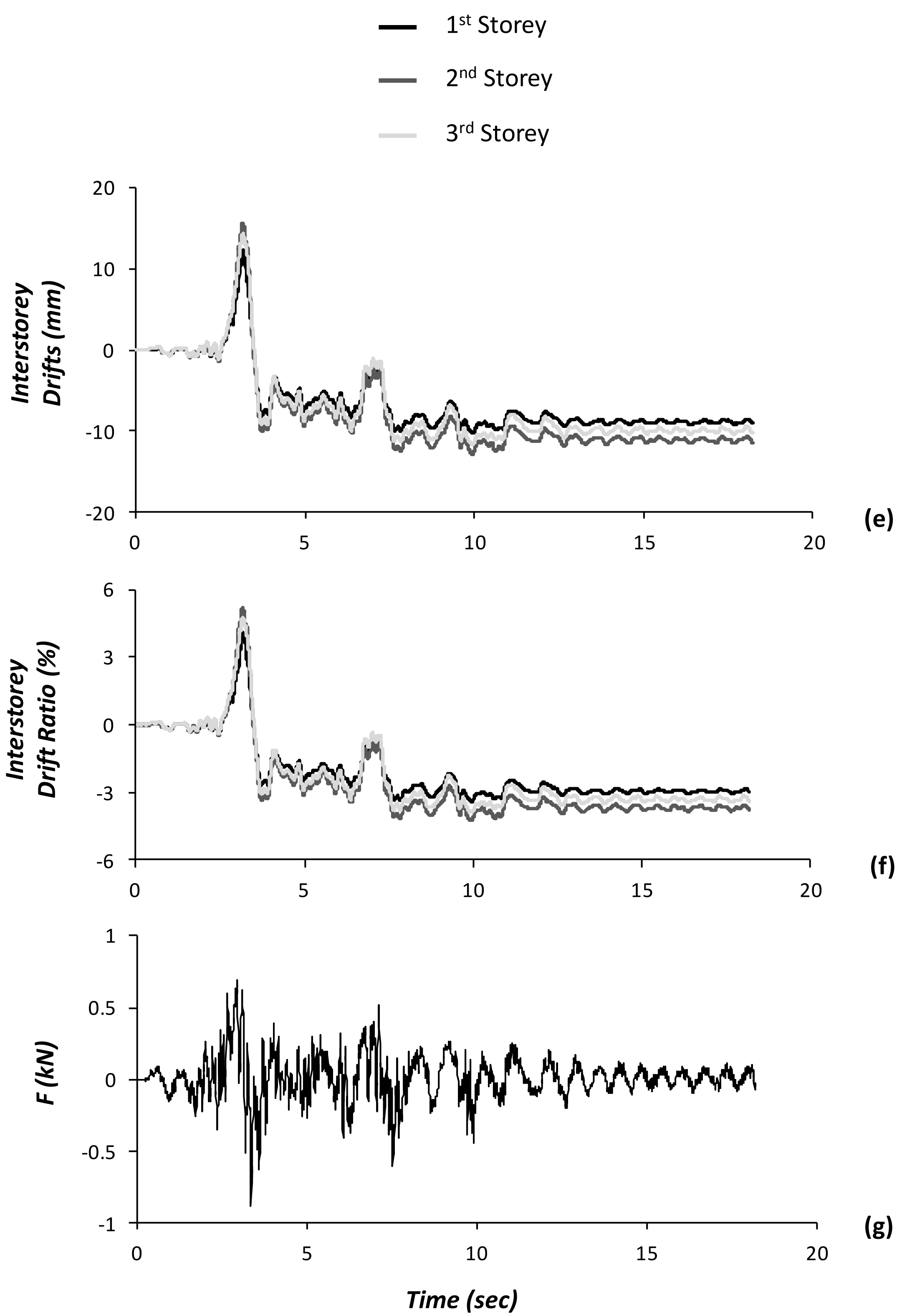

Figure 37. Time histories of **(e)** interstorey drifts at the level of each storey, **(f)** the respective drift ratios and **(g)** the total shear force the retrofitted structure receives .

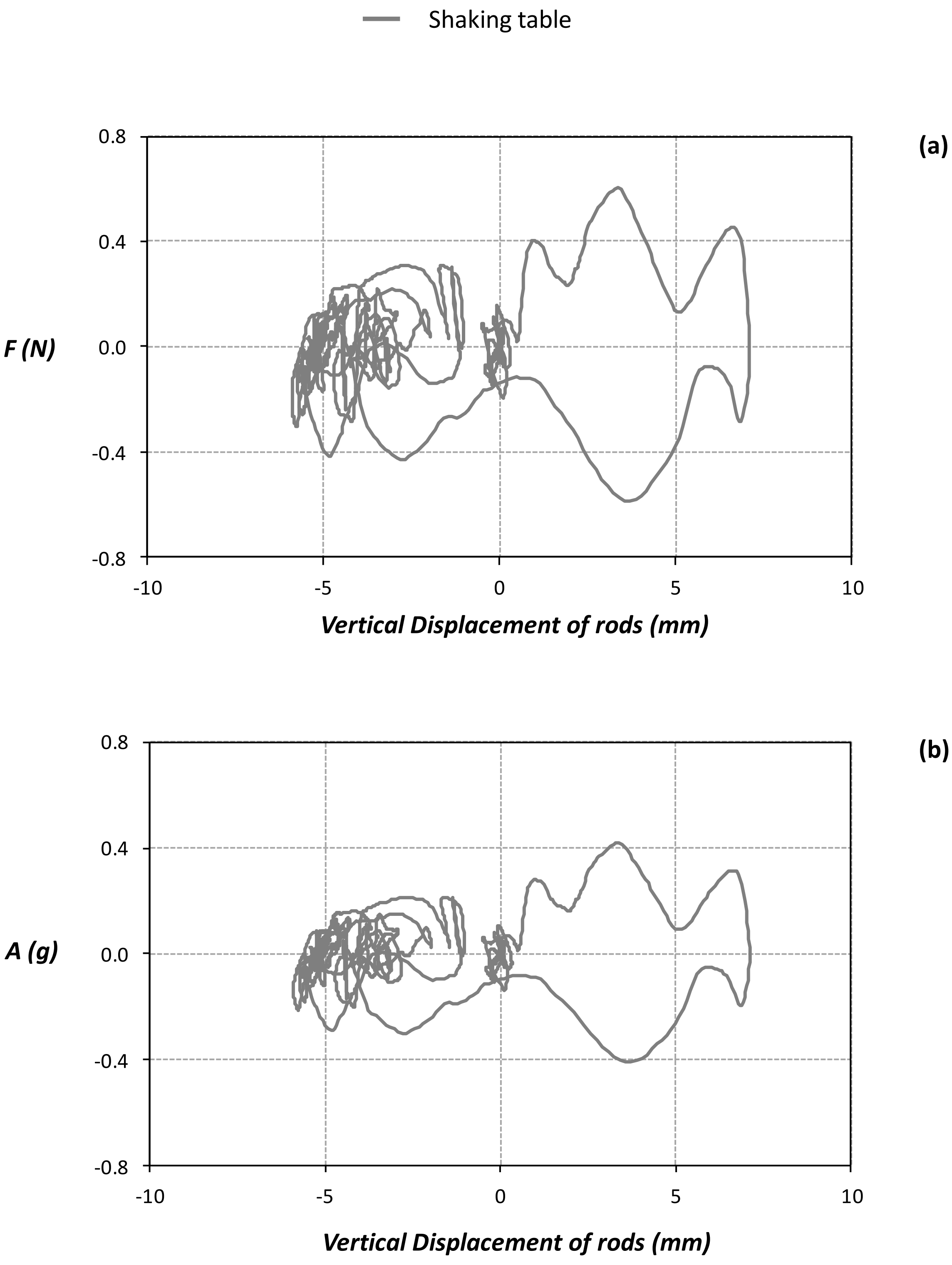

Figure 38. (a) Total shear force – relative vertical displacement of rods and **(b)** acceleration – vertical rod displacement curves.

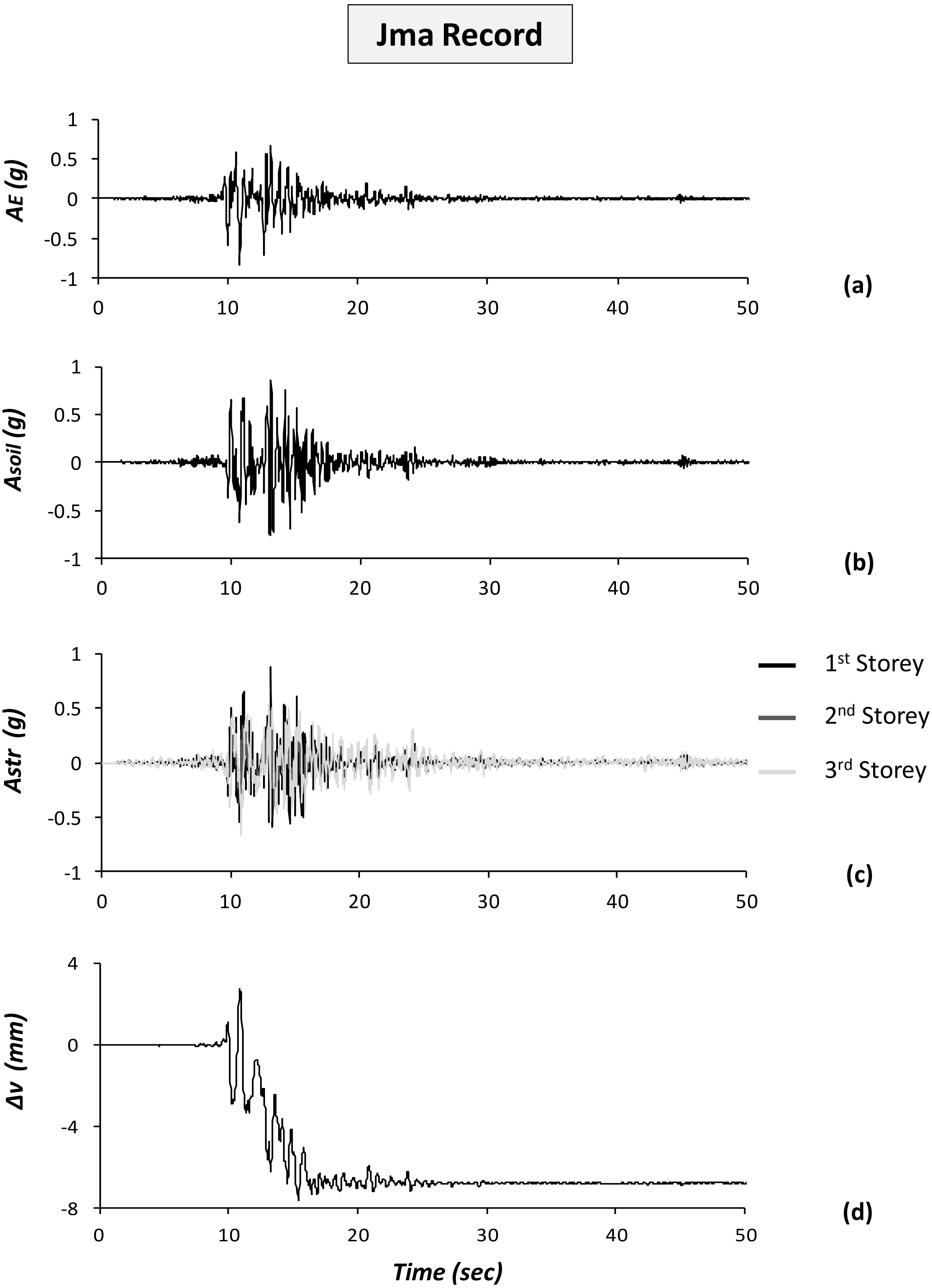

Figure 39. Time histories of **(a)** the acceleration used as bedrock excitation, **(b)** the acceleration measured in a small depth from the soil surface, **(c)** the accelerations measured at storey levels and **(d)** the vertical displacement of the rods.

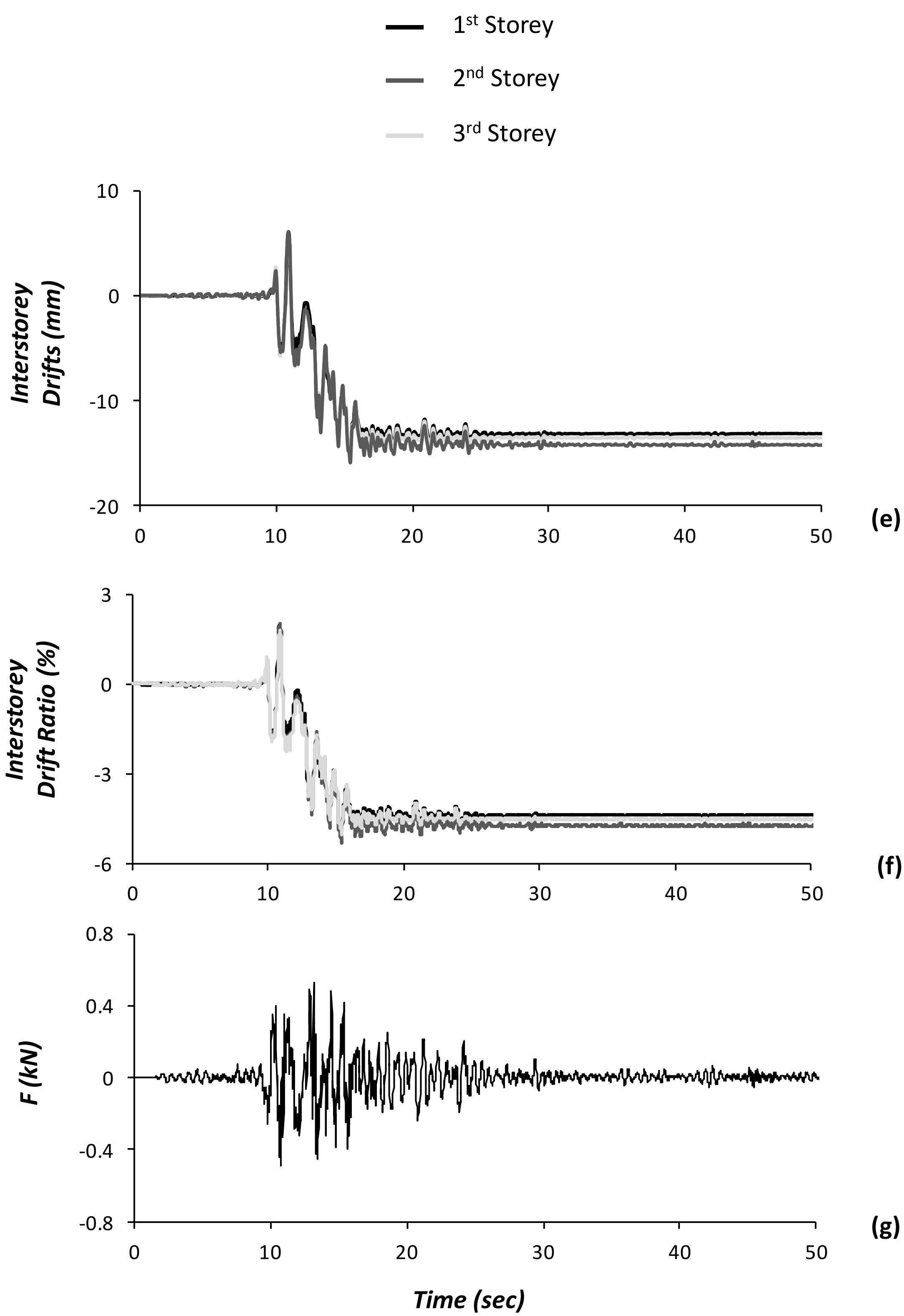

Figure 40. Time histories of **(e)** interstorey drifts at the level of each storey, **(f)** the respective drift ratios and **(g)** the total shear force the retrofitted structure receives .

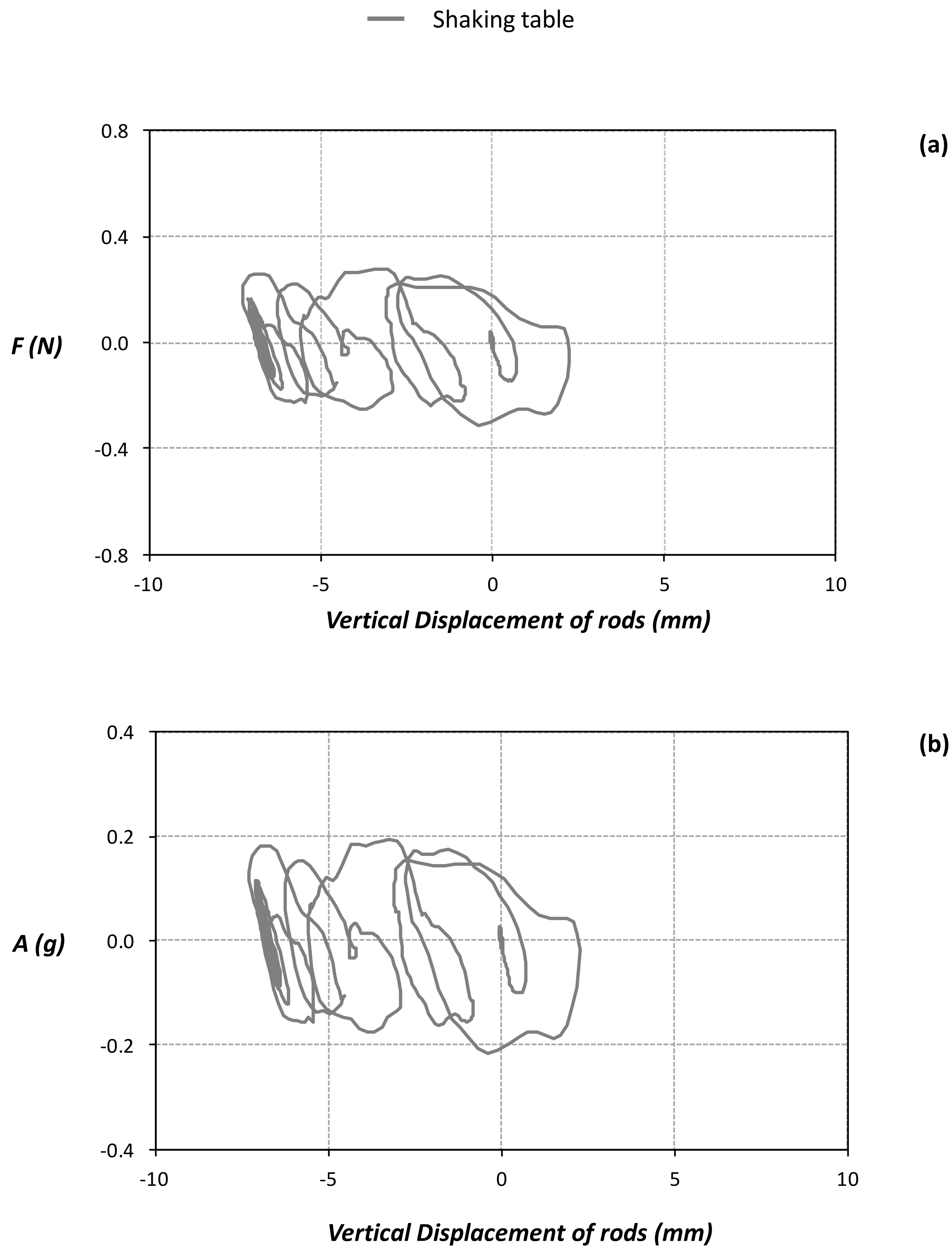

Figure 41. (a) Total shear force – relative vertical displacement of rods and **(b)** acceleration – vertical rod displacement curves.

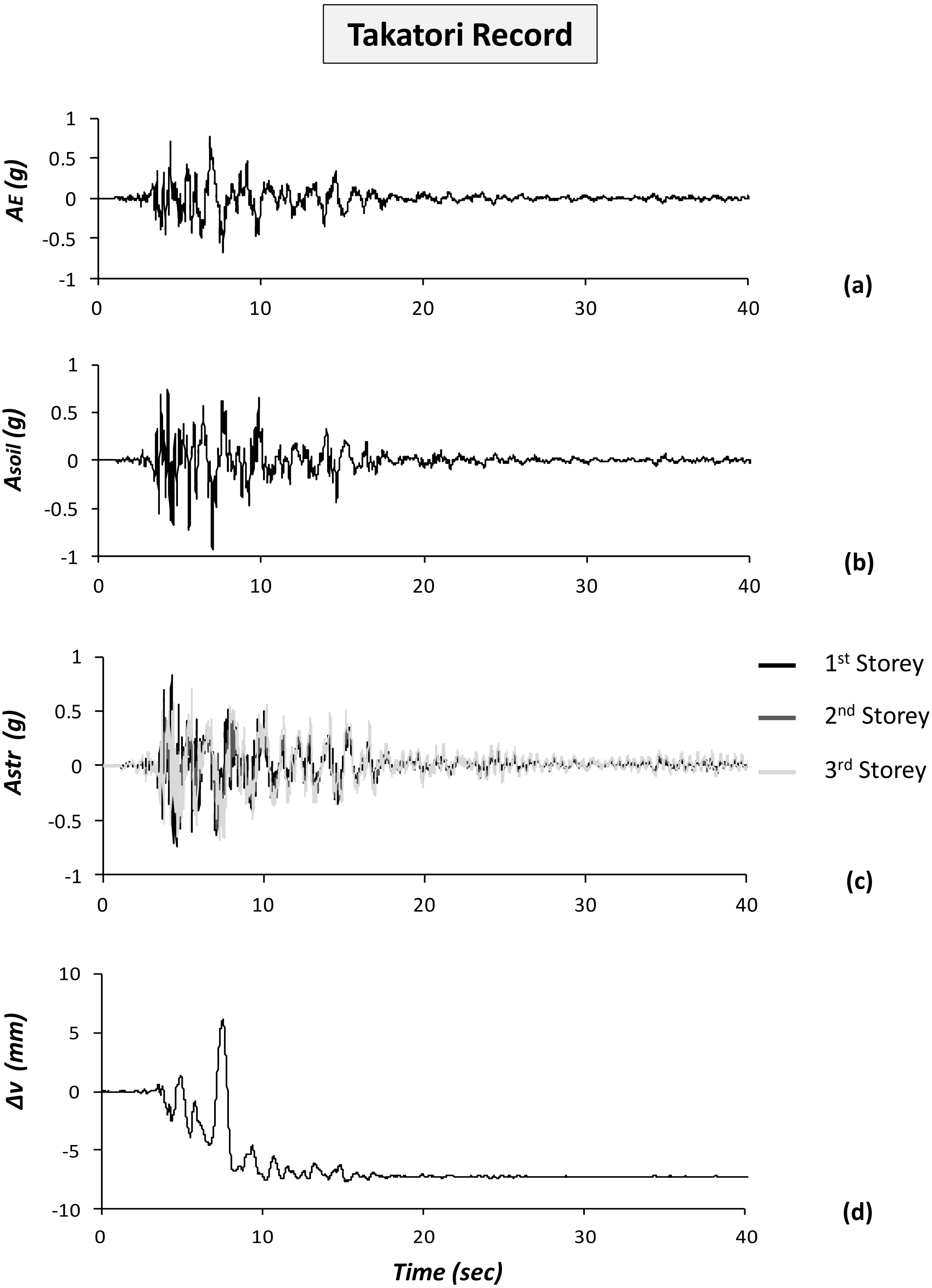

Figure 42. Time histories of **(a)** the acceleration used as bedrock excitation, **(b)** the acceleration measured in a small depth from the soil surface, **(c)** the accelerations measured at storey levels and **(d)** the vertical displacement of the rods.

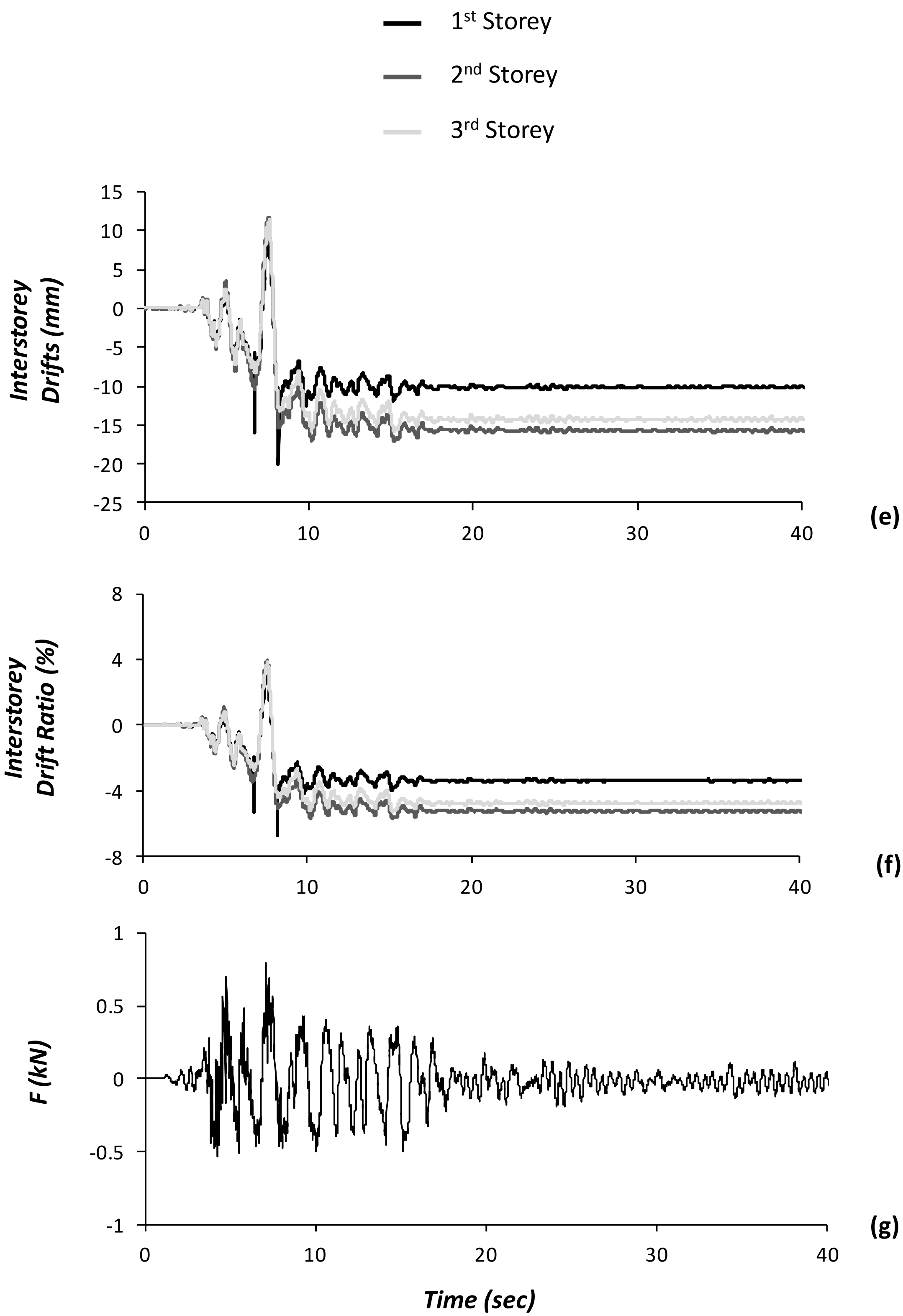

Figure 43. Time histories of **(e)** interstorey drifts at the level of each storey, **(f)** the respective drift ratios and **(g)** the total shear force the retrofitted structure receives .

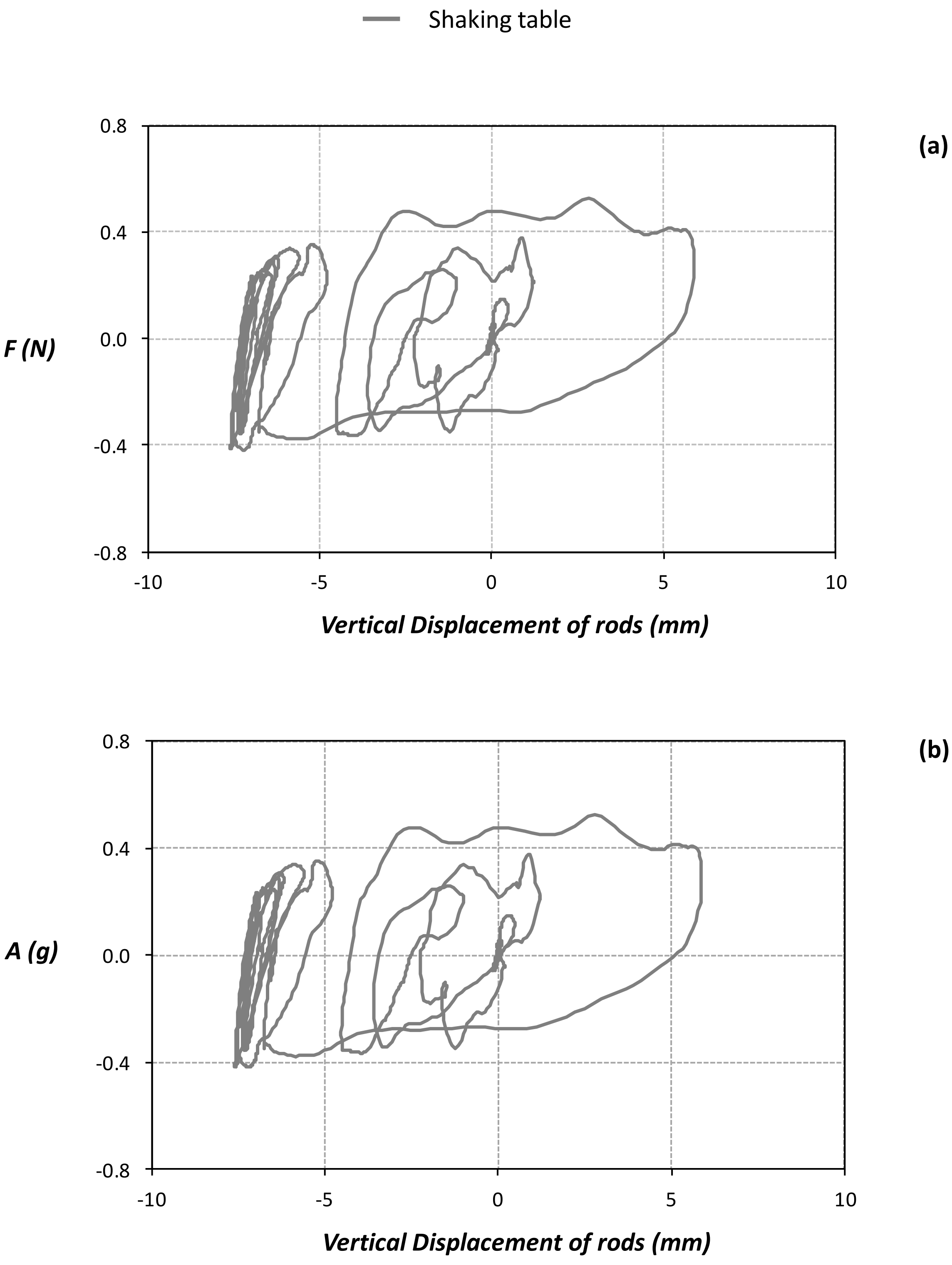

Figure 44. (a) Total shear force – relative vertical displacement of rods and **(b)** acceleration – vertical rod displacement curves.